Generation and Reactivity of Oxygen-Centred Radicals and Hydrogen Atoms in Organic Synthesis

Stefan Ivanov Chakarov

Primary supervisor: Dr Roopender Kumar

A thesis submitted in partial fulfilment of the requirements for the degree of

Doctor of Philosophy

Department of Chemistry

University College London

November 2025

Declaration

I, Stefan Ivanov Chakarov confirm that the work presented in this thesis is my own. Where information has been derived from other sources, I confirm that this has been indicated in the thesis.

Stefan I. Chakarov

31/10/2025

Abstract

This thesis explores the development of novel catalytic strategies to access highly reactive and underexplored radical intermediates. Although each project addresses a distinct synthetic challenge, together they contribute to the broader goal of expanding the toolbox for sustainable radical chemistry.

The first part focuses on the development of a strategy for novel titanium-based N-heterocyclic carbene catalysts capable of activating alcohols. Reaction design and conditions optimisation provided preliminary evidence consistent with homolytic C–O bond cleavage in primary alcohol substrates, while indicating that improved conversion and milder conditions will require further ligand optimisation.

The second part investigates strategies for generating oxygen-centred radicals aimed at anti-Markovnikov hydroxylation of terminal olefins. Pyridine N-oxides were identified as suitable precursors for radical oxygen-transfer under photoredox conditions, providing a promising approach to direct olefin hydroxylation.

Finally, the third project presents a near-UV-initiated methodology for generating a hydrogen radical. As a proof of concept, radical hydrogenation of terminal alkenes and Michael acceptors was achieved and optimised. Mechanistic studies revealed two potential pathways: (i) direct generation and radical addition of the hydrogen atom, and (ii) concerted transfer of a hydrogen radical into the olefinic π-system.

Collectively, these studies demonstrate how rational catalyst and reaction design can unlock previously unexplored radical reactivity under synthetically useful conditions.

Impact Statement

This research advances the field of sustainable organic synthesis through the development of novel catalytic strategies for accessing challenging radical intermediates. Alcohols are among the most abundant and readily available feedstocks in organic chemistry, yet their inertness under single-electron conditions has limited their direct use as radical precursors. The first part of this thesis explores metal-mediated pathways capable of overcoming this limitation, focusing on rational ligand design and metal catalyst formation to generate alkyl radicals directly from simple alcohols.

The second part of this work addresses the long-standing challenge of anti-Markovnikov hydroxylation of olefins. By harnessing the reactivity of highly oxidising oxygen-centred species, this study identifies new pathways for achieving regioselective C–O bond formation under mild, catalytic conditions. In the final chapter, a novel strategy for the controlled production of the hydrogen atom radical is described. This proof of concept establishes the feasibility of generating and harnessing the smallest radical species in a synthetically useful way. Although the demonstrated radical hydrogenation does not yet surpass existing olefin saturation methodologies, it reveals a previously underexplored mechanistic approach that could inspire future developments in hydrogen radical chemistry and radical hydrogen transfer.

Within academia, this work lays the foundation for new directions in N-heterocyclic carbene catalysis, where the systems developed here could enable previously unobserved reactivity and catalytic transformations. The proposed strategy for oxygen radical generation provides a potential route toward solving the long-standing problem of anti-Markovnikov hydroxylation, while the generation of the smallest radical introduces an untapped dimension of radical chemistry. For example, hydrogen radicals could enable atom-economical halogen abstraction and offer routes to activate strong C–F bonds, presenting opportunities for the upcycling of perfluoroalkyl substances (“forever chemicals”) with potential environmental and industrial significance.

Beyond academia, these findings could contribute to sustainable chemical manufacturing. By enabling alcohols to serve as radical precursors, this research

supports the upconversion of biomass and biomass-derived platform chemicals, facilitating the use of cheap, renewable feedstocks. The one-step anti-Markovnikov hydroxylation represents an efficient means to produce linear alcohols, valuable intermediates in bulk and fine chemical synthesis. Given the prevalence of alkenes in pharmaceutical scaffolds, these methods could also find use in late-stage functionalisation of drug candidates. Finally, radical hydrogenation has been extensively observed in coal liquification processes, thus our work could supplement current strategies for crude oil refining.

Overall, this thesis provides fundamental insight and practical strategies for selective C–O bond homolysis and formation, and hydrogen-centred radical generation, advancing both the scientific understanding and sustainable practice of modern organic synthesis.

For my family

Acknowledgments

I still struggle to fathom that my PhD journey has come to an end. It feels almost as if it were yesterday when I first stepped through the gates of the Kathleen Lonsdale Building. Nevertheless, three years filled with challenges and excitement have passed, and if I could, I would relive them all again. The countless hours spent in the lab, the thousands of experiments, and the many, many failures have shaped the scientist I am today, and I am truly grateful to have experienced it all.

Now, I would like to express my gratitude to the people who have accompanied me on this journey of personal and professional growth.

First and foremost, I would like to thank my supervisor, Dr Roopender Kumar, for your constant support and guidance throughout the course of my PhD. I will always cherish our discussions—whether about science, philosophy, or the philosophy of science—and I am deeply grateful for the many lessons you have taught me. As a mentor, you have truly inspired me to pursue my passions and dreams. I would not be where I am today without your encouragement during difficult times and your guidance when things were unclear. Thank you for the opportunity to work on such challenging and exciting projects; I hope that one day they will truly make a dent in scientific knowledge.

Over the past three years, I have had the opportunity to work with and supervise a number of ambitious Master's students, and I would like to thank them for their contributions to the lab spirit, their help with shared projects, and—most importantly—for the lessons they taught me.

In my first year of the PhD, I was very excited to supervise my first student, Qilong, and I would like to thank him for his contribution to my work and for always maintaining a positive attitude (even in the face of a hundred optimisation reactions). The next student I worked with, Ryan, taught me that the world isn't always fair, but that with patience and perseverance, one can achieve anything. It was also a great pleasure to work with Roman during my final year project, and I greatly appreciate his dedication and hard work in expanding our library of photocatalysts. Around that time, I met Annie, who reminded me always to pursue my passions—no matter the field.

I would also like to thank the rest of the Kumar group – Xuezheng, Angelica, Anas, and Alan – whose enthusiasm and curiosity made it a pleasure to briefly supervise them in their projects. Working alongside all of you has been a genuine pleasure, and your presence in the lab was always something to look forward to. I will miss each and every one of you, and I hope our paths will cross again in the future.

I would also like to acknowledge my secondary supervisor, Prof. Vijay Chudasama, for serving as part of my supervisory committee. In addition, I would like to thank the Sheppard group for organising our joint group meetings and for generously sharing their scientific insights, in particular Matt and Richard for their help in the lab with any of my questions.

I am also grateful to the other members of the research groups in the KLB for creating such a friendly and supportive working environment.

Finally, my extended thanks go to Dr. Abil Aliev for assistance with NMR spectroscopy, Dr. Kersti Karu for mass spectrometry analysis, and Dr. Alberto Collauto (Imperial College London) for EPR analysis.

Abbreviations

acac - Acetylacetonate

BDE – Bond dissociation energy

BINOL – 1,1′-Bi-2-naphthol

bpy - 2,2'-bipyridine

BQ – Benzoquinone

CDI – Carbonyldiimidazole

CHD – Cyclohexadiene

Cp – Cyclopentadienyl

DBU – 1,8-Diazabicyclo[5.4.0]undec-7-ene

DCE – 1,2-Dichloroethane

DCM – Dichloromethane

DDQ – 2,3-Dichloro-5,6-dicyano-p-benzoquinone

DFT – Density Functional Theory

DMA – Dimethylacetamide

DMF – Dimethylformamide

DMPO – 5,5-Dimethyl-1-pyrroline-N-oxide

DMSO – Dimethyl sulfoxide

EPR – Electron paramagnetic resonance

FAT – Fluorine atom transfer

Fc – Ferrocene

HAT – Hydrogen atom transfer

HBQ – Hydrobenzoquinone

HOMO – Highest occupied molecular orbital

ILCT – Intraligand charge transfer

LLCT – Ligand-to-ligand charge transfer

LMCT – Ligand-to-metal charge transfer

LUMO – Lowest unoccupied molecular orbital

MLCT – Metal-to-ligand charge transfer

mCPBA – Meta-chloroperoxybenzoic acid

MW – Microwave

NBS – N-bromo succinimide

NFSI – N-fluorobenzenesulfonimide

NHC – N-heterocyclic carbene

NHE – Normal hydrogen electrode

NMP – N-methyl-2-pyrrolidone

NR – No reaction

PC – Photocatalyst

PCET – Proton coupled electron transfer

ppy – 2-phenylpyridine

PTC – Phase transfer catalyst

Pyr – Pyridine

RHT – Radical hydrogen transfer

ROS – Reactive oxygen species

RT – Room temperature

SCE – Standard calomel electrode

SET – Single electron transfer

SHE – Standard hydrogen electrode

TBAC – tetrabutylammonium chloride

TiBALD – Titanium(IV) bis(ammonium lactato)dihydroxide

TFA – Trifluoroacetic acid

THF – Tetrahydrofuran

TMS – Trimethylsilane

TPPT – 2,4,6-Triphenylpyrylium tetrafluoroborate

UV – Ultraviolet

XAT – Halogen atom transfer

Table of Contents

List of Figures

List of Tables

List of Schemes

CHAPTER 1

Overview of Radical Chemistry: Applications and Challenges in Organic Synthesis

1.1. Overview of radical chemistry

Radicals occupy a central role in modern organic chemistry, enabling bond formations and functional group interconversions that are often inaccessible through polar pathways.

The origins of radical chemistry can be traced back to the mid-19th century with the development of the Kolbe electrolysis.[1] Although the concept of open-shell species was not yet understood, several key reactions now recognised as radical processes were discovered during this period, including the Wurtz coupling (1855)[2, 3] and the Sandmeyer reaction (1884).[4, 5] Definitive evidence for free radicals emerged in 1900, when Gomberg isolated the trityl radical ($Ph_3C^{\bullet}$), confirming the existence of discrete carbon-centred radicals.[6]

Following this, studies in the 20th century laid the foundations for understanding the reactivity of radicals, their generation and stability. The selective anti-Markovnikov addition into alkenes and Michael acceptors was the focus of studies by Kharash[7] and Giese[8] respectively. Arene radical functionalisation, such as homolytic aromatic substitution, was pioneered by Hey and Waters,[9] while Minisci later expanded this reactivity to radical additions into pyridines.[10] Bachmann introduced the concept of the persistent radical effect,[11] while the kinetic studies by Walling, Beckwith and Ingold, among others, focused on measuring the rate of radical processes and developing a variety of 'radical clocks'.[12-15] The mechanistic insights gained from these and other[16] developments transformed radicals from 'unstable curiosities' into reliable synthetic intermediates.[17]

Building on this foundation, contemporary methods have sought to broaden the range of accessible radical precursors and to achieve their generation under increasingly mild and controlled conditions.[18-20] As our understanding of radicals matured, it became evident that their intrinsic stability and reactivity depend strongly on the nature of the atom bearing the unpaired electron.

An overview of the known open-shell species revealed that radical chemistry has been primarily centred around carbon, with tens of thousands of known examples, making it the most thoroughly studied and well-understood class of radicals (Figure 1.1).[16] In contrast, nitrogen- and oxygen-centred radicals are far less represented, while synthetic reports on the hydrogen-centred radical are exceedingly rare. This disparity

in distribution can be attributed to their relative stability. Most radicals are typically stabilised through hyperconjugation, delocalisation or steric crowding, however nitrogen and oxygen radicals are inherently more destabilised relative to carbon due to their higher electronegativity. Hydrogen radical on the other hand, has no stabilising effects and populating the 1s shell with a single electron is energetically demanding owing to its proximity to the nucleus. Thus, the generation of N-, O- and H- centred radicals is significantly more challenging relative to carbon, resulting in their lesser exploration in a synthetic setting. This chapter provides a brief overview of contemporary strategies developed to access such challenging radicals in organic synthesis.

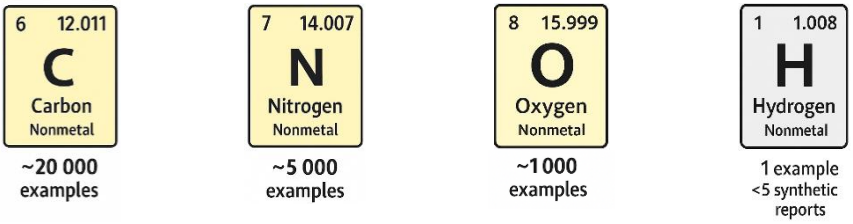

Figure 1.1. Distribution of known radical species by element.[21]

1.1.1. Generation of carbon-centred radicals

As the most extensively explored class of radical species, numerous strategies have been developed for the generation of alkyl radicals (Scheme 1.1, A). The hydrogen atom transfer (HAT) pathway enables their direct formation from simple hydrocarbons via abstraction of a hydrogen atom from a C–H bond.[22] In parallel, alkyl radicals can be accessed from prefunctionalised substrates such as halides, carboxylic acids and their derivatives, or alcohol derivatives through direct irradiation, halogen atom transfer (XAT) or single-electron transfer (SET) pathways.[23] For XAT reactions, the rate determining step is the C–X bond homolysis, which is dependent on the bond dissociation energy (BDE) and polarizability of the bond.[24] As such, alkyl iodides are easiest to activate, whereas alkyl chlorides and fluorides have been the most challenging. With regards to the latter, to date there has been a single report evoking the direct abstraction of a C–F bond (Scheme 1.1, B).[25] In the presence of an N-heterocyclic carbene (NHC)–ligated borane, trifluoromethyl arenes were shown to undergo fluorine atom transfer (FAT). Considering the exceptionally strong C–F bond dissociation energy of these substrates (~120 kcal mol^{-1}),[26] this transformation represents a remarkable example of photocatalytic C–F activation.

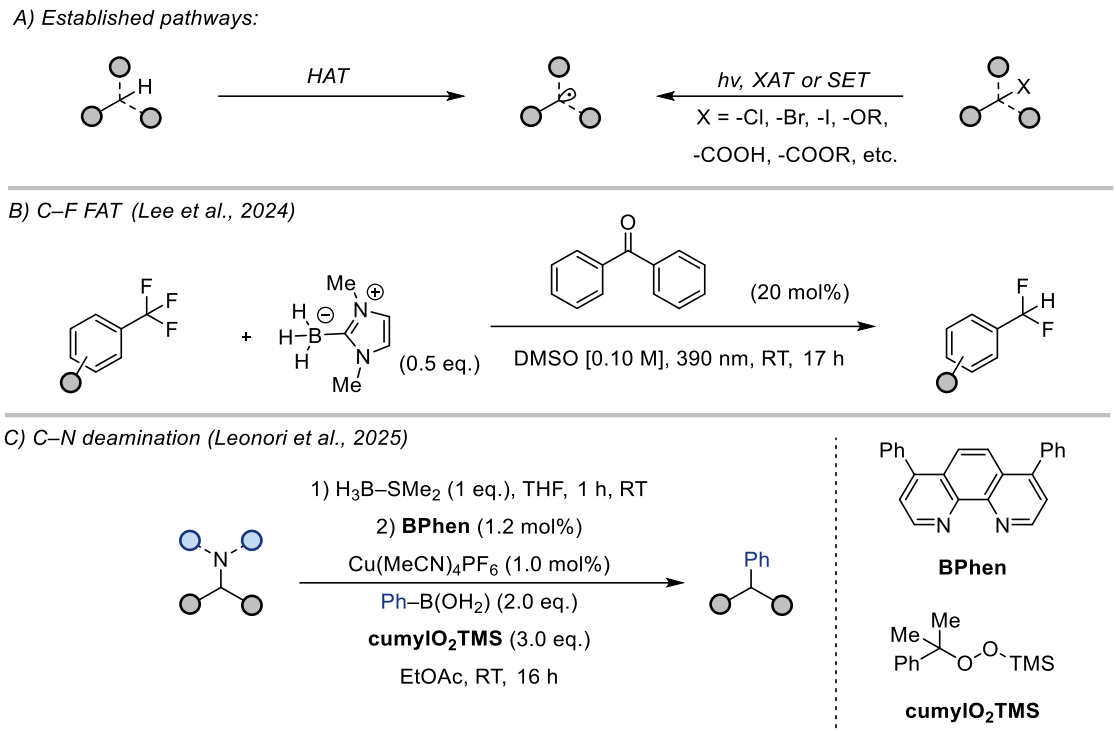

Scheme 1.1. A) Common methods for carbon radical generation. B) First example of a fluorine atom transfer. C) First example of non-activated C–N bond homolysis.

Another example of a challenging radical activation was recently published by the Leonori group (Scheme 1.1, C).[27] Alkyl amines were employed as radical precursors in a previously unseen C–N bond activation. In the presence of a borane source and stoichiometric oxidant, amine-ligated boranyl radicals were generated in situ and their ability to undergo β-scission afforded the desired carbon-centred radicals. The use of a copper catalyst employed boronic acids as coupling partners in an overall C–C bond forming transformation.

1.1.2. Generation of nitrogen-centred radicals

Similarly to carbon radical precursors, a common strategy towards nitrogen-centred radicals is the preactivation of an amine (Scheme 1.2, A).[28] Nitrogen-halogen bonds are typically weaker than carbon-halogen bonds (BDE ≈ 30–55 vs 60–90 kcal/mol, respectively)[26] thus easier to activate in a homolysis step. A classic example of this chemistry is the Hofmann–Löffler–Freytag reaction which typically involves preforming the haloamine in refluxing acid.[29, 30] Recently, milder conditions have been developed by the Nagib group (Scheme 1.2, B).[31] In the presence of an oxidant, the in situ iodination of nitrogen results in intermediate **1** which upon mild heating or visible light irradiation can undergo homolysis to generate the nitrogen-centred radical **2**. This step

is followed by 1,5-HAT, recombination with iodine radical and nucleophilic attack of nitrogen to afford pyrrolidines **3**.

Another strategy for the generation of nitrogen-centred radicals involves proton-coupled electron transfer (PCET) activation (Scheme 1.2, C).[32] In the presence of a Brønsted base, hydrogen bonding to the amide substrate activates the N–H bond toward oxidation by the excited photocatalyst. The concerted transfer of a proton and an electron results in a nitrogen-centred radical, which subsequently undergoes Kharasch-type addition to an olefin. Thiophenol serves as a hydrogen atom donor, quenching the intermediate carbon radical while regenerating both the photocatalyst and the phosphine base. Given the relative inertness of the anilide N–H bond (BDE ≈ 100 kcal mol^{-1}), the high chemoselectivity observed for PCET-mediated homolysis in the presence of a competing H-atom donor is particularly noteworthy.

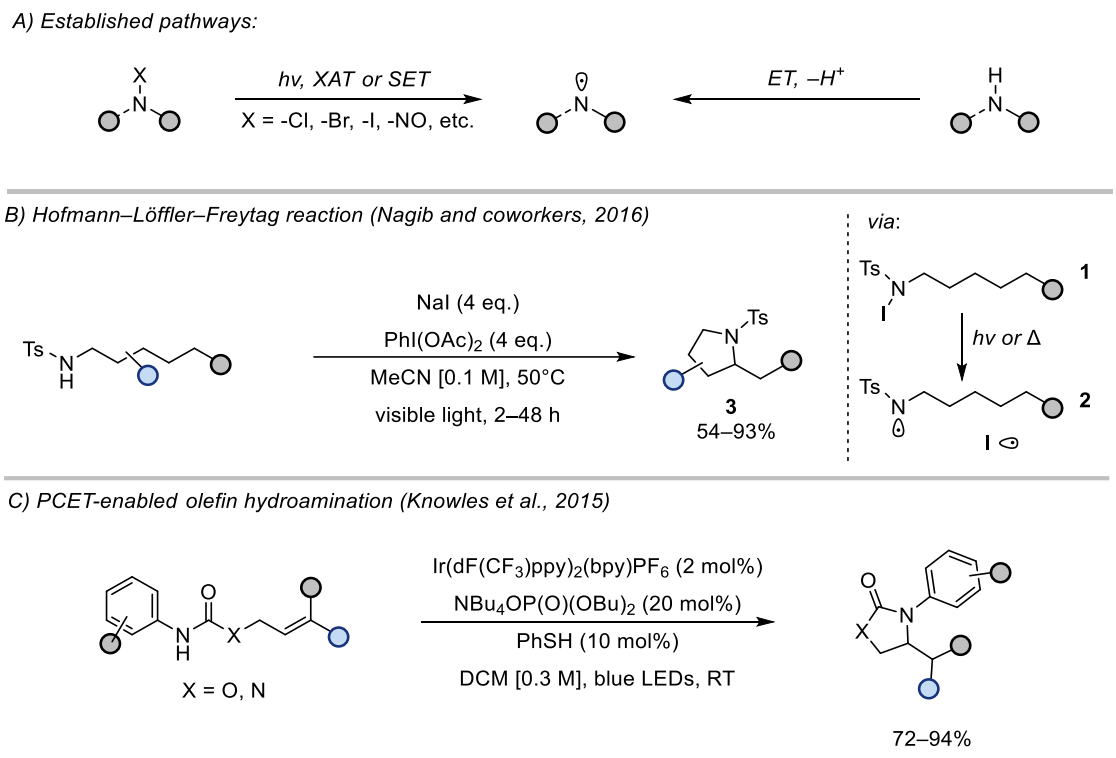

Scheme 1.2. A) Established methods for nitrogen radical generation. B) Nitrogen radicals in the Hofmann–Löffler–Freytag reaction. C) Generation of N radicals via PCET activation.

1.1.3. Generation of oxygen-centred radicals

Of the elements considered thus far, oxygen radicals are the most reactive intermediates. Among these, alkoxy radicals are long-recognised synthetic intermediates with characteristic and highly valuable reactivity. Their inherent

instability, however, often leads to β-scission or other rapid fragmentation pathways, making them challenging to control.[33] Because the aliphatic O–H bond is exceptionally strong (BDE ≈ 105 kcal/mol),[26] direct homolysis of alcohols is energetically prohibitive, and classical approaches have relied on the activation of prefunctionalised oxygen derivatives such as peroxides or redox-active esters (Scheme 1.3, A). More recently, catalytic strategies based on LMCT and PCET have enabled the direct generation of alkoxy radicals from simple alcohols under mild conditions.

In the presence of a cerium(IV) catalyst, primary alcohols can undergo radical dehydroxymethylation under visible light irradiation (Scheme 1.3, B).[34] The mechanism proceeds via LMCT activation to an oxygen-centred radical that disproportionates via β-scission, and the resulting carbon radical can be exploited in a variety of transformations such as Giese-type addition.

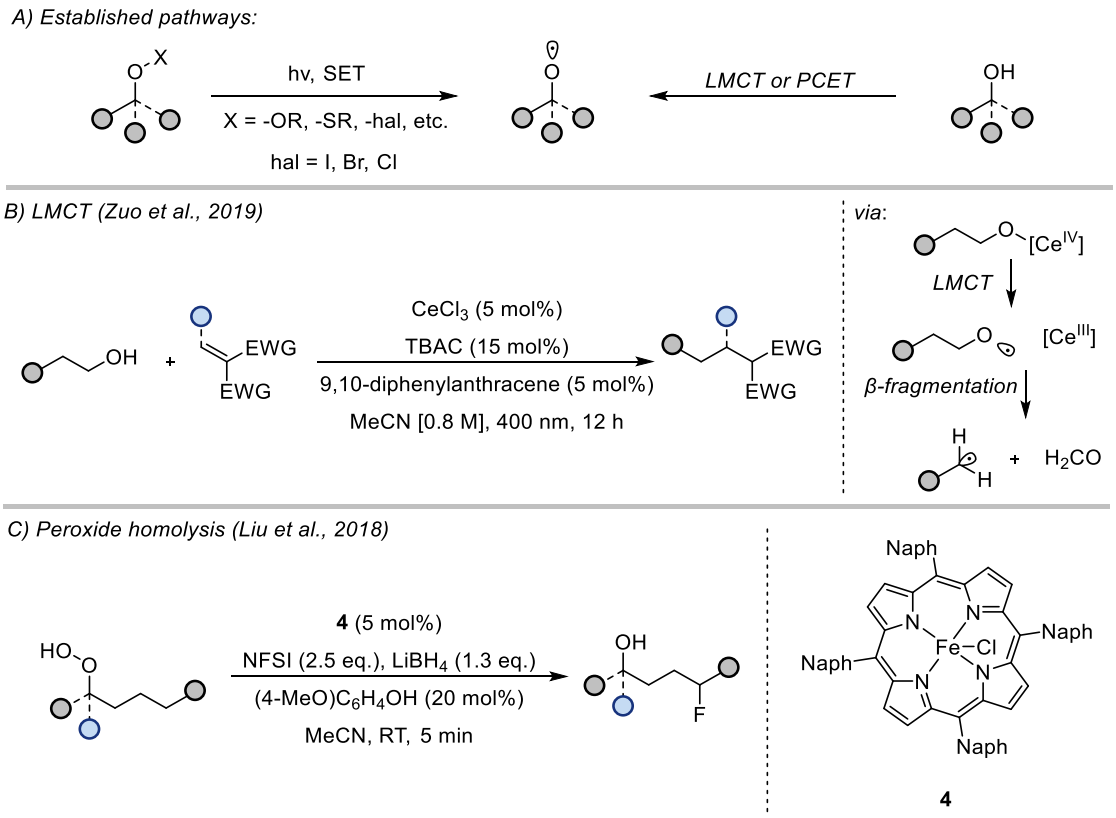

Scheme 1.3. A) Methods for oxygen radical generation. B) LMCT activation of primary alcohols. C) Peroxide reduction towards oxygen-centred radicals.

Alkyl hydroperoxides are easily accessible yet highly reactive precursors for alkoxy radicals (Scheme 1.3, C).[35] In the study by Liu et al. an iron-porphyrin catalyst (**4**) enabled the SET reduction of alkyl hydroperoxides, giving oxygen-centred radical

capable of 1,5-HAT. The resulting carbon radical can be further functionalised, for example with a fluorinating agent (NFSI).

Considering the discussion and examples above, it is evident that carbon-centred radicals have been the most extensively explored owing to their relative stability. In contrast, nitrogen-, oxygen-, and hydrogen-centred open-shell species remain underexplored in radical chemistry. As such, this work contributes to the development of new strategies for accessing some of the most challenging and less-studied radicals in organic synthesis.

Chapter 2 focuses on the design and synthesis of novel catalysts for the homolytic activation of alcoholic C–O bonds. The chapter opens with a review of existing methods, highlighting their scope, mechanistic features, and limitations, before moving on to the formulation of our hypothesis and presentation of experimental results.

Chapter 3 explores the generation of highly reactive oxygen-centred radicals and their application in anti-Markovnikov olefin hydroxylation. An overview of current alkene hydration methodologies is provided, outlining their inherent challenges and the unmet need for a more general strategy. Two new approaches developed in this work are then described in detail, together with the experimental progress achieved toward that goal.

Chapter 4 turns to the smallest radical in the periodic table – hydrogen. The chapter summarises known methods for hydrogen radical generation, discusses its distinct reactivity, and introduces our hypothesis before presenting the results and discussion arising from this investigation.

CHAPTER 2

Development of Novel Titanium N-Heterocyclic Carbene Catalysts Towards C–O Bond Activation

2.1. Introduction

Alcohol groups (C–OH) are among the most ubiquitous functionalities in nature, occurring in a wide range of molecules—from simple alcohols such as ethanol and glycerol, to carbohydrates like glucose and fructose, and more complex structures including hormones, terpenoids and biomass-derived polymers such as cellulose.[36] Their abundance and low toxicity make them valuable and sustainable feedstocks for chemical synthesis. As such, incorporating them as synthetic building blocks by exploiting the alcohol moiety has been the focus of organic chemistry since the 19th century.[37]

One of the earliest transformations developed with alcohols is the Williamson ether synthesis, which exemplifies the nucleophilic character of alkoxides formed upon deprotonation.[38] In general, alcohols can be engaged synthetically through three distinct modes of activation: (i) α-C–H bond activation, (ii) O–H bond activation, and (iii) C–O bond activation (Scheme 2.1).[39] Among these, the latter represents the greatest challenge for synthetic chemists due to the strength of the C–O bond (ca. 95 kcal/mol)[26] and poor leaving group ability of hydroxide (water $pK_a \approx 16$).[40] Indeed many polar strategies have focused on improving the latter by interconverting the alcohol moiety to a more suitable nucleofuge. The most commonly employed procedures are tosylation,[41] the Appel reaction[42] and the Mitsunobu reaction,[43] among others.[44, 45]

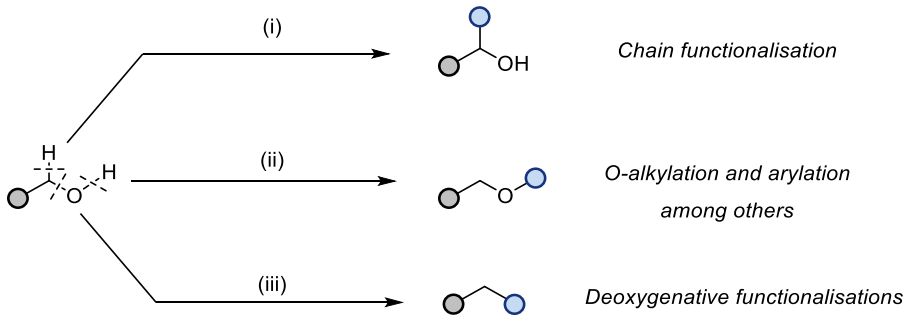

Scheme 2.1. Pathways for alcohol functionalisation.

Radical chemistry has long sought to exploit the abundance of alcohols as convenient sources of alkyl radicals. However, the high bond dissociation energy and redox stability of the C–O bond often necessitate preactivation of the substrate. A classic example is the first radical deoxygenation developed by Barton and McCombie in 1975, which involved conversion of the alcohol to a xanthate ester.[46] Due to the requirement for stoichiometric and toxic tin reagents, as well as the often harsh reaction

conditions, subsequent studies focused on developing alternative auxiliaries that could be formed under milder conditions and activated through photoredox catalysis. Representative examples include N-alkoxyphthalimides,[47] oxalates[48] and benzoate esters,[49] among others.[50] More recently, strategies enabling in situ interconversion of the alcohol have been introduced, achieving deoxygenation in a single-pot process.[51] Notable approaches include the formation of phosphoranyl radicals[52] or NHC-alcohol adducts[53] both of which promote *β*-scission of the C–O bond. The latter strategy has been able to access the most challenging primary alcohols and can be employed in conjunction with other catalytic systems,[54] including applications in late-stage drug functionalisations[55] and complex scaffolds synthesis.[56] Nevertheless, the reliance on stoichiometric activating reagents and the resulting poor atom economy highlight the continued absence of a truly direct catalytic deoxygenation strategy. In contrast, metal-catalysed activation of the alcohol C–O bond offers a promising approach for addressing this challenge.[50]

First-row transition metal complexes based on titanium, nickel, cobalt, and copper have shown particular promise in mediating single-electron pathways that enable homolytic C–O bond activation.[57] Among these, titanium-based reagents and catalysts have been most extensively explored for the activation of alcohols, owing to their inherent oxophilicity and the readily accessible Ti(III)/Ti(IV) redox couple.[58] The ability of titanium to selectively coordinate to the oxygen atom of an alcohol and promote single-electron transfer into the C–O σ* orbital has been exploited in the generation of tertiary, secondary, and, to a lesser extent, primary alkyl radicals.[57] This form of reactivity has underpinned a broad range of transformations, including reductive deoxygenation, cross-coupling, and cascade reactions.[57] However, the activation of primary alcohols remains a persistent challenge in titanium catalysis – a limitation that this work seeks to address.

This chapter explores the activation of the alcohol C–O bond through titanium-mediated homolysis. The following sections summarise key literature precedents and mechanistic insights into Ti(III)–alcohol interactions, before presenting our strategy to design novel titanium complexes for the generation of alkyl radicals from primary alcohols.

2.1.1. Low-valent titanium chloride mediated deoxygenations

Initial reports employing alcohols as coupling agents in a Ti-promoted deoxygenation date back to 1965 when Schwartz and van Tamelen published their work on the reductive coupling of benzylic alcohols (Scheme 2.2).[59] The scope of the procedure was limited due to the use of the very reactive potassium as a reductant and hence to prevent the substrate from quenching the reaction, a sodium alkoxide had to be prepared in situ which necessitated the use of another sensitive reagent – NaH. Later works have extended this methodology to prepare olefins,[60] cyclopropanes,[61] 1,3- and 1,5-dienes,[62-64]. However, these procedures still employed a strong reducing agent which restricted the substrate scope and was the main cause for reproducibility issues. Another downside was the need for stochiometric amounts of a titanium salt and reflux conditions which hinders not only the yield, selectivity and functional group tolerance, but the overall sustainability of this methodology and its application on industrial scale.

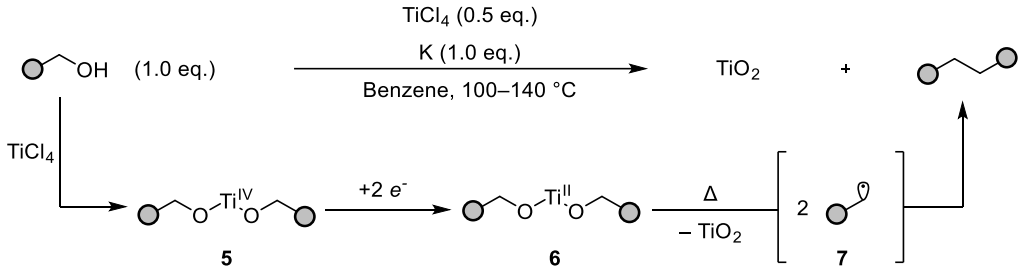

Scheme 2.2. First example involving deoxygenation of alcohols in the presence of titanium salts and mechanistic proposal by Sharpless et al.

The general understanding of these processes was that an intermediate Ti(IV)-dialkoxide **5** gets reduced to Ti(II) species **6** which undergoes double C–O bond homolysis to erect titania (TiO_2) and the resulting carbon radicals couple in the termination step of the reaction to give product **7**.[65] In some cases, there has also been evidence for a stepwise mechanism in the deoxygenation of diols.[66]

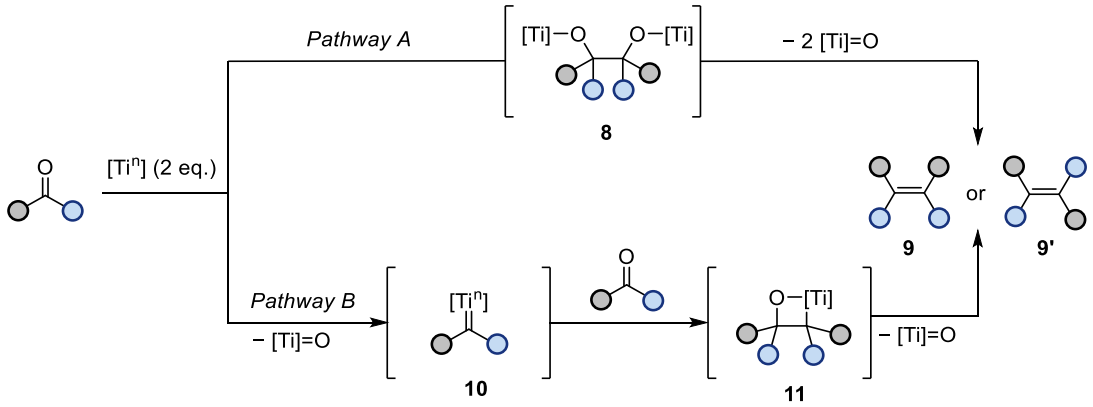

Scheme 2.3. Plausible reaction pathways in the McMurry reaction. [Ti^n] denotes the surface of a low-valent titanium particle (n<4).

This type of alcohol deoxygenation initiated by Ti is very similar to a reductive olefination that has now been established as the McMurry reaction. Since the initial reports in 1973,[67, 68] the reaction has been extensively studied by the McMurry group[60, 69-78] and has found numerous applications in the synthesis of natural and non-natural products.[79, 80] In general, a low-valent titanium species produced from the in situ reduction of $TiCl_3$ or $TiCl_4$ can activate an aldehyde or ketone towards a coupling event which precedes deoxygenation to the final olefin product. Even though the nature of the reaction intermediates depends on the reductant, solvent, temperature etc., there has been evidence towards two mechanisms that are accepted for this reaction (Scheme 6).[79, 81-83] Pathway A proceeds with the formation of a metalopinacolate intermediate **8** via a ketyl radical or alkoxide nucleophilic attack followed by deoxygenation to give a mixture of alkene products **9** and **9'**. On the other hand, Pathway B describes the initial deoxygenation to a carbene intermediate **10** which can dimerise with another carbonyl to give **11**. This is most likely carried out on the surface of a reduced titanium nanoparticle and final C–O bond homolysis gives alkene **9**. Since the McMurry reaction lies outside of the scope of this chapter it will not be further discussed here, however several critical reviews have been reported.[79, 80, 82, 84]

2.1.2. Applications of titanium chloride mediated deoxygenations

The Ukaji group investigated the Giese-type deoxygenative coupling of benzyl alcohols **12** (Scheme 2.4).[85] In the presence of stoichiometric amounts of titanium and a reductant, benzylic alcohols **12** were deoxygenated to produce resonance-stabilised radicals **13**. Giese-type addition to an electron poor olefin afforded radical intermediate **14** which can be trapped by another reduced titanium molecule to form organometallic species **15**. In the final step, protonation yields the conjugate addition product **16**. The proposed mechanism is in line with initial reports on the titanium mediated deoxygenations (vide supra Scheme 2.2).[65] Though the reactivity remains limited to activated benzylic substrates (**16a-d**), introducing a base in this reaction allows for a radical quenching step to be implemented, while minimising potential termination pathways.

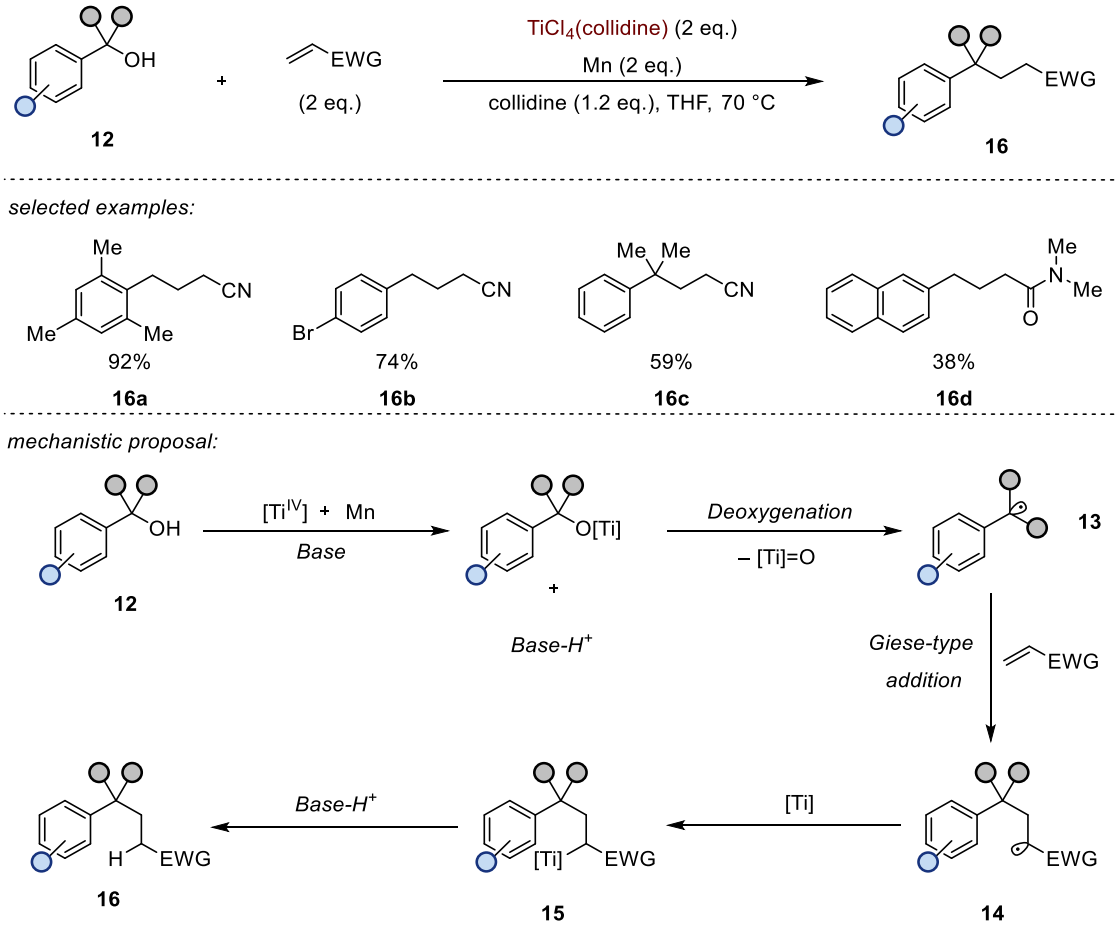

Scheme 2.4. Deoxygenation of benzyl alcohols by low-valent titanium and its application in the Giese-type addition to electron deficient olefins.

In a subsequent study, the $TiCl_4$/Mn/base system was adapted for the cross-electrophile coupling of benzyl alcohols **17** with aryl halides **18** through the

incorporation of a nickel catalytic cycle (Scheme 2.5).[86] Activation of the aryl halide (C–I) bond affords complex **19-I**, which intercepts the alkyl radical generated in the titanium-mediated deoxygenation step to form complex **19-II**. Subsequent reductive elimination from **19-II** delivers the coupled product **20** and nickel (I) species **19-III** which can be reduced to nickel(0) **19-IV** to close the catalytic cycle. A range of aryl functionalities (**20a–f**) were well tolerated; however, more sterically encumbered substrates (**17a** and **17b**) remained unreactive, restricting the scope to primary benzylic alcohols. Kinetic analysis indicated that the rate-determining step is the thermal homolysis of the C–O bond, which proceeds independently of the nickel catalyst concentration.

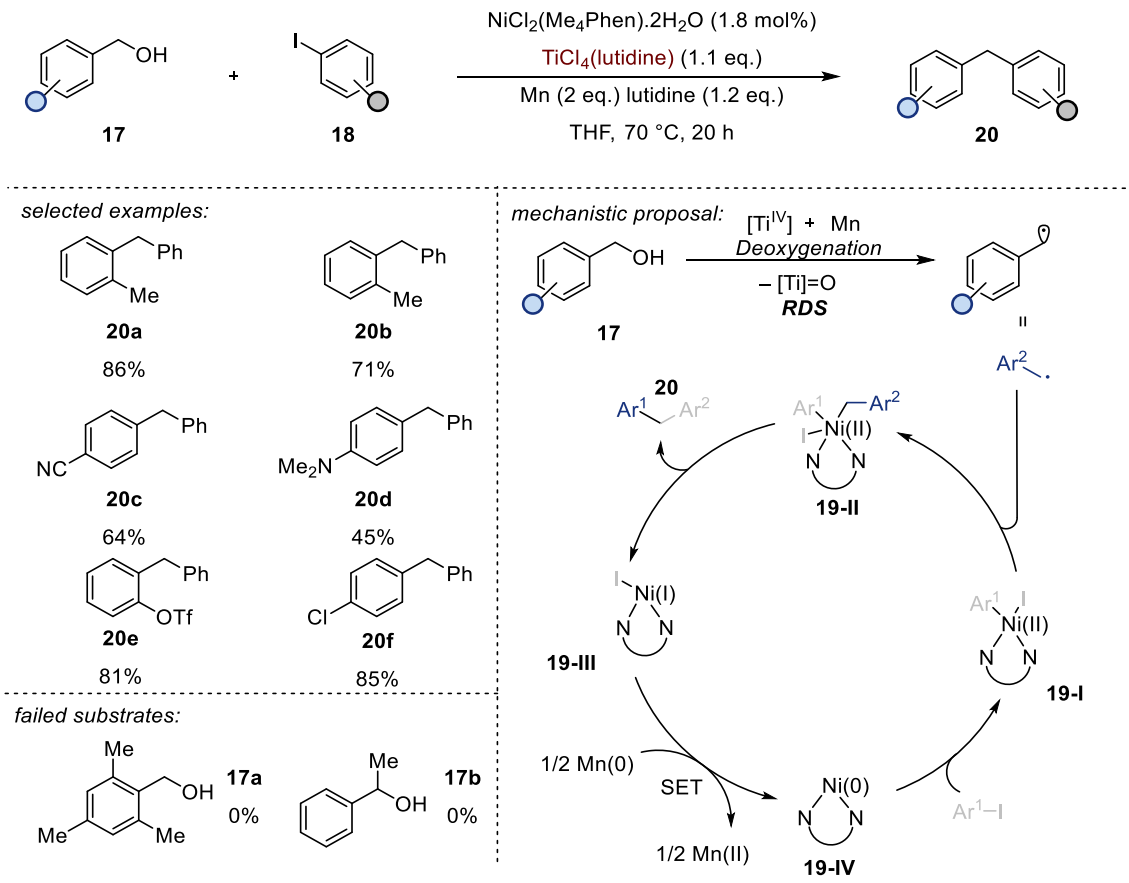

Scheme 2.5. Dual-metal promoted benzyl alcohol coupling strategy developed in the Ukaji group.

Further studies showcased the application of the $TiCl_4$/Mn/Base deoxygenation methodology in the cascade synthesis of 2-carboxyalyl acetates **21** (Scheme 2.6, A) and gem-difluoro alkenes **22** (Scheme 2.6, B).[87, 88] In both cases, the reactions proceed via deoxygenation to form benzylic radicals, addition to olefin followed by radical

trapping with titanium and a final elimination step to furnish the substituted alkene products. In the synthesis of allyl acetates **21**, E1cb elimination from enolate **23** was proposed as the most probable step. On the other hand, gem-difluoro alkenes were suggested to be the product of an unusual β-fluoride elimination from **24**.

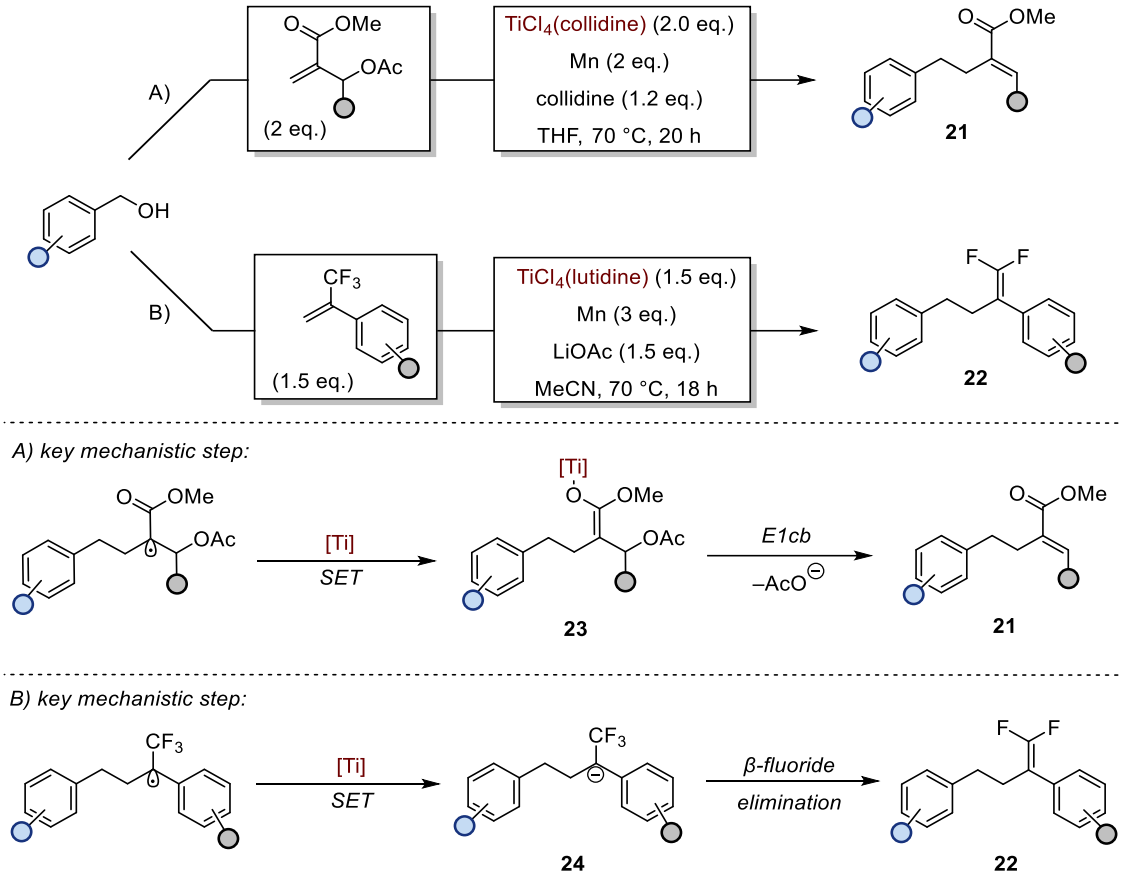

Scheme 2.6. Deoxygenation-coupling-elimination cascades towards substituted alkenes.

From the studies outlined above, several limitations can be drawn regarding the use of low-valent titanium species derived from $TiCl_4$ in alcohol deoxygenation reactions. To begin with, the reactivity of this system is largely confined to activated benzylic substrates, while tertiary, secondary, and primary alcohols lie beyond its effective scope. Moreover, Ti(II/III) has been shown to serve as an effective reductant for both α-carbonyl and benzylic carbon-centred radicals. However, stoichiometric quantities are required to promote C–O bond homolysis, indicating that $TiCl_4$ cannot function catalytically under these conditions. This limitation most likely stems from its strong affinity for oxygen atoms, which prevents regeneration of the active titanium species. As will be discussed in the following sections, introduction of a suitable ligand

framework enables regeneration of the reduced titanium complex through the use of an external oxygen trap, thereby allowing catalytic turnover.

2.1.1. Titanocene dichloride mediated deoxygenations

The shortcoming of the procedures mentioned above have been utilising stochiometric amounts of titanium salts and elevated temperatures. In addition, there seems to be an ambiguity about the low-valent titanium intermediate and mechanism of the deoxygenation step and this would be key information in the design of a catalytic version of the reaction. In 2010, the Barrero group reported the use of Nugent's reagent (Cp_2TiCl_2) and Mn for the deoxygenation of allylic and benzylic alcohols **25** (Scheme 2.7).[89] Although a similar procedure was first reported in 1980,[90] the density functional theory (DFT) calculations in the modern study supported the hypothesis that forming a Ti(III)-alkoxide complex can significantly lower the activation barrier towards C–O bond homolysis. In addition, employing chlorotrimethylsilane (TMSCl) as the final oxygen trap allowed for the reaction to be carried out with substoichiometric catalyst loadings and this w8as strongly suggestive of a $Cp_2Ti{=}O$ species formed that could be transformed back to the active chloride species. This study is the first example of a catalytic in titanium radical deoxygenation of alcohols, however the system is still limited to activated alcohols.

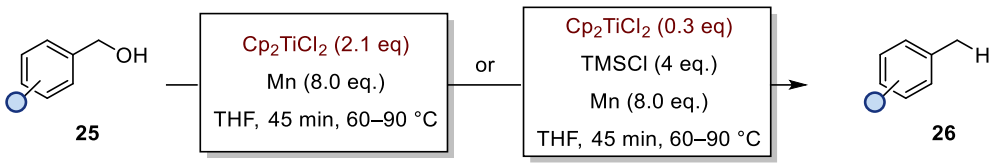

Scheme 2.7. First catalytic deoxygenation procedure from the Barrero group.

In a later study by the same group, it was reported that the hydrogen of the reduction product **26** originated from the Bronsted acids generated in situ from the starting alcohol.[91] Another application of this catalytic manifold was found in the umpolung coupling of hemiaminals with alkenes.[92] Taken together, these studies are suggestive of the following mechanism (Scheme 2.8). Single electron reduction of Cp_2TiCl_2 leads to the active Ti(III) catalyst (**T-I**), which is capable of coordinating a benzylic alcohol (**25**) in **T-II** and activating it towards C–O bond homolysis. This step yields the benzylic radical (**27**) and titanium oxide species **T-III** which can be transformed back to the starting titanocene dichloride using TMSCl as the final oxygen trap. Concurrently, the benzylic radical **27** can be trapped by another reduced titanium catalyst to give

organometallic species **28**, which gets protonated by the in situ generated acid to afford the final product **26** and regenerate the titanocene catalyst.

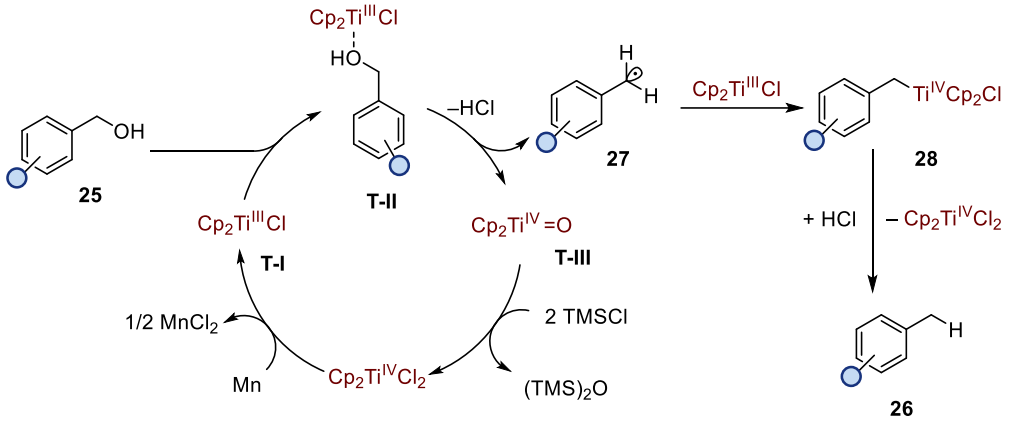

Scheme 2.8. Proposed mechanism for the titanocene catalysed deoxygenation of benzylic alcohols.

2.1.2. (Pentamethylcyclopentadienyl)titanium trichloride mediated deoxygenations

In 2020, Shu et al. published their dehydroxylative alkylation strategy of tertiary alcohols (Scheme 2.9).[93] Subjecting substrates **29** to a catalytic Cp*$TiCl_3$/Zn/TESCl system in the presence of activated alkenes **30** resulted in coupling products **31** in good to excellent yields. This was the first report of non-activated alcohols partaking in a deoxygenative-coupling process. The reaction employs molecular sieves to extract the in situ generated HCl, which otherwise leads to side alcohol dehydration reactions. The alcohol scope included cyclic and acyclic tertiary alcohols **29a** and **29b** irrespective of the substrate steric hindrance. Secondary benzylic alcohol **29c** gave diminished yield of coupling product whereas secondary alkyl and primary benzylic alcohols **29d** and **29e** remained unreactive with some product of oxygen silylation detected under the optimal conditions. However, this chemoselectivity allowed the selective deoxygenative alkylation of diols **29f** and **29g** at the more hindered hydroxy group. The procedure was also tolerable of a variety of aryl functionalities (**31a-d**), primary alkyl chloride (**30a**) and the terminal alkyne functionality in acceptor **30b**.

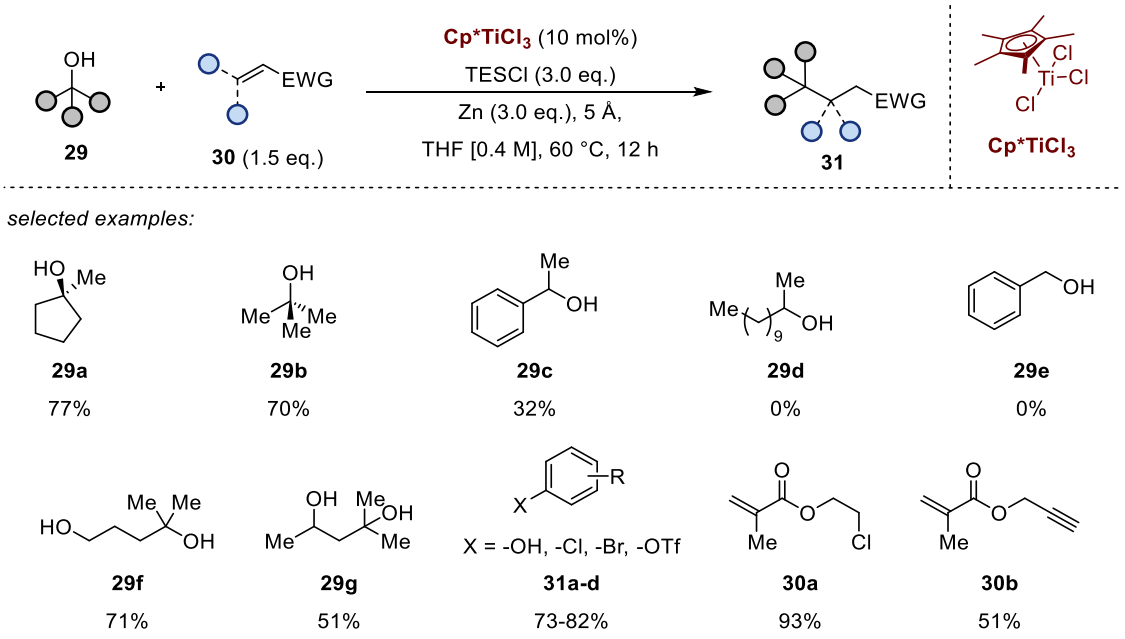

Scheme 2.9. Catalytic deoxygenation of tertiary alcohols by Shu et al.

In addition, a combination of electronic and steric factors seemed to govern catalyst reactivity (Table 2.1). During the reaction optimisation, it became apparent that a more sterically hindered titanium centre in $Cp^*_2TiCl_2$ (entry 2) reduced the reaction conversion and favoured the formation of elimination product **32**. The less electron rich Cp_2TiCl_2 and $CpTiCl_3$ further decreased the product yield (entries 3 and 4). The difference in reduction potential between $CpTiCl_3$ ($E_{red}^{(IV/III)}$ = –0.82 V vs Fc+/Fc) and Cp^*TiCl_3 ($E_{red}^{(IV/III)}$ = –1.10 V vs Fc+/Fc)[94] is another indicator for reactivity. Thus, it can be concluded that a more reducing titanium complex is necessary for the SET to unactivated alcohols.

Table 2.1. Catalyst optimization: Electronic and steric properties tuning

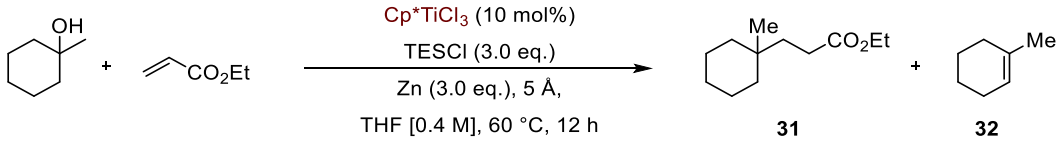

Entry	Titanium catalyst	31 (%)	32 (%)
1	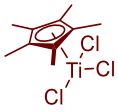 **Cp^*TiCl_3**	65	24
2	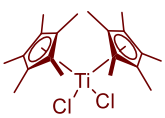 **$Cp^*_2TiCl_2$**	43	32

3	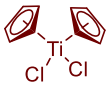	Cp_2TiCl_2	26	35
4	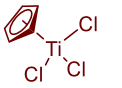	$CpTiCl_3$	24	12

The proposed reaction mechanism begins with coordination of alcohol to the reduced Ti(III) centre resulting in complex **T*-I** (Scheme 2.10). Intramolecular SET generates a carbon radical **33** that is capable of coupling to the Michael acceptor **30**, followed by titanium-assisted reduction and protonation to the final product **31**. The remaining Cp^*TiCl_2OH (**T*-II**) can react with TESCl as the final oxygen trap to regenerate Cp^*TiCl_3 (**T*-III**) and thus complete the catalytic cycle. Computational analysis revealed that the energy barrier for catalyst regeneration (28.1 kcal/mol) was the rate limiting step, therefore explaining the experimentally observed dependence of the reaction rate on the amount of chlorotriethylsilane (TESCl).

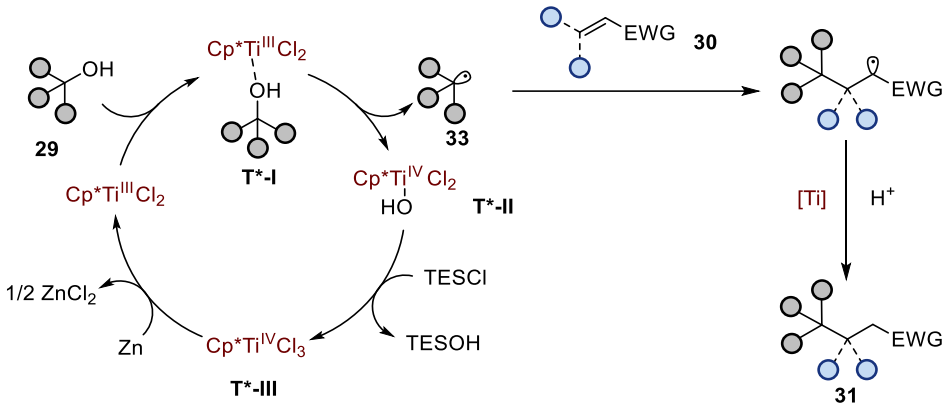

Scheme 2.10. Proposed catalytic cycle of deoxygenation of tertiary alcohols and Giese-type coupling step.

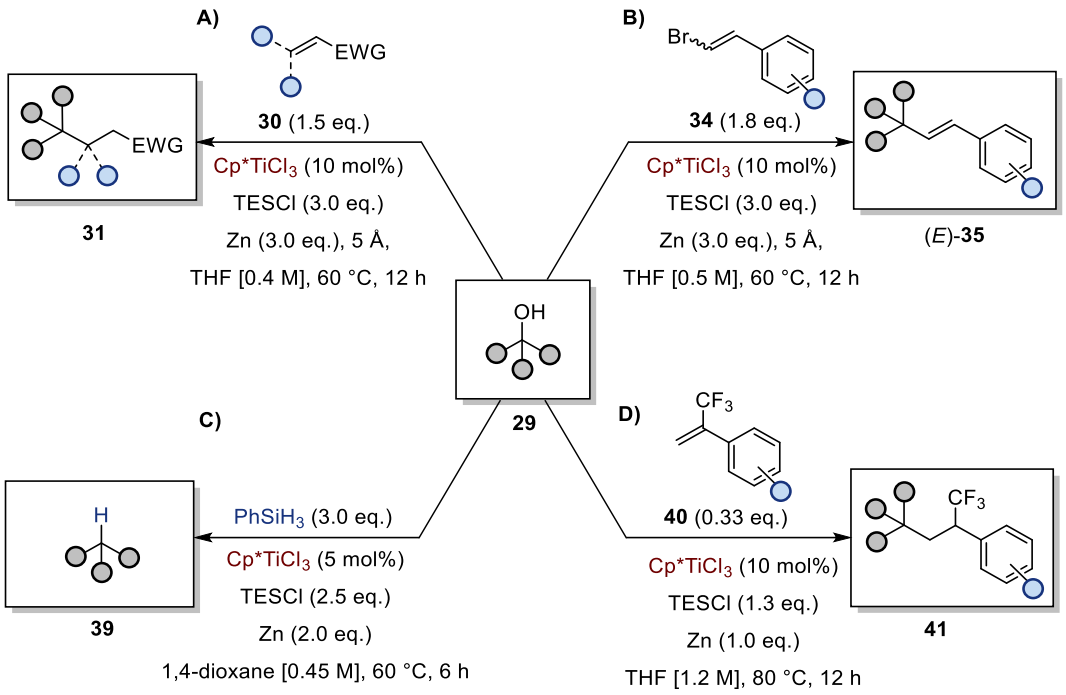

Scheme 2.11. Applications of the radical deoxygenation of tertiary alcohols in the presence of various electrophiles. A) Giese-type addition to electron deficient olefins. B) Selective radical dehydroxylative vinylation towards substituted E-alkenes. C) Reductive deoxygenation of tertiary alcohols. D) Alkylation of trifluoromethyl styrenes.

The application of the Cp*TiCl$_3$/Zn/TESCl system was extended to a variety of radical transformations (Scheme 2.11). The Giese-type coupling was showcased in the seminal work (Scheme 2.11, A), while a later study from the same group coupled tertiary radicals to halo-alkenes (Scheme 2.11, B).[95] Interestingly, employing a mixture of E- and Z-vinyl bromides **34** resulted in the stereoselective coupling product (E)-**35**. To explain the observed reactivity, it was suggested that following analogous formation of radical **33** (vide supra Scheme 2.10), addition to **34** gives either complex (E)-**36a** or (Z)-**37a** which are in equilibrium with (E)-**36b** and (Z)-**37b** respectively (Scheme 2.12). In order to place the bulky alkyl group in the least sterically hindered position, (E)-**36b** would form preferentially, and upon reduction with Ti(III) to (E)-**38** and *β*-elimination the final product (E)-**35** is obtained. As observed in the previous study,[93] the system employed was tolerable of a variety of aryl substituents alongside cyclic and acyclic tertiary alcohols leaving non-benzylic secondary and primary alcohols intact. The vinyl halide scope was favoured for all halogens (-Cl, -Br, -I) with even challenging fluoride acting as a leaving group.

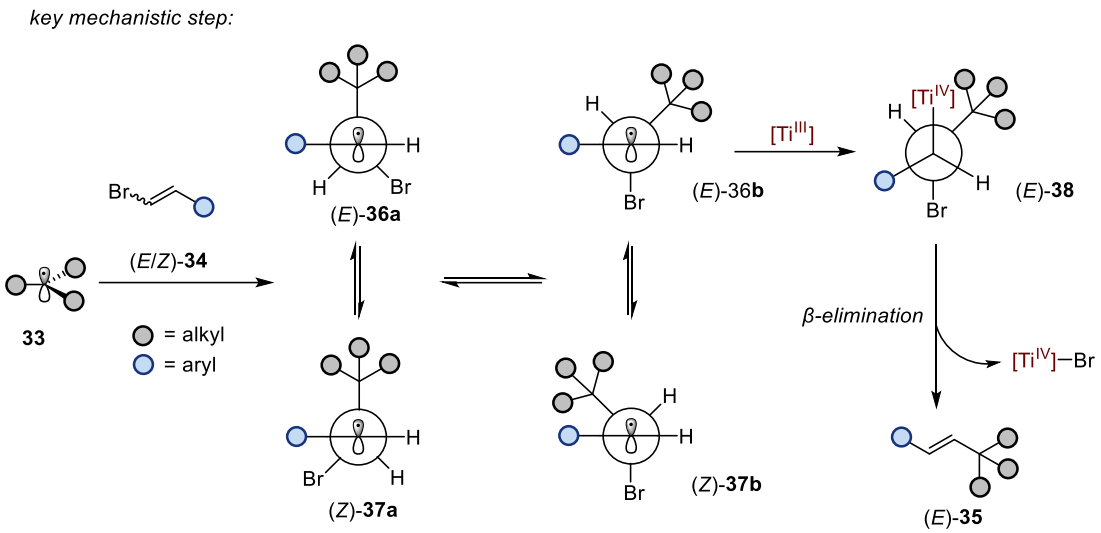

Scheme 2.12. Proposed mechanism for the (E)-selectivity in the deoxygenative coupling of tertiary alcohols to alkene halides.

In the presence of a hydrogen atom donor, the dehydroxylation of tertiary alcohols **29** to alkanes **39** was successfully achieved (vide supra Scheme 2.11, C).[96] Phenylsilane (BDE = 90 kcal/mol)[26] was identified as the optimal HAT reagent. However, during optimisation it became apparent that, even in the absence of a HAT reagent, the model substrate was still converted to product in significant yield (71%). This observation suggested that residual water present in the solvent acted as a competent quencher for the tertiary radicals (Scheme 2.13). Such behaviour could be rationalised by the notably low O–H bond dissociation energy in reduced titanium–water complexes previously reported by Oltra et al.[97]

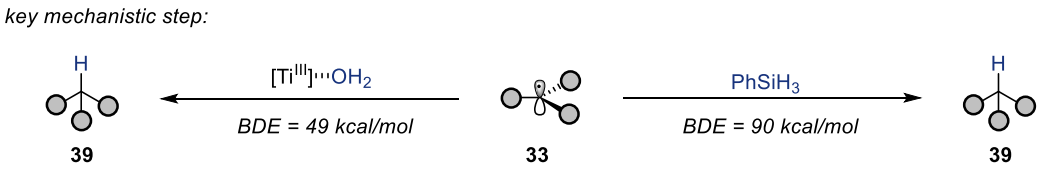

Scheme 2.13. Proposed HAT step with phenylsilane or water as the hydrogen atom donor.

The Giese-type coupling was extended to trifluoromethyl styrenes **40** (vide supra Scheme 2.11, D).[88] A variety of functionalities were tolerated (**41a**-**h**), notably, primary and secondary alcohols (**41b** and **41c**) and unactivated alkenes (**41d**) remained intact whereas primary and secondary benzylic alcohols gave bisalkylation products (Scheme 2.14). On the other hand, aryl-substituted *α,β*-unsaturated acceptors (**41f-g**) reacted well whereas *β,γ*-styrene **41h** did not take part in the coupling step. The

authors investigated the hydrogen source donor by employing a deuterated at oxygen tert-butanol which resulted in the coupling product with 72% deuteration, whereas THF-d_8 gave no deuterium incorporation. These results further support that upon deoxygenation, the resulting carbon radical can be further reduced to a carbanion and subsequently protonated under the reaction's acidic media (vide supra Scheme 2.10).

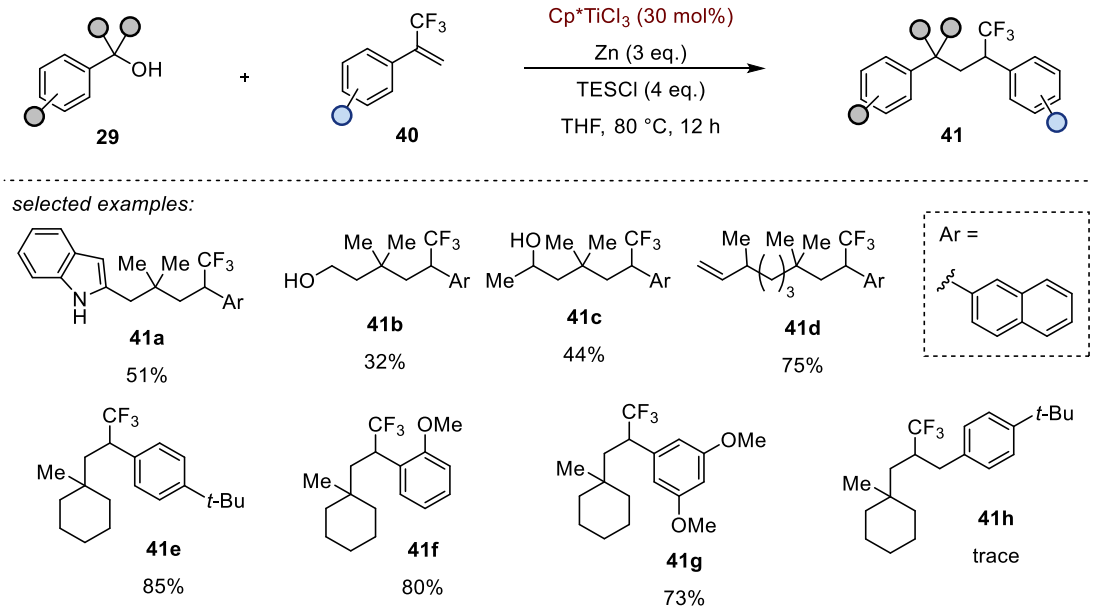

Scheme 2.14. Deoxygenative coupling of tertiary alcohols to trifluoromethyl alkenes.

The most recent work from the Ukaji group described an application of the catalytic deoxygenation of tertiary alcohols in the functionalisation of the anomeric carbon in simple sugars **42** (Scheme 2.15). The substrate scope was tolerable of furanose and pyranose rings (**43a**-**f**) regardless of the orientation of the anomeric substituent, whereas acrylamide (**43d**) and acrylates were suitable Michael acceptors. Notably, the titanium catalyst demonstrated selectivity for the anomeric carbon alcohol group while leaving the rest of the hydroxyl groups intact. In addition, all the products obtained exhibited a preference for axial addition following deoxygenation. This selectivity can be attributed to the anomeric effect of the oxygen atom in **42**: donation of electron density from the lone pair into the back lobe of the σ* orbital of the radical intermediate (**42-I**) stabilises the axial conformation (**42-II**), thereby favouring addition at the axial position.[98]

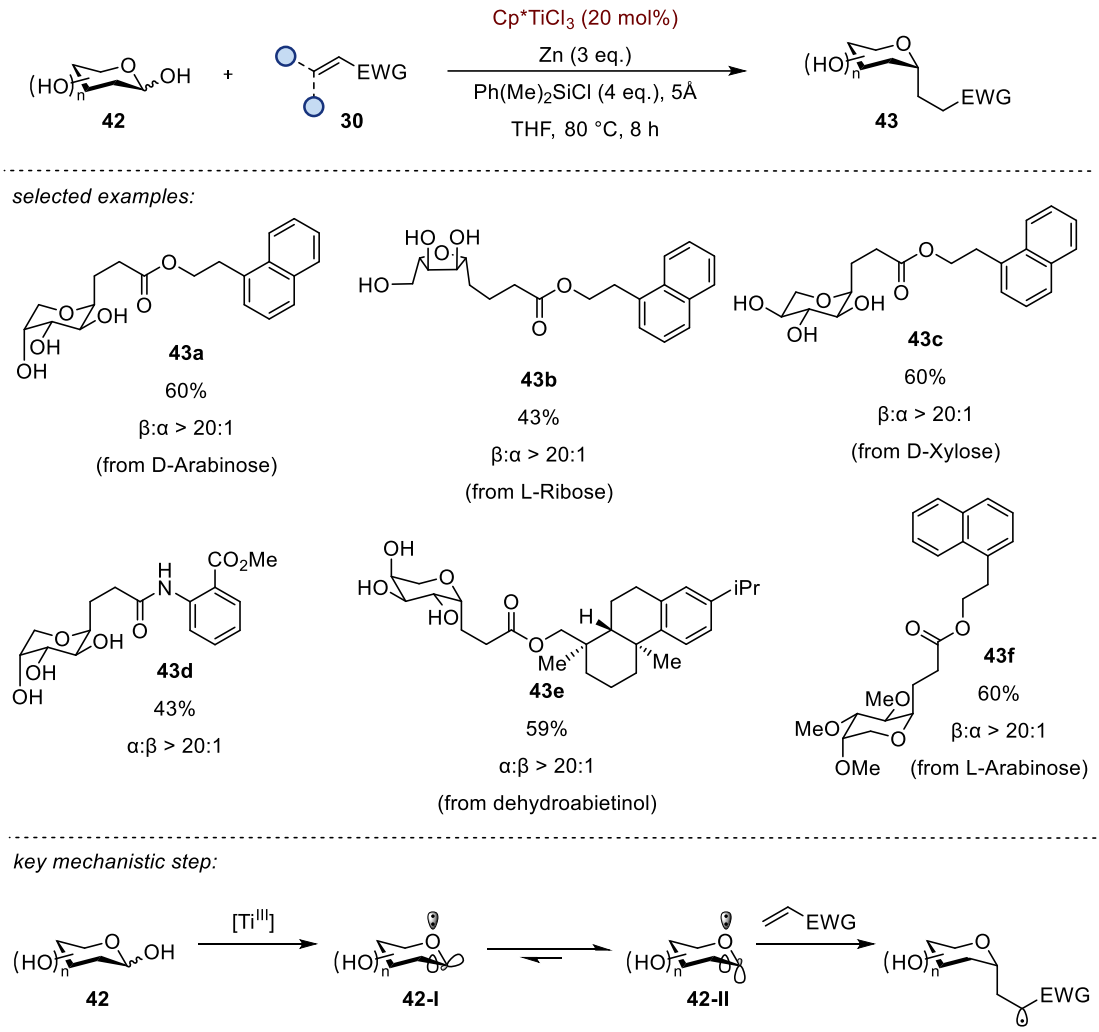

Scheme 2.15. Stereoselective deoxygenation of the anomeric alcohol in simple saccharides.

2.1.1. Titanium catecholate mediated deoxygenations

In 2022, the Ukaji group reported the first deoxygenative coupling of primary and secondary alcohols (Scheme 2.16).[99] Unactivated alcohols **44** in the presence of a titanium (IV) catecholate [**$TiCl_2$(cat)**]/Zn system were found to give products **45** in good to excellent yields which has been elusive to other titanium reagents.[85, 89, 100] However, the main limitation of the strategy is the high temperatures required for deoxygenation, which limited the substrate scope to protected amines (**44a** and **44b**), some aryl substituents (**44c-g**) and alkyl chains. It was suggested that [**$TiCl_2$(cat)**] exists as a dimer, as observed for an analogous [Ti(Oi-Pr)$_2$(cat)thf)]$_2$ system.[101] Therefore, the mechanism of reaction is initiated by a three-electron reduction of **46** to alkoxide complex **47** with the release of hydrogen gas. Direct C–O homolysis gives carbon radical **48** that can couple to an alkene resulting in **49**. A metalation-protonation sequence of **49** yields the final product **45** (Path A). Concurrently, a titanium-promoted HAT from the solvent was found to be another termination step in the reaction, as observed during deuteration experiments with DMA-d_3 (Path B).

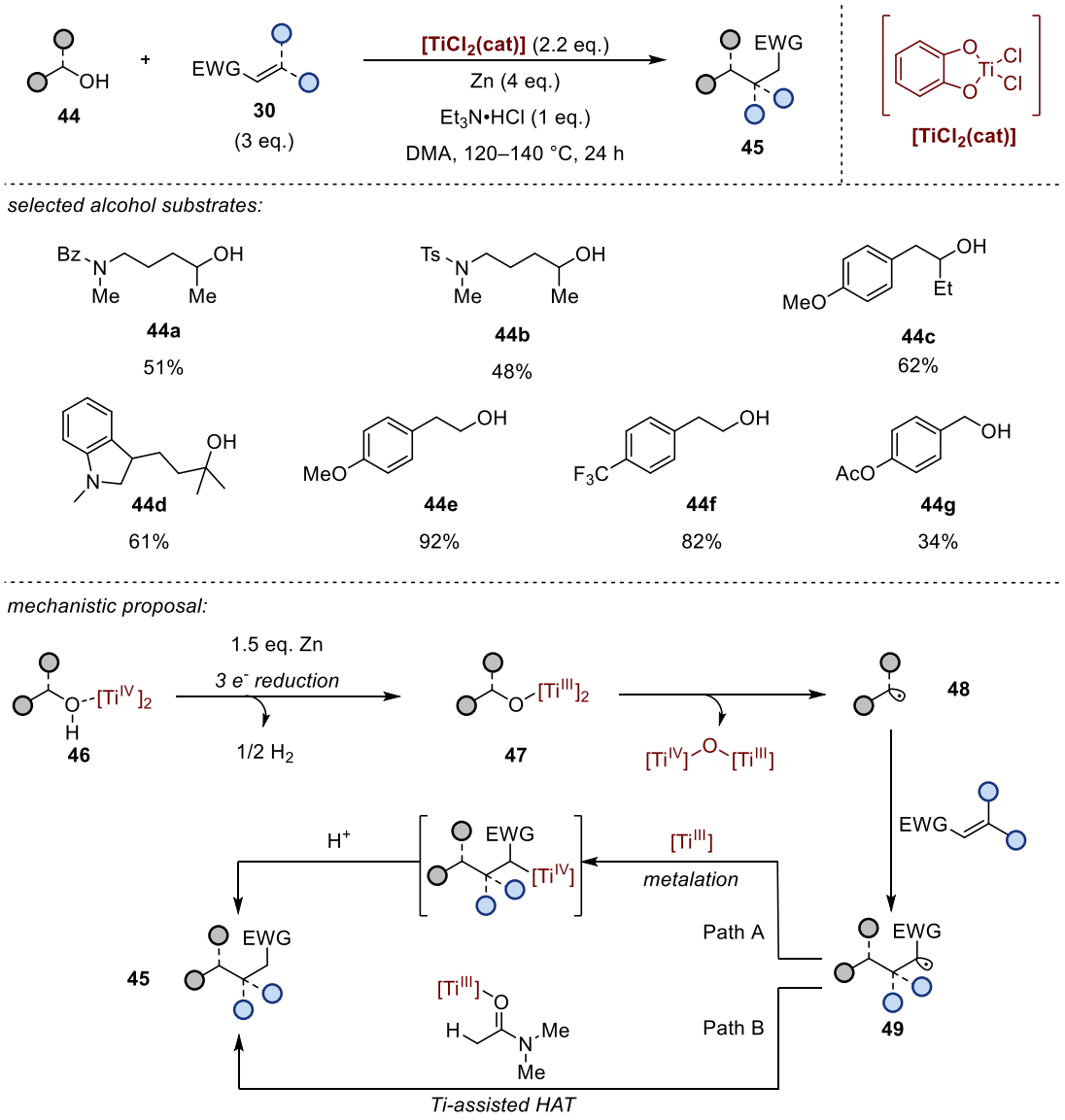

Scheme 2.16. Primary and secondary alcohols deoxygenation by low valent titanium cathecolate reagent.

Although this procedure offers the first titanium-mediated activation of primary and secondary alcohols, it suffers from poor atom economy (stoichiometric amounts of titanium reagent used) and harsh conditions that significantly minimise the functional group compatibility.

In a subsequent study from the same group, the acceptor scope was extended to disubstituted styrenes **50** (Scheme 2.17).[102] In the presence of excess 1,3,5-trimethyl-1,4-cyclohexadiene (**51**), the mono-coupling product **52** was obtained, and side product of dimerisation was avoided. The strategy was applied to a variety of primary to tertiary alcohols with some functionality present (**53a-d**), however no mechanistic

investigation was carried out and thus no further insight into the deoxygenation of alcohols can be elucidated from this study.

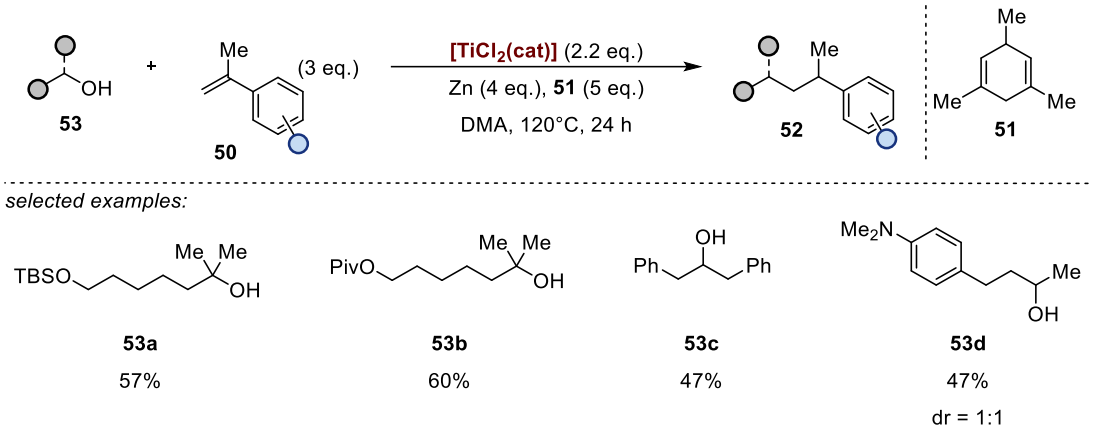

Scheme 2.17. $TiCl_2$(cat) system in the presence of a HAT reagent.

2.2. Catalyst design and hypothesis for titanium-catalysed deoxygenation

Considering the above-mentioned literature reports, there are no titanium-based strategies that can catalyse the deoxygenation of unactivated primary and secondary alcohols. How can one catalytically homolyse the strong C–O bond in a mild and selective manner to directly afford underexplored carbon radicals?

The proposition of this project is to develop novel tridentate ligands to be evaluated in the titanium-mediated deoxygenation reaction (Scheme 2.18, A). By employing a salen-type pincer architecture,[103] our design harnesses the chelating effect to achieve robust thermal and chemical stability, yet preserves open coordination sites essential for substrate binding. In addition, the structure bears an NHC core that further strengthen ligand binding while giving the titanium metal unique properties in the trans position.

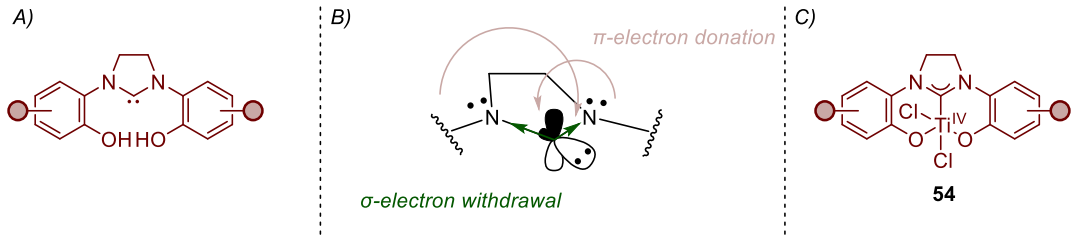

Scheme 2.18. A) Ligand design. B) Properties of NHC core. C) Catalyst design.

The NHC core contains a carbene carbon with an unfilled octet, bearing a lone pair in an sp^2 orbital (HOMO) and a vacant p orbital (LUMO) (Scheme 2.18, B).[104] The adjacent nitrogen atoms stabilise the carbene centre by lowering the HOMO energy through σ-electron withdrawal and raising the LUMO energy through π-electron donation. These resonance effects impart an overall nucleophilic character to the carbene (Schrock-type carbene), making it an excellent σ-donor ligand in transition-metal catalysis.[105, 106] In addition, the steric bulk of the nitrogen substituents further enhances the stability of the complex by suppressing carbene dimerisation.

Overall, in the presence of titanium, we aim to form NHC-titanium complex **54** (Scheme 2.18, C).[107] Upon fine-tuning the electronic properties of the ligand, we anticipate to evoke the homolytic cleavage of the C–O bond of primary and secondary alcohols.

Based on previous reports,[89, 93, 99] we propose a catalytic manifold for the deoxygenation of primary and secondary alcohols (Scheme 2.19). Initially, coordination of an alcohol substrate to catalyst **54-I** results in alkoxide complex **54-II**.

In the presence of stoichiometric zinc, reduction of catalyst **54-II** to Ti(III) species **54-III** should be facile and will result in C–O homolysis. The generated primary/secondary radical **55** can either couple to another substrate, dimerise or undergo HAT to the final product. The catalytic cycle is complete by metathesis with a radical scavenger (TMSCl) to turnover **54-IV** to the initial NHC complex **54-I**.

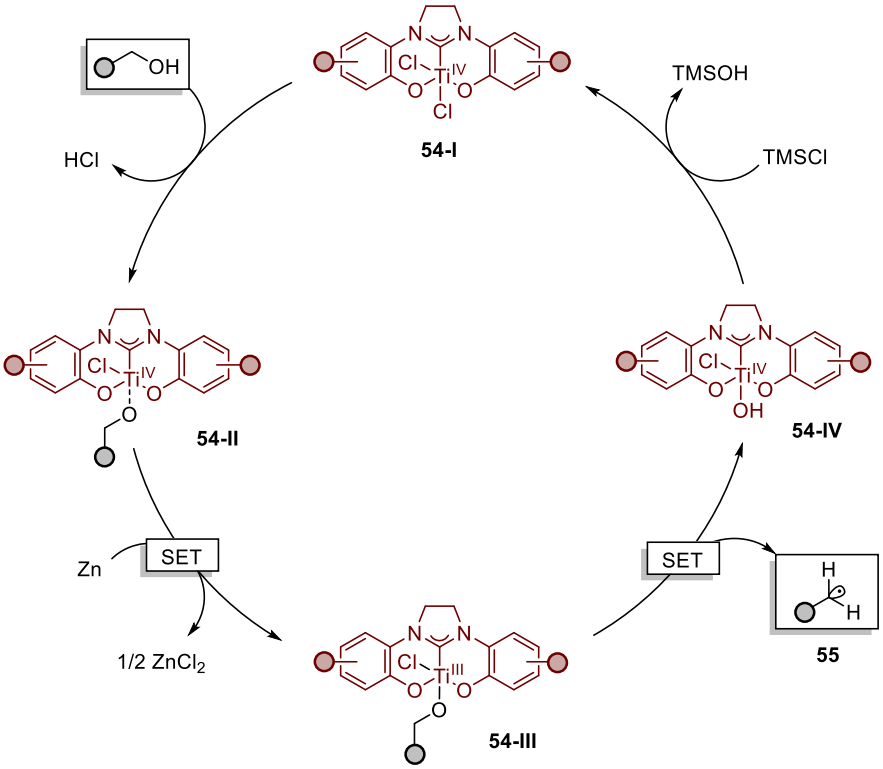

Scheme 2.19 Proposed catalytic cycle for deoxygenation of primary alcohols**.**

The homolysis step would be selective towards the substrate instead of the two phenolic C–O bonds due to the difference in their bond dissociation energies (BDEs) (Table 2.2).[108] In addition, we anticipate the final step to be the most energetically uphill and therefore rate limiting.[93] On the other hand, the formation of the strong TMS–OH (BDE of Si–O is 191 kcal/mol vs 158 kcal/mol for Ti–O)[109] should be a thermodynamic driving force of the system.

Table 2.2. Bond dissociation energies of simple alcohols

Alcohol	C–O bond BDE (kcal/mol)
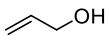	81
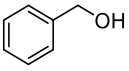	83
	94
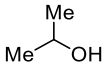	96
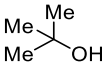	96
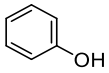	112

2.3. Planned titanium catalysts and retrosynthetic analysis

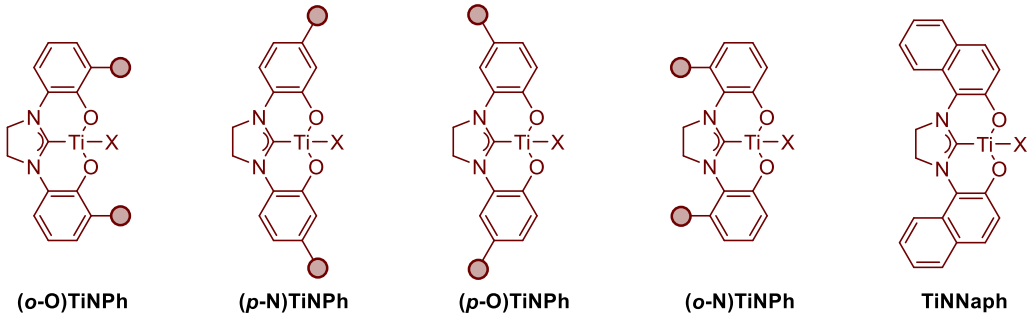

Scheme 2.20. Planned novel titanium catalysts.

The first aim of the research project was to develop a strategy for the synthesis of a library of titanium-based catalysts (Scheme 2.20). The two key designs are the Titanium N-heterocyclic carbene Phenyl (**TiNPh**) and the Titanium N-heterocyclic carbene Naphthyl (**TiNNaph**). The former will be functionalised with a variety of aromatic substituents either ortho to oxygen in **(o-O)TiNPh**, para to nitrogen in **(p-N)TiNPh**, para to oxygen in **(p-O)TiNPh** or ortho to nitrogen in **(o-N)TiNPh**. This will ensure the variety of steric and electronic properties for the catalysts.

The second aim was to investigate the catalysts in the deoxygenation of primary and secondary alcohols. We anticipate that in the presence of a suitable reductant, solvent and radical scavenger TiNPh or TiNNaph will be able to catalytically homolyse the C–O bond to afford a carbon centred radical that will be used in further transformations (vide infra Scheme 2.19).

The final aim of the project was to explore the scope of the deoxygenation strategy and probe the reaction mechanism. We anticipate that the deoxygenated substrates will participate in a Giese-type reaction with appropriate Michael acceptors.

The strategy to prepare catalysts **54** can be broken down into three key steps (Scheme 2.21). Retrosynthetically, the catalyst can be obtained from the imidazolium salt precursor **54a** via salt methatesis in the presence of base. The second disconnection would regenerate diamine **54b** that can react in the forward synthesis as the HCl-adduct with triethyl orthoformate to give **54a**. Finally, diamine **54b** can be obtained from aminophenol **54c** by a simple alkylation with dibromoethane or an alkylation/reduction with another suitable electrophile.

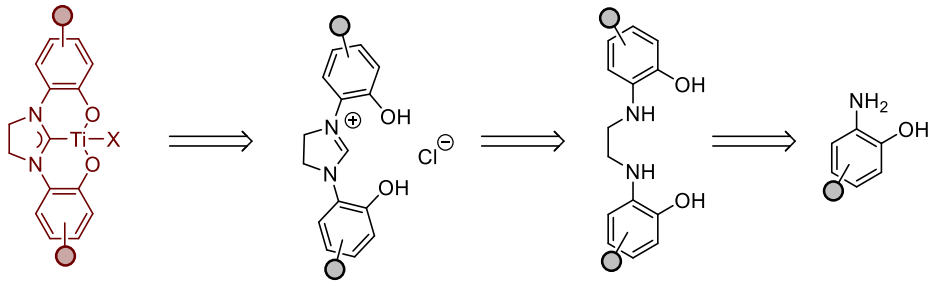

54 **54a** **54b** **54c**

Scheme 2.21. Retrosynthetic analysis of ligand precursor.

2.4. Results and Discussion

2.4.1. Synthesis of TiNPh

As a starting point, we were initially interested in preparing the non-substituted **TiNPh**. Thus, aminophenol **55** was reacted in the presence of dibromoethane under water reflux to give the resulting diaminophenol **56** in 19% yield. Although this step could be further optimised, the competing elimination reactions of the mono-alkylated intermediate and the poor substrate solubility under the reaction conditions were the reasons for the poor yield and encouraged us to seek an alternative pathway towards diamine formation as will be discussed below. Upon transformation of the diamine to the corresponding HCl-salt, cyclisation with trimethyl orthoformate afforded the phenyl imidazolium salt **57** in 64% yield. The ^{1}H NMR of **57** displayed the characteristic imidazolium C–H peak at 9.71 ppm and the O–H signal at 11.06 ppm which is in accordance to reported literature data.[110] Titanium metal templating following a literature procedure[107] afforded an orange solid of presumably **TiNPh**, however it was poorly soluble and therefore difficult to characterise. The ^{1}H NMR spectrum no longer exhibited the corresponding C–H signal, however the peaks did not match the exact reference values[107] potentially because the report by Roux et al. gave a spectrum with residual toluene solvent peaks.

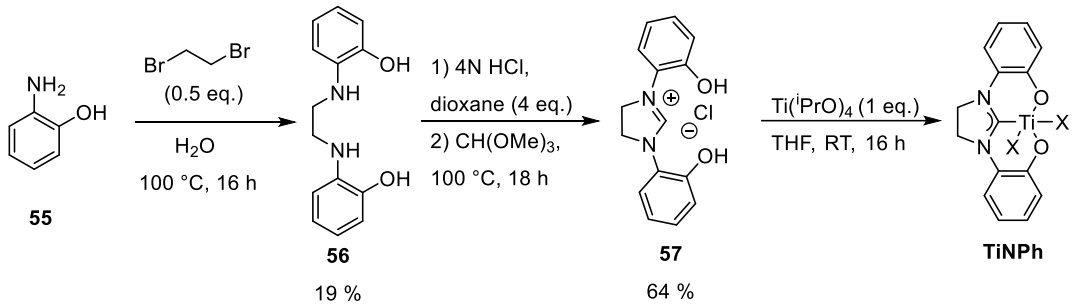

Scheme 2.22. Synthesis of **TiNPh**.

Concurrently, we were developing a strategy towards the **TiNNaph** target, which will be discussed in the next section.

2.4.2. Synthesis of TiNNaph

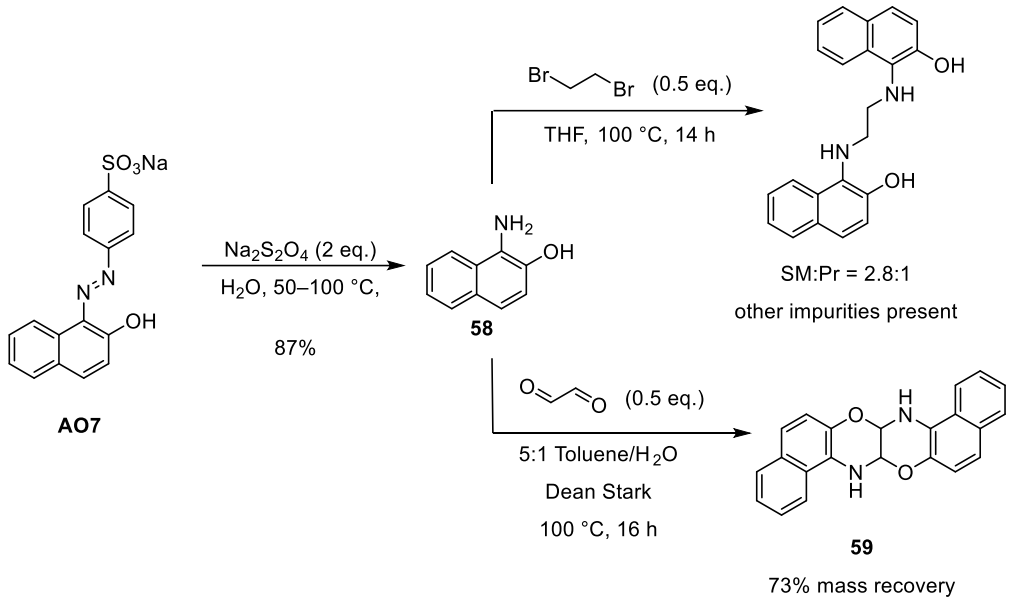

Scheme 2.23. Strategies derived from acid orange 7.

In order to access a similar starting aminophenol precursor to **TiNPh**, we identified acid orange 7 (**AO7**) as readily available source. Following a literature procedure,[111] 1-amino-2-naphthol **58** was prepared by reduction of **AO7** in the presence of sodium hydrosulphite (Scheme 2.23). As observed for aminophenol (vide infra Scheme 2.22), alkylation with dibromoethane proved to give a complex mixture due to the harsh reaction conditions and selectivity problem. Therefore, we pursued an alternative route involving condensation with glyoxal, followed by reduction to the corresponding amine. Gratifyingly, oxazine **59** was obtained in good yield and the ^{1}H NMR spectrum displayed the characteristic C–H signal at 5.55 ppm which is within the range of similar substrates.[112]

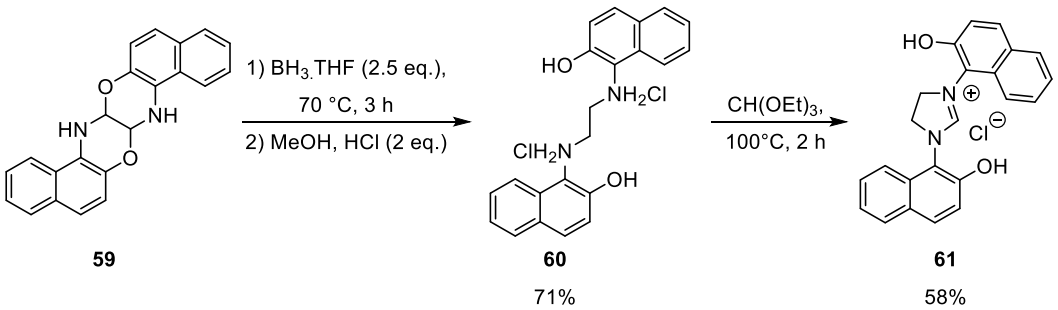

Scheme 2.24. Reduction of oxazine **59** and cyclisation with triethyl orthoformate.

Oxazine **59** was reduced to the corresponding diamine which upon reaction workup can be easily transformed to the HCl adduct **60**. As expected, cyclisation with triethyl

orthoformate afforded the desired imidazolium salt **61**, however it proved to be poorly soluble in common organic solvents which made characterisation difficult. Nonetheless, the substrate was reacted in the presence of titanium(IV) however the identity of the resulting species could not be characterised due to its inherent poor solubility.

We postulated that the poor solubility of **TiNPh** and **TiNNaph** is due to strong π-staking between the aromatic cores. Thus, we expected that introducing substitution on the rings can break the crystal packing and improve the substrate's solubility.

2.4.2 a Functionalisation of TiNNaph precursor

Attempts to functionalise oxazine **60** proved futile as the compound is unstable on silica gel and therefore isolation of products was unsuccessful due to decomposition. As a result, we decided to implement a protecting group strategy in the previous step, before we proceed to functionalise aminonaphthol **59**.

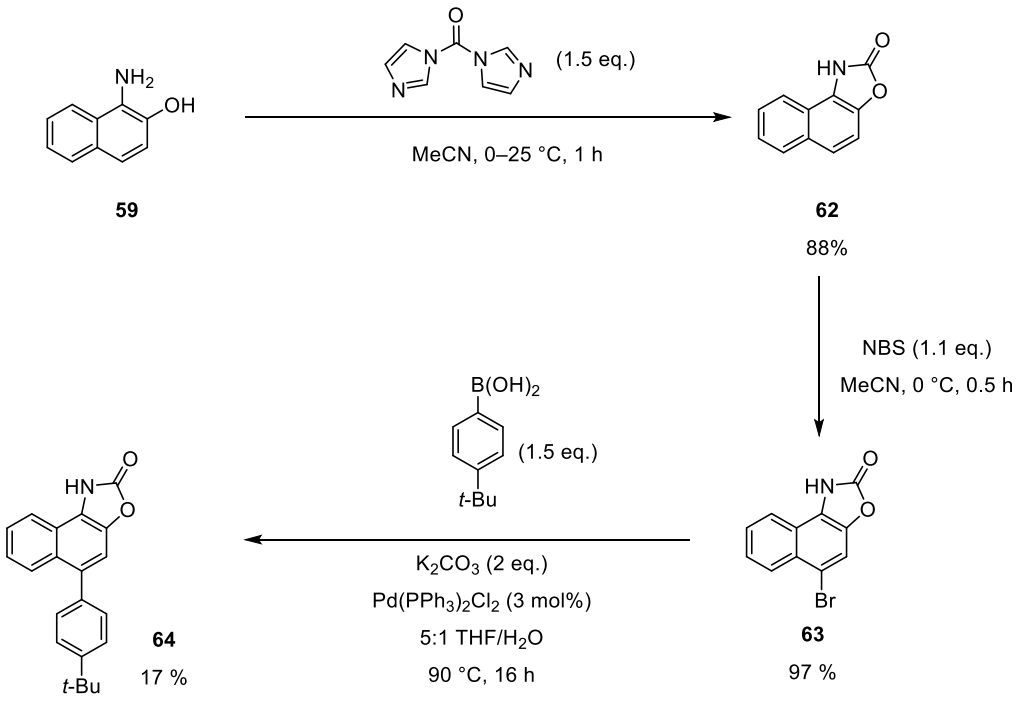

Scheme 2.25. Strategy towards functionalisation of naphthalene core (Mr Sun, *Master's thesis, 2023)*.

As such, **59** was treated with carbonyldiimidazole (CDI) to afford naphthoxazole **62** in excellent yield (Scheme 2.25). In the presence of N-bromosuccinimide, **62** reacted in exclusive para to nitrogen substitution (**63**). Our preliminary results showed that the substrate could then be employed in a Suzuki-Miyaura coupling in the presence of a

Pd catalyst to give aryl product **64**, which was further characterised and explored by Qilong Sun in his Master's thesis (2023). However, due to the poor solubility of substrate **64** it was discarded as a key target in this project. In addition, attempts to alkylate at the nitrogen of **64** proved unsuccessful since reaction with dibromoethane gave either monosubstitution in **65a** or elimination product **65b** (Scheme 2.26). Employing a more reactive electrophile such as oxalyl chloride showed complete consumption of starting material as observed in the crude ^{1}H NMR, however it was fully recovered after the reaction workup. These results suggested that either no reaction took place, or the corresponding product **66** is unstable and susceptible to hydrolysis.

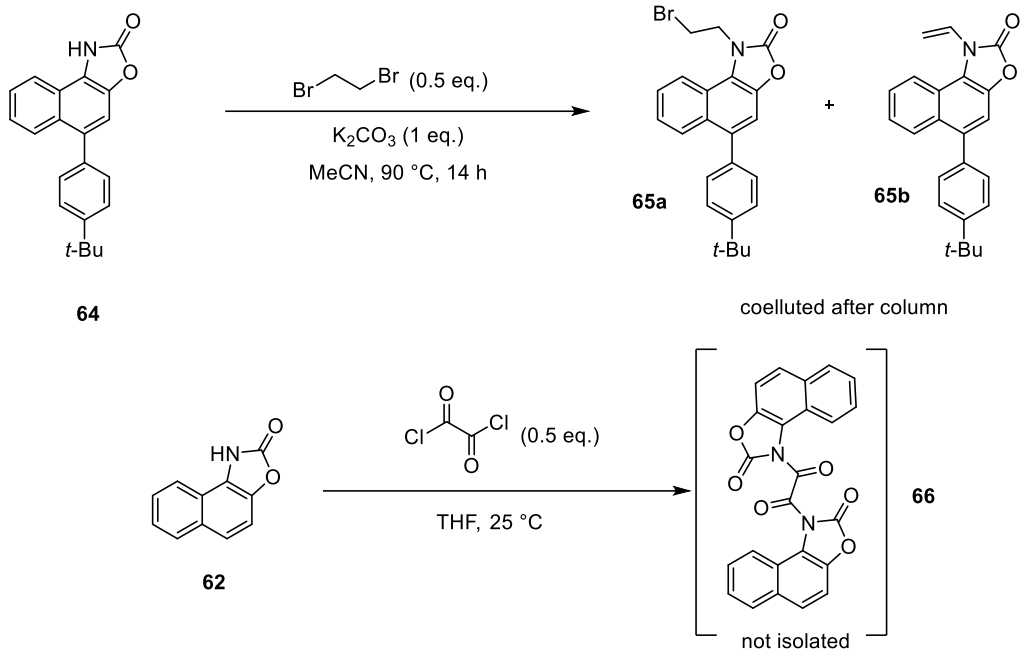

Scheme 2.26. Failed attempts at installing alkyl chain moiety.

These observations prompted us to install the diketone fragment prior to the protecting group as that would ensure the stability of the product. In addition, conversion of the amine to an amide would have a dual function as a protecting group against electrophiles and it will contain the alkyl fragment that has been elusive to the previous dibromoethane strategy.

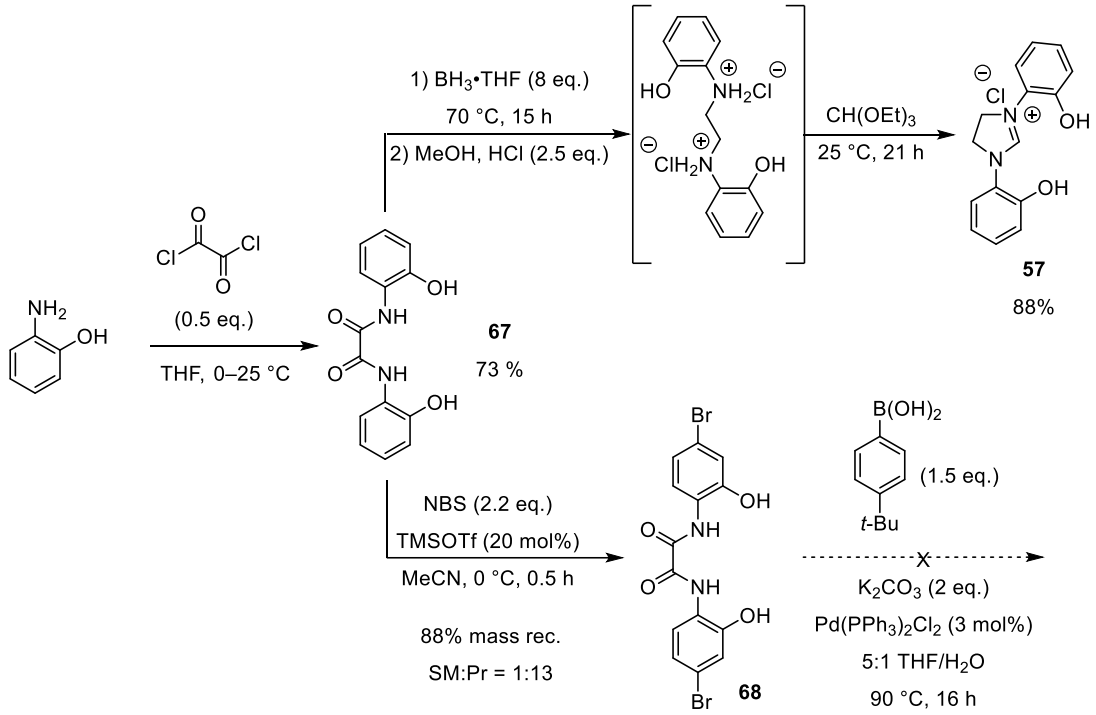

Scheme 2.27. Improved strategy for imidazolium salts synthesis.

In order to test the possibility of diketone formation, we reacted aminophenol with oxalyl chloride and to our delight the product phenyl oxalamide **67** was obtained in good yield (Scheme 2.27). Phenyl oxalamide **67** was converted directly to the corresponding imidazolium salt **57** in a one-pot two-step reaction which proceeded with excellent 88% yield.[107] On the other hand, halogenation with NBS in the presence of TMSOTf as a Lewis acid gave para to nitrogen substituted product **68** in excellent conversion with only 8% remaining starting material. Unfortunately, our attempts to subject substrate **68** to a Suzuki coupling reaction were unsuccessful with only the starting material detected. This was most likely due to the ability of the substrate to coordinate the Pd(II) catalyst and therefore prevent it from participating in the C–Br oxidative addition step.

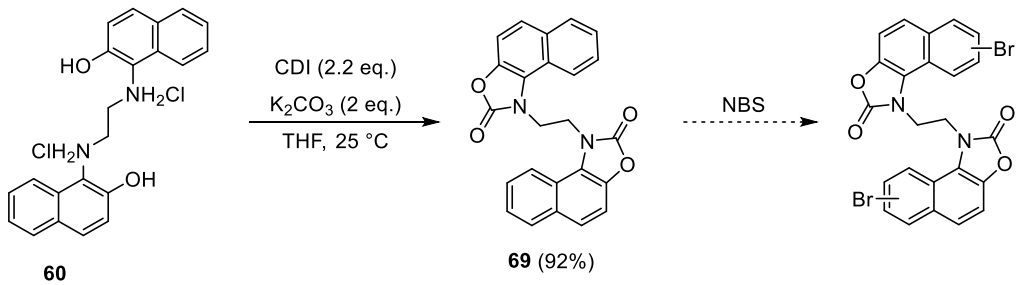

Scheme 2.28. Introducing protecting group after alkyl chain installation and attempt at derivatisation.

The inability of **68** to participate in the Suzuki coupling step indicated that the functionalisation of the cores must proceed in the presence of a protecting group at both the phenol and amine moieties. Therefore, we carried out the protection of **60** using CDI (Scheme 2.28). Although the reaction proceeded with excellent yield and selectivity, as observed for the disappearance of the phenol protons in the ^{1}H NMR, the resulting product **69** was very insoluble, and this prevented functionalisation with NBS in the subsequent step. Since the product cannot dissolve at room temperature, there would always be an excess of NBS present and that would result in polysubstitution of the core which was undesirable.

Table 2.3. Screen of brominating agent equivalents in the derivatization of phenoxazole **70**

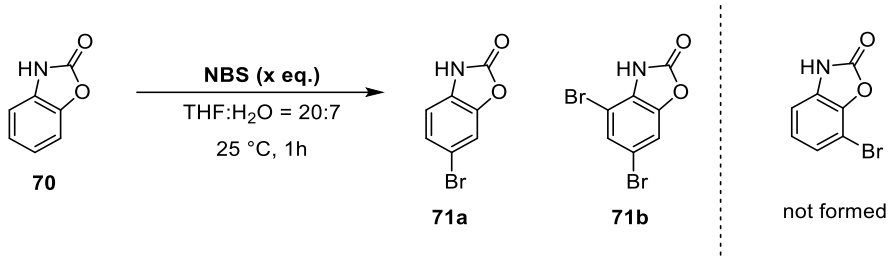

Entry	Equivalents of NBS	71a (%)*	71b (%)*
1	1.2	54	19
2	2.5	6	73

* Determined via ^{1}H NMR using 1,1,2,2-tetrachloroethane as internal standard.

In addition, bromination of phenoxazole **70** was attempted (Table 2.3). Treatment with 1.2 eq. of NBS resulted in a mixture of mono- and dibromo products which were identified as **71a** and **71b**. Unfortunately, it appeared that bromination preferentially occurs at the para position to nitrogen followed by the ortho position. Since we already observed the poor solubility of the p-N substituted phenyl oxalamide **68**, we were discouraged to investigate this substance further. On the other hand, the dibrominated substrate **71b** exhibited excellent solubility and could be a potential future target.

From the experiments above it was evident that para substitution to the nitrogen for either the phenyl or naphthyl cores decreased the substrate solubility and hindered the development of our synthetic strategy. Therefore, the next focus of the project was to introduce a substituent in one of the ortho positions.

2.4.3. Development of multistep strategy for synthesis of (o-N)TiNPh

Thus, amino-phenol **72**, presenting the bromine ortho to nitrogen, was protected with CDI (Scheme 2.29). With the amine and phenol not hindering the Pd(II) catalyst, the Suzuki coupling of **73** was carried out and product **74** was obtained in good yield and we observed improved solubility relative to p-N bromophenoxazole **71a**. The next step would be the deprotection of the amine to allow for the bridging reaction with oxalyl chloride as formation of the diketone of **66** was unfavourable (vide supra Scheme 2.26).

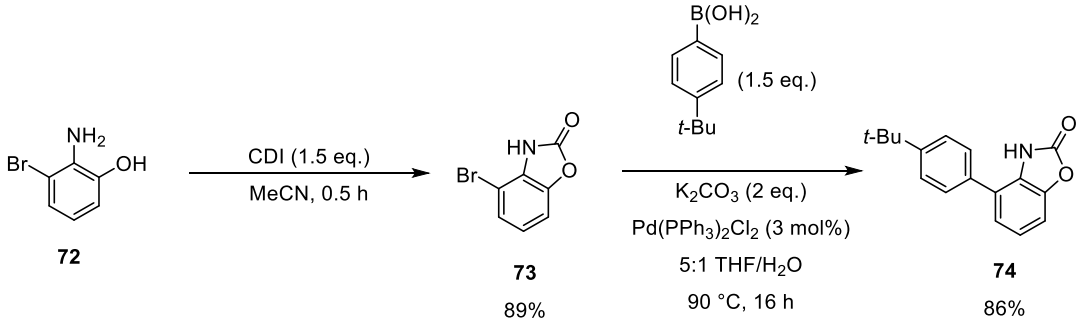

Scheme 2.29. Strategy with bromine already installed at the aromatic core.

Unfortunately, our attempts to remove the protecting group proved to be hindered by the scarcity of procedures for this type of deprotections. In addition, it was difficult to screen the reaction via crude NMR due to the hydrogen bonding of the product to water in the NMR solvent and spotting the crude reaction on TLC was presenting further challenges due to the excess of base. In addition, the aminophenol product did not seem to survive workup conditions and our best effort was to immediately take the crude reaction and load it on a silica gel column as adapted from a patent.[113] The ^{1}H NMR spectrum of the resulting aminophenol **75** exhibited the characteristic N–H and O–H signals at 4.12 ppm and 9.30 ppm respectively.

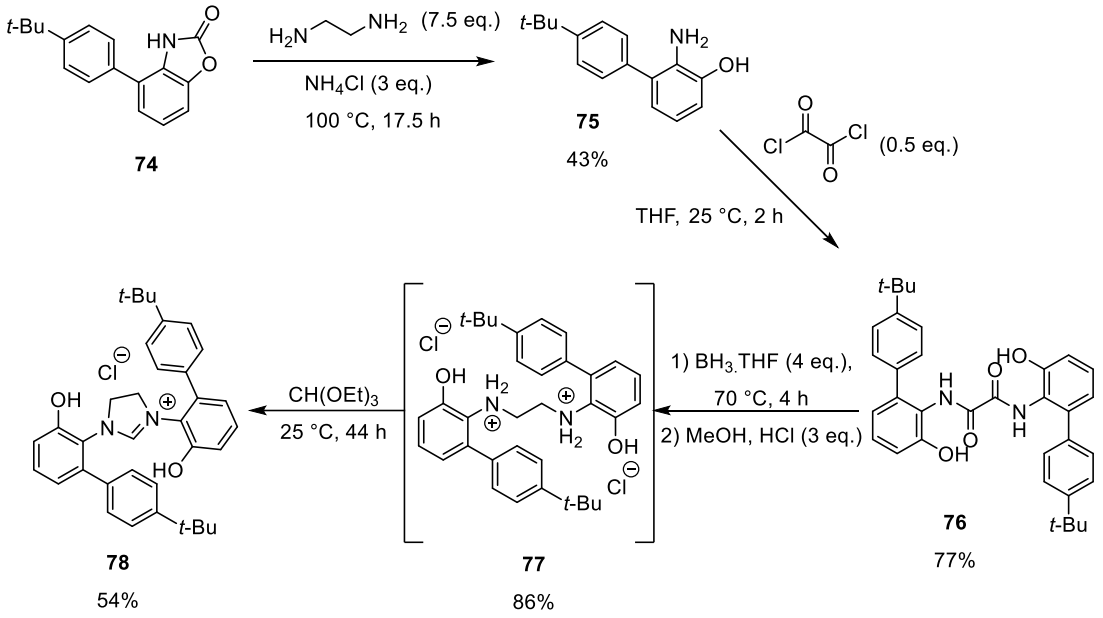

Scheme 2.30. Deprotection of carbamate followed by final strategy towards imidazolium salt X formation.

Introducing oxalyl chloride gave the expected phenyl oxalamide **76** in excellent yield. Substrate **76** was then reduced to the corresponding amine which was converted to the HCl-adduct **77**. Cyclisation with triethyl orthoformate afforded the expected imidazolium salt **78**, characterised by the sole C–H signal at 9.11 ppm in the ^{1}H NMR spectrum. Although this strategy gave promising results, the reproducibility issue associated with the deprotection of the carbamate group prompted us to investigate a different starting material. We envisioned that having a nitro group as a masked amine moiety would ensure the participation of the substrate in the Suzuki coupling step and a simple nitro reduction would efficiently afford the desired aminophenol.

This hypothesis was tested with the isomeric ortho-to-oxygen nitrophenol **79** as a more available substance (Table 2.4). Our previous conditions for Suzuki coupling (vide supra Scheme 2.29) appeared to be somewhat sluggish (entry 1), however substituting the boronic acid with the pinacol ester **80** afforded a higher yield under the same conditions (entry 2). Employing a variety of ligands for palladium (entries 3–5) showed the superiority of the tricyclohexylphosphine (entry 5) over other common ligands for this type of reaction and product **81** was obtained in 68% yield. Unfortunately, decreasing the catalyst loading (entry 6) resulted in more starting material detected in the crude NMR spectrum and that was undesirable since the product could not be purified by column chromatography due to its similar polarity with

79. On the other hand, substituting the solvent for 1,4-dioxane gave an improved 74% yield (entry 7) and increasing the temperature to 120 °C afforded ca. 90% of the product **81** and only 10% of **79** as determined from the crude NMR.

Table 2.4. Optimisation of Suzuki-Miyaura coupling conditions.

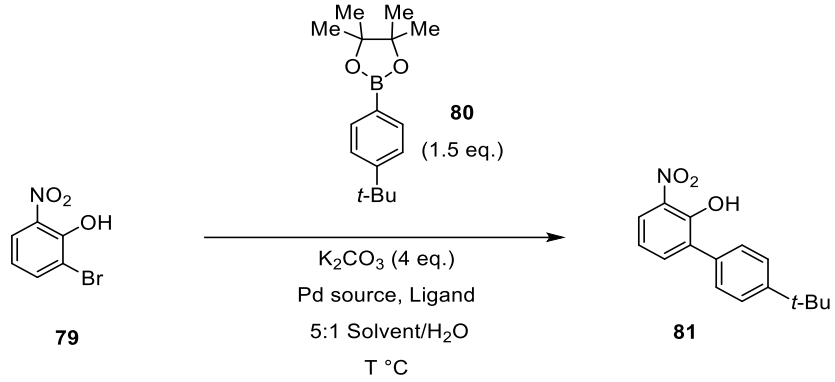

Entry[a]	Cat. (mol%)	Ligand (mol%)	Solvent	T (°C)	time (h)	**79** (%)[b]	**81** (%)[b]
1[c]	$Pd(PPh_3)_2Cl_2$ (15 mol%)	–	THF	100	12	13	45
2	$Pd(PPh_3)_2Cl_2$ (15 mol%)	–	THF	100	12	19	61
3	$Pd(OAc)_2$ (15 mol%)	SPhos (30 mol%)	THF	100	12	19	16
4	$Pd(OAc)_2$ (15 mol%)	P(o-tolyl)$_3$ (30 mol%)	THF	100	12	21	35
5[d]	$Pd(OAc)_2$ (15 mol%)	PCy_3 (30 mol%)	THF	100	12	<1	68
6[d]	$Pd(OAc)_2$ (3 mol%)	PCy_3 (6 mol%)	THF	100	16.5	29	68
7[d]	$Pd(OAc)_2$ (3 mol%)	PCy_3 (6 mol%)	1,4-dioxane	100	17.5	14	74
8[d]	$Pd(OAc)_2$ (3 mol%)	PCy_3 (6 mol%)	1,4-dioxane	120	15	10	~90

[a] Reactions run on 0.1 mmol scale using solvents purged with argon. [b] Yield determined using 1,1,2,2-tetrachloroethane as internal standard. [c] Used boronic acid instead of ester. [d] Ratio of solvent:H_2O = 4:1.

Unfortunately, the o-N substituted nitro compound **82** was not readily available and attempts to prepare it from 3-bromophenol gave the desired product but in very poor yield (Scheme 2.31). It appears that nitration with zirconyl nitrite favours the isomers **83** and **84** over the desired nitro compound **82** potentially due to the steric hindrance of that specific ortho-site.

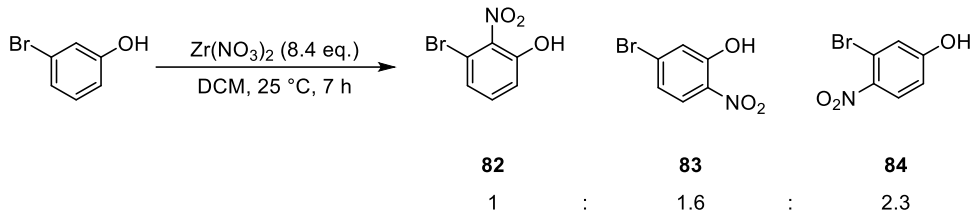

Scheme 2.31. Attempt at nitrating 3-bromophenol**.**

Considering the aforementioned limitations of the nitration strategy, the o-N substituted ligand was prepared via a different route. The symmetric nitro-2–5-diphenol **85**, was reacted in the presence of triflic anhydride to give the mono-substituted product **86**. We envisioned that substrate **86** will participate in the Suzuki-Miyaura coupling and preliminary results under the optimised conditions showed complete conversion to product **87**.

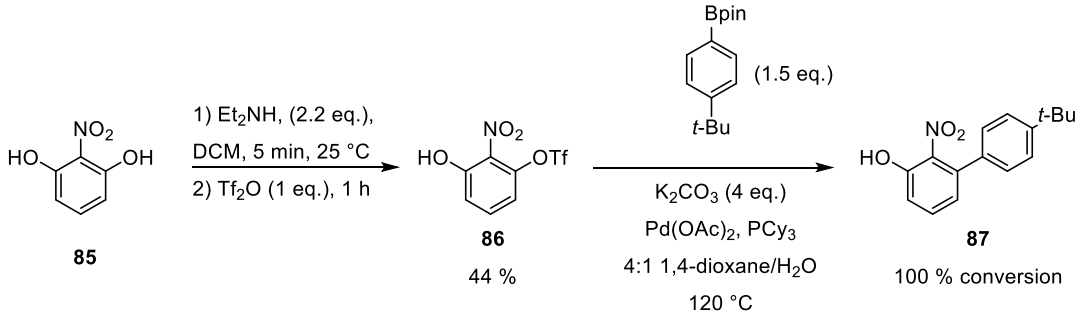

Scheme 2.32. Triflation strategy towards o-N precursor.

2.4.4. Development of multistep strategy for synthesis of (o-O)TiNPh

With substrate **81** in hand (vide supra Table 2.4), we were able to execute the reduction of the nitro group and we observed complete conversion of starting material (Scheme 2.33). Aminophenol **88** was reacted in the presence of oxalyl chloride to give the expected phenyl oxalamide **89** in excellent 76% yield. Substrate **89** was completely reduced in the presence of borane, transformed to the HCl-adduct **90** and subsequently cyclised with triethyl orthoformate to give the expected imidazolium salt **91** in 42% yield for the final step.

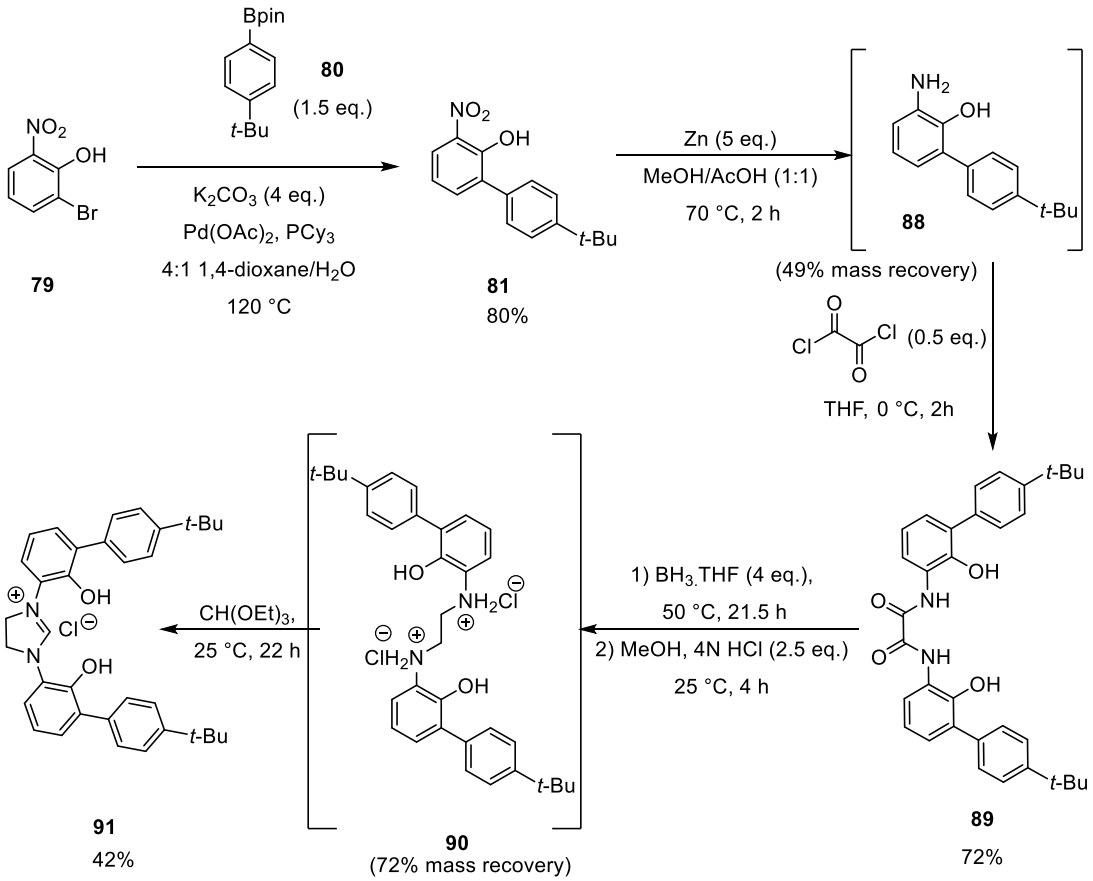

Scheme 2.33. Synthesis of o-O imidazolium salt precursor **91**.

Having established a route for imidazolium salts from amino phenol precursors, ligand **94** was prepared on gram scale (Scheme 2.34). Imidazolium **94** exhibited better solubility than the non-substituted framework (**57**) and as such we were able to investigate it as a model ligand towards the formation of **(p-O)TiNPh** catalysts.

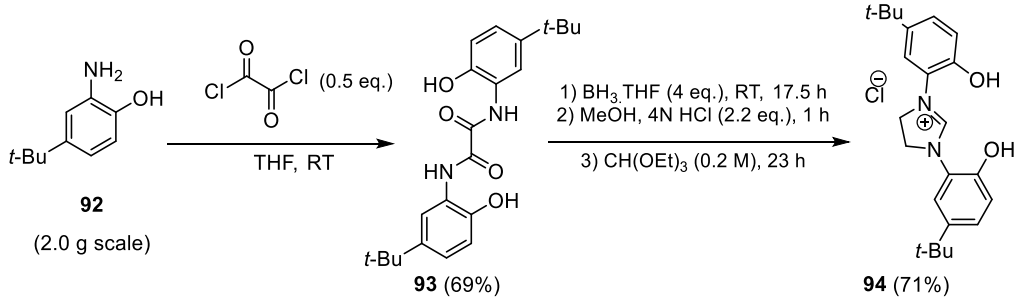

Scheme 2.34. Gram scale synthesis of imidazolium salt **94**.

2.4.5. Attempts at preparing soluble TiNPh catalysts

Table 2.5. Conditions screening towards (p-O)TiNPh catalysts

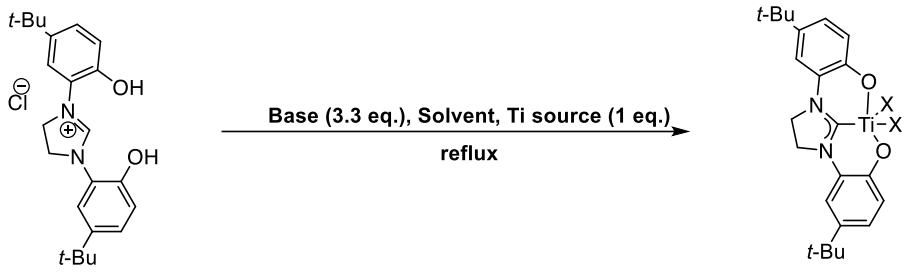

94

Entry	Conditions			Outcome*
	Base	Solvent	Ti source	
1	–	Toluene	$TiCl_4$	SM
2	–	DCM, then toluene	$ClTi(Oi\text{-}Pr)_3$	Insoluble precipitate
3	Et_3N	Toluene	$TiCl_4$	Mixture
4	NaH	Toluene	$TiCl_4$	Mixture
5	t-AmylOK	Toluene	$TiCl_4$	Mixture
6	t-BuOK	Toluene	$TiCl_4$	Mixture
7	t-BuOK	DCM	$TiCl_4$	SM
8	t-BuOK	THF	$TiCl_4$	Poorly soluble precipitate
9	t-BuOK	THF	$TiOSO_4 \cdot H_2O$	Insoluble precipitate
10	t-BuOK	THF	$Ti(Oi\text{-}Pr)_4$	Single product
11	–	THF	$Ti(Oi\text{-}Pr)_4$	SM

* Determined via ^1H NMR analysis.

An extensive evaluation of reaction conditions was conducted to access the desired **TiNPh** complex (Table 2.5). Initial attempts were guided by literature procedures reported for related diphenol-based ligands[99] and imidazolium precursors.[114] Refluxing the model ligand **94** with titanium(IV) chloride resulted only in recovery of the starting material (entry 1), while treatment with chlorotriisopropoxytitanium(IV) produced an insoluble precipitate (entry 2).

Given the presence of the imidazolium proton in **94** (pK_a ~ 24 in water),[115] it was hypothesised that deprotonation would be essential for complexation with titanium. In addition, agostic interactions with the metal centre could increase the acidity of the imidazolium proton. Therefore, several bases were screened, including triethylamine, sodium hydride, potassium tert-amylate, and potassium tert-butoxide (Table 2.5, entries 3–6). In all cases, complex mixtures were obtained, and no isolable product could be identified. Notably, reactions employing t-BuOK showed comparatively cleaner ^{1}H NMR spectra, prompting further optimisation of other reaction parameters.

Solvent screening revealed that the reaction in dichloromethane afforded only unreacted starting material (Table 2.5, entry 7), whereas performing the reaction in THF yielded a single but poorly soluble product (entry 8). Subsequent variation of the titanium source demonstrated a clear dependence on reagent identity: while $TiCl_4$ and $TiOSO_4 \cdot H_2O$ gave insoluble materials, titanium(IV) isopropoxide in the presence of t-BuOK produced a soluble species. The ^{1}H NMR spectrum of the latter (entry 10) suggested the formation of a ligand-to-metal complex as judged by the disappearance of the phenolic O–H and imidazolium C–H protons and an overall upfield shift in the aromatic proton environments. In contrast, omitting the base under otherwise identical conditions led exclusively to recovery of the starting ligand (entry 11), underscoring the critical role of deprotonation in promoting coordination to titanium.

Based on NMR analysis, two proposed structures for the complex of titanium(IV) isopropoxide (**95a** and **95b**) are shown in Scheme 2.35. Unfortunately, attempts to crystalise the compound and obtain an X-ray structure have been futile thus far, and decomposition was observed when the product was left at room temperature in air over a couple of days.

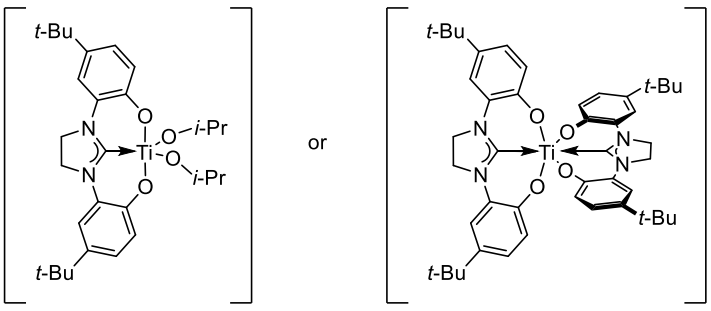

95a **95b**

Scheme 2.35. Proposed structures for (p-O)TiNPh catalyst **95a** and **95b**.

2.4.6. Investigation of novel NHC ligands in the titanium catalysed deoxygenation of primary alcohols

Table 2.6. NHC ligand screen in primary alcohol deoxygenation

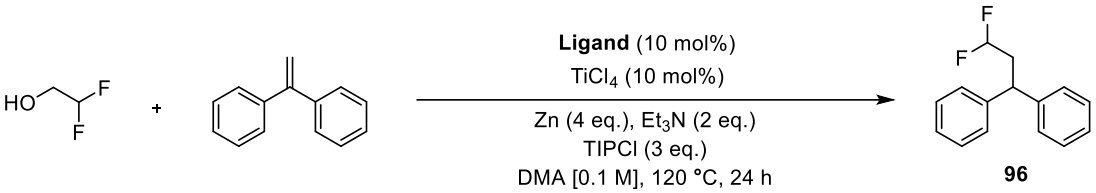

Entry	Ligand	Yield of 96*
1	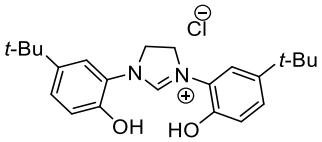 **94**	0%
2	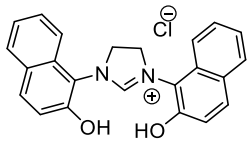 **61**	0%
3	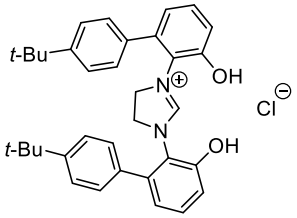 **78**	0%
4	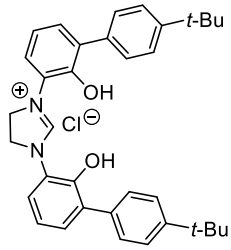 **91**	0%

* Determined via ^{19}F NMR using trifluorotoluene as internal standard.

Having achieved routes to a variety of NHC ligands, we were interested in investigating their reactivity towards alcohol deoxygenation. Since our attempts to prepare and isolate titanium-NHC catalysts led to formation of unstable or insoluble species, we hypothesized that the catalyst could be formed in situ and probed for alcohol activation. In this regard, titanium(IV) chloride, the prepared imidazolium salts and base were mixed in the presence of an alcohol (Table 2.6). Difluoroethanol was chosen as the model substrate, since the products of its deoxygenation can be easily monitored via ^{19}F NMR. In addition, stoichiometric amounts of activated zinc and triisopropylsilyl

chloride were employed to generate the active Ti(III) catalyst and ensure the recycling of the titanium-oxo species (vide supra Scheme 2.19). Diphenyl styrene was chosen as the radical trap, while the rest of the reaction conditions (dimethyl acetamide, 120 °C, 24 h) were adapted from a literature procedure.[99] Unfortunately, no product of deoxygenation (**96**) was detected (at -116.2 ppm),[116] with only a side product (at -127.4 ppm) being observed in the crude ^{19}F NMR spectrum with any of the ligands tested. We hypothesised that the alcohol udergoes silylation to **97** as a side reaction with triisopropylsilyl chloride (TIPCl), however it was not possible to isolate it due to the low boiling point of the substrate (Scheme 2.36).

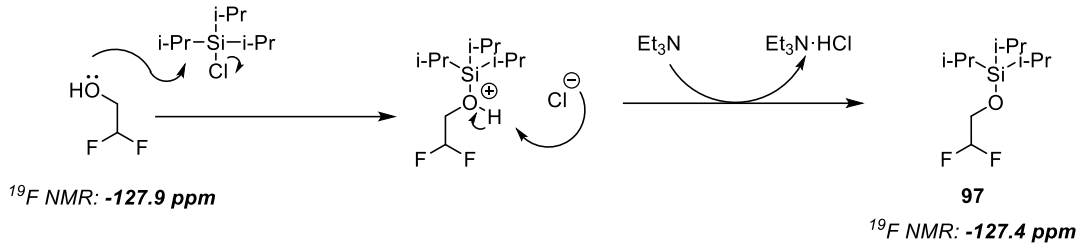

Scheme 2.36. Proposed formation of side silylation product **97**.

In addition, the effect of the solvent was examined. Common solvents in deoxygenation strategies[89, 93] such as THF and 1,4-dioxane did not afford any product (entries 1 and 2), while higher boiling solvents such as dimethyl formamide (DMF), N-methyl-2-pyrrolidone (NMP) and DMA only seemed to afford the side product with no alcohol deoxygenation observed (entries 3–5).

Table 2.7. Solvent screen in titanium deoxygenations.

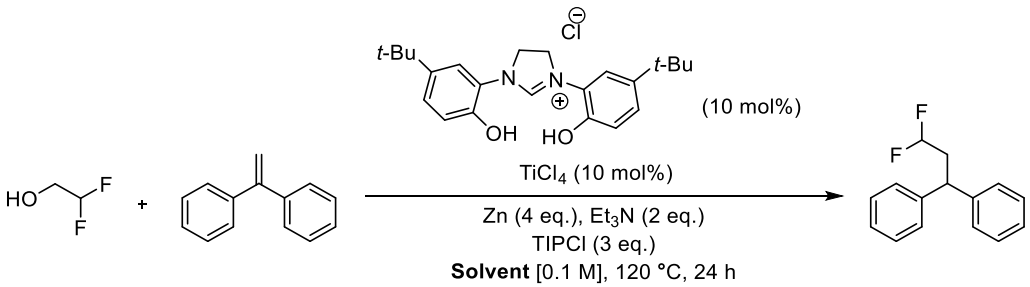

Entry	Solvent	Yield of 96*
1[a]	THF	0%
2	1,4-dioxane	0%
3	DMF	0%

4	NMP	0%
5	DMA	0%

* Determined via ^{19}F NMR using trifluorotoluene as internal standard.

[a] Reaction performed at 70°C.

The role of the base was investigated (Table 2.8). Triethylamine (entry 1), potassium tert-butoxide (entry 2), 1,8-Diazabicyclo[5.4.0]undec-7-ene (DBU) and sodium hydride (entry 4) all failed to give the deoxygenatively coupled product. Triethylamine was selected for the rest of the optimisation process due to its availability.

Table 2.8. Base screen in titanium deoxygenations.

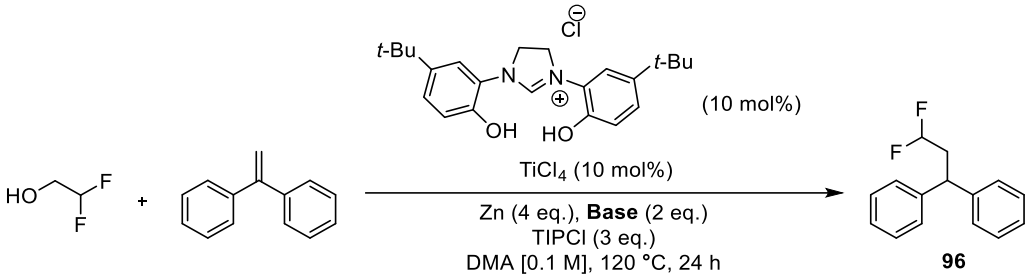

Entry	Base	Yield of 96*
1	Et_3N	0%
2	KO^tBu	0%
3	DBU	0%
4	NaH	0%

* Determined via ^{19}F NMR using trifluorotoluene as internal standard.

Finally, the reaction temperature was varied (Table 2.9). From room temperature to 70 °C the alcohol substrate remained intact with no side product forming (entries 1 and 2). Increasing the temperature up to 120 °C consumed most of the starting material but no product of deoxygenation was detected. Rising the temperature higher to 140 °C (entry 4) showed traces of the expected product with 3% being detected at 150 °C (entry 5). However, significant degradation could also be observed indicating that the deoxygenation was most likely due to the elevated temperature rather than any catalytic activity.

Table 2.9. Temperature variation in titanium deoxygenations

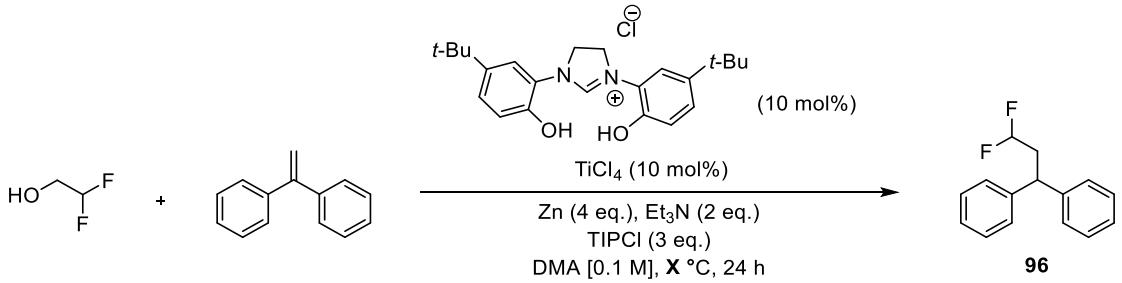

Entry	Temperature	Yield of 96*
1	RT	0%
2	70	0%
3	120	0%
4	140	Traces
5	150	3%

* Determined via ^{19}F NMR using trifluorotoluene as internal standard.

Taken together, these screenings indicated that no alcohol deoxygenation could be achieved in the presence of the model NHC ligand and titanium chloride. As such, further investigation into the preparation of a stable titanium NHC catalyst prior to deoxygenation could be able to support the hypothesis, since no evidence was present for the successful in situ preparation of a Ti NHC. Alternatively, a glove box could be employed to avoid the decomposition of air-sensitive catalysts.

2.5. Conclusion

Alcohols represent highly desirable yet challenging substrates for radical chemistry, particularly as precursors in catalytic C–O bond homolysis. While numerous strategies employing activating groups have been established, the direct catalytic cleavage of C–O bonds in primary and secondary alcohols remains an unsolved problem. To address this challenge, titanium-based catalysts and reagents have emerged as promising candidates, and this project aimed to advance the field through rational catalyst design.

In pursuit of this goal, three multistep ligand syntheses were developed toward the **TiNNaph**, **(o-N)TiNPh**, and **(o-O)TiNPh** catalyst precursors. The **TiNNaph** complex exhibited poor solubility, and further derivatisation attempts only exacerbated this issue. In contrast, the **(o-N)TiNPh** and **(o-O)TiNPh** scaffolds displayed superior solubility and showed potential as novel N-heterocyclic carbene ligands for titanium catalysis.

Preliminary investigations into the synthesis of the **(p-O)TiNPh** complex yielded promising results; however, its pronounced instability necessitated careful handling, highlighting the sensitivity of these systems.

The central objective of this work was to promote C–O bond homolysis in primary alcohols under catalytic conditions. Although initial studies using a model ligand resulted only in decomposition and side products, the findings provide valuable insights into the limitations of current systems. The observation of trace amounts of deoxygenatively coupled product indicate that with a different ligand design and suitable base, the reaction could be improved. Currently, the activation of primary alcohols toward homolytic cleavage therefore remains a key challenge and an exciting direction for future exploration in titanium-mediated radical chemistry.

CHAPTER 3

Strategies for the anti-Markovnikov Hydroxylation of Alkenes

3.1. Introduction

3.1.1. Classical hydration of alkenes

The direct and selective conversion of terminal olefins into linear alcohols via hydration is widely regarded as desirable transformation in synthetic chemistry—so much so that it has been identified as one of the “ten challenges for catalysis”.[117] This process holds significant synthetic and industrial value, as the addition of water across a double bond offers a straightforward route to alcohols.[118] Traditionally, direct hydration of alkenes is achieved using aqueous acid (Scheme 3.1). However, this method is reversible and typically exhibits Markovnikov regioselectivity, favouring the formation of branched alcohols. The underlying mechanism involves protonation of the alkene to generate a carbocation intermediate, which is then intercepted by water as a nucleophile. Since carbocation stability increases with substitution, the process inherently favours more substituted products,[119] making the synthesis of primary alcohols via this pathway especially challenging.

Alternatively, there have been many catalytic strategies developed for alkene hydration involving phosphoric acid,[120] metal oxides,[121] zeolites[122] and clays.[123] Nevertheless, these processes obey the Markovnikov rule giving preferentially the more substituted alcohol and the anti-Markovnikov product has remained elusive.

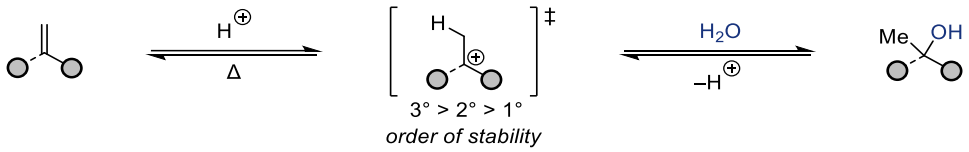

Scheme 3.1. Markovnikov addition of water across a double bond.

3.1.2. Hydroboration-oxidation sequence for the formation of anti-Markovnikov alcohols

To circumvent the carbocation intermediate and increase the selectivity for the anti-Markovnikov alcohol, a two-step strategy can be employed. Most notably, the hydroboration-oxidation of olefins has been extensively used in organic synthesis (Scheme 3.2).[124] First published in 1956 by Brown and Rao,[125] the reaction proceeds by direct addition of diborane (B_2H_6) or a borane reagent (BHR_2) across an alkene. The mechanism begins with the addition of the double bond π electrons into the empty p orbital on boron, which generates a partial positive charge on carbon. As a result, the more substituted carbon stabilises the transition state and leads to the selective

addition of boron to the less substituted end of the double bond. In addition, bulky groups on boron (such as in BHR2) can further improve the selectivity for the less sterically hindered olefinic carbon. In the second step, the borane adduct can be quantitatively oxidised to give the alcohol product at the less substituted carbon. Although this strategy can provide high degrees of primary alcohol, the oxidation step can sometimes give the secondary product (up to 6% with BH_3). Using a bulky borane reagent such as 9-BBN can improve the selectivity for the primary alcohol (only 0.1% of secondary alcohol is formed), but at the same time, it leads to a poorer atom economy.[126] In addition, hydrogen peroxide is a strong oxidant that can limit functional group tolerance, with common groups such as amines and thiols requiring a protection and deprotection.

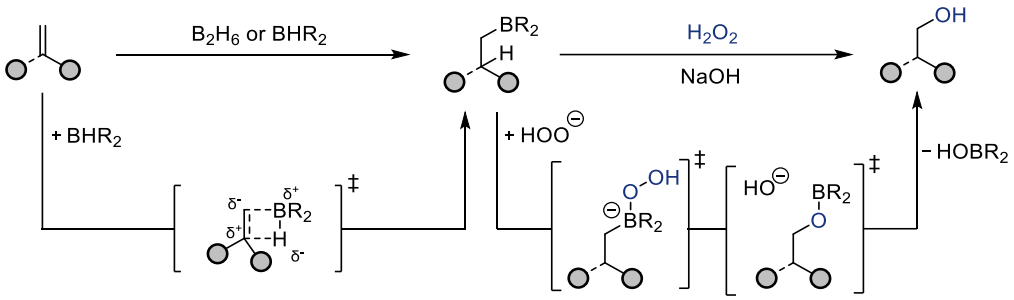

Scheme 3.2. Hydroboration-oxidation sequence for anti-Markovnikov hydration of olefins.

3.1.1. Hydroformylation–hydrogenation of olefins

A notable alternative strategy for accessing primary alcohols from terminal olefins involves the hydroformylation–hydrogenation sequence (Scheme 3.3).[127] In this tandem approach, a rhodium catalyst activates carbon monoxide from a syngas (CO/H_2) mixture under elevated temperature and pressure to promote hydroformylation of the alkene, yielding a linear aldehyde. This intermediate is then hydrogenated in situ in the presence of a ruthenium catalyst, affording the desired n-alcohol with high regioselectivity and as part of a formal one carbon extension of the alkyl chain. This strategy is very atom economical compared to epoxidation, since it is only stoichiometric in CO and H_2 gas and catalytic in all other components. On the other hand, it is best suited for terminal alkenes, with internal and activated substrates leading to branching at the aldehyde and subsequently mixtures of alcohol regioisomers.[128] Another downside is the harsh conditions employed which significantly limits the scope with some alkenes suffering from direct hydrogenation.

The carbon chain elongation could be another shortcoming in situations where only the longer chain olefin is synthetically accessible.

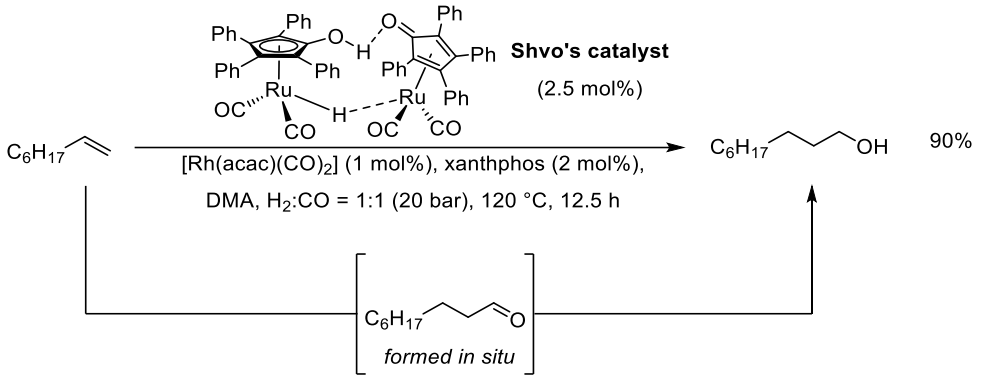

Scheme 3.3. Procedure from Nozaki et al. for the hydroformylation–hydrogenation of terminal olefins.

In an attempt to avoid the carbon chain homologation, Grubbs et al. developed a triple relay catalysis approach toward the anti-Markovnikov hydration of styrenes (Scheme 3.4).[129] Activation of the olefin (**97**) in a Wacker-type oxidation cycle generates the respective aldehyde (**98**), which can be reduced to the anti-Markovnikov alcohol (**99**). The first step is the coordination of the alkene to a palladium(II) catalyst (**Pd-I**) followed by nucleophilic attack by tert-butanol at the less hindered carbon. The steric effect of the tert-butyl group was suggested to be crucial in the selectivity of this process. The resulting complex **Pd-II** can undergo *β*-hydride elimination to yield allyl ether **100** which can undergo acid-catalysed hydrolysis to aldehyde **98**. The palladium hydride (**Pd-III**) gets deprotonated and oxidised by benzoquinone (BQ) mediated by a copper co-oxidant to the starting **Pd-I** and hydrobenzoquinone (HBQ) is formed as a side product. On the other hand, aldehyde **98** can participate in a transfer hydrogenation cycle mediated by Shvo's catalyst to form the anti-Markovnikov alcohol **99**. This procedure offers significantly milder conditions compared to the hydroformylation-hydrogenation sequence above and it also circumvents the carbon chain elongation. However, it is most suitable for terminal styrenes (**97a-d**), with aliphatic alkenes giving reduced yields and poor selectivity as seen for **97e**. Another major drawback is the use of high loadings of precious metal catalysts and stoichiometric amounts of BQ.

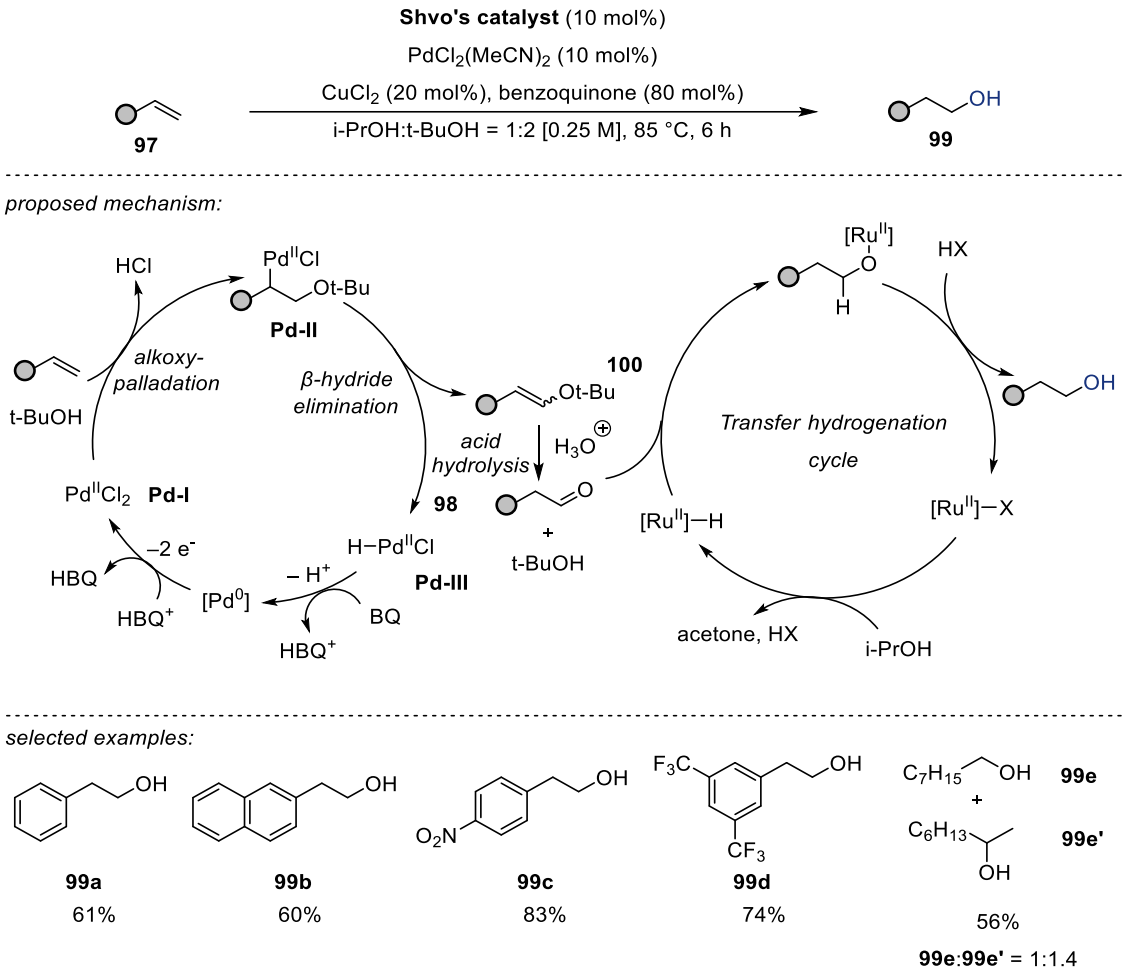

Scheme 3.4. Proposed mechanism in the formal anti-Markovnikov hydration via triple relay catalysis. X = anionic ligand (e.g. chloride, acetate).

3.1.2. Epoxides as intermediates towards anti-Markovnikov hydration

Another well-established two-step approach is the conversion of an alkene to epoxide, followed by ring opening. Typical reagents for epoxide formation are hydrogen peroxide and peroxycarboxylic acids, such as meta-chloroperoxybenzoic acid (mCPBA). More recently, metal-catalysed variants have been developed,[130] a landmark example being the enantioselective Sharpless epoxidation.[131]

Scheme 3.5. Structural classes of epoxides.

As shown in Scheme 3.5, there are 6 classes of epoxides that can be prepared from alkenes depending on their substitution pattern. For the respective anti-Markovnikov

alcohol formation, only classes **I–IV** are relevant, and their chemistry will be discussed in detail below.

The inherent ring strain of an epoxide (~28 kcal/mol for oxirane)[132] explains its reactivity towards ring opening in the presence of a nucleophile. The regioselectivity of this reaction depends on the reaction conditions[133] and nucleophilicity of reagent. Under basic conditions, a strong nucleophile undergoes S_N2 attack at the less sterically hindered β-atom. leading to the alcohol group residing on the more substituted α-carbon in the product. On the other hand, protonation of the epoxide, as is usually observed under acidic conditions, leads to elongation of the C–O bond, generating a more stabilised positive charge on the α-carbon.[134] The nucleophile attack proceeds via a 'loose S_N2' transition state, yielding the hydroxyl at the less substituted carbon.[133]

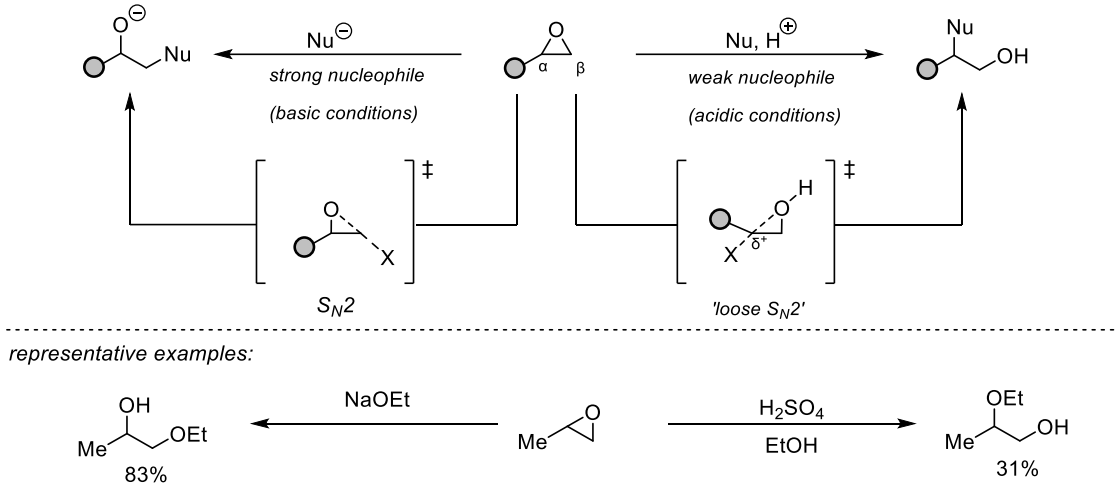

Scheme 3.6. Regioselectivity of epoxide ring opening under acidic vs. basic conditions.

Direct hydrogenolysis of epoxides offers a straightforward route to access alcohols but it comes with significant limitations. The use of excess amounts of reducing agents (such as $LiAlH_4$) typically leads to mixtures of products and stoichiometric waste[135] whereas conventional hydrogenolysis conditions (Pd/C, H_2 gas) favour formation of the undesired secondary alcohol.[136] Raney Ni has been shown to catalyse the regioselective hydrogenation of epoxides towards the anti-Markovnikov primary alcohol, though only under harsh conditions that restrict substrate scope.[137] To address these challenges, alternative catalytic strategies involving the Meinwald rearrangement have been developed.

3.1.3. Meinwald rearrangement – hydrogenation sequence as a strategy to access anti-Markovnikov alcohols from epoxides

First reported in 1963,[138] the Meinwald rearrangement describes the Lewis acid (LA) mediated activation of an epoxide, which triggers ring opening to generate a carbocation at the more stabilised carbon centre in **101** (Scheme 3.7, A). Intermediate **101** undergoes a 1,2-shift (typically hydride or aryl migration), producing an oxocarbenium ion that subsequently collapses to the corresponding carbonyl compound (**102**). When coupled with a reduction step, this transformation provides efficient access to anti-Markovnikov alcohols (**103**), a strategy that has been widely applied in synthesis.[139-143]

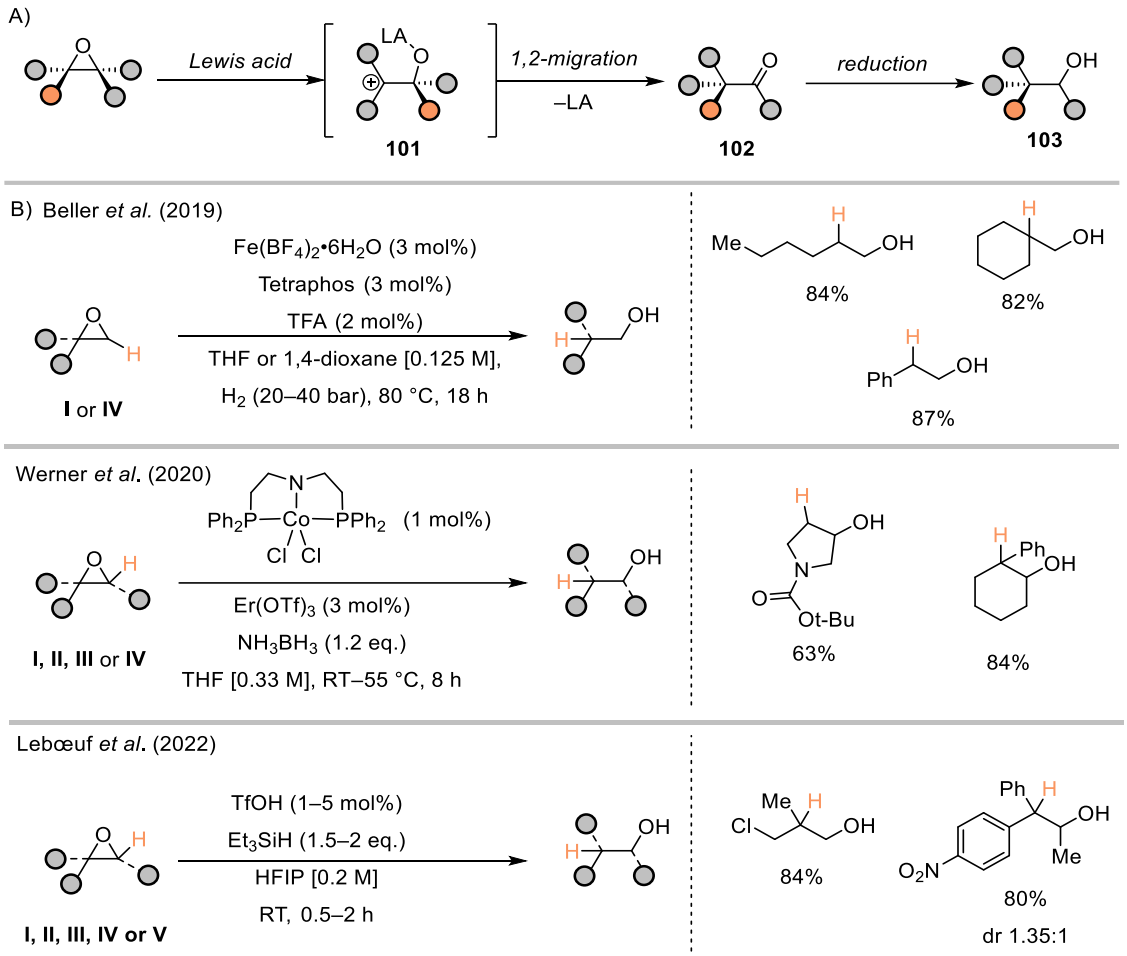

Scheme 3.7. A) Two-step mechanism of polar epoxide ring opening involving a Meinwald rearrangement and carbonyl reduction. B) Selected synthetic methods with examples showcasing the utility of this transformation. The migrating group has been highlighted in orange.

Representative procedures are highlighted in Scheme 3.7, B. In general, these methodologies are very selective towards the less substituted alcohol product and are broadly applicable to both benzylic and aliphatic epoxides bearing a variety of substitution patterns. However, the use of high pressures of hydrogen gas or stoichiometric reducing agents (NH_3BH_3, Et_3SiH) alongside the need to prepare an epoxide make these strategies unappealing for anti-Markovnikov alcohol production from olefins.

3.1.4. Radical ring opening of epoxides

Alternative to the polar strategies presented above, a radical ring opening of the epoxide can offer the desired selectivity. Homolysis of the weak C-O bond will lead to a more stable secondary radical which could be quenched to the primary alcohol. Initial studies in the radical ring-opening of epoxides involved the use of solvated alkali metals as stoichiometric reductants.[144-146] However, employing lithium or calcium as one electron donors resulted in poor product selectivity and side radical reactivity.

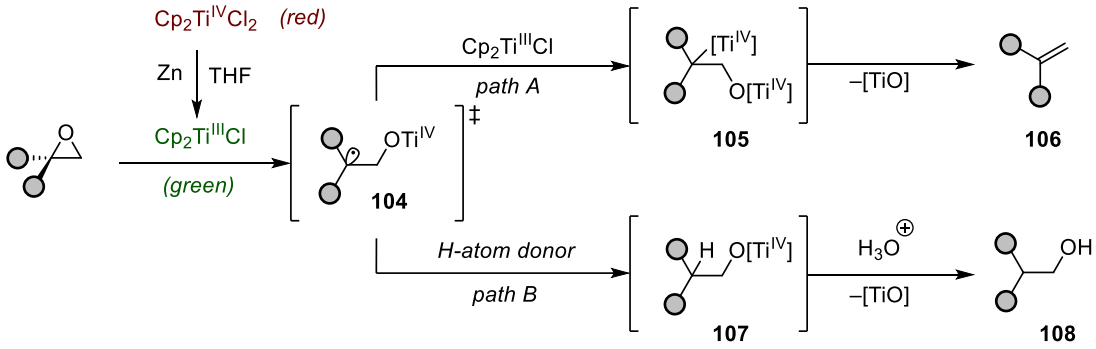

Scheme 3.8. Reactivity of the Nugent-RajanBabu reagent with epoxides.

Thus, research focus was shifted to other homogeneous metal systems that can act as milder SET reagents. A landmark discovery in the field was the development of the Nugent-RajanBabu reagent.[147] Stirring a red titanocene(IV) chloride solution in THF with powdered zinc for 15 minutes results in the quantitative formation of titanium(III), as evidenced by the lime green colour change. In the presence of an epoxide, a radical ring-opening takes place, with preferred regioselectivity for the more substituted β-titanoxy radical (Scheme 3.8). The carbon radical (**104**) can either be reduced by another equivalent of Ti(III) to give intermediate **105**, which undergoes rapid elimination to alkene **106** (Scheme 3.8, Path A), or be trapped with a hydrogen atom donor (**107**) and protonated to yield alcohol **108** (Scheme 3.8, Path B). The rate of

radical trapping in Path B needs to be faster than the radical reduction (path A) in order to improve the selectivity for the alcohol product. Thus, other less sterically hindered SET reagents (such as SmI_2) are unsuitable for this transformation as they favour the deoxygenation pathway.[148]

Another consideration is the choice of a suitable hydrogen atom donor. Although commonly used hydrogen atom donor reagents such as 1,4-cyclohexadiene (1,4-CHD),[149] 2-methylpropan-2-thiol,[147] and Bu_3SnH[150] (with BDE ~76 kcal/mol) are tolerated under the reaction conditions, they have their own drawbacks. 1,4-CHD is highly volatile, whereas thiols and tin reagents are notorious for their toxicity, and/or foul smell. Nonetheless, Oltra et al. employed water as the hydrogen atom source[97], proving that titanocene-water complexes can be used as unique HAT reagents. The group showcased that the coordination of a water molecule to a reduced titanocene metal center significantly lowers the O–H BDE from 118 kcal/mol to 49 kcal/mol.[151]

Another major drawback of the Nugent-RajanBabu reagent is the generation of stoichiometric metal and hydrogen atom donor waste. Therefore, a catalytic variant would be an attractive development to improve the atom economy of this transformation. To achieve this, several key challenges must be addressed: regenerating the active titanium(III) species and substituting the stoichiometric hydrogen atom donor reagent with a more sustainable alternative.

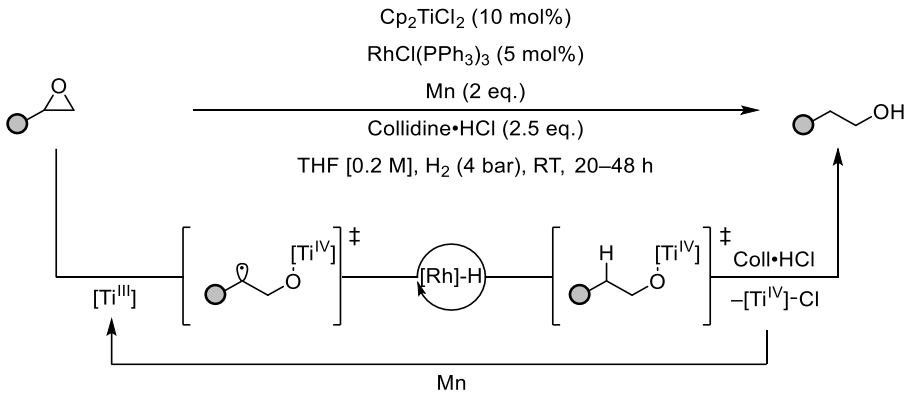

Scheme 3.9. First dual catalytic procedure for radical epoxide ring opening.

The first catalytic development in the titanocene radical opening of epoxides was published by the Gansäuer group.[149] In particular, introducing collidine hydrochloride in the reaction resulted in the regeneration of the titanium active site via protonation of the Ti–O and Ti–C bonds (Scheme 3.9). Subsequent reduction with manganese

powder renders the reaction catalytic in titanium. Another key feature of this system was using Wilkinson's catalyst ($Rh(PPh_3)_3$) as the hydrogen atom transfer mediator.[152] These advancements prevented the stoichiometric titanium and hydrogen atom donor waste; however, the use of explosive hydrogen gas, precious metal catalyst and stoichiometric reductant and H^+ source are areas that need further optimisation.

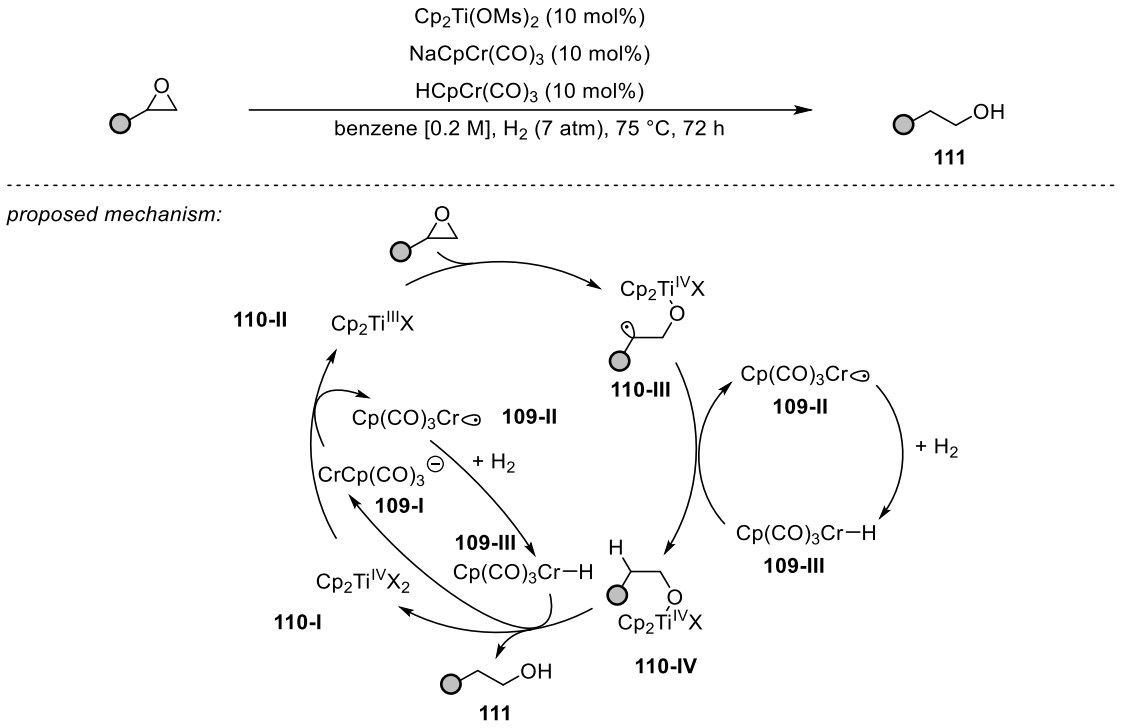

Scheme 3.10. Cooperative chromium catalysis in the radical epoxide ring opening. Proposed mechanism of the transformation.

To improve the atom economy of the epoxide ring opening reaction, a cooperative chromium catalyst was introduced (Scheme 3.10).[153] The use of $CpCr(CO)_3H$ (**109**) eliminated the need for stoichiometric metal reductant and proton source, with the only reagent in excess being hydrogen gas. The mechanism proceeds with anion **109-I** reducing titanium(IV) (**110-I**) to Ti(III) (**110-II**), which then undergoes radical epoxide ring opening to give titanium alkoxide (**110-III**). The resulting oxidised chromium catalyst (**109-II**) activates hydrogen gas to form metal hydride (**109-III**), which can then quench the carbon radical via HAT (BDE of Cr–H is 62.2 kcal/mol).[154] Simultaneously metal hydride **109-III** protonates alkoxide **110-IV** to regenerate the titanium catalyst (**110-I**) and yield the alcohol product (**111**), thus rendering the transformation catalytic in titanium and chromium.

More recent studies focused on eliminating the use of hydrogen gas[155] and even chromium co-catalyst[156] and extending the substrate scope to benzylic epoxides which have been elusive to previous strategies.[147, 149]

3.1.5. Anti-Markovnikov hydroxylation using water

Advancements in the field of photoredox catalysis have delivered multiple strategies for anti-Markovnikov hydrofunctionalisation of olefins including hydroetherification,[157] hydroamination,[158] and hydroacetoxylation[159] among others.[160] In this regard, Lei and colleagues first demonstrated that the anti-Markovnikov hydration of styrenes can be achieved by simply using water as a nucleophile.[161] This transformation has recently been extended by the Ritter group to more challenging tri- and disubstituted aliphatic alkenes (Scheme 3.11).[162]

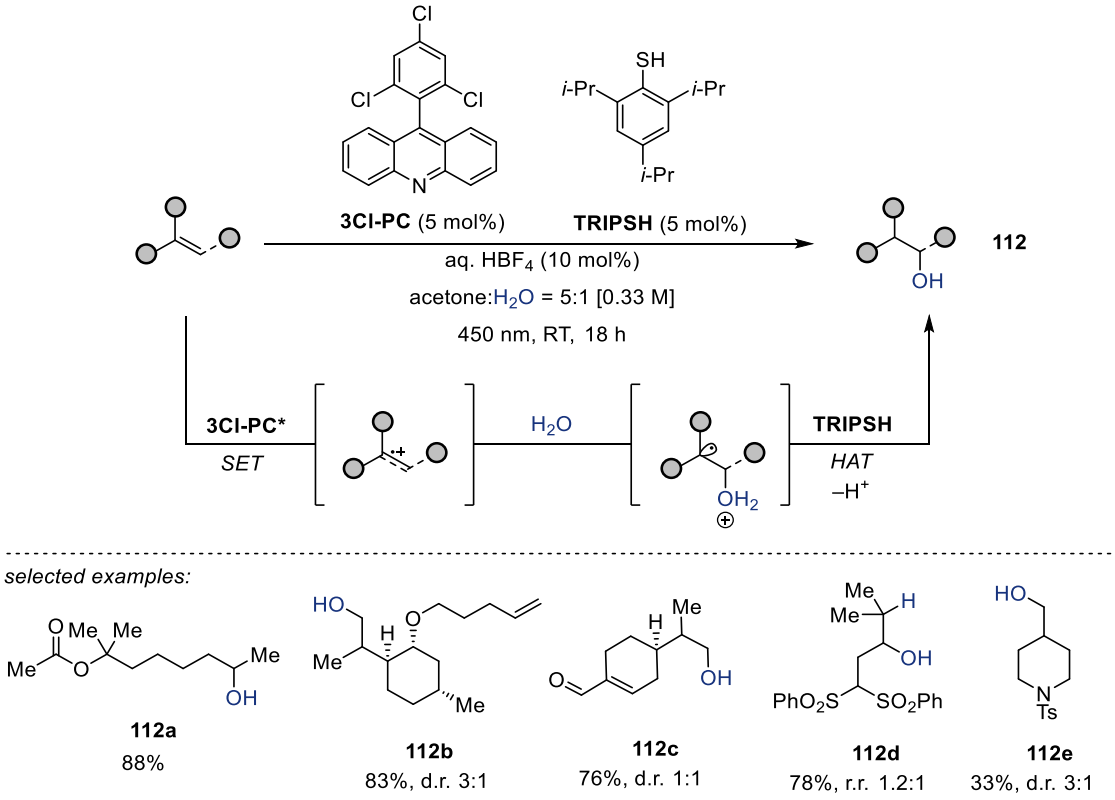

Scheme 3.11. Anti-Markovnikov hydration of alkenes under oxidative conditions.

The mechanism of the hydration reaction involves SET from the alkene substrate to the excited state of the photocatalyst (**3Cl-PC***). The resulting cation radical can be captured by nucleophilic attack of a water molecule and quenched with a HAT catalyst (**TRIPSH**) leading to the final alcohol product. The reaction is catalytic in all components and it offers excellent regioselectivity towards the anti-Markovnikov

adduct in a one-pot transformation. Although the conditions are very mild (room temperature, visible light irradiation), the use of a highly oxidising PC (E^*_{red} = 2.28 V vs SCE)[162] is limiting the substrate scope and functional group compatibility. Since this approach relies on the direct oxidation of the olefin, substrates that fall outside of the oxidation window of the PC, such as terminal and electron-deficient alkenes, remain inaccessible (**112b** and **112c**). Furthermore, the poor nucleophilicity of water allows more nucleophilic species (e.g., amines, thiols) to compete in side reactions, thus they remain not tolerated in this system and protecting groups must be employed (**112d** and **112e**).

Although a wide range of approaches has been explored, a broadly applicable, catalytic, sustainable, and selective anti-Markovnikov hydroxylation continues to present a formidable synthetic challenge. In this work, we attempt to develop a new strategy to overcome this limitation.

3.2. Hypothesis for anti-Markovnikov hydroxylation via hydroxyl radical

The most efficient and atom economical way to produce anti-Markovnikov alcohols from alkenes is to form the C–O bond directly in a single step. Given our previous interest in alcohol bond homolysis (Chapter 2), we hypothesised that a radical C–O bond formation would be feasible between a hydroxyl radical (HO•) and an olefin (Scheme 3.12). The resulting carbon centred radical can be quenched via HAT to yield the product.

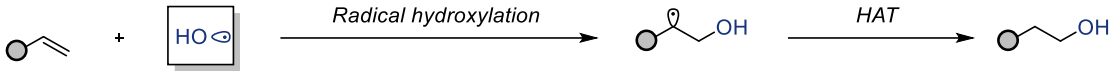

Scheme 3.12. Radical addition of hydroxyl radical into olefin followed by HAT

The design of such a reaction needs to address three main challenges. Firstly, the system must be able to generate the HO• under synthetically useful conditions. Secondly, the reaction environment must tolerate most organic molecules and minimise degradation of substrates and catalysts. Finally, a suitable HAT catalyst must be employed that can preferentially react with the carbon centred radical to avoid the quenching of the oxygen radicals.

One approach to this is to directly activate water via oxidation or HAT (Scheme 3.13). However, its inherently high oxidation potential (E° > 3 V vs NHE) and the strength of the O–H bond (BDE = 118.2 kcal/mol) render it rather inert in most reaction systems. Thus, to produce HO• from water under mild conditions, it needs to be preactivated, for example by coordination to a metal centre.

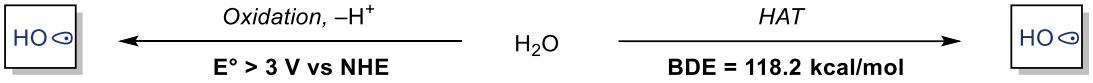

Scheme 3.13. Methods for generating hydroxyl radical from water.

With recent advancements in the photochemistry of first-row transition metals,[163-165] we were attracted to the photoreactivity of their charge transfer excited states. These are categorised as metal-to-ligand charge transfer (MLCT), ligand-to-metal charge transfer (LMCT), intraligand charge transfer (ILCT) and ligand-to-ligand charge transfer (LLCT).[166] Notably, LMCT states lead to the activation of nucleophilic entities into open-shell radical species. By promoting an electron from ligand (p/π) or a metal-ligand (dσ) bond into a vacant antibonding orbital (d*/ dσ*) at the metal centre, a formal 1

electron oxidation of the ligand and reduction of the metal is evoked.[167] We hypothesise that this mode of reactivity can be exploited to induce the formal oxidation of water leading to the generation of HO•.

Key considerations in designing such systems include the use of high-valent metal centres and strong σ- and/or π-donor ligands. In particular, LMCT states of high-valent, electron-deficient first-row transition metal complexes (e.g., Ti^{IV}, V^{III}, Fe^{III}, Co^{III}, Cu^{II}) have been extensively explored,[167] since their low-lying empty d orbitals can be readily populated via electron transfer from donor ligands. The nature of the ligand crucially determines the magnitude of the ligand field splitting: strong σ- and π-donors typically produce a small to moderate splitting, allowing both t_{2g} and e_g orbitals to be accessed by LMCT transitions. In these systems, the bonding orbitals are primarily ligand-centred, whereas the corresponding antibonding orbitals are metal-centred.[166] Consequently, population of the metal-based antibonding orbital through LMCT excitation can promote homolytic cleavage of the M–X bond.

Water itself is a weak to moderate field ligand, however in the form of hydroxide, it acts as both a strong σ- and π-donor. Consequently, LMCT excitation leading to HO• generation is more likely to proceed from a metal–hydroxide than from a metal–aqua complex, as the higher-lying O-based orbitals of the hydroxide facilitate electron transfer to the metal centre. Moreover, because this charge transfer occurs within an inner-sphere complex, the oxidising equivalent remains localised, thereby minimising overoxidation of other solution-phase species. These considerations address the first two out of the three challenges posed above.

Finally, to circumvent the chemoselectivity problem of the HAT step, water can be employed as the hydrogen atom donor. In the radical ring opening of epoxides, Oltra et al. showed that coordination of a water molecule to a reduced Ti^{III} centre can significantly lower its BDE and hence allow it to participate in HAT with carbon-centred radicals.[97] Thus, we can formulate the final version for the anti-Markovnikov LMCT hydroxylation hypothesis (Scheme 3.14).

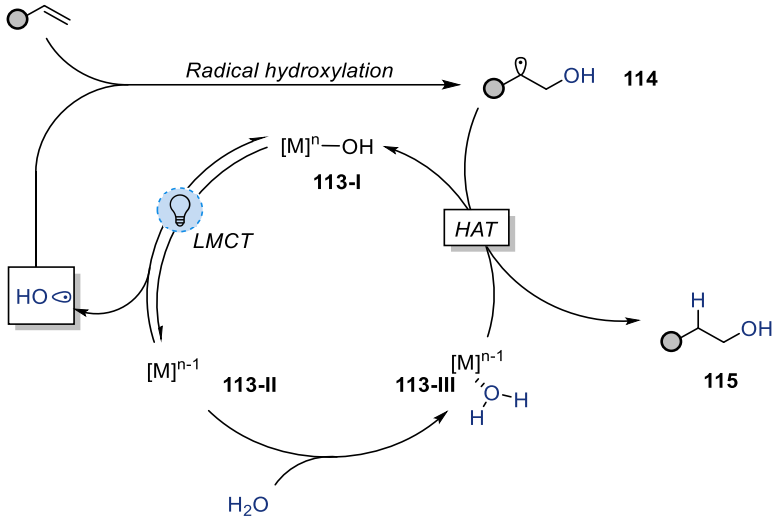

Scheme 3.14. Proposed hypothesis for anti-Markovnikov hydroxylation via hydroxyl radical mediated by LMCT.

Light irradiation of a metal-hydroxide complex (**113-I**) leads to an LMCT state from which M-O bond homolysis takes place to yield the hydroxyl radical and reduced metal centre (**113-II**). HO• undergoes anti-Markovnikov Kharasch addition resulting in the more stable carbon-centered radical (**114**). Coordination of a water molecule to the reduced metal centre (**113-II**) produces the active HAT catalyst (**113-III**). **113-III** can quench radical **114** to give the terminal alcohol product (**115**) and regenerate the starting metal-hydroxide complex (**113-I**), thus completing the catalytic cycle.

Titanium(IV) and its complexes present an ideal platform for investigating this reactivity. Owing to the hard Lewis acidic character and d^0 configuration of Ti(IV), electron transfer from oxygen-based ligands is thermodynamically accessible and can be photochemically induced under LMCT excitation. This behaviour is well established in heterogeneous systems such as titania, where Ti–O LMCT processes drive the formation of reactive oxygen species (ROS) during photocatalytic water oxidation and pollutant degradation.[168-170] By translating these principles into a homogeneous framework, we aimed to explore whether analogous Ti–O LMCT events could mediate hydroxyl radical generation and subsequent anti-Markovnikov hydroxylation of alkenes.

3.3. Results and discussion on hydroxylation via hydroxyl radical

As an initial study, the LMCT hydroxylation was attempted at alkene **116** in mixtures of MeCN and water (Table 3.1). In the presence of either titanium chloride (entries 1–3) or titanocene chloride (entry 4), no desired hydroxylation product (**117**) was observed. Given its comparable d^0 configuration, zirconium chloride was also investigated, however no reaction occurred (entry 5).

Table 3.1. Attempts to evoke LMCT from water

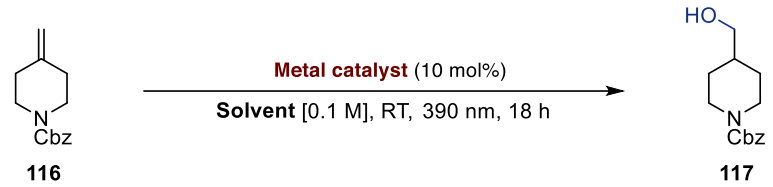

116 **117**

Entry	Metal catalyst	Solvent	Outcome*
1	$TiCl_4$	9:1 MeCN/H_2O	NR
2	$TiCl_4$	1:1 MeCN/H_2O	NR
3	$TiCl_4$	MeCN (+1 eq. H_2O)	NR
4	$TiCp_2Cl_2$	9:1 MeCN/H_2O	NR
5	$ZrCl_4$	9:1 MeCN/H_2O	NR

* Determined via ^1H NMR using 1,1,2,2-tetrachloroethane as internal standard.

It was of interest to examine whether the NHC ligands previously prepared (see section 2.4. would exhibit any reactivity in this system (**Table 3.2**). Coordination of a polydentate ligand to the metal centre was anticipated to lower the energy of the LMCT excited state through extended conjugation. However, upon addition of ligands **78**, **91**, and **94**, no hydroxylation product was detected.

Table 3.2. Attempts to evoke LMCT from water in the presence of an NHC ligand

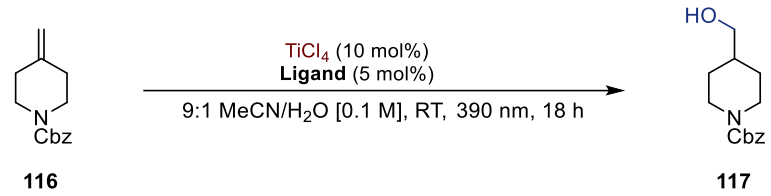

116 **117**

Entry	Ligand	Outcome*
1	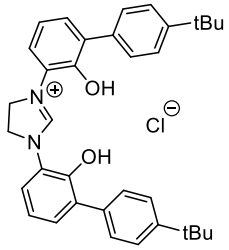 **91**	NR
2	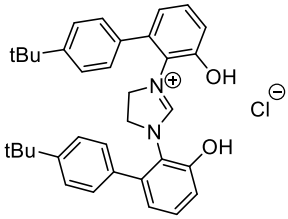 **78**	NR
3	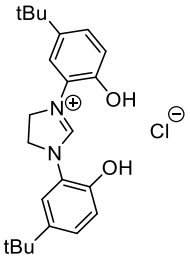 **94**	NR

* Determined via ^{1}H NMR using 1,1,2,2-tetrachloroethane as internal standard.

Having observed no changes to the substrate in reactions with water, we hypothesised that introducing a source of hydroxide could improve the formation of metal-hydroxide complex and evoke LMCT reactivity (Table 3.3). As such, different amounts of potassium hydroxide were tested but none of the reaction mixtures were productive towards hydroxylation. Excess of base was chosen as standard procedure in the end to ensure that the equilibrium of metal hydroxide formation lies towards hydroxide complex.

Table 3.3. Introduction of base and varying equivalents

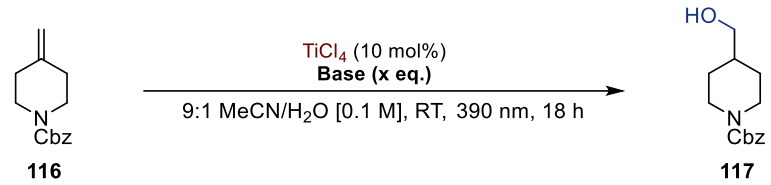

116 **117**

Entry	Amount of KOH	Outcome*
1	5 mol%	NR
2	1 eq.	NR
3	2 eq.	NR
4	5 eq.	NR
5	10 eq.	NR

* Determined via ^{1}H NMR using 1,1,2,2-tetrachloroethane as internal standard.

We then examined other high-valent metal centres capable of undergoing LMCT activation (Table 3.4). Accordingly, metal precatalysts based on vanadium(III), manganese(II), iron(II), cobalt(II), nickel(II), copper(II), zirconium(IV) and indium(III) were evaluated in the presence of excess hydroxide. In all cases, no hydroxylation product was detected and the starting material remained untouched. Titanocene(IV) chloride was also examined under these conditions but, once again, no reactivity was observed (entry 10).

Table 3.4. Screening of metal catalysts towards LMCT

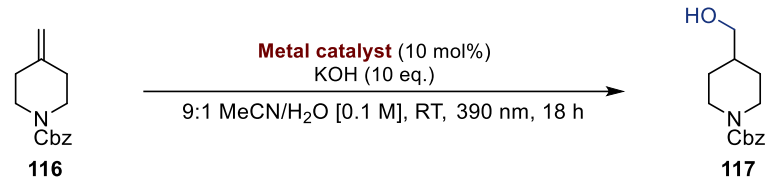

116 **117**

Entry	Amount of KOH	Outcome*
1	$V(acac)_3$	NR
2	$MnCl_2$	NR
3	$FeCl_3$	NR
4	$Fe(acac)_3$	NR
5	$Co(acac)_2$	NR
6	$NiCl_2$	NR
7	$CuCl_2$	NR
8	$ZrCl_4$	NR
9	$InCl_3$	NR
10	$TiCp_2Cl_2$	NR

* Determined via ^1H NMR using 1,1,2,2-tetrachloroethane as internal standard.

The NHC ligands were also trialed in the current system (Table 3.5) in the presence of titanium (entries 1 and 2) or zirconium (entries 3 and 4) but no reactivity was observed.

Table 3.5. Attempts to evoke LMCT from hydroxide in the presence of an NHC ligand

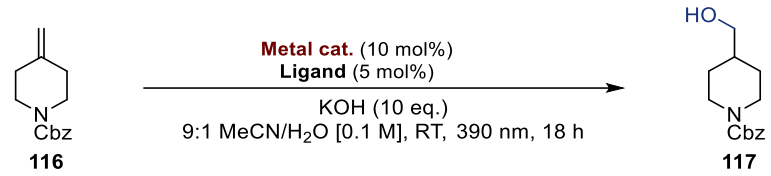

Entry	Metal catalyst	Ligand	Outcome*
1	$TiCl_4$	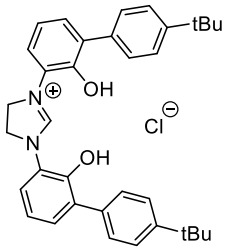 **91**	NR
2	$TiCl_4$	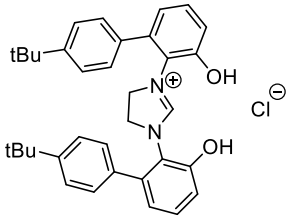 **78**	NR
3	$ZrCl_4$	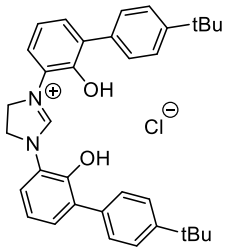 **91**	NR
4	$ZrCl_4$	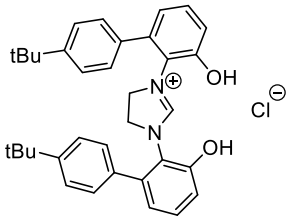 **78**	NR

* Determined via ^1H NMR using 1,1,2,2-tetrachloroethane as internal standard.

Since no product of LMCT hydroxylation had been observed thus far, it was hypothesised that the biphasic nature of the reaction medium might inhibit formation of the active metal–hydroxide species. To address this limitation, a preformed metal hydroxide complex was employed. Titanium(IV) bis(ammonium lactato)dihydroxide (TiBALD) was therefore used as an aqueous solution in a range of solvent mixtures (Table 3.6). However, no hydroxylation product was detected under any of the conditions examined.

Table 3.6. LMCT with preformed titanium metal hydroxide: Solvent screen

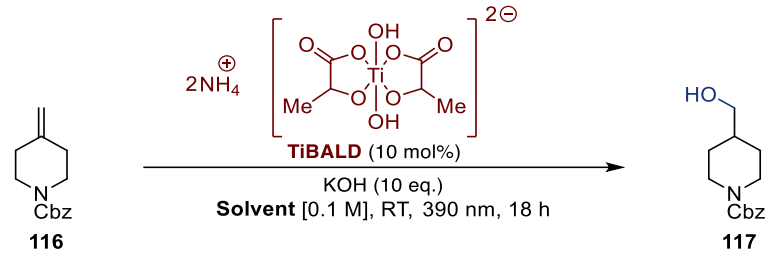

Entry	Solvent	Outcome*
1	9:1 MeCN/H_2O	NR
2	3:1 MeCN/H2O	NR
3	1:1 MeCN/H_2O	NR
4	1:9 MeCN/H_2O	NR

* Determined via ^{1}H NMR using 1,1,2,2-tetrachloroethane as internal standard.

Activation of the preformed titanium hydroxide complex was next explored in the presence of various ligands (Table 3.7). Catechol **118** (entry 1) and its derivative **119** (entry 2) were evaluated but proved unsuccessful. Similarly, 1,1′-bi-2-naphthol (BINOL) **120** was tested but showed no evidence of reactivity. NHC ligands **61**, **78**, and **91** were likewise investigated; however, none promoted hydroxylation under the examined conditions.

Table 3.7. LMCT with preformed titanium metal hydroxide: Ligand screen

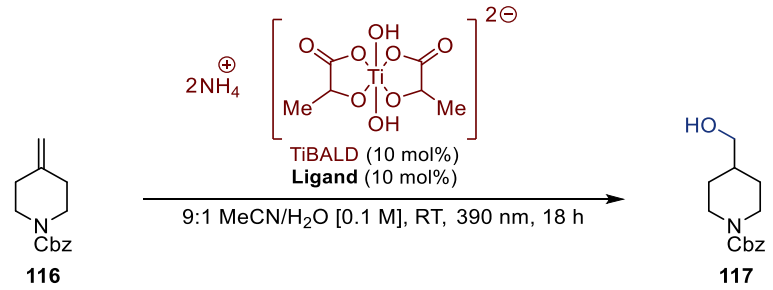

Entry	Ligand	Outcome*
1	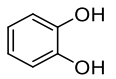 **118**	NR
2	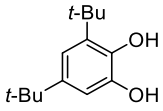 **119**	NR

3	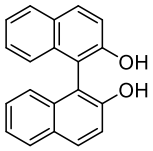	**120**	NR
4	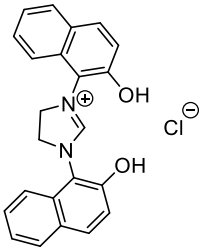	**61**	NR
5	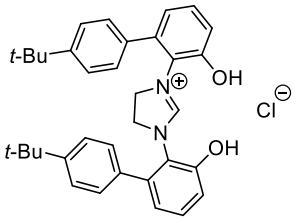	**78**	NR
6	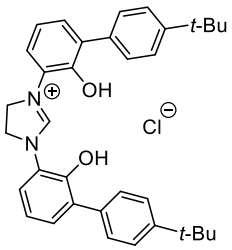	**91**	NR

[*] Determined via ^{1}H NMR using 1,1,2,2-tetrachloroethane as internal standard.

As an alternative to potassium hydroxide as the hydroxide source, we envisioned that a sufficiently strong organic base could deprotonate water at the interface of the two layers and thereby bring the desired hydroxide species in the organic phase. Accordingly, a range of organic-soluble (super)bases was evaluated (Table 3.8). N,N-Dimethylguanidine (**121**) and proton sponge (**122**), with conjugate acid pK_a values of approximately 25 in MeCN,[171] should in principle be capable of deprotonating water ($pK_a \approx 16$). However, neither base promoted any detectable reactivity. The less basic potassium tert-butoxide was also tested but proved ineffective. Finally, tetraethylammonium hydroxide was employed as a direct source of hydroxide, yet no hydroxylation product was observed.

Table 3.8. Screen of superbases in the presence of titanium

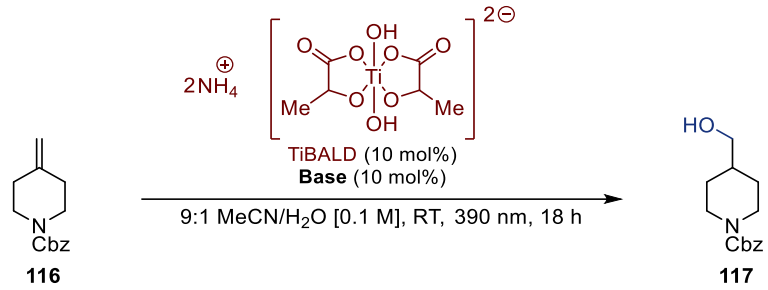

Entry	Base	Outcome*
1	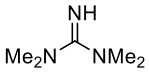 **121**	NR
2	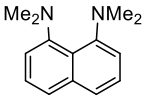 **122**	NR
3	KOtBu	NR
4	Et_4NOH	NR

* Determined via ^1H NMR using 1,1,2,2-tetrachloroethane as internal standard.

Given the biphasic nature of our system, we hypothesised that our inability to observe the product of hydroxylation is due to insufficient transfer of hydroxide anions between the two phases. As such, this hypothesis prompted us to investigate phase transfer catalysts (PTC) as carriers for hydroxide into the organic layer (Table 3.9). Crown ether **123** was selected due to its complementary cavity towards potassium cations,[172] but no reactivity was observed (entry 1). Other common PTCs such as tetrabutylammonium hexafluorophosphonate ($TBAPF_6$) and tetraphenylphosphonium chloride (Ph_4PCl) proved ineffective in this system (entries 2 and 3). Finally, cyclopropenium salt **124** was synthesised and employed, but the reaction gave no product of hydroxylation. The same set of experiments in Table 3.9 was carried out by substituting TiBALD with: $VO(acac)_2$, $Sc(acac)_3$ and $ZrCl_4$ but none of them gave any sign of reactivity.

Table 3.9 Screen of PTCs in the presence of titanium

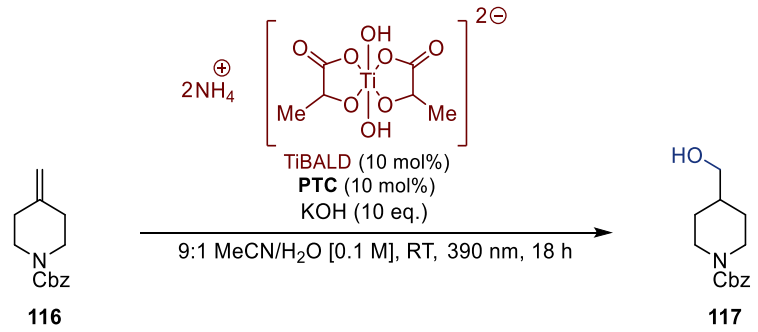

Entry	PTC	Outcome*
1	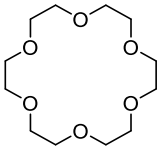 **123**	NR
2	$TBAPF_6$	NR
3	Ph_4PCl	NR
4	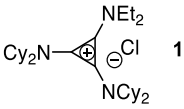 **124**	NR

* Determined via ^1H NMR using 1,1,2,2-tetrachloroethane as internal standard.

Recent reports in the highly oxidising nature of the cyclopropenium radical cation (E^*_{red} = 3.33 V vs SCE)[173, 174] produced in the one electron oxidation of **124**, encouraged us to investigate **124** further as a photooxidant of water/hydroxide. As such, cyclopropenium **124** was screened in the presence of a variety of high valent metal salts (Table 3.10). Unfortunately, no product of hydroxylation was identified with the starting material remaining untouched.

Table 3.10. Cyclopropenium as hydroxide surrogate with different high valent metals

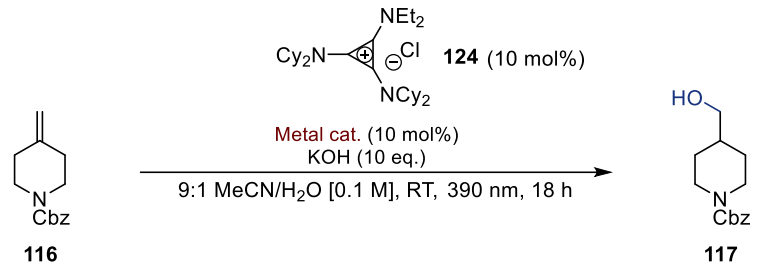

Entry	Metal catalyst	Outcome*
1	$Sc(acac)_3$	NR

2	TiBALD	NR
3	$VO(acac)_2$	NR
4	VCl_3	NR
5	$Co(acac)_3$	NR
6	$ZrCl_4$	NR

* Determined via ^{1}H NMR using 1,1,2,2-tetrachloroethane as internal standard.

A recent study published by the Sanford group showed that the oxidation properties of first row Lewis acids in the presence of acridine (**125**) can be significantly enhanced.[175] As such, we attempted to employ this highly oxidising system (E^*_{red} = 2.47 V in MeCN vs SCE for scandium)[175] for the generation of HO• from a preformed organic hydroxide (Table 3.11). Lewis acids based on scandium, titanium, indium and aluminium were tested but only traces of decomposition products were detected in the crude reaction mixtures.

Table 3.11. Screen of Lewis acid – acridine complexes towards generation of hydroxyl radical

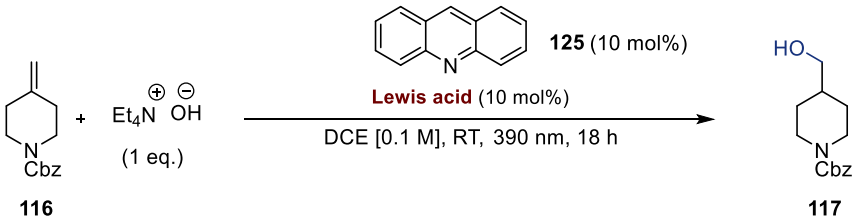

116 117

Entry	Lewis acid	Outcome*
1	$Sc(acac)_3$	NR
2	$TiCl_6(PPh_4)_2$	NR
3	$In(OTf)_3$	NR
4	$Al(acac)_3$	NR

* Determined via analysis of crude ^{1}H NMR.

Overall, the anti-Markovnikov hydroxylation via LMCT activation was not realised within the scope of this study. Despite extensive screening of metal precursors, ligands, bases, solvents, and phase-transfer additives, the alkene substrate remained unreactive under all tested conditions. While no hydroxylation products were detected, these results highlighted the inherent difficulty of promoting efficient HO• generation through visible light LMCT excitation in titanium complexes. Consequently, this

prompted us to reconsider our approach to oxygen-centred radical formation and explore the use of alternative radical species capable of mimicking hydroxyl radical reactivity, as discussed in the following section.

3.4. Hypothesis for anti-Markovnikov hydroxylation via hydroxyl radical surrogate

As all efforts to produce HO• in situ and exploit its reactivity proved futile, we sought to generate an alternative oxygen-centred radical capable of emulating the reactivity of HO•. Inspired by recent reports on the anti-Markovnikov hydrooxygenation of unactivate olefins,[176-179] we postulated that tethering the oxygen radical to a cleavable leaving-group (LG) handle could deliver comparable reactivity under much milder conditions (Scheme 3.15). The resulting radical intermediate (**126**) could undergo quenching via a HAT step, followed by LG cleavage to unveil the corresponding alcohol functionality.

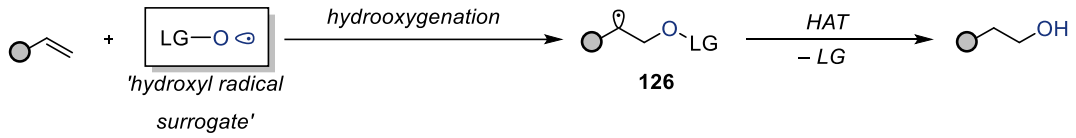

Scheme 3.15. Proposed addition of hydroxyl radical surrogate into alkene, followed by HAT and functional handle cleavage.

A recent study by Deng et al. serves as proof of concept for the hydroxyl radical surrogate (Scheme 3.16).[180] In this work, the authors achieved the anti-Markonikov hydroxylation of alkenes using pyridine N-oxides as the source of oxygen radicals, however the resulting alcohols underwent chain extension. The reaction proceeds with the one electron oxidation of **127** to electrophilic radical **127-I** which can undergo a polarity-matched radical addition to an electron rich olefin. The resulting intermediate (**127-II**) can be trapped with an electron deficient olefin in a Giese-type reaction leading to intermediate **127-III**. Rapid SET with the reduced photocatalyst results in anion **127-IV** which be protonated by the trifluoroacetic acid forming the acetate salt **127-V**. In the final step, nucleophilic attack of water kicks out the alcohol product (**128**) and regenerates the starting N-oxide catalyst (**127**).

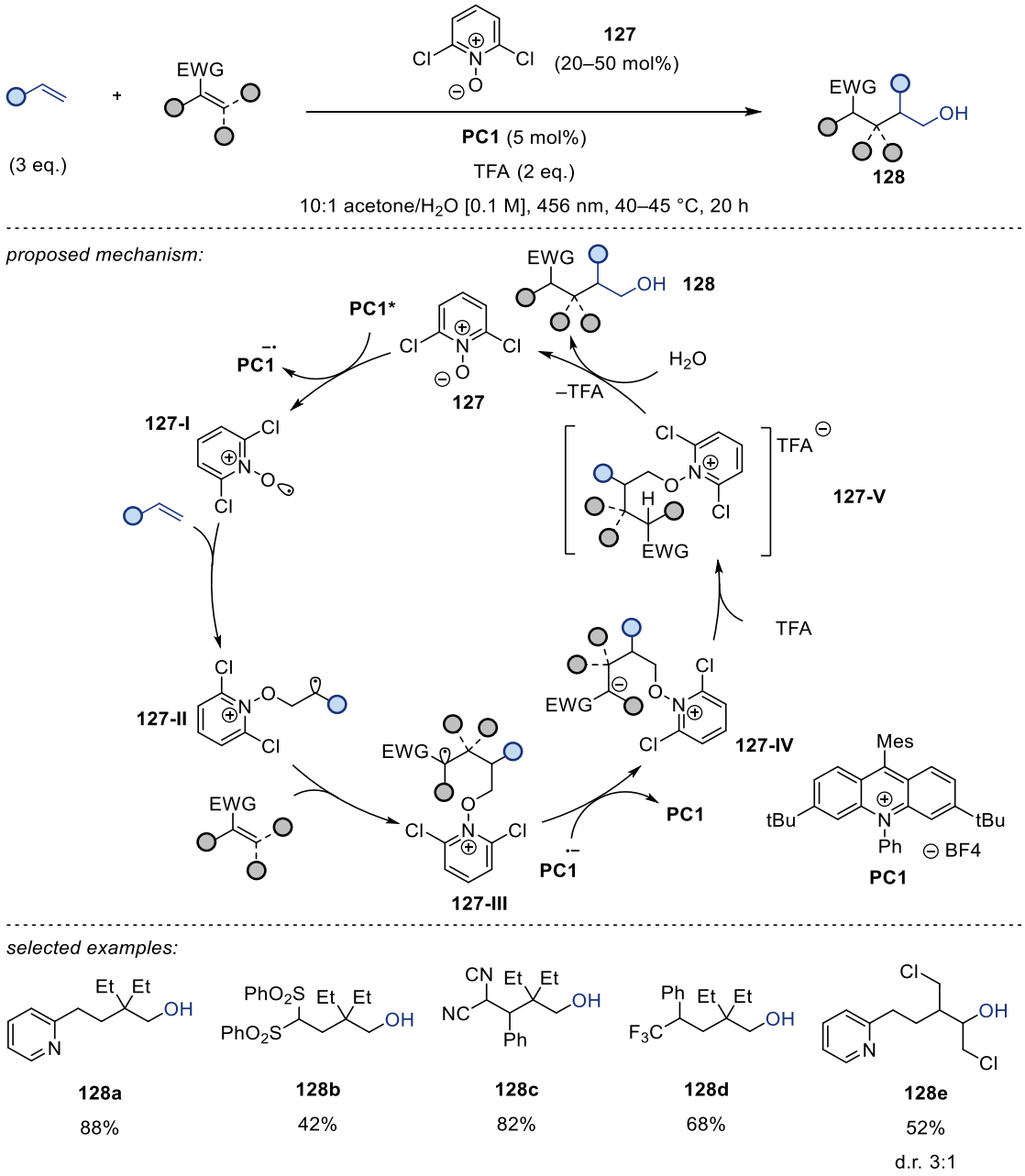

Scheme 3.16. Anti-markovnikov carbohydroxylation of olefins under pyridine N-oxide/photoredox catalysis.

The downside of this reaction is the necessary chain extension with an electron deficient alkene (**128a-e**). The electrophilic radical **127-I** prefers to react with the electron rich alkene however the resulting carbon radical is not a sufficient oxidant for the reduced photocatalyst. To ensure catalytic turnover of the photocatalyst, a more oxidative carbon-centred radical is generated in **127-IV**. We believe that it is possible to involve a third catalytic manifold in this transformation to stop the reaction at **127-II** and thus generate the short chain anti-Markovnikov alcohol.

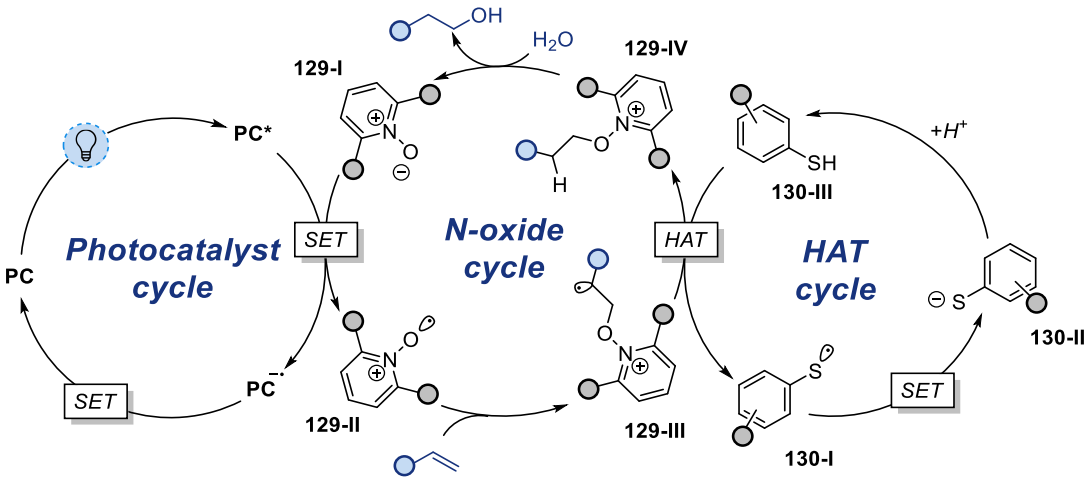

Scheme 3.17. Proposed triple catalytic mechanism for the anti-Markovnikov hydroxylation of olefins.

Our proposed hypothesis, involving three interconnected catalytic manifolds, is illustrated in Scheme 3.17. The reaction is initiated by oxidation of pyridine N-oxide **129-I** by the excited state of a photocatalyst (**PC***) generating the N-oxy radical (**129-II**) and the reduced photocatalyst (**PC**$^{\bullet-}$). **129-II** serves as a surrogate for the hydroxyl radical and undergoes Kharasch-type addition into an olefin leading to intermediate **129-III**. Incorporation of a HAT catalyst at this stage enables quenching of the carbon-centred radical, furnishing the 1,2-hydrated product (**129-IV**) without extending the carbon chain. Subsequent nucleophilic attack of water closes the N-oxide catalytic cycle, affording the terminal alcohol. Concurrently, a complementary SET between the thiyl radical **130-I**, formed in the HAT step, and the reduced photocatalyst (**PC**$^{\bullet-}$) regenerates both the ground-state photocatalyst (**PC**) and the thiolate species (**130-II**), which upon protonation reforms the active thiol HAT catalyst (**130-III**). Thus, the process operates catalytically in all three cycles: photo-, HAT-, and N-oxide-mediated hydroxylation.

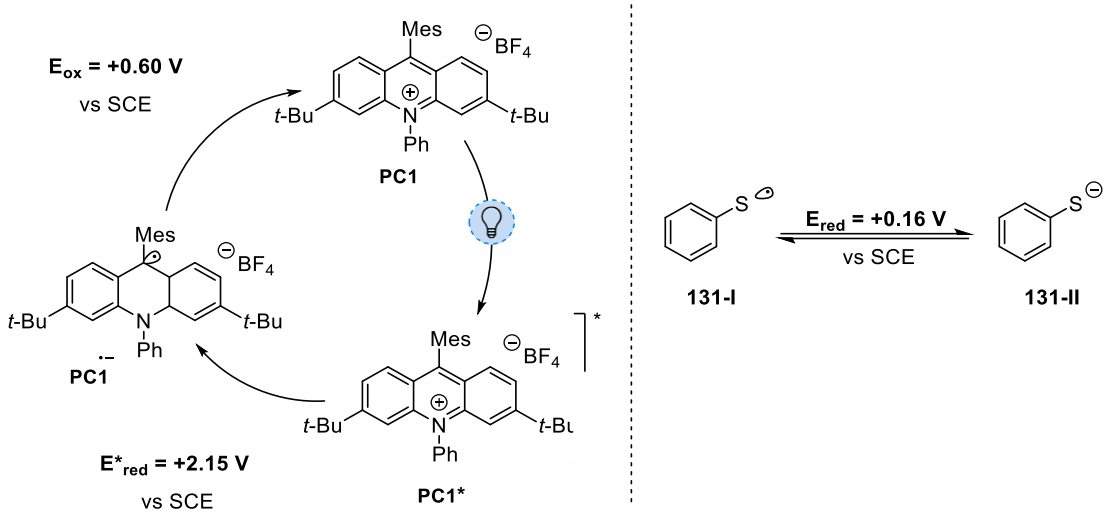

Scheme 3.18. Oxidation potential alignment between acridinium photocatalyst and thiphenol HAT catalyst.

To ensure efficient catalytic turnover, we sought to exploit the redox complementarity of the acridinium/thiolate pair (Scheme 3.18). The excited-state acridinium catalyst **PC1*** is a potent photooxidant (E^*_{red} = +2.15 V vs SCE),[181] capable of oxidising pyridine N-oxide (E_{ox} = +1.84 V vs SCE).[182] Meanwhile, the reduced form, **PC1**$^{\bullet-}$ (E_{ox} = +0.60 V vs SCE)[181] can be readily reoxidised by the thyil radical **131-I** (E_{red} = +0.16 V vs SCE).[183] Such a redox interplay between the excited acridinium and the thiolate system has been previously demonstrated in related hydrofunctionalisation reactions.[160]

3.5. Results and discussion on hydroxylation via hydroxyl radical surrogate

At the onset of our investigation, a variety of photocatalysts were synthesized. The library was comprised of **Acr$^+$-Mes BF$_4$**, **4CzIPN** and **PC2** that were synthesized following literature procedures (see Appendix to Chapter 4) whereas 9-phenyl acridine (**9-Ph-Acr**), 2,3-dichloro-5,6-dicyano-p-benzoquinone (**DDQ**) and 2,4,6-triphenylpyrylium tetrafluoroborate (**TPPT**) were commercially available (Scheme 3.19).

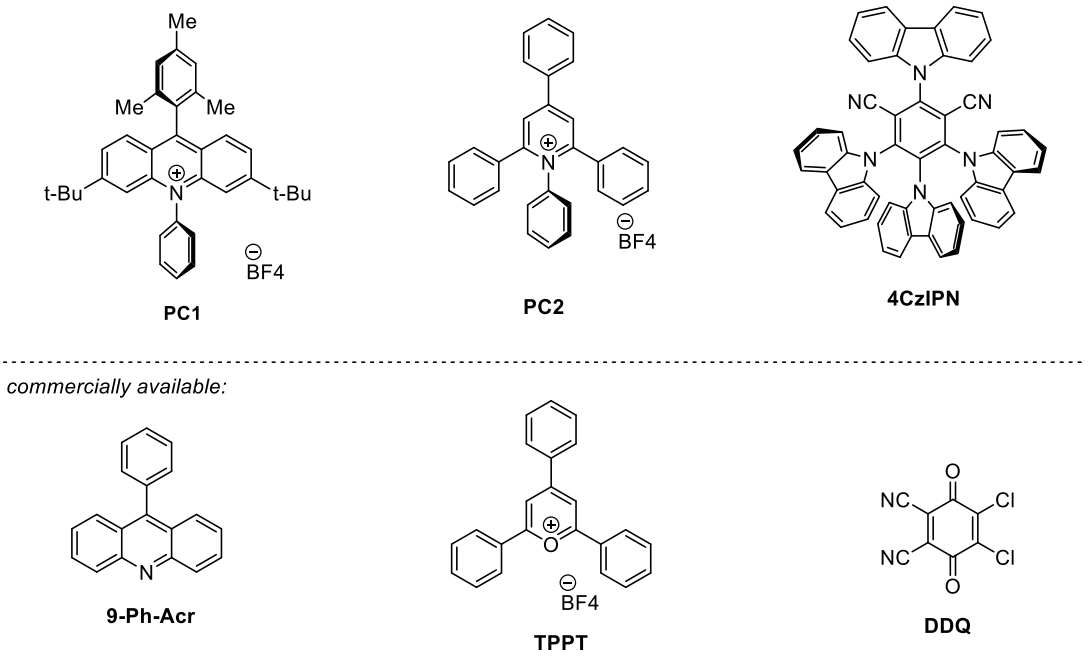

Scheme 3.19. Photocatalysts library.

In accord with our hypothesis, reacting methyl undecanoate **132** in the presence of pyridine N-oxide **127**, **PC1** and phenyl disulfide the hydroxylation product was detected in 8% NMR yield (Table 3.12, entry 1). **132** was selected as optimal substrate to avoid side oxidation with the photocatalyst. Alongside the hydroxylation product **133a**, a side product of chlorination (**133b**) was detected (mechanism of formation is discussed below). Changing the photocatalyst to 9-Ph-Acr only resulted in trace amounts of product **133a**, with 7% of **133b** (entry 2). Other catalysts did not afford any reactivity and the starting material remained untouched (entries 3–6).

Table 3.12. Evaluation of photocatalysts in the N-oxide hydroxylation

Entry	HAT catalyst	Outcome*	
		133a	133b
1	**PC1**	8%	21%
2	**9-Ph-Acr**	Traces	7%
3	**PC2**	–	–
4	**DDQ**	–	–
5	**4CzIPN**	–	–
6	**TPPt**	–	–

* Determined via ^{1}H NMR using 1,1,2,2-tetrachloroethane as internal standard.

Both **133a** and **133b** were prepared via known procedures to confirm their presence in the crude NMR analysis (Scheme 3.20). The α-proton of **133a** displayed a characteristic triplet at 3.63 ppm whereas the same environment appeared for **133b** at 3.52 ppm. Thus, we were able to quantify the amount of each species by integrating with respect to an internal standard.

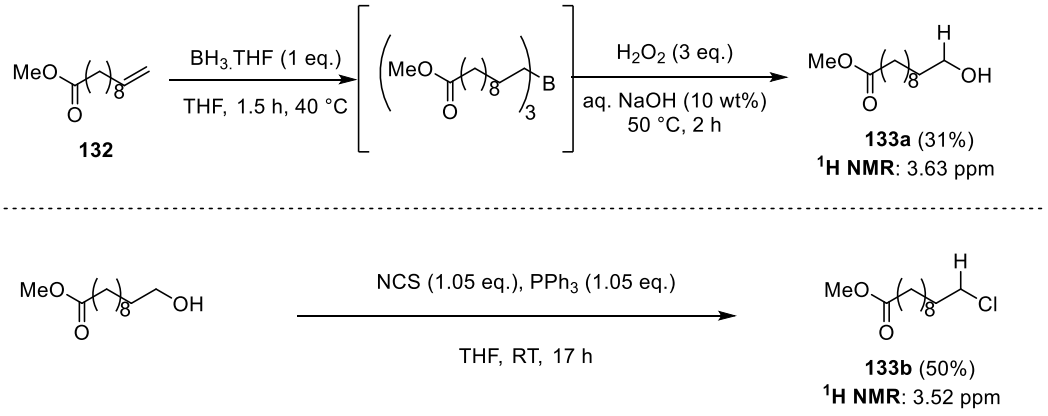

Scheme 3.20. Synthesis of **133a** and **133b**.

From the cosolvents screen in this reaction (Table 3.13), the optimal choice was acetonitrile (entry 1), with acetone and ethyl acetate giving only traces of product

(entries 2 and 3), while DCM afforded only the product of chlorination in 17% NMR yield (entry 4).

Table 3.13. Screen of cosolvents in the N-oxide hydroxylation.

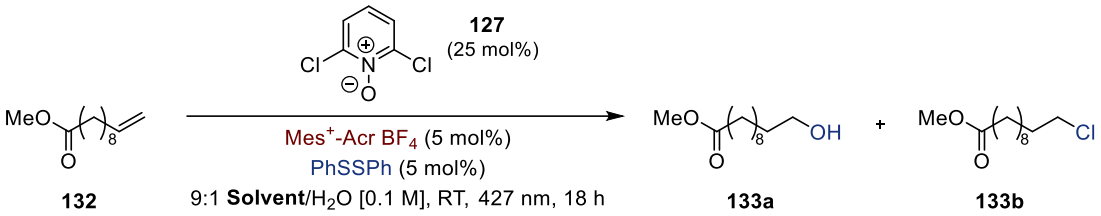

Entry	Cosolvent	Outcome*	
		133a	133b
1	MeCN	8%	21%
2	Acetone	Traces	Traces
3	EtOAc	Traces	Traces
4	DCM	–	17%

* Determined via ^{1}H NMR using 1,1,2,2-tetrachloroethane as internal standard.

As part of the optimisation study, a variety of electron rich and deficient pyridine N-oxide catalysts were prepared (Scheme 3.21). Details of the synthesis of N-oxides **127**, **134–142** can be found in the Appendix section. Catalysts **143–145** were commercially available.

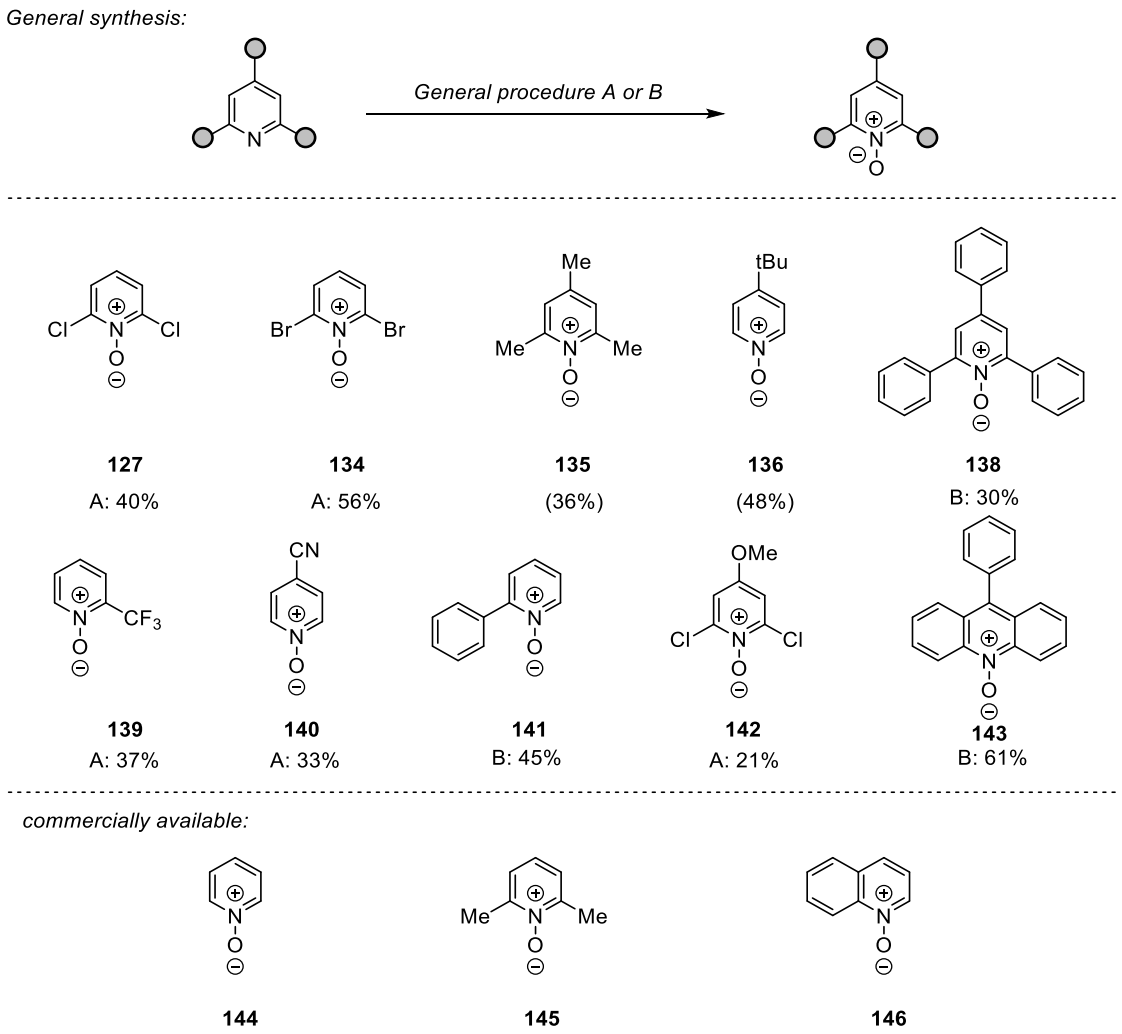

Scheme 3.21. Pyridine N-oxide synthesis.

To probe the effects of electronics and sterics on the reaction selectivity, the neutral and electron rich N-oxides were initially screened (Table 3.14). Non-substituted pyridine N-oxide **144** did not afford any product (entry 1), whereas in the reaction with 2,6-disubstituted **145** and **135** traces of hydroxylation product could be detected (entry 2 and 3). More sterically hindered and electron rich catalysts did not exhibit any reactivity towards the desired product, however deoxygenation at nitrogen was observed (entries 4–8).

Table 3.14. Screening of neutral and electron rich N-oxide catalysts

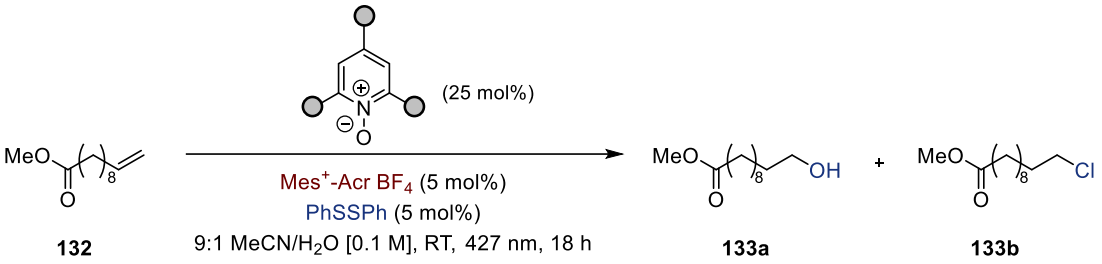

Entry	N-oxide catalyst	Outcome*	
		133a	133b
1	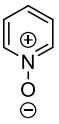 **144**	–	–
2	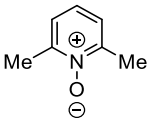 **145**	6%	–
3	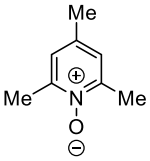 **135**	Traces	–
4	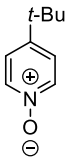 **136**	–	–
5	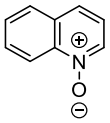 **146**	–	–
6	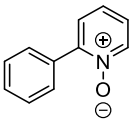 **141**	–	–
7	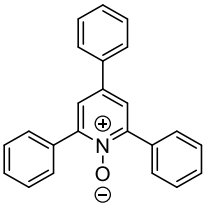 **138**	–	–

8	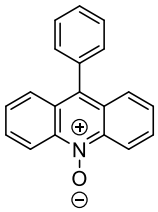	**143**	–	–

* Determined via ^{1}H NMR using 1,1,2,2-tetrachloroethane as internal standard.

On the other hand, electron deficient N-oxides were investigated (Table 3.15). Catalyst **139** remained unreactive in this transformation (entry 1), whereas **140** showed products of decomposition with no hydroxylation product formed (entry 2). Dichloro N-oxide **127** showed by far the highest yield (8%), however significant amount of side product of chlorination was also observed (entry 3). Installing an electron donating group in the para position in **142** hindered reactivity (entry 4), whereas dibromo N-oxide **134** only gave traces of product and underwent some deoxygenation (entry 5).

Table 3.15. Screening of electron deficient N-oxide catalysts

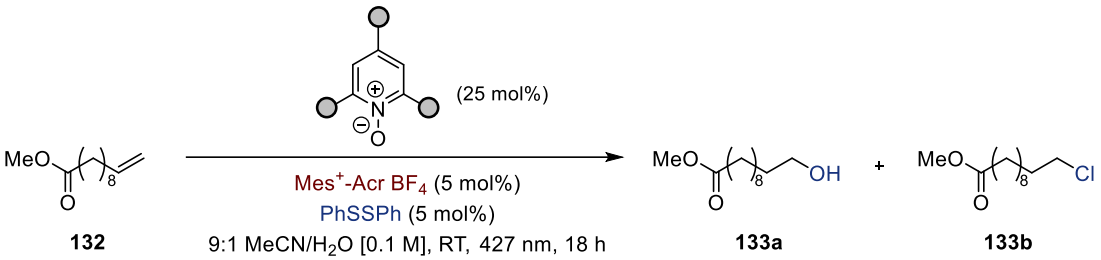

Entry	N-oxide catalyst	Outcome* 133a	Outcome* 133b
1	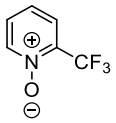 **139**	–	–
2	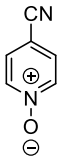 **140**	–	–
3	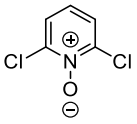 **127**	8%	21%
4	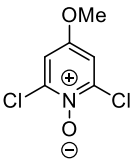 **142**	–	–

5	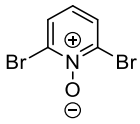 **134**	Traces	–

* Determined via ^{1}H NMR using 1,1,2,2-tetrachloroethane as internal standard.

Subsequently, the loading of the N-oxide catalyst was varied (Table 3.16). Lower loading was detrimental to overall reactivity since only traces of hydroxylation and chlorination product were detected (entry 1). On the other hand, increasing the amount of 2,6-dichloro N-oxide favored the formation of **133b** with only trace amounts of **133a** being detected (entries 3 and 4).

Table 3.16. Screening of N-oxide catalyst loading

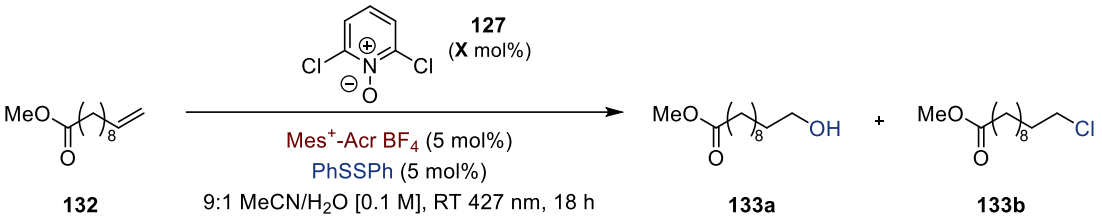

Entry	N-oxide loading (mol%)	Outcome*	
		133a	133b
1	12.5	Traces	4%
2	25	8%	21%
3	50	Traces	30%
4	100	Traces	40%

* Determined via ^{1}H NMR using 1,1,2,2-tetrachloroethane as internal standard.

Finally, the effect of the HAT catalyst was probed (Table 3.17). Electron withdrawing group in the para position of **148** seemed to increase conversion to both products (entry 2), while electron rich catalyst **149** favoured the formation of chlorinated adduct **133b** (entry 3). 2-aminophenyl disulfide **150** seemed to decrease conversion to chlorinated product **133b** while retaining similar yields for the hydroxylation product (entry 4). Ester or amide substituents in **151** and **152** respectively, afforded only **133b**, with traces of **133a** detected in the crude NMR (entries 5 and 6). Malonitrile **153** did not give any product, and the starting material was fully recovered (entry 7).

Table 3.17. HAT catalyst screen in the N-oxide hydroxylation

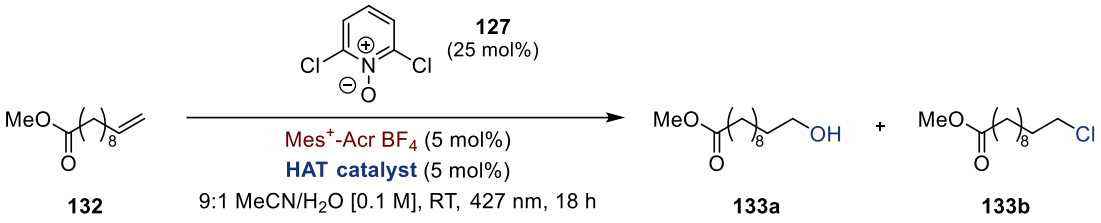

Entry	HAT catalyst	Outcome*	
		133a	133b
1	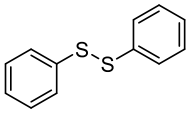 **147**	8%	21%
2	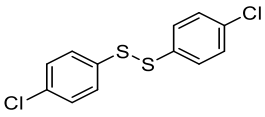 **148**	16%	27%
3	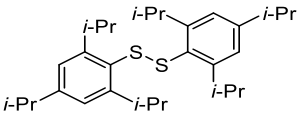 **149**	4%	28%
4	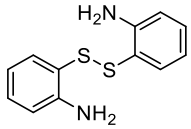 **150**	8%	8%
5	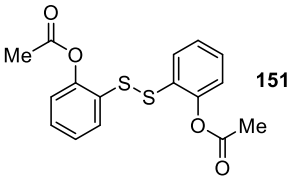 **151**	Traces	8%
6	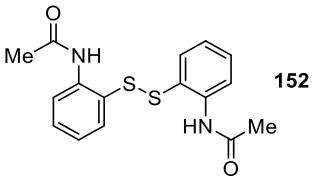 **152**	Traces	15%
7	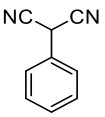 **153**	NR	NR

* Determined via ^{1}H NMR using 1,1,2,2-tetrachloroethane as internal standard.

HAT catalysts **151**–**153** were synthesized following literature procedures (see Appendix) whereas **147**–**150** were commercially available. At this stage, no clear effect of the HAT catalyst can be established since any observable increase in product yield fall within the 5–10% margin error of integration of crude NMR. Since no other

improvements were observed throughout the optimisation of other reaction components, the study was discontinued.

The results of the N-oxide electronics and loading investigations (vide supra Table 3.15 and Table 3.16) indicated that the product of chlorination **133b** is only observed in the presence of the chlorinated pyridine N-oxide **127**. This could be due to the presence of chloride anions in the reaction, that have been previously shown to be oxidizable in the presence of acridinium photocatalysts.[184] Thus, the following mechanism can be proposed (Scheme 3.22). Acridinium **PC1** undergoes anion exchange with chloride anions to give complex **PC1-Cl**. Upon photoexcitation, the excited state **PC1-Cl*** undergoes outer sphere electron transfer to generate acridinyl radical **PC**$^{\bullet-}$ and chloride radical that can undergo radical addition into alkene **132**. Subsequently, the HAT catalyst (**PhSH**) quenches the carbon radical to yield the chlorinated product **133b**, and the resulting thyil radical (**PhS**$\bullet$) can reoxidise **PC**$^{\bullet-}$ back to the starting position. The presence of chloride anions is most likely due to elimination from N-oxide **127** that could be as a result of decomposition or nucleophilic aromatic substitution.

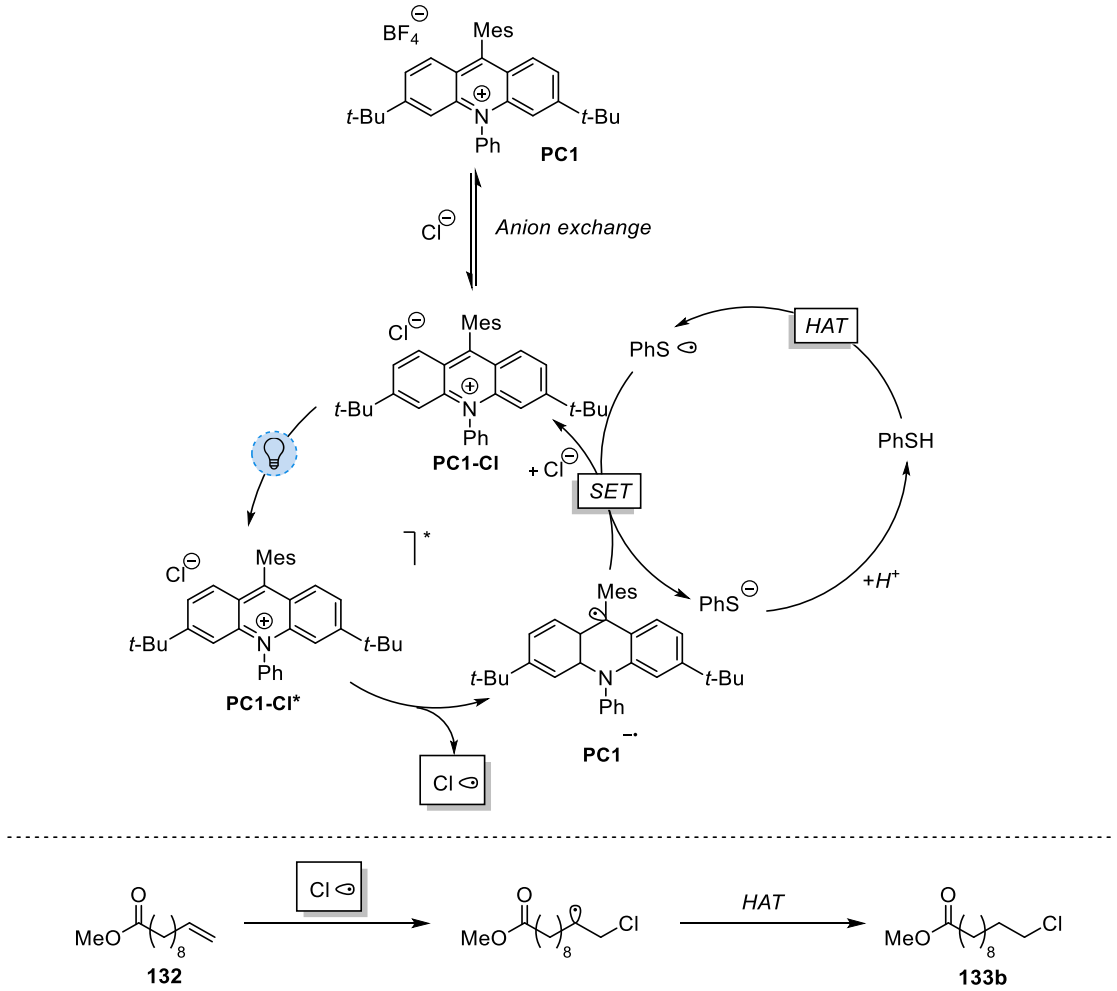

Scheme 3.22. Proposed mechanism for the formation of hydrochlorinated product **133b.**

Further investigation into this reaction could increase the yield of the alcohol product. In particular, rational design of the N-oxide catalyst might improve the selectivity towards hydroxylation while avoiding side product formation. One appealing target is 2,6-difluoropyridine N-oxide (**154**), however given the poor nucleophilicity of the parent pyridine, we were unable to generate it.

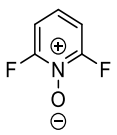

154

Scheme 3.23. N-oxide **154** as a potential target for future investigations.

3.6. Conclusion

The production of anti-Markovnikov alcohols from terminal olefins is an attractive yet challenging synthetic transformation. While most established strategies rely on two-step substrate preactivation, the single step anti-Markovnikov hydroxylation of alkenes is ineffective for primary and electron-deficient olefins. The aim of this project was to develop novel strategies to overcome this limitation.

In the first part of the study, the visible-light generation of hydroxyl radicals was explored as a means to achieve direct radical addition into olefins. Specifically, we investigated the potential for LMCT activation of metal hydroxides to generate HO• species. A range of metal catalysts were screened, with particular focus on group 4 and first-row transition metals. Titanium(IV) emerged as the most promising candidate and was examined under various ligand, solvent, base, and phase-transfer conditions. However, across all experiments, no hydroxylation product was detected, and the model substrate remained unreacted.

The second part of the project focused on developing a suitable hydroxyl radical surrogate capable of promoting the desired anti-Markovnikov hydroxylation. Pyridine N-oxides were identified as promising candidates, and their implementation within a triple catalytic system yielded encouraging preliminary results. Nonetheless, reaction optimisation revealed that the hydroxylation pathway was not dominant, with a competing chlorination process prevailing under the tested conditions.

Overall, this study provides initial evidence for the feasibility of single-step anti-Markovnikov hydration of terminal olefins. Although the current system suffers from poor selectivity, the findings highlight the potential of pyridine N-oxides as capable of inducing hydroxylation. Future work focused on catalyst design and mechanistic understanding may ultimately enable selective and efficient hydroxylation, addressing this long-standing challenge in synthetic chemistry.

CHAPTER 4

Generation and Reactivity of Hydrogen Radical

4.1. Introduction

4.1.1. The discovery of hydrogen

Hydrogen (H), the most prevalent element in the universe, constitutes approximately 75% of the mass of ordinary (non-dark) matter.[185] Under standard conditions, it exists as a diatomic molecule (H_2), forming a colourless, odourless, and highly flammable gas. Due to its low molecular weight, H_2 readily escapes Earth's gravitational pull, resulting in its low atmospheric concentration of about 1 part per million by volume.[186] Despite this, hydrogen is abundantly found in nature, often in combination with other elements such as carbon in hydrocarbons and oxygen in water (H_2O).

The discovery of hydrogen as a distinct chemical element is attributed to Henry Cavendish, who successfully isolated it in 1766 during experiments involving the reaction of various metals with acids.[187] While this process was well known by that time – dating back to at least the early 16th century – it had not previously been associated with the generation of a unique gaseous substance. The earliest documented instance of the metal–acid reaction was reported by Paracelsus (circa 1520s)[188] and subsequently investigated by Jan Baptist van Helmont, who introduced the term ‘gas’ and noted that the evolved gas was highly flammable in air, yet incapable of sustaining combustion on its own. Further observations were made by Robert Boyle in 1671, who described the formation of gas bubbles from the reaction of steel filings with oil-of-vitriol (archaic for sulfuric acid).[189] Despite these early contributions, it took nearly a century for the scientific community to recognize hydrogen (H_2) as a discrete entity. Cavendish referred to the substance as “inflammable air,” and demonstrated that its combustion in the presence of atmospheric oxygen resulted in the formation of water—a key observation that later contributed to the overthrow of phlogiston theory.[190] The gas was formally named hydrogène by Antoine Lavoisier in 1783, from the Greek hydro (water) and genes (creator), in recognition of its role in the synthesis of water.

Following Lavoisier’s redefinition of hydrogen as an element, its fundamental properties became a subject of intensive study throughout the 19th and 20th centuries. The hydrogen atom—being the simplest atomic system—was central to the development of atomic theory. In 1913, Niels Bohr introduced a model describing hydrogen’s electron in quantized orbits,[191] building on earlier work by Rutherford[192] and Planck,[193] and laying the foundation for quantum mechanics. This model was further refined by Schrödinger’s wave mechanics[194] and Heisenberg’s matrix mechanics,[195]

using hydrogen as a key benchmark system. These developments provided the theoretical basis for understanding hydrogen's electronic structure and chemical behaviour.

In parallel to physics, the reactivity of hydrogen was of great interest to synthetic chemists. Given its electronic configuration ($1s^1$), hydrogen can adopt three different oxidation states that span from +1 (proton), through 0 (elemental), to -1 (hydride). In the +1 oxidation state, hydrogen exists as a proton (H^+) that can react with nucleophiles – an observation that laid the foundations of the Brønsted–Lowry acid–base theory in 1923.[196, 197] On the other hand, hydride (-1 oxidation state) is a strong base and powerful reducing reagent, which is most often bound to other elements,[198] with very few examples reported on a 'naked' H^-.[199, 200]

4.1.2. Reactivity of molecular hydrogen

The zeroth oxidation state of hydrogen is most encountered in the diatomic molecule (H_2), which is very stable and chemically inert. This is due to the high bond dissociation energy (104 kcal/mol) also evident from its short bond length of 74 pm.[201] Due to the proximity of the two hydrogen atoms, homolytic cleavage of the bond (eq. 1) is more thermodynamically feasible over heterolytic cleavage (400 kcal/mol) (eq. 2).[202] Therefore, activation of the hydrogen molecule typically requires either harsh conditions (high pressure and temperature) or metal catalysis.

$$H_2(g) \rightarrow H^0(g) + H^0(g) \quad \Delta_r H^{\ominus} = +104 \text{ kcal/mol} \qquad (1)$$

$$H_2(g) \rightarrow H^+(g) + H^-(g) \quad \Delta_r H^{\ominus} = +400 \text{ kcal/mol} \qquad (2)$$

Given these challenges in hydrogen activation, the development of metal-catalysed hydrogenation processes represented a transformative advance in both synthetic and industrial chemistry.[203] A foundational breakthrough was achieved by Paul Sabatier in the late 19th century, who significantly advanced the field of catalytic hydrogenation (Scheme 4.1, A). Building upon earlier observations by James Boyce,[204] Sabatier demonstrated that the use of catalytic quantities of nickel markedly enhanced the addition of hydrogen to unsaturated organic compounds via a heterogeneous reaction pathway.[205] Shortly thereafter, Fritz Haber demonstrated that atmospheric nitrogen (N_2) could be catalytically reduced to ammonia (NH_3) under high temperatures and pressures in the presence of an iron catalyst (Scheme 4.1, B).[206] This reaction was subsequently scaled to industrial levels by Carl Bosch, giving rise to the Haber–Bosch

process, which profoundly transformed the agricultural industry by enabling large-scale synthetic fertiliser production. Hydrogen has also found applications in the refining industry for pure metal production from ores or high-value hydrocarbons from crude oil and biomass (Scheme 4.1, C).[203, 207] Another invaluable utilisation of hydrogen is in the Fischer-Tropsch synthesis, where a highly pressurised gaseous mixture of H_2 and carbon monoxide (CO) undergoes multiple transformations in the presence of metal catalysts to yield industrially useful liquid organic molecules (Scheme 4.1, D).[208, 209]

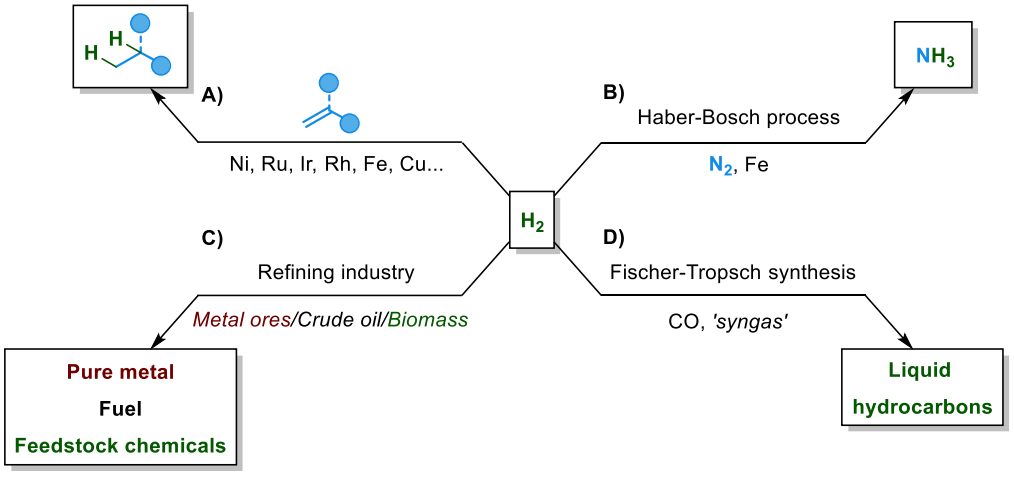

Scheme 4.1. Applications of molecular hydrogen in heterogeneous catalysis.

These seminal discoveries laid the groundwork for subsequent developments in homogeneous catalysis, culminating in the first successful homogeneous hydrogenation[210] reported in 1961 and the isolation of the first well-defined metal hydride complex by Vaska in 1962.[211] Further progress came with the development of Wilkinson's catalyst in 1965, a rhodium complex capable of catalysing the hydrogenation of unactivated olefins under mild conditions.[212] The first asymmetric rhodium-catalysed hydrogenations were later introduced by William Knowles in 1968,[213] marking the beginning of enantioselective hydrogenation and opening new possibilities for asymmetric synthesis. Other pioneers in this filed, Robert H. Crabtree and Ryōji Noyori, subsequently developed their infamous catalysts based on iridium and ruthenium respectively.[214, 215] Recent advancements in hydrogenation methodologies have facilitated the use of earth-abundant metals such as iron[216] and copper[217] for olefin saturation. Concurrently, hydrogenation techniques have been successfully extended to a wide array of functional groups, including alkynes,[218] carbonyls,[219] and imines, among others.[220]

4.1.3. Generation of hydrogen atoms

The generation of atomic hydrogen (H•) from its molecular form, can be accomplished by direct homolysis of the strong H–H bond (BDE 104 kcal/mol).[26] Indeed, the first person to observe that was Irving Lagmuir who in the beginning of the 20th century managed to fortuitously break the hydrogen molecule. In his study,[221] he observed that the heat conductivity of a tungsten wire in a hydrogen atmosphere increased dramatically upon heating above 2100 °K. This effect was attributed to the thermal dissociation of molecular hydrogen on the surface of the hot wire, resulting in the formation of atomic hydrogen. The atomic species subsequently diffused from the surface and recombined, releasing energy as heat, thereby contributing to the observed enhancement in thermal conductivity. Another thermal approach was the use of shock waves to obtain the rate of hydrogen dissociation in a temperature range of 3000 to 4500 °K.[222]

4.1.3 a From molecular hydrogen

Since Langmuir's initial observation, many methods have been developed to produce H• from molecular hydrogen. In 1920, during the study of the Balmer series of hydrogen,[223] Robert Wood applied an electric glow discharge current inside a tube filled with hydrogen gas at a potential of 25 000 V. Activation of H_2 can also be achieved when the molecule is bombarded with electrons in a Faraday cup.[224, 225] These experiments were conducted at much lower ionisation potentials (16–18 V), and instead of homolysis or reduction of the molecule, the formation of dihydrogen cation (H_2^+) was observed.[226] The oxidised species can either decompose to form the hydrogen atom (eq. 3) or collide with another H_2 molecule resulting in a trihydrogen cation (H_3^+) and H• (eq. 4).

$$H_2^+(g) \rightarrow H^+(g) + H^0(g) \quad (3)$$

$$H_2^+(g) + H_2(g) \rightarrow H_3^+(g) + H^0(g) \quad (4)$$

Another approach to break the H–H bond is via photoexcitation. The minimum absorption wavelength of hydrogen that can lead to homolysis is not at the BDE of ~436 kJ/mol (~275 nm), but rather in the Lyman–Werner bands (~91–110 nm), where the molecule undergoes dipole-allowed electronic transitions.[227] However, such activation is not fully efficient: only about 10–15% of absorptions result in dissociation, as most excited molecules return to the ground state via fluorescence (the Solomon process) or non-dissociative decay pathways.[228] Moving towards more ionising

irradiation, soft X-rays in the 100–1000 eV region can induce photoionisation of hydrogen to H_2^+ followed by fragmentation similar to the electron-bombardment experiments (vide supra eq. 3).[229] On the other side of the visible spectrum, non-ionising irradiation can also be employed in the form of a radiofrequency[230] or microwave (MW) discharge.[231, 232] Although, the former has been found to give good dissociation efficiency (50–60%), a MW pulse can be easily implemented in a gas injection setup with improved efficiencies of H• generation (60–80%).[233]

To achieve a milder set of conditions for hydrogen atom production, a metal catalyst can be employed. In particular, the mercury-photosensitized decomposition of hydrogen offers by far the mildest procedure for direct H_2 activation. Pioneered by Franck and Cario[234] in 1922 and later developed by Crabtree,[235] it involves the saturation of a mercury drop with hydrogen gas, which is then irradiated with a 254 nm lamp. In the presence of an organic substrate as the limiting reagent, products of hydrogen atom reactivity were obtained in moderate to excellent yields (vide infra Section 4.1.5.).

4.1.3 b From inorganic and organic molecules

Beyond molecular hydrogen, H• can be generated from other hydrogen-rich inorganic and organic molecules. Among these, H_2O represents perhaps the most abundant and ubiquitous source, although it has a significantly high BDE (118 kcal/mol)[26] thus requires even harsher activation conditions than the hydrogen molecule. Indeed, techniques based on radiolysis,[236, 237] electron field induction,[238] sonication[239] and UV-light irradiation[240] have been demonstrated to generate atomic hydrogen, but due to the extreme nature of the conditions, very little synthetic utility has been reported.

Similarly, other molecules can be directly activated to evoke the homolysis of a H–X bond. From the inorganic acids, HCl,[241] HBr,[242] HI,[243] H_2S,[244] are known to undergo photodecomposition to atomic hydrogen under strong UV light irradiation (185–254 nm).

In addition to the inorganic precursors mentioned above, a variety of organic molecules can also serve as sources of hydrogen radicals. For instance, in the γ-radiolysis of hydrocarbons, the induced C–H bond homolysis led to generation of hydrogen gas,[245] or products of reaction with a hydrogen radical.[246] Cvetanovic and Jennings observed the formation of H• during the mercury-photosensitized decomposition of

hydrocarbons[247] and fluorohydrocarbons.[248, 249] Similarly, direct photolysis of organic molecules provides another efficient source: formaldehyde (HCHO) readily undergoes photodecomposition to yield H• alongside CO,[250] while thiols are known to undergo S–H bond cleavage under UV excitation (254–275 nm).[251, 252] In addition, certain organic peroxides such as tert-butyl peroxyformate can fragment upon irradiation (300 nm), releasing hydrogen atoms as part of its radical decomposition cascades.[253] Benzylic compounds may produce H• through homolytic C–H cleavage (at 295–320 nm iradiation) facilitated by the relative stability of the benzylic radical intermediate.[254]

4.1.4. Fundamental properties of the hydrogen radical

Given the open shell configuration of the hydrogen atom ($1s^1$), it has a fleeting nature with lifetime of ca. 1 microsecond in solution.[255] Nonetheless, in the radiolysis of water, some of its properties have been recorded such as its pK_a of 9.6 and high reduction potential of –2.31 V vs SHE.[256, 257]

Under current spectroscopic techniques it is impossible to detect directly and often its products are observed. Thus, many studies have focused on measuring the rates of reaction of H• with different solutes.[245, 246, 258-266] A detailed account of the currently known reactivity of hydrogen atom is given in the following section.

4.1.5. Chemical reactivity of the hydrogen radical

Radical polarity has emerged as a valuable framework for predicting the selectivity of radical transformations.[267] In a recent study, Nagib and co-workers systematically calculated the global electrophilicities (ω) of over 550 radical intermediates, using the hydrogen atom radical as a reference point.[268] While the authors did not explicitly classify its intrinsic polarity, the data suggest that H• occupies a midpoint on the polarity scale – exhibiting neither strong nucleophilic nor electrophilic tendencies. Compared to most well-characterized radicals, hydrogen radical is slightly electrophilic, however it exhibits reactivity typical of both electrophilic and nucleophilic species (Scheme 4.2).

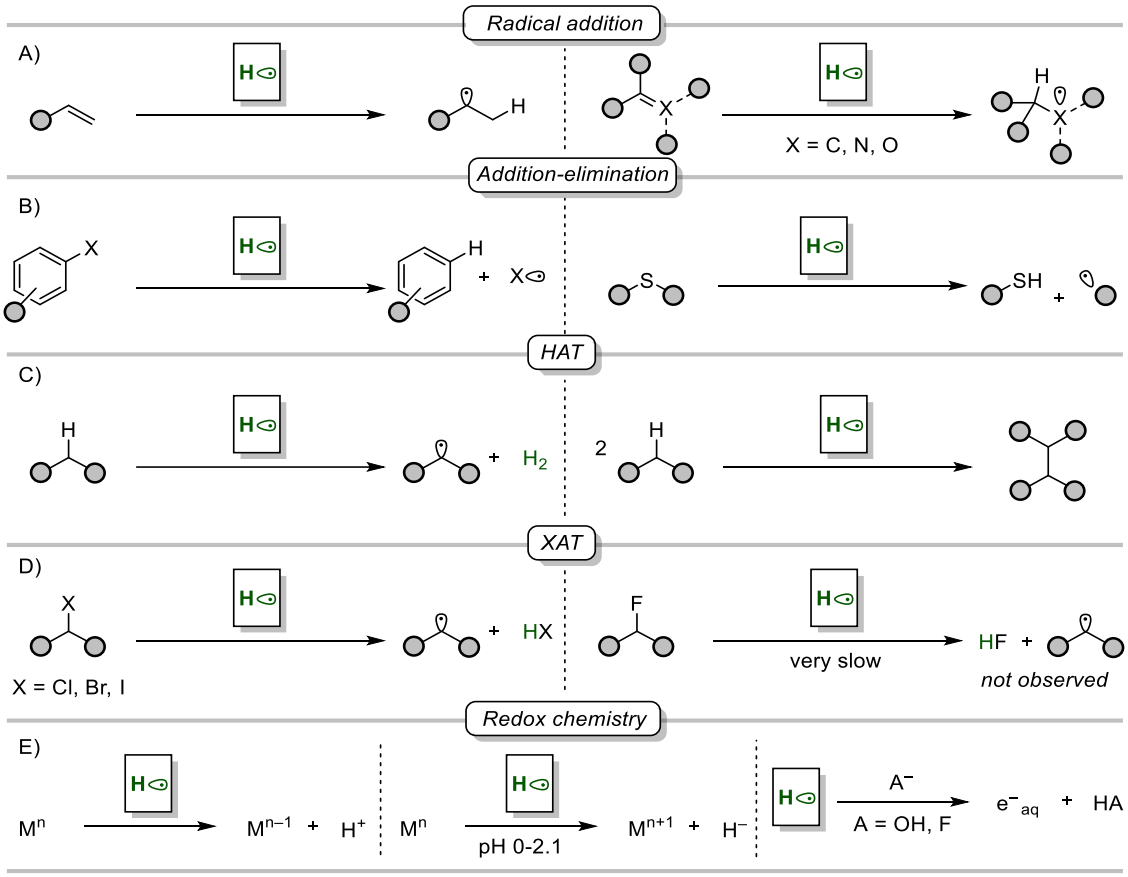

Scheme 4.2. The solution state reactivity of hydrogen radical with different organic and inorganic species.

The hydrogen radical is capable of radical addition into double bonds (Scheme 4.2, A).[264, 269-272] Like most radicals, H• undergoes anti-Markovnikov Kharasch addition resulting in the more stable carbon-centered radical, which can recombine with another hydrogen atom, disproportionate, add into another alkene or dimerise.[235, 271, 273] The reaction is facile at room temperature with terminal and substituted alkenes[264], but lower conversions are typically observed with alkynes[274] and aromatic compounds.[270] Few examples are reported in literature for the H• addition into C=O[246] and C=N[275] bonds.

In some cases, addition-elimination reactions have been reported (Scheme 4.2, B).[246, 276-278] The hydrogen radical inserts into the aromatic ring resulting in an intermediate cyclohexadienyl radical that can extrude a radical leaving group. This has been observed in coal liquification at elevated temperatures (vide infra Section 4.1.6.)[279, 280] and in the homolytic cleavage of alkyl sulfides.[281]

Perhaps the most observed reactivity of H• is the HAT reaction (Scheme 4.2, C).[237, 245, 282-284] Governed by the thermodynamic driving force of a strong H–H bond formation (BDE = 104 kcal/mol), the selectivity of HAT follows the formation of the most stabilised radical.[235] This inherent property of radicals has been applied in the synthesis of dehydrodimerisation products.[285]

Another intriguing reactivity of the hydrogen radical is its ability to abstract halogen atoms (Scheme 4.2, D). Similarly to tin and silicon centered radicals,[24] XAT with H• is preferential in the order I > Br > Cl in alignment with the strength of the respective carbon-heteroatom bond.[263] In the case of alkyl bromides, H• was simulated to exibit the lowest theromodynamic barrier towards XAT relative to other common abstracting radicals (·$SnMe_3$ and ·$SiMe_3$).[286] Abstraction of the smallest of halogens (fluorine) is an attractive possibility using hydrogen radical, given the stark difference in BDE of the C–F (120 kcal/mol) and H–F bonds (136 kcal/mol).[26] However, it has been estimated that the activation energy for such a reaction is too high to proceed at room temperature,[287] thus any hydrofluoric acid observed in the treatment of fluorohydrocarbons with H• comes from a disproportionation pathway.[248]

Considering its high reduction potential (–2.31 V vs. SHE), the hydrogen radical can be expected to display pronounced redox activity (Scheme 4.2, E). In reactions with metal ions, H• predominantly acts as a reductant, consistent with reported redox data.[259] However, its behaviour appears to be of dual character: in strongly acidic media (pH 0–2.1) H• has been observed to function as an oxidant.[288] Under basic conditions, such as in the presence of hydroxide or fluoride anions, the hydrogen atom can disproportionate to a proton and hydrated electron (e_{aq}^-).[289] These studies highlight the ambivalent redox nature of this species and its dependence on the reaction pH.

4.1.6. Radical hydrogen transfer (RHT)

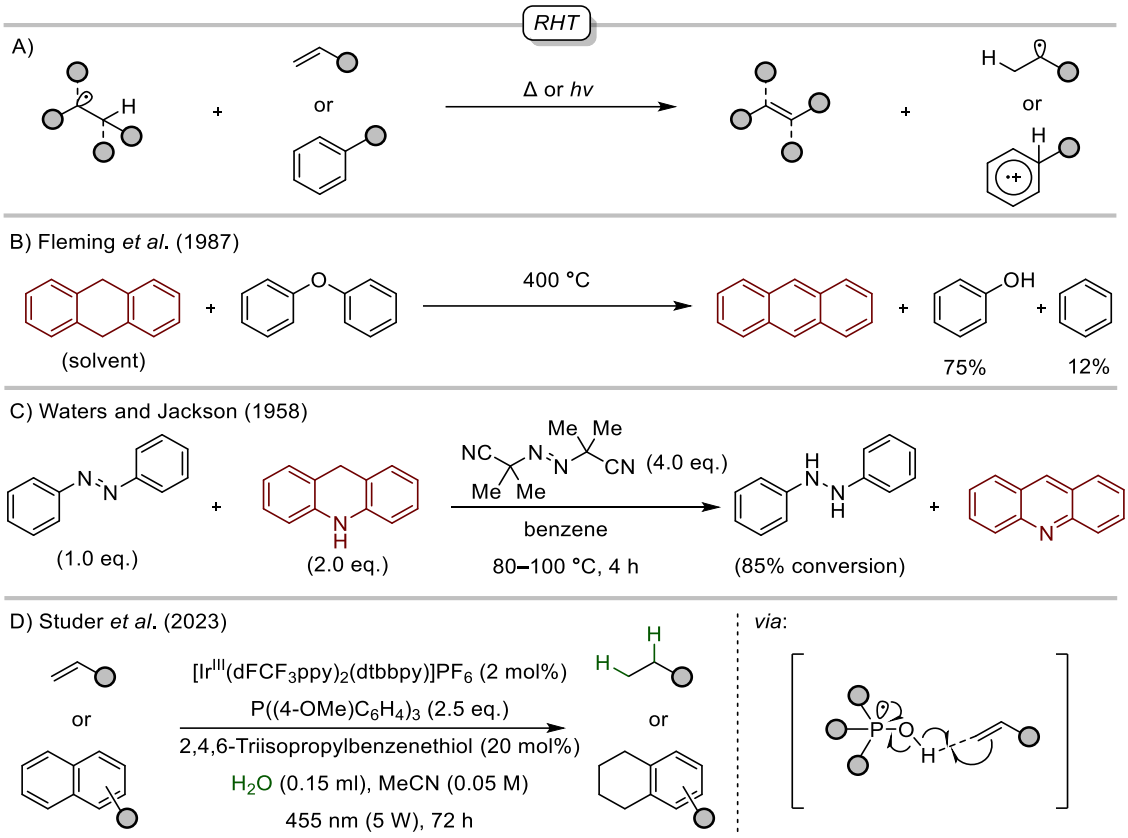

Scheme 4.3. A) General mechanism for radical hydrogen transfer (RHT). B) RHT in donor solvent systems as part of coal liquification processes. C) RHT reduction of diazo compounds exploiting the proaromaticity of acridan. D) Phosphoranyl radical-mediated water activation achieves RHT reduction of olefins and naphtalenes.

The intermediacy of a hydrogen radical has been recognised in coal liquification processes.[280] Fleming et al. studied the decomposition pathways of a variety of aromatic molecules in the presence of a hydrogen donor solvent. The authors recognised that the generation of proaromatic radical intermediates from the solvent was leading to the formal addition of a hydrogen radical to the ipso position of substituted benzenes and that was resulting in the scission of strong C–C and C–O bonds (Scheme 4.3, B).[279] The term radical hydrogen transfer (RHT) was coined to describe the concerted *β*-hydrogen radical elimination and addition into aromatic ring. Metzger recognised the same reactivity between alkyl radicals and olefins,[290] whereas Waters and Jackson observed an aromaticity driven through-N hydrogen atom elimination (Scheme 4.3, C).[291] In a recent study from the Studer group,[292] the reactivity of phosphoranyl radicals towards water activation was exploited for radical hydrogenation (Scheme 4.3, D). Upon oxidation of the intermediate R_3P–OH, a β-

scission occured resulting in a formal transfer of H• into the π-system of alkenes and arenes. The relatively mild conditions of the study allowed for a broad substrate scope exploration, unlike other studies involving RHT.[293]

It is worth concluding that even though the hydrogen atom has been reported to have a broad variety of reactivity, due to the harsh nature of H• generation, very few of these methodologies have been applied in a synthetic setting. Notably, the hydro- and dehydrodimerizations from Crabtree et al.,[273, 285] and radical hydrogenation by Studer et al.[292] are the only studies to date to show application in organic synthesis, though the latter involves a hydrogen radical intermediate and has no evidence towards a 'naked' H atom.

4.2. Hypothesis for H• generation

Thus, we set out to develop a strategy for the generation of a free H• in a synthetically useful setting. To this end, the design was required to meet three key criteria: (i) employ a readily available and atom-economical H• precursor; (ii) enable the desired reactivity under mild and selective conditions; and (iii) rely on a catalytic system that obviates the use of stoichiometric reagents other than the hydrogen atom source.

Suitable precursor for the H• could be a small molecule rich in hydrogen atoms that can be easily manipulated. As discussed in the section above, hydrogen gas, though a suitable candidate, requires harsh conditions for activation. Another alternative is formic acid (HCOOH). It has been previously observed[294] that the photodissociation of formic acid proceeds via two distinct channels:

$$HCOOH(g) + h\nu \rightarrow CO(g) + H_2O(g) \qquad (5)$$

$$HCOOH(g) + h\nu \rightarrow CO_2(g) + H_2(g) \qquad (6)$$

In (6), the homolysis of the O–H bond leads to the generation of a 'hot' hydrogen atom that can roam around the molecule, undergo hydrogen abstraction and terminate further reactivity. So direct activation is not only challenging but very likely to not yield a detectable amount of single H-atoms. However, it has been reported that if formic acid is transformed into a peroxide **155**, homolysis of the weak O–O bond leads to the generation of a formyloxy radical **156** (Scheme 4.4). Species **156** can undergo β-scission to generate H• as suggested by Pryor and Henderson.[253]

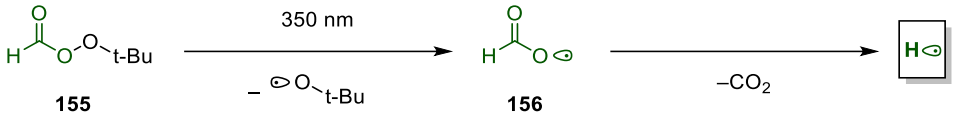

Scheme 4.4: Homolysis of tert-butyl peroxiformate as means to generate hydrogen radical.

Inspired by these early studies, we envisioned that if we could generate the formyloxy radical from formic acid in situ, followed by a radical decarboxylation step, we would be able generate a ‘naked’ hydrogen atom.

With recent developments in the fields of photoredox metal- and organocatalysis,[295, 296] we envisaged that we could exploit the carboxyl moiety and evoke the radical decarboxylation under mild conditions. Multiple strategies based on Ir,[297] Ru,[298] Fe[299] and other photocatalysts[300] for the activation of carboxylic acids have been developed. However, recent advancements in acridine and acridinium chemistries attracted our attention to develop a metal-free approach.

Aza-arenes and in particular acridine and its derivatives, have been shown to serve as photocatalysts and evoke the radical decarboxylation of alkyl carboxylic acids (Scheme 4.5). Seminal works by Noyori[301] and Oda[302] used UV light irradiation to induce the desired reactivity, while recently the groups of Larionov[303] and Dilman[304] have extended the reactivity into the visible region. Given the availability and tunability of acridines, we found them an attractive opportunity to develop as a catalytic platform.

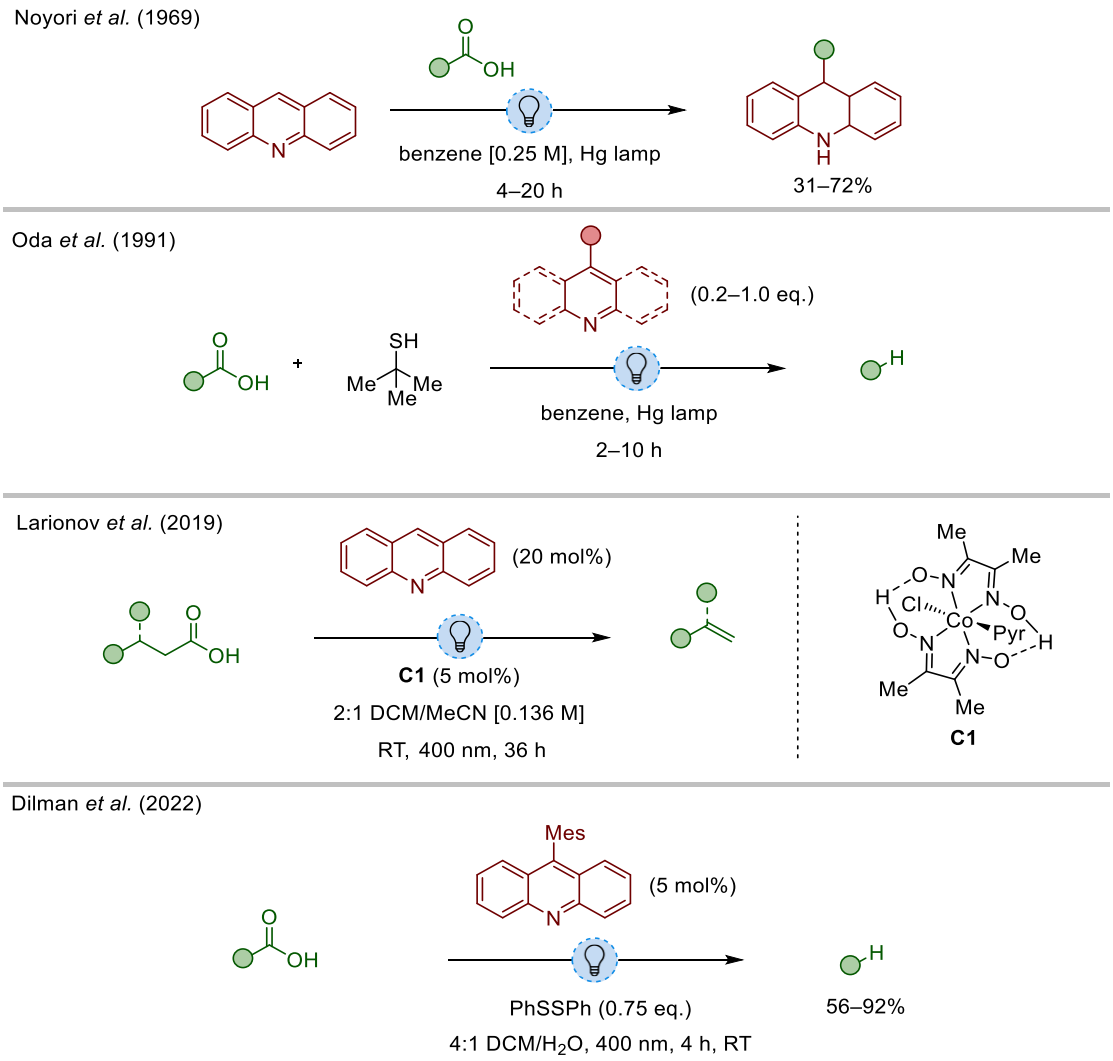

Scheme 4.5. Aza-arenes in the radical decarboxylation of carboxylic acids.

It has been suggested that acridine photocatalysts activate primary carboxylic acids via a proton-coupled electron transfer (PCET) pathway (Scheme 4.6).[305] Extending this rationale, we expect that with formic acid the acridine catalyst **157** will form a hydrogen-bonded complex, which upon photoexcitation undergoes electron transfer. The resulting formyloxy radical **156** can then decarboxylate, providing the targeted H• and acridinyl radical **158**. Finally, a suitable oxidant needs to be employed to regenerate the starting acridine **157** and close the catalytic cycle.

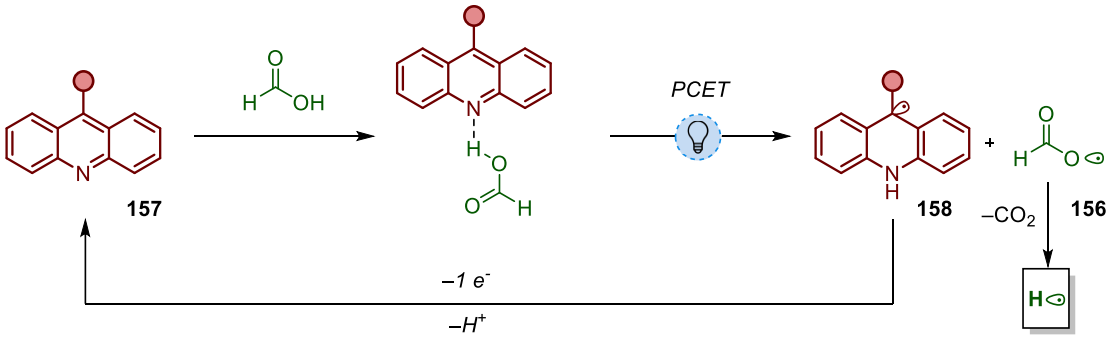

Scheme 4.6. Proposed generation of hydrogen radical from formic acid and acridine-type photocatalyst via PCET.

To confirm the generation of a hydrogen atom, we expect that it will readily react with olefins (Scheme 4.7). Anti-Markovnikov addition of H• in alkene **159** will result in a carbon centred radical **160** which can participate in a HAT step to generate alkane **161**. A suitable HAT catalyst could be thiophenol **130-III** which offers a polarity-matched HAT step and the resulting thiyl radical **130-I** has been shown to be a sufficient oxidant for acridinyl radicals.[306] Thus, we expect it to be able to regenerate the starting photocatalyst and HAT catalyst after electron transfer and proton exchange.

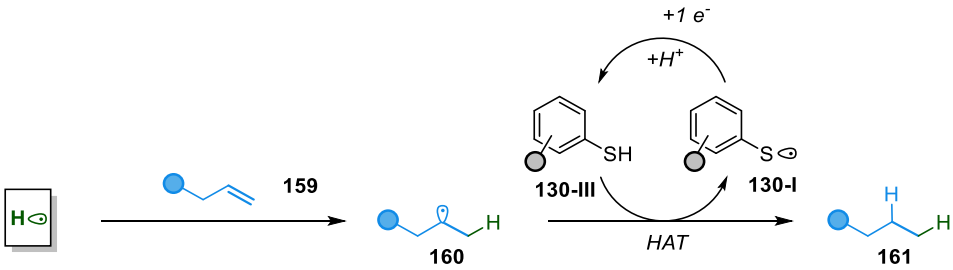

Scheme 4.7. Proposed trapping of hydrogen radical and regeneration of photocatalyst.

4.3. Results and discussion

4.3.1. Discovery and optimisation of the radical hydrogenation reaction of 4-phenyl-1-butene

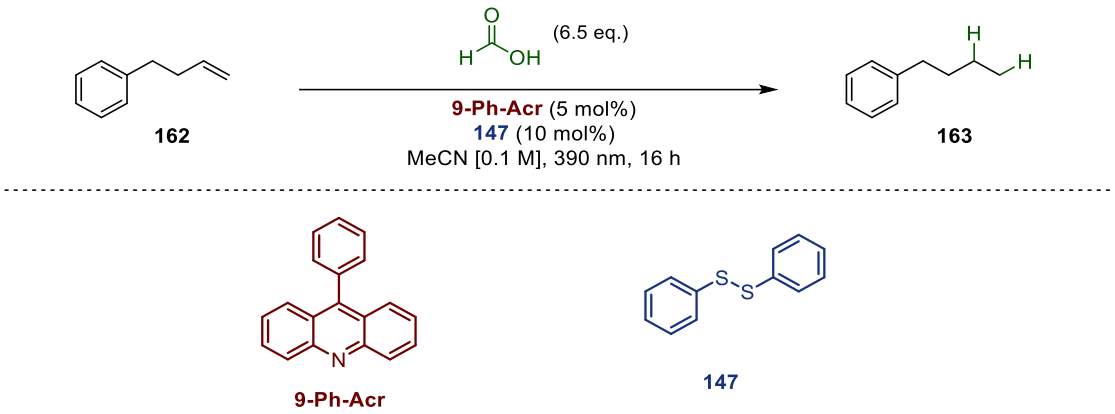

Scheme 4.8. Initial discovery of radical hydrogenation reaction by Dr Roopender Kumar (2024).

Taking a simple terminal alkene **162** in the presence of formic acid, 9-Ph-Acr as the photocatalyst (PC) and phenyl disulfide (**147**) as the HAT catalyst we observed the formation of the hydrogenation product **163** under 390 nm blue light irradiation. Although the initially observed crude NMR yield was very low (10%), the formation of alkane **163** was consistent with our hypothesis and motivated further investigation into the optimal reaction conditions.

To begin the reaction optimisation, we screened a variety of solvents (Table 4.1). Our initial choice of acetonitrile allowed for the reaction to proceed (entry 1), whereas substituting it for propionitrile decreased reactivity (entry 2). Ethyl acetate was also favourable in this reaction (entry 3), though it gave lower yield. Other polar solvents led to the consumption of the starting material (entries 4–6), however those were mostly undesired side reactions and only traces of hydrogenated product were observed. Interestingly, employing water as solvent resulted in the almost complete consumption of starting material and the formation of 5-phenylpentanoic acid. The reaction likely proceeds via the thiyl radical abstracting from formic acid, followed by radical addition and HAT as previously observed in similar systems.[307] 1,4-dioxane was also ineffective in this transformation, with only traces of product observed (entry 7). On the other hand, non-polar solvents such as toluene and fluorobenzene (entries 8–9) completely shut down the reaction.

Among the solvents evaluated, acetonitrile gave the best results and was therefore selected as the optimal medium.

Table 4.1: Solvent screen in the radical hydrogenation

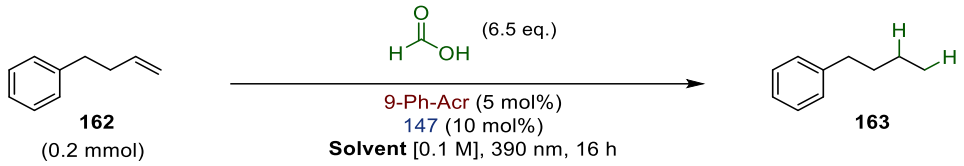

162
(0.2 mmol)

163

Entry	Solvent	Product yield*
1	MeCN	10%
2	EtCN	Traces
3	EtOAc	5%
4	DMSO	Traces**
5	Formic acid	Traces**
6	Water	Traces**
7	1,4-dioxane	Traces
8	Toluene	NR
9	Fluorobenzene	NR

* Determined via ^{1}H NMR using 1,1,2,2-tetrachloroethane as internal standard.

** Starting material was partially consumed

NR = No reaction

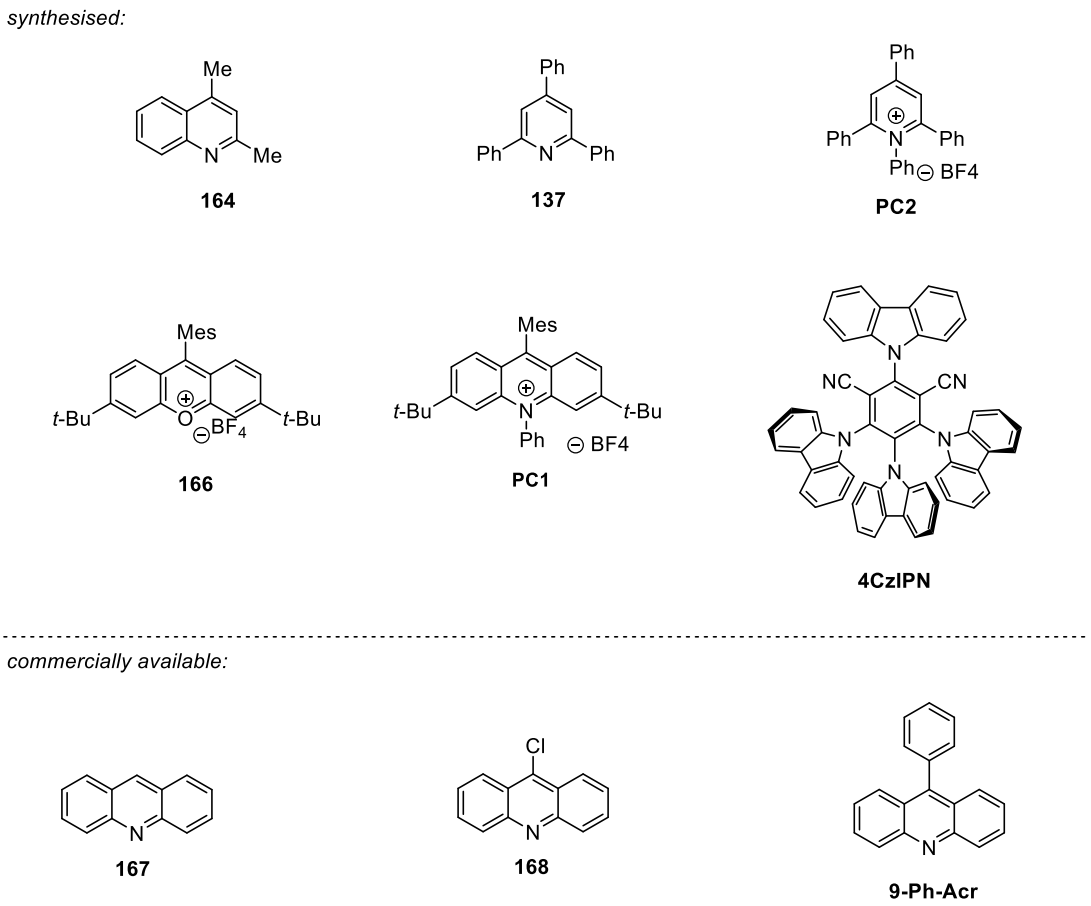

Scheme 4.9. Aza-heteroarene photocatalyst library.

Our next optimisation was focused on altering the 9-Ph-Acr skeleton to investigate which class of aza-heteroarene is necessary for reactivity (Scheme 4.9). Removing the phenyl group from the 9-position in **167** and **168** (Table 4.2, entries 1 and 2) or reducing the number or main aromatic cores to quinoline **164** and pyridine **137** (entries 3 and 4) resulted in no reaction. These observations can be attributed to the decreased conjugation of the scaffold, which shifts the absorption profile towards the UV region and renders the catalysts non-excitable under the reaction irradiation wavelength. Substitution at nitrogen, as in the case of pyridinium **PC2** and acridinium **PC1** catalysts (entries 5 and 6), prevented coordination of formic acid and thereby suppressed the reaction. Similarly, swapping the nitrogen for an oxygen in xanthilium **166** (entry 7) eliminated the Lewis basicity of the catalyst and thus impeded reactivity. Employing a carbazole-based photocatalyst **4CzIPN** (entry 8) was also unfavourable. Finally, to reduce errors arising from NMR integration and to improve product isolation, the optimal 9-Ph-Acr catalyst was employed on a slightly bigger scale reaction (0.40 mmol), which afforded a comparable outcome to the initial hit (entry 9).

Table 4.2: Photocatalyst class screen

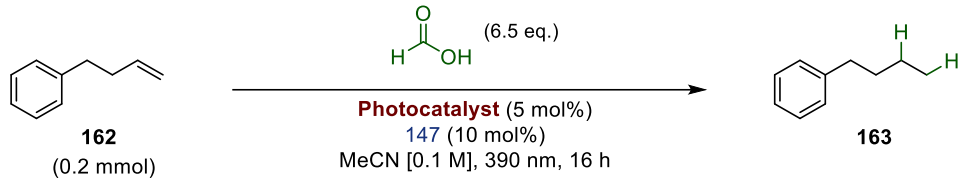

Entry	Photocatalyst	Product yield*
1	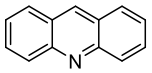 **167**	NR
2	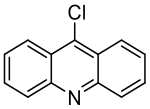 **168**	NR
3	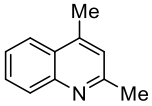 **164**	NR
4	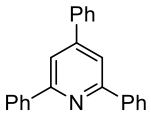 **137**	NR
5	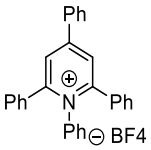 **PC2**	NR
6	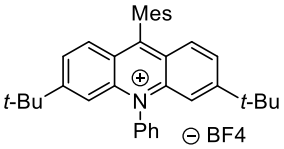 **PC1**	NR
7	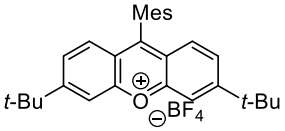 **166**	NR
8	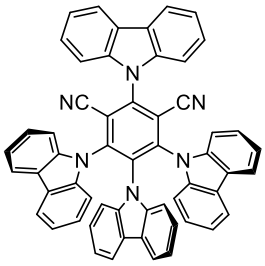 **4CzIPN**	NR

9**	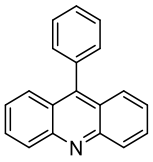	**9-Ph-Acr**	10%

* Determined via ^{1}H NMR using 1,1,2,2-tetrachloroethane as internal standard.
** Reaction carried out at 0.4 mmol scale.

In an attempt to improve reaction efficiency, the HAT catalyst loading was reduced fourfold (entry 1), which led to a decrease in yield. In contrast, use of 2-aminophenyl disulfide **150** (entry 2) resulted in a noticeable improvement and was selected as the optimal catalyst from this set. By comparison, aliphatic disulfide **169** (entry 3) and thiol **170** (entry 4) both gave lower yields, accompanied by the formation of side products.

Table 4.3: Preliminary HAT catalyst screen

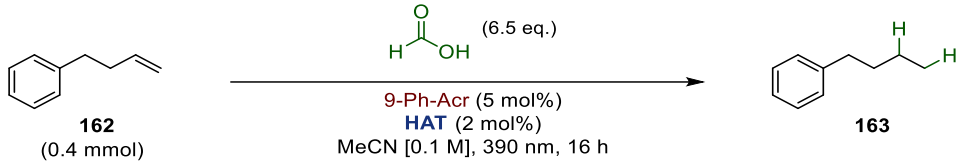

162 (0.4 mmol) → **163**

Entry	HAT catalyst	Product yield*
1	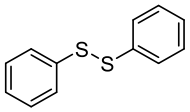 **147**	5%
2	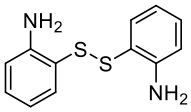 **150**	8%
3	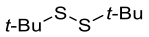 **169**	4% (Complex)
4**	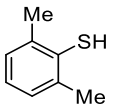 **170**	4% (Complex)

* Determined via ^{1}H NMR using 1,1,2,2-tetrachloroethane as internal standard.

** Using 4 mol% of HAT catalyst

We evaluated the source of irradiation and that proved to be crucial for the success of this reaction (Table 4.4). A red shift in the irradiation wavelength at 427 nm (entry 2) completely terminated the reaction, whereas a blue shift in the UV-A region improved the reactivity threefold (entry 3). Addition of a second light source significantly increased the reaction yield (entry 4). This was a productive development in the conditions optimisation and was adopted for subsequent experiments. Notably, the use of two lamps led to increase in temperature which ranged in 60–80 °C.

Table 4.4: Light wavelength and photon flux

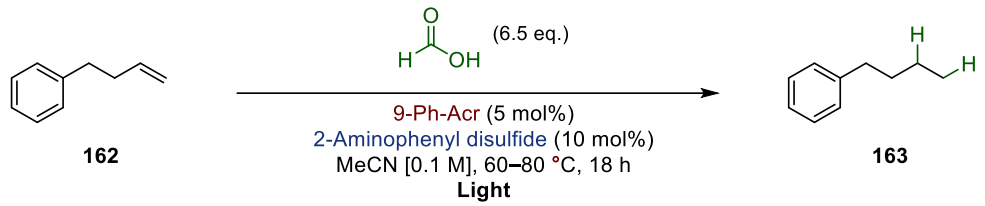

Entry	Light wavelength and flux	Product yield*
1	1 × 390 nm	10%
2	1 × 427 nm	0%
3	1 × 370 nm	27%
4	2 × 370 nm	47%

* Determined via ^{1}H NMR using 1,1,2,2-tetrachloroethane as internal standard.

To explain the improvement in reactivity, the UV-vis absorption spectrum of the photocatalyst was investigated (Figure 4.1). A blue shift in irradiation wavelength is favourable since it is moving towards the absorption maximum of the photocatalyst (λ_{max} = 359 nm). On the other hand, at 427 nm there is no absorbance hence no reactivity was observed.

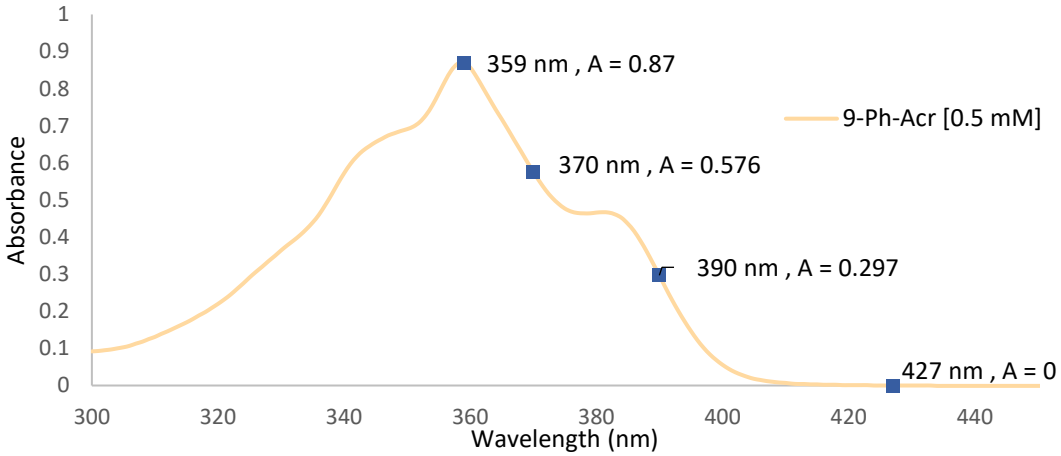

Figure 4.1: UV–vis absorption spectrum of 0.5 mM 9-Ph-Acr in acetonitrile.

A more detailed investigation of catalyst loading revealed that decreasing the HAT catalyst from 10 mol% to 5 mol% improved the product yield (Table 4.5, entries 1–3), whereas further reductions had no beneficial effect. In contrast, a PC loading of 10 mol% was found to be optimal (entry 6), with higher loadings providing no further improvement.

Table 4.5: Loading of PC and HAT catalysts

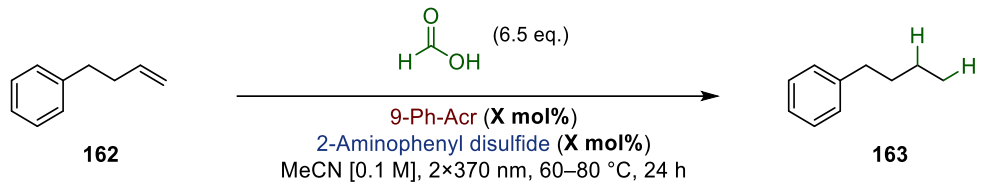

162 163

Entry	PC (mol%)	150 (mol%)	Product yield*
1	5	10	50%
2	5	7.5	36%
3	5	5	58%
4	5	2.5	48%
5	7.5	5	55%
6	10	5	66%
7	12.5	5	67%
8	15	5	58%

* Determined via ^{1}H NMR using 1,1,2,2-tetrachloroethane as internal standard.

With the optimized catalyst loadings identified, attention was directed to the electronic effects of the HAT catalyst (Table 4.6). Removing the amino group from the ortho-position (entry 2) was detrimental to reaction yield. On the other hand, introducing an electron rich substituent such as methyl (**171**) or methoxy (**172**) (entries 3 and 4) offered and improvement in reactivity, while sterically hindered and electron rich triisopropyl disulfide (**149**) (entry 5) performed similarly to the optimal catalyst. It became apparent that electron rich substituents are favoured over the non-substituted variant and to confirm this hypothesis, we tested some electron deficient catalysts (entries 6–8). Not surprisingly, the results were lower or similar to the parent phenyl disulfide **147** (entry 2).

Table 4.6: Screening the electronics of the HAT catalyst

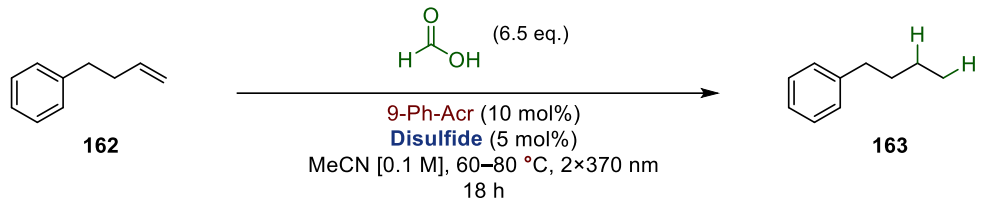

162 163

Entry	Disulfide	Product yield*
1	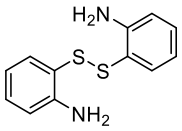 **150**	50%
2	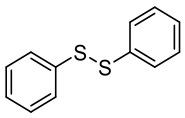 **147**	21%
3	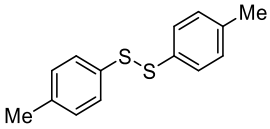 **171**	38%
4	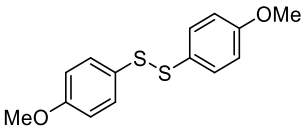 **172**	33%
5	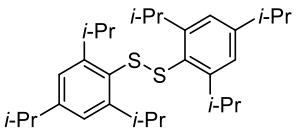 **149**	43%
6	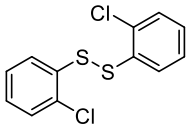 **173**	14%
7	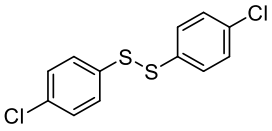 **148**	23%
8	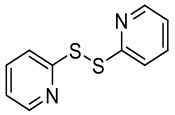 **174**	13%

* Determined via ^{1}H NMR using 1,1,2,2-tetrachloroethane as internal standard.

All catalysts were commercially available, except for **173** (entry 6, see Appendix).

The optimal reaction time was investigated (Table 4.7). After 18 h, the reaction had proceeded nearly to completion (entry 1), with the maximum product yield obtained after 24 h of irradiation (entry 2). Extending the reaction beyond 24 h did not result in

further improvement (entry 3), thus 24 h was selected for optimal in subsequent optimisations.

Table 4.7: Reaction time

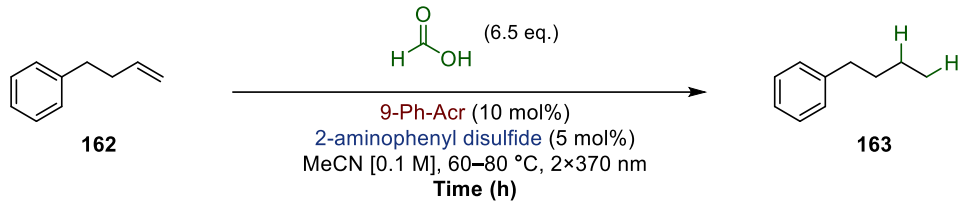

Entry	Reaction time (h)	Product yield*
1	18	50%
2	24	66%
3	48	64%

* Determined via ^{1}H NMR using 1,1,2,2-tetrachloroethane as internal standard.

To showcase the necessity of each component of the reaction a set of control experiments was performed (Table 4.8). Heating the reaction in the dark led to no product forming (entry 2). Similarly, irradiation in the absence of formic acid or photocatalyst afforded no reactivity (entries 3 and 4), whereas omitting the HAT catalyst gave traces of product (entry 5). This is most likely due to the role of the thiyl radical in the recycling of the photocatalyst intermediate radical. Finally, oxalic acid was shown to be a suitable source of H• (entry 6) presumably undergoing a double radical decarboxylation.

Table 4.8: Control experiments

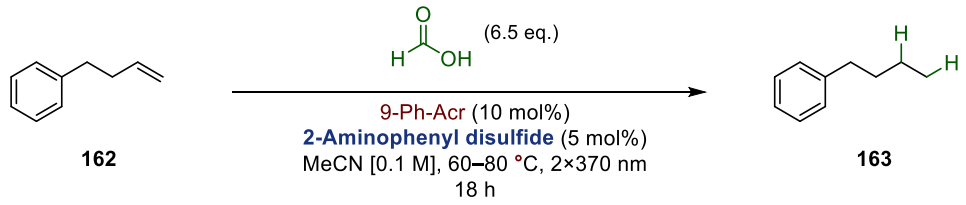

Entry	Change from standard conditions	Product yield*
1	–	50%
2	No light	NR
3	No formic acid	NR
4	No PC	NR
5	No HAT	Traces

6	Oxalic acid instead of formic acid	40%

* Determined via ^{1}H NMR using 1,1,2,2-tetrachloroethane as internal standard.

Having optimised the reaction parameters, a substrate class screen was carried out (Table 4.9). Under a slightly more concentrated condition, the model substrate afforded a good 70% yield (entry 1). When the same conditions were applied to other terminal alkenes **132**, **175** and **176**, the reaction performance declined significantly to moderate 44–33% yields (entries 2–4). Disubstituted and activated alkenes **116** and **177** offered a much higher conversion of starting material (entries 5 and 6), while styrene **178** underwent complete polymerisation in the first 3 hours of reaction (entry 7).

Table 4.9: Preliminary substrate scope

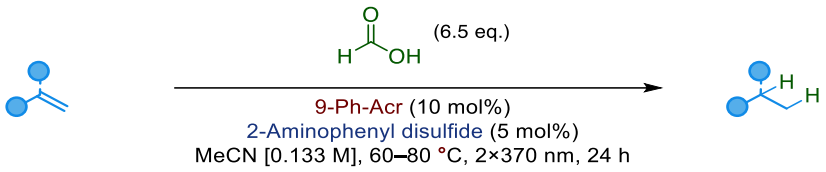

Entry	Substrate	Outcome*	
		Remaining SM	Product
1**	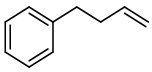 **162**	20%	70%
2	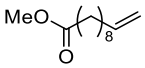 **132**	67%	33%
3**	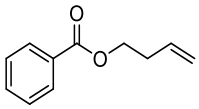 **175**	62%	40%
4**	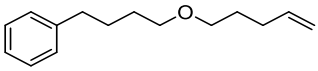 **176**	56%	44%
5	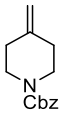 **116**	10%	N/A
6	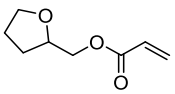 **177**	17%	50%
7	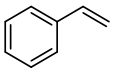 **178**	0%	0%

* Determined via ^{1}H NMR using 1,1,2,2-tetrachloroethane as internal standard.

**See Appendix for substrate synthesis details.

Although promising conversions were observed for substrates **116** and **177**, we were sceptical towards those results given the inability to isolate the product from the reaction mixture. At the time, we were aware that disubstituted alkene **116** might be susceptible to oxidation and given the highly oxidising nature of our system, that could be a reason for the observed conversion. On the other hand, acrylate **177** is volatile (bpt = 87 °C) and that led to the poor product recovery. As such, **116** and **177** were not optimal for further reaction optimisation.

Efforts to isolate the model substrate **162**, alongside the poor performance of other similar substrates motivated us to investigate the reaction conditions in more detail. Thus, non-volatile alkene **132** was selected as the model substrate for subsequent optimisations.

4.3.2. Re-optimisation of radical hydrogenation reaction employing methyl undecanoate as model substrate

Seeing that the reaction outcome is strongly dependent on the HAT catalyst electronics, we decided to investigate it in further depth (Table 4.10). The presence of the ortho-amino group proved to be ubiquitous and one potential explanation could be due to its chelating properties. Thus, disulfides bearing other coordinating groups such as phenol (**180**), ester (**151**) and amide (**152**) were probed (entries 1–3) but failed to deliver an improvement over the standard 2-aminophenyl disulfide.

Table 4.10: Screen of chelating groups on HAT catalyst

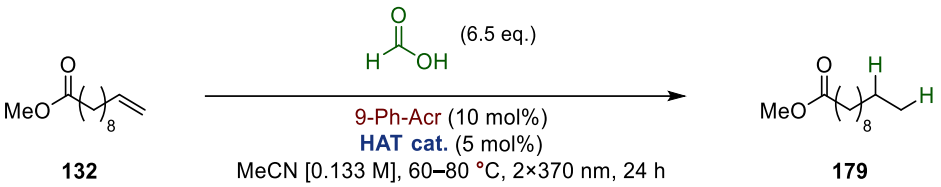

132 **179**

Entry	HAT catalyst	Product yield*
1**	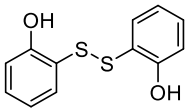 **180**	17%
2**	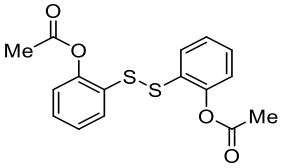 **151**	Traces

3**	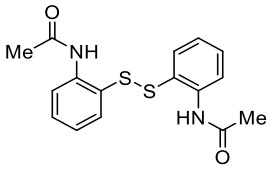	**152**	19%

* Determined via ^{1}H NMR using 1,1,2,2-tetrachloroethane as internal standard.

**See Appendix for catalyst synthesis details.

Thus, we turned our attention to other classes of HAT catalysts. We hypothesised that the electron rich nature of a naphthalene core could offer an improvement over a non-substituted phenyl ring. Unfortunately, catalysts **181** and **182** exhibited poor reactivity and solubility under the reaction conditions (entries 4 and 5). Substituting the sulfur with a softer selenium centre in **183** proved to be reactive but not optimal (entry 6). Finally, 2-phenylmalonitrile **153** (BDE = 77 kcal/mol),[26] that has been particularly effective in other acridinium systems,[157, 308] was probed (entry 7). Although it has a very similar BDE to thiophenol (79 kcal/mol) its only gave traces of product in this transformation.

Table 4.11: Other classes of HAT catalysts

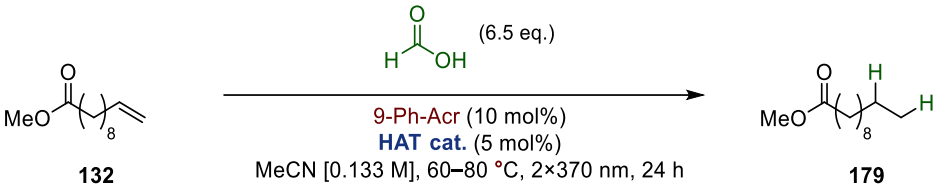

132 **179**

Entry	HAT catalyst	Product yield*
1**	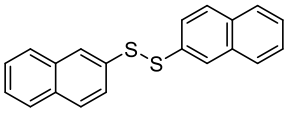 **181**	15%
2**	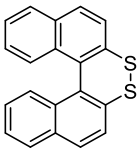 **182**	12%
3	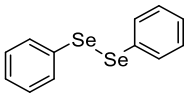 **183**	18%
4**	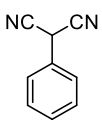 **153**	Traces

* Determined via ^{1}H NMR using 1,1,2,2-tetrachloroethane as internal standard.

**See Appendix for catalyst synthesis details.

To confirm the role of intermediate thiol as the HAT catalyst, reaction was carried out with respective amount of 2-aminothiophenol **184** (entry 1). Pleasingly, the reaction proceeded though in decreased yield (33%). As a control experiment to further validate the role of the sulfur in this transformation, the reaction was conducted in the presence of 2-aminophenols **185–187** (entries 2–4). Evidently, no reactivity was observed when the sulfur atom was substituted for oxygen and it was clear that the disulfide catalyst performed more efficiently.

Table 4.12: Thiols and phenols evaluation as HAT catalysts

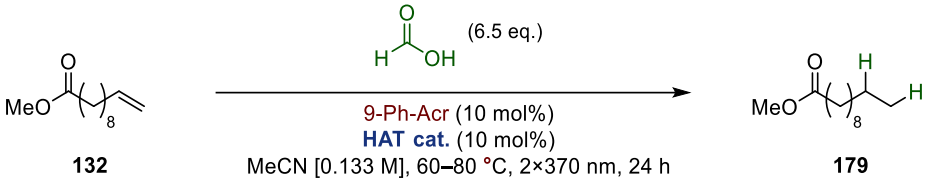

Entry	HAT catalyst	Product yield*
1	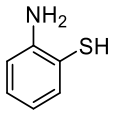 **184**	33%
2	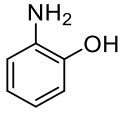 **185**	NR
3	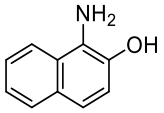 **186**	NR
4	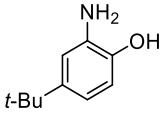 **187**	NR

* Determined via ^{1}H NMR using 1,1,2,2-tetrachloroethane as internal standard.

Increasing the number of light sources seemed to improve the reaction yield from 23% (entry 1) for one light source to 47% (entry 2) under two lamp irradiation, in line with previous observations (vide supra Table 4.4). This could be due to an increase in the photon flux at the reaction medium thereby enhancing the number of photoexcitation events. However, we noticed that the temperature also increased (vials felt much hotter at the end of the reaction), which is most likely stemming from non-radiative relaxation pathways taking place in the reaction or from the heat generated at the lamp source (note distance from the vial is only 2–4 cm). The elevated temperature led us to believe that the yield improvement is not necessarily coming from the higher photon flux (entry

3–4) but from the reaction having more thermal energy to overcome the potentially high activation barrier for decarboxylation. Thus, the effect of temperature was investigated next.

Table 4.13: Photon flux

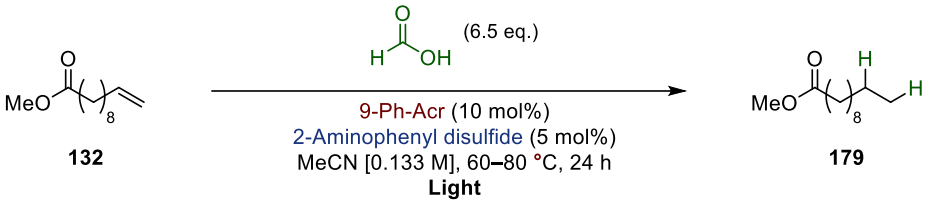

Entry	LEDs	Product yield*
1	1 × 370 nm	23%
2	2 × 370 nm	47%
3	3 × 370 nm	72%
4	4 × 370 nm	71%

* Determined via ^{1}H NMR using 1,1,2,2-tetrachloroethane as internal standard.

Lights were placed equidistantly from reaction vial (2 cm).

To ensure a more rigorously controlled thermal environment during the course of the transformation, the experimental setup was modified such that the reaction vials were placed within an oil bath. This adjustment was made to mitigate uncontrolled temperature fluctuations that might otherwise arise from localised heating under irradiation. When the reaction was performed under irradiation with a single light source at ambient conditions, we observed a steady increase in temperature, reaching values in the range of 50–60 °C within the first hour of irradiation (Table 4.14). Under these conditions, the yield obtained after 24 hours of reaction time was recorded as shown in entry 1. Conducting the reaction at a fixed oil bath temperature of 60 °C produced a very similar outcome (entry 2), suggesting that the reaction progress under irradiation at room temperature is in fact driven, to some extent, by the temperature rise induced by the light source. Elevating the oil bath temperature further to 80 °C led to a marked improvement in efficiency, affording the optimal yield (entry 3). Attempts to carry out the transformation at temperatures above this threshold resulted in higher conversion, albeit at the expense of significant substrate decomposition (entry 4). Finally, when the optimized thermal conditions (80 °C) were combined with the previously identified optimal photon flux setup (vide supra, Table 4.13), the reaction

delivered its highest yield of 48%, notably without any detectable substrate degradation (entry 5). These observations highlight the interplay between photon input and thermal control and underscore the importance of balancing these two factors to achieve the most effective reaction outcome. Thus, the remaining optimisations were carried out in the aforementioned experimental setup.

Table 4.14: Temperature effect on reaction yield

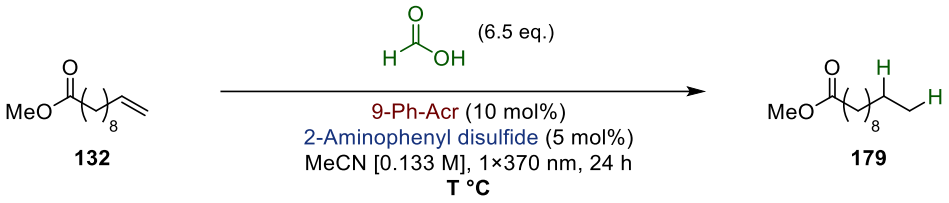

132 179

Entry	Temperature (°C)	Product yield*
1	RT	23%
2	60	28%
3	80	40%
4	100	48% (complex)
5**	80	48%

* Determined via ^{1}H NMR using 1,1,2,2-tetrachloroethane as internal standard.

** Reaction under 2 lamp irradiation.

To improve photon flux, the reaction was diluted (Table 4.15, entry 1), but this had little effect on yield. In contrast, doubling the amount of HAT catalyst enhanced the reactivity (entry 2), whereas further increases led to a poorer outcome (entry 3). Increasing the photocatalyst loading did not significantly affect the reaction outcome (entry 4).

Table 4.15: PC and HAT catalyst loading

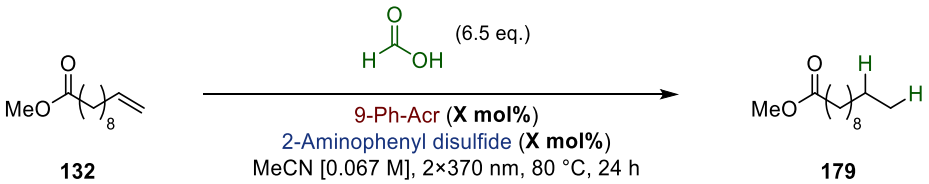

132 179

Entry	PC (mol%)	HAT (mol%)	Product yield*
1	10	5	48%
2	10	10	67%
3	10	20	29%

4	20	10	61%

* Determined via ^{1}H NMR using 1,1,2,2-tetrachloroethane as internal standard.

The quantity of formic acid was determinant for the overall efficiency of the transformation. Careful evaluation of different loadings revealed that the use of 6.5 equivalents provided the most favourable condition, affording the highest degree of conversion (entry 3). When the reaction was carried out with reduced quantities of acid, a pronounced decline in product formation was observed (entries 1 and 2), suggesting that insufficient acid loading hinders the productive pathway. Conversely, increasing the amount of acid beyond the optimal threshold did not translate into any appreciable enhancement in conversion (entries 4 and 5). This observation indicates that excessive acid loading does not further promote reactivity once a sufficient buffer amount is present.

Table 4.16: Formic acid equivalents

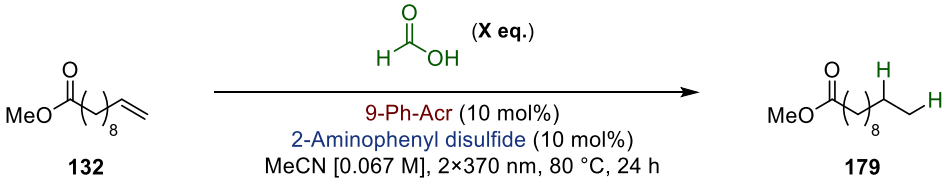

Entry	Acid (eq.)	Conversion*
1	1	13%
2	3	36%
3	6.5	66%
4	13	70%
5	20	70%

* Determined from the starting material to product ratio in the crude ^{1}H NMR

Under the current optimal setup (vide supra Table 4.15, entry 2), a short solvent variation was carried out. As previously observed (vide supra Table 4.1) polar aprotic solvents were productive with acetonitrile offering the best yield (entry 1), while ethyl acetate and 1,2-dichloroethane (DCE) led to a decrease in reaction performance (entries 2 and 3). Conversely, non-polar toluene completely ceased reactivity (entry 4). Taken together these results favourably validate the previous solvent optimisation.

Table 4.17: Solvent variations

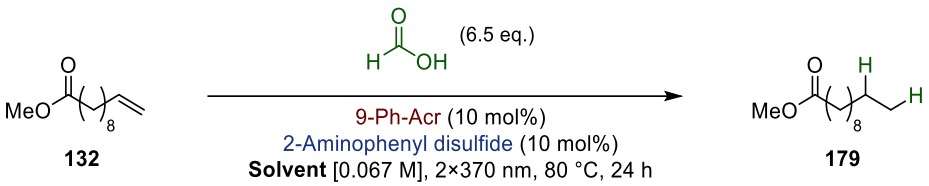

Entry	Solvent	Product yield*
1	MeCN	67%
2	EtOAc	23%
3	DCE	14%
4	Toluene	NR

* Determined via ^{1}H NMR using 1,1,2,2-tetrachloroethane as internal standard.

Under the current optimal catalyst loading (Table 4.15, entry 2), the concentration of the solvent was varied (Table 4.18). The range of 0.05–0.1 M was favourable for the reaction (entries 1–3), with 0.067 M selected as optimal solvent concentration. However, moving towards more concentrated solutions diminishes the productivity of the system (entry 4).

Table 4.18: Concentration variations

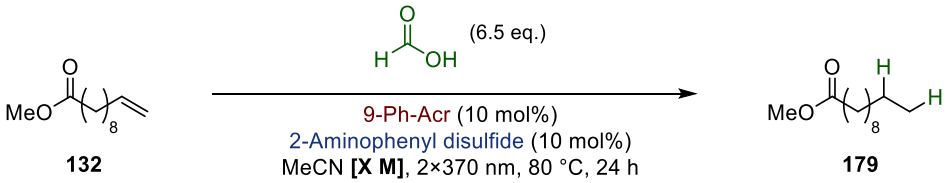

Entry	Concentration [M]	Product yield*
1	0.05	58%
2	0.067	67%
3	0.1	63%
4	0.2	28%

* Determined via ^{1}H NMR using 1,1,2,2-tetrachloroethane as internal standard.

In our initial HAT catalyst evaluation (vide supra, Table 4.16), 2-aminophenyl disulfide (**150**) emerged as the optimal candidate. These studies also indicated that electron-rich phenyl disulfides were generally superior to electron-deficient analogues, a key observation that guided subsequent optimisation efforts. To substantiate these findings, we conducted further variations under the current optimal conditions (Table

4.19). Alternative catalysts **147**, **148** and **188** (entries 1–3) underperformed relative to the optimal choice **150** (entry 4), and relocating the amino substituent in **189** diminished the yield considerably (entry 5), underscoring the critical role of the ortho-amino group. Attempts to modify the catalyst framework further revealed that N-methylation in **190** (entry 6) reduced reactivity, likely due to steric hindrance. In line with our earlier conclusions, we introduced additional electron-donating groups while retaining the 2-amino substituent. However, methyl (**191**) and tert-butyl groups (**192**) (entries 7 and 8) led to modest decreases in efficiency, while the methoxy group in **193** (entry 9) completely suppressed reactivity. Collectively, these results reaffirm that 2-aminophenyl disulfide remains the optimal HAT catalyst for this transformation.

Table 4.19: Extended study of HAT catalyst variations and structural optimisation

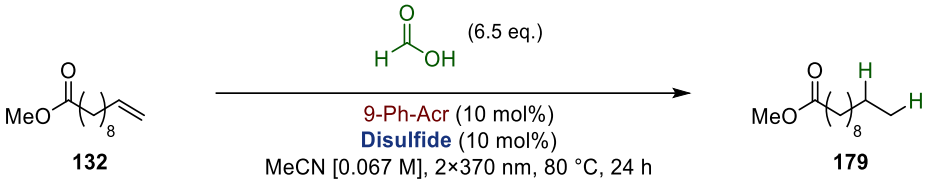

132 → **179**

Entry	Disulfide	Product yield*
1	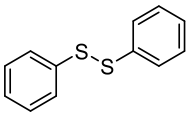 **147**	33%
2	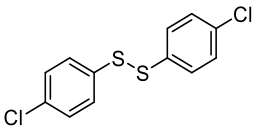 **148**	23%
3**	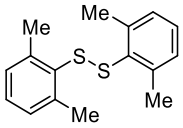 **188**	25%
4	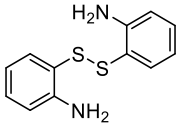 **150**	67%
5	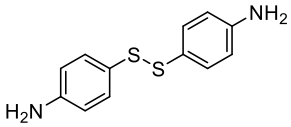 **189**	36%
6**	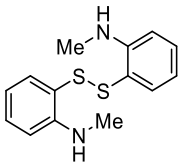 **191**	46%
7**	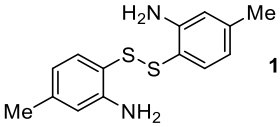 **192**	52%
8**	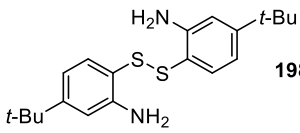 **198**	55%
9**	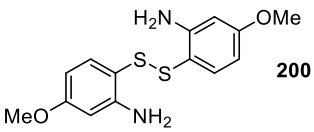 **200**	Traces

* Determined via ^{1}H NMR using 1,1,2,2-tetrachloroethane as internal standard.

**See Appendix for catalyst synthesis details.

Having previously identified the 9-Ph-Acr scaffold as essential for this transformation (vide supra Table 4.2), we decided to introduce different substituents to fine tune the properties of the catalyst (Table 4.20). Substituting the 9-phenyl ring with tert-butyl in **202** did not impact the reaction significantly (entry 2), whereas the mesityl group in **203** led to a reduction in yield (entry 3). Introducing electron rich substituents at the main core in **204** completely shut down reactivity (entry 4) while substitution at both the phenyl and main core in **205** (entry 5) offered an improvement over **204** but still did not perform better than the non-substituted catalyst (**9-Ph-Acr**). No clear trend was established in the evaluation of electron-rich substituents. On the other hand, the effect of electron withdrawing groups was investigated. Substituting the phenyl ring with a single fluorine atom in **206** did not affect the reaction progress (entry 6), however a second fluorine in **207** displayed a decrease in reactivity (entry 7). Other electron-withdrawing groups such as chlorine (**208**) and trifluoromethyl (**209**) led to a reduction in yield (entries 8 and 9) and at the very end of the spectrum, a catalyst with two trifluoromethyl groups was prepared and tested (**210**), though it inhibited the reaction further (entry 10). We established that electron-deficient groups are detrimental to the outcome of the transformation with more electron withdrawal leading to a lower yield of hydrogenated product. To note, the synthesis of catalysts **202**, **203**, **204**, **205** and **208** (entries 2, 3, 4, 5, 8) can be found in the appendix, whereas catalysts **206**, **207**, **209** and **210** (entries 6,7,9,10) were prepared by Roman Tinkov and their synthesis and data characterisation is described in his master's thesis (2025). Finally, the non-substituted catalyst **9-Ph-Acr** was chosen as optimal.

Table 4.20: Photocatalyst variations

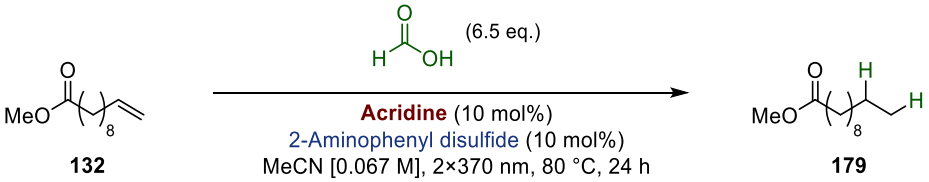

Entry	Acridine	Product yield*
1	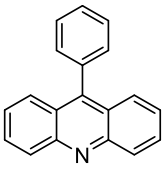 **9-Ph-Acr**	67%
2	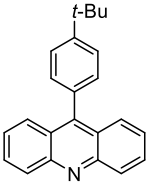 **202**	62%
3	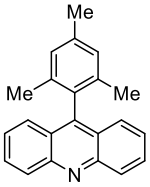 **203**	50%
4	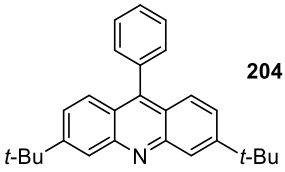 **204**	Traces
5	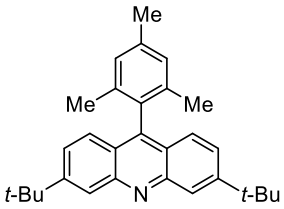 **205**	60%
6	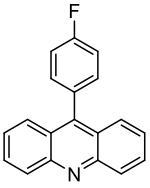 **206**	65%
7	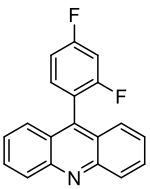 **207**	62%

8	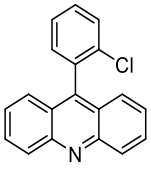	**208**	55%
9	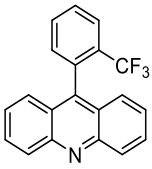	**209**	49%
10	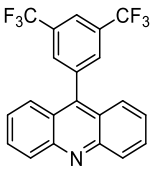	**210**	30%

* Determined via ^{1}H NMR using 1,1,2,2-tetrachloroethane as internal standard.

The necessity of each reaction component was evaluated by performing control experiments (Table 4.21). As previously observed (vide supra Table 4.8) removal of one of the reaction elements (PC, HAT catalyst, formic acid or light) resulted in the complete disappearance of hydrogenation product.

Table 4.21: Control experiments

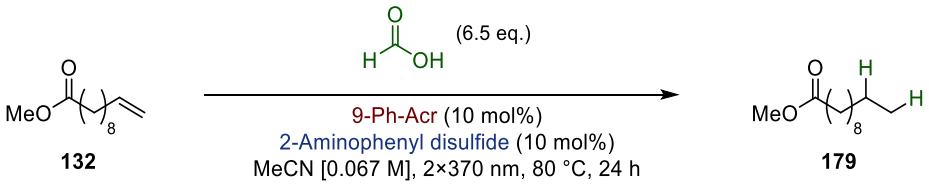

132 **179**

Entry	Change from standard conditions	Outcome*
1	No PC	NR
2	No HAT catalyst	NR
3	No acid	NR
4	No light	NR

* Determined via ^{1}H NMR using 1,1,2,2-tetrachloroethane as internal standard.

Having varied every possible component of the reaction, we were not able to increase the conversion of the starting material above 67%. Our hypothesis for this problem was that one of the reaction catalysts is being deactivated in an unproductive side reaction pathway. To restart the hydrogenation reaction, we attempted to introduce each catalyst as an additive after 24 h (Table 4.22). Thus, following one day of irradiation, the reaction was spiked with another dose of PC, HAT catalyst or formic acid and left

to react for another 24 h (entries 2–4). Unfortunately, no significant improvement was observed in the reaction yield. However, when all three components were introduced after the first irradiation cycle (entry 4), the product was obtained in almost quantitative yield, with traces of starting material remained. Notably, introducing only PC and HAT (entry 6), did not improve the reaction. We have already tested carrying out the reaction with the same amount of formic acid (13 eq.) from the beginning (vide supra Table 4.16, entry 4) or higher loading of PC (vide supra, Table 4.5 and Table 4.15) and HAT catalyst (see Table 4.5). However, these variations did not offer such a stark improvement in yield. Thus, sequential addition of extra formic acid in combination with the rest of the reagents is optimal for this transformation and was adopted as a standard procedure in the substrate scope evaluation below.

Table 4.22: Sequential reagents addition

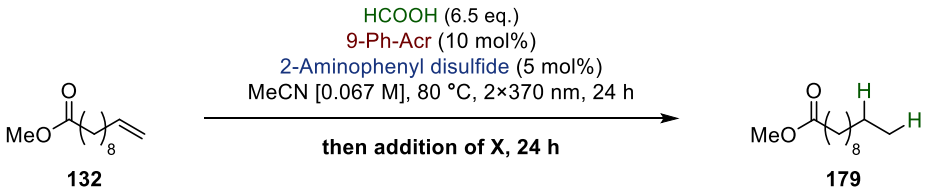

Entry	Additive at 24 h	Yield*
1	none	67%
2	PC (10 mol%)	72%
3	HAT (10 mol%)	61%
4	HCOOH (6.5 eq.)	75%
5	PC (10 mol%), HAT (10 mol%), HCOOH (6.5 eq.)	95%
6	PC (10 mol%), HAT (10 mol%)	70%

* Determined via ^{1}H NMR using 1,1,2,2-tetrachloroethane as internal standard.

The optimal reaction conditions were applied to a variety of terminal alkene substrates (Table 4.23). Pleasingly, most of this class of substrates performed well resulting in conversions above 80%. In terms of functional group tolerance, aliphatic (**132**) and aromatic esters (**175**) are tolerated (entries 1 and 2) as well as ethers in **176** (entry 3). Alkyl bromide **213** gave poorer mass recovery, due to coelution with the starting material (entry 4), whereas alcohol **215** participated in a side reaction with formic acid giving the respective formate ester (entry 4). Perhaps lowering the temperature of reaction for this substrate can eliminate the esterification side product. N-protected

amines (**217**) and pyridines (**219**) were also well tolerated (entries 6 and 7). Attempts to hydrogenate the disubstituted alkene moiety in **221** resulted in high conversion but poor mass recovery of product (entry 8).

Table 4.23: Substrate scope: Terminal alkenes

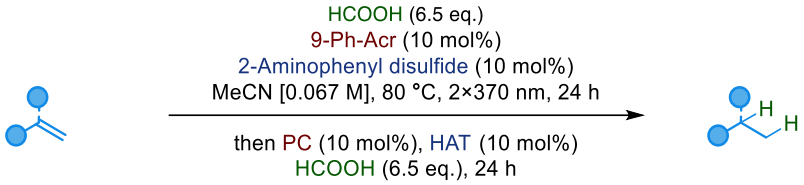

Entry	Alkene	Product	Yield*
1	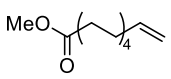 **132**	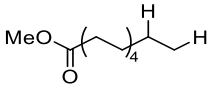 **179**	60% (95%)
2	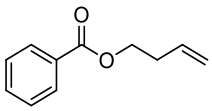 **175**	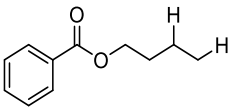 **211**	66% (90%)
3	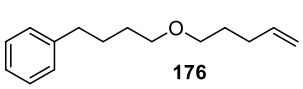 **176**	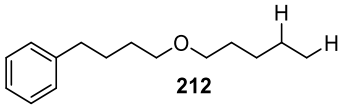 **212**	54% (100%)
4**	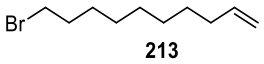 **213**	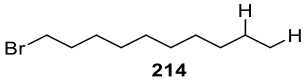 **214**	34% (82%)
5	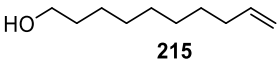 **215**	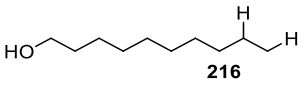 **216**	27% (90%)
6**	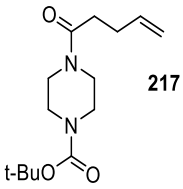 **217**	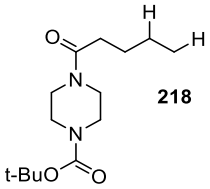 **218**	56% (83%)
7	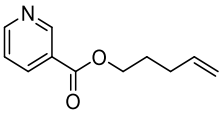 **219**	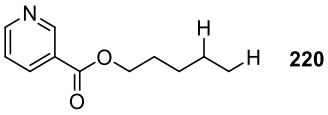 **220**	27% (80%)
8	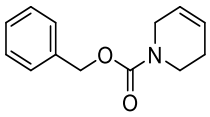 **221**	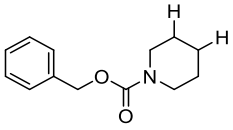 **222**	8% (90%)

* Isolated yields reported. Conversion (in parenthesis) is based on uptake of starting material from crude ^{1}H NMR with respect to internal standard (1,1,2,2-tetrachloroethane or nitromethane).

** Product coeluted alongside remaining starting material.

Conjugated olefins were also tolerated in the reaction (Table 4.24). Substrates **224**, **226** and **228** were isolated in moderate yields, although the conversion of the SM was quantitative. This could be due to a background thermal decomposition reaction, which was observed at high temperatures and thus the radical hydrogenation scope of Michael acceptors was performed at a lower temperature (60 °C). In addition, a mixture of diastereomers was observed which most likely comes from epimirisation of the stereocentres with H•.

Table 4.24: Substrate scope: Activated alkenes

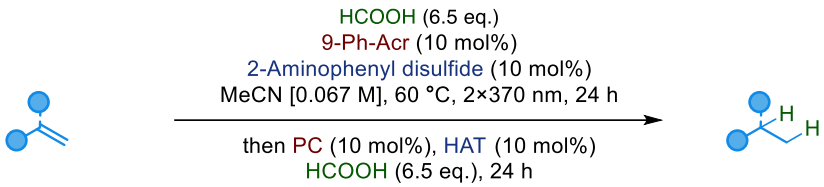

Entry	Alkene	Product	Yield*
1	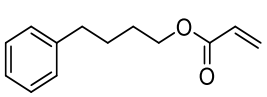 **223**	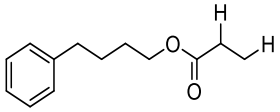 **224**	41% (100%)
2	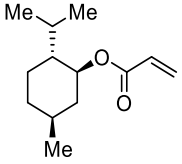 **225**	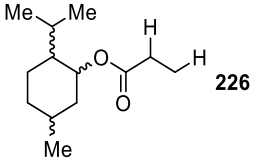 **226**	26% (100%)
3	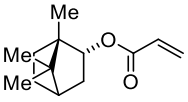 **227**	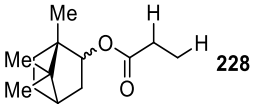 **228**	32% (100%) (dr = 5.3:1)

* Determined via ^{1}H NMR using 1,1,2,2-tetrachloroethane as internal standard. Values in parentheses indicate conversion of starting material.

A set of unsuccessful substrates is presented in Table 4.25. Activated alkenes **177**, **229** and **230** were compatible in the reaction, however their low boiling points made it impossible to isolate any product (entries 1–3). On the other hand, trisubstituted alkenes **231–233** were fully consumed but no product was identified in the crude mixture (entries 4–6). This observation was explained by the oxidation potential (ca. E_{ox} = 2 V vs SCE)[309] which makes them susceptible to SET to the PC. Similarly, alkene **116** did not afford any product although conversion was quantitative (entry 7). Styrene (**178**) was unstable under the reaction conditions and fully decomposed after 2.5 h of irradiation time (entry 8). Taken together these results highlight the limitations of the radical hydrogenation: i) the substrate must be photo- and/or thermally stable, ii) the

alkene must lie outside of the oxidation potential of the PC and iii) oxidisable functional groups are susceptible to side reactions.

Table 4.25. Substrate scope: Unsuccessful substrates

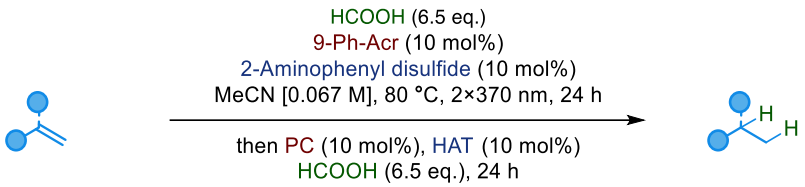

Entry	Substrate	Limitation*
1†	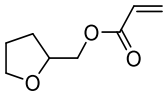 **177**	Volatile
2	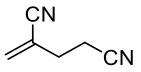 **229**	Volatile
3†	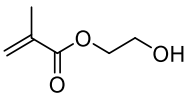 **230**	Volatile
4	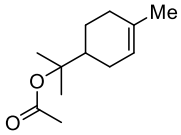 **231**	Oxidisable
5	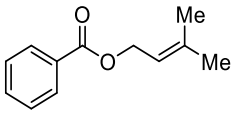 **232**	Oxidisable
6	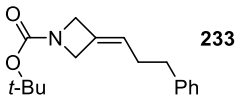 **233**	Oxidisable
7	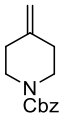 **116**	Oxidisable
8†	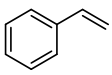 **178**	Unstable

* Determined via ^{1}H NMR using 1,1,2,2-tetrachloroethane as internal standard. Values in brackets indicate conversion of starting material.

† Reaction carried out at 60 °C.

The substrates in Scheme 4.10 were synthesised during the course of the project in order to be evaluated as part of the substrate scope.

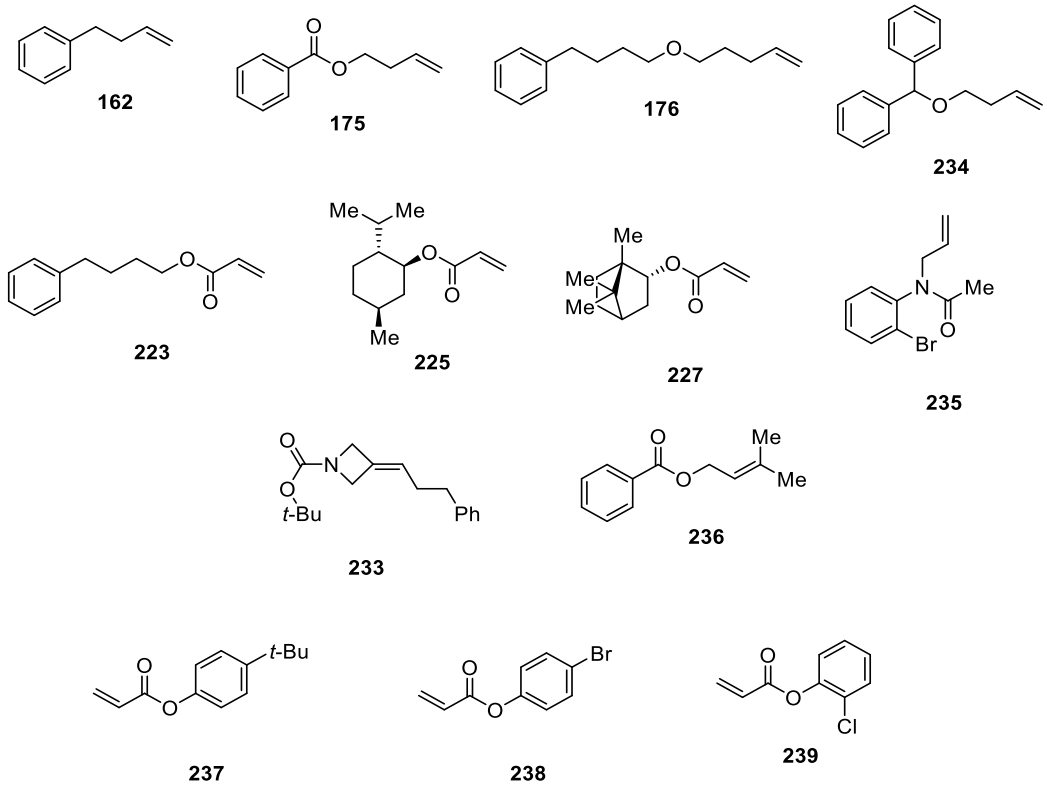

Scheme 4.10. Synthesised substrate library.

4.4. Mechanistic investigation

To gain further insight into the reaction and its mechanism, we studied it in a bit more detail. A typical reaction setup is shown in Figure 4.2. Upon addition of formic acid to suspension A), a clear yellow solution is obtained in B). Following light irradiation, the reaction mixture turns into a brown-orange murky suspension and a significant amount of carbonation is observed in C). Syringing the overlying gas, passing it through deuterated chloroform and analysing it via ^{1}H NMR revealed the presence of hydrogen gas. This could be a product of H• recombination, as previously observed in studies of hydrogen radical generation from hydrocarbons.[245]

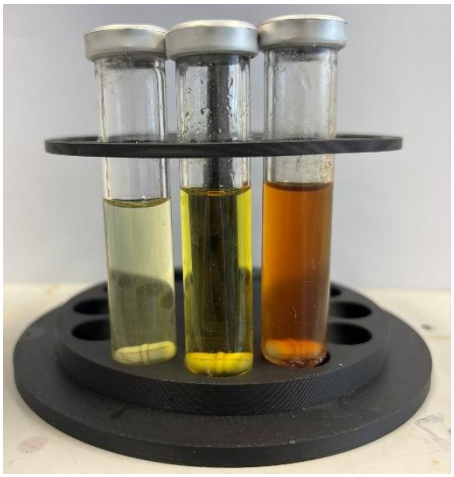

Figure 4.2: A pictorial of the reaction setup at different stages. A) Reaction mixture before addition of formic acid. B) After addition of formic acid. C) Reaction crude after 24 h of irradiation under 370 nm.

To confirm that the formed hydrogen gas is not involved in the hydrogenation reaction, we performed a control experiment where formic acid was eliminated from the reaction and the solution was saturated with and left to react under hydrogen gas atmosphere (Scheme 4.11). This change led to termination of the reaction as no product was detected and we concluded that H_2 is not responsible for the observed reactivity.

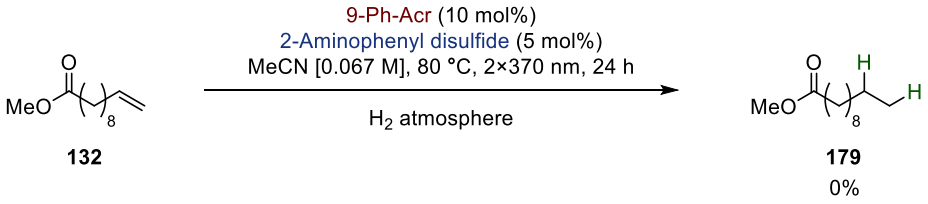

Scheme 4.11. Control experiment under hydrogen atmosphere in the absence of formic acid.

On the other hand, we sought to confirm that decarboxylation was occurring by detecting the release of CO_2. However, NMR spectroscopy was not suitable for this purpose, as the dissolved concentration of CO_2 in chloroform is extremely low due to its poor solubility. Consequently, the signal remained below the detection limit of the spectrometer, especially since ^{13}C NMR is intrinsically less sensitive than ^{1}H NMR. Thus, a qualitative technique was adopted to confirm the presence of CO_2 in the gas phase of the reaction post irradiation. Passing the headspace of the vial through a clear aqueous solution of barium hydroxide resulted in the precipitation of barium carbonate as a white solid.

4.4.1. Radical clock and spin trapping of hydrogen radical

In order to confirm the radical nature of the hydrogenation reaction, a radical clock experiment was conducted (Scheme 4.12, A). Pleasingly, subjecting malonate **241** to the standard reaction conditions for 1 day afforded the cyclised product in 64% NMR yield and a diastereomeric ratio (dr) of 4.4:1 with the major cis-isomer. A proposed mechanism of cyclisation is shown in Scheme 4.12, B. Addition of H• into one of the olefins results in a carbon centered radical that is able to undergo a rapid 5-exo-trig cyclisation with the other alkene, giving a primary radical that can be quenched in the HAT step.

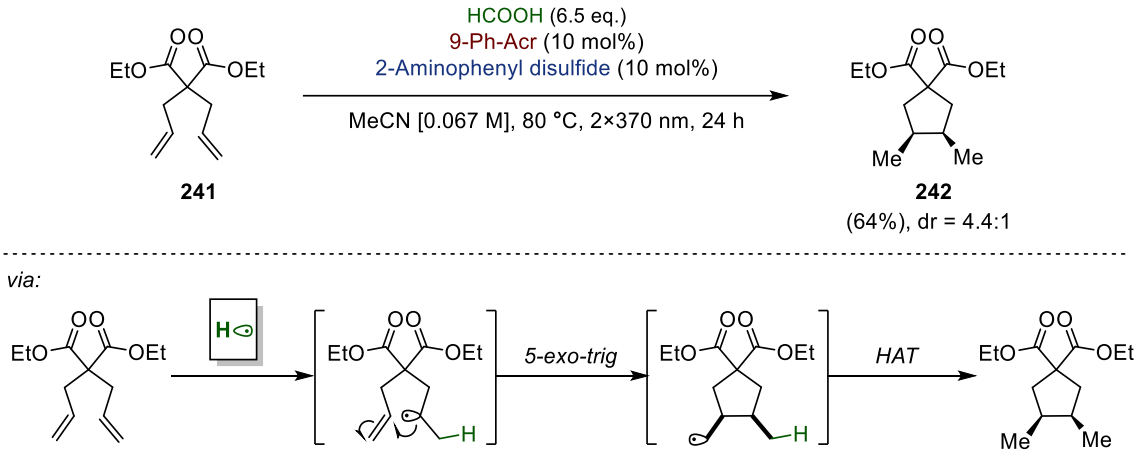

Scheme 4.12: A) Radical clock experiment using malonate **241.** B) Proposed mechanism.

Electron Paramagnetic Resonance (EPR) spectroscopy is arguably the most widely used analytical technique for detecting radical intermediates. Given the high reactivity

of hydrogen radical,[259] it would be impossible to observe its unpaired electron directly. However, a spin trapping agent that can react with H• to afford a stable adduct can be used. Thus, we selected 5,5-dimethyl-1-pyrroline-N-oxide (DMPO) which has been shown to capture H• at a rather high rate ($k = 3.8 \times 10^9\ M^{-1}\ s^{-1}$).[259] The resulting open shell species (DMPO-H) has been previously recorded to have a half-life of several minutes,[255] allowing sufficient time for an EPR spectrum to be recorded. The calculated reference data for the coupling constants of DMPO-H is α_N = 1.64 mT and α_H = 2.24 mT with a of g-factor of 2.0067,[255] which is in accord with experimentally obtained data.[310]

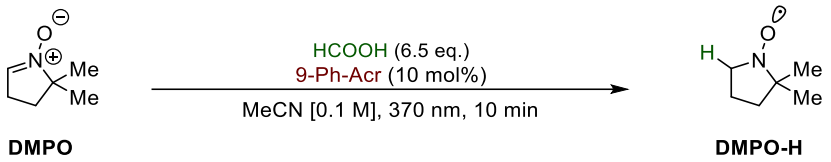

Scheme 4.13. Spin-trapping experiment of hydrogen radical using DMPO.

Upon mixing of photocatalyst with formic acid and DMPO, we observed a weak signal for the expected DMPO-H adduct. Unfortunately, the concentration of the species was too low to allow for accurate data to be recorded and the signal-to-noise ratio was too big for the coupling constants and g-factor to be correctly estimated.

4.4.2. Analysis of the photocatalyst and its deactivation pathways

To obtain further understanding of the reaction mechanism and its deactivation pathways, the photocatalyst was investigated before and after light irradiation. The ^{1}H NMR spectrum of **9-Ph-Acr** possesses a characteristic peak for H_β at 7.91 ppm displayed in Figure 4.3, A. Upon addition of formic acid (B), a downfield shift is observed from 8.20 ppm to 8.38 ppm, indicative of an interaction between the two species. A similar deshielding effect is also evident in the spectrum of the PC with the much more acidic trifluoroacetic acid (TFA) in C).

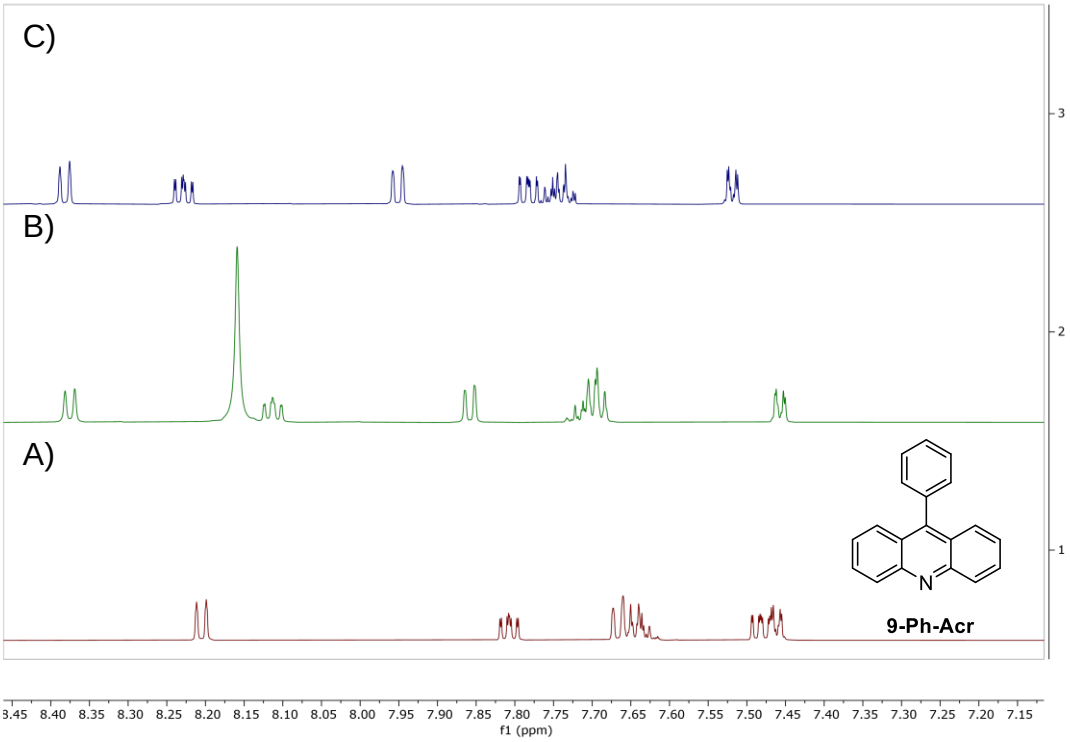

Figure 4.3. ^{1}H NMR spectra. A) **9-Ph-Acr**, B) **9-Ph-Acr** with 1 eq. formic acid and C) **9-Ph-Acr** with 1 eq. TFA.

To confirm whether **9-Ph-Acr** is coordinating or deprotonating the acid, we also investigated the nitrogen shift in ^{15}N NMR (Table 4.26). Upon addition of acid, the chemical shift undergoes a significant shift from 304 ppm for the acridine (entry 1) to 187 and 172 ppm in the presence of formic acid and TFA respectively (entries 2–3). This stark change is indicative of a protonated nitrogen, for reference, the reported chemical shift of the nitrogen in pyridine is 306 ppm whereas protonated pyridine is at 206 ppm.[311]

Table 4.26. ^{15}N Chemical shift of **9-Ph-Acr** in the presence of acids

Entry	Acid	^{15}N NMR (ppm)*
1	None	304
2	HCOOH	187
3	TFA	172

*NMR was conducted in d^{3}-MeCN.

The NMR data above would lead us to conclude that the photocatalyst exists as a formate salt under the reaction conditions. However, in our attempts to crystalise the salt and obtain its X-ray structure, we were only able to obtain 9-Ph-Acr crystals. To

explain this anomaly, the Bronsted-Lowry theory can be used. At first glance, the reported pK_a values for acridine (pK_{aH+} = 5.6)[312] and formic acid (pK_a = 3.7)[313] suggest that a facile deprotonation should take place upon mixing of the two. However, this data is in water and since the reaction solvent is MeCN, there is a significant shift in the acid-base pair equilibrium. Indeed, **9-Ph-Acr** has been reported to have a slightly higher basicity (pK_{aH+} = 12.7),[312] whereas formic acid is estimated to be significantly less acidic (pK_a = 20.9)[314] in acetonitrile. Thus, no deprotonation is possible between the PC and formic acid in the reaction medium and a hydrogen-bonded complex (**243**) is what leads to the observed shift in the ^{15}N NMR (Scheme 4.14).

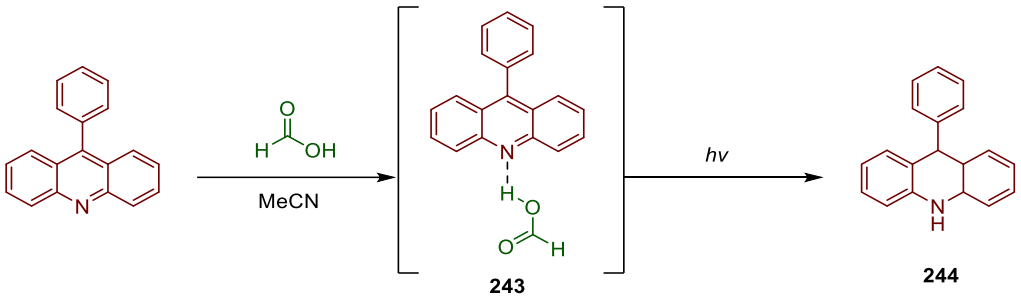

Scheme 4.14. Interactions between formic acid and 9-Ph-Acr.

Upon irradiation of complex **243** with 370 nm light, we witnessed the formation of acridan **244** in the crude NMR. This observation was confirmed by reducing **9-Ph-Acr** with a hydride source in the presence of a Lewis acid and isolating the pure product (see Appendix). The formation of **244** in the radical hydrogenation reaction is in support of our hypothesis and can be explained via the recombination of acridinyl radical with the H• (Scheme 4.15).

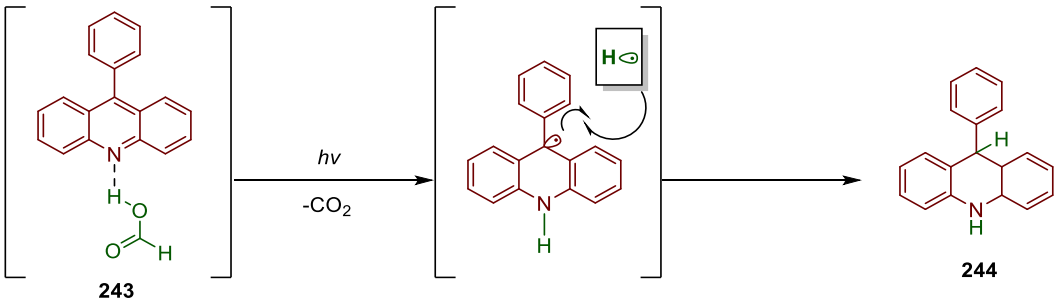

Scheme 4.15. Proposed mechanism for 9-phenyl acridan **244** formation.

The formation of acridan **244** could be a potential deactivation pathway which explains why the reaction stops after 24 h. To test this proposal, acridan **244** was employed as the photocatalyst in the hydrogenation reaction. Surprisingly, the product of

hydrogenation was obtained in similar yield to the reaction using 9-Ph-Acr, disproving the hypothesis above. In fact, irradiation of a mixture of acridan **244** with 2-aminophenyl disulfide **150** afforded **9-Ph-Acr** as product (Scheme 4.16). This control experiment proved that the HAT catalyst is a sufficient oxidant to regenerate the PC during the course of the reaction.

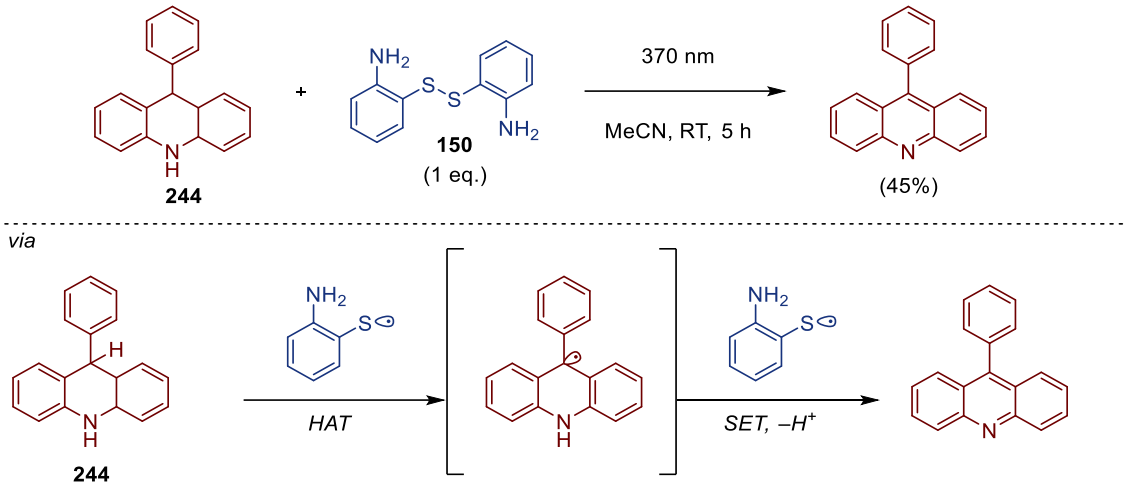

Scheme 4.16. Control experiment between 9-phenyl acridan (x) and 2-aminophenyl disulfide. Proposed mechanism involves an initial HAT step followed by SET (oxidation) of acridinyl radical.

In the absence of formic acid, acridan **244** can still afford the product of hydrogenation (Scheme 4.17). In a separate control experiment, a higher loading of acridan **244** (20 mol%) was used to generate detectable amounts of product outside of error of integration. Notably, this reaction does not proceed without HAT catalyst and it highlights a potential unique mechanistic pathway outside of the original hypothesis. Further discussion is provided in section 4.5.

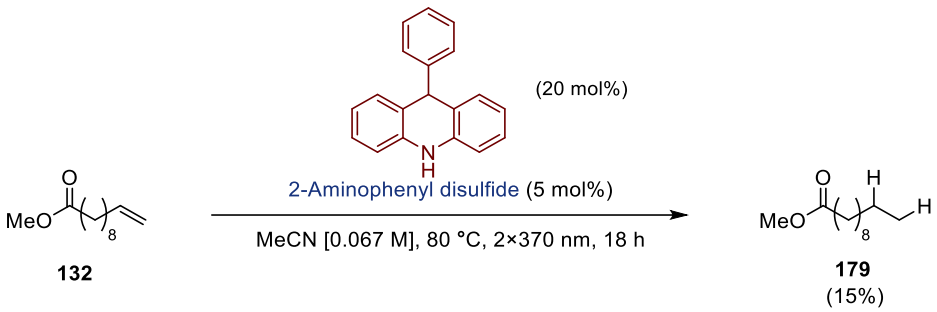

Scheme 4.17. Radical hydrogenation with 9-phenyl acridan in the absence of formic acid.

Our next goal was to establish how the PC is deactivated in the course of the reaction. We have already observed that radical recombination between the acridinyl radical and H• is a potential side reaction that is not a deactivation pathway in the presence of HAT catalyst. However, we hypothesised that there is another side reaction involving acridinyl radical that is poisoning the PC and prohibiting it from further reactivity.

To monitor changes in the PC, we analysed the crude reaction mixture by ^{1}H NMR. However, this approach proved challenging due to the complex spectrum of 9-Ph-Acr (vide supra Figure 4.3, A) and additional signals from other species present in the crude mixture. To overcome this limitation, we introduced a single fluorine atom at the ortho-position of the phenyl ring in **F-PC** (Scheme 4.18). Since a para-fluoro substituent had previously been shown to be well-tolerated under the reaction conditions (vide supra Table 4.20, entry 6), we reasoned that relocating it closer to the acridinyl radical centre would provide a more sensitive spectroscopic probe of structural changes. That is, since only the PC bears a fluorine label, monitoring the reaction by ^{19}F NMR would directly reveal changes to the photocatalyst as the reaction progresses.

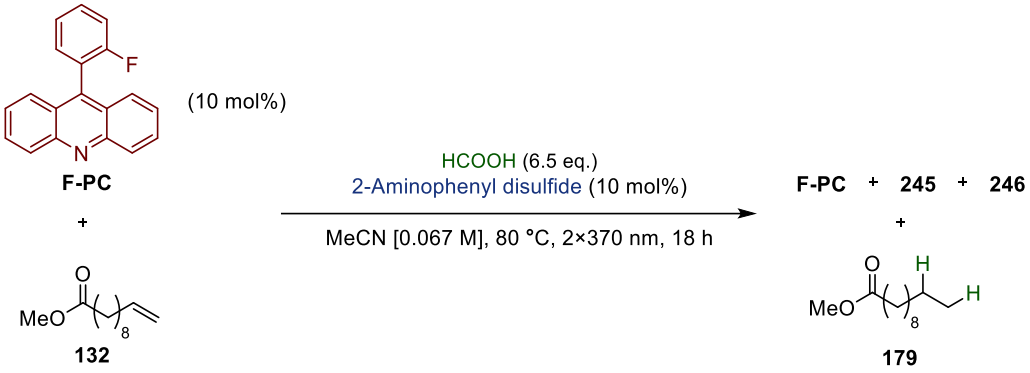

Scheme 4.18. Radical hydrogenation reaction with labelled **F-PC**.

The radical hydrogenation was carried out in the presence of **F-PC** (Scheme 4.18). The ^{19}F NMR spectrum displayed 3 major peaks: at -119 ppm assigned to the reduced **F-PC** (**245**), -113 ppm coming from remaining **F-PC** and an unidentified compound at -106 ppm (**246**) (Figure 4.4, A). Attempts to purify the latter were unsuccessful due to

coelution with other impurities, however the ^{1}H NMR gave us a hint towards a potential structure (Figure 4.4, B).

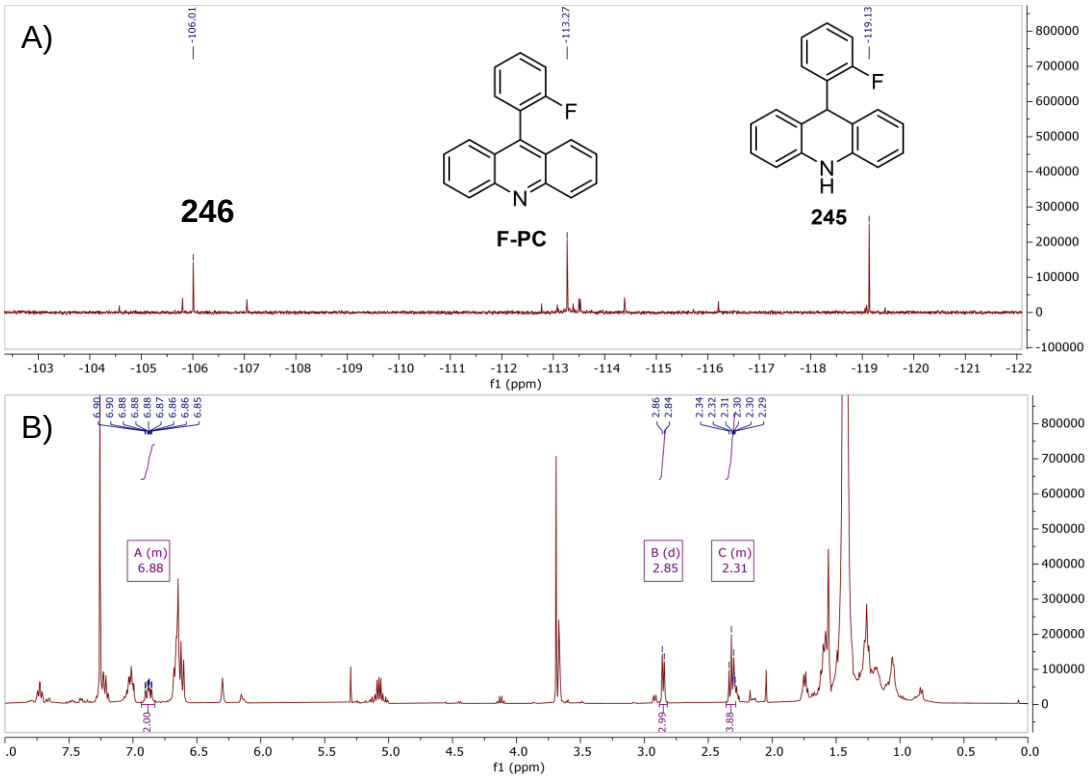

Figure 4.4. NMR analysis. A) ^{19}F NMR of crude reaction mixture. B) ^{1}H NMR of **246**.

Based on the spectrum it is clear that **246** has a significant amount of aliphatic protons. Since only the alkene substrate possesses a hydrocarbon chain, we hypothesised that a radical addition of the acridinyl radical into the olefin or recombination with a carbon centred radical has taken place. In addition, carrying out the reaction in the absence of HAT catalyst afforded mostly the reduced PC with traces of **246**. In the absence of thiyl radical, it is impossible to generate the acridinyl radical, thus the major product observed is the reduced acridine. Potential structures are shown in Scheme 4.19.

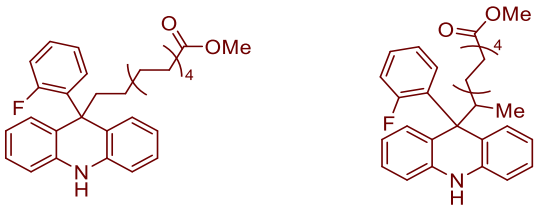

Scheme 4.19. Proposed structures of **246**.

To further prove that **246** is a product of acridinyl radical bonded to a secondary carbon centre, a radical decarboxylation of **F-PC** in the presence of cyclobutanoic acid was carried out (Scheme 4.20). Based on a literature precedent,[301] the reaction afforded

dihydroacridine **247** with a characteristic ^{19}F peak at -104 ppm. This product confirms our hypothesis that the acridinyl radical is participating in an irreversible side reaction with a secondary carbon radical that is leading to the catalyst death in the radical hydrogenation.

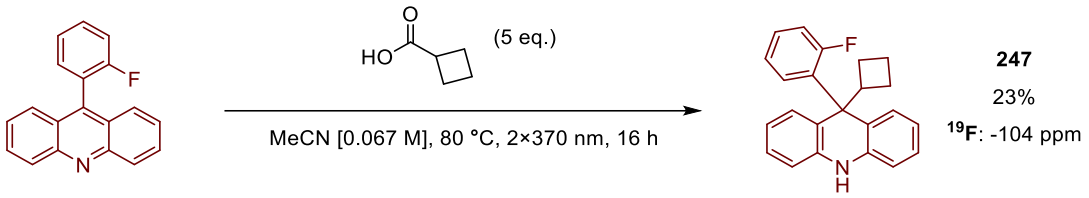

Scheme 4.20. Trapping of acridinyl radical with a secondary carbon radical.

4.5. Proposed mechanism

Taking together all the results outlined above, one potential reaction mechanism is depicted in Scheme 4.21.

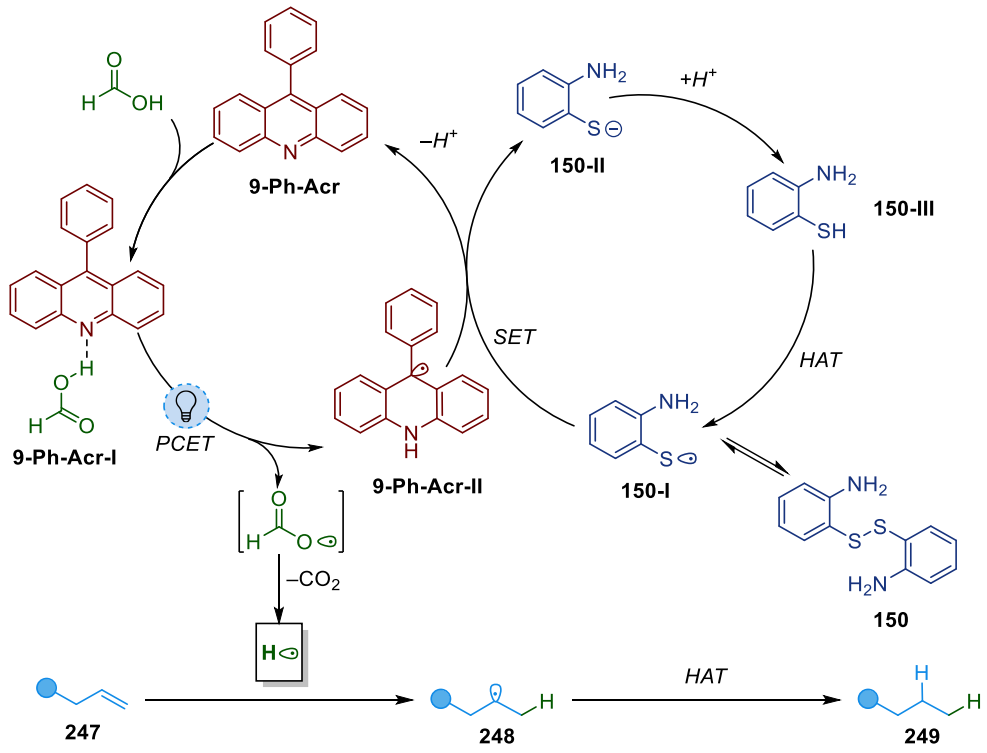

Scheme 4.21. Proposed reaction mechanism for the radical hydrogenation involving the generation of a free hydrogen atom.

Upon addition of formic acid to **9-Ph-Acr**, a photoredox-active hydrogen-bonded complex (**9-Ph-Acr-I**) is formed, as inferred from the difference in their pK_a values. Irradiation at 370 nm then triggers a PCET event, generating the formyloxy radical together with the acridinyl radical (**9-Ph-Acr-II**). The presence of (**9-Ph-Acr-II**) was

shown in the control experiment between formic acid and **9-Ph-Acr** (vide supra Scheme 4.14). Concurrently, 2-aminophenyl disulfide **150** undergoes S–S homolysis under light irradiation[160] to generate thiyl radical **150-I**. SET between acridinyl radical **9-Ph-Acr-II** and thiyl radical **150-I** followed by proton exchange generates the starting 9-Ph-Acr and the thiol HAT catalyst (**150-III**) overall completing the net redox neutral PC cycle. Evidence towards this oxidation event comes from the control experiment above (see Scheme 4.16), as well as literature precedent in similar systems.[162, 184]

Although, the reduction potentials of acridinyl radical **9-Ph-Acr-II** and thiyl radical **150-I** have not been previously reported, an estimate can be derived from similar previously studied intermediate species. For example, ortho-chlorine substituted acridinyl radical (derived from **208**) has been calculated to have a reduction potential $E_{1/2}^{red}$ = -0.33 V vs SHE[305] or $E_{1/2}^{red}$ = -0.57 V vs SCE (potential was converted by subtracting 0.24 V).[315] On the other hand, PhS• was experimentally determined to have $E_{1/2}^{red}$ = +0.16 V vs SCE[183] and since we observed it to be a sufficient oxidant of radical **9-Ph-Acr-II** (vide supra Scheme 4.16) we suggest that a facile electron transfer from **9-Ph-Acr-II** into the thiyl radical **150-I** takes place in our system.

The formyloxy radical undergoes radical decarboxylation expunging CO_2 gas, confirmed in the barium hydroxide experiment, and yielding the free hydrogen atom. H• can then undergo radical addition into an olefin (**247**), resulting in a carbon centred radical (**248**) that can participate with thiol **150-III** in a HAT reaction, regenerating the thiyl radical **150-I** and yielding the product of hydrogenation (**249**).

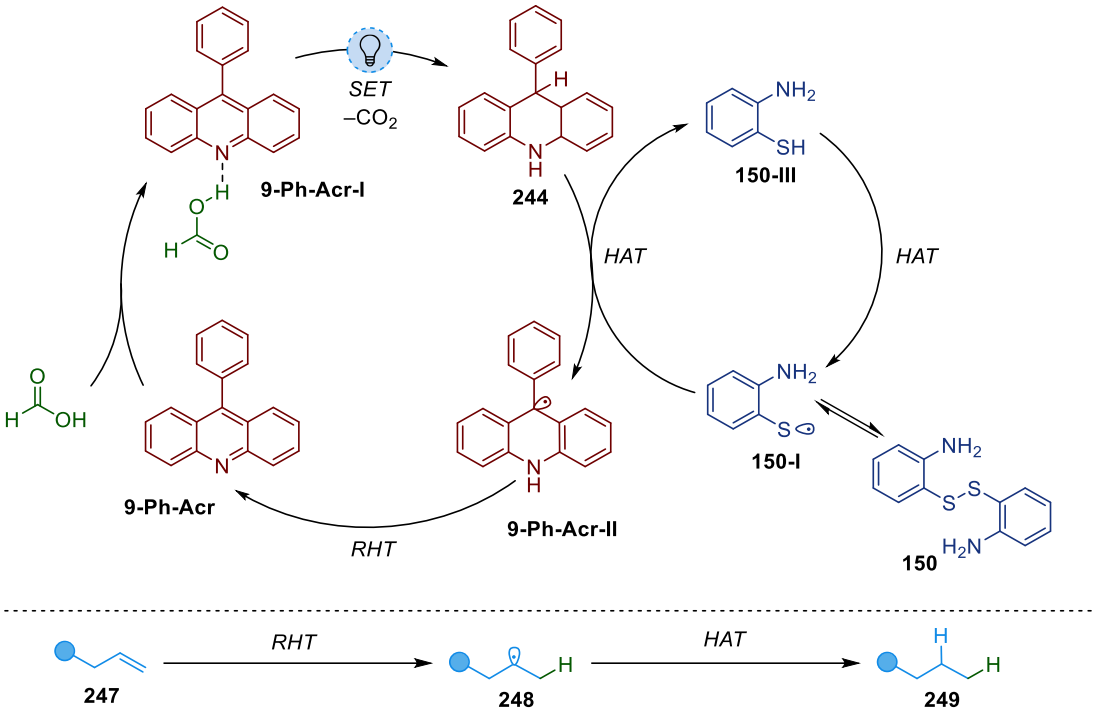

Scheme 4.22. Proposed reaction mechanism involving an RHT step.

To explain why acridan **244** is capable of hydrogenating alkenes in the absence of formic acid (vide supra Scheme 4.17) an alternative mechanism can be proposed. Following SET and radical decarboxylation, acridan **244** is formed in situ. Thiyl radical **150-I** can then undergo HAT with acridan **244** yielding acridinyl radical **9-Ph-Acr-II**. Driven by its proaromaticity, **9-Ph-Acr-II** can transfer a hydrogen atom to an olefin in a concerted RHT step.[291] This closes the PC cycle and the resulting carbon centred radical **248** can participate in another HAT with the thiol to close the HAT catalyst cycle thus yielding the hydrogenation product **249**.

4.6. Conclusion

The existence of the hydrogen atom radical has been recognised for over a century. However, the destructive nature of most methodologies for its generation, have made the smallest radical underexplored in radical chemistry. The aim of this chapter was to develop a novel strategy for the generation of H• under synthetically compatible conditions and explore its reactivity.

Towards this goal, a near-UV light-initiated radical hydrogenation of olefins was developed exploiting the radical decarboxylation of formic acid. The cooperative use of photocatalysis and HAT catalysis enabled sufficient generation of H• without the need for stoichiometric reagents to ensure catalytic turnover. Systematic optimisation identified the optimal photo- and HAT catalysts and resulted in nearly quantitative conversion of the model substrate. Substrate scope studies revealed the compatibility of the different classes of alkenes: terminal and electron deficient olefins afforded the best results while electron rich substrates were poorly tolerated.

Compelling experimental evidence confirmed the involvement of the hydrogen radical. Electron paramagnetic resonance (EPR) spectroscopy and radical clock experiments supported its transient formation, while isolation of the reduced photocatalyst provided independent verification of H• generation. Further mechanistic investigations indicated that catalyst deactivation arises primarily through recombination with carbon-centred radicals rather than reduction of the photocatalyst itself.

Two mechanistic scenarios were proposed for the radical hydrogenation: (i) direct addition of a free hydrogen atom to the alkene, consistent with the initial hypothesis, and (ii) a recombination pathway in which H• first associates with the reduced photocatalyst, followed by an RHT step to the substrate.

Taken together, this work represents the first demonstration of hydrogen radical generation and utilisation under synthetically relevant conditions. The findings establish a foundation for future developments in mild generation of H• and open new opportunities to harness its reactivity in selective transformations.

Appendix

All reactions were carried out in oven-dried glassware under an argon atmosphere unless otherwise indicated. All chemicals were used as supplied unless otherwise indicated. Column chromatography was carried out using BDH (40–60 μm) silica gel and analytical thin layer chromatography was carried out using Merck Keiselgel aluminium-backed plates coated with silica gel. Components were visualised using combinations of ultra-violet lights, iodine, ceric ammonium molybdate, phosphomolybdic acid and potassium permanganate. Melting points were determined using a Reichert hot-stage apparatus and are uncorrected. Infrared (IR) spectra were recorded on a Perkin-Elmer 1605 Fourier transform spectrometer or a Perkin-Elmer spectrum 100 FT-IR spectrometer as thin films. ^{1}H NMR spectra were recorded at 300 MHz on a Bruker AMX300 spectrometer, at 400 MHz on a Bruker AMX400 or Avance 400 spectrometer, at 500 MHz on a Bruker Avance 500 spectrometer, or at 600 MHz on a Bruker Avance 600 spectrometer in the stated solvent using residual protic solvent $CHCl_3$ (d = 7.26 ppm, s), DMSO (d = 2.56 ppm, qn) or D_2O (4.79, s) as the internal standard. Chemical shifts are quoted in ppm using the following abbreviations: s, singlet; d, doublet; t, triplet; q, quartet; qn, quintet; m, multiplet; br, broad or a combination of these. The coupling constants (J) are measured in Hertz. ^{13}C NMR spectra were recorded at 75 MHz on a Bruker AMX300 spectrometer, at 100 MHz on a Bruker AMX400 or Avance 400 spectrometer, at 125 MHz on a Bruker Avance 500 spectrometer or at 150 MHz on a Bruker Avance 600 spectrometer in the stated solvent using the central reference of $CHCl_3$ (d = 77.0 ppm, t), DMSO (d = 39.52 ppm, septet) as the internal standard. Chemical shifts are reported to the nearest 0.1 ppm. Mass spectra were obtained using either a VG70-SE or MAT 900XP spectrometer at the Department of Chemistry, University College London. Elemental analyses were performed at the Department of Chemistry, University College London. Absorbance spectroscopy was performed on a Shimazu UV-3600i Plus spectrophtometer using a Hellma Macro quartz cuvette, 100-QS with a 2 mm path length and the spectra were recorded with a 1 nm step, in the 300–1000 nm range.

The spectra of the Kessil lamps were taken from the Kessil website:

https://www.kessil.com/products/science_PR160L.php

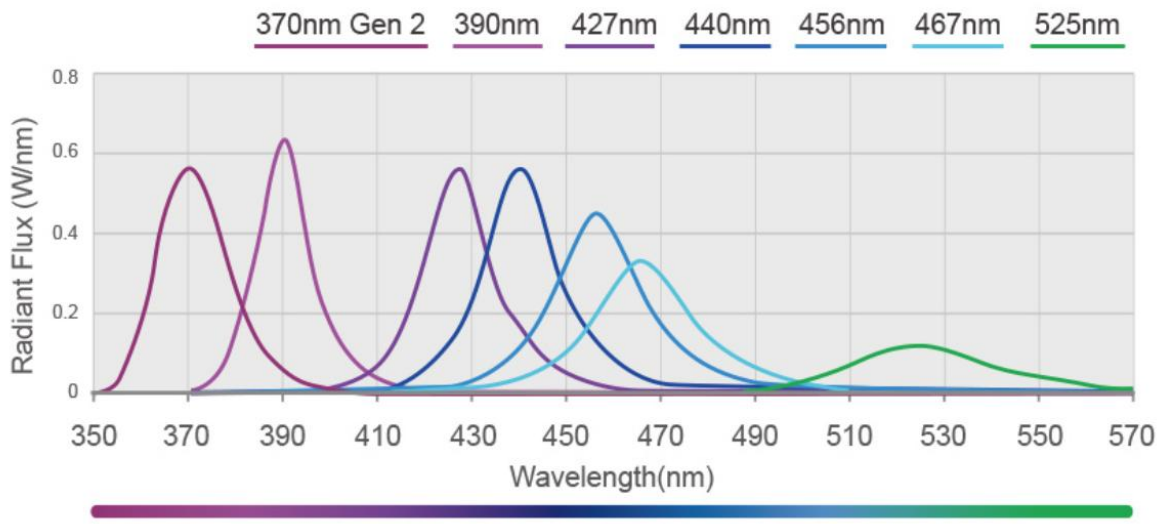

Experimental for Chapter 2

2,2'-(Ethane-1,2-diylbis(azanediyl))diphenol (56)

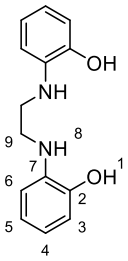

A suspension of 2-aminophenol (5.00 g, 45.8 mmol), 1,2-dibromoethane (1.79 mL, 22.9 mmol) and degassed water (20 mL) was stirred under argon at 100 °C for 16 h. The resulting precipitate was washed with EtOAc (25 mL), cyclohexane (25 mL), dried under vacuum and recrystalised from hot MeOH and washed with 10% MeOH in DCM to give diamine **56** as a purple solid (1.08 g, 19%).

^{1}H NMR (400 MHz, DMSO) δ 9.21 (s, 2H, OH), 6.68 – 6.59 (m, 4H, H5, H6), 6.54 (d, J = 7.6 Hz, 2H, H3), 6.40 (t, J = 7.5 Hz, 2H, H4), 4.79 (s, 2H, NH), 3.27 (s, 4H, H9).

^{13}C NMR (101 MHz, DMSO) δ 144.1 (C2), 137.4 (C7), 119.7 (C5), 115.7 (C4), 113.4 (C6), 109.6 (C3), 42.2 (C9).

IR ν_{max}/cm^{-1}: 3305 (w, OH), 2920 (w), 1723 (s, C–O), 1595, 1508, 1445, 1408, 1358, 1255, 1107.

1,3-Bis(2-hydroxyphenyl)-4,5-dihydro-1H-imidazol-3-ium chloride (57)

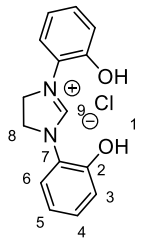

To a solution of diamine **56** (1.00 g, 4.09 mmol) in 1,4-dioxane (20 mL) was added HCl (4N in dioxane, 4.09 mL, 16.36 mmol) and resulting solution was stirred at room temperature for 15 min before it was evaporated under reduced pressure. Resulting diamine hydrochloride was not isolated but used directly in the next step. Redissolved crude with trimethyl orthoformate (20 mL) and stirred at 100 °C for 18 h. The resulting green solution was cooled in an ice-bath, triturated with ice-cold pentane (30 mL) and filtered to afford imidazolium salt **57** as a grey powder (0.76 g, 64%).

^{1}H NMR (400 MHz, DMSO): δ 11.06 (s, 2H, OH) 9.71 (s, 1H, H9), 7.40–7.38 (d, J = 7.9 Hz, 2H, H3), 7.25–7.22 (t, J = 7.9, 7.5 Hz, 2H, H4), 7.15–7.13 (d, J = 8.0 Hz, 2H, H6), 6.98–6.94 (t, J = 7.7, 7.5 Hz, 2H, H5), 4.54 (s, 4H, H8).

^{13}C NMR (101 MHz, DMSO): δ 156.2 (C9), 149.9 (C2), 128.7 (C4), 123.6 (C7), 122.8 (C3), 119.8 (C5), 116.9 (C6), 49.4 (C8).

IR (neat) ν_{max}/cm^{-1}: 3311 (br., O–H), 2942 (sp^2 C–H), 2831 (sp^3 C–H), 1449, 1415, 1115, 1022 (s, C–O).

1-Aminonaphthalen-2-ol (58)

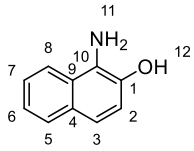

Sodium hydrasulfite (19.9 g, 114.2 mmol) was added portionwise to a solution of acid orange 7 (20 g, 57.1 mmol) in deionised water (200 mL) at 50 °C. Resulting suspension was stirred at 100 °C for 1 h before it was cooled in an ice-bath. The precipitate was filtered, washed with ice-cold water and dried under vacuum to afford **58** (7.95 g, 87%) as a pink solid.

^{1}H NMR (500 MHz, DMSO): δ 9.13 (br. s, OH), 7.94–7.93 (d, J = 8.5 Hz, 1H, H8), 7.66–7.64 (d, J = 8.1 Hz, 1H, H5), 7.31–7.28 (t, J = 8.1 Hz, 1H, H6), 7.21–7.18 (t, J = 7.5 Hz, 1H, H7), 7.09–7.05 (m, 2H, H2–3), 4.91 (br. s, 2H, NH).

^{13}C NMR (126 MHz, DMSO): δ 138.9 (C1), 128.9 (C9), 128.5 (C4), 127.8 (C5), 123.77 (C6), 123.74 (C10), 122.3 (C7), 121.5 (C8), 117.6 (C2), 116.0 (C3).

IR (neat) ν_{max}/cm^{-1}: 3385 (s), 3313 (s), 3050 (sp^2 C–H), 2619 (br.), 1632, 1604, 1574, 1361, 1329, 1275, 1255, 1179.

7a,8,15a,16-Tetrahydronaphtho[2,1-b]naphtho[1',2':5,6][1,4]oxazino[2,3-e][1,4]oxazine (59)

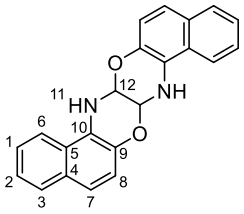

To a solution of aminonaphthol **58** (1.99 g, 12.5 mmol) in toluene (10 mL) was added water (2 mL) and glyoxal (40% wt in H_2O, 0.91 g, 6.26 mmol). The suspension was stirred under reflux in a Dean-Stark apparatus for 16 h. The resulting brown solid was filtered, washed with water and triturated from acetone with ice-cold water to give a yellow-brown powder of oxazine **59** (1.56 g, 73%).

^{1}H NMR (400 MHz, DMSO): δ 8.08–8.06 (d, J = 8.5 Hz, 2H), 7.83–7.82 (d, J = 4.2 Hz, 2H, NH), 7.79–7.77 (d, J = 8.2 Hz, 2H), 7.48–7.45 (t, J = 7.6 Hz, 2H), 7.37–7.33 (t, J = 7.8 Hz, 2H), 7.28–7.26 (d, J = 8.7 Hz, 2H), 7.02–6.99 (d, J = 8.7 Hz, 2H), 5.56–5.55 (d, J = 4.2 Hz, 2H).

^{13}C NMR (101 MHz, DMSO): δ 136.3, 129.4, 128.1, 125.1, 123.6, 122.88, 122.87, 120.4, 118.8, 118.3, 75.4.

IR (neat) ν_{max}/cm^{-1}: 3315 (br.), 2943, 2831, 1449, 1415, 1114, 1022 (s, C–O).

1,1'-(Ethane-1,2-diylbis(chloro-l5-azanediyl))bis(naphthalen-2-ol) (60)

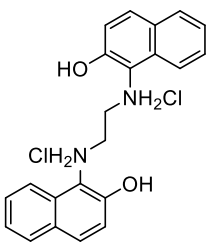

An oven-dried two-neck flask equipped with a condenser was charged with oxazine **59** (3.83 g, 11.3 mmol) and cooled under Ar. A solution of borane (1M in THF, 28.1 mL, 28.1 mmol) was introduced dropwise in an ice-bath and the mixture was stirred under reflux for 3 h. The reaction was quenched with MeOH (8 mL) at 0 °C and to the resulting green solution was introduced HCl (4N in dioxane, 5.63 mL, 22.5 mmol) and stirred at room temperature for 1h. The resulting suspension was diluted with DCM, filtered and dried under vacuum to give **60** (2.76 g, 71%) as a green solid.

^{1}H NMR (400 MHz, DMSO): 11.14 (br. s, 2H, OH), 8.17–8.16 (d, J = 8.5 Hz 2H), 7.91–7.89 (d, J = 8.1 Hz 2H), 7.83–7.81 (d, J = 8.9 Hz 2H), 7.58–7.55 (t, J = 7.6 Hz 2H), 7.42–7.38 (t, J = 7.6 Hz 2H), 7.37–7.34 (d, J = 8.9 Hz, 2H), 3.79 (br. s, 4H, NH_2), 3.72 (s, 4H).

^{13}C NMR (101 MHz, DMSO) δ 148.7, 129.2, 128.7, 128.1, 127.4, 127.3, 123.6, 120.5, 118.0, 54.9, 46.4.

IR (neat) ν_{max}/cm^{-1}: 3129, 2952, 2697, 1651, 1556, 1288.

1,3-Bis(2-hydroxynaphthalen-1-yl)-4,5-dihydro-1H-imidazol-3-ium chloride (61)

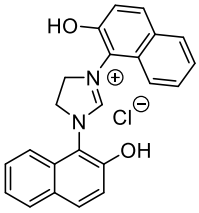

Diamine hydrochloride **60** (0.80 g, 2.05 mmol) was dissolved in triethyl orthoformate (30 mL) and stirred at 100 °C for 2 h. The resulting green solution was cooled to room temperature and triturated with ice-cold pentane. Filtration afforded imidazolium salt **61** (0.47 g, 58%) as a yellow solid.

^{1}H NMR (400 MHz, MeOD): δ 9.17 (s, 1H), 8.08–8.06 (d, J = 8.5 Hz, 2H), 7.98–7.96 (d, J = 9.0 Hz, 2H), 7.94–7.92 (d, J = 8.0 Hz, 2H), 7.72–7.68 (t, J = 7.6 Hz, 2H), 7.49–7.46 (t, J = 7.7 Hz, 2H), 7.35–7.32 (d, J = 9.0 Hz, 2H), 4.71 (s, 4H).

Note: solid was poorly soluble for ^{13}C NMR.

IR (neat) ν_{max}/cm^{-1}: 3317 (br.), 2943, 2832, 1449, 1416, 1114, 1021 (s. C–O).

Titanium isopropoxide complex of 61

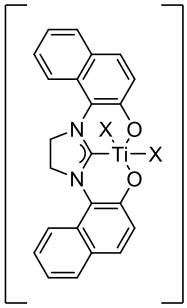

Imidazolium chloride **61** (390 mg, 1 mmol) was mixed with potassium carbonate (415 mg, 3 mmol) in THF (4 mL) under argon at room temperature. Reaction was cooled to 0°C and titanium(IV) isopropoxide (0.3 mL, 1 mmol) was added dropwise and resulting brown suspension was stirred for 14 h. Reaction was quenched with a few drops of water, evaporated under reduced pressure and crude was washed with water to give a brown solid that was insoluble in common organic solvents and could not be purified or characterised further.

1H-benzo[e][1,3]benzoxazol-2-one (62)

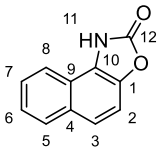

To a solution of 1-aminonaphthalen-2-ol **59** (8.00g, 50 mmol) in acetonitrile (100 mL) was added 1,1'-carbonyldiimidazole (12.2 g, 75 mmol) at 0°C and suspension was stirred for 1 h. The reaction was diluted with water (500 mL), filtered and dried under vacuum to give **62** (8.15g, 88%) as a pink solid.

^{1}H NMR (400 MHz, $CDCl_3$): δ 10.99 (br. s, 1H, NH), 7.98–7.96 (d, J = 8.3 Hz, 1H, H5/H8), 7.92–7.89 (d, J = 8 Hz, 1H, H5/H8), 7.67–7.65 (d, J = 8.8 Hz, 1H, H2), 7.61–7.57 (t, J = 7.4 Hz, 1H, H6/H7), 7.51–7.48 (t, J = 7.8 Hz, 1H, H6/H7), 7.48–7.46 (d, J = 8.8 Hz, 1H, H3),

^{13}C NMR (101 MHz, $CDCl_3$): δ 157.2 (C12), 142.2 (C1), 130.7 (C4/C9), 129.0 (C5/C8), 127.2 (C6/C7), 125.5 (C6/C7), 124.2 (C10), 123.3 (C2), 120.9 (C5/C8), 119.6 (C4/C9), 110.6 (C3).

IR (neat) ν_{max}/cm^{-1}: 3130, 3052, 1748 (s, C=O), 1462, 1432, 1377, 1277.

5-Bromo-1H-benzo[e][1,3]benzoxazol-2-one (63)

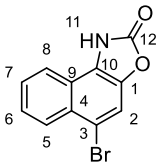

To a solution of **62** (92.5 mg, 0.5 mmol) in MeCN (2.5 mL) was added N-bromosuccinimide (98 mg, 0.55 mmol) portionwise and the resulting suspension was stirred for 30 min at 0 °C. Reaction was diluted with water (20 mL) and extracted with EtOAc (3x30 mL). Combined organic was washed with water (20 mL), brine (20 mL), dried over $MgSO_4$, filtered and evaporated under reduced pressure to give **63** (128 mg, 97%) as an orange solid. Used directly in the next step without further purification.

^{1}H NMR (500 MHz, DMSO): δ 12.58 (s, 1H, NH), 8.18–8.17 (d, J = 8.1 Hz, 1H, H8), 8.08 (s, 1H, H2), 8.08–8.06 (d, J = 8.3 Hz, 1H, H5), 7.72–7.64 (m, 2H, H6, H7).

^{13}C NMR (126 MHz, DMSO): δ 154.6 (C12), 139.1 (C1), 127.8 (C4), 127.6 (C7), 127.4 (C8), 126.9 (C6), 125.3 (C3), 121.8 (C5), 119.7 (C9), 114.9 (C2), 113.8 (C10).

IR (neat) ν_{max}/cm^{-1}: 3138, 3074, 2836, 1742, 1463, 1303.

5-(4-(Tert-butyl)phenyl)naphtho[1,2-d]oxazol-2(1H)-one (64)

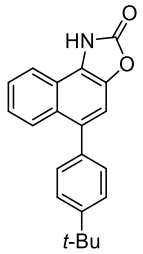

A two-neck flask equipped with a condenser was charged with 5-bromo-1H-benzo[e][1,3]benzoxazol-2-one **63** (79 mg, 0.3 mmol), (4-(tert-butyl)phenyl)boronic acid (80.1 mg, 0.45 mmol), potassium carbonate (82.9 mg, 0.6 mmol), bis(triphenylphosphine)palladium(II) dichloride (21.1 mg, 3 mol%) and water (0.2 mL). Resulting mixture was degassed by performing three cycles of evacuation and flushing with argon. Tetrahydrofuran (1 mL) was introduced, and reaction was stirred at 90 °C for 16 h. The crude NMR showed complete conversion of the starting material. Purification and full characterisation was carried out by one of our master students – Qilong Sun.

^{1}H NMR (400 MHz, DMSO): δ 12.45 (s, 1H, NH), 8.09–8.07 (d, J = 8.3 Hz, 1H), 7.86–7.84 (d, J = 8.6 Hz, 1H), 7.64–7.63 (t, J = 7.5 Hz, 1H) 7.56–7.54 (d, J = 8.1 Hz, 2H), 7.52 (s, 1H), 7.49–7.45 (t, J = 8.1 Hz, 1H), 7.41–7.39 (d, J = 8.1 Hz, 2H), 1.36 (s, 9H).

^{13}C NMR (101 MHz, DMSO): δ 155.0, 149.9, 139.1, 136.6, 134.2, 129.8, 127.9, 126.7, 126.6, 125.3, 124.3, 121.5, 119.3, 111.3, 34.4, 31.2.

1-(2-Bromoethyl)-5-(4-(tert-butyl)phenyl)naphtho[1,2-d]oxazol-2(1H)-one (65a) and 5-(4-(tert-butyl)phenyl)-1-vinylnaphtho[1,2-d]oxazol-2(1H)-one (65b)

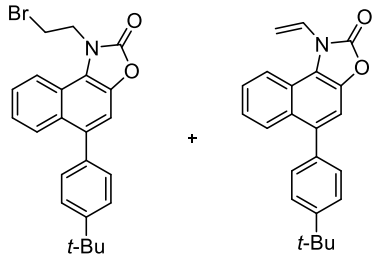

Dibromoethane (9.4 mg, 0.05 mmol) was introduced to a mixture of 5-(4-(tert-butyl)phenyl)naphtho[1,2-d]oxazol-2(1H)-one **64** (31.7 mg, 0.1 mmol) and potassium carbonate (13.8 mg, 0.1 mmol) in MeCN (0.8 mL). Resulting suspension was stirred under reflux for 14 h. Reaction mixture was diluted with water (20 mL) and extracted with DCM (3x20 mL). Combined organic was washed with water (3x20 mL), brine (20 mL), dried over $MgSO_4$, evaporated and reduced under vacuum. Column over silica gel (0–3% MeOH in DCM) gave **65a** and **65b** as an equimolar mixture.

Note: Ratio of products was determined by the presence of two triplet peaks at 4.7 and 3.8 ppm assigned to **65a** and two dublets at 6.0 and 5.6 ppm assigned to **65b**. See below for ^{1}H NMR spectrum.

N^1, N^2-Bis(2-hydroxyphenyl)oxalamide (67)

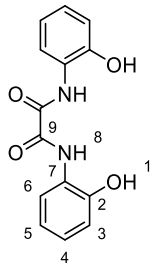

A solution of oxalyl chloride (1.29 mL, 15 mmol) was added dropwise to a suspension of 2-aminophenol (3.27 g, 30 mmol) in THF (25 mL) at 0 °C under Ar. The resulting mixture was stirred at room temperature for 3 h until complete consumption of starting material. Reaction was quenched with water (3 mL), solvent was evaporated and resulting crude was washed with water and recrystalised from hot EtOH to give phenyl oxalamide **67** (73%) as a pink solid.

^{1}H NMR (400 MHz, DMSO): δ 10.38 (s, 2H, OH), 9.87 (s, 2H, NH), 8.11–8.09 (d, J = 7.9, 1.3 Hz, 2H, H6), 7.05–7.02 (t, J = 7.9, 1.5 Hz, 2H, H5) 6.96–6.94 (d, J = 8.1, 1.2 Hz, 2H, H3), 6.89–6.85 (t, J = 8.1, 1.1 Hz, 2H, H4).

^{13}C NMR (101 MHz, DMSO): δ 157.1 (C9), 147.3 (C7), 125.5 (C5), 124.7 (C2), 119.9 (C6), 119.3 (C4), 115.1 (C3).

IR (neat) ν_{max}/cm^{-1}: 3352 (s, O–H), 2924, 2853, 1724 (s C=O), 1594 (s, C–O), 1538, 1457, 1338, 1286, 1228, 1191, 1095.

1,3-Bis(2-hydroxyphenyl)-4,5-dihydro-1H-imidazol-3-ium chloride (57)

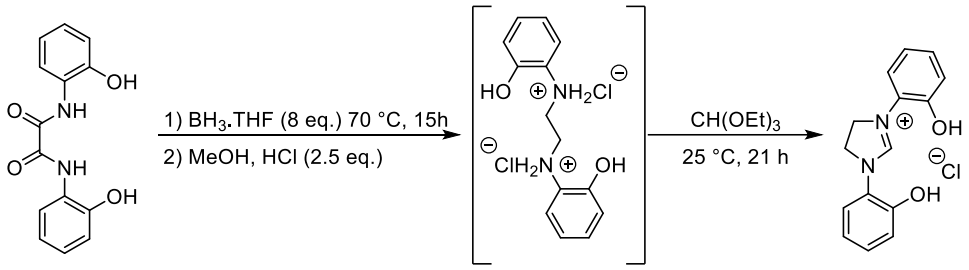

Phenyl oxalamide **67** (54.4 mg, 0.2 mmol) was dissolved in a solution of borane (1M in THF, 1.6 mL, 1.6 mmol) and heated at 70 °C under Ar atmosphere for 15 h. The reaction was quenched with MeOH (3 mL) and HCl (4N in dioxane, 0.13 mL, 0.5 mmol) was introduced and stirred at room temperature for 30 min. The suspension was evaporated to dryness and the resulting white solid was used directly in the next step without further purification. In the same reaction flask, triethyl orthoformate (0.5 mL) was introduced and the solution was stirred at room temperature under argon atmosphere for 21 h. The resulting suspension was triturated with pentane, filtered, and dried under vacuum to afford imidazolium salt **57** (51.1 mg, 88%).

N^{1},N^{2}-Bis(4-bromo-2-hydroxyphenyl)oxalamide (68)

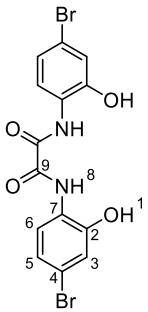

To a solution of phenyl oxalamide **67** (1.09 g, 4 mmol) and N-bromosuccinimide (1.57 g, 8.8 mmol) in acetonitrile (10 mL) was added trimethylsilyl trifluoromethanesulfonate

(0.15 mL, 20 mol%) dropwise at 0 °C. The reaction was stirred under argon atmosphere for 3 h before it was quenched with water (50 mL). The resulting precipitate was filtered and dried under vacuum to afford a mixture of bromo-phenyl oxalamide **68** (1.52 g, 13:1 ratio of product to starting material) which was used directly in the next step without further purification.

^{1}H NMR (400 MHz, DMSO): δ 10.80 (s, 2H, OH), 9.83 (s, 2H, NH), 8.25–8.24 (d, J = 2.0 Hz, 2H, H3), 7.23–7.20 (dd, J = 8.6, 2.0 Hz, 2H, H5), 6.92–6.90 (d, J = 8.6 Hz, 2H, H6).

^{13}C NMR (101 MHz, DMSO): δ 157.1 (C9), 146.8 (C7), 128.0 (C5), 126.2 (C2), 122.3 (C3), 116.9 (C6), 109.9 (C4).

IR (neat) ν_{max}/cm^{-1}: 3357 (s, O–H), 2931, 1773, 1655 (s, C–O), 1589, 1522, 1485, 1419, 1269, 1104.

1,1'-(Ethane-1,2-diyl)bis(naphtho[1,2-d]oxazol-2(1H)-one) (69)

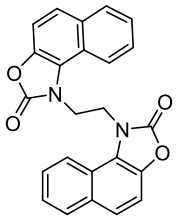

To a suspension of diamine hydrochloride **60** (2.1 g, 5.04 mmol) and potassium carbonate (1.46g, 10.6 mmol) in THF (15 mL) was introduced a solution of CDI (1.8 g, 11.1 mmol) in THF (33 mL) and reaction was stirred at room temperature for 3.5 h. The resulting suspension was poured over ice-water, filtered and dried under vacuum to afford product **69** (1.83 g, 92%) as an off-white solid.

^{1}H NMR (400 MHz, DMSO): δ 8.23–8.21 (d, J = 8.3 Hz, 2H), 8.05–8.03 (d, J = 8.0 Hz, 2H), 7.78–7.76 (d, J = 8.7 Hz, 2H), 7.57–7.55 (d, J = 8.7 Hz, 2H), 7.52–7.49 (t, J = 7.1 Hz, 2H), 7.45–7.42 (t, J = 7.9 Hz, 2H), 7.01 (s, 2H), 4.79 (s, 4H).

Note: Compound was poorly soluble for ^{13}C NMR.

IR (neat) ν_{max}/cm^{-1}: 3056, 1744, 1472, 1270, 999.

71a and 71b

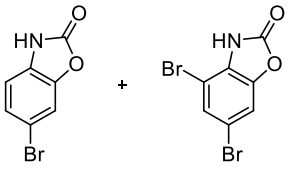

71a **71b**

To a suspension of N-bromosuccinimide (3.34 g, 18.75 mmol) in THF (20 mL) and water (7 mL) was added dropwise a solution of phenoxazole **70** (1.01 g, 7.5 mmol) in THF (5 mL). The resulting suspension was stirred at room temperature for 1 h. The reaction was quenched with water (20 mL), extracted with EtOAc (3x30 mL), combined organic was washed with water (3x30 mL), brine (50 mL), dried over $MgSO_4$, filtered and reduced under vacuum to give a mixture of 73% of **71b** and 6% of **71a**.

Note: Yield of products was identified using internal standard and identity of products was confirmed with the help of reported data.[316]

4-Bromobenzo[d]oxazol-2(3H)-one (73)

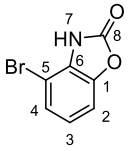

1,1'-Carbonyldiimidazole (6.08 g, 37.5 mmol) was added portion-wise to an ice-cold solution of 2-amino-3-bromophenol **72** (4.70 g, 25 mmol) in acetonitrile (45 mL). The resulting suspension was stirred for 30 min to ensure complete consumption of starting material. The reaction was poured over ice-water, filtered and dried under vacuum to give product **73** (4.75 g, 89% yield) as a yellow solid.

^{1}H NMR (400 MHz, $CDCl_3$): δ 9.06 (br. s, 1H, NH), 7.30–7.28 (d, J = 8.3 Hz, 1H, H), 7.17–7.15 (d, J = 8.0 Hz, 1H), 7.05–7.01 (t, J = 8.2 Hz, 1H).

^{13}C NMR (101 MHz, $CDCl_3$): δ 154.2, 143.9, 129.7, 126.9, 123.8, 109.2, 101.9.

IR (neat) ν_{max}/cm^{-1}: 3175, 3112, 1758 (s, C=O), 1484, 1256, 1119.

4-(4-(Tert-butyl)phenyl)benzo[d]oxazol-2(3H)-one (74)

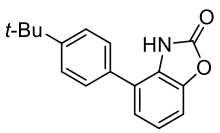

A suspension of bromophenoxazole **73** (1.24 g, 5.8 mmol), 4-tert-butylphenylboronic acid (1.55 g, 8.7 mmol), potassium carbonate (1.60 g, 11.6 mmol) and bis(triphenylphosphine)palladium(II) dichloride (116 mg, 3 mol%) in THF (6 mL) and water (1.5 mL) was stirred under argon atmosphere at 90 °C for 15 h. The reaction was cooled to room temperature, diluted with water (50 mL) and extracted with DCM (3x30ml). Combined organic was washed with water (3x30 mL), brine, dried over $MgSO_4$, filtered and evaporated under reduced pressure. Flash column chromatography over silica gel in cyclohexane then 15% EtOAc/cyclohexane afforded product **74** (1.30 g, 83%) as a white solid.

^{1}H NMR (400 MHz, $CDCl_3$): δ 9.54 (s, 1H), 7.56–7.54 (m, 2H), 7.49–7.47 (m, 2H), 7.27–7.25 (m, 1H), 7.18–7.17 (m, 2H), 1.38 (s, 9H).

^{13}C NMR (101 MHz, $CDCl_3$): δ 155.8, 151.5, 144.3, 133.4, 127.5, 127.2, 126.4, 124.9, 123.9, 122.9, 108.8, 34.8, 31.4.

IR (neat) ν_{max}/cm^{-1}: 3216, 2959 (N–H), 1766 (s, C=O), 1452, 1272, 954.

2-Amino-4'-(tert-butyl)-[1,1'-biphenyl]-3-ol (75)

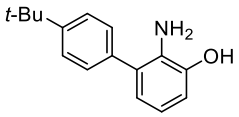

A microwave vial was charged with phenoxazole **74** (0.80 g, 3 mmol) and ammonium chloride (0.48 g, 9 mmol) and sealed under argon atmosphere. Introduced ethylene diamine (1.5 mL, 22.4 mmol) and resulting bubbling mixture was stirred at 100 °C for 17.5 h. The vial was cooled to room temperature and the resulting slurry was immediately loaded on a silica gel column (50% EtOAc/hex) resulting in aminophenol **75** (314 mg, 43%) as a white solid.

^{1}H NMR (400 MHz, DMSO): δ 9.29 (s, 1H, OH), 7.47–7.45 (d, J = 8.0 Hz, 2H), 7.37–7.35 (d, J = 8.0 Hz, 2H), 6.68–6.66 (d, J = 6.7 Hz, 1H), 6.54–6.48 (m, 2H), 4.12 (s, 2H, NH).

^{13}C NMR (101 MHz, DMSO): δ 149.0, 144.4, 136.8, 133.1, 128.2, 126.4, 125.4, 120.8, 116.8, 113.2, 34.3, 31.2.

IR (neat) ν_{max}/cm^{-1}: 3388, 2959, 2028, 1499, 1287, 802.

N^1,N^2-Bis(4'-(tert-butyl)-3-hydroxy-[1,1'-biphenyl]-2-yl)oxalamide (76)

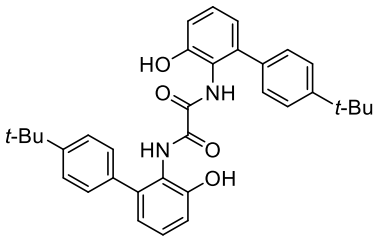

To a solution of aminophenol **75** (355 mg, 1.47 mmol) in THF (5 mL) was added a solution of oxalyl chloride (1M in THF, 0.74 mL, 0.74 mmol) dropwise at room temperature under argon atmosphere. The reaction was stirred for 2 h before it was diluted with water (20 mL) and extracted with EtOAc (3x30 mL). Combined organic was washed with water (3x30 mL), brine (30 mL), dried over $MgSO_4$, filtered and evaporated under reduced pressure. Purification via flash column chromatography (cyclohexane then 15% EtOAc/cyclohexane) afforded phenyl oxamide **76** (304 mg, 73%) as a white solid.

^{1}H NMR (400 MHz, DMSO): δ 9.69 (s, 2H), 9.52 (s, 2H), 7.37–7.35 (d, J = 8.0 Hz, 4H), 7.28–7.26 (d, J = 8.0 Hz, 4H), 7.20–7.16 (t, J = 7.9, 7.7 Hz, 2H), 6.90–6.88 (d, J = 7.9 Hz, 2H), 6.78–6.76 (d, J = 7.7 Hz, 2H), 1.31 (s, 18H).

The compound was poorly soluble for a ^{13}C NMR to be recorded.

IR (neat) ν_{max}/cm^{-1} : 2959, 2150, 1774, 1666, 1530, 1469, 1263.

1,3-Bis(4'-(tert-butyl)-3-hydroxy-[1,1'-biphenyl]-2-yl)-4,5-dihydro-1H-imidazol-3-ium chloride (78)

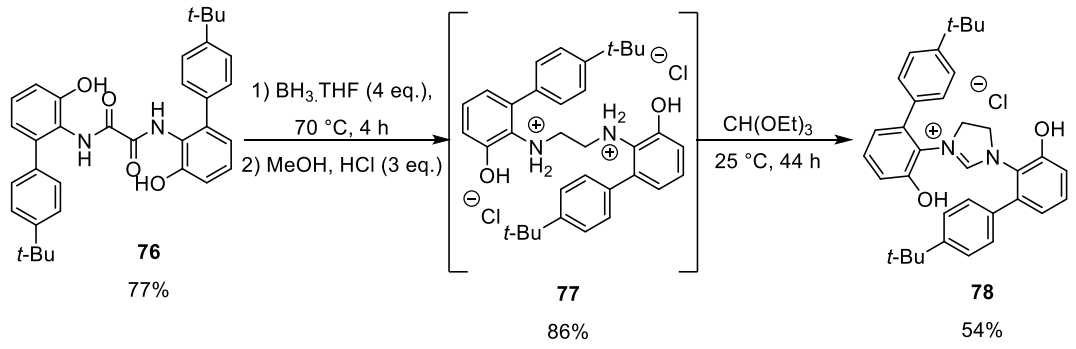

Phenyl oxalamide **76** (304 mg, 0.57 mmol) was dissolved in a solution of borane (1M in THF, 2.3 mL, 2.3 mmol) and stirred at 25 °C under Ar atmosphere for 18.5 h. The reaction was cooled in an ice-bath and quenched with MeOH (1.5 mL) and HCl (4N in dioxane, 0.43 mL, 1.72 mmol) was introduced and stirred at room temperature for 30

min. The suspension was diluted with ice-cold pentane (20 mL), filtered and dried under vacuum to give diamine salt **77** (244 mg, 86%) as a white solid. Used directly in the next step without further purification or characterisation.

77 (244 mg, 0.42 mmol) was dissolved in triethyl orthoformate (2.5 mL) under an argon atmosphere and stirred at room temperature for 44 h. Resulting suspension was diluted with pentane, filtered and triturated from hot methanol with toluene to give imidazolium salt **78** (126 mg, 54%) as an off-white solid.

^{1}H NMR (400 MHz, DMSO): δ 10.81 (s, 2H, OH), 9.11 (s, 1H),7.52–7.50 (d, 4H), 7.39–7.35 (t, 2H), 7.34–7.32 (d, 4H), 7.08–7.06 (d, 2H), 6.91–6.89 (d, 2H), 3.77 (s, 4H), 1.34 (s, 18H).

^{13}C NMR (101 MHz, DMSO): δ 153.2, 150.6, 139.4, 134.2, 130.6, 128.9, 128.3, 128.2, 125.5, 125.3, 121.0, 120.7, 115.5, 50.7, 34.4, 31.1, 21.1.

HRMS m/z (ESI) calculated for $C_{35}H_{39}O_2N_2$ [M^+] 519.3006; found 519.3002.

IR (neat) ν_{max}/cm^{-1} : 3002 (br. O–H), 2867, 1632, 1469, 1215, 1262, 1091.

2-(4-(Tert-butyl)phenyl)-4,4,5,5-tetramethyl-1,3,2-dioxaborolane (80)

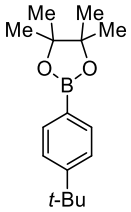

To a solution of pinacol (2.13 g, 18 mmol) in diethyl ether (35 mL), was added (4-(tert-butyl)phenyl)boronic acid and reaction was stired at room temperature for 16 h. Crude was reduced under vacuum and column over silica gel (0–10% EtOAc in cyclohexane) afforded ester **80** (3.78 g, 97%) as a white solid.

^{1}H NMR (400 MHz, $CDCl_3$): δ 7.77–7.51 (d, J = 7.8 Hz, 2H), 7.42–7.40 (d, J = 7.8 Hz, 2H), 1.33 (s, 12H), 1.32 (s, 9H).

^{13}C NMR (101 MHz, $CDCl_3$): δ 154.6, 134.8, 124.8, 83.7, 34.9, 31.3, 24.9.

80 is a known compound and its NMR spectra are in accord with published data.[317]

Reaction with $Zr(NO_3)_2$:

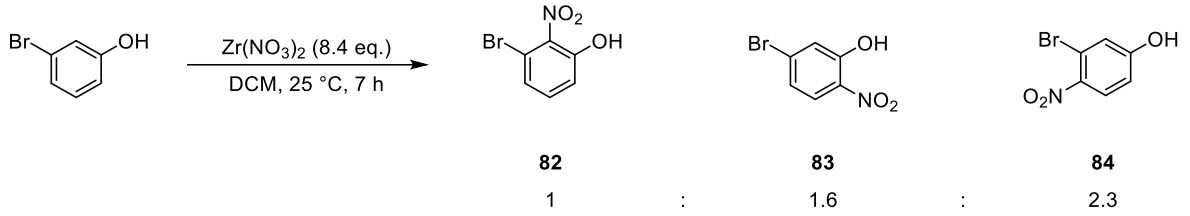

To a solution of 3-bromophenol (176 mg, 1 mmol) in DCM (2 mL) was introduced dropwise zirconyl nitrate (0.6 mL, 8.4 mmol) and reaction was stirred at room temperature for 7 h until complete consumption of starting material. Crude NMR analysis gave products **82**, **83** and **84** as a mixture of isomers in a 1:1.6:2.3 ratio.

Note: Identity of **83** and **84** was confirmed from reported data.[318, 319]

3-Hydroxy-2-nitrophenyl trifluoromethanesulfonate (86)

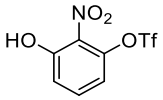

Diethylamine (230 µL, 2.2 mmol) was added dropwise to a solution of 2-nitrobenzene-1,3-diol **85** (155 mg, 1 mmol) in DCM (2 mL) and stirred for 5 min. Resulting black solution was cooled to 0 °C and trifluoromethanesulfonic anhydride (165 µL, 1 mmol) was introduced dropwise. Reaction was stirred for 30 minutes before it was quenched with aq. HCl (1M, 5 mL). Aqueous was extracted with DCM (3x20 mL) and combined organic was washed with water (3x20 mL), brine (20 mL), dried over $MgSO_4$, filtered and evaporated under reduced pressure. Column over silica gel (EtOAc in hexane 0–20%, then 100%) gave product **86** (126 mg, 44%) as a red oil.

^{1}H NMR (400 MHz, $CDCl_3$): δ 10.52 (br. s, 1H, OH), 7.57–7.53 (t, J = 8.5, 8.4 Hz, 1H), 7.21–7.19 (d, J = 8.7 Hz, 1H), 6.94–6.92 (d, J = 8.2 Hz, 1H).

^{13}C NMR (101 MHz, $CDCl_3$): 156.3, 142.6, 135.8, 120.6, 117.0, 115.3, 29.8.

^{19}F NMR (376 MHz, $CDCl_3$): δ -73.08.

IR (neat) ν_{max}/cm^{-1}: 3200 (br. O–H), 2929, 1705, 1623, 1580, 1429, 1350, 1212, 1135, 1009.

4'-(Tert-butyl)-3-nitro-[1,1'-biphenyl]-2-ol (81)

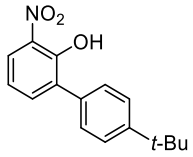

The reaction was carried out in 5 separate vials which were combined in the workup and purification step. A MW vial was charged with 2-bromo-6-nitrophenol **79** (218 mg, 1 mmol), pinacol ester **80** (390 mg, 1.5 mmol), palladium acetate (6.7 mg, 3 mol%), and tricyclohexylphosphine (16.8 mg, 6 mol%), 1,4-dioxane (3.2 mL) and introduced potassium carbonate (332 mg, 2.4 mmol) in degassed water (0.8 mL). Reaction was stirred at 120 °C under argon atmosphere for 24 h. Introduced aq. HCl (1M, 20 mL) and aqueous layer was extracted with DCM (3x50 mL). Combined organic was washed with water (50 mL), brine (50 mL), dried over $MgSO_4$, filtered and evaporated under reduced pressure. Analysis of crude NMR with 1,1,2,2-tetrachloroethane as internal standard confirmed the product yield (~90%). Column over silica gel (0–2% EtOAc in cyclohexane) followed by recrystallisation from EtOH afforded the purified product (1.09 g, 80%) as a yellow solid.

^{1}H NMR (400 MHz, $CDCl_3$): δ 11.16 (s, 1H, OH), 8.13–8.11 (d, J = 8.5 Hz, 1H), 7.66–7.64 (d, J = 7.4 Hz, 1H), 7.50 (m, 4H), 7.07–7.03 (t, J = 8.2 Hz, 1H), 1.38 (s, 9H).

^{13}C NMR (101 MHz, $CDCl_3$): δ 152.9, 151.3, 138.4, 134.2, 133.1, 132.9, 129.1, 125.4, 124.1, 119.9, 34.7, 31.4.

IR (neat) ν_{max}/cm^{-1} : 3100, 2962, 1725, 1604, 1539, 1446, 1300, 1016.

3-Amino-4'-(tert-butyl)-[1,1'-biphenyl]-2-ol (88)

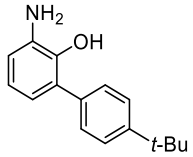

To a solution of nitrophenol **81** (1.66 g, 6.12 mmol) in MeOH/AcOH (1:1, 16 mL) was added zinc powder (2 g, 30. 6 mmol) portionwise and reaction was stirred at 70 °C for 2 h. Resulting mixture was filtered over celite and concentrated under reduced pressure. Solid was dissolved in DCM (50 mL) and washed with water (5x50 mL), brine (20 mL), dried over $MgSO_4$, filtered and evaporated under reduced pressure to afford

crude **88** (720 mg, 49%) that was used directly into the next step without further purification.

Note: the compound is unstable if kept in solution for >1 day so should be treated as soon as possible or stored as a solid at low temperature under inert atmosphere.

N^1,N^2-bis(4'-(tert-butyl)-2-hydroxy-[1,1'-biphenyl]-3-yl)oxalamide (89)

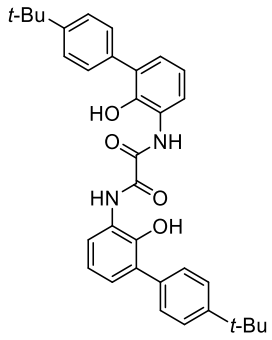

To a solution of aminophenol **88** (720 mg, 2.98 mmol) in THF (6 mL) was added a solution of oxalyl chloride (1M in THF, 1.49 mL, 1.49 mmol) dropwise at 0 °C under argon atmosphere. The reaction was stirred for 2 h before it was diluted with water (20 mL) and extracted with EtOAc (3x30 mL). Combined organic was washed with water (3x30 mL), brine (30 mL), dried over $MgSO_4$, filtered and evaporated under reduced pressure. Purification via flash column chromatography (DCM) afforded phenyl oxamide **89** (578 mg, 72%) as a white solid.

^{1}H NMR (400 MHz, $CDCl_3$): δ 9.88 (s, 2H, OH), 8.13–8.11 (d, J = 7.9 Hz, 2H), 7.54–7.52 (d, J = 8.0 Hz, 4H), 7.43–7.41 (d, J = 8.0 Hz, 4H), 7.13–7.11 (d, J = 7.5 Hz, 2H), 7.05–7.01 (t, J = 7.9 Hz, 2H), 6.25 (s, 2H, NH). 1.38 (s, 18H).

Note: The compound was poorly soluble for ^{13}C NMR.

1,3-Bis(4'-(tert-butyl)-2-hydroxy-[1,1'-biphenyl]-3-yl)-4,5-dihydro-1H-imidazol-3-ium chloride (91)

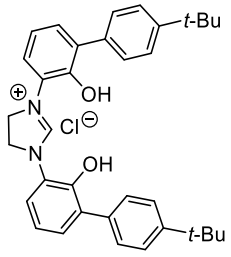

Phenyl oxalamide **89** (578 mg, 1.08 mmol) was dissolved in a solution of borane (1M in THF, 6.48 mL, 6.48 mmol) and stirred at 50 °C under Ar atmosphere for 20 h. The reaction was cooled in an ice-bath and quenched with MeOH (5 mL) and HCl (4N in dioxane, 0.6 mL, 2.4 mmol) was introduced and stirred at room temperature for 30 min. The suspension reduced under pressure and triturated with ice-cold pentane (20 mL), filtered and dried under vacuum to give diamine salt **90** (416 mg, 72% mass recovery). Used directly in the next step without further purification or characterisation.

Introduced triethyl orthoformate (11 mL) under an argon atmosphere and stirred at room temperature for 22 h. Resulting suspension was diluted with pentane, filtered and washed with methanol and cyclohexane to give imidazolium salt **91** (250 mg, 42%) as a white solid.

^{1}H NMR (400 MHz, $CDCl_3$): δ 9.85 (s, 2H), 9.35 (s, 2H), 7.45 (s, 10H), 7.37–7.35 (d, J = 7.6 Hz, 2H), 7.12–7.08 (t, J = 7.6 Hz, 2H), 4.52 (s, 4H), 1.33 (s, 18H).

^{13}C NMR (101 MHz, $CDCl_3$): δ 149.8, 148.5, 134.5, 131.7, 131.1, 128.9, 125.7, 125.1, 124.7, 120.7, 51.2, 34.3, 31.2.

IR (neat) ν_{max}/cm^{-1}: 3074, 2961, 2867, 1725, 1632, 1464, 1266, 1220, 1011.

HRMS m/z (ESI) calculated for $C_{35}H_{39}O_2N_2$ [M^+] 519.3006; found 519.3002.

N^1,N^2-bis(5-(tert-butyl)-2-hydroxyphenyl)oxalamide (93)

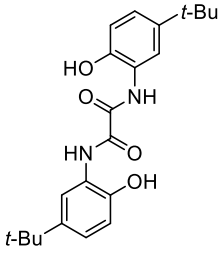

To a solution of 2-amino-4-(tert-butyl)phenol **92** (1.98 g, 12 mmol) in dry THF (14 mL) was added a solution of oxalyl chloride (1M in THF, 6 mL, 6 mmol) dropwise at 0 °C under argon atmosphere. The reaction was stirred for 3 h before it was diluted with water (20 mL) and extracted with EtOAc (3x30 mL). Combined organic was washed with water (3x30 mL), brine (30 mL), dried over $MgSO_4$, filtered and evaporated under reduced pressure. The crude was triturated with pentane (x3) and dried under vacuum to afford phenyl oxamide **93** (1.59 g, 69%) as an off-white solid.

^{1}H NMR (400 MHz, DMSO) δ 10.18 (s, 2H), 9.85 (s, 2H), 8.24 (d, J = 2.4 Hz, 2H), 7.05 (dd, J = 8.5, 2.4 Hz, 2H), 6.87 (d, J = 8.4 Hz, 2H), 1.26 (s, 18H).

^{13}C NMR (101 MHz, DMSO) δ 157.1, 144.8, 141.6, 124.2, 122.1, 116.7, 114.5, 33.9, 31.3.

93 is a known compound and its NMR spectra are in accord with published data.[320]

1,3-Bis(5-(tert-butyl)-2-hydroxyphenyl)-4,5-dihydro-1H-imidazol-3-ium chloride (94)

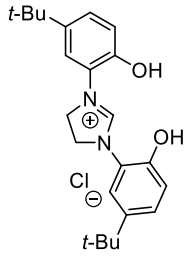

Phenyl oxalamide **93** (1.59 g, 4.14 mmol) was dissolved in a solution of borane (1M in THF, 16.6 mL, 16.6 mmol) and stirred at 50 °C under Ar atmosphere for 5 h. The reaction was cooled in an ice-bath and quenched with MeOH (5 mL) and HCl (1N in EtOAc, 9.10 mL, 9.10 mmol) was introduced and stirred at room temperature for 30 min. The suspension reduced under pressure, redissolved in MeOH and evaporated under vacuum for a total of three cycles. The crude was used directly in the next step without further purification or characterisation.

Introduced triethyl orthoformate (14 mL) under an argon atmosphere and stirred at room temperature for 19 h. Resulting suspension was diluted with ice-cold pentane, filtered, washed with ice-cold pentane and dried under vacuum to give imidazolium salt **94** (1.19 g, 71%) as an orange solid.

^{1}H NMR (500 MHz, DMSO) δ 10.61 (d, J = 2.1 Hz, 2H), 9.48 (s, 1H), 7.38 (d, J = 2.4 Hz, 2H), 7.28 (dd, J = 8.6, 2.3 Hz, 2H), 7.00 (d, J = 8.5 Hz, 2H), 4.57 (s, 4H), 1.28 (s, 18H).

^{13}C NMR (126 MHz, DMSO) δ 156.7, 147.9, 142.5, 125.9, 123.1, 120.4, 116.6, 49.9, 34.1, 31.3.

94 is a known compound and its NMR spectra are in accord with published data.[321]

Titanium isopropoxide complex of 94 (95)

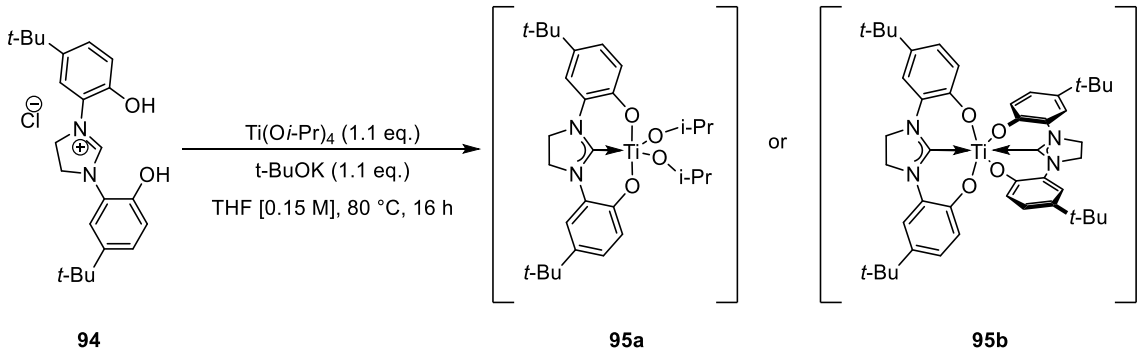

94 **95a** **95b**

To a solution of imidazolium salt **94** (60 mg, 0.15 mmol) and potassium tert-butoxide (19 mg, 0.165 mmol) in anhydrous THF (1 mL) was added a solution of titanium(IV) isopropoxide (1M in THF, 0.165 mL, 0.165 mmol) under Ar atmosphere. The reaction was stirred at 80 °C for 16 h, before it was concentrated under reduced pressure. The crude was triturated with ice-cold pentane to afford complex **95** (48 mg, 60%) as judged by the disappearance of the phenolic O–H and imidazolium C–H protons.

Note: The structure was not determined and two proposed structures (**95a** and **95b**) are given.

^{1}H NMR (400 MHz, $CDCl_3$) δ 6.98 (s, 2H), 6.81 (d, J = 8.6 Hz, 2H), 6.25 (d, J = 8.5 Hz, 2H), 4.46 (s, 4H), 1.31 (s, 18H).

^{13}C NMR (101 MHz, $CDCl_3$) δ 200.6, 152.9, 140.7, 129.2, 120.7, 116.6, 112.6, 47.4, 34.3, 31.8.

General procedure for deoxygenation reactions

A MW vial was charged with ligand (10 mol%), base (0.2 mmol), zinc powder (26.1 mg, 0.4 mmol) and $TiCl_4$ (0.1 mL, 0.1 M in DCM) under Ar. The solvent was evaporated under reduced pressure and 2,2-difluoroethanol (6.3 µL, 0.1 mmol), 1,1-diphenylethylene (35 µL, 0.2 mmol) and triisopropylsilyl chloride (64.2 µL, 0.3 mmol) were added under Ar. Introduced solvent (1 mL) and the reaction was stirred at the indicated temperature for 24 h. The internal standard was added directly and an aliquot taken for NMR analysis.

NMR spectra for Chapter 2

2,2'-(Ethane-1,2-diylbis(azanediyl))diphenol (56)

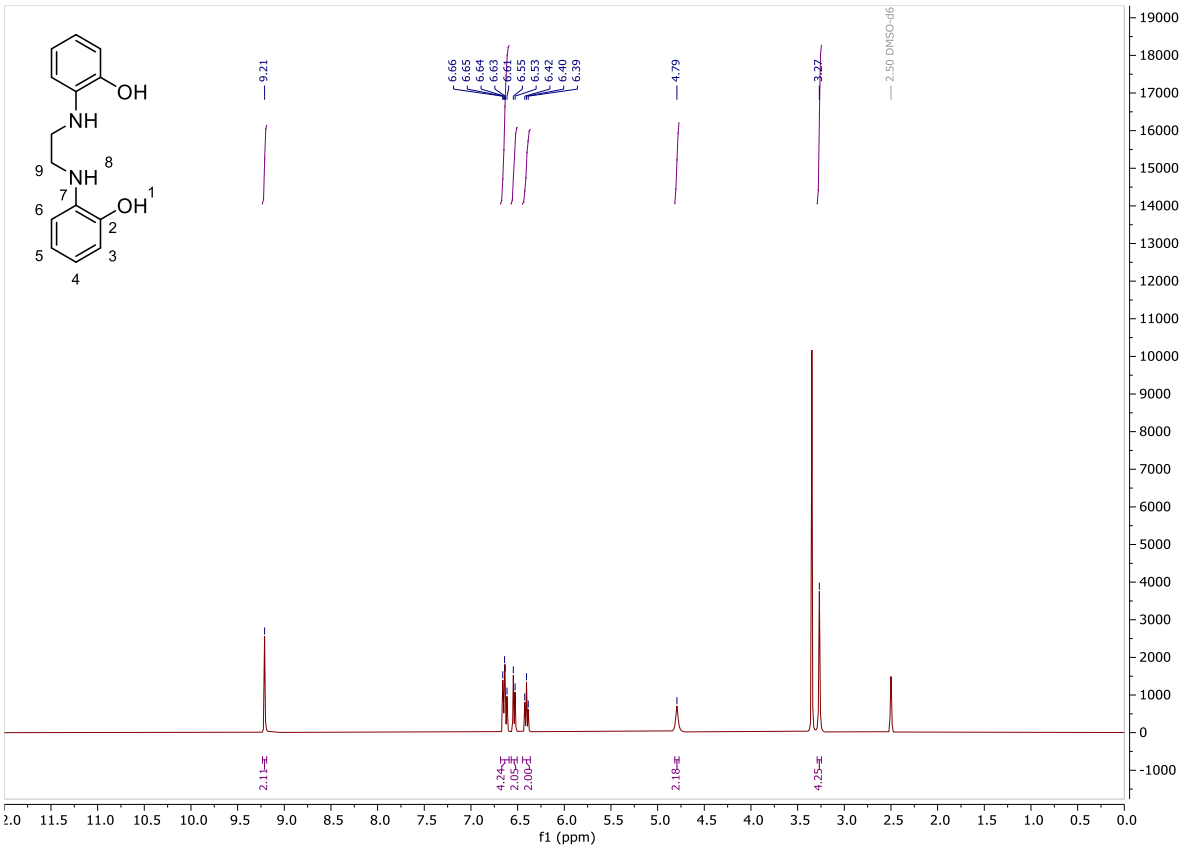

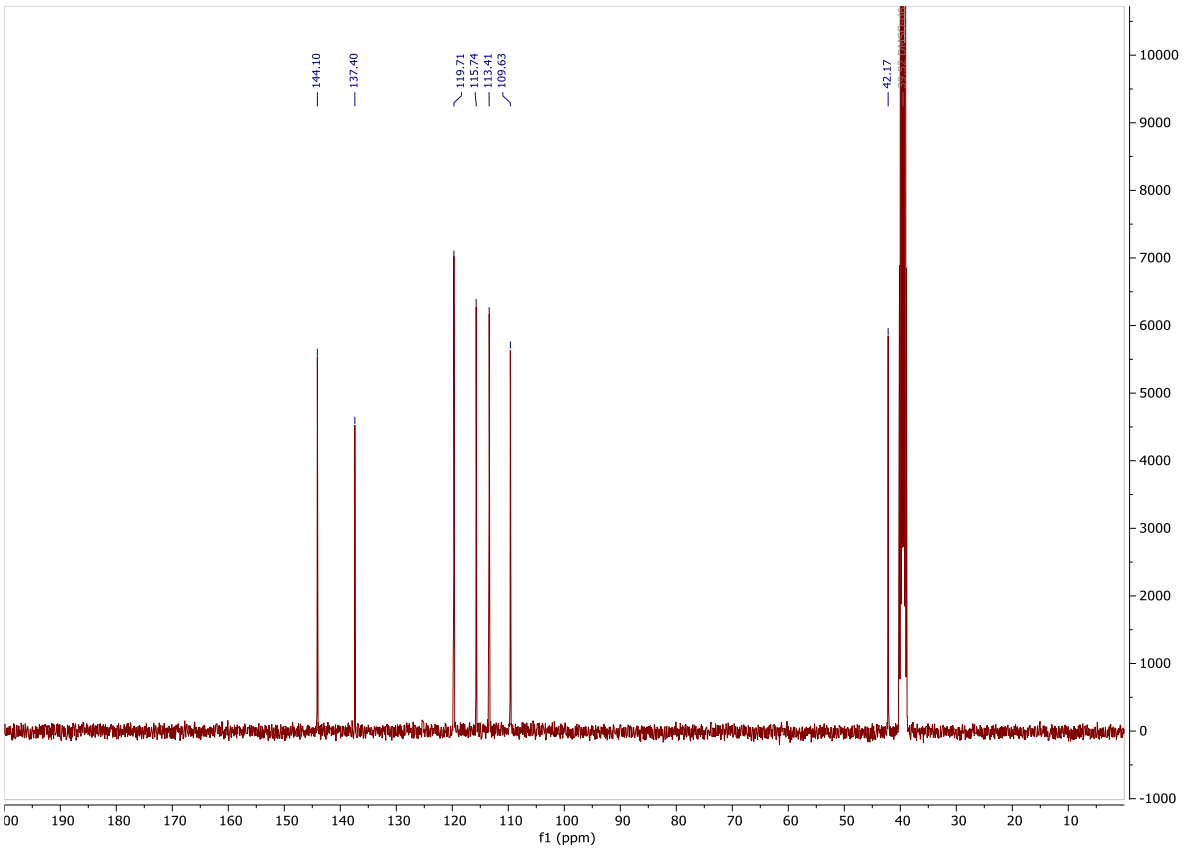

1,3-Bis(2-hydroxyphenyl)-4,5-dihydro-1H-imidazol-3-ium chloride (57)

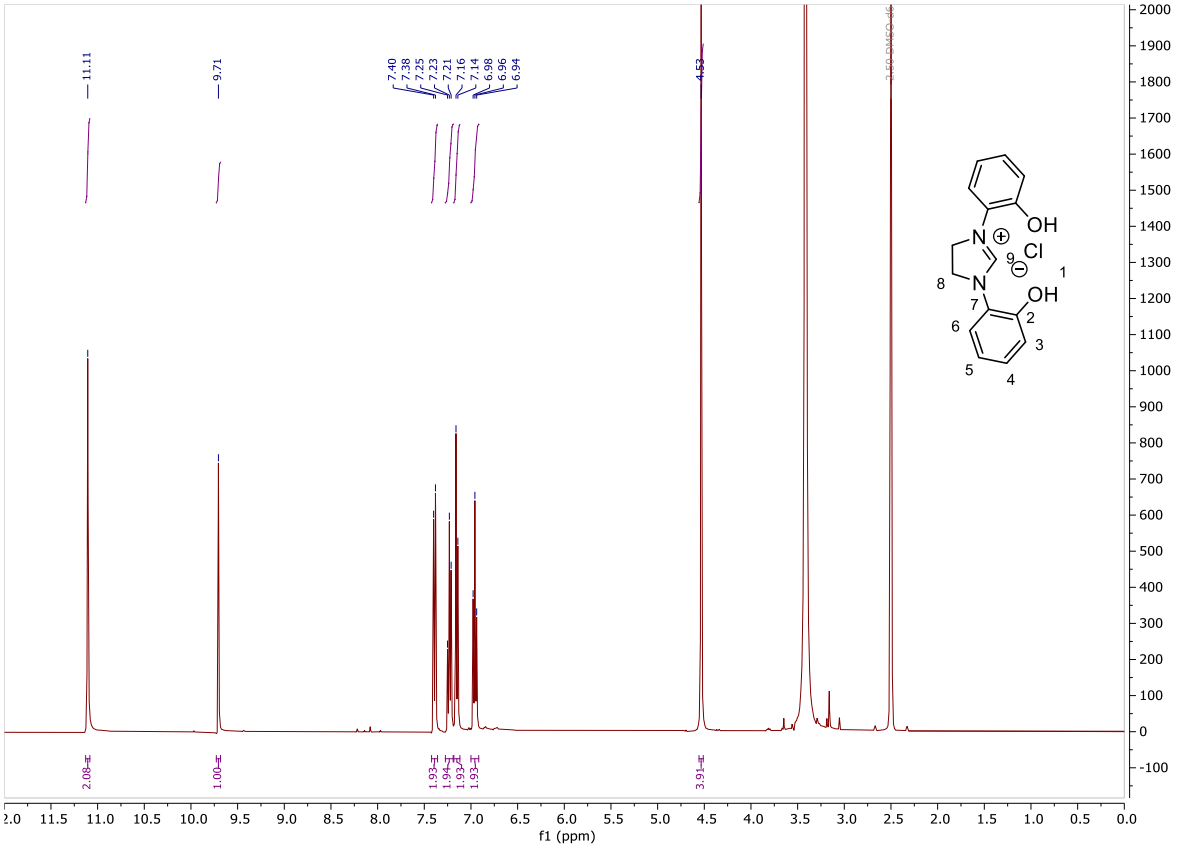

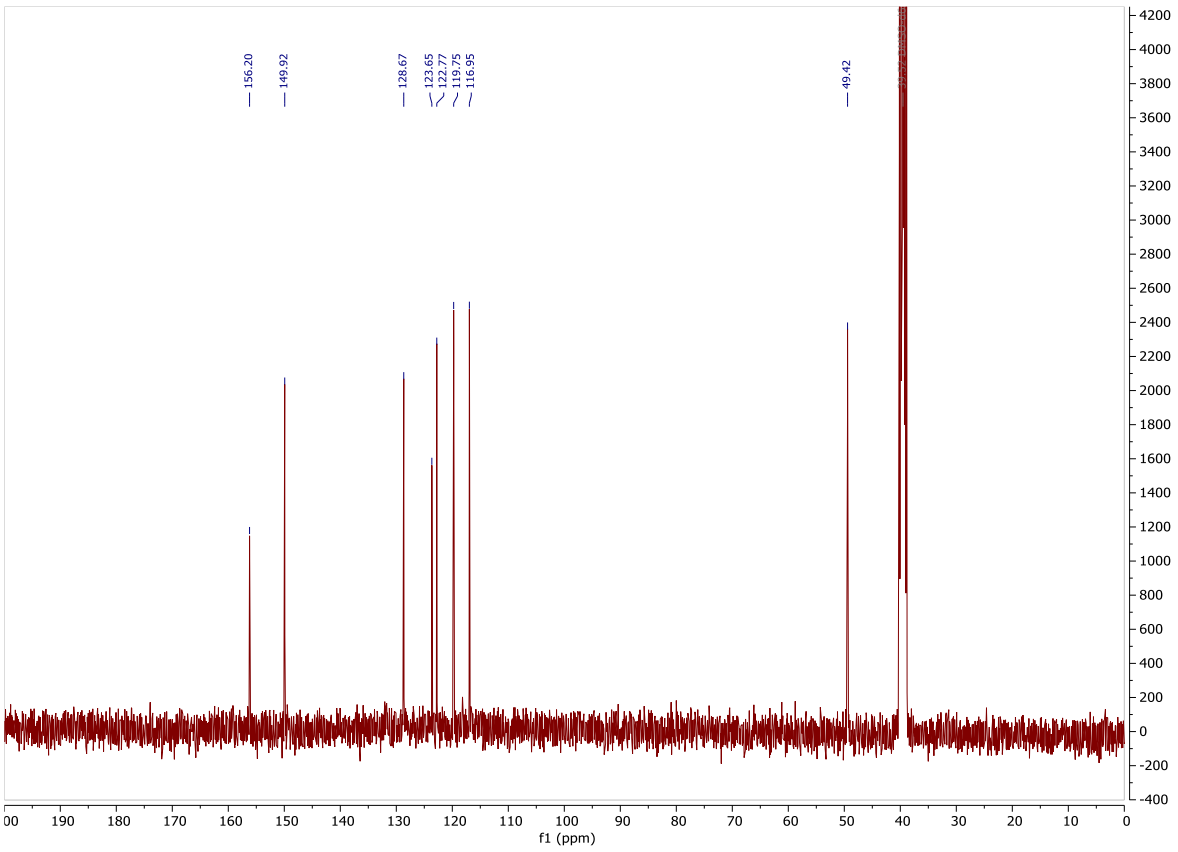

1-Aminonaphthalen-2-ol (58)

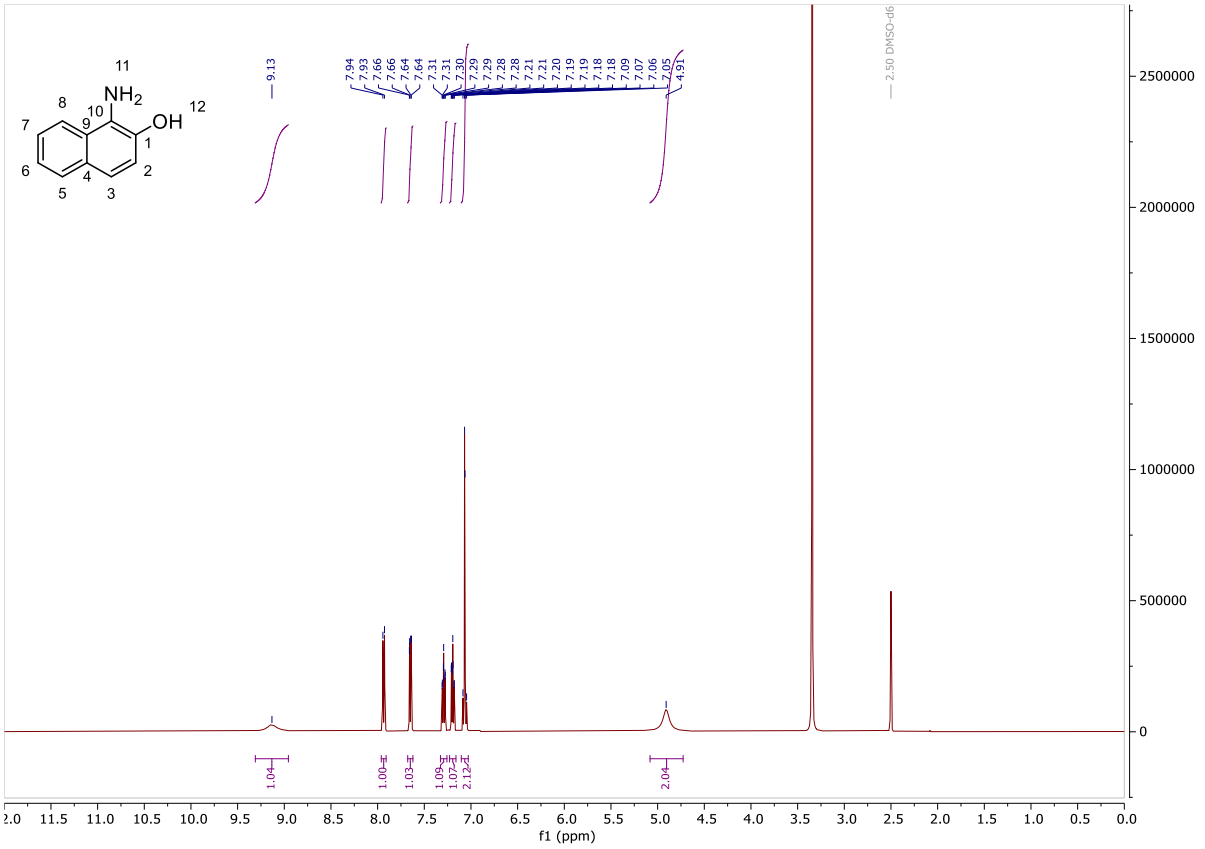

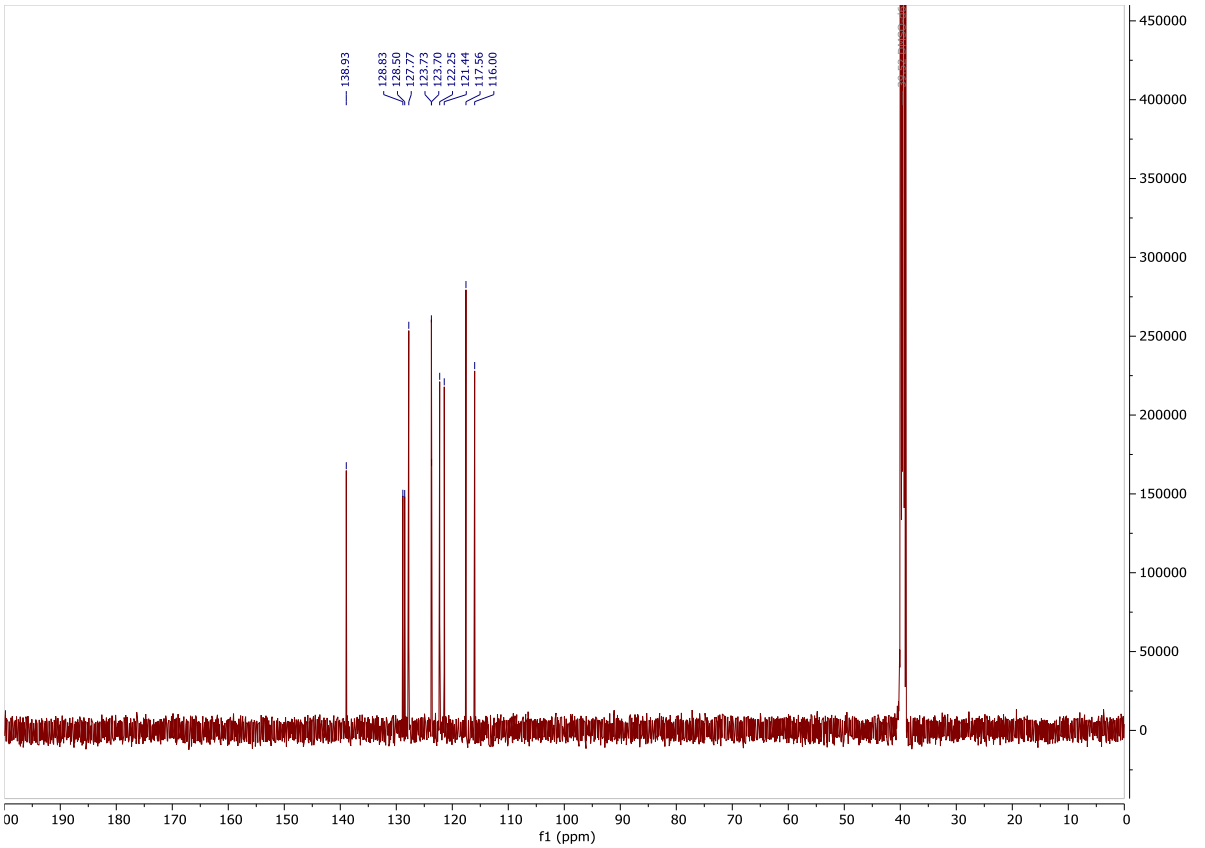

7a,8,15a,16-Tetrahydronaphtho[2,1-b]naphtho[1',2':5,6][1,4]oxazino[2,3-e][1,4]oxazine (59)

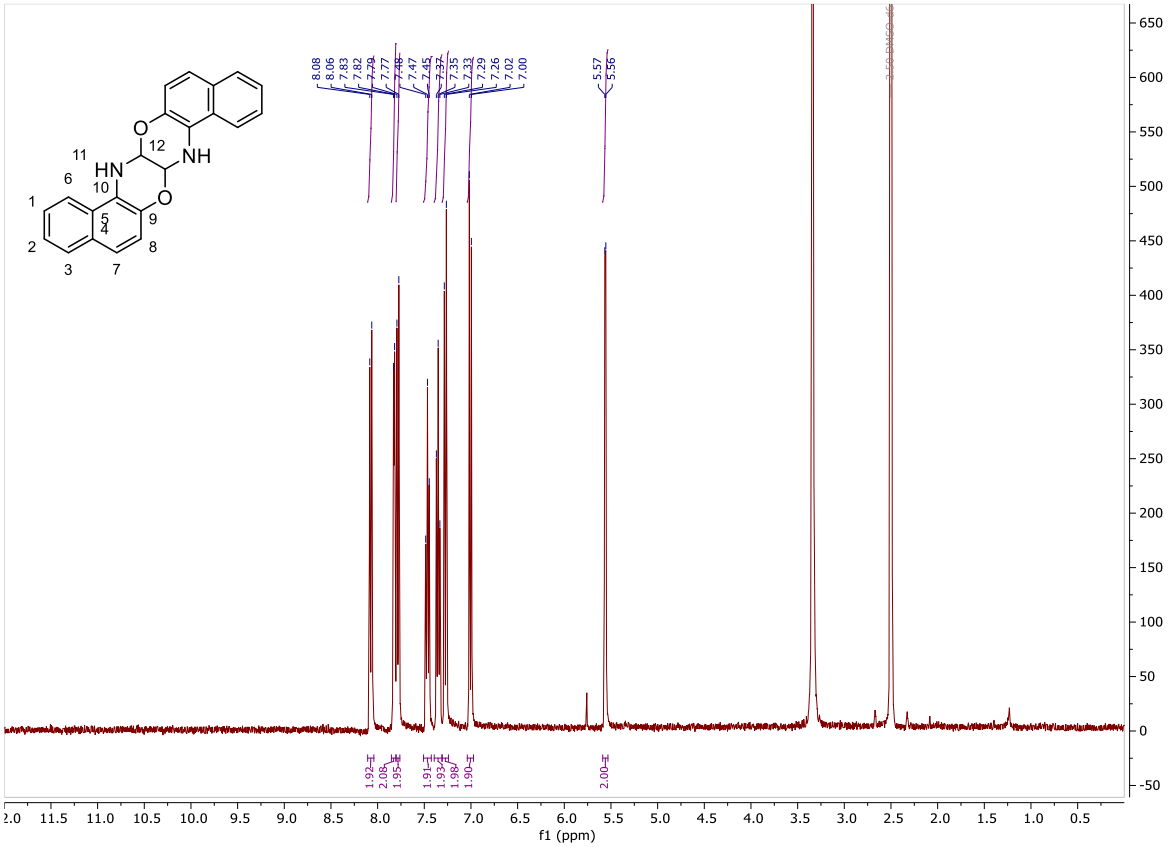

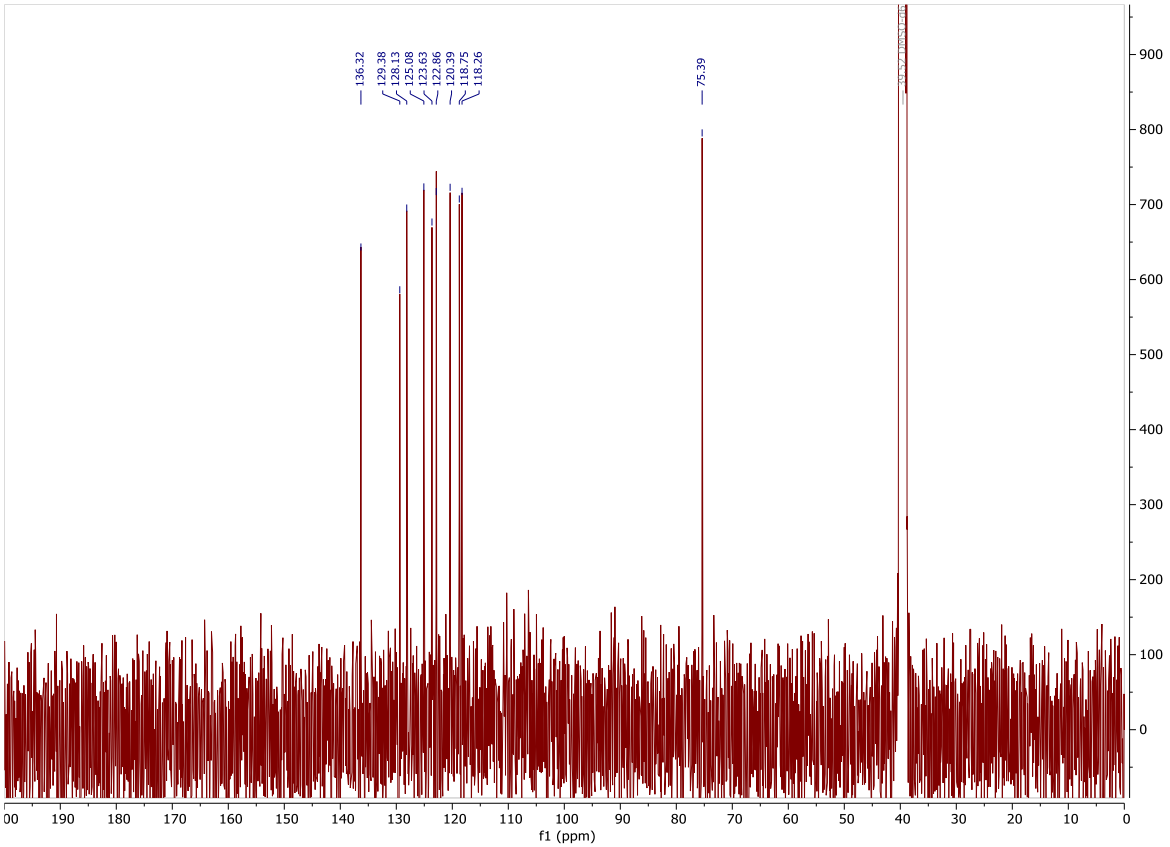

1,1'-(Ethane-1,2-diylbis(chloro-l5-azanediyl))bis(naphthalen-2-ol) (60)

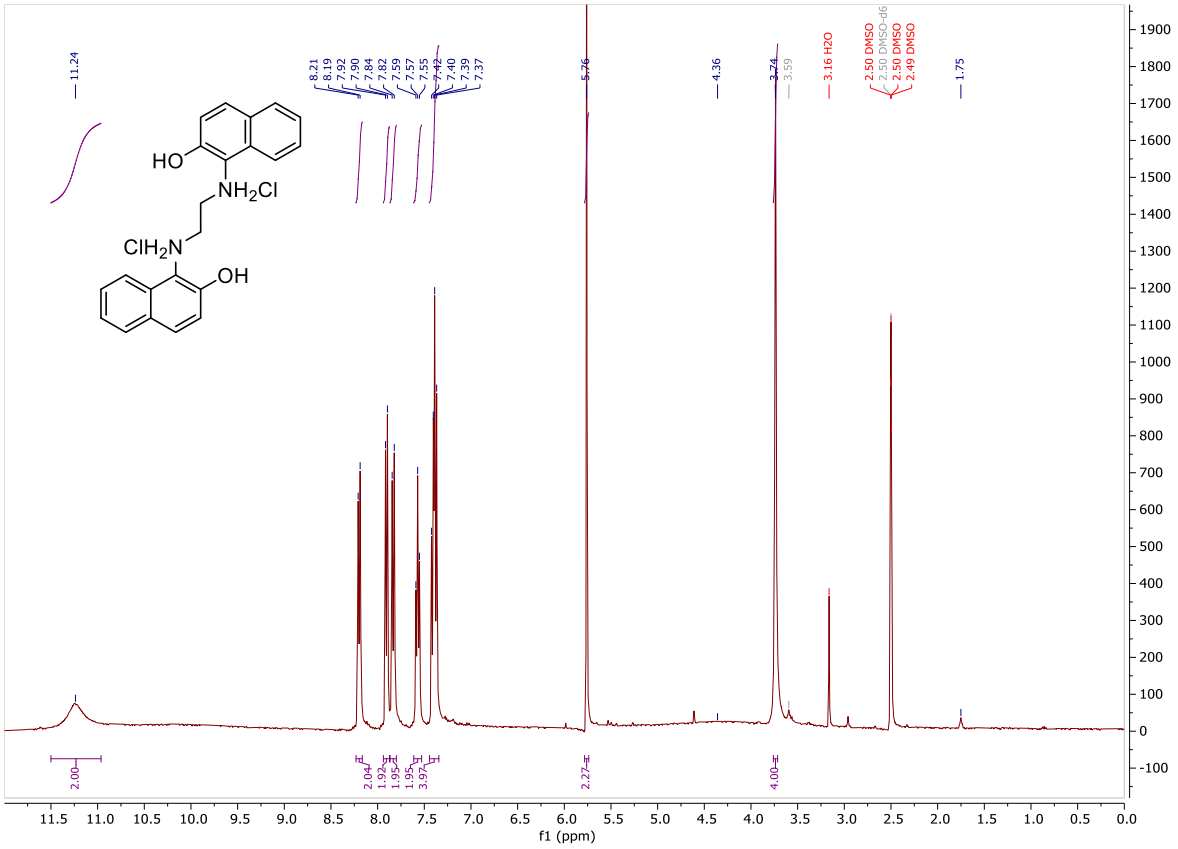

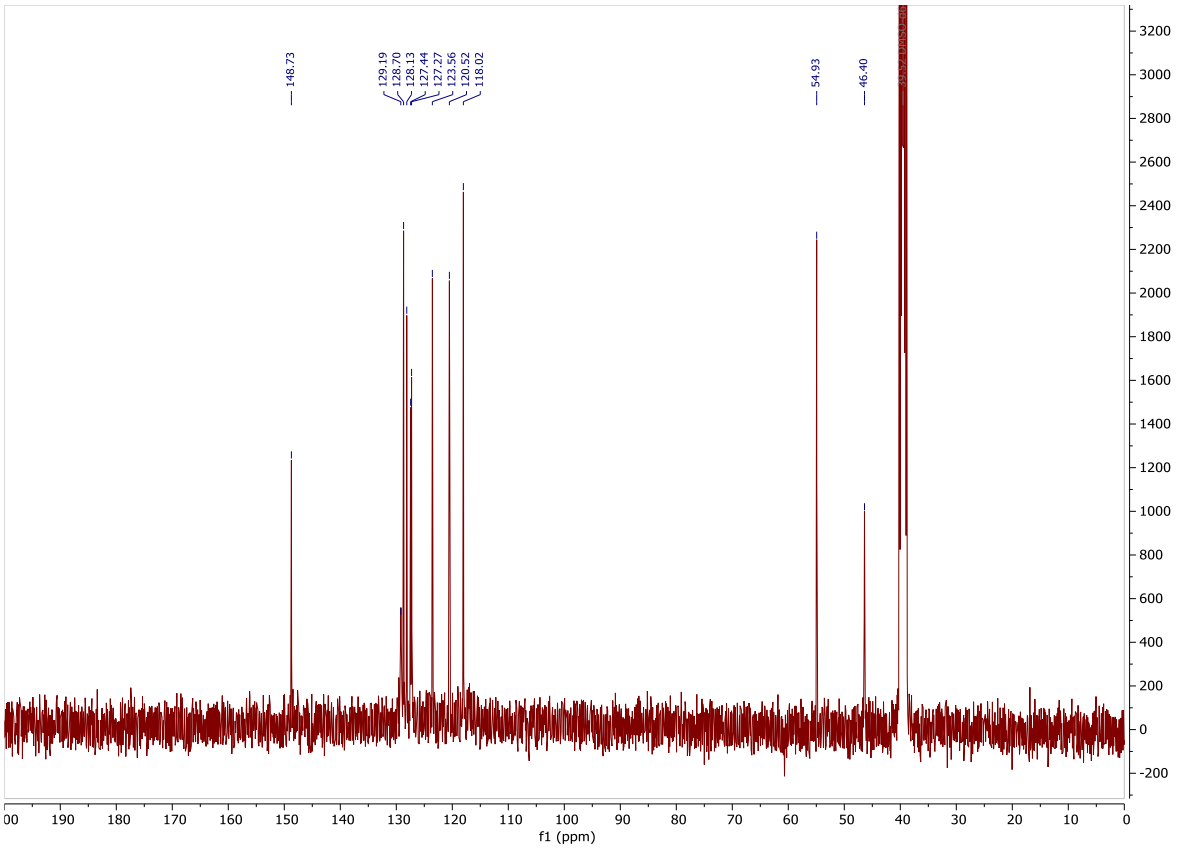

1,3-Bis(2-hydroxynaphthalen-1-yl)-4,5-dihydro-1H-imidazol-3-ium chloride (61)

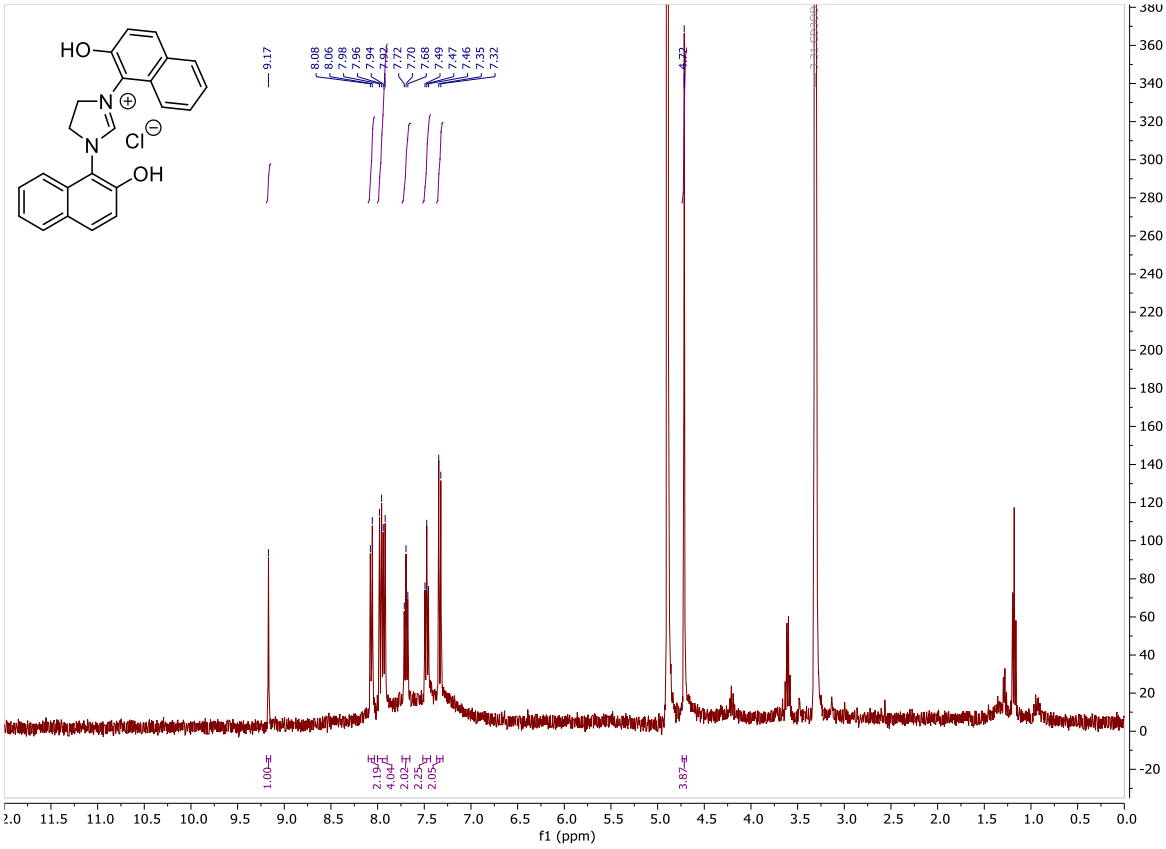

1H-benzo[e][1,3]benzoxazol-2-one (62)

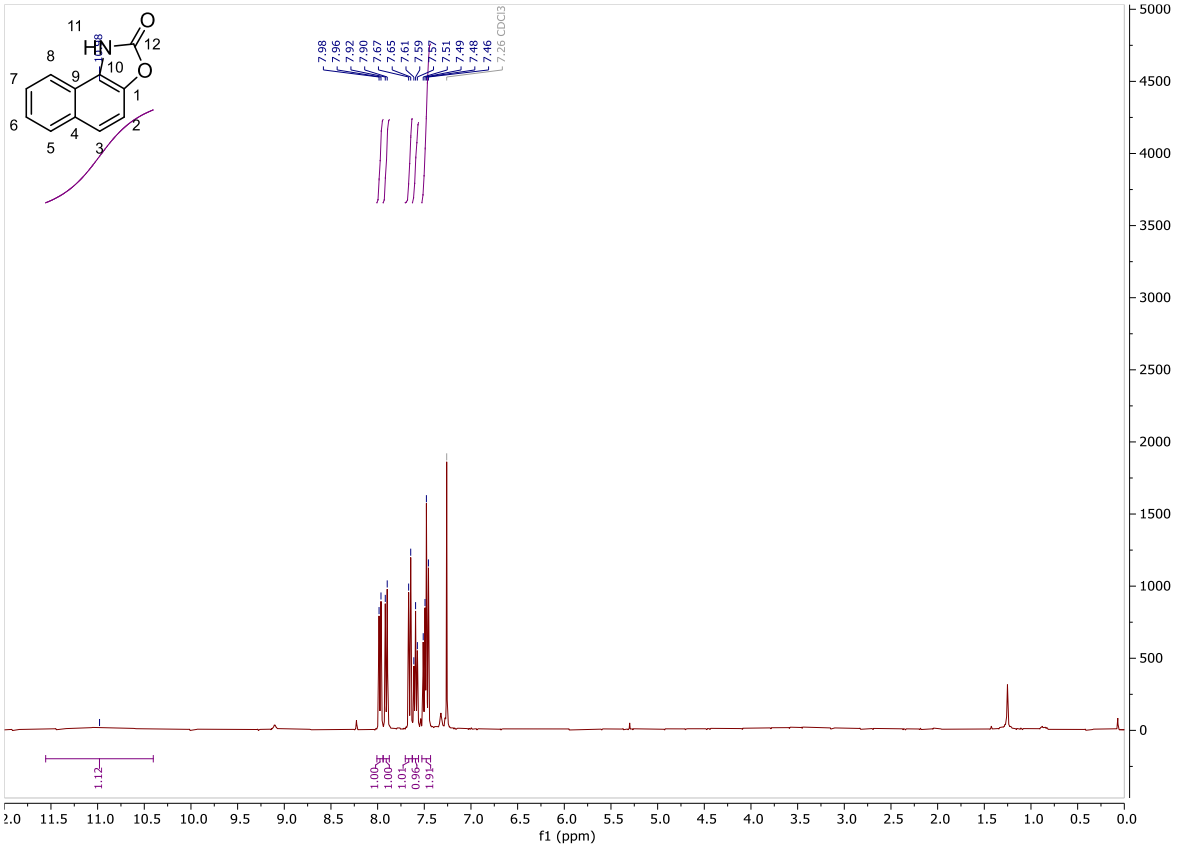

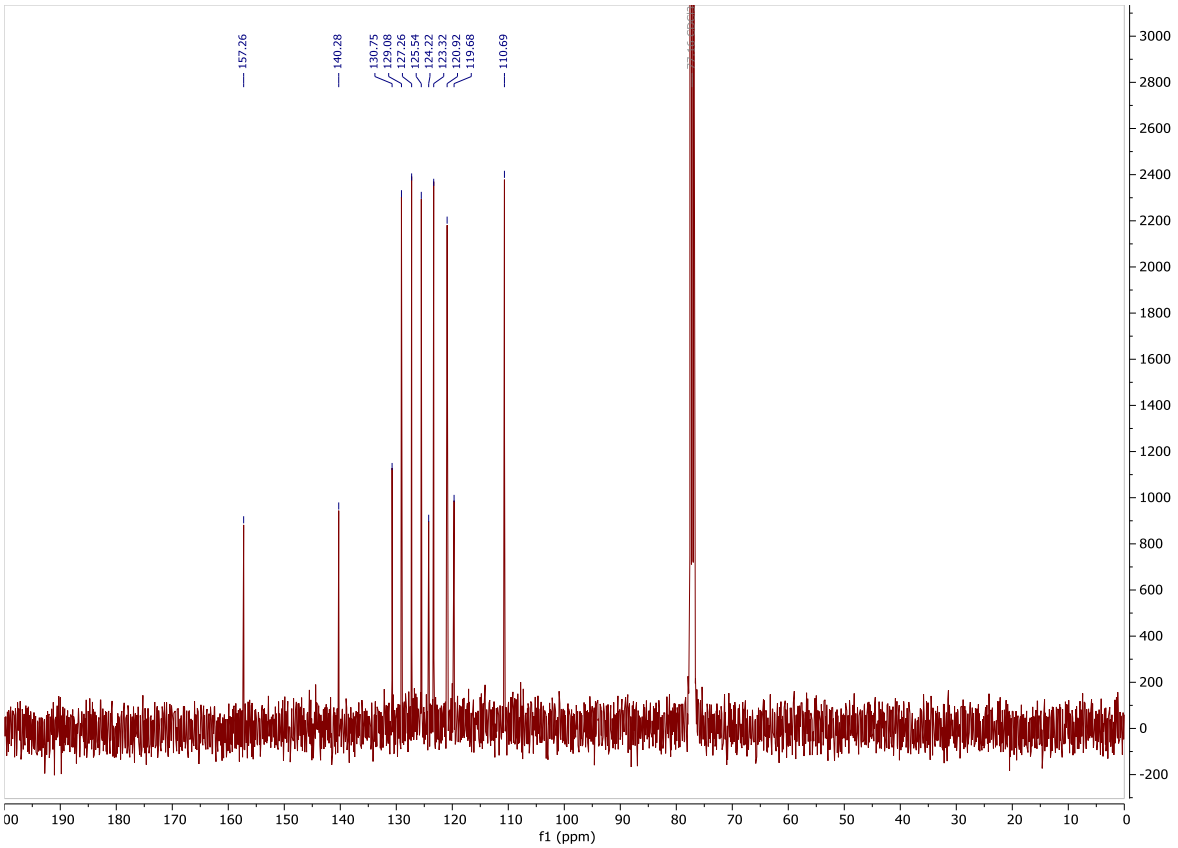

5-Bromo-1H-benzo[e][1,3]benzoxazol-2-one (63)

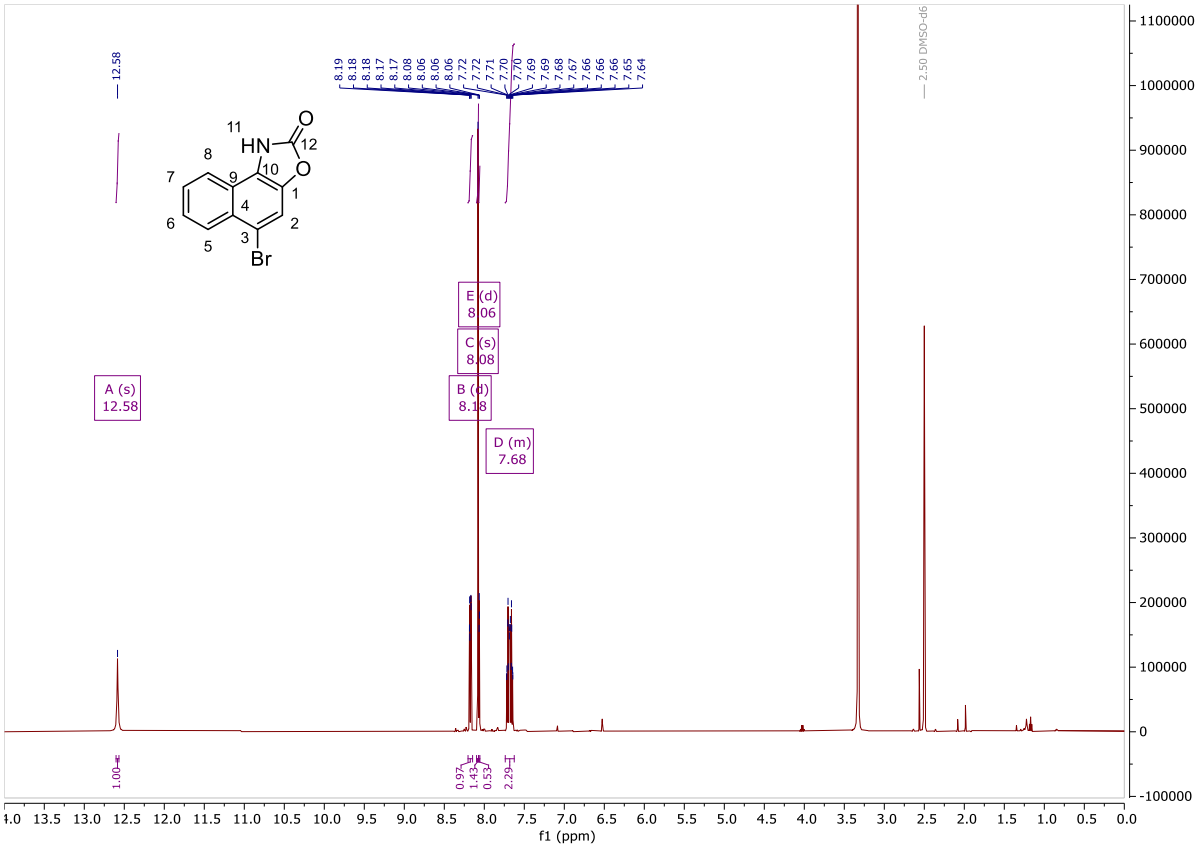

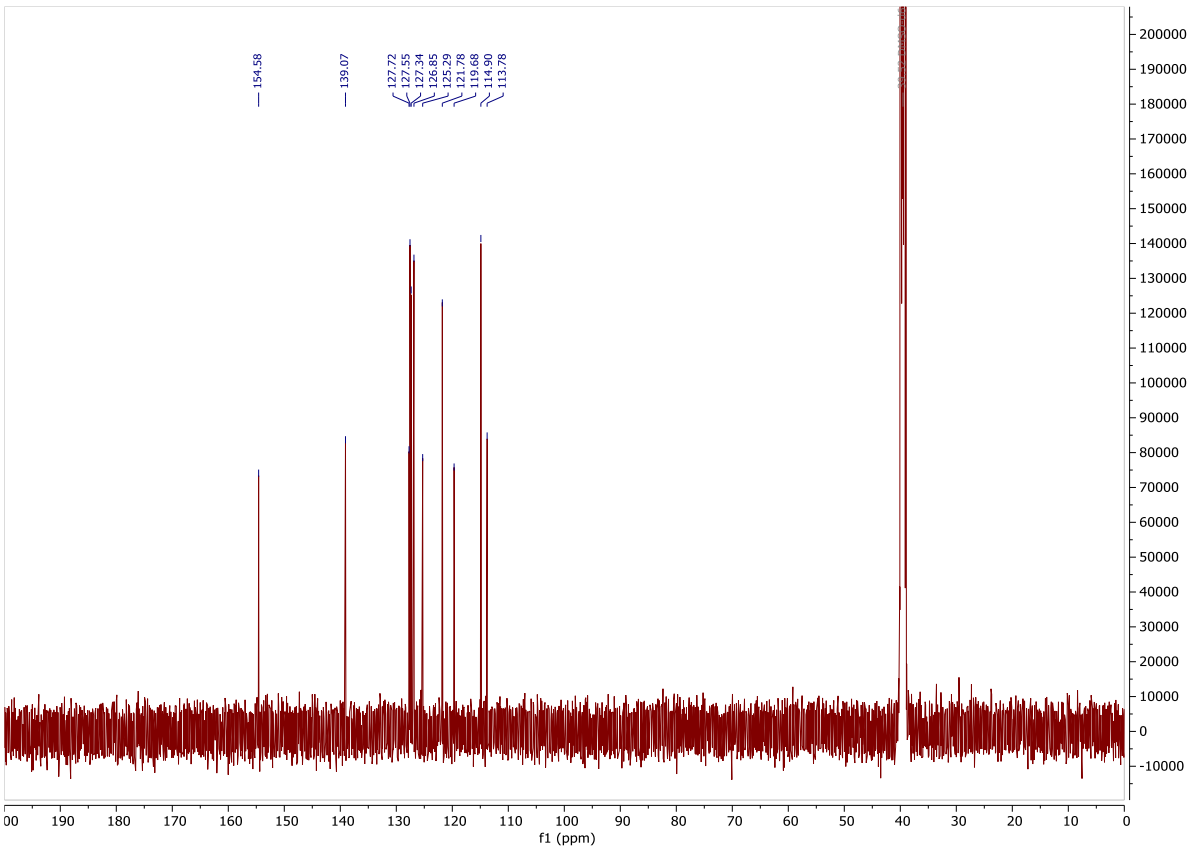

5-(4-(Tert-butyl)phenyl)naphtho[1,2-d]oxazol-2(1H)-one (64)

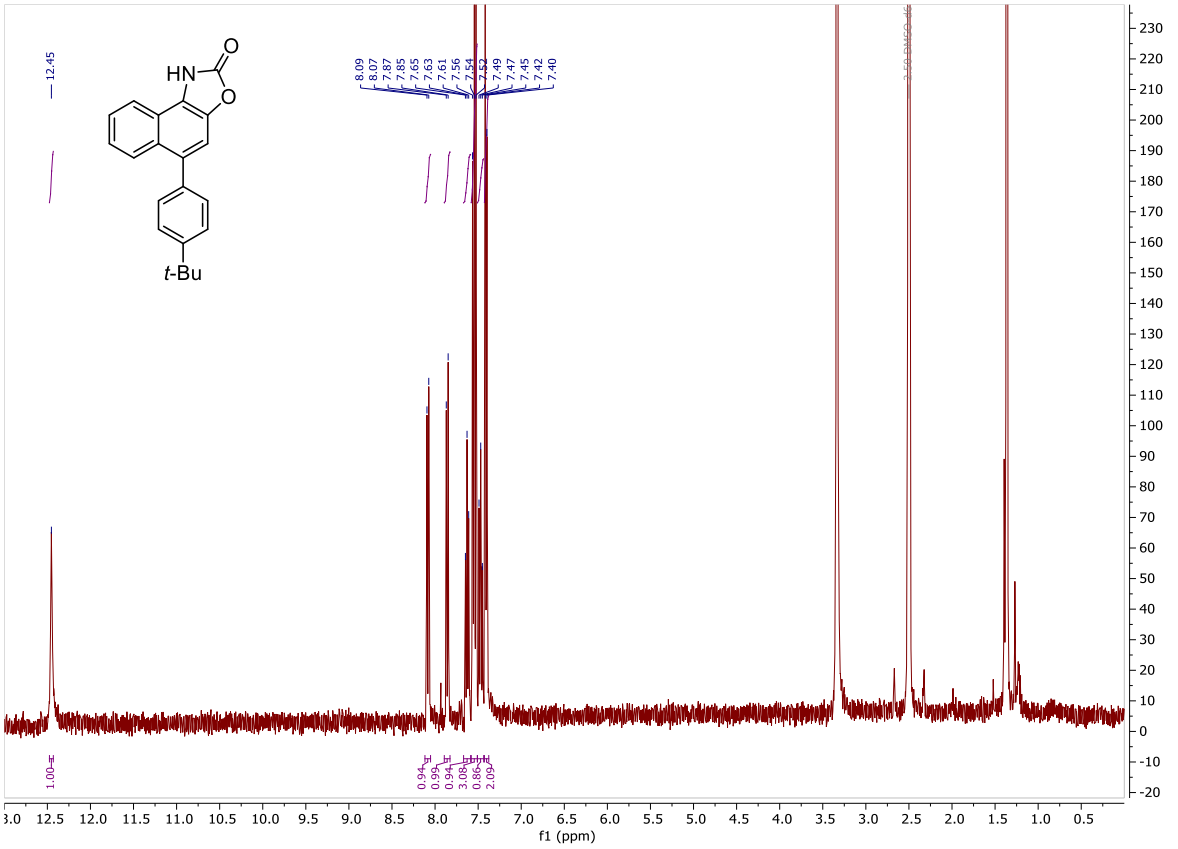

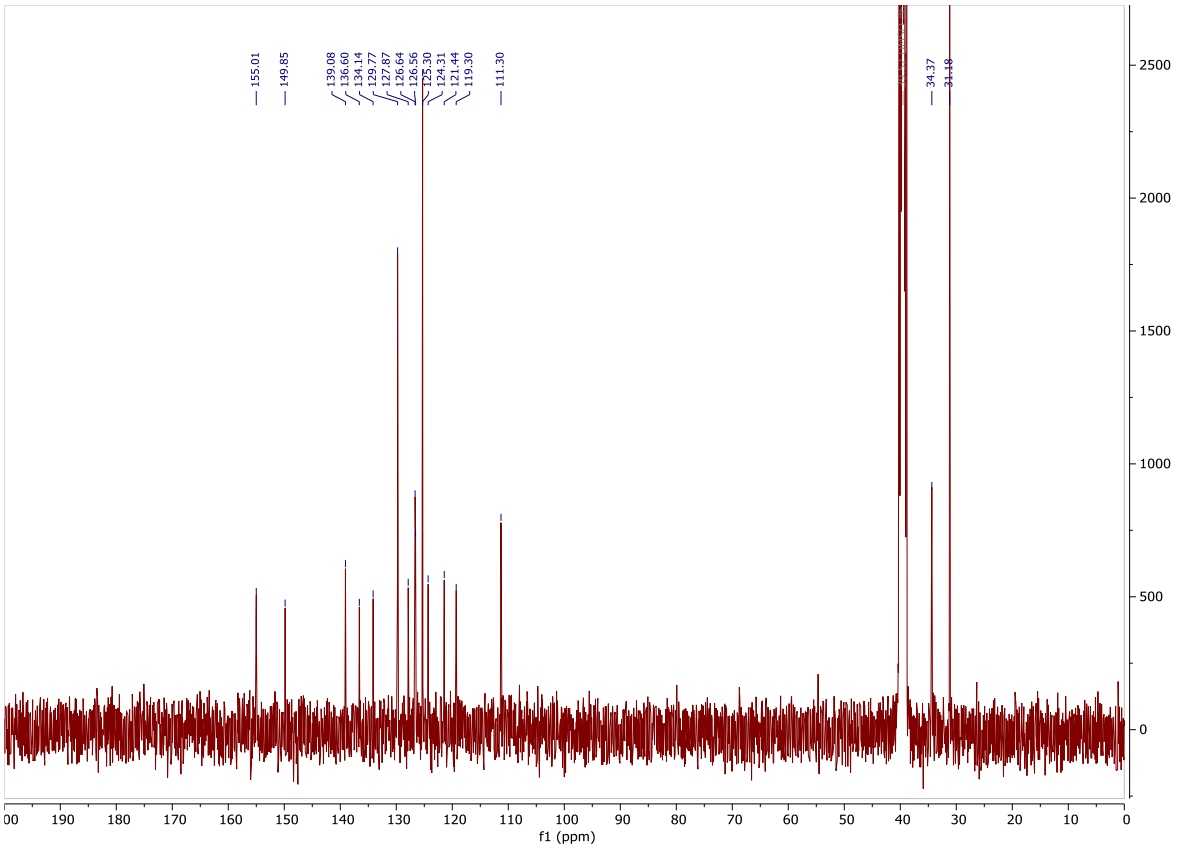

1-(2-Bromoethyl)-5-(4-(tert-butyl)phenyl)naphtho[1,2-d]oxazol-2(1H)-one (65a) and 5-(4-(tert-butyl)phenyl)-1-vinylnaphtho[1,2-d]oxazol-2(1H)-one (65b)

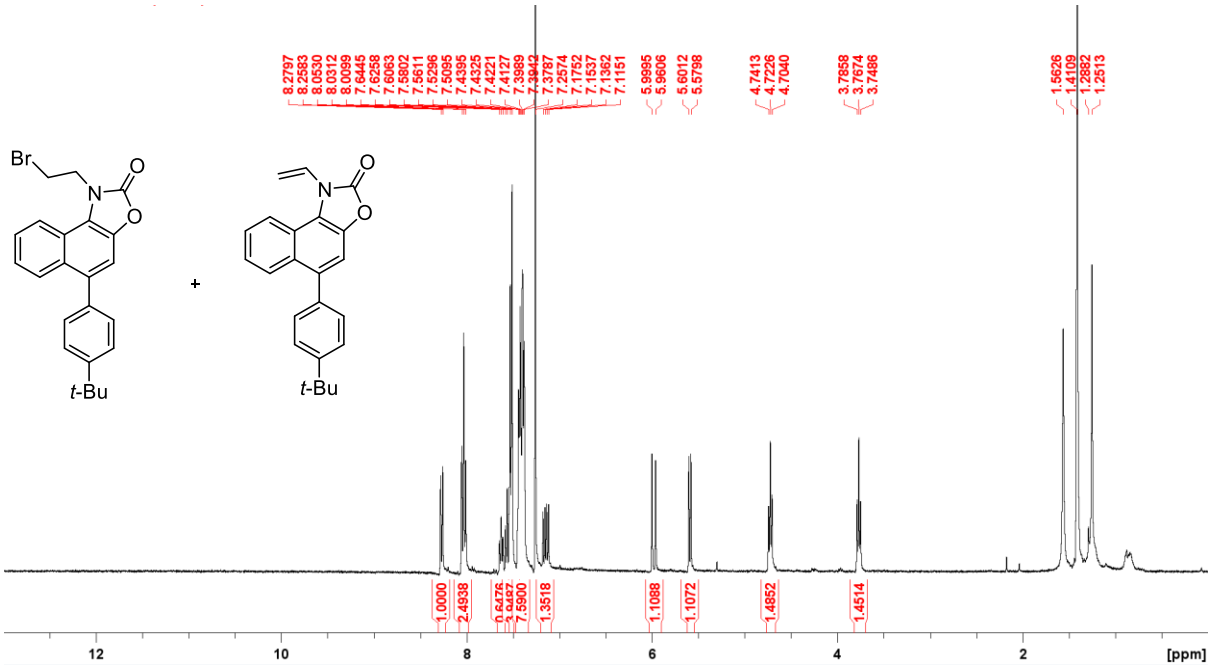

N^1, N^2-bis(2-hydroxyphenyl)oxalamide (67)

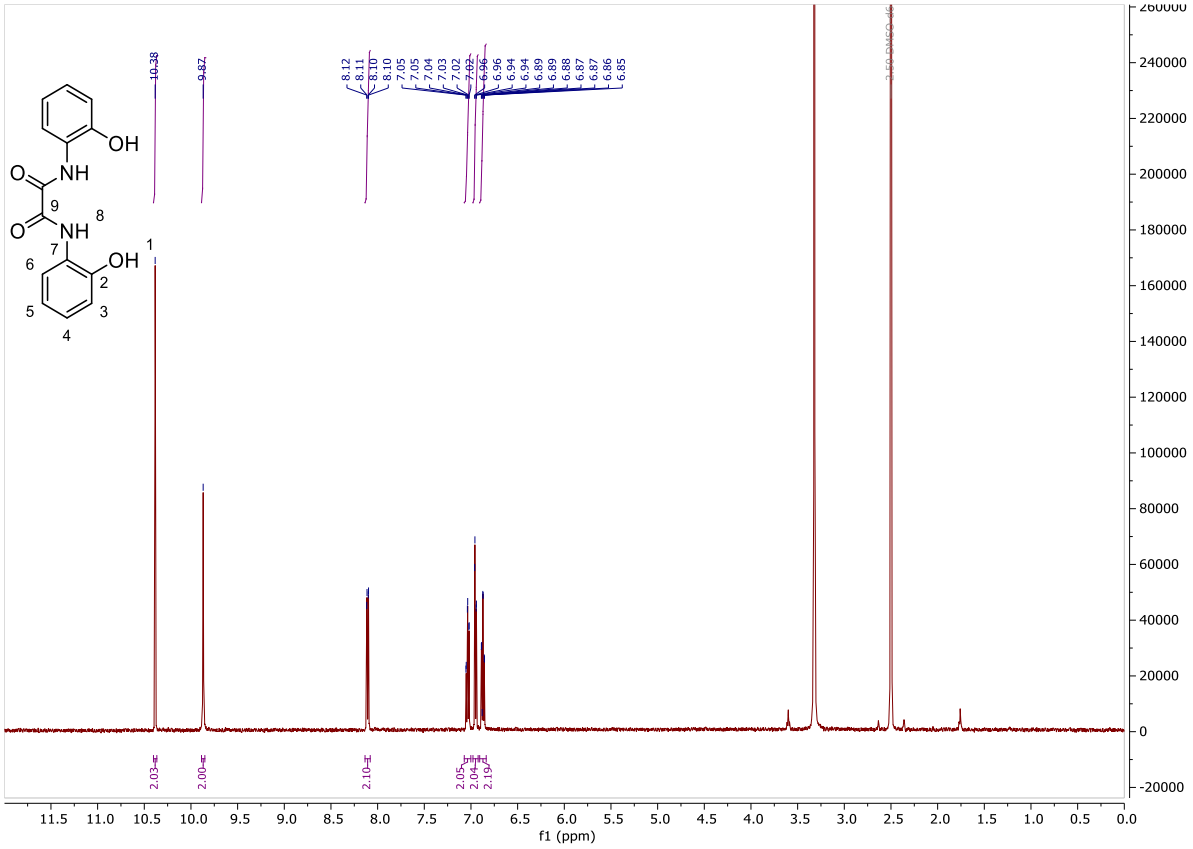

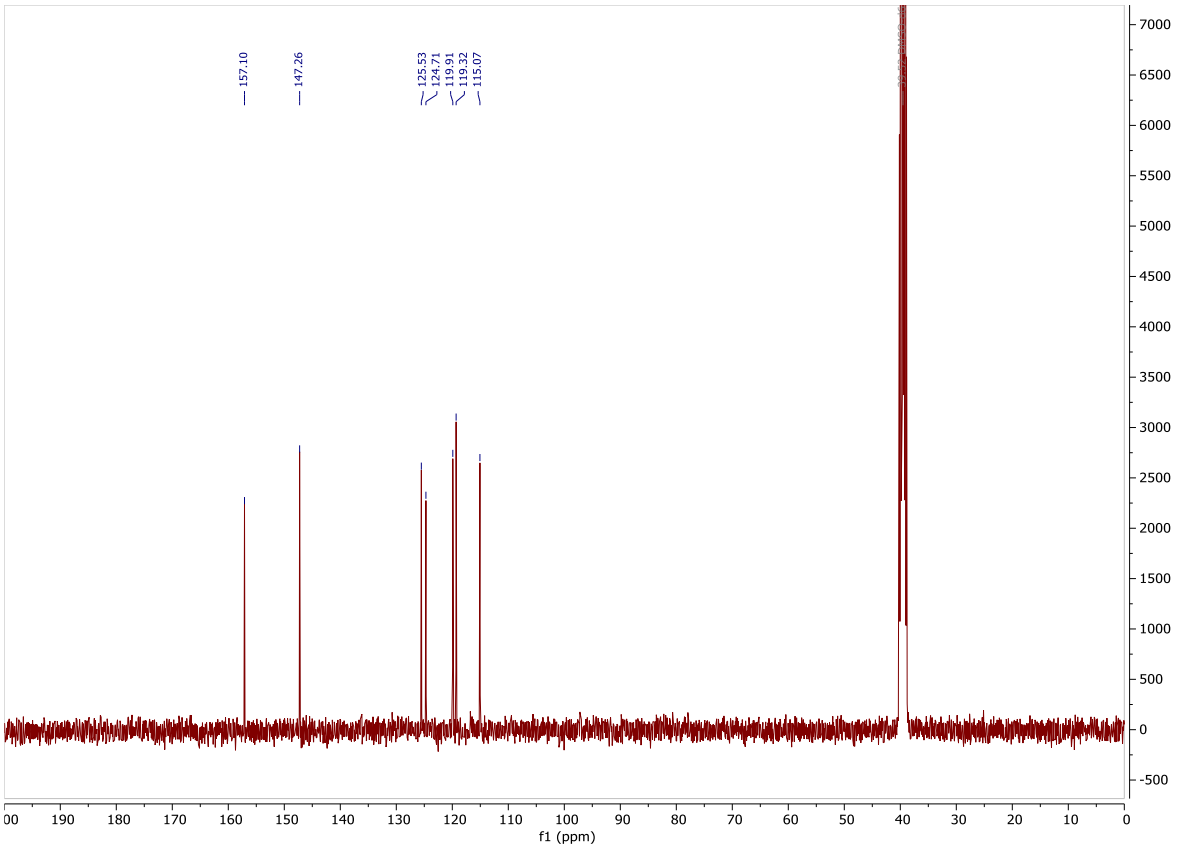

N^1,N^2-bis(4-bromo-2-hydroxyphenyl)oxalamide (68)

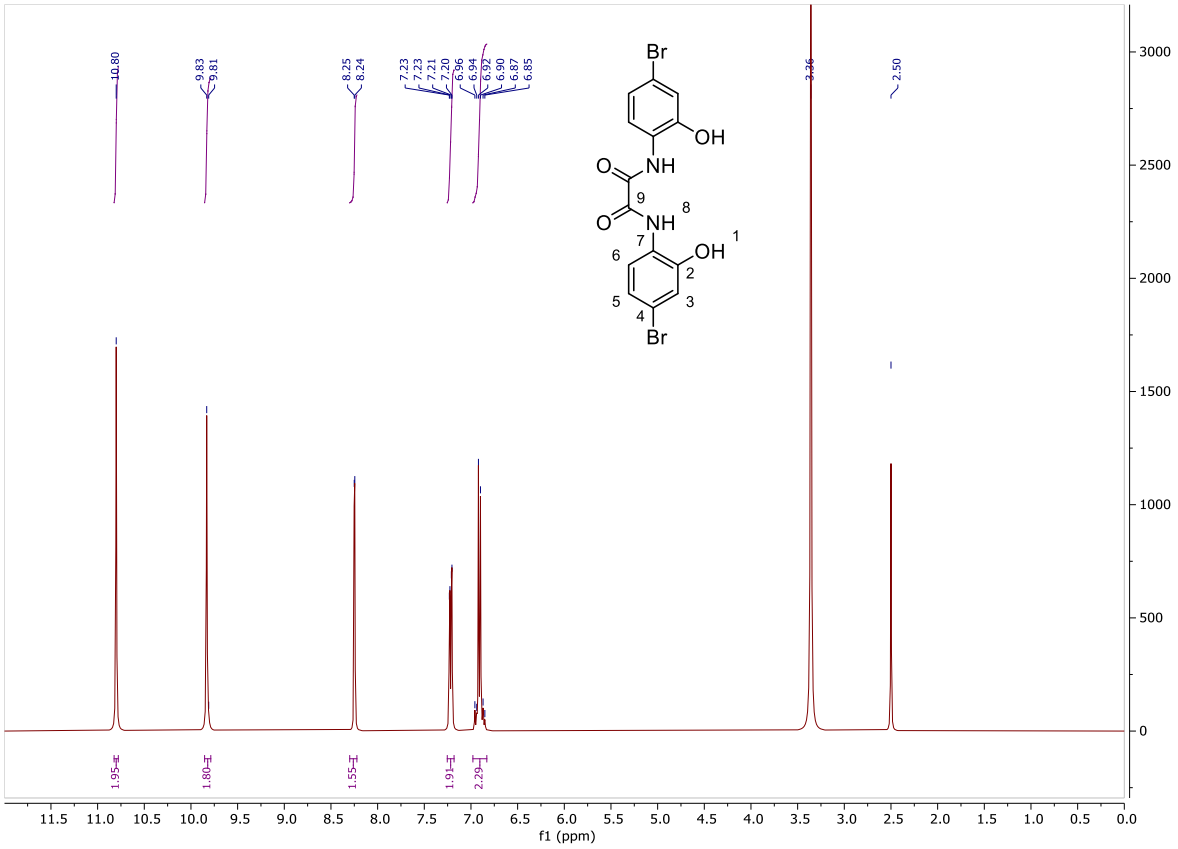

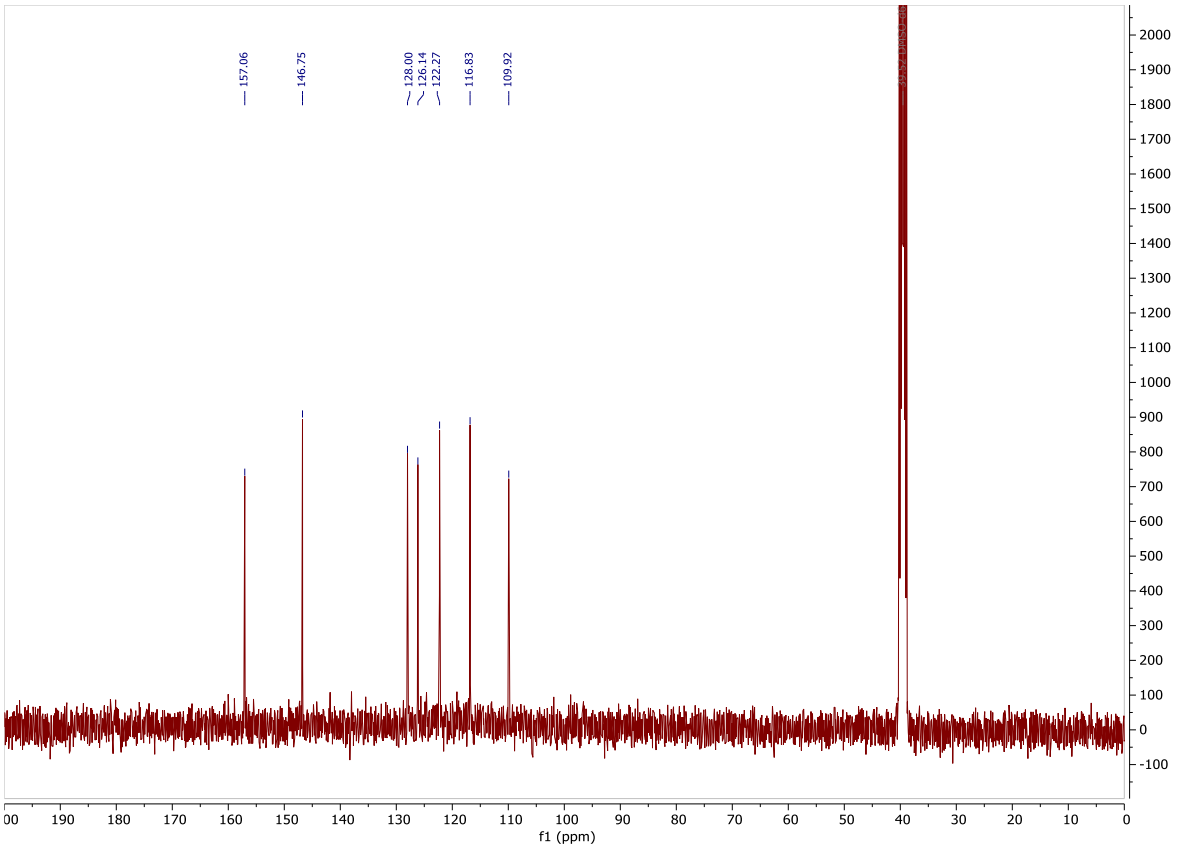

1,1'-(Ethane-1,2-diyl)bis(naphtho[1,2-d]oxazol-2(1H)-one) (69)

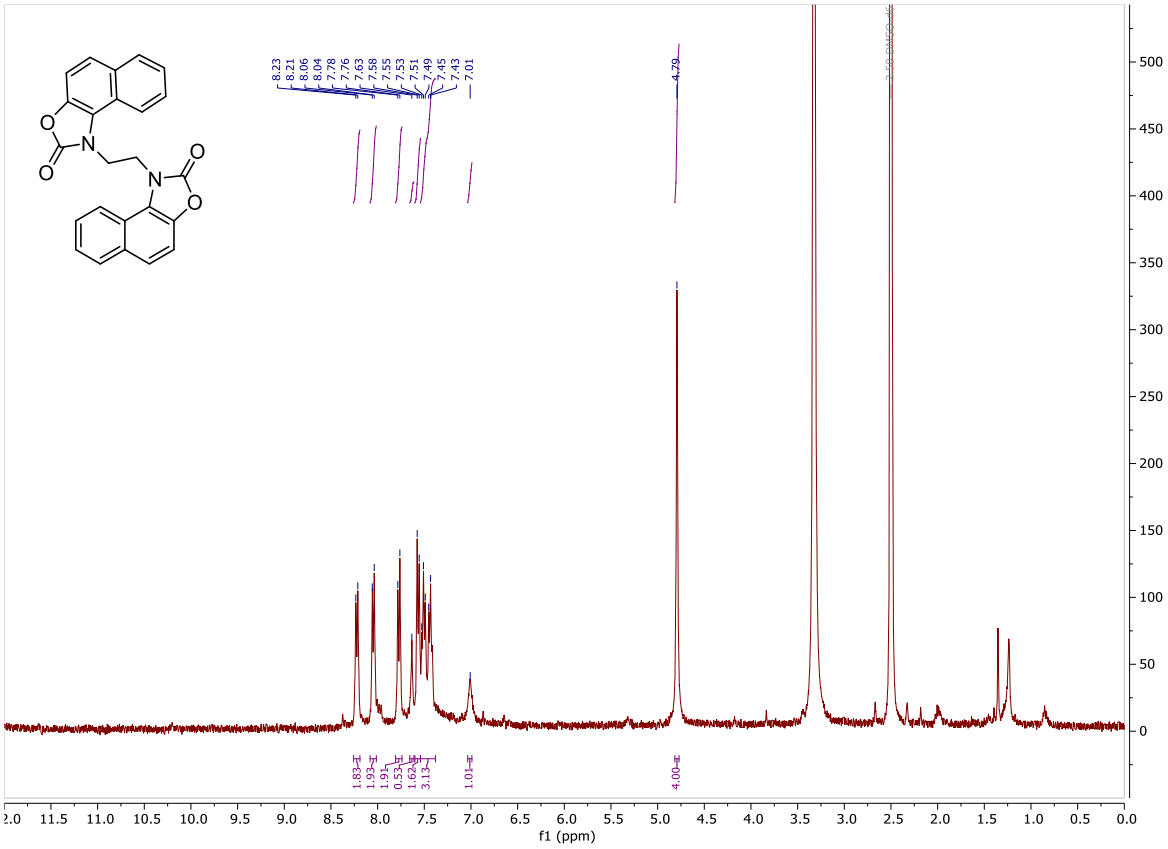

4-Bromobenzo[d]oxazol-2(3H)-one (73)

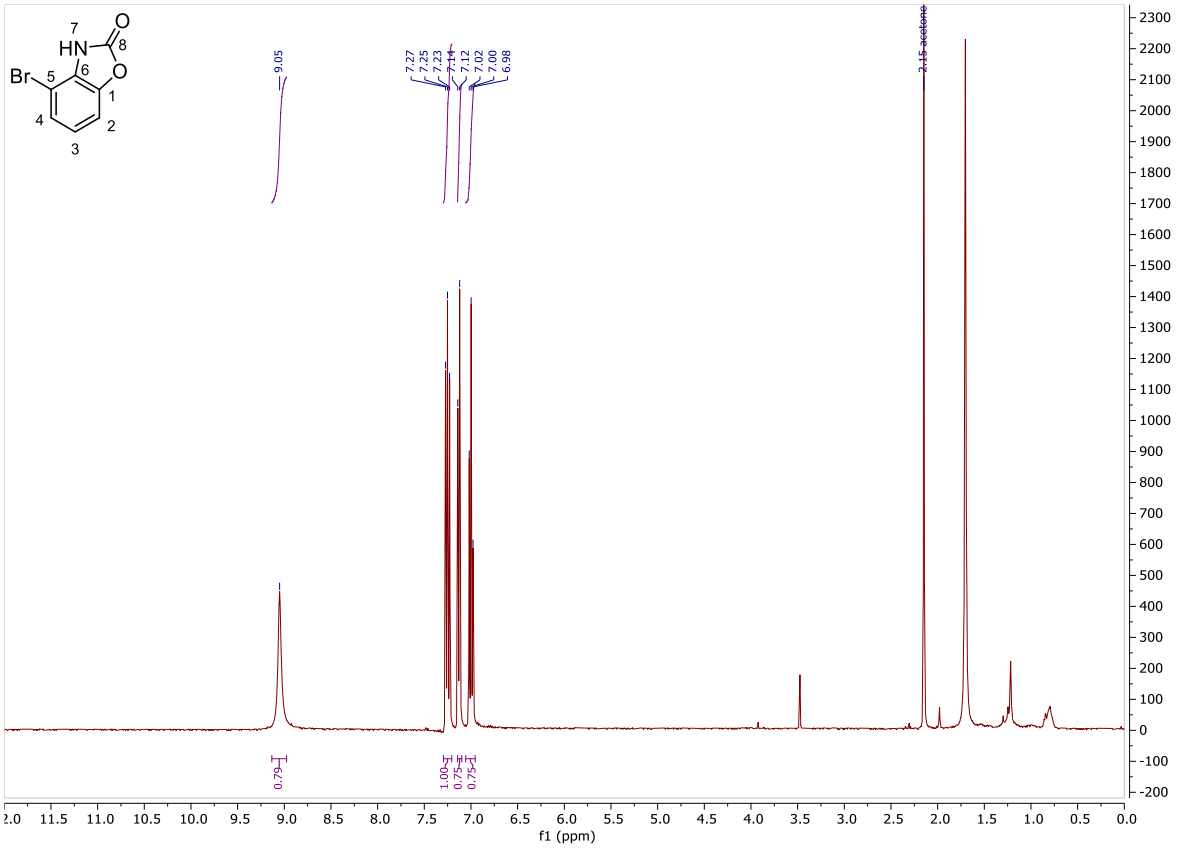

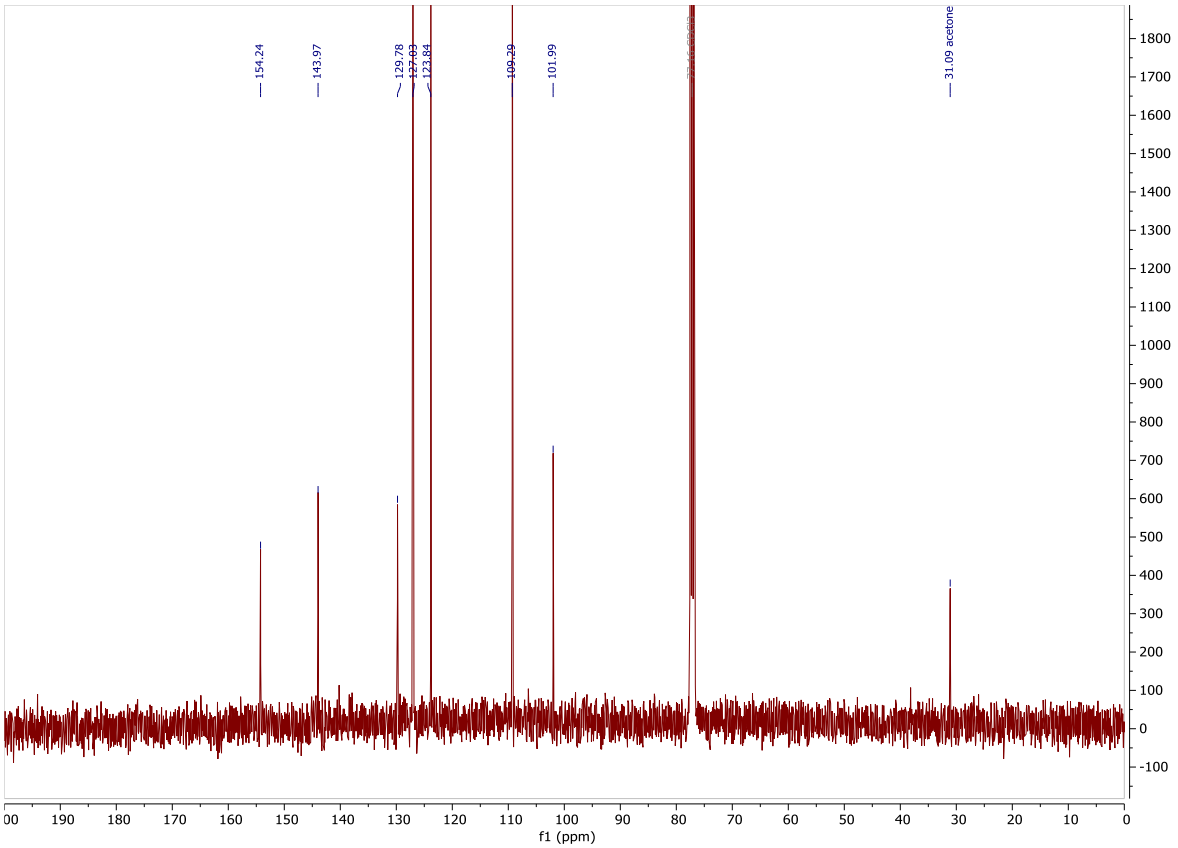

4-(4-(Tert-butyl)phenyl)benzo[d]oxazol-2(3H)-one (74)

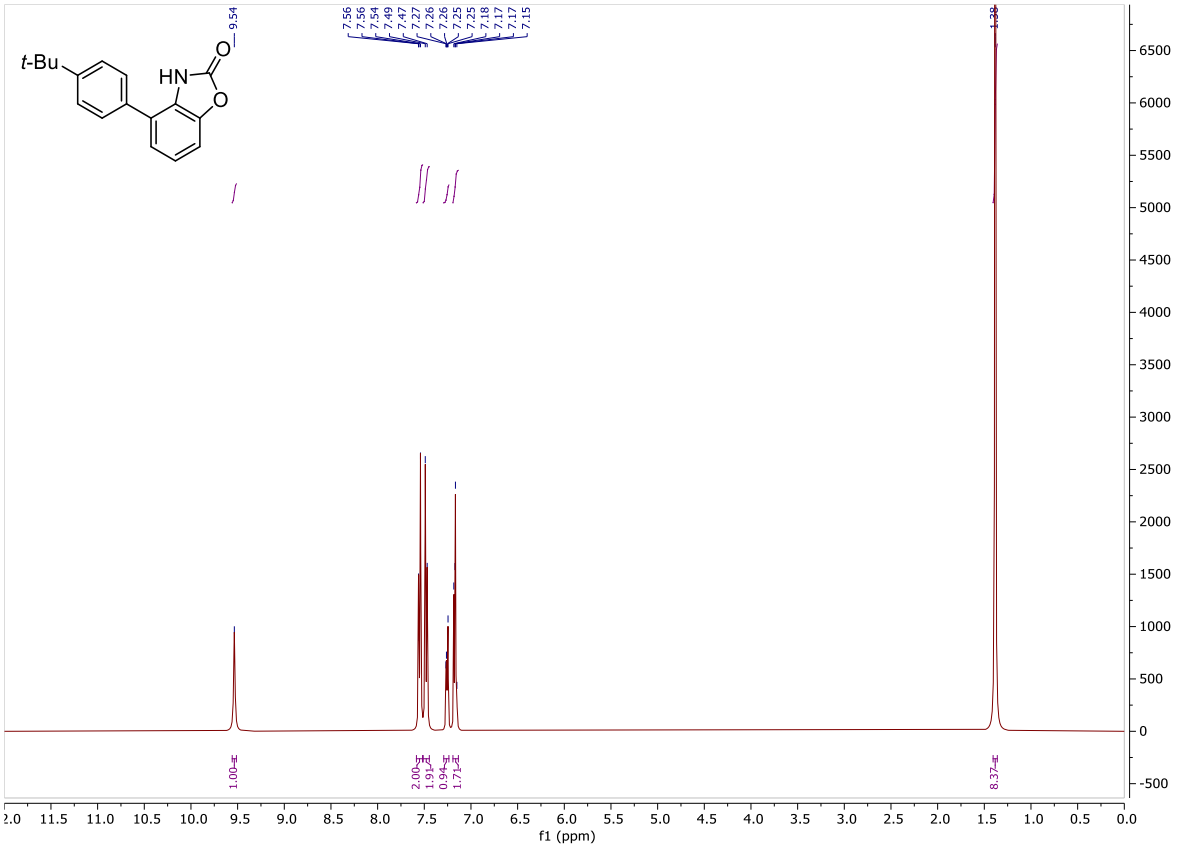

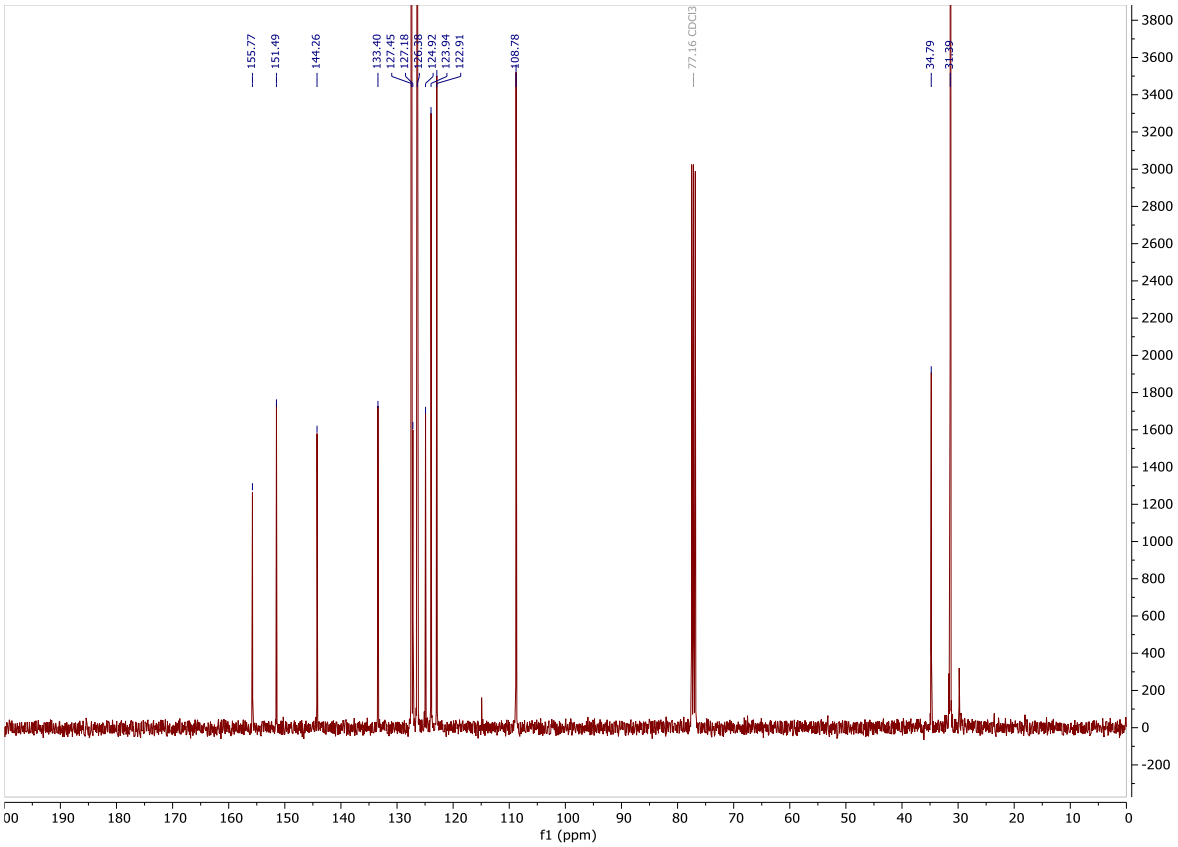

2-Amino-4'-(tert-butyl)-[1,1'-biphenyl]-3-ol (75)

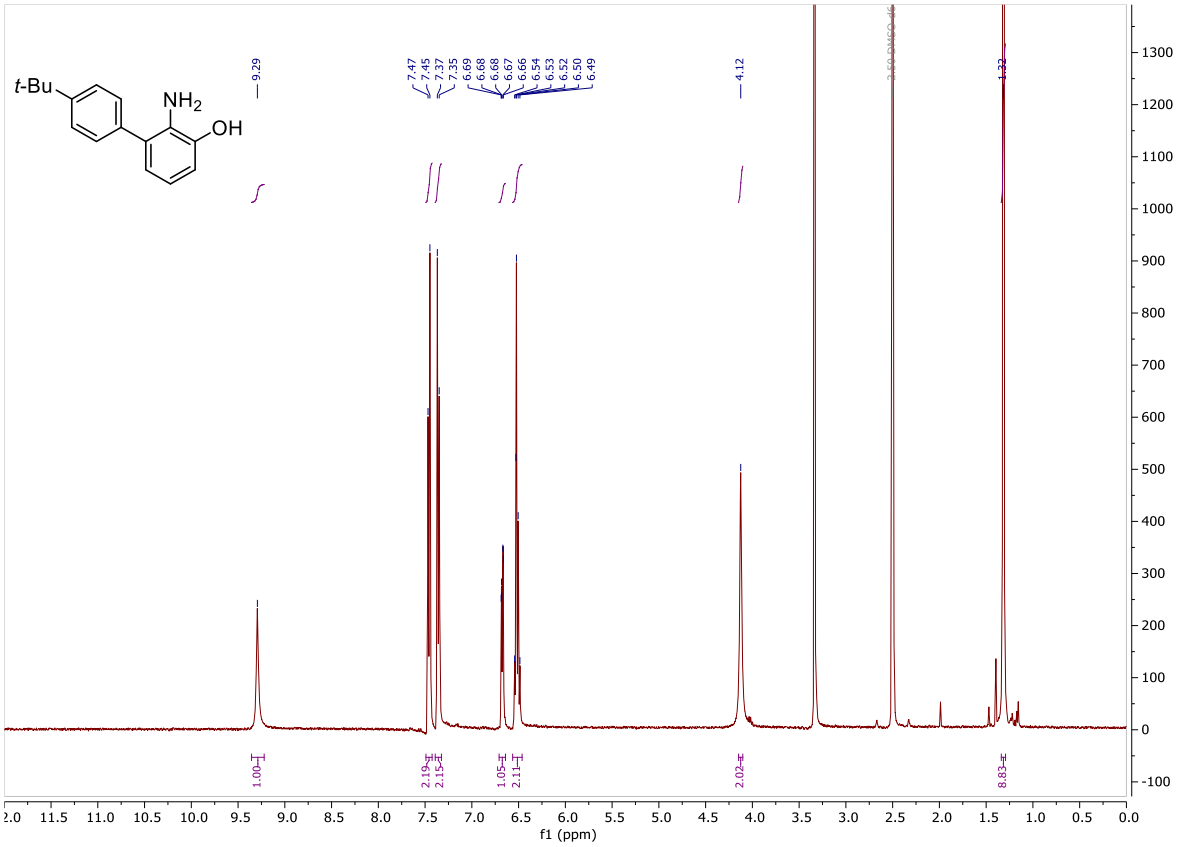

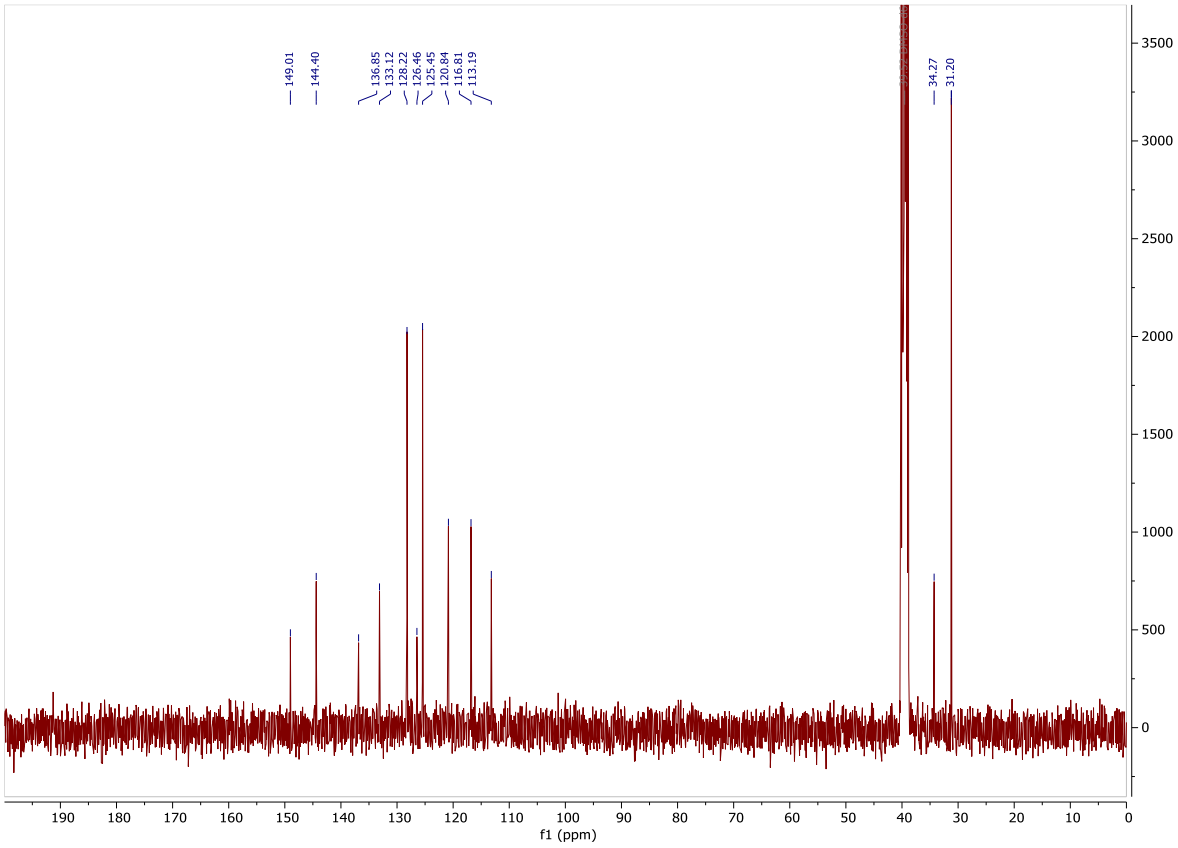

N^1,N^2-bis(4'-(tert-butyl)-3-hydroxy-[1,1'-biphenyl]-2-yl)oxalamide (76)

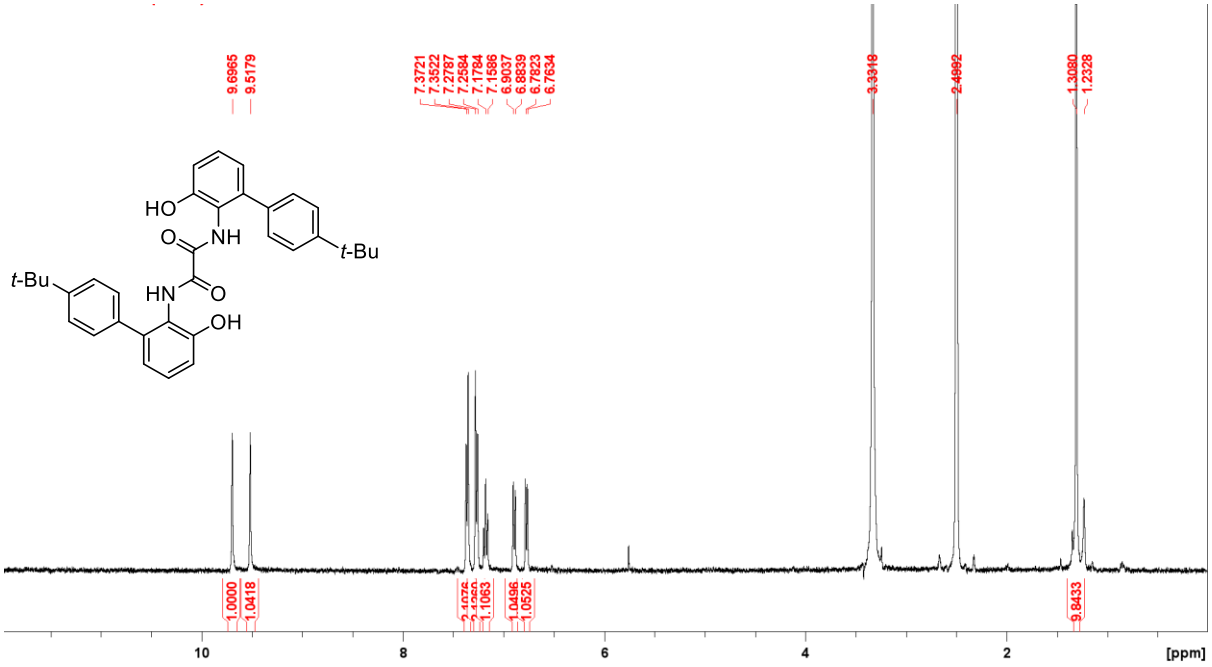

1,3-Bis(4'-(tert-butyl)-3-hydroxy-[1,1'-biphenyl]-2-yl)-4,5-dihydro-1H-imidazol-3-ium chloride (78)

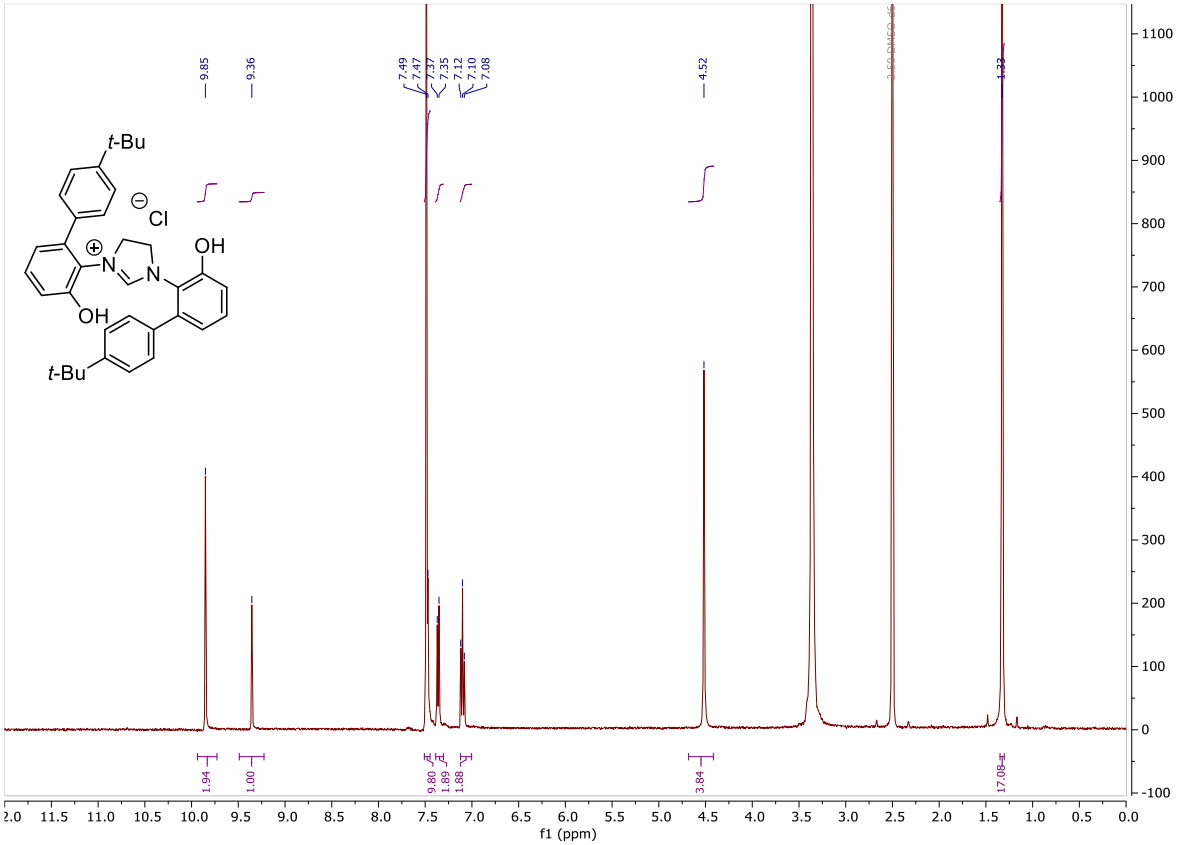

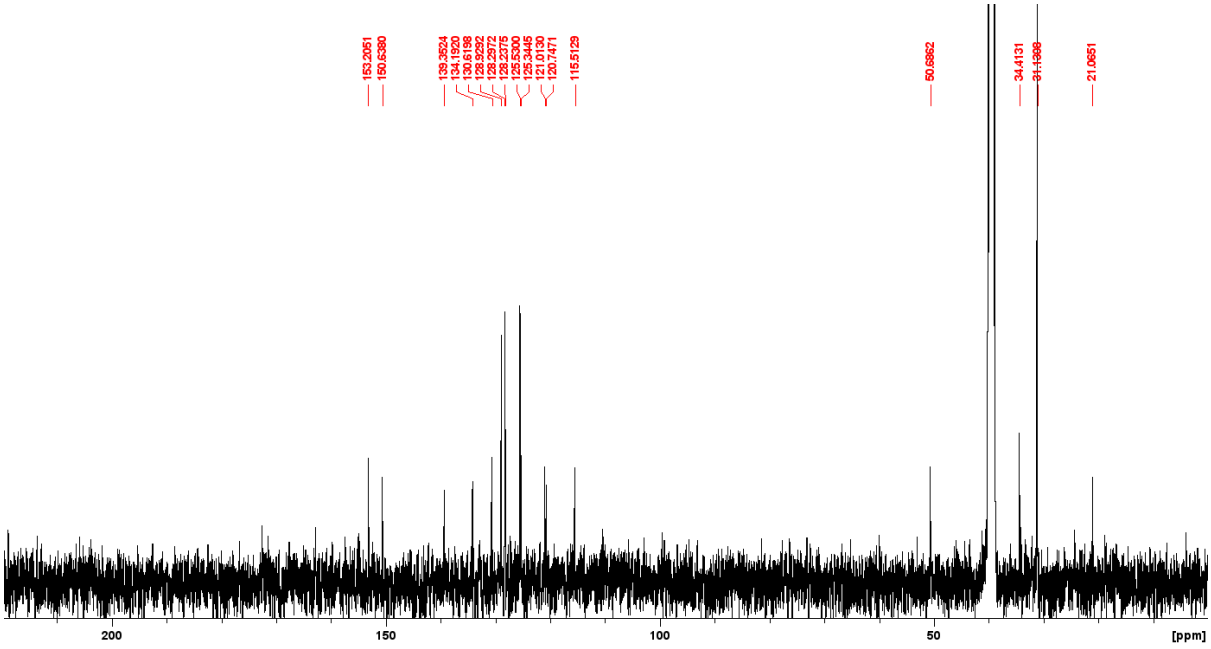

2-(4-(Tert-butyl)phenyl)-4,4,5,5-tetramethyl-1,3,2-dioxaborolane (80)

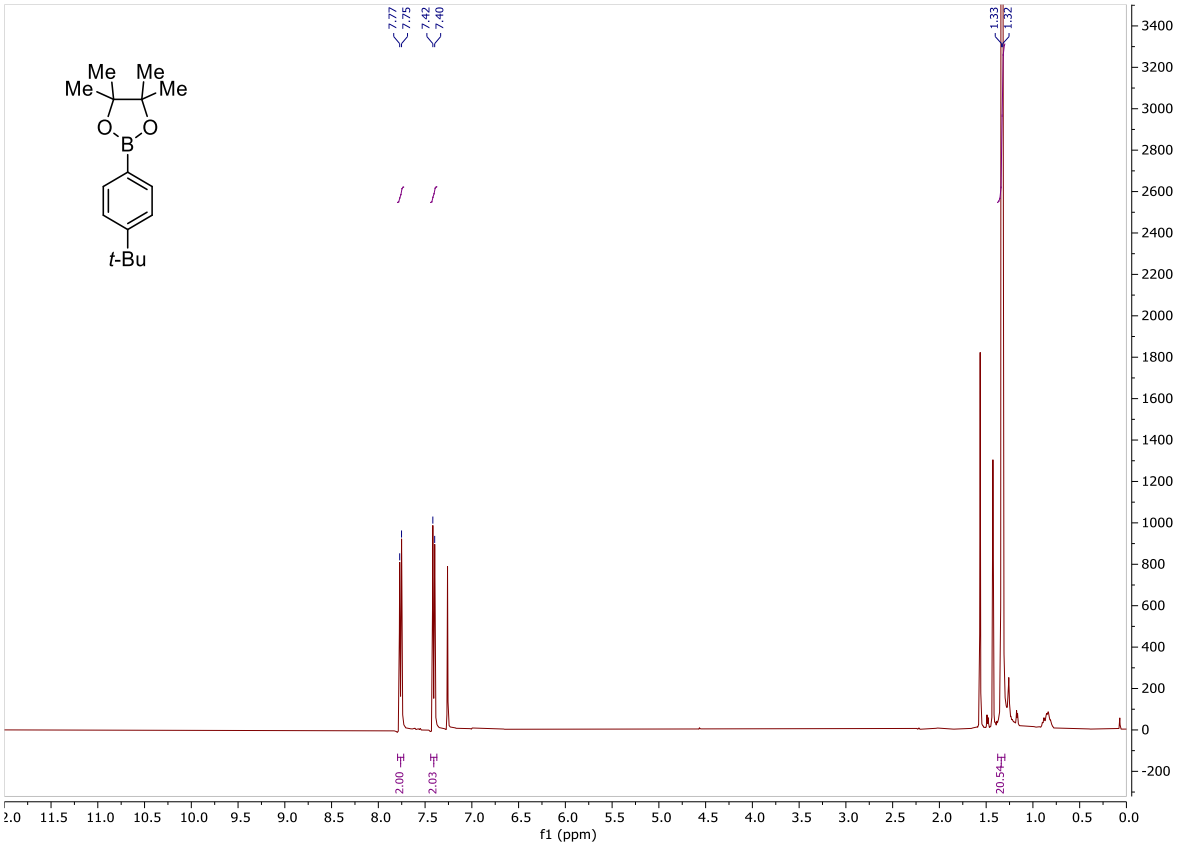

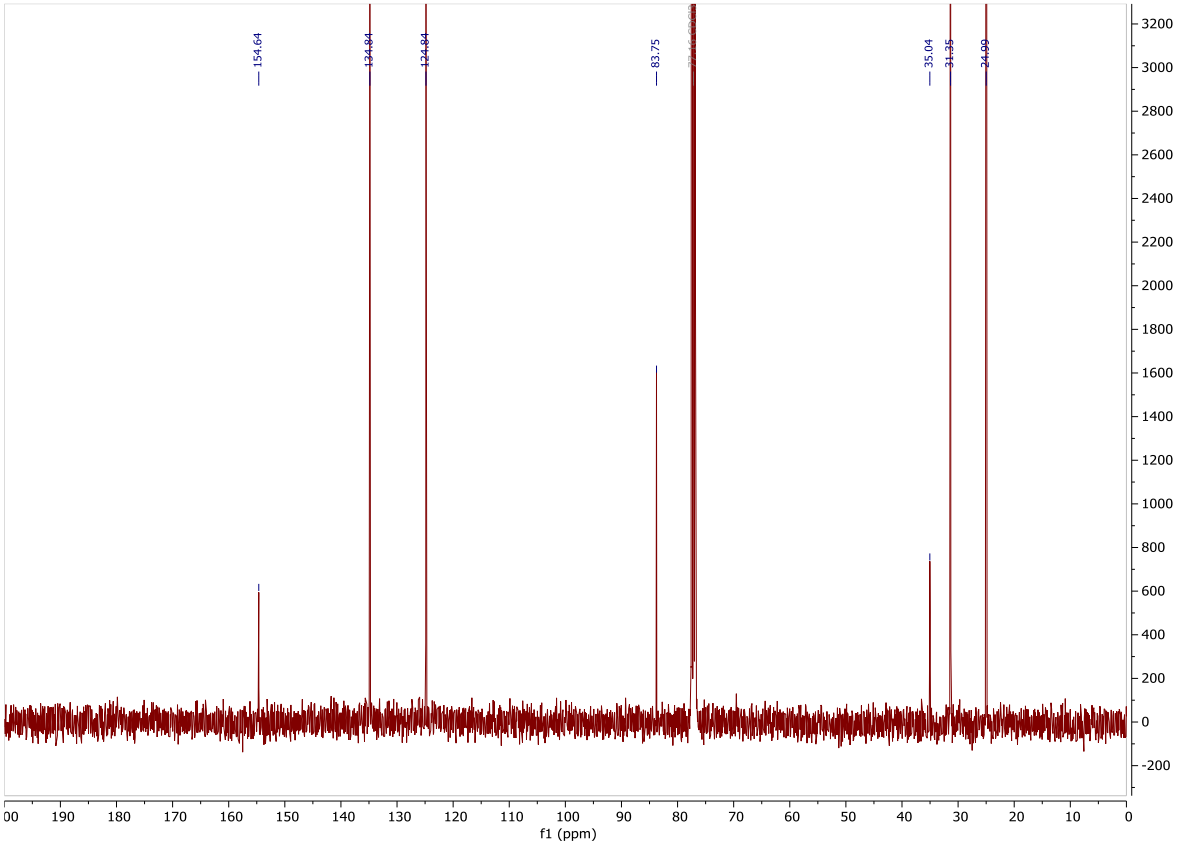

3-Hydroxy-2-nitrophenyl trifluoromethanesulfonate (86)

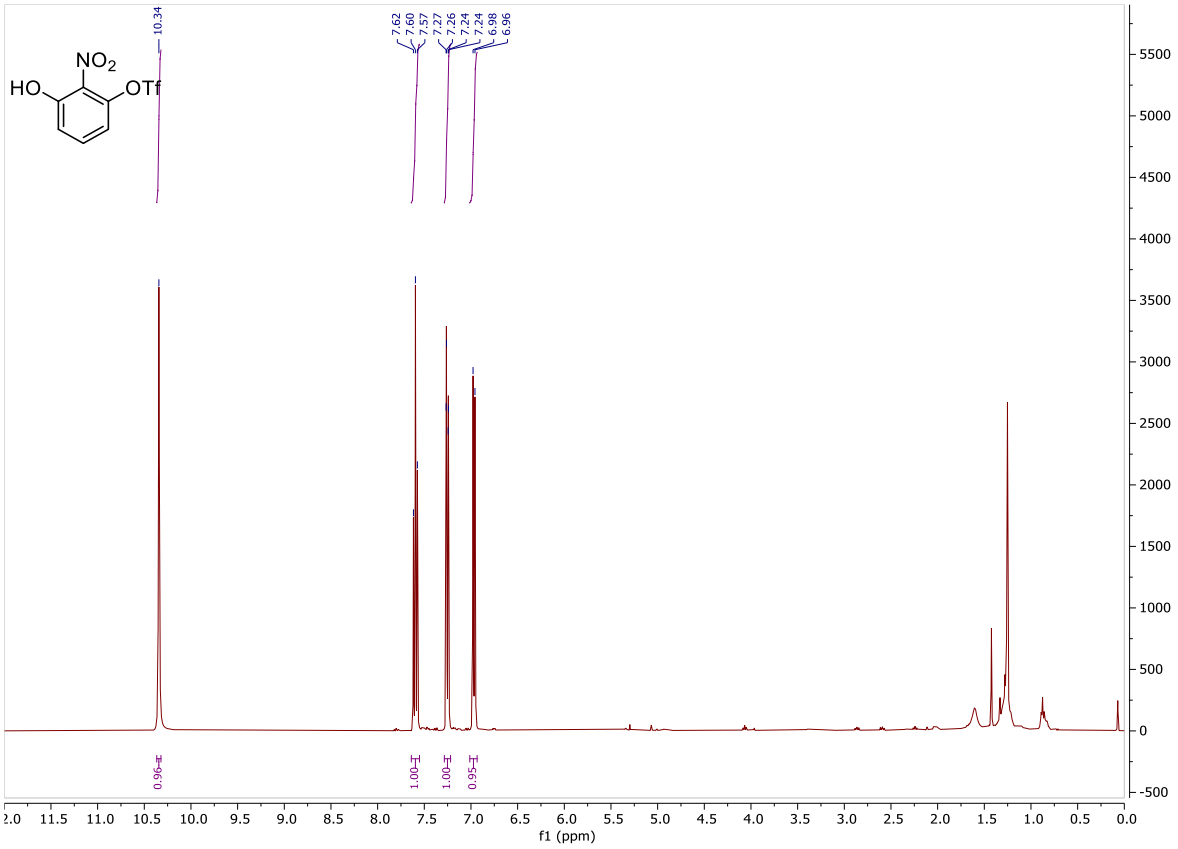

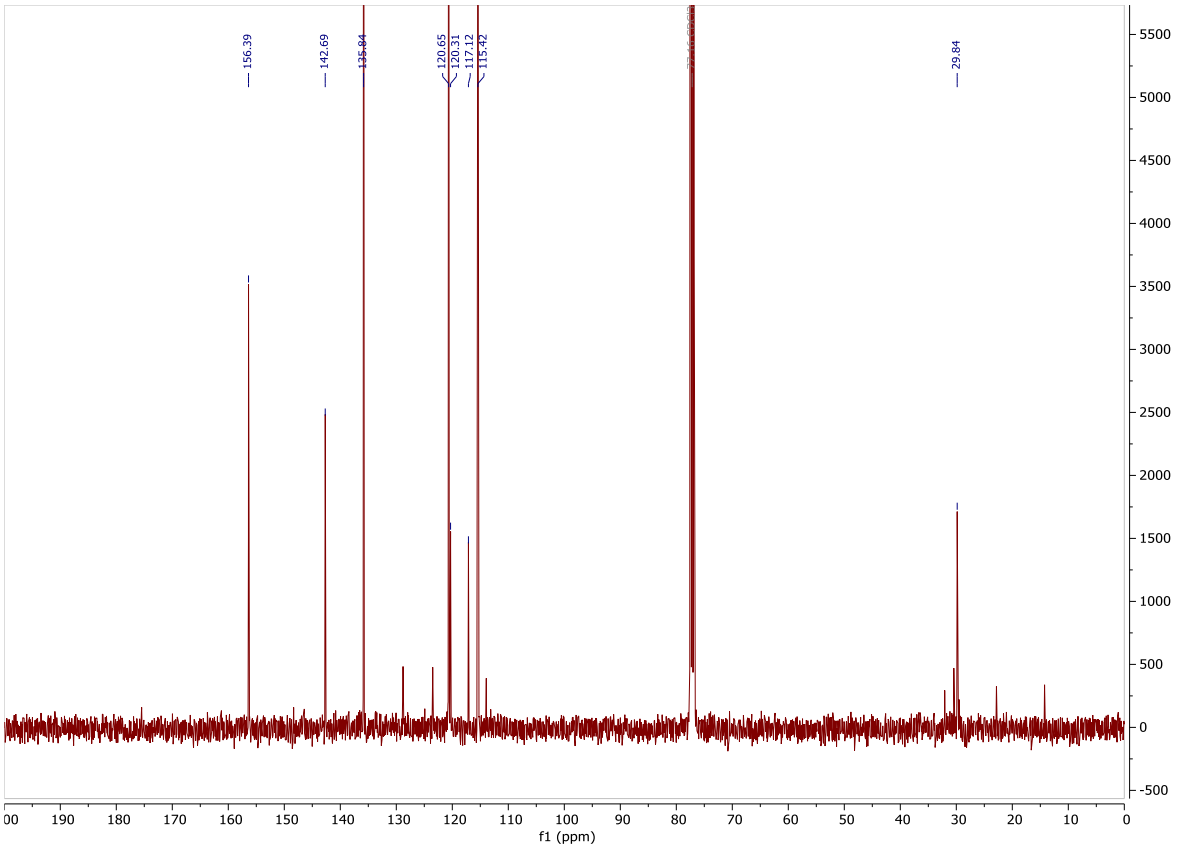

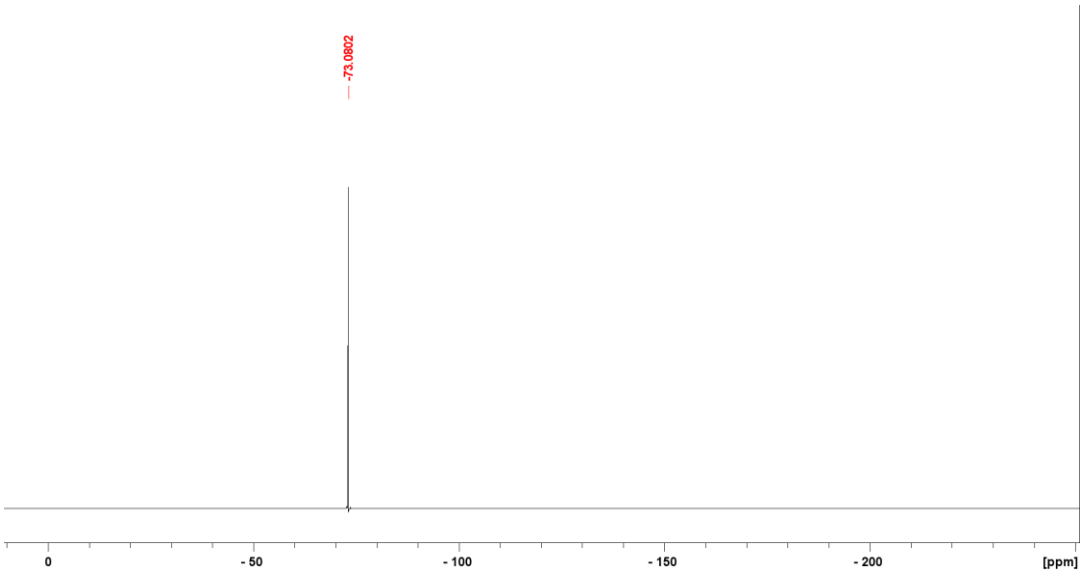
-73.0802
0
- 50
- 100
- 150
- 200
[ppm]

4'-(Tert-butyl)-3-nitro-[1,1'-biphenyl]-2-ol (81)

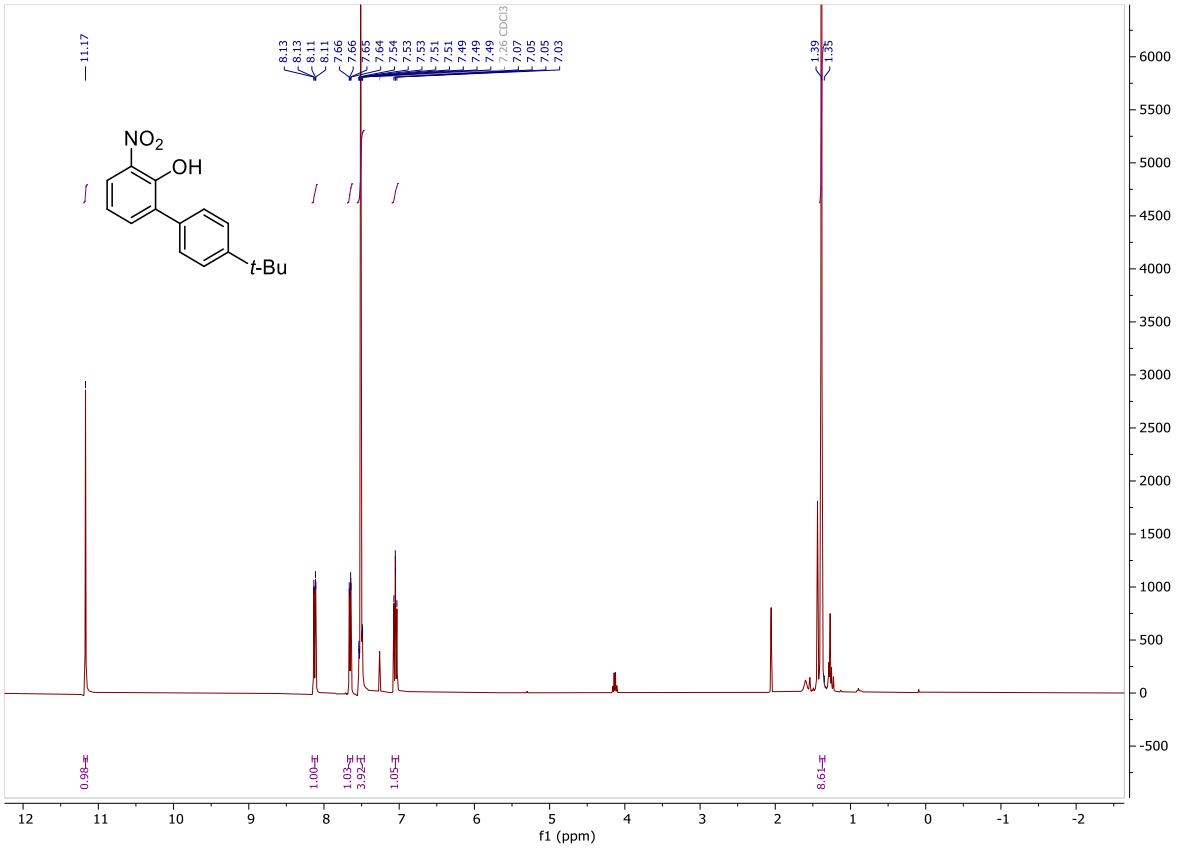

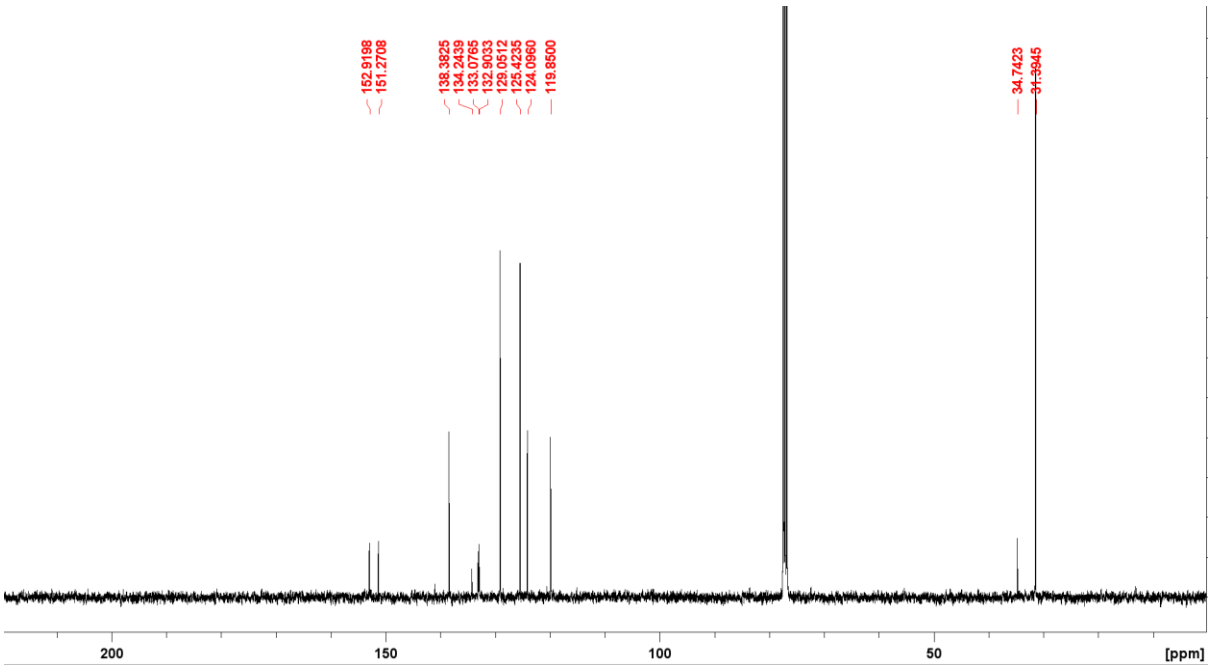

N^1,N^2-bis(4'-(tert-butyl)-2-hydroxy-[1,1'-biphenyl]-3-yl)oxalamide (89)

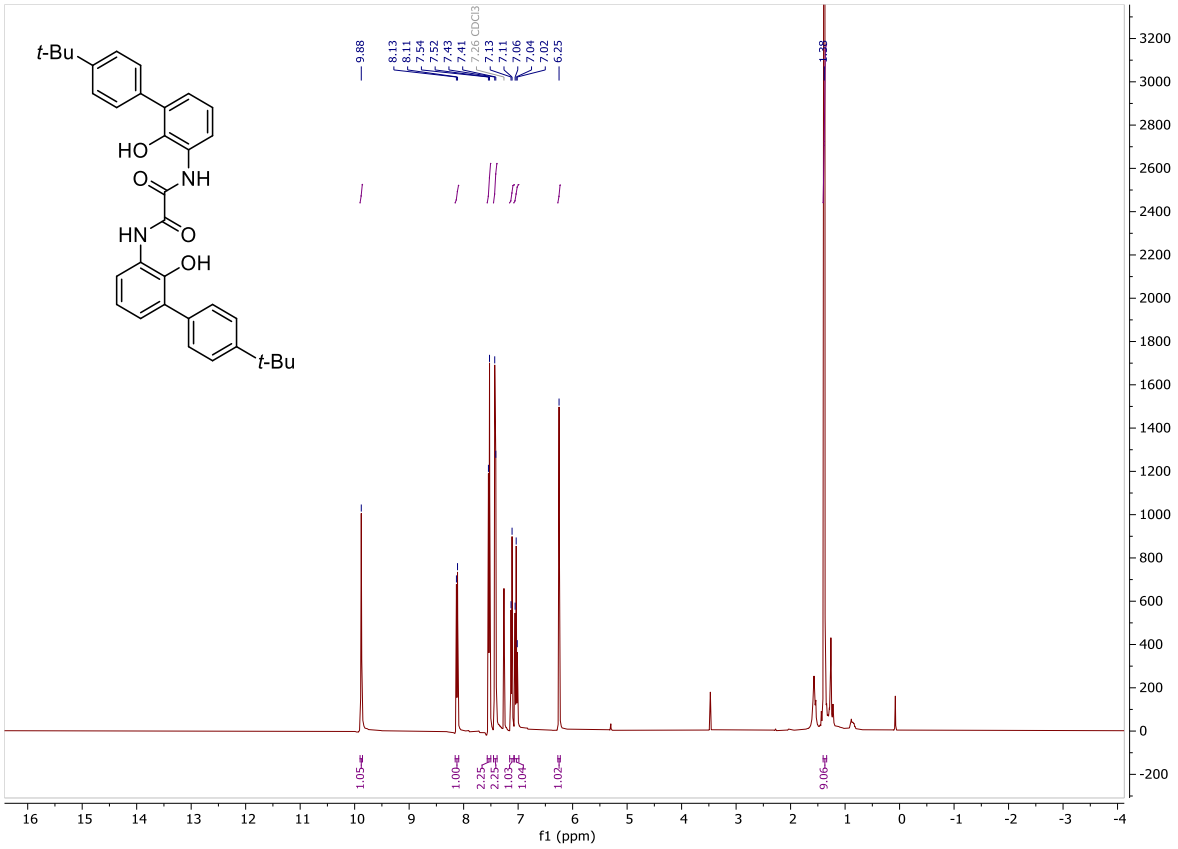

1,3-Bis(4'-(tert-butyl)-2-hydroxy-[1,1'-biphenyl]-3-yl)-4,5-dihydro-1H-imidazol-3-ium chloride (91)

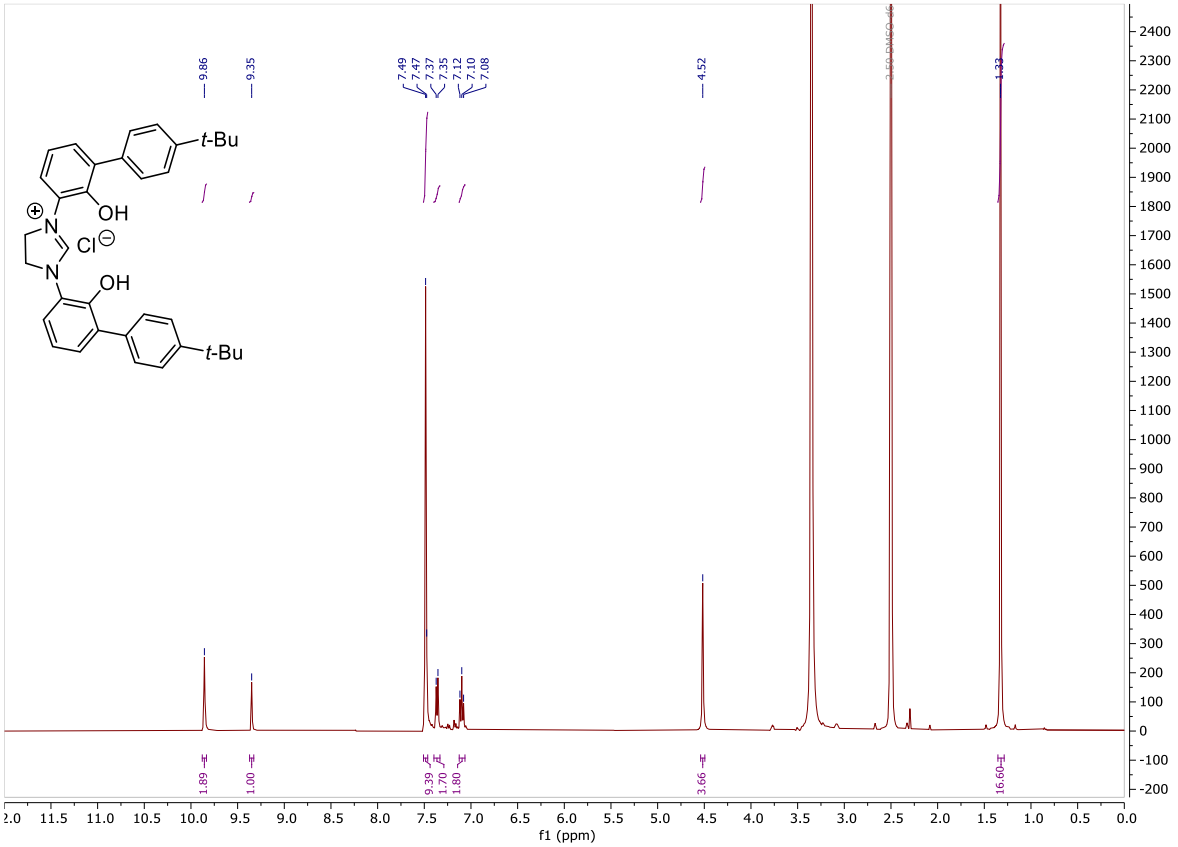

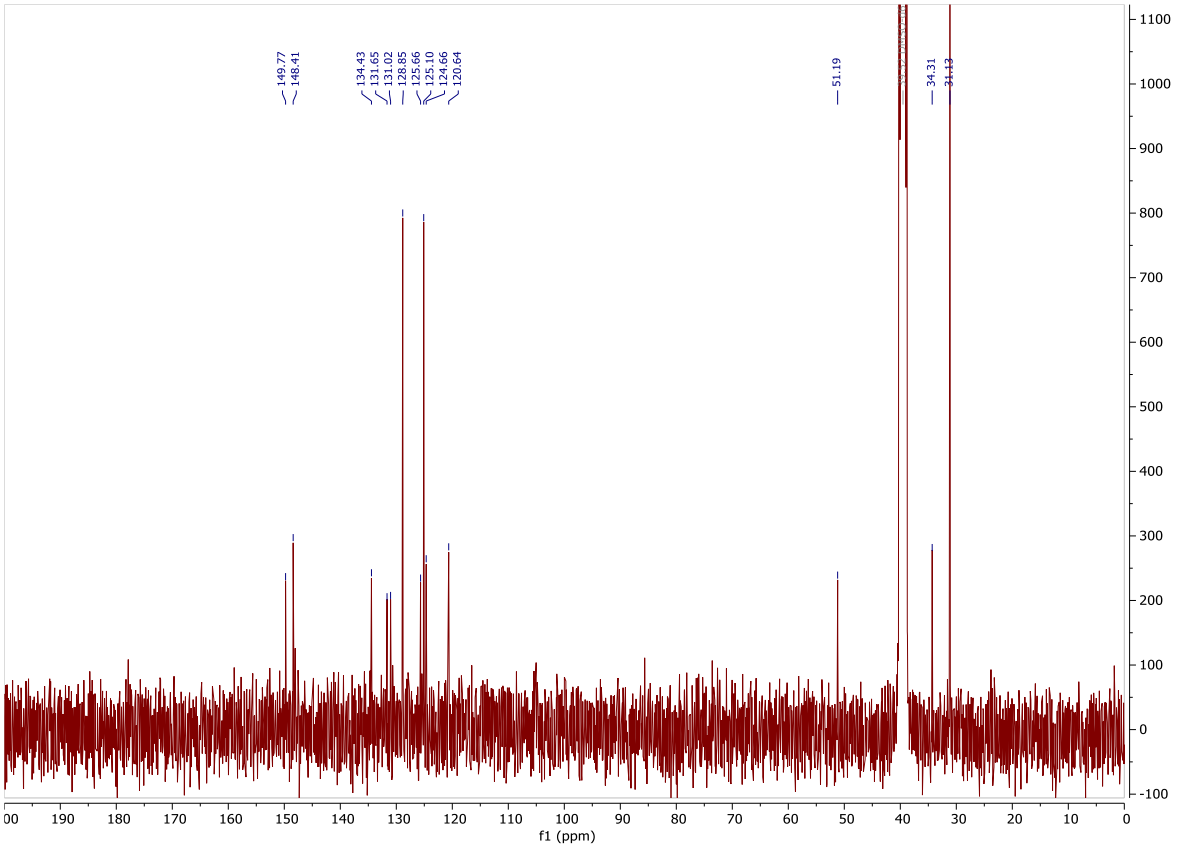

N^1,N^2-bis(5-(tert-butyl)-2-hydroxyphenyl)oxalamide (93)

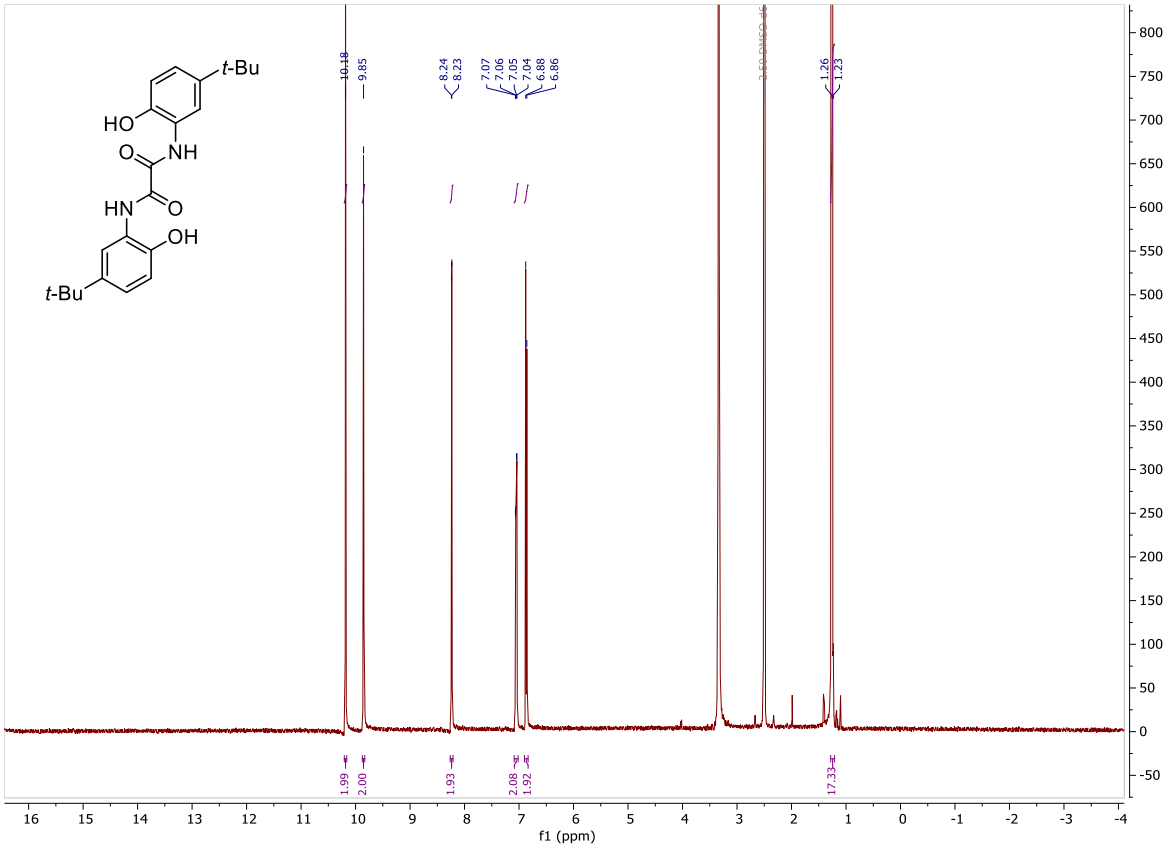

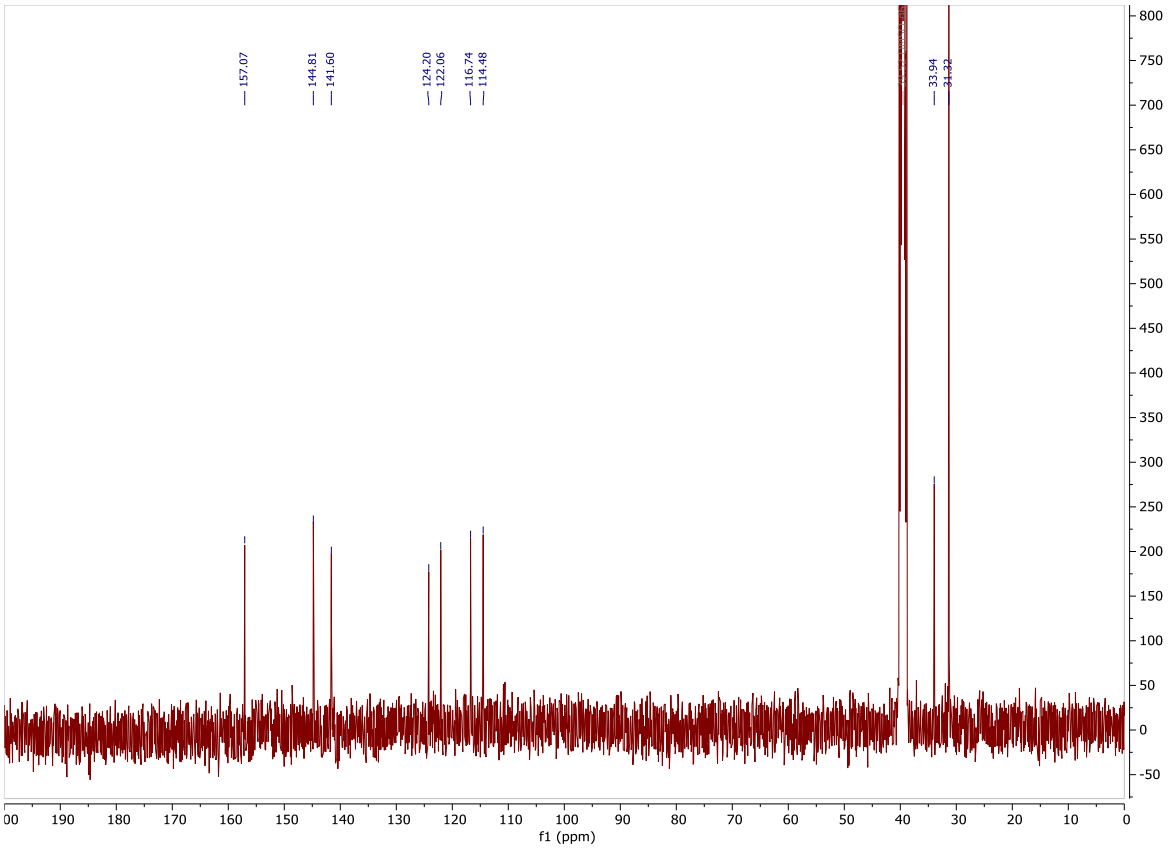

1,3-Bis(5-(tert-butyl)-2-hydroxyphenyl)-4,5-dihydro-1H-imidazol-3-ium chloride (94)

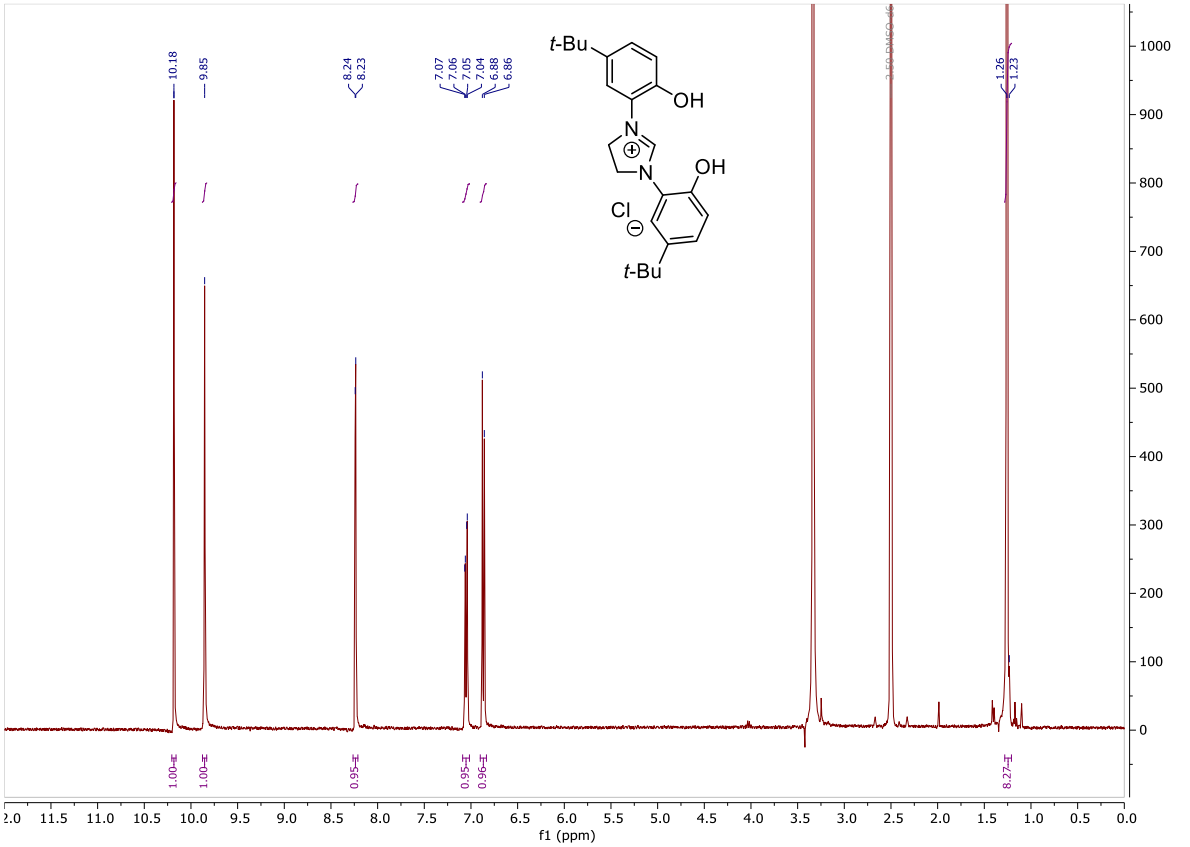

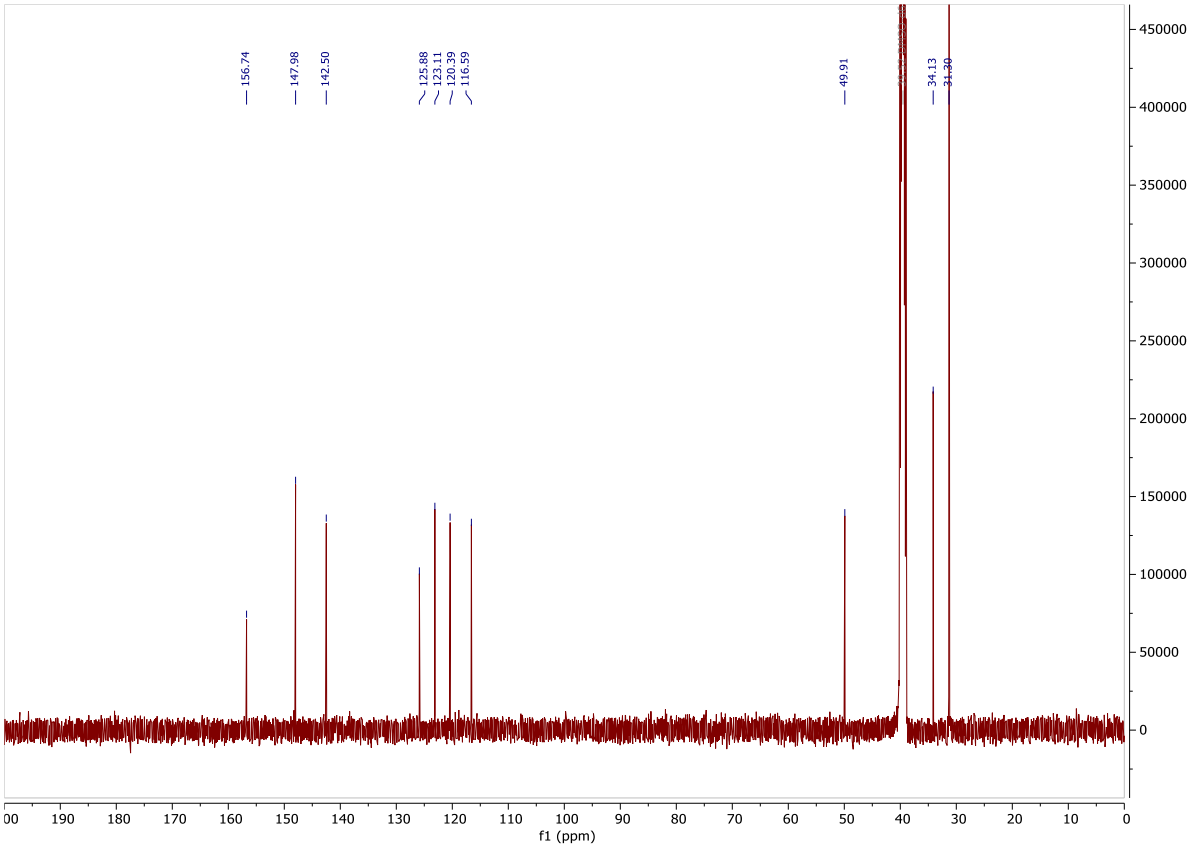

Titanium isopropoxide complex of 94 (95)

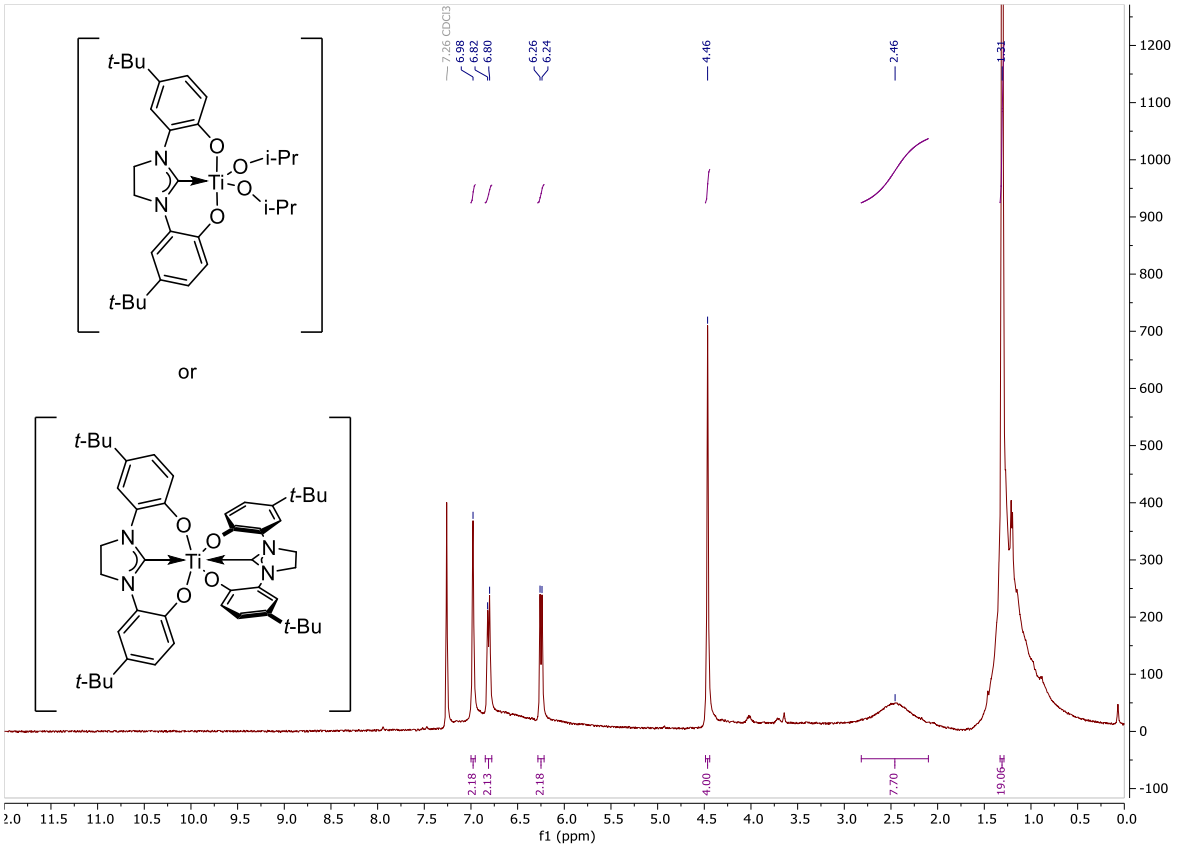

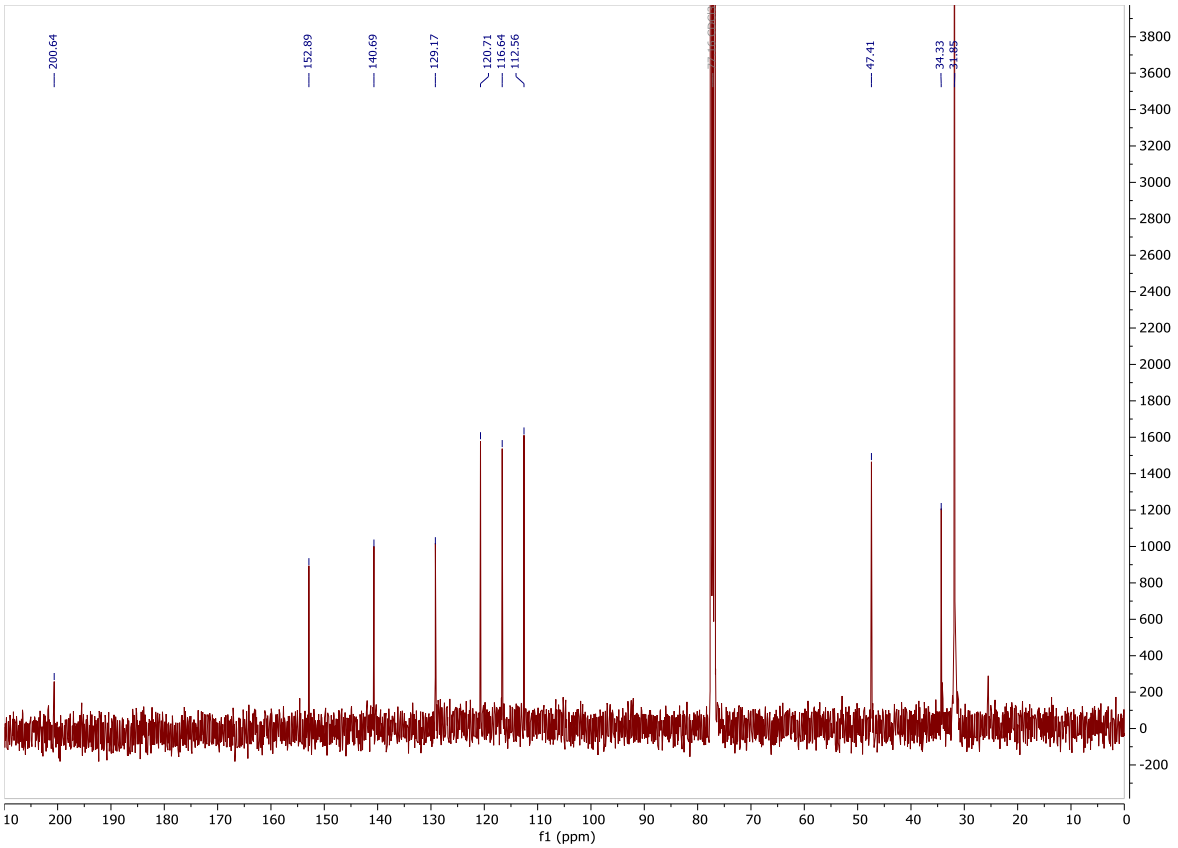

Experimental for Chapter 3

General procedure for anti-Markovnikov LMCT hydroxylation

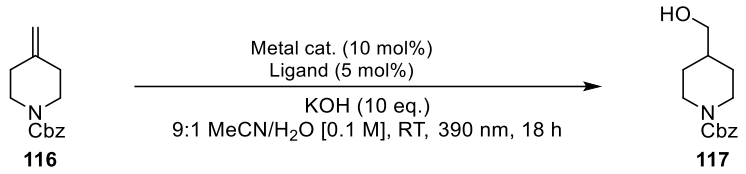

A microwave vial was charged with benzyl 4-methylidenepiperidine-1-carboxylate (41.5 µL, 0.2 mmol), metal catalyst (10 mol%), ligand (5 mol%) and any other additives. A mixture of acetonitrile (1.8 mL) and aq. KOH (10 M, 0.2 mL) was added and the reaction was bubbled with argon for 5 min. The reaction was stirred at RT under 390 nm light irradiation for 18 h, before the internal standard was introduced and aliquot taken for NMR analysis.

N-cyclohexyl-N-(2-(dicyclohexylamino)-3-(diethylamino)cyclopropylidene)cyclohexanaminium chloride (124)

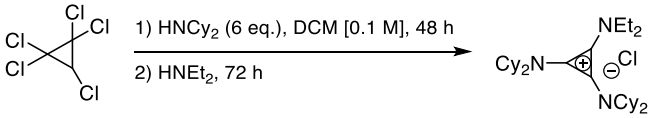

Prepared according to a literature procedure.[322]

A solution of pentrachlorocyclopropane (1.28 mL, 10 mmol) in DCM (100 mL) was sparged with argon for 10 min and cooled to 0 °C. Dicyclohexylamine (12 mL, 60 mmol) was added dropwise and the reaction was stirred for 48 h at RT. To the mixture, diethylamine (2.06 mL, 20 mmol) was added dropwise and the reaction was stirred for 72 h before it was quenched with conc. HCl (40 mL) at 0 °C. The resulting precipitate was filtered and washed with aq. HCl (1 M, 100 mL) and hot chloroform (100 mL). The combined organic was washed with aq. HCl (5x100 mL), water (50 mL) and brine (50 mL), dried over Na_2SO_4, filtered and evaporated to afford **124** as a solid (4.03 g, 79%).

^{1}H NMR (400 MHz, $CDCl_3$) δ 4.12 (q, J = 7.2 Hz, 4H), 3.61 (q, J = 7.2 Hz, 4H), 3.35 (t, J = 12.4 Hz, 4H), 1.96 – 1.01 (m, 42H).

^{13}C NMR (101 MHz, $CDCl_3$) δ 119.7, 118.7, 60.9, 46.4, 32.5, 25.9, 24.9, 14.7.

124 is a known compound and its NMR spectra are in accord with published data.[322]

General procedure for anti-Markovnikov N-oxide hydroxylation

A microwave vial was charged with methyl undecanoate (40 mg, 0.2 mmol), photocatalyst (5 mol%), HAT catalyst (5 mol%) and pyridine N-oxide (25 mol%). A mixture of acetonitrile (3.6 mL) and water (0.4 mL) was added and the reaction was bubbled with argon for 5 min. The reaction was stirred at RT under 427 nm light irradiation for 18 h. The solvent was removed under reduced pressure, and the crude was dissolved in $CDCl_3$ and taken for NMR analysis.

Methyl 11-Hydroxyundecanoate (133a)

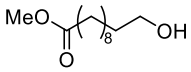

Adapted from literature procedure.[323]

To an oven-dried two-neck flask was added methyl undecanoate (595 mg, 3 mmol) under argon atmosphere. A solution of borane-THF (1M in THF, 3 mL, 3 mmol) was added dropwise at 0°C and the reaction was warmed to 40 °C and stirred for 1.5 h. Aqueous sodium hydroxide (10 wt%, 1.08 mL, 3 mmol) was added, followed by dropwise addition of hydrogen peroxide (30 wt%, 0.61 mL, 6 mmol) and the reaction was stirred at 50 °C for 2 h. The mixture was quenched with saturated potassium carbonate, and the aqueous layer was extracted with EtOAc (3x10 mL). The combined organic was washed with brine (20 mL), dried over $MgSO_4$, filtered and evaporated under reduced pressure. Purification via silica plug eluting with pentane (100 mL) and EtOAc (100 mL) afforded the purified product as a colourless oil (200 mg, 31%).

^{1}H NMR (400 MHz, $CDCl_3$) δ 3.68 – 3.59 (m, 5H), 2.30 (t, J = 7.5 Hz, 2H), 1.67 – 1.50 (m, 5H), 1.28 (m, J = 4.0 Hz, 12H).

^{13}C NMR (101 MHz, $CDCl_3$) δ 174.5, 63.2, 51.6, 34.3, 32.9, 29.6, 29.5, 29.5, 29.3, 29.3, 25.8, 25.1.

133a is a known compound and its NMR spectra are in accord with published data.[324]

Methyl 11-chloroundecanoate (133b)

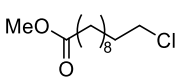

Adapted from literature procedure.[325]

To an oven-dried round bottom flask was added N-chlorosuccinimide (70 mg, 0.53 mmol, 1.05 equiv.), THF (3.2 mL, 0.26 M) and triphenylphosphine (139 mg, 0.53 mmol, 1.05 equiv.) sequentially. The resulting pink slurry was stirred for 30 minutes at room temperature in the dark. Alcohol **133a** (108 mg, 0.5 mmol, 1 equiv.) in THF (3.2 mL) was then added to the reaction mixture and the resulting slurry was stirred at room temperature for 17 hours, at which point the reaction turned into a burgundy solution. The reaction mixture was diluted with water (10 mL) and extracted with EtOAc (3x10 mL). Combined organic was washed with water (10 mL) and brine (10 mL), dried over MgSO4, filtered and evaporated under reduced pressure. Purification via silica plug eluting with pentane (50 mL) afforded **133b** (59 mg, 50%) as a colourless oil.

^{1}H NMR (400 MHz, $CDCl_3$) δ 3.66 (s, 3H), 3.52 (t, J = 6.8 Hz, 2H), 2.30 (t, J = 7.5 Hz, 2H), 1.81 – 1.70 (m, 2H), 1.67 – 1.54 (m, 3H), 1.42 (s, 3H), 1.33 – 1.23 (m, 12H).

^{13}C NMR (101 MHz, $CDCl_3$) δ 174.5, 51.6, 45.3, 34.2, 32.8, 29.5, 29.4, 29.3, 29.3, 28.9, 27.0, 25.1.

General procedure A for N-oxide synthesis:

To a solution of pyridine (10 mmol) in TFA (20 mL) was added a solution of hydrogen peroxide (30 wt% in water, 5.9 mL) and the reaction was stirred at 100 °C for 4 h. The solution was cooled to room temperature and poured over ice-water. The resulting suspension was extracted with DCM, the organic layer was washed with aq. $NaHCO_3$ and brine, dried over $MgSO_4$, filtered and evaporated under reduced pressure. The crude was passed through a short silica plug (eluting with DCM, then 10% MeOH/DCM) to afford the pure product.

General procedure B for N-oxide synthesis:

To a solution of pyridine (10 mmol) in chloroform (10 mL) was added meta-chloroperbenzoic acid (3.44 g, 20 mmol) and the reaction was stirred at 70 °C overnight. The resulting suspension was neutralised with sodium bicarbonate and extracted with DCM (20 mL). The combined organic was washed with aq. Sodium bicarbonate (20 mL), water (20 mL) and brine (20 mL), dried over $MgSO_4$, filtered and evaporated under reduced pressure. The crude was passed through a short silica plug (eluting with DCM, then 10% MeOH/DCM) to afford the pure product.

2,6-Dichloropyridine 1-oxide (127)

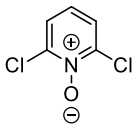

Prepared following general procedure A on a 23.4 mmol scale and purified by trituration from DCM with pentane as the antisolvent. Dried under suction to afford **127** as an off-white solid (1.55 g, 40% yield).

^{1}H NMR (400 MHz, $CDCl_3$) δ 7.46 (d, J = 8.1 Hz, 2H), 7.13 (t, J = 8.1 Hz, 1H).

^{13}C NMR (101 MHz, $CDCl_3$) δ 143.0, 125.0, 124.8.

127 is a known compound and its NMR spectra are in accord with published data.[326]

2,6-Dibromopyridine 1-oxide (134)

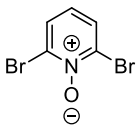

Prepared following general procedure A on a 11.7 mmol scale and purified by passing through a short silica plug (eluting with DCM then 10% MeOH in DCM) to **134** (1.66 g, 56% yield) as an orange solid.

^{1}H NMR (400 MHz, $CDCl_3$) δ 7.65 (d, J = 8.0 Hz, 2H), 6.94 (t, J = 8.0 Hz, 1H).

^{13}C NMR (101 MHz, $CDCl_3$) δ 133.9, 129.7, 125.1.

134 is a known compound and its NMR spectra are in accord with published data.[327]

2,4,6-Trimethylpyridine 1-oxide (135)

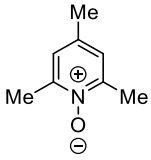

To a solution of 2,4,6-collidine (2.64 mL, 20 mmol) in acetic acid (20 mL) was added a solution of hydrogen peroxide (30 wt% in water, 8.5 mL, 75 mmol) and the reaction was stirred at 100 °C for 12 h. The solution was cooled reduced under vacuum and neutralised with aq. $NaHCO_3$. Extracted with DCM (3x20 mL), combined organic was washed with water (2x20 mL) and brine (20 mL), dried over $MgSO_4$, filtered and evaporated under reduced pressure. The crude was passed through a short silica plug

(eluting with EtOAc, then 10% MeOH/DCM) to afford **135** (975 mg, 36%) as a yellow solid.

^{1}H NMR (400 MHz, $CDCl_3$) δ 6.96 (s, 2H), 2.51 (s, 6H), 2.28 (s, 3H).

^{13}C NMR (126 MHz, $CDCl_3$) δ 148.3, 136.5, 124.9, 20.3, 18.3.

135 is a known compound and its NMR spectra are in accord with published data.[328]

4-(Tert-butyl)pyridine 1-oxide (136)

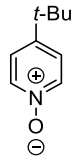

To a solution of 4-tert-butyl pyridine (18 mL, 123 mmol) in acetic acid (135 mL) was added hydrogen peroxide (30 wt% in water, 200 mL) portionwise and the reaction was stirred at 110 °C for 16 h. The solvent was distilled off and the remaining crude was neutralised with aq. $NaHCO_3$ (1 M, 50 mL) and extracted with DCM (3x30 mL). The combined organic was washed with water (3x30 mL) and brine (30 mL), dried over $MgSO_4$, filtered and evaporated. Purification over a short pad of silica gel (eluting with EtoAc, then 10% MeOH in DCM) afforded **136** (9 g, 48%) as an orange solid.

^{1}H NMR (400 MHz, $CDCl_3$) δ 8.12 (d, J = 6.4 Hz, 2H), 7.25 (d, J = 6.2 Hz, 2H), 1.29 (s, 9H).

^{13}C NMR (101 MHz, $CDCl_3$) δ 150.9, 138.6, 123.2, 34.6, 30.6.

136 is a known compound and its NMR spectra are in accord with published data.[329]

2,4,6-Triphenylpyridine (137)

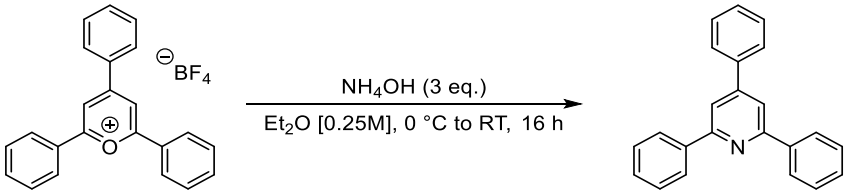

To a suspension of 2,4,6-triphenylpyrylium tetrafluoroborate (1.98 g, 5 mmol) in diethyl ether (20 mL) was added ammonium hydroxide (28–30% wt. in water, 1.95 mL, 15 mmol) at 0 °C. The resulting solution was allowed to warm up to room temperature and stirred for 16 h. The reaction was diluted with water (20 mL) and extracted with diethyl ether (50 mL). Combined organic was washed with water (20 mL), brine (20 mL), dried

over $MgSO_4$, filtered and evaporated to afford the crude product. Purification through a short silica plug (eluting with DCM) gave the pure product (1.51 g, 98% yield).

^{1}H NMR (400 MHz, $CDCl_3$) δ 8.25 – 8.17 (m, 4H), 7.90 (s, 2H), 7.80 – 7.72 (m, 2H), 7.58 – 7.42 (m, 9H).

^{13}C NMR (101 MHz, $CDCl_3$) δ 157.6, 150.4, 139.7, 139.2, 129.29, 129.23, 129.16, 128.9, 127.35, 127.31, 117.3.

137 is a known compound and its NMR spectra are in accord with published data.[330]

2,4,6-Triphenylpyridine 1-oxide (138)

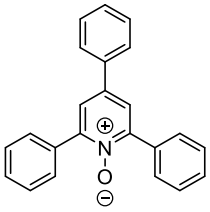

Prepared according to general procedure B on 4 mmol scale. Purification via silica plug (eluting with DCM, then 10% MeOH/DCM) afforded product **138** (388 mg, 30% yield) and recovered **137** (790 mg, 2.57 mmol).

^{1}H NMR (400 MHz, $CDCl_3$) δ 7.91 – 7.86 (m, 4H), 7.68–7.67 (m, 1H), 7.66 (s, 3H), 7.52 – 7.41 (m, 9H).

^{13}C NMR (101 MHz, $CDCl_3$) δ 149.9, 137.8, 136.8, 133.5, 129.7, 129.5, 129.4, 129.0, 128.2, 126.5, 123.9.

138 is a known compound and its NMR spectra are in accord with published data.[331]

2-(Trifluoromethyl)pyridine 1-oxide (139)

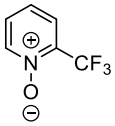

Prepared according to general procedure A on 10 mmol scale. Purification via silica plug (eluting with DCM, then 10% MeOH/DCM) afforded product **139** (595 mg, 37% yield) as yellow oil.

^{1}H NMR (400 MHz, $CDCl_3$) δ 8.31 (d, J = 6.5 Hz, 1H), 7.70 (dd, J = 8.0, 2.1 Hz, 1H), 7.45 (td, J = 7.2, 2.1 Hz, 1H), 7.34 (t, J = 7.8 Hz, 1H).

^{19}F NMR (376 MHz, $CDCl_3$) δ -69.14.

139 is a known compound and its NMR spectra are in accord with published data.[332]

4-Cyanopyridine 1-oxide (140)

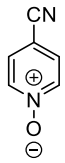

Prepared according to general procedure B. Product **140** was isolated (397 mg, 33% yield) after workup without the need for further purification. Some of the yield was lost due to the compound being soluble in water.

^{1}H NMR (400 MHz, $CDCl_3$) δ 8.27 – 8.20 (m, 2H), 7.56 – 7.49 (m, 2H).

^{13}C NMR (101 MHz, $CDCl_3$) δ 140.4, 129.1, 115.9, 107.8.

140 is a known compound and its NMR spectra are in accord with published data.[333]

2-Phenylpyridine 1-oxide (141)

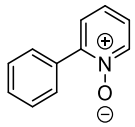

Prepared according to general procedure B on 10 mmol scale. Product **141** was isolated (775 mg, 45% yield) as an off-white solid after workup without the need for further purification.

^{1}H NMR (400 MHz, $CDCl_3$) δ 8.35 (dd, J = 6.5, 1.3 Hz, 1H), 7.85 – 7.77 (m, 2H), 7.56 – 7.41 (m, 4H), 7.34 (td, J = 7.7, 1.3 Hz, 1H), 7.29 – 7.21 (m, 1H).

^{13}C NMR (126 MHz, $CDCl_3$) δ 149.3, 140.5, 132.7, 129.6, 129.3, 128.3, 127.5, 125.7, 124.6.

141 is a known compound and its NMR spectra are in accord with published data.[334]

2,6-Dichloro-4-methoxypyridine 1-oxide (142)

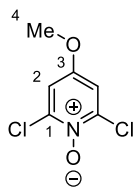

Prepared according to general procedure A on 10 mmol scale. Purification via silica plug (eluting with DCM, then 10% MeOH/DCM) afforded product **142** (400 mg, 21% yield) as an orange solid.

^{1}H NMR (400 MHz, $CDCl_3$) δ 7.02 (s, 2H, H2), 3.86 (s, 3H, H4).

^{13}C NMR (101 MHz, $CDCl_3$) δ 155.8 (C3), 143.8 (C1), 111.6 (C2), 56.8 (C4).

IR (neat) ν_{max}/cm^{-1}: 3082, 3059, 3019, 2961, 1607, 1547, 1400, 1240, 1159, 1096, 1028.

HRMS m/z (ESI) calculated for $C_6H_6Cl_2NO_2$ $[M+H]^+$ 193.9776, found: 193.9773

9-Phenylacridine 10-oxide (143)

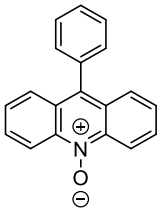

Prepared according to general procedure B. Recrystallisation from hot MeOH:$CHCl_3$ = 1:1 (ca. 100 mL) afforded product **143** (1.64 g, 61% yield)

^{1}H NMR (400 MHz, $CDCl_3$) δ 8.99 (d, J = 9.1 Hz, 2H), 7.80 (ddd, J = 9.1, 6.6, 1.3 Hz, 2H), 7.72 (dd, J = 8.9, 1.3 Hz, 2H), 7.66 – 7.56 (m, 3H), 7.52 – 7.42 (m, 4H).

^{13}C NMR (101 MHz, $CDCl_3$) δ 139.4, 135.4, 131.1, 130.8, 128.8, 128.8, 127.6, 127.1, 126.8, 120.0.

143 is a known compound and its NMR spectra are in accord with published data.[335]

The following substrates did not react under standard conditions A to form the respective N-oxide:

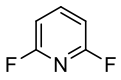

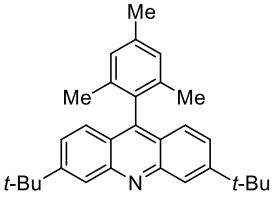

The following N-oxides did not form under standard conditions B:

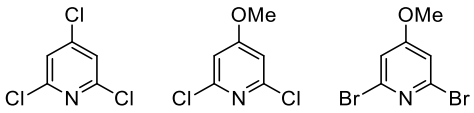

Dimethyl 2,2'-disulfanediyldibenzoate (151)

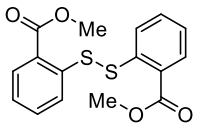

To a suspension of thiosalicylate (0.69 mL, 5 mmol) in DCM:H_2O = 1:1 (0.5 M) was added $KHCO_3$ (1 eq.) and reaction was kept in a water bath. Introduced bromine (0.5 eq.) dropwise and the resulting suspension was stirred at room temperature for 30 min. The reaction was extracted with DCM (30 mL) and the combined organic was washed with water (20 mL) and brine (10 mL), dried over $MgSO_4$, filtered and evaporated to afford the pure disulfide **151** (666 mg, 80%) as a white solid.

^{1}H NMR (400 MHz, $CDCl_3$) δ 8.00 (d, J = 7.6, Hz, 2H), 7.69 (d, J = 8.2 Hz, 2H), 7.34 (t, J = 8.2 Hz, 2H), 7.17 (d, J = 7.6 Hz, 2H), 3.92 (s, 6H).

^{13}C NMR (101 MHz, $CDCl_3$) δ 167.1, 140.5, 133.2, 131.6, 127.4, 126.0, 125.6, 52.6.

151 is a known compound and its NMR spectra are in accord with published data.[336]

N,N'-(disulfanediylbis(2,1-phenylene))diacetamide (152)

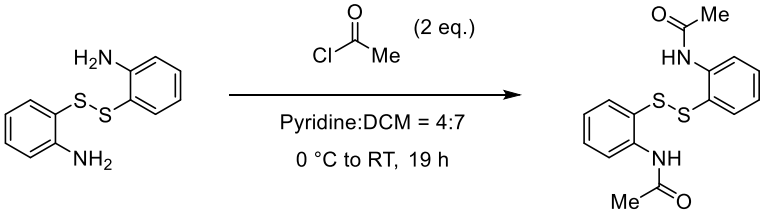

152

To a solution of 2-aminophenyl disulfide (1 g, 4 mmol) in pyridine:DCM = 4:7 (11 mL) was added acetyl chloride (0.57 mL, 8 mmol) dropwise at 0 °C and the reaction was stirred at RT for 19 h. The crude was poured into water (20 mL) and extracted with DCM (3x20 mL). The combined organic was washed with aq. HCl (1M, 2x20 mL), water (20 mL) and brine (20 mL), dried over $MgSO_4$, filtered and evaporated. The resulting solid was washed with pentane and dried under vacuum to afford **152** (1 g, 75%) as an off-white solid.

^{1}H NMR (400 MHz, $CDCl_3$) δ 8.35 (d, J = 8.3 Hz, 2H), 7.91 (s, 2H), 7.41 (t, J = 7.6 Hz, 4H), 7.02 (t, J = 7.3 Hz, 2H), 1.98 (s, 6H).

^{13}C NMR (126 MHz, $CDCl_3$) δ 168.6, 139.9, 136.5, 132.2, 124.5, 123.9, 121.3, 24.7.

152 is a known compound and its NMR spectra are in accord with published data.[337]

2-Phenylmalononitrile (153)

Synthesized following a modified literature procedure.[338]

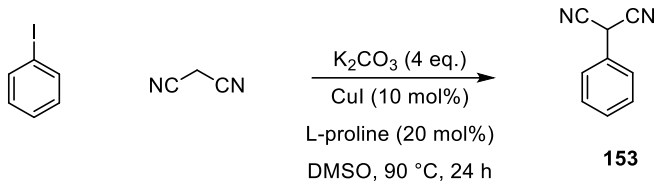

In a flame-dried and argon filled round bottom flask potassium carbonate (5.53 g, 40.0 mmol, 4.0 eq.), copper iodide (190 mg, 1.0 mmol, 10 mol%), L-proline (0.23 g, 2.0 mmol, 20 mol%) and malononitrile (1.98 g, 30.0 mmol, 3.0 eq.) were suspended in dry DMSO (40 mL). After the addition of iodobenzene (1.12 mL, 10.0 mmol, 1.0 eq.), the flask was sealed with a sureseal and stirred for 24 h at 90 °C. After cooling to room temperature, the reaction was neutralised with aq. HCl. The aqueous layer was extracted with EtOAc (3x100 mL). The combined organic layers were washed with water (2x100 mL) and brine (2x100 mL), dried over $MgSO_4$, filtered, and the solvent was removed under reduced pressure. The product was purified by column chromatography (dry loading on celite, eluting with gradient 30% to 100% DCM in cyclohexane), **153** was obtained as a white solid (352 mg, 25%).

^{1}H NMR (400 MHz, $CDCl_3$) δ 7.51 (m, 5H), 5.07 (s, 1H).

^{13}C NMR (101 MHz, $CDCl_3$) δ 130.5, 130.2, 127.3, 126.3, 111.9, 28.2.

153 is a known compound and its NMR spectra are in accord with published data.[338]

NMR spectra for Chapter 3

N-cyclohexyl-N-(2-(dicyclohexylamino)-3-(diethylamino)cyclopropylidene)cyclohexanaminium chloride (124)

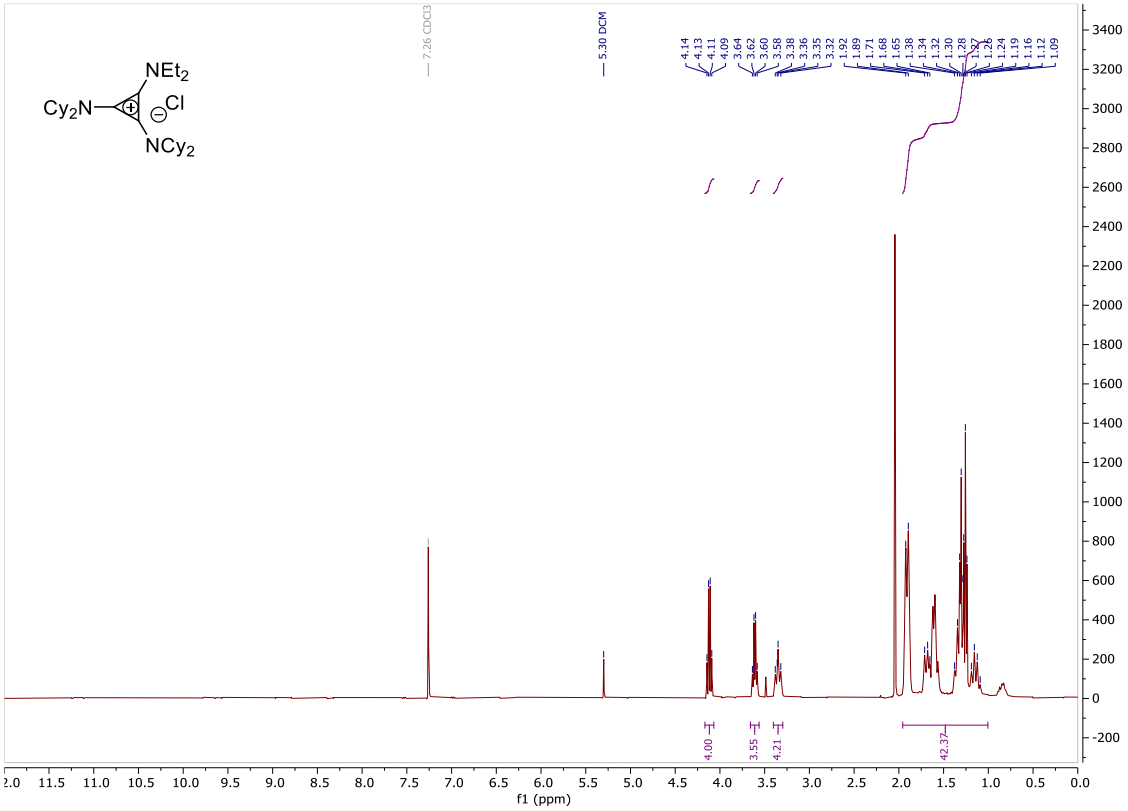

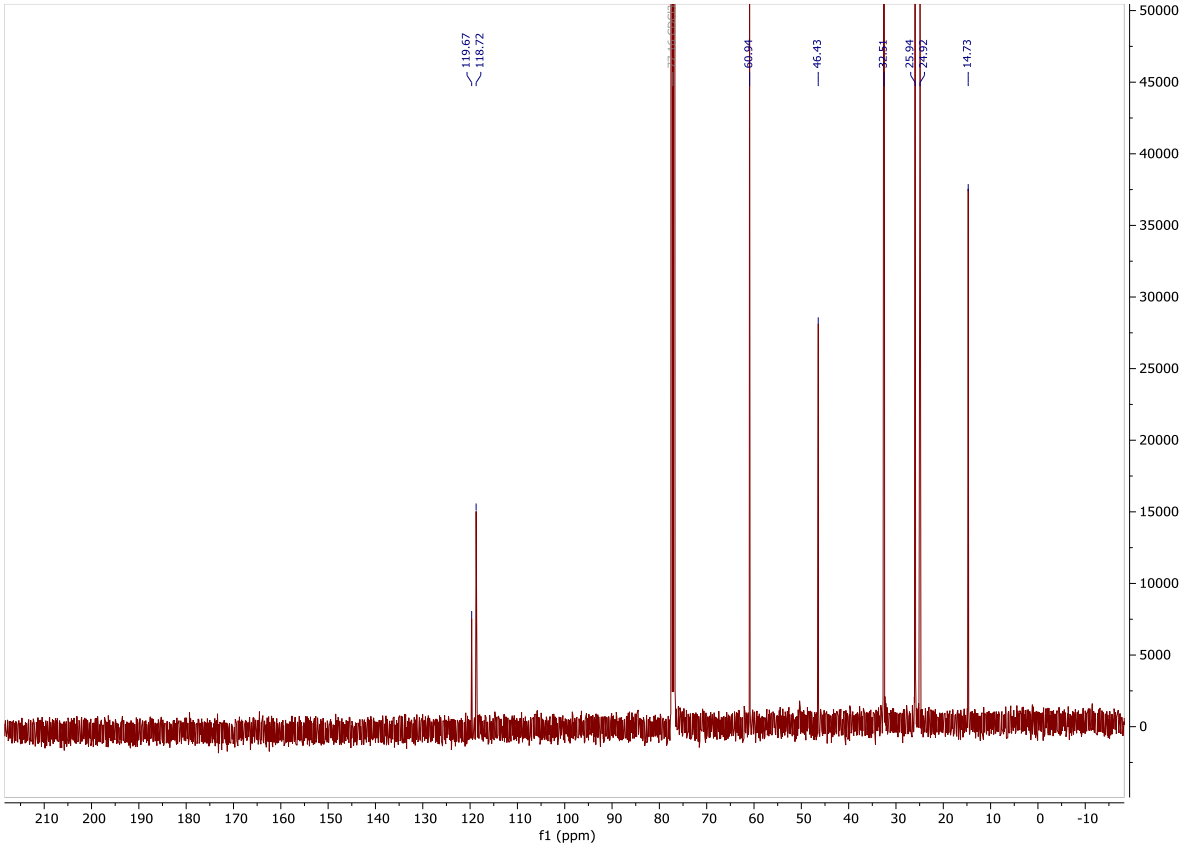

Methyl 11-Hydroxyundecanoate (133a)

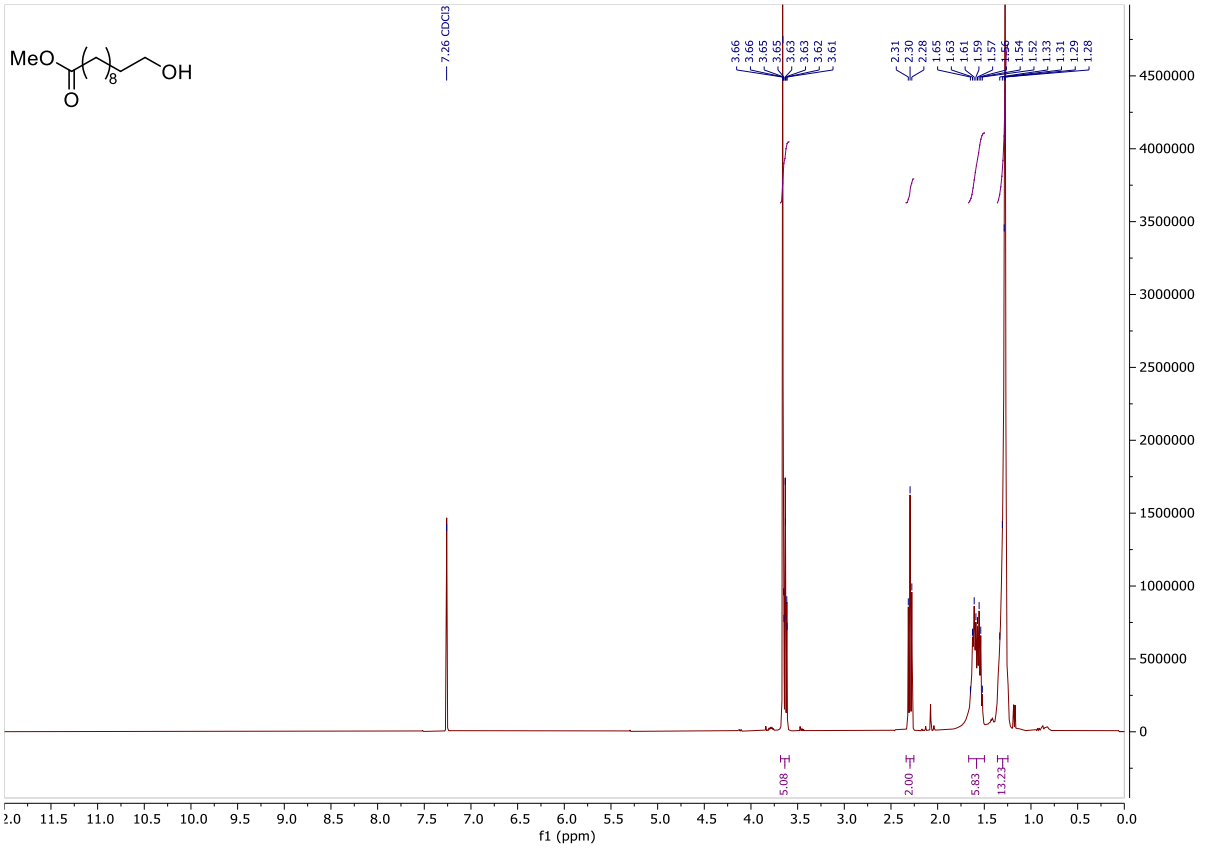

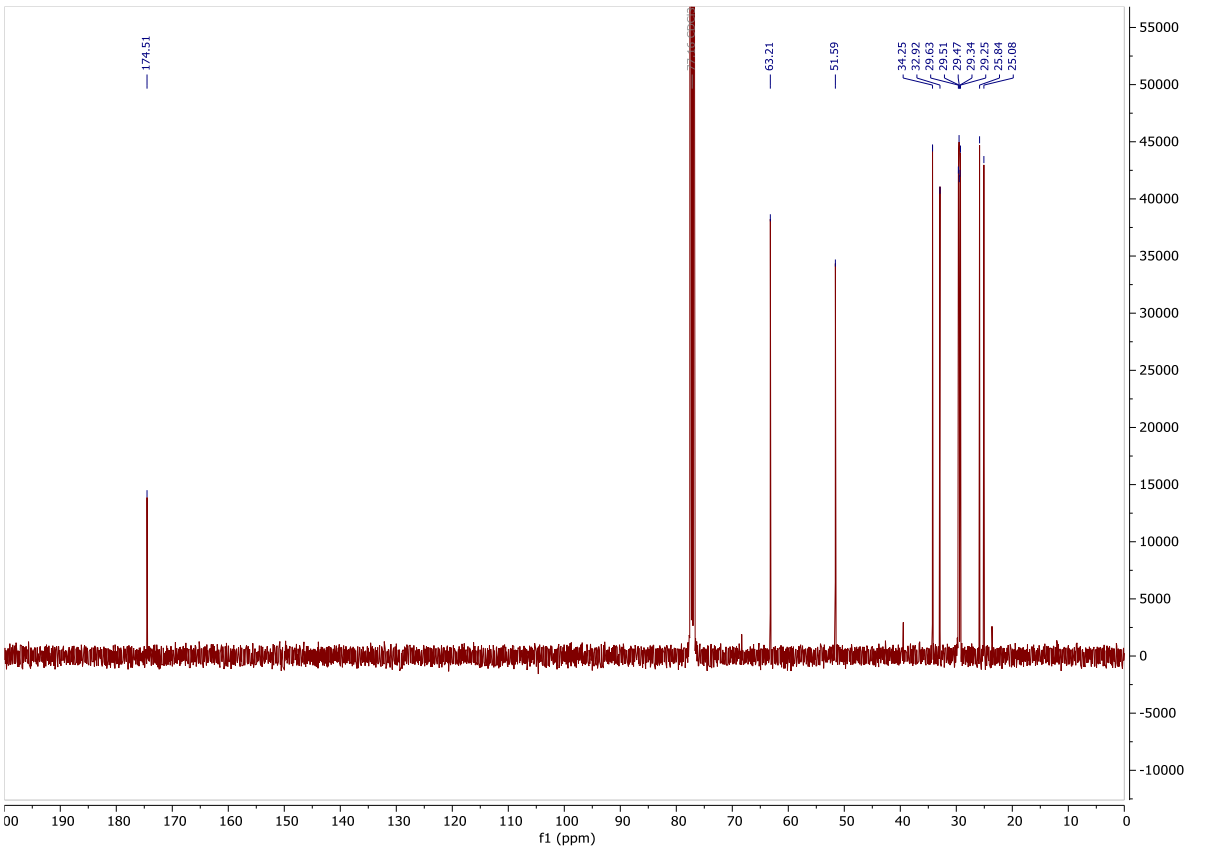

Methyl 11-chloroundecanoate (133b)

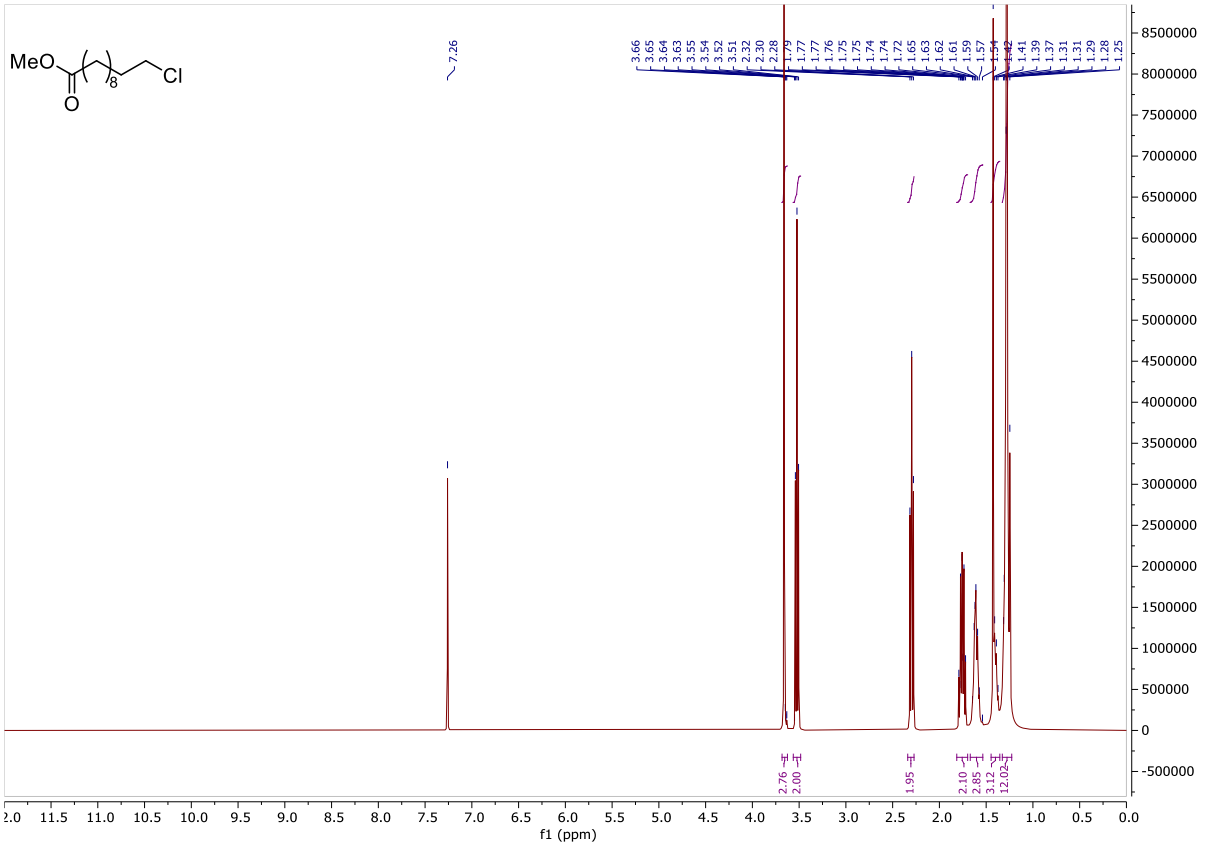

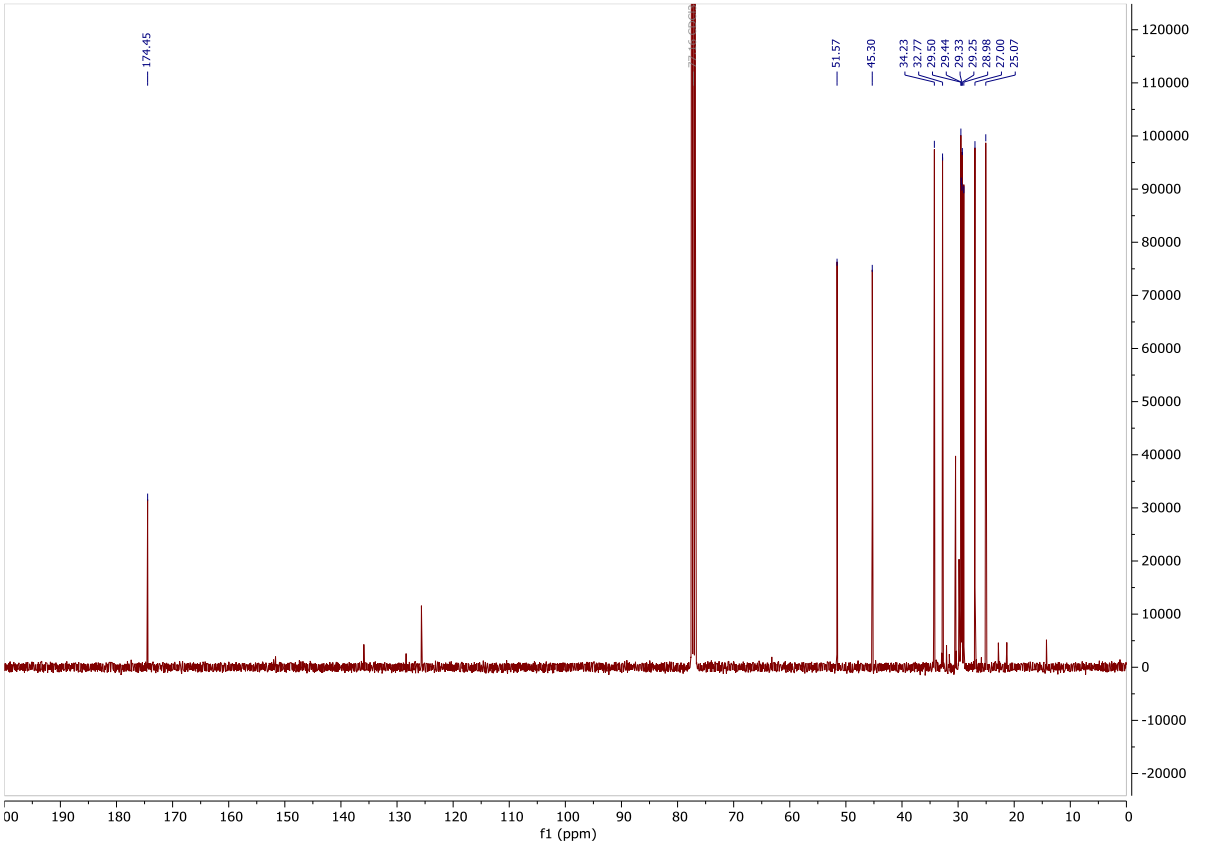

2,6-Dichloropyridine 1-oxide (127)

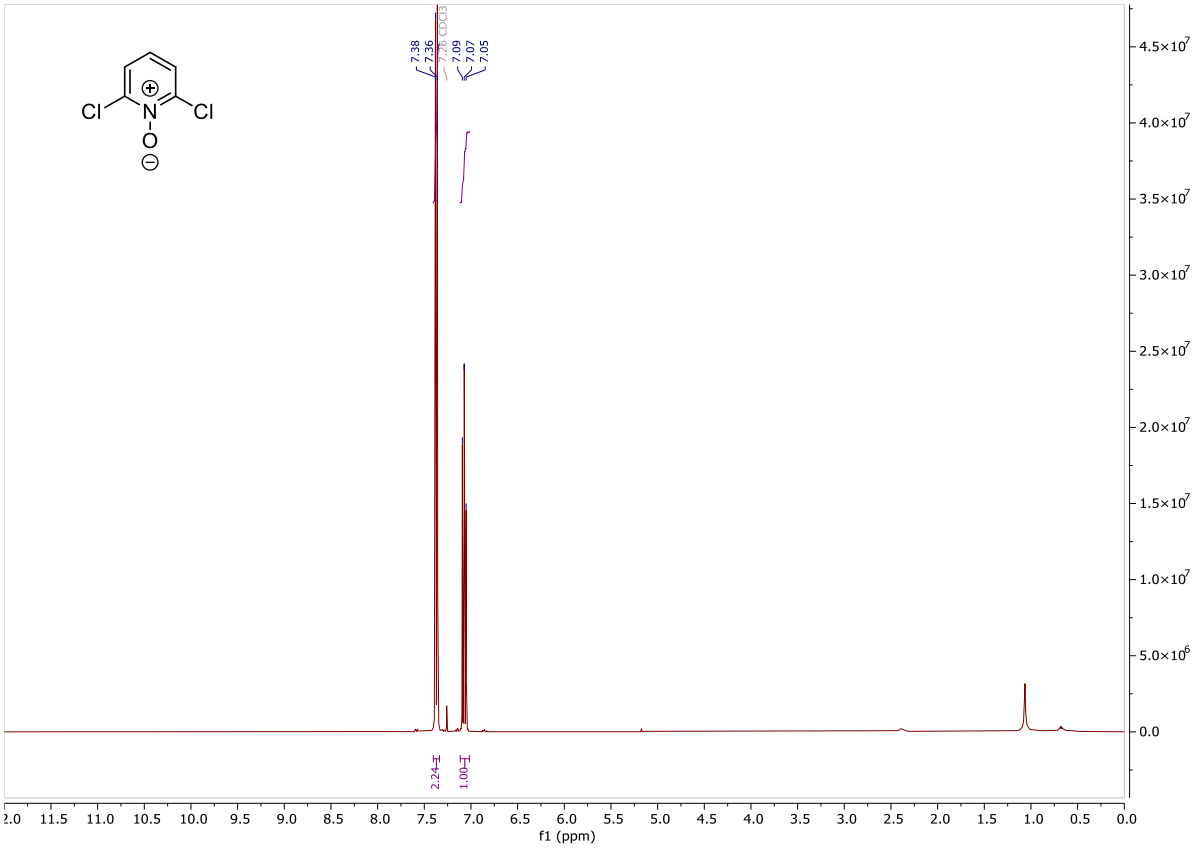

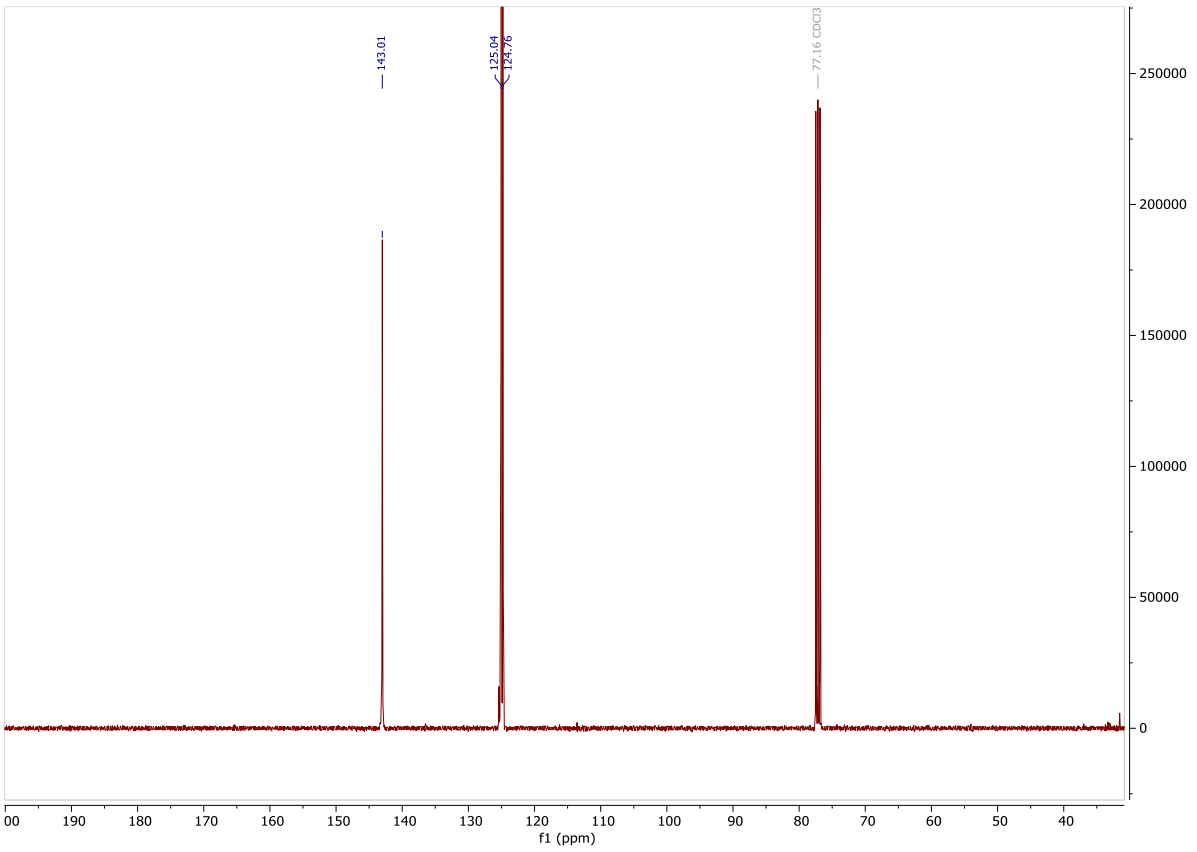

2,6-Dibromopyridine 1-oxide (134)

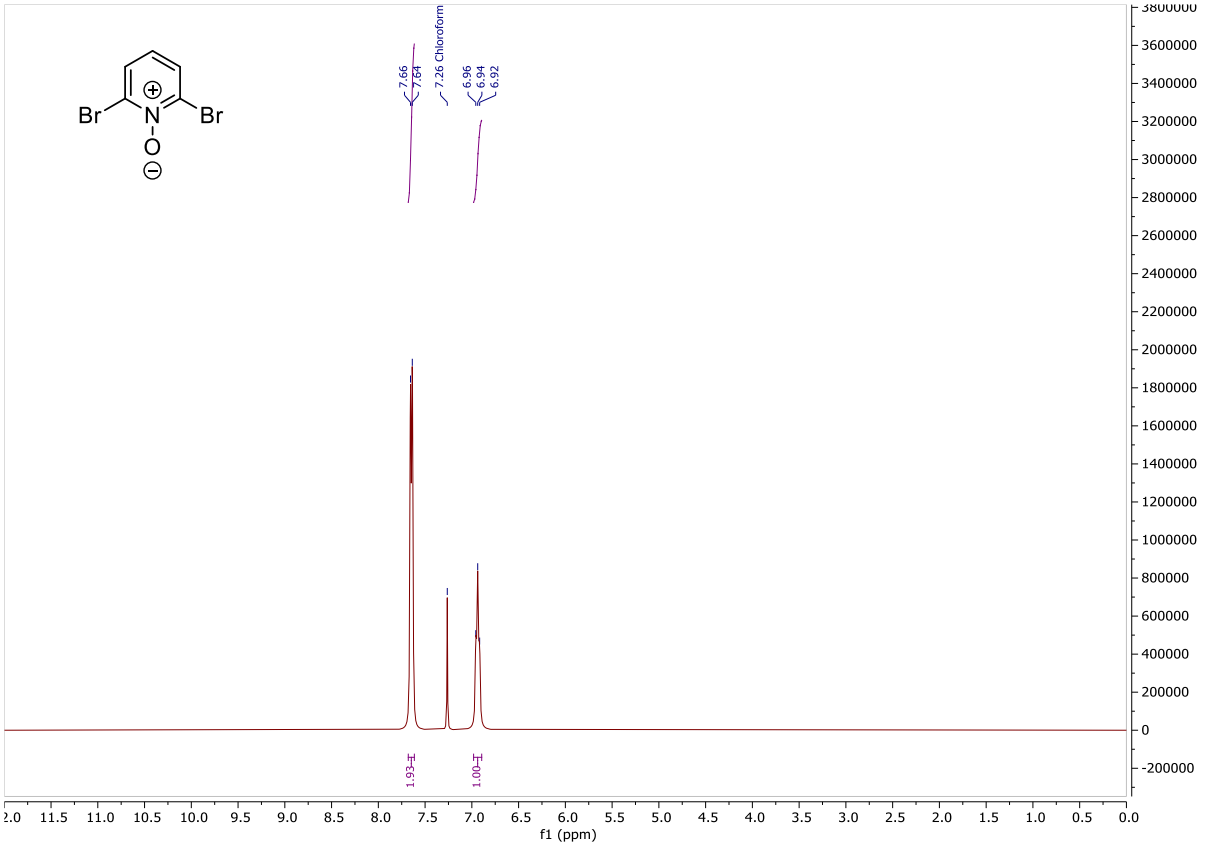

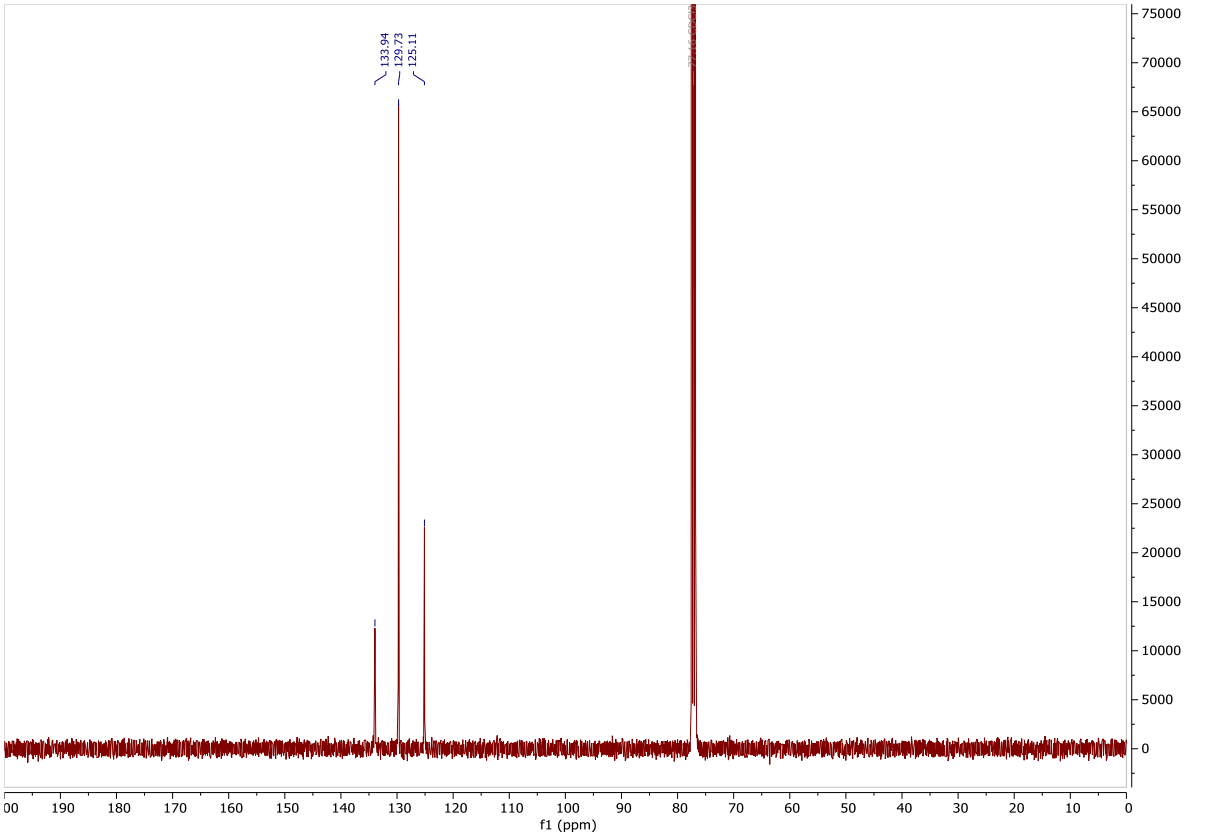

2,4,6-Trimethylpyridine 1-oxide (135)

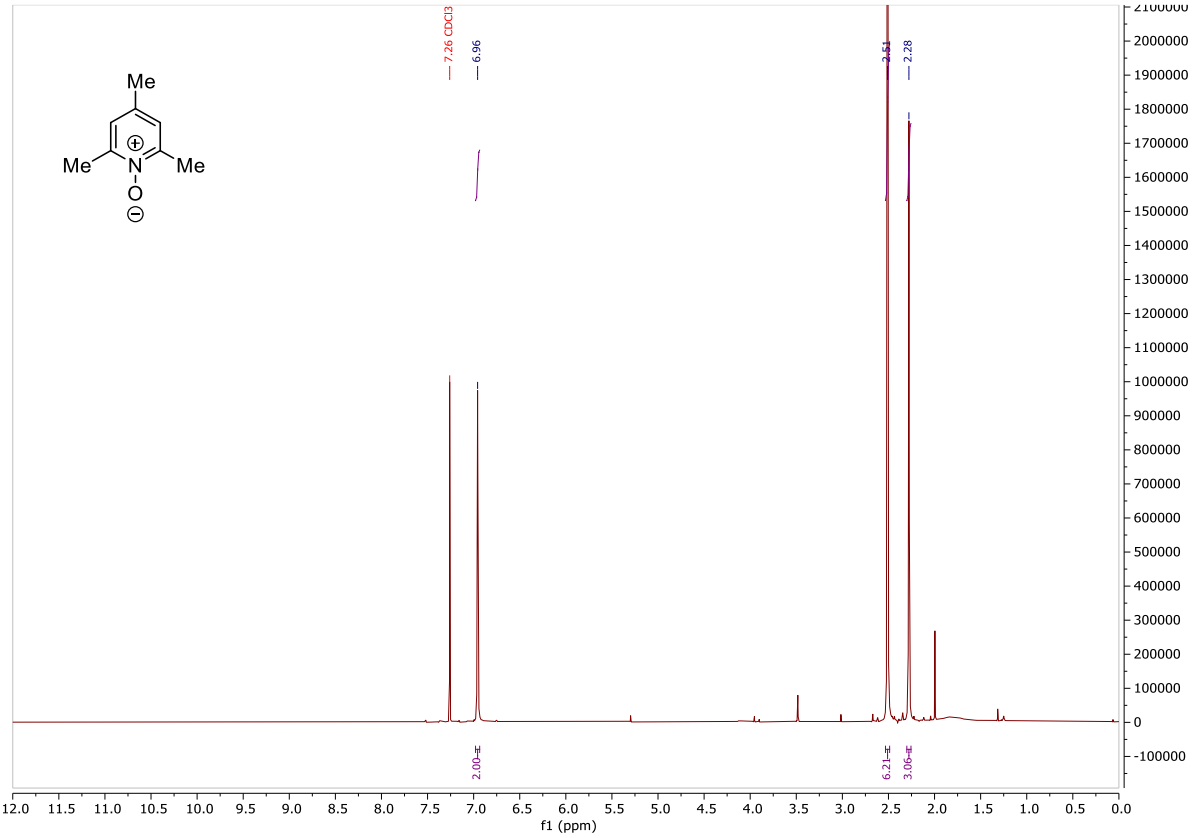

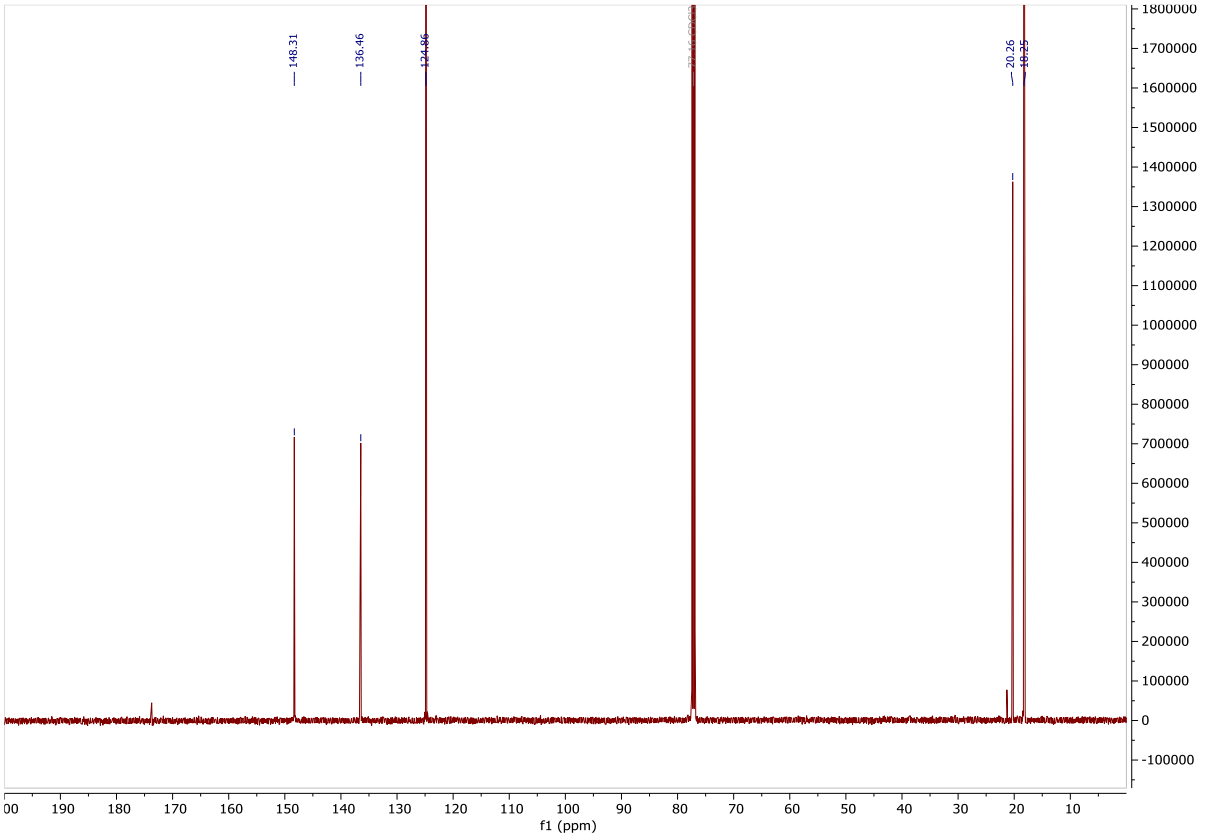

4-(Tert-butyl)pyridine 1-oxide (136)

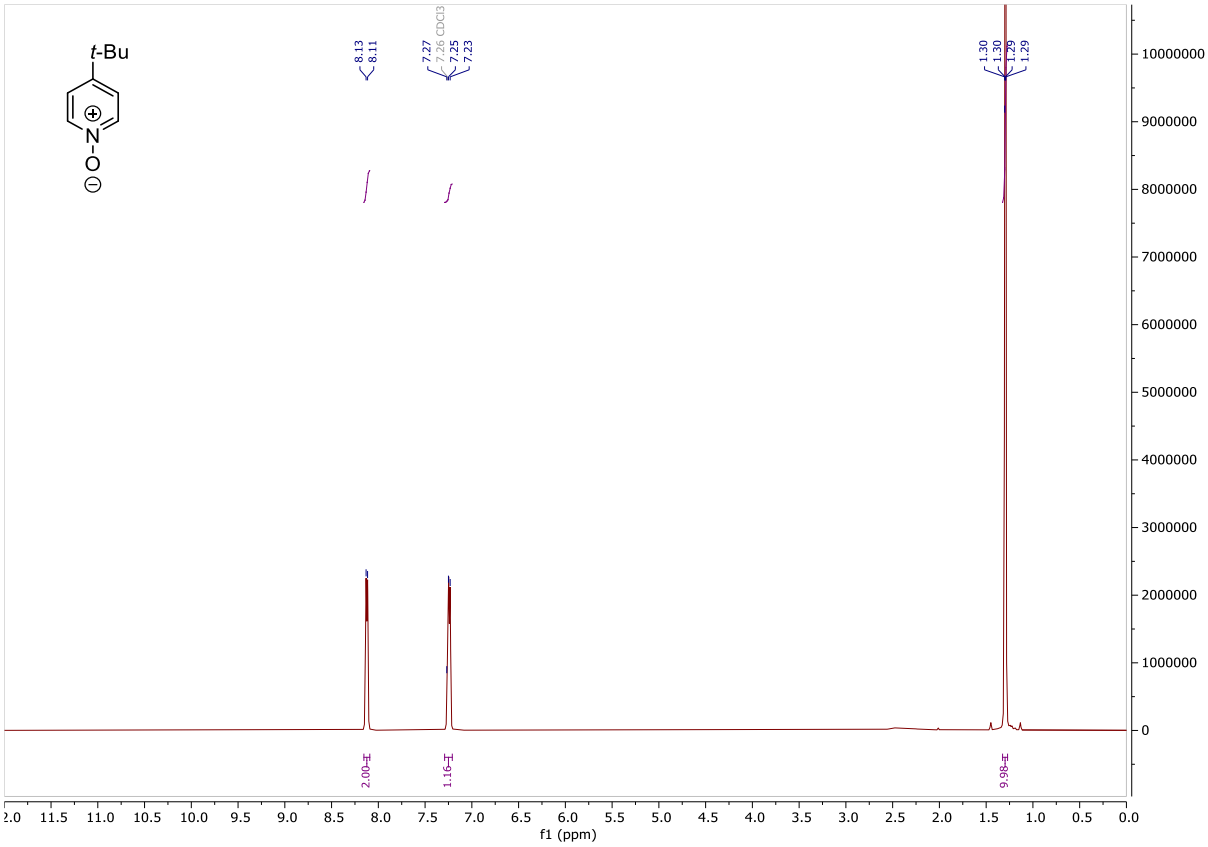

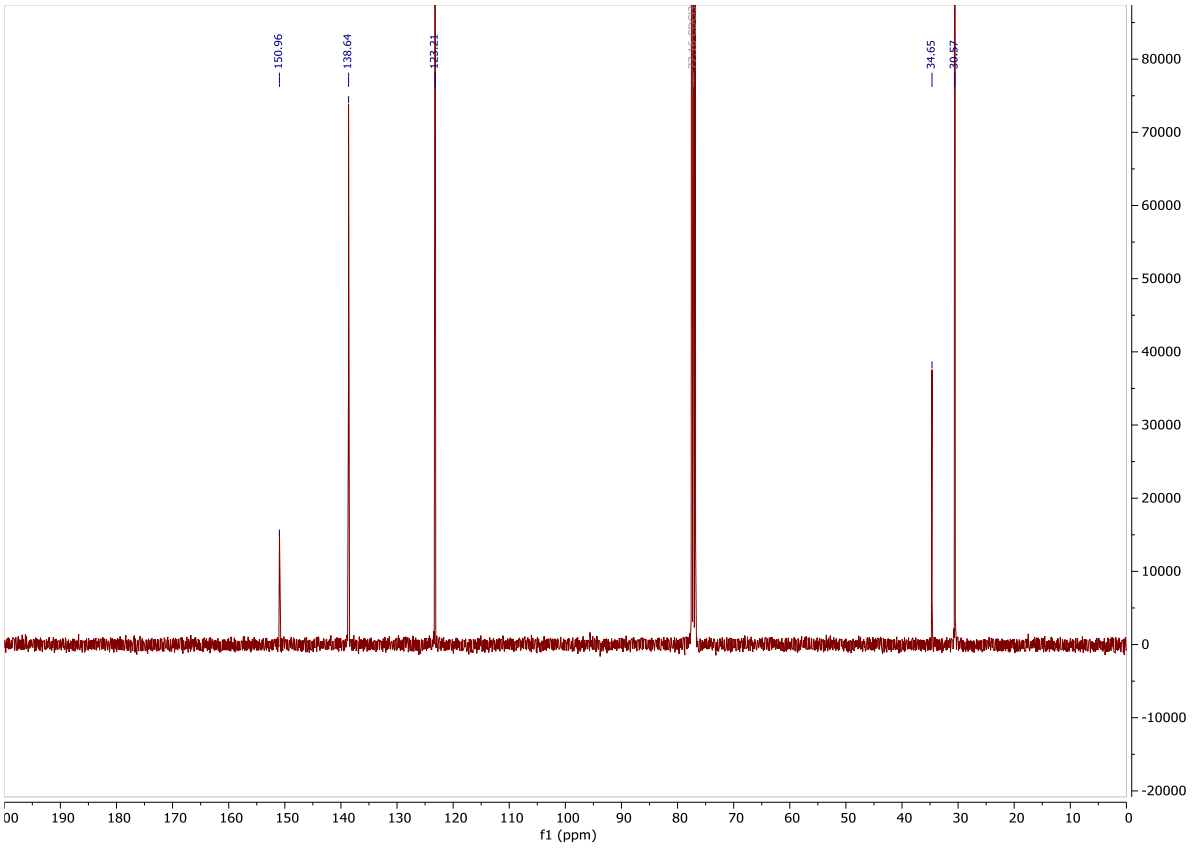

2,4,6-Triphenylpyridine (137)

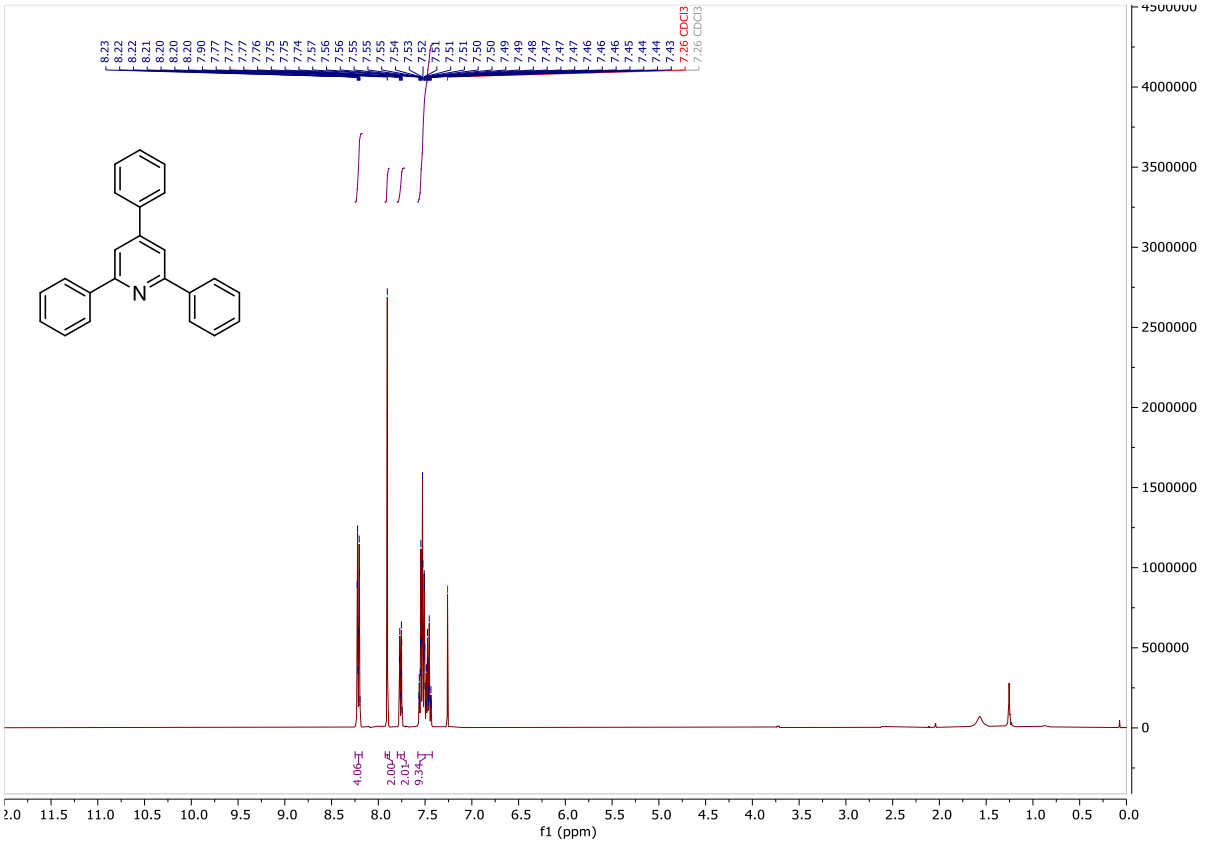

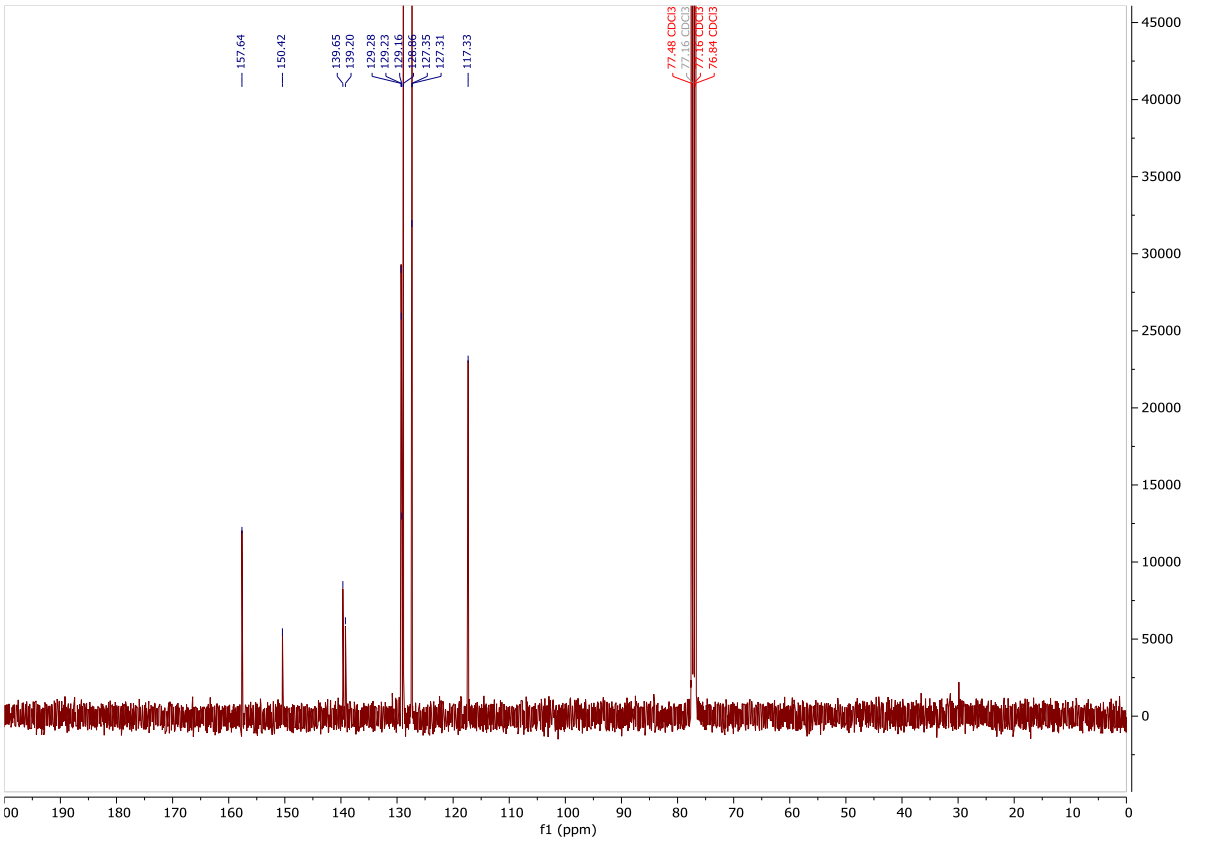

2,4,6-Triphenylpyridine 1-oxide (138)

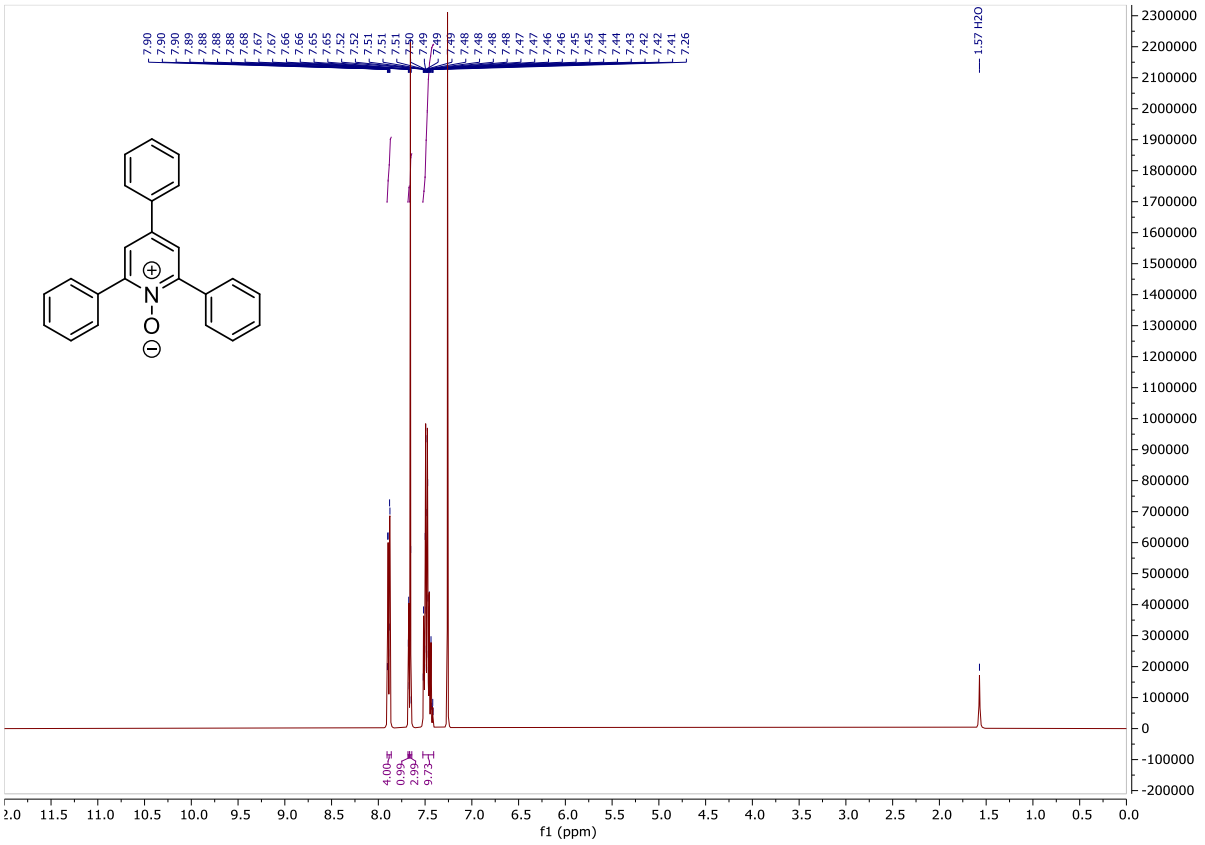

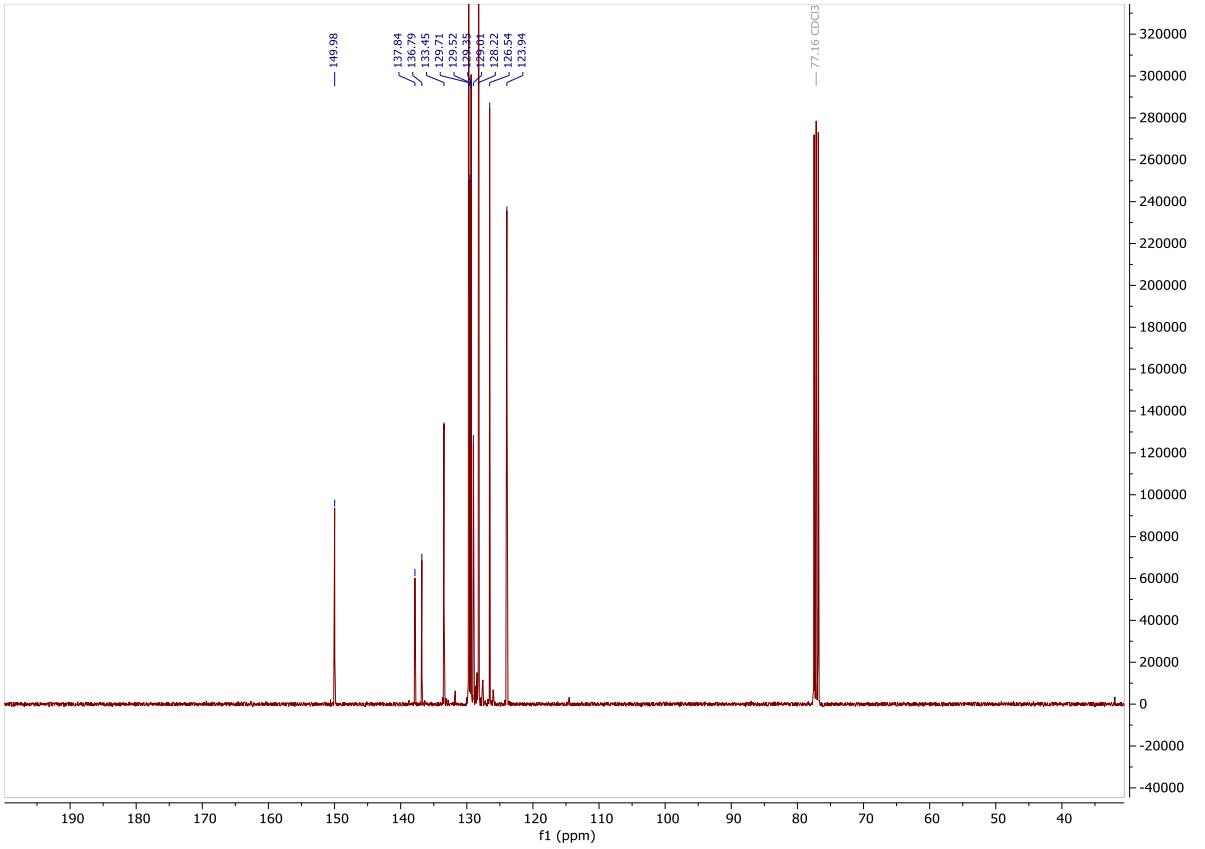

2-(Trifluoromethyl)pyridine 1-oxide (139)

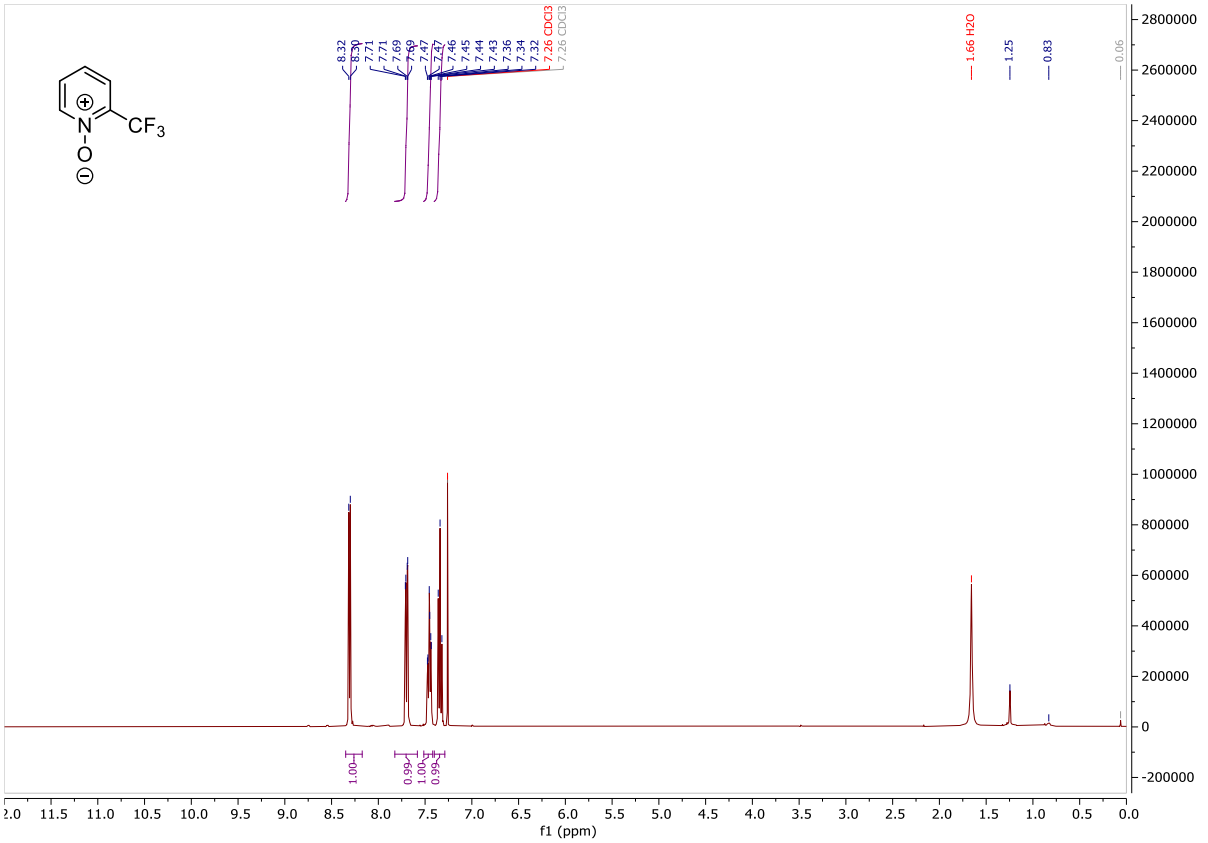

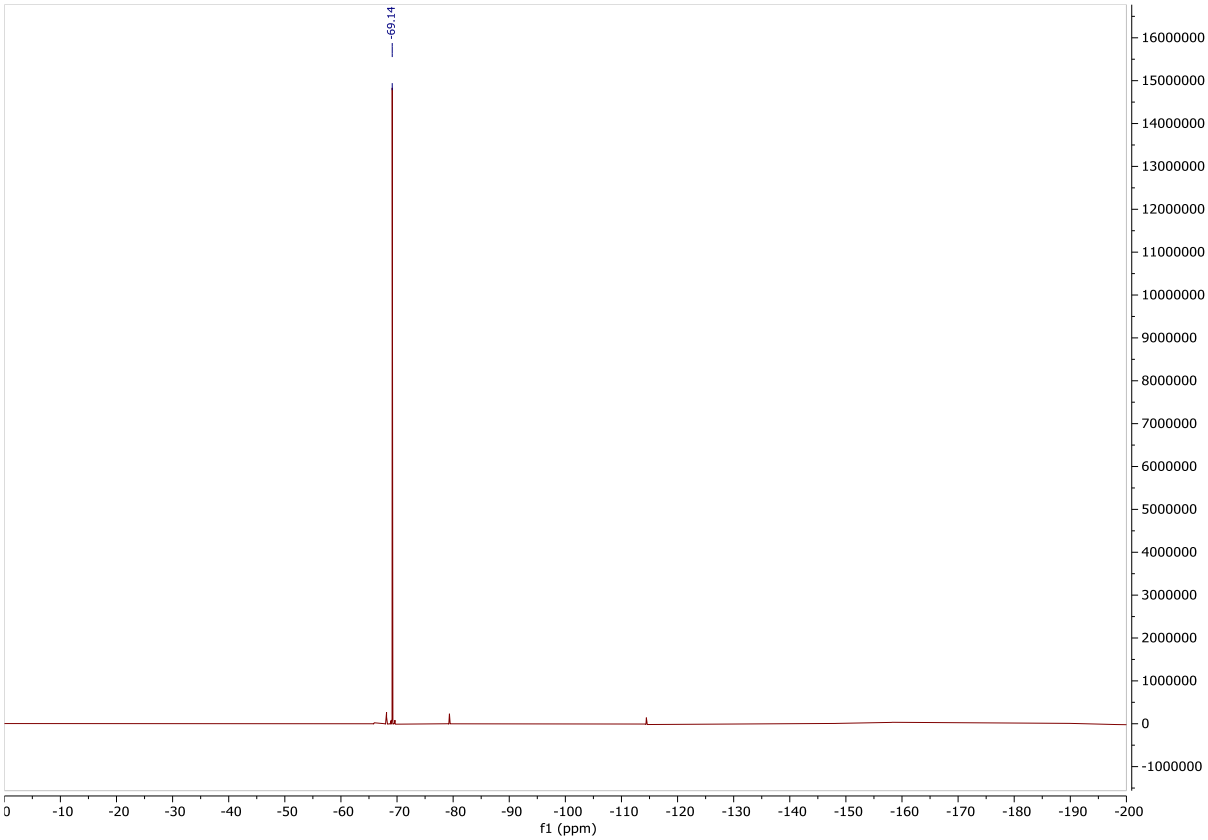

4-Cyanopyridine 1-oxide (140)

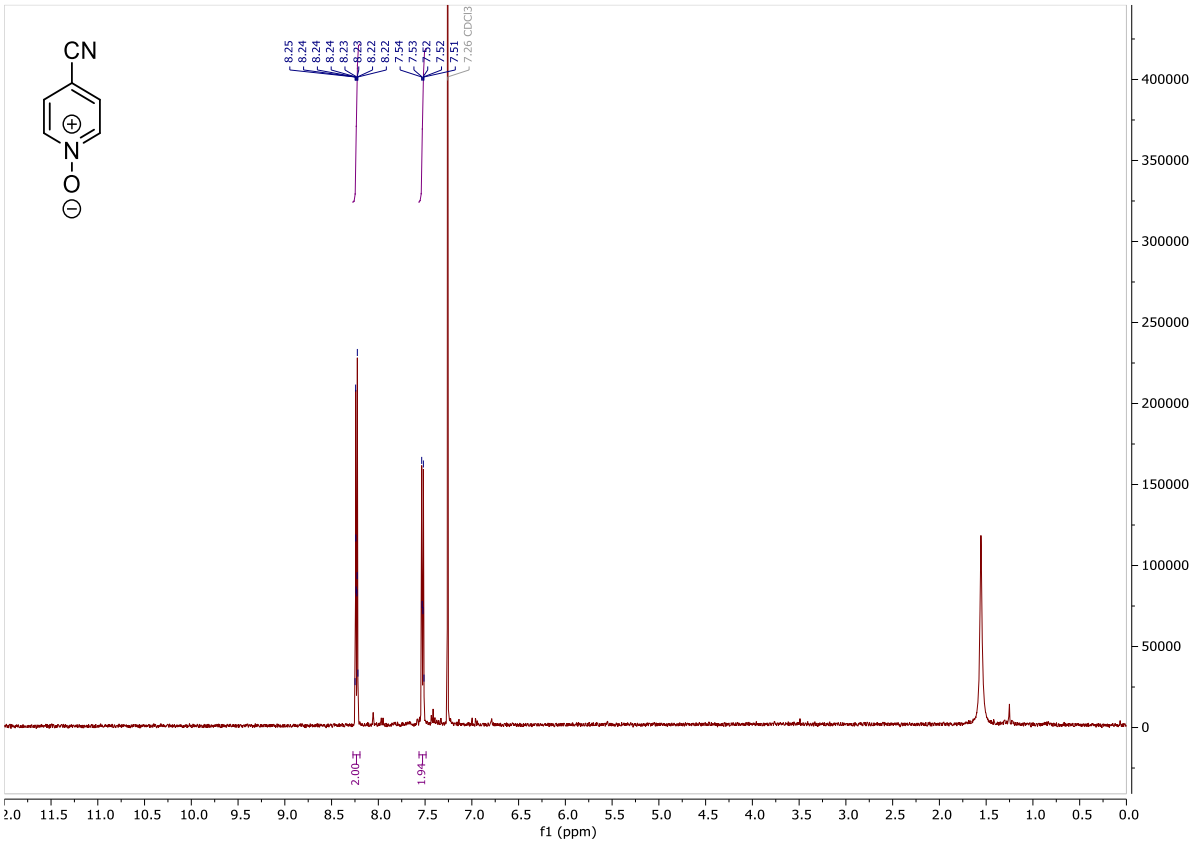

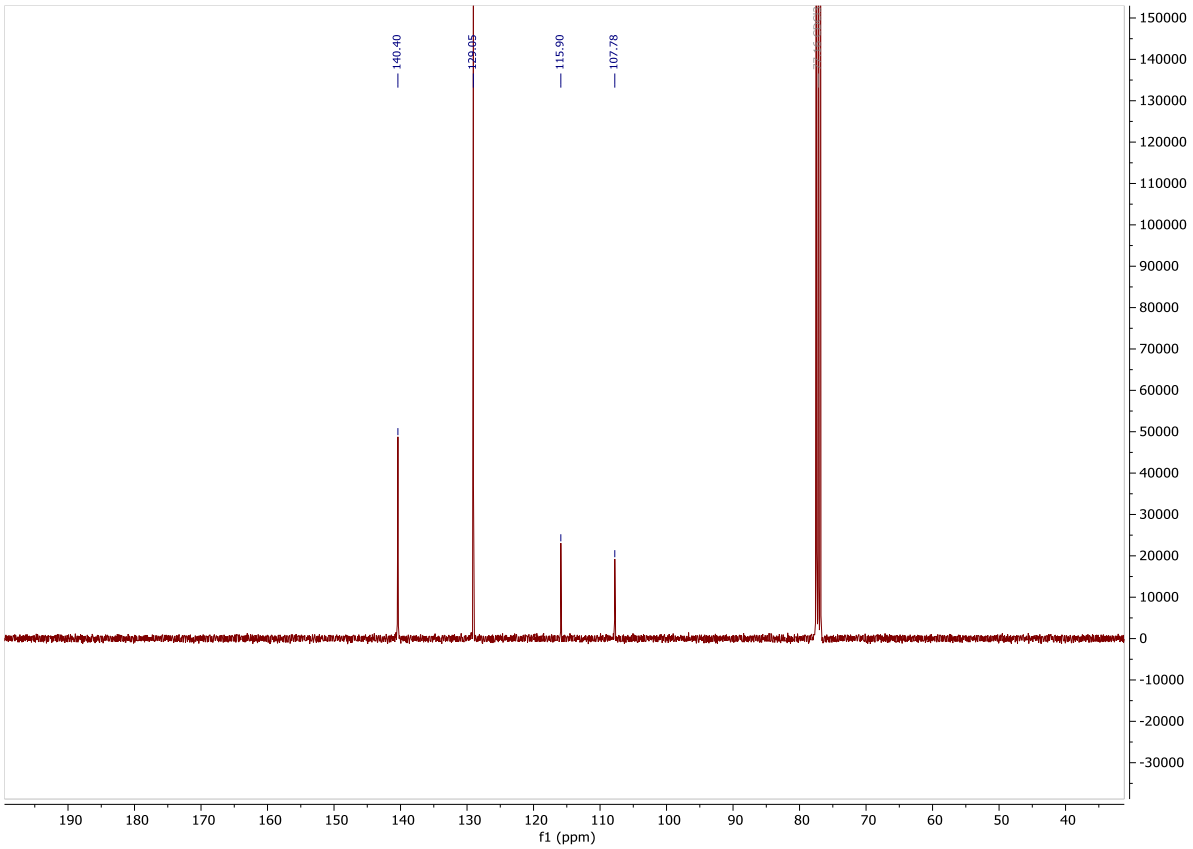

2-Phenylpyridine 1-oxide (141)

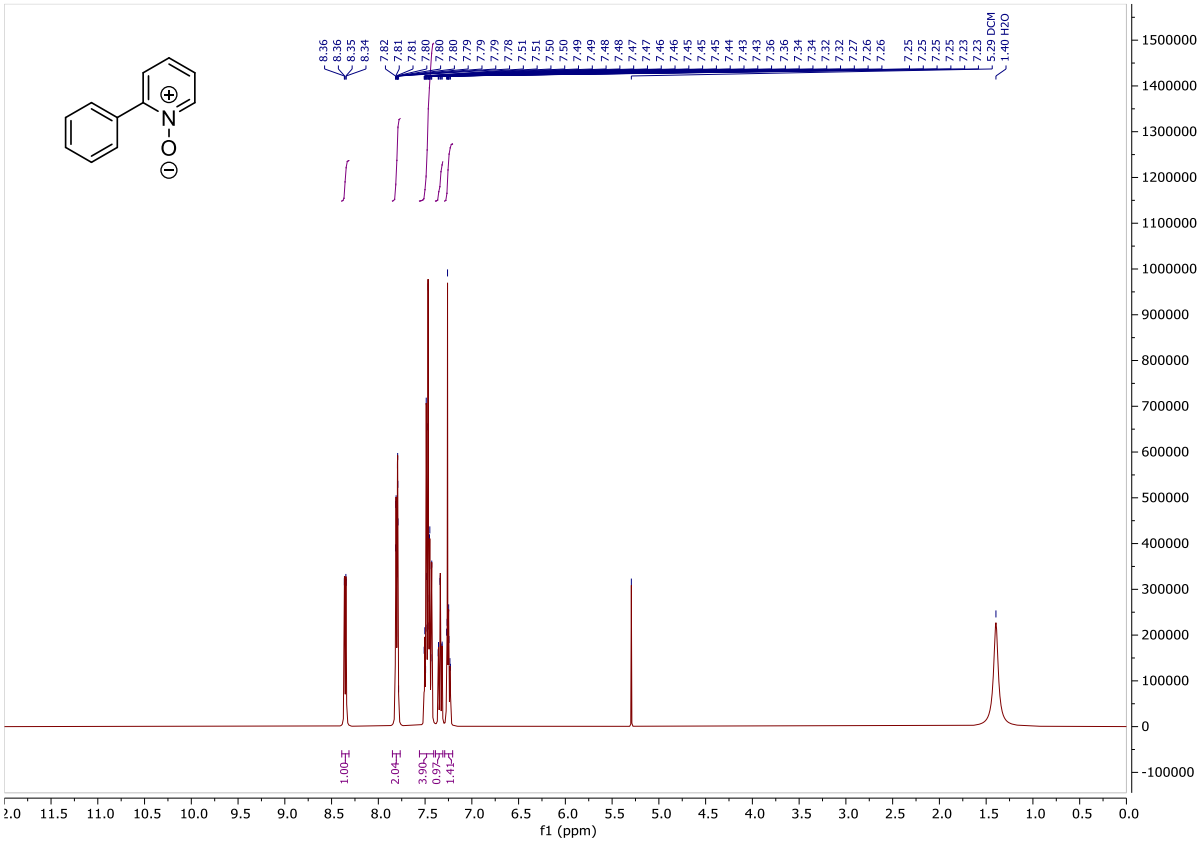

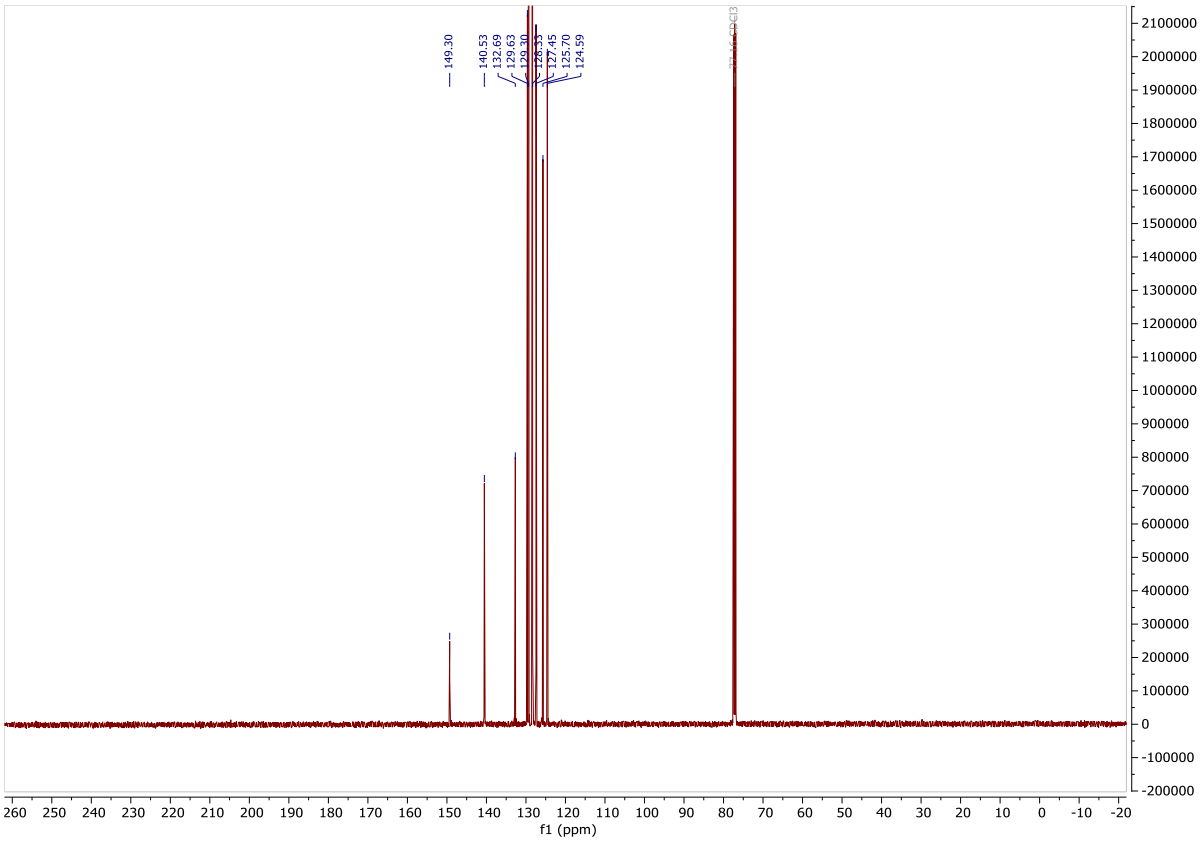

2,6-Dichloro-4-methoxypyridine 1-oxide (142)

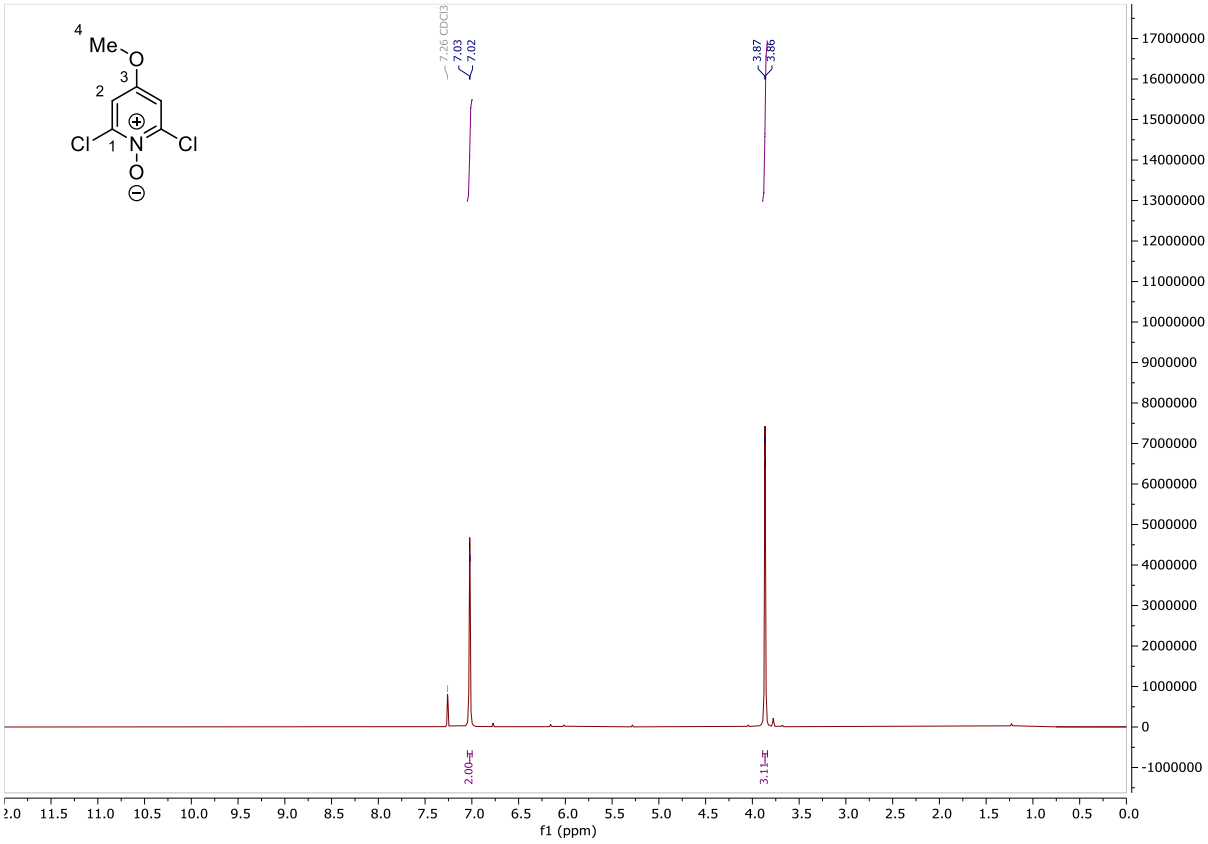

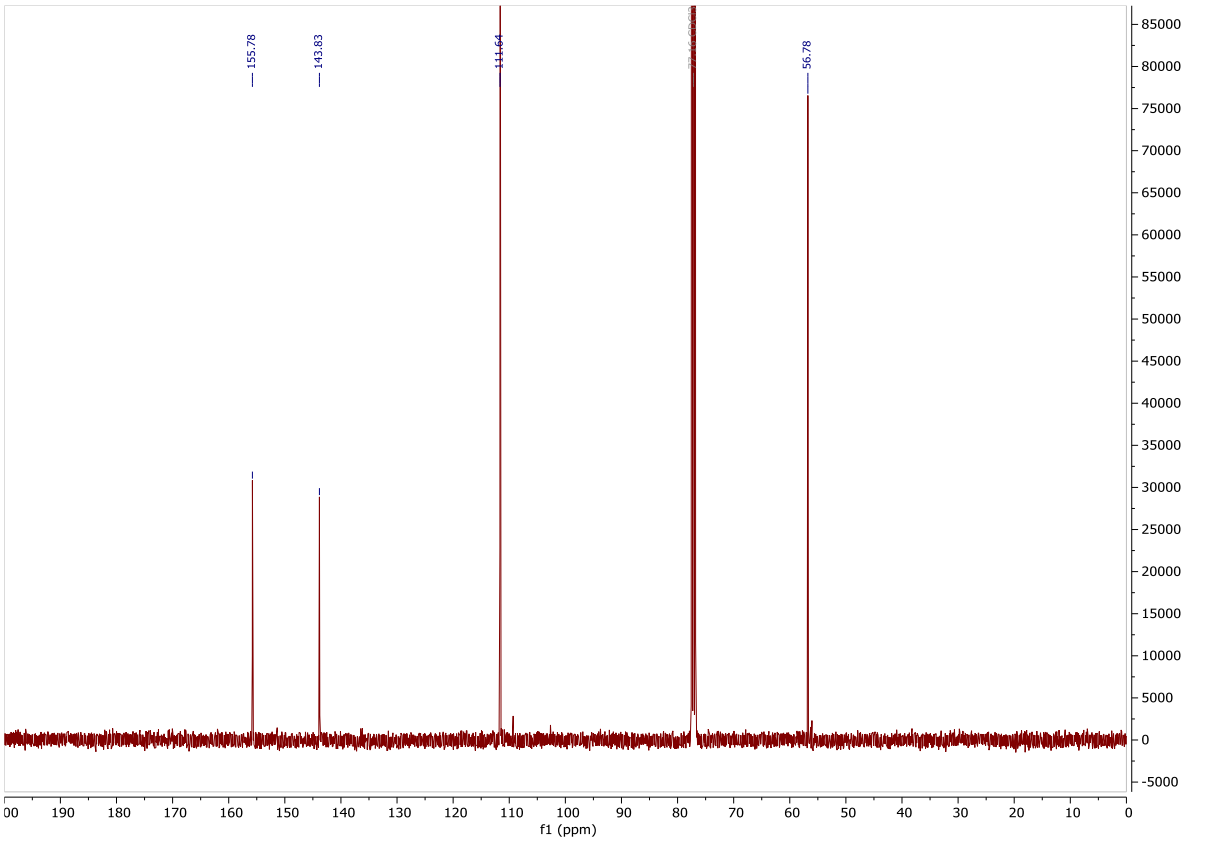

9-Phenylacridine 10-oxide (143)

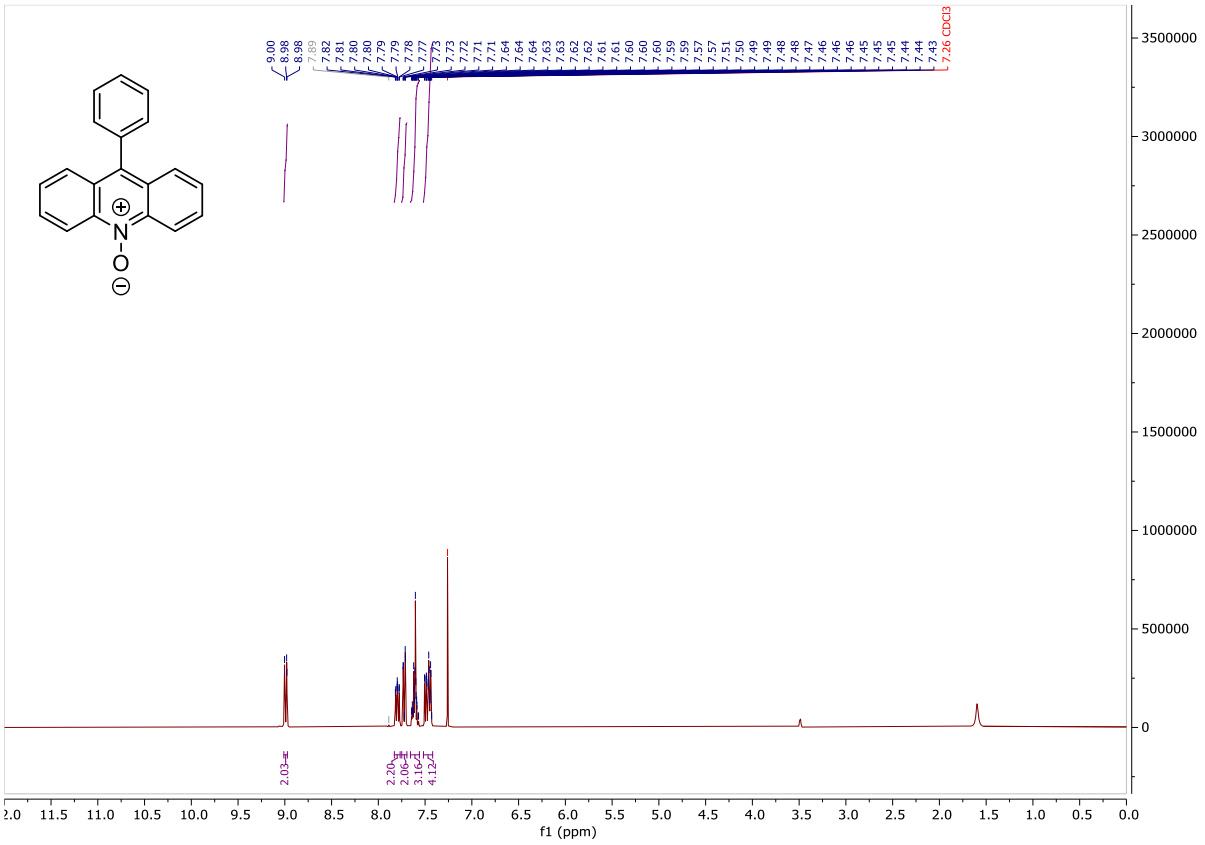

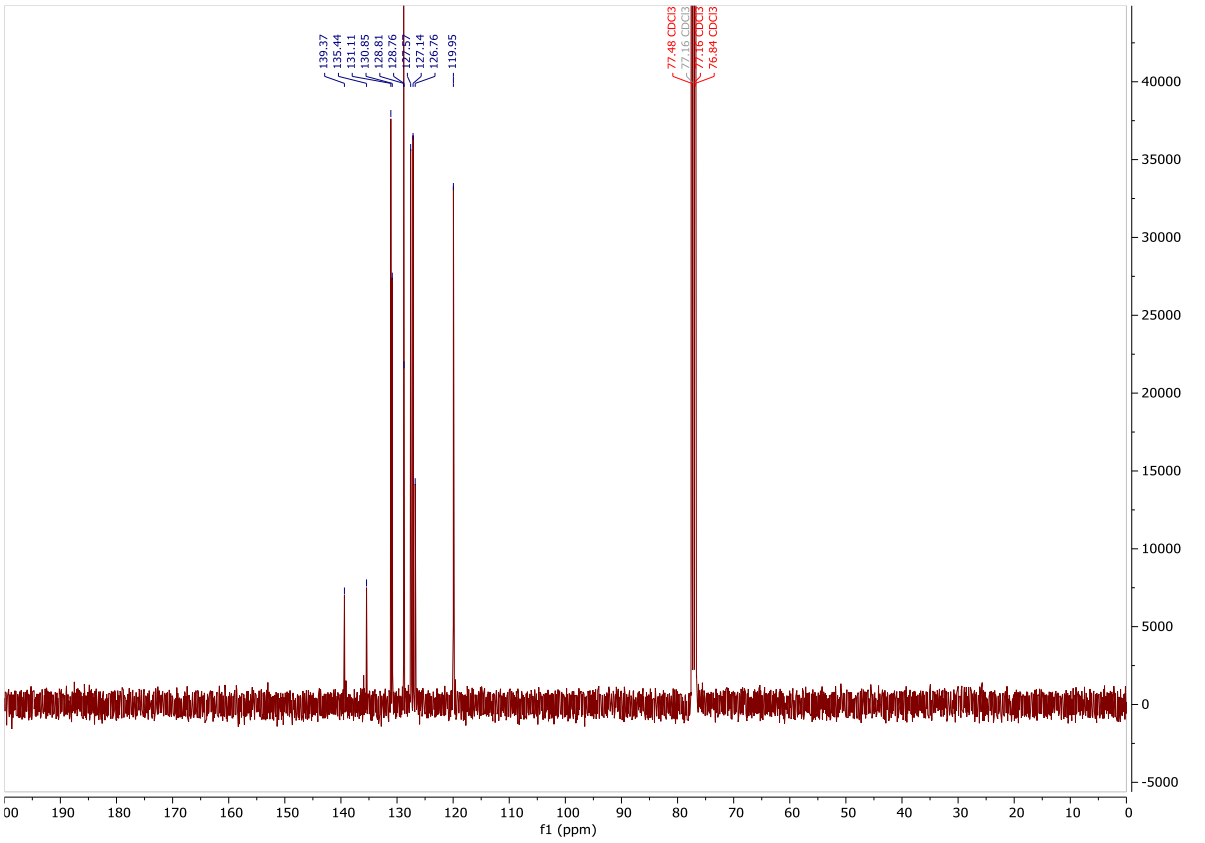

Dimethyl 2,2'-disulfanediyldibenzoate (151)

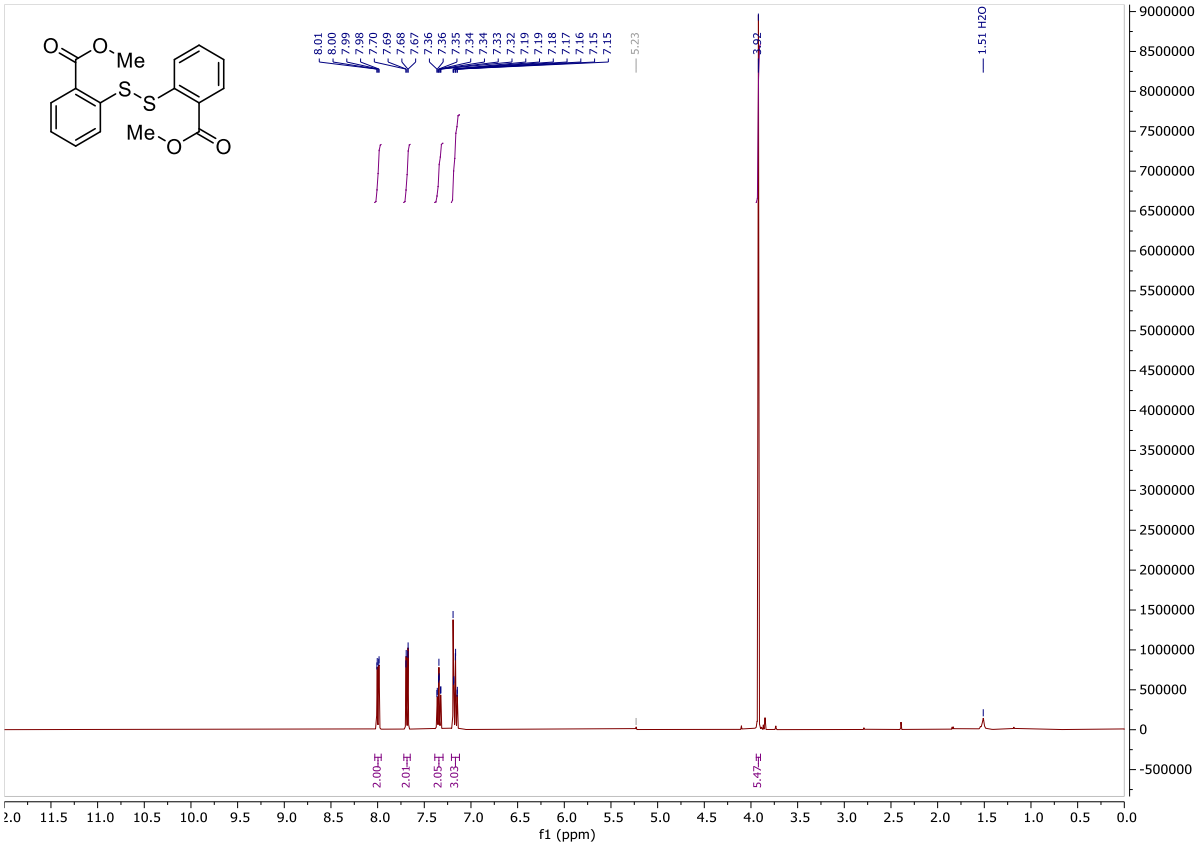

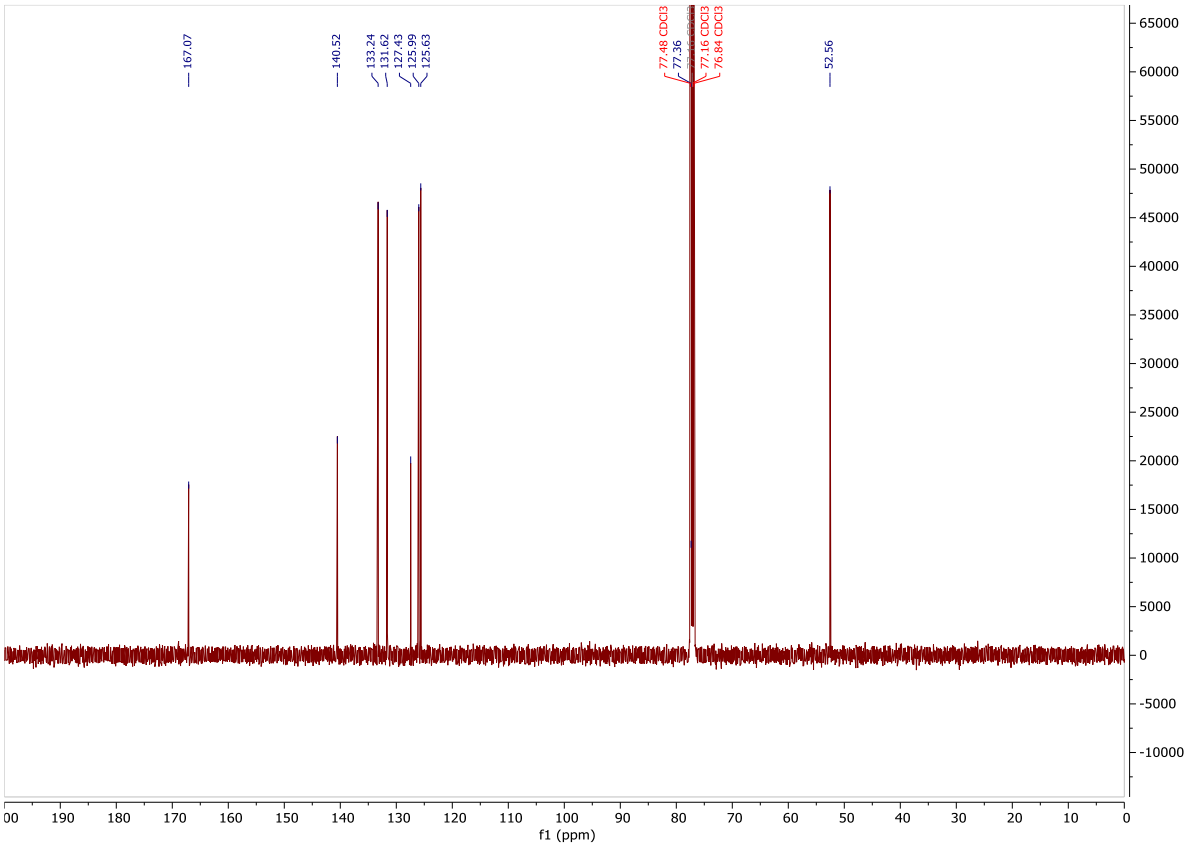

N,N'-(disulfanediylbis(2,1-phenylene))diacetamide (152)

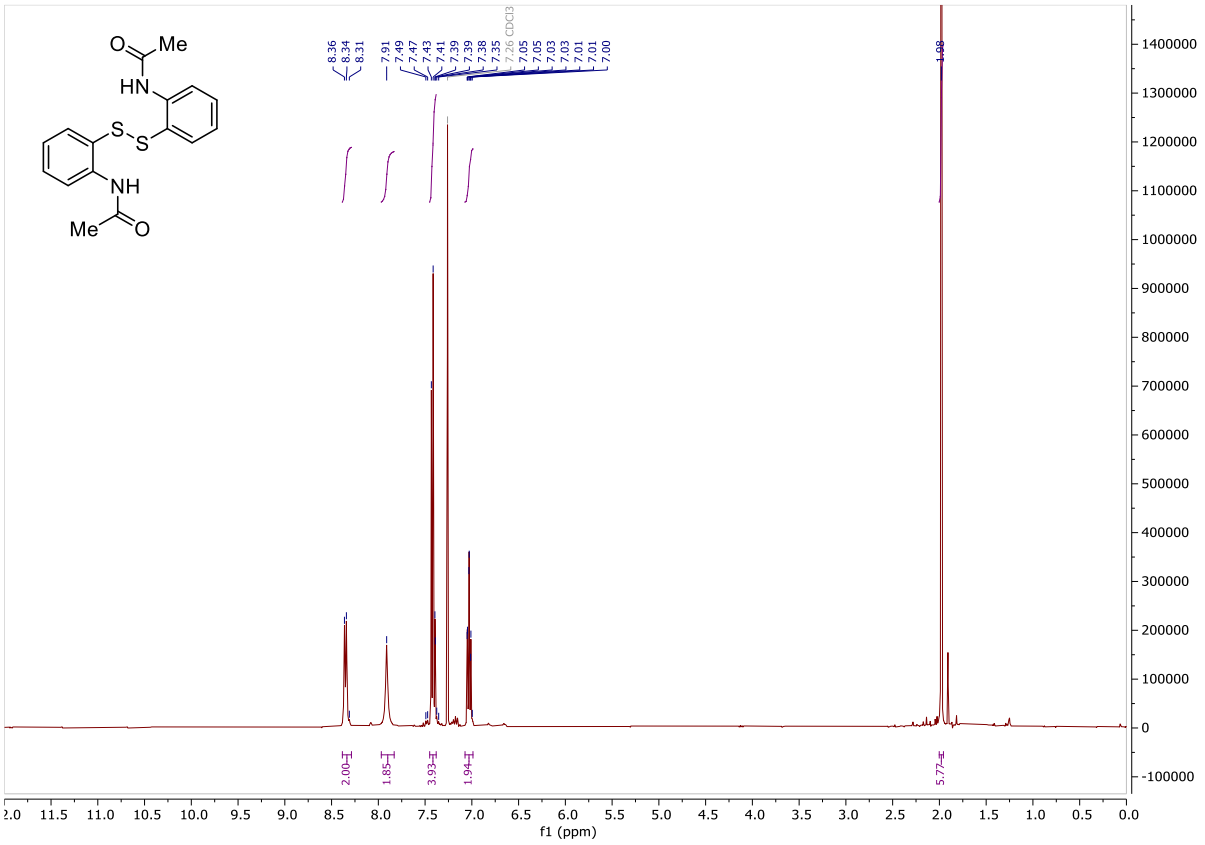

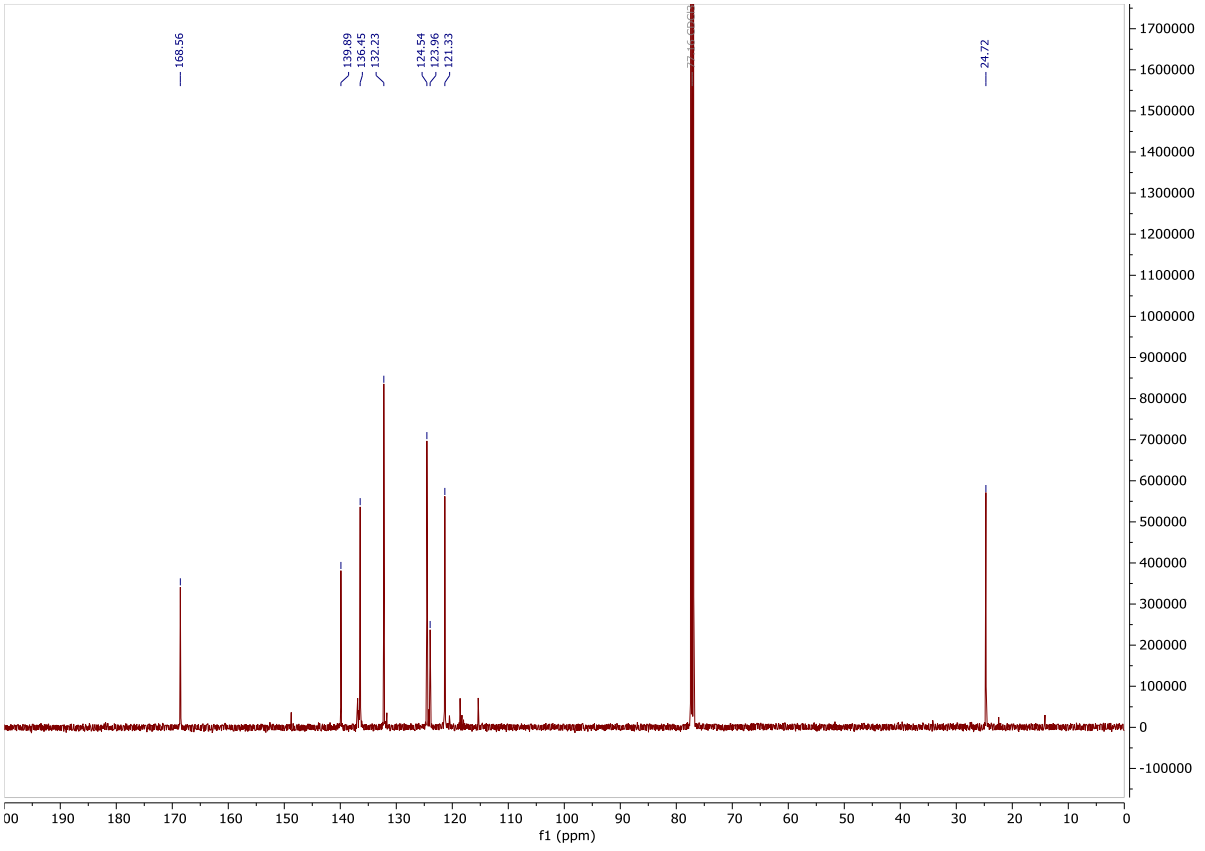

2-Phenylmalononitrile (153)

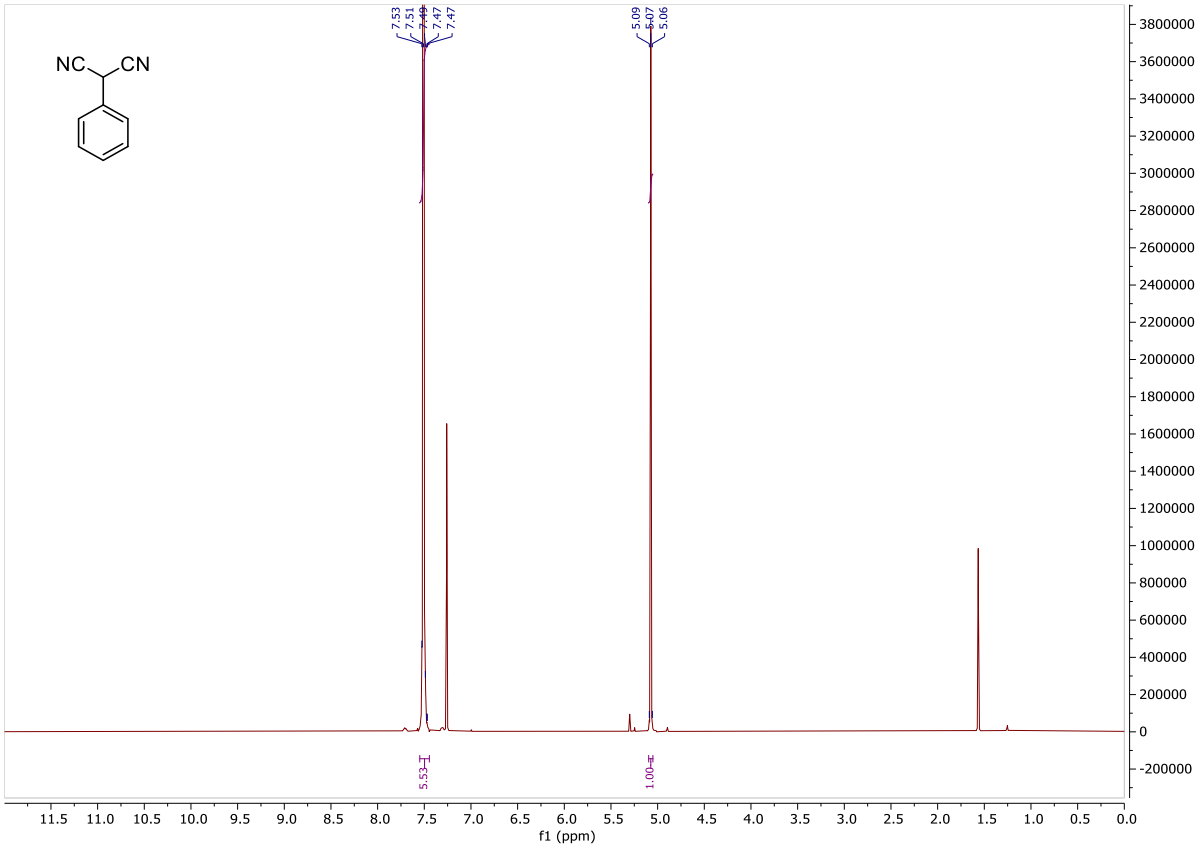

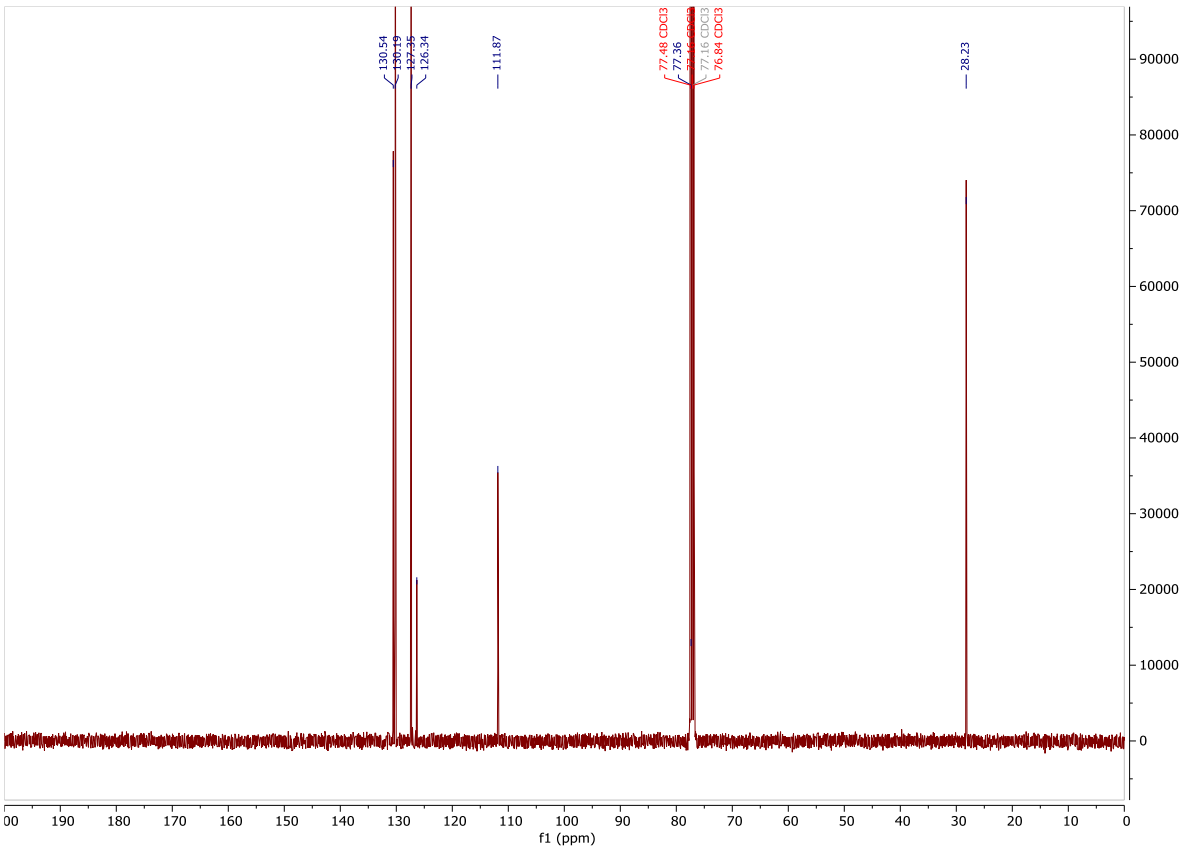

Experimental for Chapter 4

2,4,5,6-Tetra(9H-carbazol-9-yl)isophthalonitrile (4CzIPN)

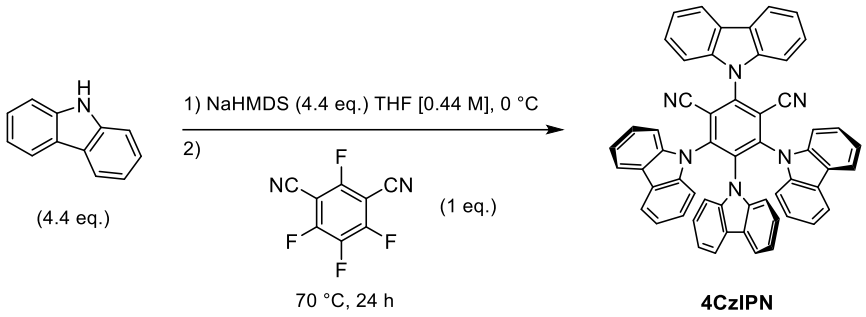

Prepared according to literature procedure.[339]

An oven-dried two-neck flask was charged with carbazole (3.68 g, 22 mmol) and sealed under argon. Diethyl ether (40 mL) was introduced and the suspension was cooled to 0 °C. Sodium bis(trimethylsilyl)amide (2M in THF, 10.5 mL, 21 mmol) was added dropwise and the resulting suspension was stirred at RT for 30 min. A solution of tetrafluoroisophthalonitrile (1 g, 5 mmol) in Et_2O:THF = 5:1 (6 mL) was added dropwise and the reaction was stirred under reflux (62 °C) for 24 h. The solvent was removed under vacuum and the resulting solid was washed with diethyl ether (200 mL) and extracted with chloroform (340 mL). The chlorinated organic was concentrated and triturated with pentane, filtered and dried under suction to afford **4CzIPN** (2.70 g, 69%) as a yellow solid.

^{1}H NMR (500 MHz, $CDCl_3$) δ 8.23 (d, J = 7.8 Hz, 2H), 7.76 – 7.66 (m, 8H), 7.53 – 7.46 (m, 2H), 7.33 (d, J = 7.6 Hz, 2H), 7.25 – 7.19 (m, 4H), 7.13 – 7.03 (m, 8H), 6.87 – 6.79 (m, 4H), 6.67 – 6.60 (m, 2H).

^{13}C NMR (126 MHz, $CDCl_3$) δ 145.4, 144.8, 140.1, 138.3, 137.1, 134.9, 127.1, 125.9, 125.1, 124.9, 124.7, 123.9, 122.5, 122.1, 121.6, 121.1, 120.6, 119.8, 116.5, 111.8, 110.1, 109.6, 109.6.

4CzIPN is a known compound and its NMR spectra are in accord with published data.[340]

2,4-Dimethylquinoline (164)

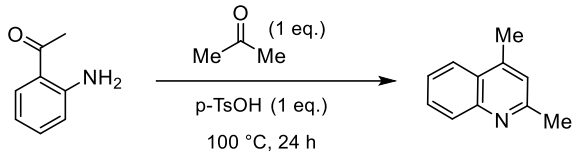

Prepared according to a literature procedure.[341]

A microwave vial was charge with 2-aminoacetophenone (1.21 mL, 10 mmol), acetone (0.74 mL, 10 mmol) and p-toluenesulfonic acid monohydrate (1.90 g, 10 mmol), sealed and stirred at 100 °C for 24 h. The reaction was neutralised with aq. NaOH (1M) and extracted with DCM (3x10 mL). The combined organic layer was washed with aq. NaOH (1M, 3x10 mL), water (2x20 mL) and brine (20 mL), dried over $MgSO_4$, filtered and evaporated. Purification via flash column chromatography over silica gel (eluting with gradient 50% to 100% DCM in cyclohexane) afforded **164** (240 mg, 15%) as a brown oil.

^{1}H NMR (500 MHz, $CDCl_3$) δ 8.07 (d, J = 8.5 Hz, 1H), 7.96 (dd, J = 8.2, 1.4 Hz, 1H), 7.69 (ddd, J = 8.4, 6.8, 1.4 Hz, 1H), 7.52 (ddd, J = 8.3, 6.8, 1.3 Hz, 1H), 7.16 (d, J = 1.2 Hz, 1H), 2.72 (s, 3H), 2.68 (d, J = 1.0 Hz, 3H).

^{13}C NMR (101 MHz, $CDCl_3$) δ 158.8, 147.8, 144.3, 129.3, 129.2, 126.7, 125.6, 123.7, 122.8, 25.4, 18.7.

164 is a known compound and its NMR spectra are in accord with published data.[341]

3,3'-Oxybis(tert-butylbenzene) (165)

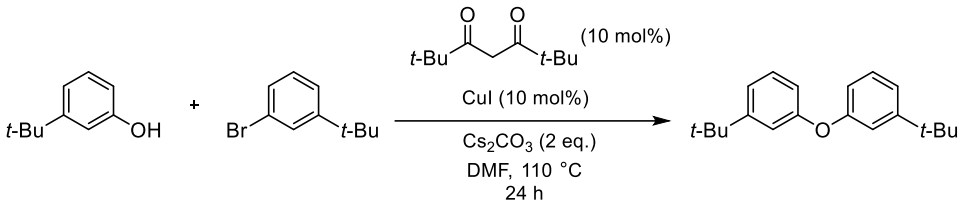

Prepared according to a literature procedure.[342]

A flask was charged with 1-bromo-3-(tert-butyl)benzene (10 g, 46.9 mmol), 3-tert-butylphenol (10.6 g, 70.4 mmol), caesium carbonate (30.6 g, 93.8 mmol), 2,2,6,6,-tetramethyl heptane-3,5-dione (0.98 mL, 10 mol%), copper(I) iodide (894 mg, 10 mol%) and DMF (30 mL). The reaction was stirred at 135 °C for 24 h. The resulting suspension was passed through a short celite plug, eluting with diethyl ether (200 mL).

The combined organic was washed with water (5x200 mL) and brine (300 mL), dried over $MgSO_4$, filtered and evaporated. Purification via flash column chromatography (dry loaded on celite, eluting with gradient 0% to 2% EtOAc in pentane) afforded **165** (8.15 g, 61%) as a colourless oil.

^{1}H NMR (400 MHz, $CDCl_3$) δ 7.28 – 7.22 (m, 3H), 7.13 (ddd, J = 7.8, 2.0, 1.0 Hz, 2H), 7.09 (t, J = 2.1 Hz, 2H), 6.79 (ddd, J = 8.0, 2.4, 1.0 Hz, 2H), 1.30 (s, 18H).

^{13}C NMR (101 MHz, $CDCl_3$) δ 157.2, 153.5, 129.3, 120.2, 116.4, 115.6, 34.9, 31.4.

165 is a known compound and its NMR spectra are in accord with published data.[342]

3,6-Di-tert-butyl-9-mesitylxanthylium tetrafluoroborate (166)

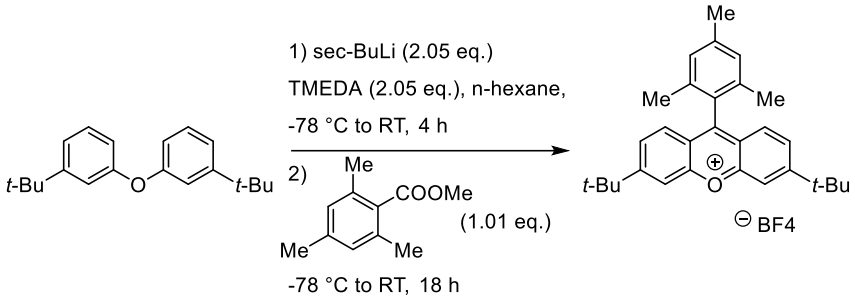

Prepared according to a literature procedure.[342]

To a solution of 3,3'-oxybis(tert-butylbenzene) (3.62 g, 12.8 mmol) and N,N,N′,N′-tetramethylethylenediamine (3.94 mL, 26.3 mmol) in n-hexane (13 mL) was added sec-BuLi (1.4 M in cyclohexane, 19 mL, 26.3 mmol) portion wise at 0 °C. The reaction was taken out of the ice-bath and stirred for 4 h at RT. The resulting suspension was cooled to -78 °C and a solution of methyl 2,4,6-trimethylbenzoate (2.56 g, 14.4 mmol) in n-hexane (10 mL) was added dropwise. The reaction was stirred at RT for 18 h before it was quenched with water (20 mL). Extracted with diethyl ether (3x30 mL), combined organic was washed with water (2x60 mL) and brine (60 mL). Introduced conc. HCl (6 mL) to the organic layer and the reaction was stirred at RT for 1 h after which it was diluted with water (50 mL). The organic layer was extracted with water until the washings became colourless and sodium tetrafluoroborate (1.16 g, 10.6 mmol) was added to the combined aqueous layer. The resulting yellow solution was extracted with DCM (ca. 1 L) until the aqueous became colourless, and the solvent was concentrated to ca. 20 mL. Tetrafluoroboric acid diethyl ether complex (1.76 mL, 12.8 mmol) was introduced, the organic layer was swirled for 2 min, washed with water (20 mL), aq.

$NaBF_4$ (1M, 20 mL) and dried over solid $NaBF_4$, filtered and evaporated. Trituration from cyclohexane/pentane afforded xanthilium **166** (3.90, 61%) as a yellow solid.

^{1}H NMR (400 MHz, $CDCl_3$) δ 8.50 (d, J = 1.7 Hz, 2H), 7.88 (dd, J = 9.0, 1.7 Hz, 2H), 7.72 (d, J = 8.9 Hz, 2H), 7.15 (s, 2H), 2.47 (s, 3H), 1.85 (s, 6H), 1.52 (s, 18H).

^{13}C NMR (101 MHz, $CDCl_3$) δ 174.2, 171.1, 158.8, 141.4, 135.6, 129.2, 128.6, 127.7, 122.2, 117.1, 37.7, 30.6, 21.4, 20.4.

^{19}F NMR (376 MHz, $CDCl_3$) δ -153.91, -153.96.

166 is a known compound and its NMR spectra are in accord with published data.[342]

3,6-Di-tert-butyl-9-mesityl-10-phenylacridin-10-ium tetrafluoroborate (PC1)

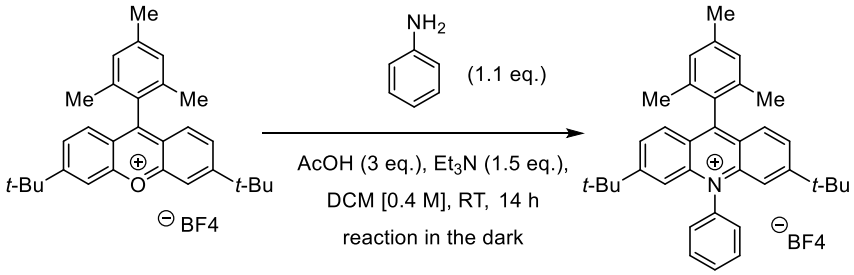

Prepared according to a literature procedure.[342]

To a solution of xanthilium **166** (997 mg, 2 mmol) in anh. DCM (5 mL) was added acetic acid (0.34 mL, 6 mmol), triethylamine (0.42 mL, 3 mmol) and aniline (0.22 mL, 2.4 mmol) under argon atmosphere and the reaction was stirred at RT for 14 h in the dark. The resulting solution was diluted with water (15 mL) and organic layer was washed with sat. $NaHCO_3$. The resulting DCM layer was stirred with $HBF_4 \cdot Et_2O$ complex (0.27 mL, 2 mmol) until a homogeneous mixture was obtained. Organic layer was washed with water (20 mL) and aq. $NaBF_4$ (1M, 20 mL), dried over $NaBF_4$, filtered and evaporated under reduced pressure. Trituration from cyclohexane/pentane afforded **PC1** (715 mg, 62%) as a yellow solid.

^{1}H NMR (400 MHz, $CDCl_3$) δ 8.00 – 7.85 (m, 3H), 7.83 – 7.69 (m, 6H), 7.42 (s, 2H), 7.16 (s, 2H), 2.49 (s, 3H), 1.87 (s, 6H), 1.29 (s, 18H).

^{19}F NMR (376 MHz, $CDCl_3$) δ -154.40, -154.45.

PC1 is a known compound and its NMR spectra are in accord with published data.[342]

1,2,4,6-Tetraphenylpyridin-1-ium tetrafluoroborate (PC2)

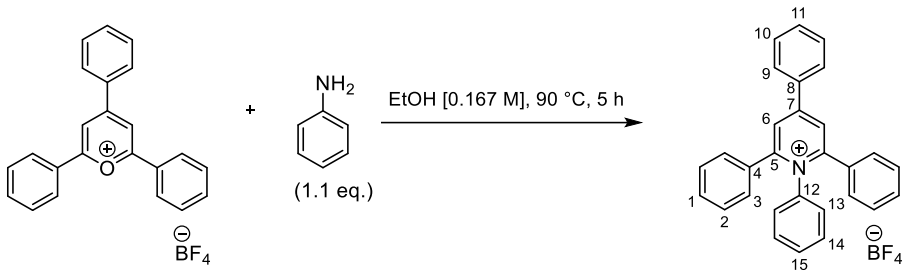

PC2

Prepared according to a literature procedure.[343]

To a suspension of 2,4,6-triphenylpyrylium tetrafluoroborate (1.98 g, 5 mmol) in ethanol (30 mL) was added aniline (0.5 mL, 5.5 mmol) and the reaction was stirred at 90 °C for 5 h. The solvent was evaporated and the crude was triturated with cyclohexane and pentane and dried under vacuum to afford **PC2** (2.26 g, 96%) as a yellow solid.

^{1}H NMR (400 MHz, $CDCl_3$) δ 7.99 (s, 2H, H6), 7.80 (d, J = 7.5 Hz, 2H, H13), 7.57 – 7.43 (m, 3H, H3), 7.40 (d, J = 7.2 Hz, 4H, H3), 7.31 – 7.17 (m, 8H), 7.11 – 7.04 (m, 3H).

^{13}C NMR (101 MHz, $CDCl_3$) δ 157.9 (C12), 156.8 (C5), 139.1 (q), 134.8 (q), 133.1 (q), 132.1, 130.2, 129.97, 129.91, 129.79, 129.04, 128.8, 128.6, 128.5, 126.5 (C6).

^{19}F NMR (376 MHz, $CDCl_3$) δ -153.10 – -153.17 (m).

IR (neat) ν_{max}/cm^{-1}: 3063, 1622, 1598, 1490, 1448, 1362, 1281, 1234, 1161, 1109, 1080.

HRMS m/z (ESI) calculated for $C_{29}H_{24}N^+$ $[M+H_2]^+$ 386.1903 found: 386.1899.

9-(4-(Tert-butyl)phenyl)acridine (202)

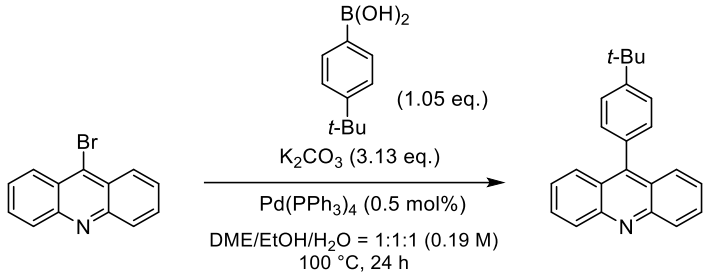

A Schlenk tube was charged with 9-chloroacridine (1.07 g, 5 mmol), 4-(tert-butyl)benzene boronic acid (935 mg, 5.25 mmol), potassium carbonate (2.16 g, 15.7 mmol), tetrakis(triphenylphosphine)palladium (29 mg, 0.5 mol%) and a DME:H_2O:EtOH = 1:1:1 mixture (27 mL). The resulting suspension was sparged with argon for 10 min before it was stirred at 90 °C for 24 h. The reaction was cooled to RT and extracted with DCM (3x20 mL). The combined organic was washed with water (2x20 mL) and brine (10 mL), dried over $MgSO_4$, filtered and evaporated. Purification via flash column chromatography over silica gel (eluting with 50% DCM in cyclohexane) afforded **202** (1.22 g, 78%) as a pale-yellow solid.

^{1}H NMR (500 MHz, $CDCl_3$) δ 8.29 (d, J = 8.7 Hz, 2H), 7.81 – 7.74 (m, 4H), 7.65 – 7.59 (m, 2H), 7.46 – 7.41 (m, 2H), 7.40 – 7.36 (m, 2H), 1.47 (s, 9H).

^{13}C NMR (101 MHz, $CDCl_3$) δ 151.5, 148.9, 147.7, 132.9, 130.4, 130.0, 129.7, 127.2, 125.5, 125.4, 34.9, 31.6.

202 is a known compound and its NMR spectra are in accord with published data.[344]

9-Mesitylacridine (203)

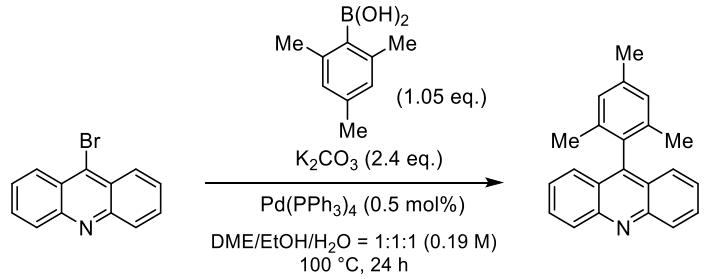

A Schlenk tube was charged with 9-chloroacridine (1.07 g, 5 mmol), mesitylbenzene boronic acid (861 mg, 5.25 mmol), potassium carbonate (2.16 g, 15.7 mmol), tetrakis(triphenylphosphine)palladium (29 mg, 0.5 mol%) and a DME:H_2O:EtOH = 1:1:1 mixture (27 mL). The resulting suspension was sparged with argon for 10 min

before it was stirred at 100 °C for 24 h. The reaction was cooled to RT and extracted with DCM (3x20 mL). The combined organic was washed with water (2x20 mL) and brine (10 mL), dried over $MgSO_4$, filtered and evaporated. Purification via flash column chromatography over silica gel (eluting with 10% EtOAc, 1% Et_3N in cyclohexane) followed by trituration with pentane afforded **203** (80 mg, 5%) as a pale-yellow solid.

^{1}H NMR (400 MHz, $CDCl_3$) δ 8.31 (d, J = 8.8 Hz, 2H), 7.78 (d, J = 7.8 Hz, 2H), 7.52 (d, J = 8.7 Hz, 2H), 7.45 – 7.37 (m, 2H), 7.09 (s, 2H), 2.45 (s, 3H), 1.71 (s, 6H).

^{13}C NMR (101 MHz, $CDCl_3$) δ 148.8, 138.2, 136.8, 132.0, 130.5 (2 C overlapping), 129.6 (2 C overlapping), 128.5, 126.2, 126.1, 125.2, 21.3, 20.1.

203 is a known compound and its NMR spectra are in accord with published data.[345]

3,6-Di-tert-butyl-9-phenylacridine (204)

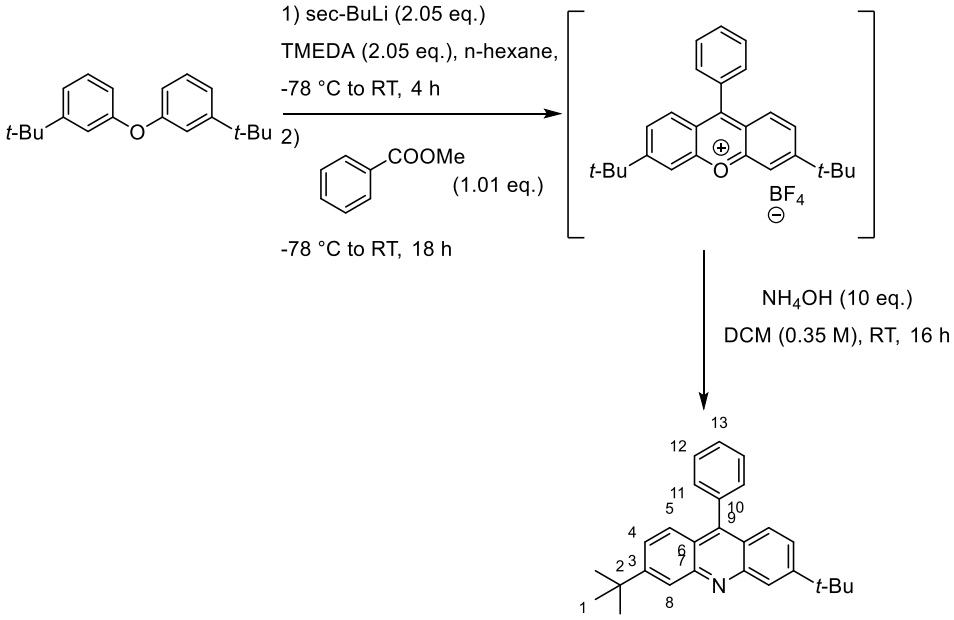

Prepared according to a modified literature procedure.[342]

To a solution of 3,3'-oxybis(tert-butylbenzene) (1 g, 3.54 mmol) and N,N,N′,N′-tetramethylethylenediamine (1.08 mL, 7.2 mmol) in n-hexane (3.5 mL) was added sec-BuLi (1.4 M in cyclohexane, 5.2 mL, 7.3 mmol) dropwise at 0 °C. The reaction was taken out of the ice-bath and stirred for 4 h at RT. The resulting suspension was cooled to -78 °C and a solution of methyl benzoate (487 mg, 3.58 mmol) in n-hexane (3.5 mL) was added dropwise. The reaction was stirred at RT for 18 h before it was quenched with water (10 mL). Extracted with diethyl ether (3x10 mL), combined organic was washed with water (2x20 mL) and brine (20 mL). Introduced conc. HCl (3 mL) to the

organic layer and the reaction was stirred at RT for 1h after which it was diluted with water (20 mL). The organic layer was extracted with water (3x20 mL) and sodium tetrafluoroborate (1.16 g, 10.6 mmol) was added to the combined aqueous layer. The resulting yellow solution was extracted with DCM (ca. 200 mL) until the aqueous became colourless, and the solvent was concentrated to ca. 20 mL. Tetrafluoroboric acid diethyl ether complex (0.48 mL, 3.54 mmol) was introduced, the organic layer was swirled for 2 min, washed with water (20 mL), aq. $NaBF_4$ (1M, 20 mL) and dried over solid $NaBF_4$, filtered and evaporated to afford crude xanthilium which was used directly in the next step without further purification.

To a solution of crude xanthilium (3.54 mmol) in DCM (10 mL) was added aq. ammonium hydroxide (28 wt%, 4 mL, 35.4 mmol) and the reaction was stirred at RT for 16 h. The suspension was extracted with DCM (3x20 mL), combined organic was washed with water (2x20 mL), brine (20 mL), dried over $MgSO_4$, filtered and evaporated. Purification over silica gel (eluting with gradient 20% to 50% DCM in cyclohexane) afforded acridine **204** (224 mg, 17% over 2 steps) as a yellow solid.

^{1}H NMR (400 MHz, $CDCl_3$) δ 7.47 – 7.39 (m, 2H, H4), 7.29 (t, J = 7.9 Hz, 2H), 7.27 – 7.16 (m, 5H, H8, H13), 7.08 (dd, J = 8.3, 1.9 Hz, 2H, H4), 1.32 (s, 18H, H1).

^{13}C NMR (101 MHz, $CDCl_3$) δ 152.8, 149.7 (q), 148.1 (q), 128.6, 127.9, 126.7, 126.6, 124.4 (q), 121.1, 113.2 (C8), 70.5 (C3), 34.8 (C2), 31.4 (C1).

IR ν_{max}/cm^{-1}: 2962, 2904, 2868, 1612, 1406, 1364, 1319, 1098.

HRMS m/z (ESI) calculated for $C_{27}H_{31}N$ [M+H2] 369.2456 found: 369.2451.

3,6-Di-tert-butyl-9-mesitylacridine (205)

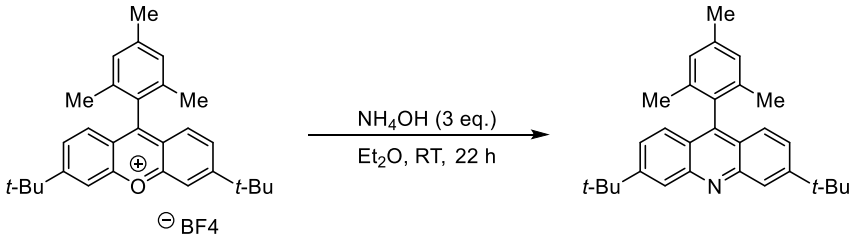

To a solution of 3,6-di-tert-butyl-9-mesitylxanthylium tetrafluoroborate (997 mg, 2 mmol) in diethyl ether (10 mL) was added aq. ammonium hydroxide (28wt%, 0.8 mL, 6 mmol) and the reaction was stirred at RT for 22 h, before it was diluted with water (10 mL) and the organic layer was separated. The aqueous layer was extracted with

Et_2O (3x10 mL), combined organic was washed with water (3x20 mL), brine (20 mL), dried over $MgSO_4$, filtered and evaporated. Purification over a short pad of silica gel (eluting with DCM) afforded **205** (737 mg, 90%) as a yellow solid.

^{1}H NMR (400 MHz, $CDCl_3$) δ 8.19 (s, 2H), 7.50 – 7.38 (m, 4H), 7.07 (s, 2H), 2.45 (s, 3H), 1.72 (s, 6H), 1.46 (s, 18H).

^{13}C NMR (101 MHz, $CDCl_3$) δ 153.1, 149.6, 145.8, 137.9, 136.9, 132.4, 128.4, 125.7, 125.1, 124.4, 123.4, 35.4, 31.0, 21.4, 20.2.

205 is a known compound and its NMR spectra are in accord with published data.[346]

9-(2-Chlorophenyl)acridine (208)

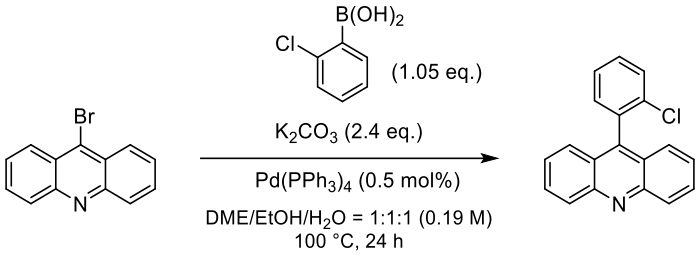

A Schlenk tube was charged with 9-chloroacridine (1.07 g, 5 mmol), 2-chlororobenzene boronic acid (822 mg, 5.25 mmol), potassium carbonate (2.16 g, 15.7 mmol), tetrakis(triphenylphosphine)palladium (29 mg, 0.5 mol%) and a DME:H_2O:EtOH = 1:1:1 mixture (27 mL). The resulting suspension was sparged with argon for 10 min before it was stirred at 100 °C for 24 h. The reaction was cooled to RT and extracted with DCM (3x20 mL). The combined organic was washed with water (2x20 mL) and brine (10 mL), dried over $MgSO_4$, filtered and evaporated. Purification via flash column chromatography over silica gel (eluting with 50% DCM in cyclohexane) afforded **208** (477 mg, 33%) as a pale-yellow solid.

^{1}H NMR (500 MHz, $CDCl_3$) δ 8.32 (d, J = 8.8 Hz, 2H), 7.79 (ddd, J = 8.8, 6.5, 1.4 Hz, 2H), 7.67 (dd, J = 8.0, 1.3 Hz, 1H), 7.60 – 7.42 (m, 6H), 7.36 (dd, J = 7.4, 1.8 Hz, 1H).

^{13}C NMR (126 MHz, $CDCl_3$) δ 148.8, 144.4, 135.1, 134.3, 132.1, 130.3, 130.3, 130.1, 129.8, 127.0, 126.4, 126.2, 125.1.

208 is a known compound and its NMR spectra are in accord with published data.[347]

9-Phenyl-9,10-dihydroacridine (244)

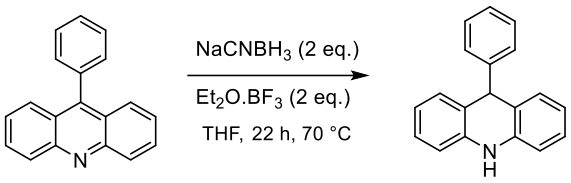

Prepared according to a literature procedure.[348]

To a suspension of 9-phenyl-acridine (384 mg, 1.5 mmol) and sodium cyanoborohydride (189 mg, 3 mmol) in THF (5 mL) was added boron trifluoride diethyl etherate (0.36 mL, 3 mmol) under argon atmosphere and the reaction was stirred at 70 °C for 22 h. The resulting mixture was cooled to 0 °C, quenched with aq. ammonia (25 wt%, 4 mL) and stirred for 10 min at RT. Extracted with diethyl ether (3x10 mL), combined organic was washed with water (2x20 mL), brine (20 mL), dried over $MgSO_4$, filtered and reduced under vacuum. Purification over silica gel (eluting with gradient 20% to 50% DCM in cyclohexane) afforded **244** (376 mg, 96%) as an off-white solid.

^{1}H NMR (400 MHz, $CDCl_3$) δ 7.29 – 7.19 (m, 4H), 7.19 – 7.05 (m, 5H), 6.85 (t, J = 7.5 Hz, 2H), 6.77 (d, J = 7.9 Hz, 2H), 6.13 (s, 1H), 5.31 (s, 1H).

^{13}C NMR (101 MHz, $CDCl_3$) δ 147.2, 139.0, 129.7, 128.7, 127.9, 127.4, 126.4, 123.7, 120.9, 113.9, 47.6.

244 is a known compound and its NMR spectra are in accord with published data.[349]

9-(2-Fluorophenyl)acridine (F-PC)

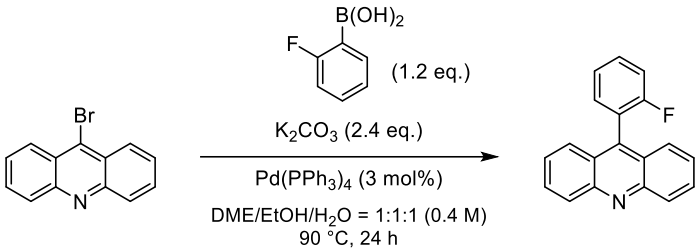

A Schlenk tube was charged with 9-chloroacridine (1.07 g, 5 mmol), 2-fluorobenzene boronic acid (840 mg, 6 mmol), potassium carbonate (1.66 g, 12 mmol), tetrakis(triphenylphosphine)palladium (173 mg, 3 mol%) and a DME:H_2O:EtOH = 1:1:1 mixture (12 mL). The resulting suspension was sparged with argon for 10 min before it was stirred at 90 °C for 24 h. The reaction was cooled to RT and extracted with DCM (3x20 mL). The combined organic was washed with water (2x20 mL) and brine (10

mL), dried over $MgSO_4$, filtered and evaporated. Purification via flash column chromatography over silica gel (eluting with 50% DCM in cyclohexane) afforded **F-PC** (1.09 g, 80%) as a yellow solid.

^{1}H NMR (500 MHz, $CDCl_3$) δ 8.31 (d, J = 8.8 Hz, 1H), 7.79 (ddd, J = 8.8, 6.5, 1.4 Hz, 1H), 7.66 (d, J = 8.7 Hz, 1H), 7.64 – 7.57 (m, 1H), 7.47 (ddd, J = 8.8, 6.5, 1.2 Hz, 1H), 7.43 – 7.38 (m, 1H), 7.35 (t, J = 8.8 Hz, 1H).

^{13}C NMR (126 MHz, $CDCl_3$) δ 160.3 (d, J = 247.8 Hz), 148.8, 141.2, 132.6 (d, J = 3.2 Hz), 130.9 (d, J = 7.8 Hz), 130.3, 129.8, 126.4, 126.2, 125.4, 124.4 (d, J = 3.6 Hz), 123.4 (d, J = 16.9 Hz), 116.3 (d, J = 21.6 Hz).

^{19}F NMR (282 MHz, $CDCl_3$) δ -112.83.

F-PC is a known compound and its NMR spectra are in accord with published data.[347]

9-(Perfluorophenyl)acridine

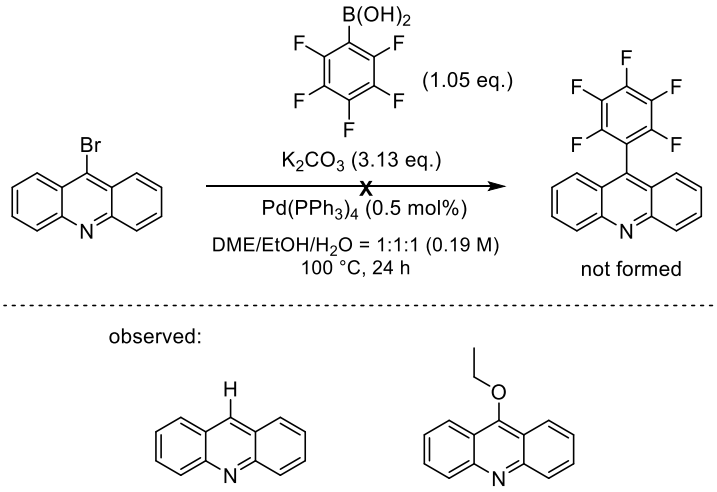

Did not form under the Suzuki coupling conditions described above due to hydrolysis of the boronic acid.

9-(2-Fluorophenyl)-9,10-dihydroacridine (245)

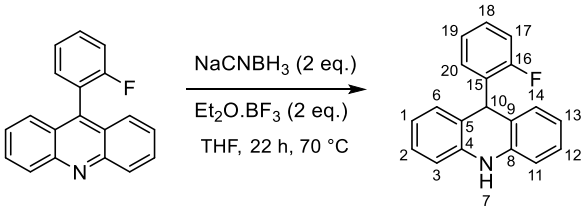

Prepared according to a literature procedure.[348]

To a suspension of 9-(2-fluorophenyl)acridine (137 mg, 0.5 mmol) and sodium cyanoborohydride (63 mg, 1 mmol) in THF (2 mL) was added boron trifluoride diethyl etherate (0.12 mL, 1 mmol) under argon atmosphere and the reaction was stirred at 70 °C for 22 h. The resulting mixture was cooled to 0 °C, quenched with aq. ammonia (25 wt%, 1 mL) and stirred for 10 min at RT. Extracted with diethyl ether (3x10 mL), combined organic was washed with water (2x20 mL), brine (20 mL), dried over $MgSO_4$, filtered and reduced under vacuum. Purification over silica gel (eluting with gradient 20% to 50% DCM in cyclohexane) afforded **245** (125 mg, 91%) as a pale-yellow powder.

Note: Upon standing in chloroform solution overnight the sample oxidises back to the starting acridine.

^{1}H NMR (400 MHz, $CDCl_3$) δ 7.17 – 7.07 (m, 5H,), 7.07 – 6.92 (m, 3H,), 6.83 (t, J = 7.6 Hz, 2H,), 6.76 (d, J = 7.9 Hz, 2H, H3, H11), 6.13 (s, 1H, H7), 5.76 (s, 1H, H10).

^{13}C NMR (101 MHz, $CDCl_3$) δ 159.3 (d, J = 245.1 Hz, C16), 139.3 (q), 134.2 (d, J = 14.3 Hz, C15), 130.6 (d, J = 4.2 Hz), 129.6 (d, J = 1.6 Hz), 127.9 (d, J = 8.1 Hz,), 127.6, 124.6 (d, J = 3.5 Hz), 122.7, 121.1, 115.5 (d, J = 22.5 Hz, C17), 113.9 (C3, C11), 39.8 (d, J = 2.5 Hz, C10).

^{19}F NMR (376 MHz, $CDCl_3$) δ -119.06.

9-Cyclobutyl-9-(2-fluorophenyl)-9,10-dihydroacridine (247)

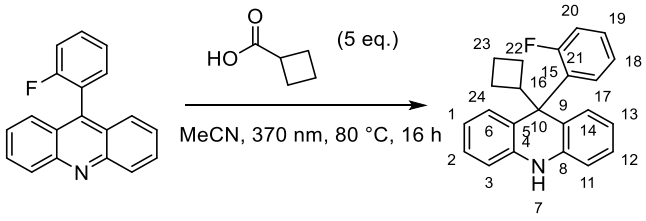

To a solution of **245** (109 mg, 0.4 mmol) in anh. MeCN (6 mL) was added cyclobutene carboxylic acid (0.19 mL, 2 mmol) and the reaction was sparged with Ar for 5 min, before it was heated to 80 °C and irradiated with 370 nm light for 16 h. The reaction was quenched with aq. $NaHCO_3$ (10 mL), extracted with DCM (3x20 mL) and the combined organics were dried under vacuum. Purification over silica gel (eluting with 50% DCM in cyclohexane) followed by trituration with ice-cold pentane afforded **247** as a white solid (30 mg, 23%).

Note: The compound is unstable under air atmosphere and discoloration was observed in solution within an hour. Trituration with pentane purifies the compound, but it is best stored as a solid under inert atmosphere.

^{1}H NMR (400 MHz, $CDCl_3$) δ 7.64 (td, J = 7.9, 2.0 Hz, 1H, H17), 7.32 – 7.24 (m, 2H), 7.20 (t, J = 7.5 Hz, 1H, H19), 7.08 (t, J = 7.5 Hz, 2H, H1, H13), 6.88 (ddd, J = 11.5, 7.8, 1.5 Hz, 1H, H20), 6.76 – 6.65 (m, 4H, H2, H3, H11, H12), 6.59 (d, J = 7.7 Hz, 2H, H6, H14), 6.08 (s, 1H, N-H7), 3.14 (p, J = 8.6 Hz, 1H, H16), 1.92 – 1.74 (m, 4H, H22, H24), 1.68 (p, J = 8.9 Hz, 1H, H23), 1.40 (q, J = 9.4 Hz, 1H, H23).

^{13}C NMR (101 MHz, $CDCl_3$) δ 161.1 (d, J = 250.9 Hz, C21), 138.6 (C5, C9), 136.4 (d, J = 9.1 Hz, C15), 129.1 (C3/C11), 128.7–128.6 (overlapping C6,C14, C17, C18), 127.2 (C1, C13), 124.9 (C4, C8), 123.0 (d, J = 3.7 Hz, C19), 119.9 (C2, C12), 117.1 (d, J = 21.9 Hz, C20), 113.0 (C3/C11), 49.2 (C10), 49.16 (C16), 24.6 (C22, C24), 18.4 (C23).

^{19}F NMR (376 MHz, $CDCl_3$) δ -104.26.

HAT catalysts synthesys

General procedure C for disulfide synthesis:

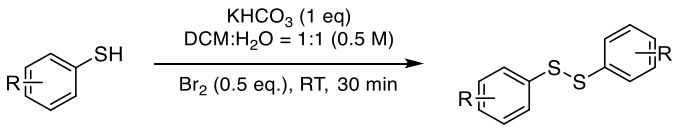

To a suspension of thiophenol (1 eq.) in DCM:H_2O = 1:1 (0.5 M) was added $KHCO_3$ (1 eq.) and reaction was kept in a water bath. Introduced bromine (0.5 eq.) dropwise and the resulting suspension was stirred at room temperature for 30 min. The reaction was extracted with DCM (30 mL) and the combined organic was washed with water (20 mL) and brine (10 mL), dried over $MgSO_4$, filtered and evaporated to afford the pure disulfide product.

1,2-Bis(2-chlorophenyl)disulfide (173)

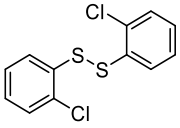

Prepared according to general procedure C using 2-chlorothiophenol (578 mg, 4 mmol). The pure disulfide (500 mg, 87%) was obtained as an off-white solid.

^{1}H NMR (400 MHz, $CDCl_3$) δ 7.55 (dd, J = 7.9, 1.6 Hz, 2H), 7.37 (dd, J = 7.8, 1.5 Hz, 2H), 7.23 (td, J = 7.6, 1.5 Hz, 2H), 7.16 (td, J = 7.6, 1.7 Hz, 2H).

^{13}C NMR (101 MHz, $CDCl_3$) δ 134.5, 132.0, 129.9, 128.0, 127.7, 127.4.

173 is a known compound and its NMR spectra are in accord with published data.[350]

2,2'-Disulfanediyldiphenol (180)

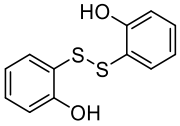

Prepared according to general procedure **180** using 2-mercaptophenol (0.2 mL, 2 mmol). The pure disulfide (230 mg, 92%) was obtained as a yellow oil.

^{1}H NMR (400 MHz, $CDCl_3$) δ 7.35 (t, J = 8.0 Hz, 2H), 7.23 (d, J = 7.5 Hz, 2H), 7.00 (d, J = 8.0 Hz, 2H), 6.83 (t, J = 7.5 Hz, 2H), 6.23 (s, 2H).

^{13}C NMR (101 MHz, $CDCl_3$) δ 157.1, 136.4, 133.4, 121.2, 120.1, 115.9.

180 is a known compound and its NMR spectra are in accord with published data.[351]

1,2-Di(naphthalen-2-yl)disulfide (181)

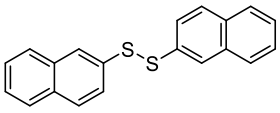

Prepared according to general procedure C using naphthalene-2-thiol (960 mg, 6 mmol). The combined organic layer was washed with additional aq. NaOH (3x20 mL), water (20 mL) and brine (10 mL), dried over $MgSO_4$, filtered and evaporated to afford disulfide **181** (740 mg, 77%) as an off-white solid.

^{1}H NMR (400 MHz, $CDCl_3$) δ 7.99 (d, J = 1.9 Hz, 2H), 7.84 – 7.77 (m, 4H), 7.76 – 7.71 (m, 2H), 7.62 (dd, J = 8.7, 1.9 Hz, 2H), 7.50 – 7.40 (m, 4H).

^{13}C NMR (101 MHz, $CDCl_3$) δ 134.4, 133.6, 132.7, 129.1, 127.9, 127.6, 126.9, 126.71, 126.4, 125.8.

181 is a known compound and its NMR spectra are in accord with published data.[352]

Dinaphtho[2,1-c:1',2'-e][1,2]dithiine (182)

Prepared according to a literature procedure.[353]

To a solution of naphthalene-2-thiol (320 mg, 2 mmol) in DCM (20 mL) was added manganese dioxide (174 mg, 2 mmol) and trifluoroacetic acid (1.53 mL, 20 mmol) and the reaction was stirred at RT for 19 h. The reaction was diluted with water (20 mL) and extracted with DCM (3x20 mL). The combined organic was washed with water (2x20 mL), brine (20 mL), dried over $MgSO_4$, filtered and evaporated. The crude was triturated from DCM/cyclohexane to afford **182** (72 mg, 23%) as a white solid.

^{1}H NMR (400 MHz, $CDCl_3$) δ 8.51 (d, J = 8.5 Hz, 2H), 7.85 (d, J = 8.1 Hz, 2H), 7.76 (d, J = 8.5 Hz, 2H), 7.67 (d, J = 8.5 Hz, 2H), 7.62 (d, J = 8.0 Hz, 2H), 7.52 (d, J = 8.1 Hz, 2H).

^{13}C NMR (101 MHz, $CDCl_3$) δ 134.1, 133.5, 133.7, 132.2, 128.5, 127.9, 127.3, 126.7, 126.5, 124.5.

182 is a known compound and its NMR spectra are in accord with published data.[353]

1,2-Bis(2,6-dimethylphenyl)disulfide (188)

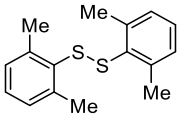

Prepared according to general procedure C using 2,6-dimethylbenzenethiol (0.67 mL, 5 mmol). The pure disulfide **188** (600 mg, 87%) was obtained as an off-white solid.

^{1}H NMR (400 MHz, $CDCl_3$) δ 7.11 (d, J = 7.5 Hz, 2H), 7.01 (d, J = 7.5 Hz, 4H), 2.23 (s, 12H).

^{13}C NMR (101 MHz, $CDCl_3$) δ 143.6, 134.9, 129.4, 128.2, 21.6.

188 is a known compound and its NMR spectra are in accord with published data.[354]

2,2'-Disulfanediylbis(N-methylaniline) (191)

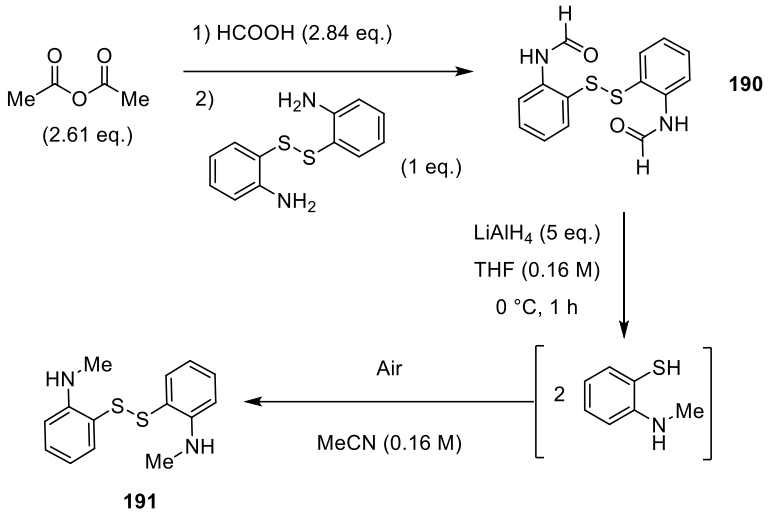

To acetic anhydride (3 mL, 31.7 mmol) was added formic acid (1.46 mL, 34.4 mmol) at 0 °C. The solution was heated to 60 °C and stirred for 30 min before it was cooled to – 10 °C and diluted with THF (3 mL). A solution of 2-aminophenyl disulfide (3 g, 12,1 mmol) in THF (6 mL) was introduced dropwise, the resulting slurry was diluted with THF (10 mL) and stirred at RT for 60 min. The resulting suspension was diluted with EtOAc (20 mL) and washed with water (40 mL), $NaHCO_3$ (40 mL) and brine (20 mL). The resulting crude was dried under vacuum to give solid **190** (3 g, 82% mass rec.) that was used directly in the next step without further purification.

To a solution of crude **190** (500 mg, 1.65 mmol) in anh. THF (8 mL) was added dropwise a solution of lithium aluminium hydride (4 M in diethyl ether, 2.1 mL, 8.4 mmol) at 0 °C under argon atmosphere. The resulting solution was stirred for 1 h at 0 °C before it was quenched with aqueous HCl (10 mL) and extracted with EtOAc (60 mL). The combined organic was washed with water (40 mL) and brine (20 mL), dried over $MgSO_4$, filtered and evaporated under reduced pressure. The resulting crude was passed through a silica plug (eluting DCM) and only the yellow fraction was evaporated under reduced pressure. The solid was dissolved in MeCN (10 mL) and stirred at RT under air atmosphere for 20 h. Purification via flash column chromatography over silica gel (eluting 30% DCM/cyclohexane then DCM) afforded **191** (320 mg, 70% over 2 steps) as a yellow solid.

^{1}H NMR (400 MHz, $CDCl_3$) δ 7.26 (t, J = 7.6 Hz, 2H), 7.20 (d, J = 7.6 Hz, 2H), 6.59 (d, J = 8.0 Hz, 2H), 6.54 (t, J = 8.0 Hz, 2H), 4.91 (s, 2H), 2.79 (d, J = 3.7 Hz, 6H).

^{13}C NMR (101 MHz, $CDCl_3$) δ 150.5, 137.1, 132.2, 118.5, 116.3, 109.9, 30.5.

191 is a known compound and its NMR spectra are in accord with published data.[355]

6,6'-Disulfanediylbis(3-methylaniline) (192)

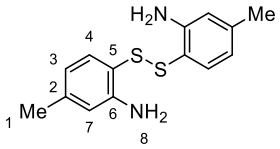

Prepared according to general procedure **192** using 2-amino-4-methylbenzenethiol (150 mg, 1.07 mmol). Purification via flash column chromatography over silica gel (eluting with DCM) afforded the pure disulfide (123 mg, 83%) as an off-white solid.

^{1}H NMR (400 MHz, $CDCl_3$) δ 7.06 (d, J = 8.0 Hz, 2H, H4), 6.54 (s, 2H, H7), 6.42 (d, J = 8.0 Hz, 2H, H3), 4.27 (br s, 4H, H8), 2.25 (s, 6H, H1).

^{13}C NMR (101 MHz, $CDCl_3$) δ 148.6 (C5), 142.2 (C6), 136.9 (C4), 119.6 (C3), 116.1 (C2), 115.9 (C7), 21.6 (C1).

IR (neat) ν_{max}/cm^{-1}: 3387, 3307, 3178, 2916, 1597, 1481, 1419, 1292, 1249, 1172.

HRMS m/z (ESI) calculated for $C_{14}H_{17}N_2S_2^+$ $[M+H]^+$ 277.0828 found: 277.0828.

4-(Tert-butyl)-2-nitrophenol (193)

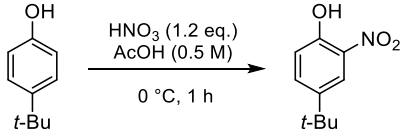

193

Nitric acid (69%, 1 mL, 15.4 mmol) was added dropwise to a solution of 4-tert-butyl phenol (2.58 g, 16.5 mmol) in acetic acid (30 mL) at 0 °C. Upon complete addition, the reaction was stirred at RT for 1 h. The solution was poured over ice-water and extracted with EtOAc (100 mL). The combined organic was washed with water (60 mL), brine (20 mL), dried over $MgSO_4$, filtered and evaporated under reduced pressure. Column over silica gel (eluting in cyclohexane then 5% EtOAc/cyclohexane) afforded nitrophenol **193** (2.54 g, 79%) as a yellow oil.

^{1}H NMR (400 MHz, $CDCl_3$) δ 10.48 (s, 1H), 8.06 (d, J = 2.3 Hz, 1H), 7.64 (dd, J = 8.8, 2.3 Hz, 1H), 7.10 (d, J = 8.8 Hz, 1H), 1.32 (s, 9H).

^{13}C NMR (101 MHz, $CDCl_3$) δ 153.2, 143.9, 135.6, 133.2, 121.1, 119.7, 77.5, 77.4, 77.1, 76.8, 34.5, 31.2.

193 is a known compound and its NMR spectra are in accord with published data.[356]

O-(4-(tert-butyl)-2-nitrophenyl) dimethylcarbamothioate (194)

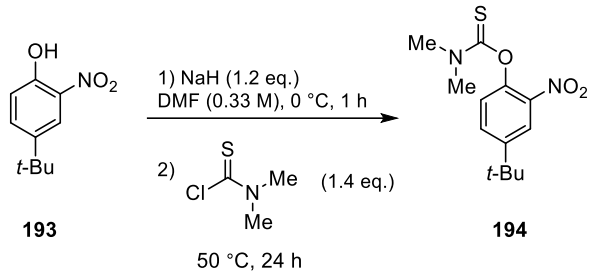

Prepared via modifying a literature procedure.[357]

A two-neck flask equipped with an addition funnel was charged with sodium hydride (60% dispersion in oil, 490 mg, 12.2 mmol) and DMF (15 mL) under argon atmosphere. A stock solution of nitrophenol **193** (2 g, 10.2 mmol) in DMF (8 mL) was added dropwise at 0 °C over 1 h. Upon complete addition, a stock solution of dimethylthiocarbamoyl chloride (1.78 g, 14.3 mmol) in DMF (8 mL) was added portionwise and the reaction was stirred for 24 h at 50 °C. The mixture was diluted with ice-cold water and extracted with Et_2O (100 mL). The combined organic was washed with aq. NaOH (200 mL), aq. HCl (2 M, 10 mL), water (40 mL), brine (20 mL), dried over $MgSO_4$, filtered and concentrated. Eluting through a short pad of silica gel afforded crude **194** (1.9 g, 66% mass rec.), which was used directly in the next step without further purification.

^{1}H NMR (400 MHz, $CDCl_3$) δ 8.09 (t, J = 2.1 Hz, 1H), 7.66 (d, J = 8.5 Hz, 1H), 7.17 (d, J = 8.4 Hz, 1H), 3.45 (s, 3H), 3.38 (s, 3H), 1.36 (s, 9H).

^{13}C NMR (101 MHz, $CDCl_3$) δ 186.2, 150.3, 144.9, 141.5, 131.7, 126.0, 122.6, 43.6, 39.2, 34.9, 31.2.

194 is a known compound and its NMR spectra are in accord with published data.[357]

S-(4-(tert-butyl)-2-nitrophenyl) dimethylcarbamothioate (195)

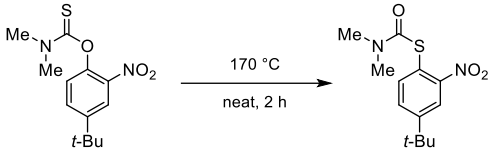

195

Prepared according to literature procedure.[358]

Three microwave vials were each charged with **194** (500 mg, 1.77 mmol), sealed and stirred at 170 °C for 2 h. The three crudes were combined and passed through a pipette column eluting with DCM to give **195** (1.37 g, 91%) as a yellow oil.

^{1}H NMR (400 MHz, $CDCl_3$) δ 7.92 (s, 1H), 7.60 (m, 2H), 3.07 (m, 6H), 1.35 (s, 9H).

^{13}C NMR (101 MHz, $CDCl_3$) δ 164.9, 154.3, 152.5, 138.0, 129.6, 122.1, 120.8, 43.3, 37.3, 35.3, 31.1.

195 is a known compound and its NMR spectra are in accord with published data.[357]

6,6'-Disulfanediylbis(3-(tert-butyl)aniline) (198)

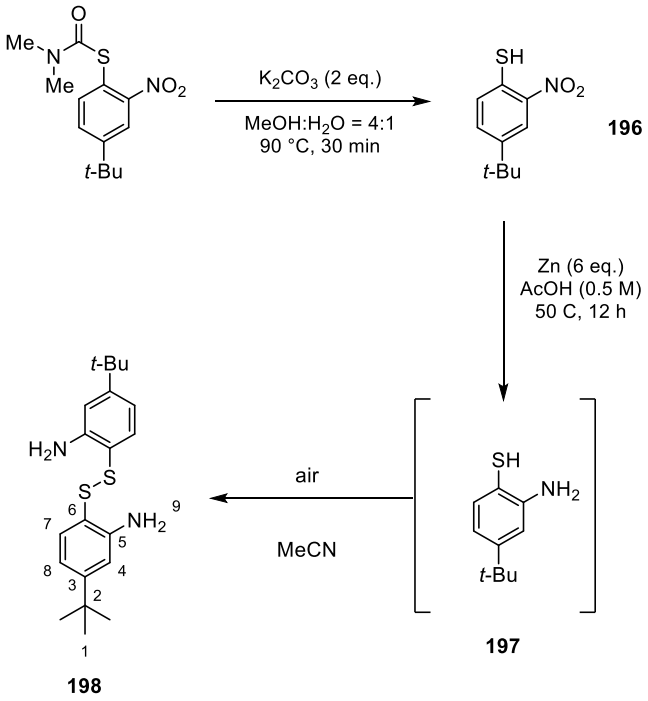

To a solution of S-(4-(tert-butyl)-2-nitrophenyl) dimethylcarbamothioate (1.37 g, 4.85 mmol) in methanol (28 mL) and water (7 mL) was added potassium carbonate (1.34 g, 9.7 mmol) and the reaction was stirred at 90 °C for 30 min. The resulting mixture was acidified with aq. HCl (2M) to a pH of 4 and extracted with diethyl ether (100 mL).

Combined organic was extracted with aq. NaOH (5 wt%, 100 mL) until the extracts became colourless. The combined aqueous was acidified with aq. HCl (2M) and extracted with diethyl ether (100 mL). Combined organic was washed with aq. HCl (2M, 20 mL), water (20 mL) and brine (20 mL), dried over $MgSO_4$, filtered and evaporated to afford crude 4-(tert-butyl)-2-nitrobenzenethiol **196** (620 mg, 60%) that was used directly in the next step without further purification.

A solution of 4-(tert-butyl)-2-nitrobenzenethiol **196** (620 mg, 2.93 mmol) in acetic acid (6 mL) was sparged with argon for 5 min. Zinc powder (1.15 g, 17.6 mmol) was introduced and the resulting suspension was stirred at 50 °C for 12 h. The reaction was neutralised with aq. $NaHCO_3$ and extracted with DCM (60 mL). The combined organic layer was washed with aq. $NaHCO_3$ (60 mL), water (40 mL), and brine (20 mL), dried over anhydrous $MgSO_4$, filtered and evaporated to give crude oil of 2-amino-4-(tert-butyl)benzenethiol **197** (260 mg, 49% mass rec.). Leaving the crude stirring in MeCN (5 mL) exposed to air for 14 h led to complete conversion to disulfide, which was extracted with DCM (20 mL), washed with water (60 mL) and brine (20 mL) to give **198** (203 mg, 78%) as a yellow solid.

^{1}H NMR (400 MHz, $CDCl_3$) δ 7.14 (d, J = 8.2 Hz, 2H, H7), 6.74 (s, 2H, H4), 6.64 (d, J = 8.2 Hz, 2H, H8), 4.28 (s, 4H, H9), 1.27 (s, 18H, H1).

^{13}C NMR (101 MHz, $CDCl_3$) δ 155.4 (C6), 148.4 (C5), 136.5 (C7), 116.3 (C3), 116.1 (C8), 112.6 (C4), 34.8 (C2), 31.3 (C1).

IR (neat) ν_{max}/cm^{-1}: 3404, 3367, 3318, 2959, 2903, 2864, 2361, 2343, 1607, 1589, 1483, 1417, 1360, 1296, 1201, 1159.

HRMS m/z (ESI) calculated for $C_{20}H_{29}N_2S_2^+$ $[M+H]^+$ 361.1767 found: 361.1765.

4-Methoxy-2-nitrobenzenethiol (199)

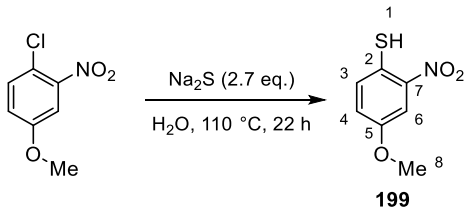

199

A suspension of 4-chloro-3-nitroanisole (938 mg, 5 mmol) and anhydrous sodium sulfide (1.65 g, 13.5 mmol) in water (10 mL) was sparged with argon for 5 minutes and stirred at 110 °C for 22 hours. Upon completion of the reaction, the suspension was

neutralised with aqueous HCl (1M) and extracted with DCM (30 mL). The combined organic layer was washed with water (20 mL) and brine (10 mL), dried over $MgSO_4$, filtered, and evaporated to yield **199** (762 mg, 98%).

^{1}H NMR (400 MHz, $CDCl_3$) δ 7.43 (d, J = 8.9 Hz, 1H, H3), 7.39 (d, J = 2.9 Hz, 1H, H6), 7.06 (ddd, J = 8.9, 2.9, 0.8 Hz, 1H, H4), 5.30 (d, J = 0.8 Hz, 1H, H1), 3.86 (d, J = 0.8 Hz, 3H, H8).

^{13}C NMR (101 MHz, $CDCl_3$) δ 158.6 (C5), 148.36 (C7), 132.5 (C3), 120.1 (C4), 118.4 (C6), 110.5 (C2), 56.2 (C8).

6,6'-Disulfanediylbis(3-methoxyaniline) (201)

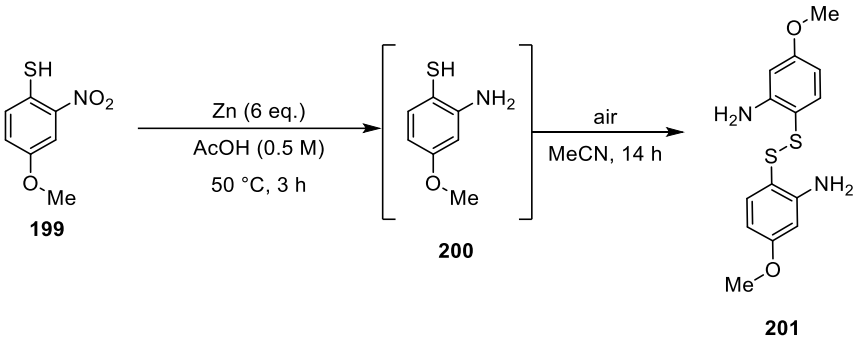

A solution of nitrothiophenol **199** (762 mg, 4.11 mmol) in acetic acid (10 mL) was sparged with argon for 5 min. Zinc powder (2.74 g, 29.5 mmol) was introduced and the resulting suspension was stirred at 50 °C for 3 h. The reaction was filtered over a short pad of silica gel, neutralised with aq. $NaHCO_3$ and extracted with DCM (60 mL). The combined organic layer was washed with aq. $NaHCO_3$ (60 mL), water (40 mL), and brine (20 mL), dried over anhydrous $MgSO_4$, filtered and evaporated to give crude oil of aminothiophenol **200** (555 mg, 87% mass rec.). The crude was stirred in MeCN (10 mL) exposed to air for 14 h, extracted with DCM (20 mL), washed with water (60 mL) and brine (20 mL), dried over $MgSO_4$, filtered and evaporated. Purification via flash column chromatography over silica gel (eluting with gradient of EtOAc 0% to 10 % in cyclohexane) afforded **201** (250 mg, 46%) as a yellow oil.

^{1}H NMR (400 MHz, $CDCl_3$) δ 7.12 (d, J = 8.9 Hz, 2H), 6.33 (d, J = 2.7 Hz, 2H), 6.28 (dd, J = 8.9, 2.7 Hz, 3H), 4.38 – 3.83 (br s, 4H), 3.75 (s, 6H).

^{13}C NMR (101 MHz, $CDCl_3$) δ 159.5, 143.8, 129.9, 111.5, 105.0, 101.5, 55.5.

201 is a known compound and its NMR spectra are in accord with published data.[359]

Alkenes synthesis

But-3-en-1-ylbenzene (162)

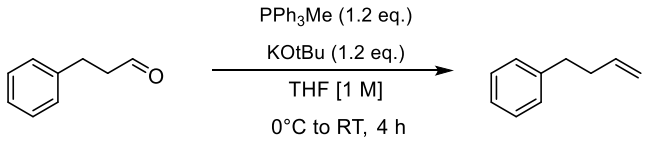

An oven-dried two-neck flask was charged with methyltriphenylphosphonium bromide (12.86 g, 36 mmol) in anh. THF (30 mL) under argon and cooled to 0 °C. Potassium tert-butoxide (4.04 g, 36 mmol) was introduced portion wise and the reaction was stirred for 1 h at 0 °C. To the resulting suspension, 3-phenylpropanal (3.98 mL, 30 mmol) was added dropwise and the reaction was stirred for 4 h at RT. The crude was passed through a short silica plug (eluting cyclohexane), reduced under vacuum and triturated with pentane. The precipitate was filtered off and the filtrate was concentrated and purified via flash column chromatography (eluting pentane) to afford **162** (3.33 g, 70%) as a colourless oil.

^{1}H NMR (400 MHz, $CDCl_3$) δ 7.35 – 7.25 (m, 2H), 7.25 – 7.18 (m, 3H), 5.88 (ddt, J = 16.9, 10.2, 6.6 Hz, 1H), 5.12 – 4.96 (m, 2H), 2.73 (t, J = 6.7 Hz, 2H), 2.45 – 2.34 (m, 2H).

^{13}C NMR (101 MHz, $CDCl_3$) δ 142.0, 138.3, 128.6, 128.4, 125.9, 115.0, 35.7, 35.5.

162 is a known compound and its NMR spectra are in accord with published data.[360]

But-3-en-1-yl benzoate (175)

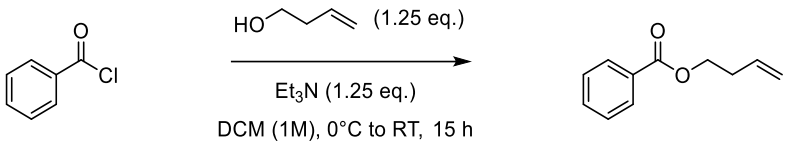

To a solution of benzoyl chloride (5.81 mL, 50 mmol) and triethylamine (8.66 mL, 62.5 mmol) in DCM (100 mL) was added 3-buten-1-ol (5.38 mL, 62.5 mmol) at 0 °C over 5 min. The reaction was stirred at RT for 15 h, before it was diluted with water (100 mL). The organic layer was separated and aqueous was extracted with DCM (3x30 mL). The combined organic layer was washed with water (3x30 mL), brine (30 mL), dried over $MgSO_4$, filtered and evaporated. Purification via flash column chromatography (eluting with gradient 1% to 2% EtOAc in cyclohexane) afforded alkene **175** (6.81 g, 77%) as a colourless oil.

^{1}H NMR (400 MHz, $CDCl_3$) δ 8.05 (d, J = 7.3 Hz, 2H), 7.55 (t, J = 7.4 Hz, 1H), 7.44 (t, J = 7.6 Hz, 2H), 5.88 (ddt, J = 17.0, 10.2, 6.7 Hz, 1H), 5.23 – 5.07 (m, 2H), 4.38 (t, J = 6.7 Hz, 2H), 2.53 (q, J = 6.8 Hz, 2H).

^{13}C NMR (101 MHz, $CDCl_3$) δ 166.7, 134.2, 133.0, 130.5, 129.7, 128.5, 117.5, 64.1, 33.3.

175 is a known compound and its NMR spectra are in accord with published data.[361]

(4-(Pent-4-en-1-yloxy)butyl)benzene (176)

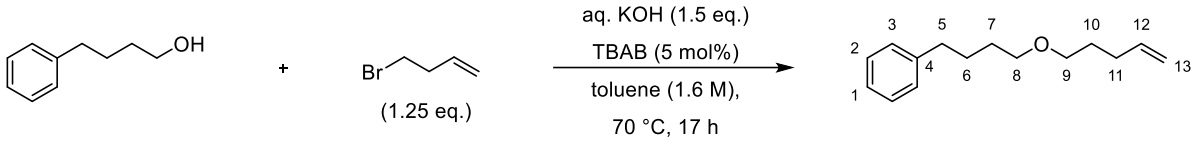

Procedure adapted from literature.[362]

To a solution of 4-phenyl butenol (2.5 g, 16.6 mmol) in toluene (10 mL) was added tetrabutylammonium bromide (270 mg, 0.84 mmol) followed by aq. KOH (50 wt%, 2.8 g, 25 mmol) and stirred at RT for 30 min. Introduced 5-bromo-1-pentene (2.48 mL, 20.8 mmol) and stirred at 70 °C for 17 h. Purification over silica gel (eluting with gradient of 2% to 5% EtOAc in cyclohexane) afforded alkene **176** (630 mg, 17%) as a colourless oil.

^{1}H NMR (400 MHz, $CDCl_3$) δ 7.33 – 7.24 (m, 2H, H3), 7.22 – 7.13 (m, 3H, H1, H2), 5.82 (ddt, J = 16.9, 10.2, 6.6 Hz, 1H, H12), 5.07 – 4.92 (m, 2H, H13), 3.41 (q, J = 6.5 Hz, 4H, H8, H9), 2.64 (t, J = 7.5 Hz, 2H, H5), 2.17 – 2.07 (m, 2H, H11), 1.76 – 1.56 (m, 6H, H6, H7, H10).

^{13}C NMR (101 MHz, $CDCl_3$) δ 142.6 (C4), 138.5 (C12), 128.6 (C1/C2), 128.4 (C3), 125.8 (C1/C2), 114.8 (C13), 70.9 (C8/C9), 70.3 (C8/C9), 35.9 (C5), 30.5 (C11), 29.6 (C6/C7/C10), 29.1 (C6/C7/C10), 28.2 (C6/C7/C10).

IR (neat) ν_{max}/cm^{-1}: 2928, 2847, 2264, 1497, 1454, 1377, 1112.

HRMS: m/z calculated for $C_{15}H_{23}O$ $[M+H]^+$ 219.1743; found 219.1745.

((But-3-en-1-yloxy)methylene)dibenzene (234)

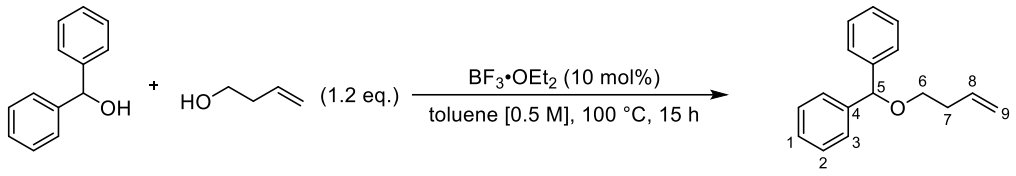

The following reaction was carried out in two separate Schlenk tubes.

To a solution of benzhydrol (1.84 g, 10 mmol) and 3-buten-1-ol (1.22 mL, 12 mmol) in toluene (20 mL) was added boron trifluoride diethyl etherate (0.12 mL, 10 mol%) and the reaction was stirred at 100 °C for 15 h. The suspension was quenched with aq. $NaHCO_3$ (5 mL) and extracted with diethyl ether (3x20 mL). The combined organic layer was washed with aq. $NaHCO_3$ (20 mL), water (2x20 mL) and brine (20 mL), dried over $MgSO_4$, filtered and evaporated. The two crudes were combined and purified via flash column chromatography (eluting with gradient 0% to 10% EtOAc in pentane) afforded alkene **234** (1.58 g, 33%) as a pale-yellow oil.

^{1}H NMR (400 MHz, $CDCl_3$) δ 7.48 – 7.36 (m, 8H, H2, H3), 7.35 – 7.27 (m, 2H, H1), 5.96 (ddt, J = 17.0, 10.2, 6.7 Hz, 1H, H8), 5.44 (s, 1H, H5), 5.24 – 5.09 (m, 2H, H9), 3.60 (t, J = 6.8 Hz, 2H, H6), 2.51 (q, J = 6.7 Hz, 2H, H7).

^{13}C NMR (101 MHz, $CDCl_3$) δ 142.5 (C4), 135.5 (C8), 128.4 (C2/C3), 127.5 (C1), 127.1 (C2/C3), 116.4 (C9), 83.7 (C5), 68.6 (C6), 34.5 (C7).

IR (neat) ν_{max}/cm^{-1}: 3063, 3028, 2970, 2859, 2361, 1740, 1493, 1450, 1365, 1228, 1093, 1074.

N-(2-bromophenyl)acetamide (240)

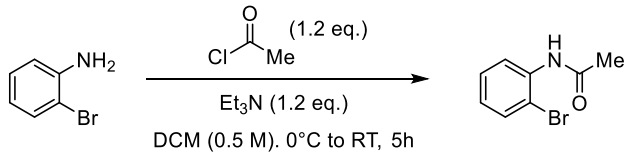

To a suspension of acetyl chloride (1 mL, 14 mmol) and triethylamine (0.97 mL, 7 mmol) in DCM (10 mL) was added 2-bromoaniline (0.66 mL, 5.81 mmol) dropwise at 0 °C. The reaction was warmed to RT and stirred for 5 h after which it was quenched with water (10 mL). The organic layer was separated and the aqueous was extracted with DCM (3x10 mL). The combined organic layer was washed with water (3x20 mL), brine (20 mL), dried over $MgSO_4$, filtered and evaporated. Purification via flash column

chromatography (eluting with gradient 10% to 20% EtOAc in cyclohexane) afforded **240** (897 mg, 72%) as a colourless oil.

^{1}H NMR (400 MHz, $CDCl_3$) δ 8.33 (d, J = 8.5 Hz, 1H), 7.60 (br s, 1H), 7.53 (d, J = 8.0 Hz, 1H), 7.31 (t, J = 8.0 Hz, 1H), 6.98 (t, J = 7.7 Hz, 1H), 2.24 (s, 3H).

240 is a known compound and its NMR spectra are in accord with published data.[363]

Tert-butyl 3-(3-phenylpropylidene)azetidine-1-carboxylate (233)

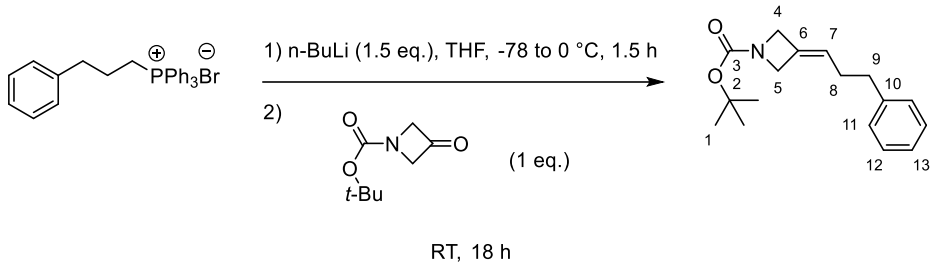

To a suspension of triphenyl(3-phenylpropyl)phosphonium bromide (2.08 g, 4.5 mmol) in THF (25 mL) at -78 °C was added n-BuLi (1.6 M in cyclohexane, 2.8 mL, 4.5 mmol) dropwise and the reaction was stirred for 30 min, then warmed up to 0 °C and stirred for another 1 hour. Introduced tert-butyl 3-oxoazetidine-1-carboxylate (516 mg, 3 mmol) dropwise and the suspension was stirred at RT for 18 h. The reaction was quenched with water (20 mL) and extracted with EtOAc (3x20 mL). The combined organic was washed with water (3x20 mL), brine (20 mL), dried over $MgSO_4$, filtered and evaporated under reduced pressure. Purification over silica gel (eluting with DCM) afforded **233** (592 mg, 72%) as a colourless oil.

^{1}H NMR (400 MHz, $CDCl_3$) δ 7.28 (dd, J = 8.2, 6.8 Hz, 2H, H11), 7.24 – 7.13 (m, 3H, H12, H13), 5.35 – 5.30 (m, 1H), 4.40 (s, 2H, H4/H5), 4.34 (s, 2H, H4/H5), 2.66 (t, J = 7.6 Hz, 2H, H9), 2.21 (q, J = 7.6 Hz, 2H, H8), 1.44 (s, 9H, H1).

^{13}C NMR (101 MHz, $CDCl_3$) δ 156.6 (C3), 141.6 (C10), 128.68 (C6), 128.55 (C11/C12), 128.50 (C11/C12), 126.1 (C13), 121.6 (C7), 79.6 (C2), 57.2 (C4/C5), 56.5 (C4/C5), 35.5 (C9), 30.6 (C8), 28.5 (C1).

IR (neat) ν_{max}/cm^{-1}: 3377 (br), 2976, 2932, 2361, 2341, 1686 (s),1497, 1454, 1392, 1368, 1250, 1157 (s).

N-allyl-N-(2-bromophenyl)acetamide (235)

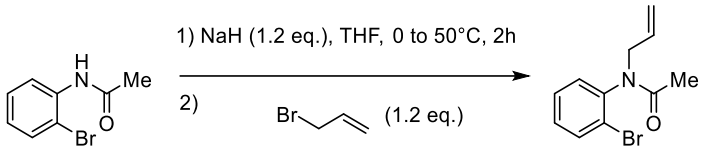

To a suspension of sodium hydride (192 mg, 4.8 mmol) in THF (3 mL) was added dropwise a solution of N-(2-bromophenyl)acetamide (856 mg, 4 mmol) in THF (7 mL) at 0 °C under argon atmosphere. The reaction was stirred at 50 °C for 2h before it was cooled to 0 °C and allyl bromide (0.42 mL, 4.8 mmol) was introduced dropwise. The reaction was heated to 50 °C and stirred for 3 h before it was quenched with water. The organic layer was separated and the aqueous was extracted with DCM (3x10 mL). The combined organic layer was washed with water (3x20 mL), brine (20 mL), dried over $MgSO_4$, filtered and evaporated. Purification via flash column chromatography (eluting with 10% EtOAc in cyclohexane) afforded **235** (914 mg, 89%) as a colourless oil.

^{1}H NMR (400 MHz, $CDCl_3$) δ 7.68 (d, J = 8.0 Hz, 1H), 7.35 (t, J = 7.2 Hz, 1H), 7.22 (ddd, J = 9.5, 7.6, 1.7 Hz, 2H), 5.88 (dddd, J = 17.4, 10.2, 7.6, 5.6 Hz, 1H), 5.13 – 4.99 (m, 2H), 4.82 – 4.72 (m, 1H), 3.71 (dd, J = 14.7, 7.6 Hz, 1H), 1.81 (s, 3H).

^{13}C NMR (101 MHz, $CDCl_3$) δ 170.2, 141.5, 133.9, 132.9, 131.2, 129.8, 128.6, 124.1, 118.6, 50.9, 22.6.

235 is a known compound and its NMR spectra are in accord with published data.[364]

4-Methylpent-3-en-1-yl benzoate (236)

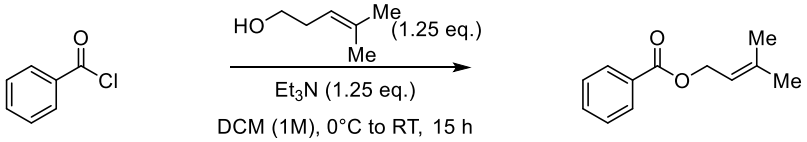

To a solution of benzoyl chloride (0.58 mL, 5 mmol) and triethylamine (0.87 mL, 62.5 mmol) in DCM (10 mL) was added 3-methyl-2-buten-1-ol (0.63 mL, 6.25 mmol) at 0 °C over 5 min. The reaction was stirred at RT for 15 h, before it was diluted with water (10 mL). The organic layer was separated and aqueous was extracted with DCM (3x10 mL). The combined organic layer was washed with water (3x10 mL), brine (10 mL), dried over $MgSO_4$, filtered and evaporated. Purification via flash column

chromatography (eluting with gradient 1% to 2% EtOAc in cyclohexane) afforded alkene **236** (744 mg, 78%) as a colourless oil.

^{1}H NMR (400 MHz, $CDCl_3$) δ 8.05 (d, J = 7.5 Hz, 2H), 7.55 (d, J = 7.1 Hz, 1H), 7.43 (t, J = 7.5 Hz, 2H), 5.47 (t, J = 7.1 Hz, 1H), 4.82 (d, J = 7.1 Hz, 2H), 1.78 (d, J = 6.7 Hz, 6H).

^{13}C NMR (101 MHz, $CDCl_3$) δ 166.8, 139.3, 132.9, 130.6, 129.7, 128.4, 118.8, 62.0, 25.9, 18.3.

236 is a known compound and its NMR spectra are in accord with published data.[365]

General procedure D for acrylates synthesis:

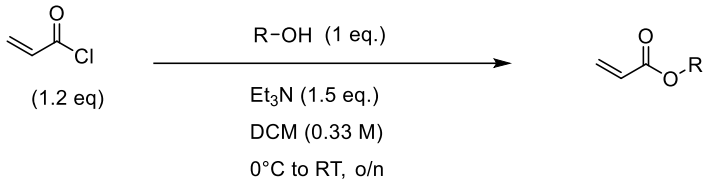

To a solution of alcohol or phenol (5 mmol) and triethylamine (1.01 mL, 7.25 mmol) in anh. DCM (15 mL) was added acryloyl chloride (0.49 mL, 6 mmol) dropwise at 0 °C and the reaction was stirred at room temperature overnight. The resulting suspension was diluted with DCM (10 mL), transferred to a separatory funnel and washed with water (2x20 mL) and brine (20 mL). The organic layer was dried over $MgSO_4$, filtered and reduced under vacuum. Purification via flash column chromatography afforded the purified product.

4-Phenylbutyl acrylate (223)

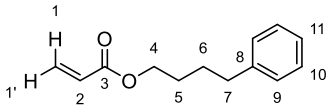

Prepared according to general procedure D using 4-phenyl-1-butanol (751 mg, 5 mmol) as alcohol substrate. Purification over silica gel (eluting with gradient 10% to 30% EtOAc in cyclohexane) afforded **223** as a colourless oil (761 mg, 75%)

^{1}H NMR (400 MHz, $CDCl_3$) δ 7.34 – 7.24 (m, 2H, H9), 7.23 – 7.15 (m, 3H, H10, H11), 6.40 (dd, J = 17.3, 1.5 Hz, 1H, H1), 6.12 (dd, J = 17.3, 10.4 Hz, 1H, H2), 5.82 (dd, J = 10.4, 1.5 Hz, 1H, H1'), 4.22 – 4.14 (m, 2H, H4), 2.71 – 2.59 (m, 2H, H7), 1.78 – 1.65 (m, 4H, H5, H6).

^{13}C NMR (101 MHz, $CDCl_3$) δ 166.4 (C3), 142.2 (C8), 130.7 (C1), 128.7 (C2), 128.53 (C9/C10), 128.49 (C9/C10), 126.0 (C11), 64.6 (C4), 35.6 (C7), 28.4 (C6), 27.9 (C5).

IR (neat) ν_{max}/cm^{-1}: 3026, 2941, 2860, 1722 (s), 1497, 1454, 1408, 1296, 1271, 1190.

(1R,2S,5R)-2-isopropyl-5-methylcyclohexyl acrylate (225)

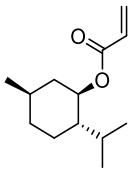

Prepared according to general procedure D using (L)-menthol (781 mg, 5 mmol) as alcohol substrate. Purification over silica gel (eluting with gradient EtOAc 0% to 15% in cyclohexane) afforded **225** as a colourless oil (469 mg, 45%)

^{1}H NMR (500 MHz, $CDCl_3$) δ 6.38 (dd, J = 17.3, 1.5 Hz, 1H), 6.10 (dd, J = 17.3, 10.4 Hz, 1H), 5.79 (dd, J = 10.4, 1.5 Hz, 1H), 4.76 (td, J = 10.9, 4.4 Hz, 1H), 2.07 – 1.99 (m, 1H), 1.87 (heptd, J = 6.9, 2.7 Hz, 1H), 1.74 – 1.64 (m, 2H), 1.56 – 1.46 (m, 1H), 1.45 – 1.38 (m, 1H), 1.14 – 0.95 (m, 2H), 0.90 (t, J = 7.0 Hz, 6H), 0.77 (d, J = 6.9 Hz, 3H).

^{13}C NMR (126 MHz, $CDCl_3$) δ 166.0, 130.3, 129.2, 74.5, 47.2, 41.0, 34.4, 31.5, 26.5, 23.7, 22.2, 20.9, 16.6.

225 is a known compound and its NMR spectra are in accord with published data.[366]

(1S,2R)-1,7,7-trimethylbicyclo[2.2.1]heptan-2-yl acrylate (227)

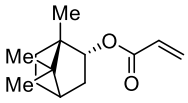

Prepared according to general procedure D using (-)-borneol (771 mg, 5 mmol) as alcohol substrate. Purification over silica gel eluting (eluting with gradient EtOAc 0% to 15% in cyclohexane) afforded **227** as a colourless oil (765 mg, 74%)

^{1}H NMR (500 MHz, $CDCl_3$) δ 6.39 (dd, J = 17.4, 1.5 Hz, 1H), 6.14 (dd, J = 17.3, 10.4 Hz, 1H), 5.81 (dd, J = 10.4, 1.5 Hz, 1H), 4.96 (ddd, J = 10.0, 3.6, 2.2 Hz, 1H), 2.44 – 2.34 (m, 1H), 2.02 – 1.93 (m, 1H), 1.81 – 1.71 (m, 1H), 1.69 (t, J = 4.6 Hz, 1H), 1.37 – 1.28 (m, 1H), 1.28 – 1.21 (m, 1H), 1.02 (dd, J = 13.8, 3.5 Hz, 1H), 0.92 (s, 3H), 0.88 (s, 3H), 0.85 (s, 3H).

^{13}C NMR (126 MHz, $CDCl_3$) δ 166.7, 130.2, 129.2, 80.2, 49.0, 48.0, 45.1, 36.9, 28.2, 27.3, 19.9, 19.0, 13.7.

227 is a known compound and its NMR spectra are in accord with published data.[367]

4-(tert-Butyl)phenyl acrylate (237)

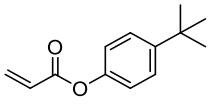

Prepared according to general procedure D using 4-(tert-butyl)phenol (751 mg, 5 mmol) as alcohol substrate. Purification over silica gel (eluting with gradient 0% to 10% EtOAc in cyclohexane) afforded **237** as a colourless oil (380 mg, 37%).

^{1}H NMR (400 MHz, $CDCl_3$) δ 7.44 – 7.35 (m, 2H), 7.09 – 7.01 (m, 2H), 6.60 (d, J = 17.3 Hz, 1H), 6.33 (dd, J = 17.3, 10.4 Hz, 1H), 6.00 (d, J = 10.4 Hz, 1H), 1.32 (s, 9H).

^{13}C NMR (101 MHz, $CDCl_3$) δ 164.9, 148.8, 148.4, 132.5, 128.2, 126.5, 120.9, 34.6, 31.6.

237 is a known compound and its NMR spectra are in accord with published data.[368]

4-Bromophenyl acrylate (238)

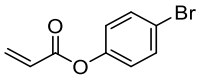

Prepared according to general procedure D using 4-bromophenol (865 mg, 5 mmol) as alcohol substrate. Purification over silica gel (eluting with 10% EtOAc in cyclohexane) afforded **238** as a colourless oil (902 mg, 79%).

^{1}H NMR (400 MHz, $CDCl_3$) δ 7.55 – 7.46 (m, 2H), 7.07 – 6.99 (m, 2H), 6.61 (d, J = 17.3 Hz, 1H), 6.30 (dd, J = 17.3, 10.5 Hz, 1H), 6.04 (d, J = 10.4 Hz, 1H).

^{13}C NMR (101 MHz, $CDCl_3$) δ 164.3, 149.7, 133.2, 132.6, 127.7, 123.5, 119.1.

238 is a known compound and its NMR spectra are in accord with published data.[368]

2-Chorophenyl acrylate (239)

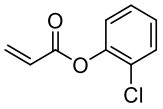

Prepared according to general procedure D using 2-chlorophenol (0.51 mL, 5 mmol) as alcohol substrate. Purification over silica gel (eluting with 10% EtOAc in cyclohexane) afforded **239** as a colourless oil (800 mg, 88%).

^{1}H NMR (400 MHz, $CDCl_3$) δ 7.46 (dd, J = 7.8, 1.6 Hz, 1H), 7.30 (td, J = 7.8, 1.6 Hz, 1H), 7.24 – 7.16 (m, 2H), 6.67 (dt, J = 17.3, 0.9 Hz, 1H), 6.37 (dd, J = 17.3, 10.5 Hz, 1H), 6.08 (dt, J = 10.5, 0.9 Hz, 1H).

^{13}C NMR (101 MHz, $CDCl_3$) δ 163.7, 147.0, 133.5, 130.5, 127.9, 127.3, 127.2, 127.1, 123.8.

239 is a known compound and its NMR spectra are in accord with published data.[368]

General procedure E for radical hydrogenation:

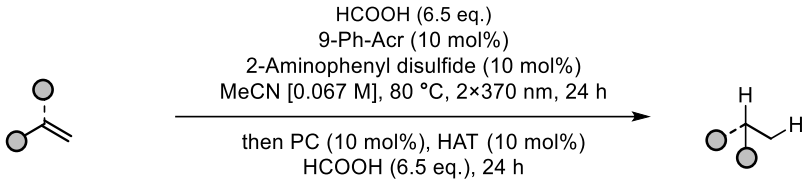

A microwave vial was charged with alkene (0.4 mmol), 9-phenyl acridine (10 mg, 10 mol%) and 2-aminophenyl disulfide (10 mg, 10 mol%). Sealed under argon atmosphere and introduced anh. MeCN (6 mL) followed by formic acid (0.1 mL, 2.6 mmol). The reaction vial was placed in a colourless oil bath (80 °C) and irradiated under 2x370 nm for 24 h (Lamp source was placed 2 cm away from the vial). The reaction was allowed to cool to RT, the pressure was released by piercing the septum with a needle, and a stock solution of 9-phenyl acridine (10 mg, 10 mol%), 2-aminophenyl disulfide (10 mg, 10 mol%) and formic acid (0.1 mL, 2.6 mmol) in MeCN (0.3 mL) was added. The reaction was sparged with argon for 5 min before it was placed back into the oil bath (80 °C) and irradiated for 24 h.

Following this, the reaction was neutralised with aq. $NaHCO_3$ and extracted with ethyl acetate (3x5 mL). Combined organic layer was washed with water (10 mL), brine (10 mL), dried over $MgSO_4$, filtered and evaporated under reduced pressure. Purification via flash column chromatography afforded the pure product.

Methyl undecanoate (179)

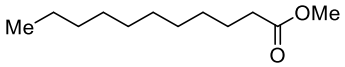

Prepared according to general procedure E using **132** (79 mg, mmol). Purification over silica gel (eluting with cyclohexane) afforded **179** as a colourless oil (48 mg, 60%).

^{1}H NMR (400 MHz, $CDCl_3$) δ 3.66 (s, 3H), 2.29 (t, J = 7.4 Hz, 2H), 1.61 (t, J = 7.5 Hz, 2H), 1.35 – 1.18 (m, 14H), 0.87 (t, J = 7.0 Hz, 3H).

^{13}C NMR (101 MHz, $CDCl_3$) δ 174.5, 51.6, 34.3, 32.0, 29.7, 29.6, 29.5, 29.4, 29.3, 25.1, 22.8, 14.3.

179 is a known compound and its NMR spectra are in accord with published data.[369]

Butyl benzoate (211)

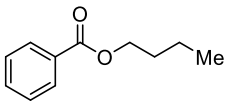

Prepared according to general procedure E using **175** (70 mg, 0.4 mmol). Purification over silica gel (eluting with gradient 0% to 10% EtOAc in pentane) afforded **211** as a colourless oil (47 mg, 66%).

^{1}H NMR (400 MHz, $CDCl_3$) δ 8.05 (d, J = 7.3 Hz, 2H), 7.55 (t, J = 7.2 Hz, 1H), 7.44 (t, J = 7.5 Hz, 2H), 4.33 (t, J = 6.6 Hz, 2H), 1.81 – 1.70 (m, 2H), 1.48 (h, J = 7.4 Hz, 2H), 0.98 (t, J = 7.4 Hz, 3H).

^{13}C NMR (101 MHz, $CDCl_3$) δ 166.8, 132.9, 130.7, 129.7, 128.5, 64.9, 30.9, 19.4, 13.9.

211 is a known compound and its NMR spectra are in accord with published data.[370]

(4-(Pentyloxy)butyl)benzene (212)

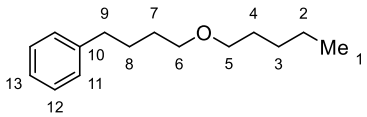

Prepared according to general procedure E using **176** (87 mg, 0.4 mmol). Purification over silica gel (eluting with gradient 0% to 10% EtOAc in pentane) afforded **212** as a colourless oil (43 mg, 49%).

^{1}H NMR (400 MHz, $CDCl_3$) δ 7.31 – 7.22 (m, 2H, H12), 7.21 – 7.12 (m, 3H, H11, H13), 3.45 – 3.33 (m, 4H H5, H6), 2.67 – 2.58 (m, 2H, H9), 1.74 – 1.49 (m, 4H, H7, H8), 1.37 – 1.23 (m, 6H, H2, H3, H4), 0.93 – 0.84 (m, 3H, H1).

^{13}C NMR (101 MHz, $CDCl_3$) δ 142.7 (C10), 128.6 (C11), 128.4 (C12), 125.8 (C13), 71.2 (C5/C6), 70.8 (C5/C6), 35.9 (C9), 29.6, 29.6, 28.5, 28.2, 22.7 (C2), 14.2 (C1).

IR (neat) ν_{max}/cm^{-1}: 2930, 2857, 1497, 1454, 1377, 1112.

1-Bromo undecane (214)

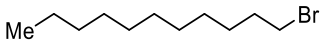

Prepared according to general procedure E using **213** (93 mg, 0.4 mmol). Purification over silica gel (eluting with cyclohexane) afforded a mixture of alkene **213** (9 mg) and alkane **214** (33 mg, 35 %).

Yield determined by dividing the total mass recovered by the NMR ratio of product and starting material.

^{1}H NMR (400 MHz, $CDCl_3$) δ 3.41 (t, J = 7.0 Hz, 2H), 1.85 (p, J = 7.0 Hz, 2H), 1.41 (m, 2H), 1.35 – 1.19 (m, 14H), 0.88 (t, J = 6.7 Hz, 3H).

214 is a known compound and its NMR spectra are in accord with published data.[371]

Undecan-1-ol (216)

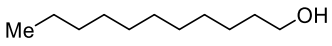

Prepared according to general procedure E using **215** (68 mg, 0.4 mmol). Purification over silica gel (eluting with cyclohexane) afforded **216** as a colourless oil (19 mg, 27%).

^{1}H NMR (400 MHz, $CDCl_3$) δ 3.64 (t, J = 6.9 Hz, 2H), 1.56 (p, J = 6.9 Hz, 2H), 1.39 – 1.21 (m, 17H), 0.88 (t, J = 6.6 Hz, 3H).

^{13}C NMR (101 MHz, $CDCl_3$) δ 63.3, 32.9, 32.0, 29.8, 29.6, 29.5, 25.9, 22.8, 14.3.

216 is a known compound and its NMR spectra are in accord with published data.[372]

Tert-butyl 4-pentanoylpiperazine-1-carboxylate (218)

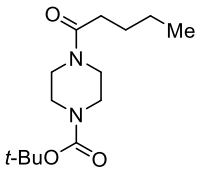

Prepared according to general procedure E using **217** (107 mg, 0.4 mmol). Purification over silica gel (eluting with cyclohexane) afforded **218** as a colourless oil (70 mg, 65% mass recovery) mixed with **217** (9%).

^{1}H NMR (400 MHz, $CDCl_3$) δ 3.61 – 3.53 (m, 2H), 3.40 (d, J = 17.1 Hz, 7H), 2.31 (t, J = 8.0 Hz, 2H), 1.66 – 1.53 (m, 2H), 1.45 (s, 11H), 1.35 (h, J = 7.4 Hz, 2H), 0.91 (t, J = 6.8 Hz, 3H).

Pentyl nicotinate (220)

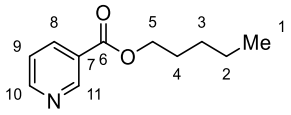

Prepared according to general procedure E using **219** (77 mg, 0.4 mmol). Purification over silica gel (eluting with 10% EtOAc in pentane) afforded **220** as a colourless oil (21 mg, 27%).

^{1}H NMR (400 MHz, $CDCl_3$) δ 9.23 (s, 1H, H8), 8.77 (s, 1H, H10), 8.33 – 8.26 (m, 1H, H9), 7.44 – 7.33 (m, 1H, H11), 4.39 – 4.30 (m, 2H, H5), 1.84 – 1.74 (m, 2H, H4), 1.46 – 1.33 (m, 4H), 0.97 – 0.88 (m, 3H, H1).

^{13}C NMR (101 MHz, $CDCl_3$) δ 165.5 (C6), 153.5 (C10), 151.1 (C8), 137.1 (C9), 126.5 (C7), 123.4 (C11), 65.7 (C5), 28.5 (C4), 28.3 (C2/C3), 22.5 (C2/C3), 14.1 (C1).

IR (neat) ν_{max}/cm^{-1}: 2959, 2932, 2872, 2363, 1722 (s), 1591, 1468, 1420, 1279, 1111.

HRMS: m/z calculated for $C_{11}H_{16}NO_2$ $[M+H]^+$ 194.1176; found 194.1178.

Benzyl piperidine-1-carboxylate (222)

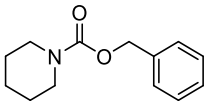

Prepared according to general procedure E using **221** (73 mg, 0.4 mmol). Purification over silica gel (eluting with gradient 20% to 40% EtOAc in pentane) afforded **222** as a colourless oil (7 mg, 8%).

^{1}H NMR (400 MHz, $CDCl_3$) δ 7.39 – 7.27 (m, 5H), 5.12 (s, 2H), 3.44 (t, J = 5.4 Hz, 4H), 1.67 – 1.44 (m, 6H).

^{13}C NMR (101 MHz, $CDCl_3$) δ 155.5, 137.2, 128.6, 128.0, 127.9, 67.0, 45.0, 25.8, 24.5.

222 is a known compound and its NMR spectra are in accord with published data.[373]

4-Phenylbutyl propionate (224)

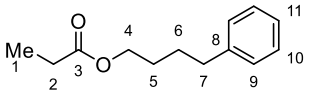

Prepared according to general procedure E using **223** (82 mg, 0.4 mmol). Purification over silica gel (eluting with gradient 0% to 10% EtOAc in cyclohexane) afforded **224** as a colourless oil (34 mg, 41%).

^{1}H NMR (500 MHz, $CDCl_3$) δ 7.32 – 7.26 (m, 2H), 7.22 – 7.15 (m, 3H, H9, H11), 4.09 (t, J = 6.0 Hz, 2H, H4), 2.65 (t, J = 7.1 Hz, 2H, H7), 2.32 (q, J = 7.5 Hz, 2H, H2), 1.75 – 1.63 (m, 4H, H5, H6), 1.14 (t, J = 7.5 Hz, 3H, H1).

^{13}C NMR (126 MHz, $CDCl_3$) δ 174.7 (C3), 142.2 (C8), 128.54 (C9/C10), 128.49 (C9/C10), 126.0 (C11), 64.3 (C4), 35.6 (C7), 28.4 (C5/C6), 27.9 (C5/C6), 27.8 (C2), 9.3 (C1).

IR (neat) ν_{max}/cm^{-1}: 3063, 2939, 2860, 1732 (s), 11493, 1454, 1351, 1182.

(1R,2S,5R)-2-isopropyl-5-methylcyclohexyl propionate (226)

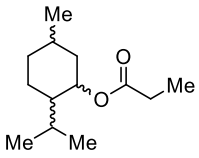

Prepared according to general procedure E using **225** (84 mg, 0.4 mmol). Purification over silica gel (eluting with gradient 0% to 10% EtOAc in pentane) afforded **226** as a colourless oil (22 mg, 26%, mixture of diastereoisomers).

See below for NMR spectra.

226 is a known compound and its NMR spectra are in accord with published data.[374]

(1S,2R)-1,7,7-trimethylbicyclo[2.2.1]heptan-2-yl propionate (228)

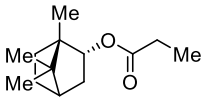

Prepared according to general procedure E using **227** (83 mg, 0.4 mmol). Purification over silica gel (eluting with gradient 0% to 10% EtOAc in pentane) afforded **228** as a colourless oil (32 mg, 38%, dr = 5.3:1).

See below for NMR spectra.

Diethyl (3R,4S)-3,4-dimethylcyclopentane-1,1-dicarboxylate (242)

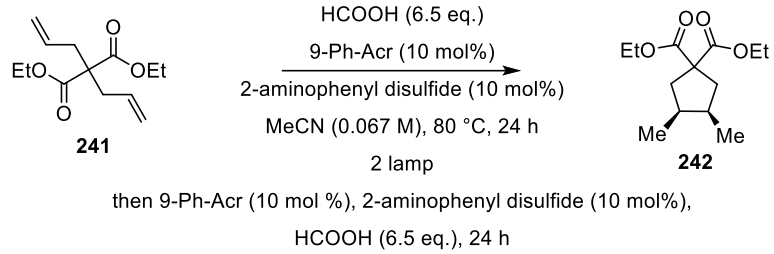

Prepared according to general procedure E using X (mg, 0.4 mmol) from diethyl 2,2-diallylmalonate **241**. Purification over silica gel (eluting with gradient 0% to 10% EtOAc in pentane) afforded **242** as a colourless oil (22 mg, 23%, 4.4:1 dr).

Data for major isomer:

^{1}H NMR (400 MHz, $CDCl_3$) δ 4.16 (d, J = 7.1 Hz, 4H), 2.38 (dd, J = 13.5, 6.3 Hz, 2H), 2.18 – 2.02 (m, 2H), 1.95 (dd, J = 13.5, 6.7 Hz, 2H), 1.23 (t, J = 7.1 Hz, 6H), 0.86 (d, J = 6.3 Hz, 6H).

^{13}C NMR (101 MHz, $CDCl_3$) δ 173.3, 173.1, 61.4, 61.4, 59.4, 42.9, 41.8, 41.1, 36.9, 17.5, 15.0, 14.2.

242 is a known compound and its NMR spectra are in accord with published data.[375]

Miscellaneous

Methyl 2,4,6-trimethylbenzoate (250)

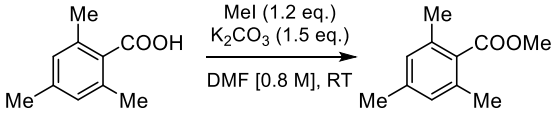

To a suspension of 2,4,6-trimethylbenzoic acid (13.1 g, 80 mmol) and potassium carbonate (16.6 g, 120 mmol) in DMF (100 mL) was added iodomethane (6 mL, 96 mmol) dropwise. The reaction was stirred at RT for 14 h, before it was diluted with water (100 mL) and extracted with diethyl ether (3x100 mL). The combined organic layer was washed with water (5x100 mL) and brine (100 mL), dried over $MgSO_4$, filtered and evaporated to afford **250** (14.0 g, 98%) as a yellow oil that was used directly without the need for any further purification.

^{1}H NMR (400 MHz, $CDCl_3$) δ 6.85 (s, 2H), 3.89 (s, 3H), 2.28 (s, 6H).

^{13}C NMR (126 MHz, $CDCl_3$) δ 170.7, 139.4, 135.3, 130.9, 128.5, 51.9, 21.3, 19.9.

250 is a known compound and its NMR spectra are in accord with published data.[376]

Methyl 2-fluorobenzoate (251)

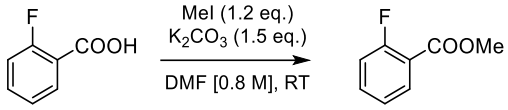

To a suspension of 2-fluorobenzoic acid (701 mg, 5 mmol) and potassium carbonate (1.04 g, 7.5 mmol) in DMF (6 mL) was added iodomethane (0.37 mL, 6 mmol) dropwise. The reaction was stirred at RT for 18 h, before it was diluted with water (10 mL) and extracted with diethyl ether (3x20 mL). The combined organic layer was washed with water (5x20 mL) and brine (20 mL), dried over $MgSO_4$, filtered and evaporated to afford **251** (505 mg, 66%) as a colourless oil that was used directly without the need for any further purification.

^{1}H NMR (400 MHz, $CDCl_3$) δ 7.94 (t, J = 7.6 Hz, 1H), 7.57 – 7.47 (m, 1H), 7.20 (t, J = 7.6 Hz, 1H), 7.17 – 7.09 (m, 1H), 3.93 (s, 3H).

^{13}C NMR (101 MHz, $CDCl_3$) δ 165.1 (d, J = 3.7 Hz), 162.1 (d, J = 259.9 Hz), 134.6 (d, J = 9.1 Hz), 132.3, 124.1 (d, J = 4.0 Hz), 118.8 (d, J = 9.8 Hz), 117.1 (d, J = 22.5 Hz), 52.5.

^{19}F NMR (376 MHz, $CDCl_3$) δ -109.62.

251 is a known compound and its NMR spectra are in accord with published data.[377]

Methyl 2,3,4,5,6-pentafluorobenzoate (252)

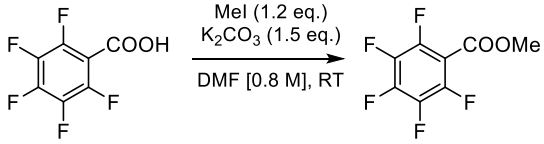

To a suspension of 2,3,4,5,6-pentafluorobenzoic acid (1.06 g, 5 mmol) and potassium carbonate (1.04 g, 7.5 mmol) in DMF (6 mL) was added iodomethane (0.37 mL, 6 mmol) dropwise. The reaction was stirred at RT for 18 h, before it was diluted with water (10 mL) and extracted with diethyl ether (3x20 mL). The combined organic layer was washed with water (5x20 mL) and brine (20 mL), dried over $MgSO_4$, filtered and evaporated to afford **252** (760 mg, 67%) as a colourless oil that was used directly without the need for any further purification.

^{1}H NMR (400 MHz, $CDCl_3$) δ 3.98 (s, 3H).

^{19}F NMR (376 MHz, $CDCl_3$) δ -138.10 (m), -148.40 (tt, J = 21.2, 4.6 Hz), -160.30 (m).

252 is a known compound and its NMR spectra are in accord with published data.[378]

4-Phenylbutyl 4-methylbenzenesulfonate (253)

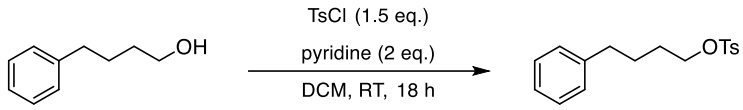

A solution of 4-phenyl-1-butanol (0.38 mL, 2.5 mmol) and tosyl chloride (715 mg, 3.75 mmol) in DCM (5 mL) was charged with pyridine (0.4 mL, 5 mmol) and stirred at RT for 18 h. The reaction was quenched with aq. HCl (1M, 5 mL) and the organic layer was separated. The aqueous was extracted with DCM (3x10 mL), combined organic was washed with water (2x20 mL), brine (20 mL), dried over $MgSO_4$, filtered and evaporated. Purification over silica gel (eluting with a gradient 0 to 20% DCM in cyclohexane) afforded **253** (428 mg, 56%) as a colourless oil.

^{1}H NMR (400 MHz, $CDCl_3$) δ 7.82 – 7.74 (m, 2H), 7.33 (d, J = 8.1 Hz, 2H), 7.25 (t, J = 7.4 Hz, 4H), 7.18 (t, J = 7.2 Hz, 1H), 7.11 (d, J = 7.1 Hz, 2H), 4.03 (t, J = 5.9 Hz, 2H), 2.56 (t, J = 7.0 Hz, 2H), 2.44 (s, 3H), 1.71 – 1.60 (m, 4H).

^{13}C NMR (101 MHz, $CDCl_3$) δ 144.8, 141.7, 133.3, 129.9, 128.5, 128.0, 126.0, 70.5, 35.2, 28.5, 27.2, 21.8.

253 is a known compound and its NMR spectra are in accord with published data.[379]

Triphenyl(3-phenylpropyl)phosphonium bromide (254)

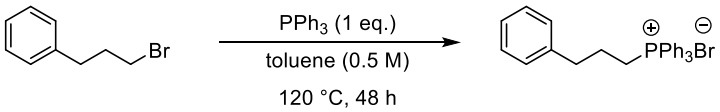

A solution of (3-bromopropyl)benzene (3.8 mL, 25 mmol) and triphenylphoshine (6.56 g, 25 mmol) in toluene (50 mL) was stirred at 120 °C for 48 hours. The resulting suspension was cooled to 0 °C, triturated with pentane (100 mL), filtered and washed with pentane and diethyl ether. The precipitate was dried under vacuum to afford phosphonium bromide (5.9 g, 51%) as an off-white solid.

^{1}H NMR (400 MHz, $CDCl_3$) δ 7.82 – 7.72 (m, 10H), 7.70 – 7.61 (m, 5H), 7.28 – 7.22 (m, 2H), 7.22 – 7.14 (m, 3H), 3.96 – 3.87 (m, 2H), 3.03 (t, J = 6.9 Hz, 2H), 1.94 (h, J = 7.7 Hz, 2H).

^{13}C NMR (101 MHz, $CDCl_3$) δ 140.4, 135.1 (d, J = 3.1 Hz), 133.8 (d, J = 9.9 Hz), 130.56 (d, J = 12.5 Hz), 129.1, 128.7, 126.5, 118.5 (d, J = 86.0 Hz), 35.7 (d, J = 16.7 Hz), 24.7 (d, J = 3.9 Hz), 21.8 (d, J = 50.2 Hz).

^{31}P NMR (162 MHz, $CDCl_3$) δ 24.54.

254 is a known compound and its NMR spectra are in accord with published data.[380]

(3-(Benzoyloxy)propyl)triphenylphosphonium bromide (255)

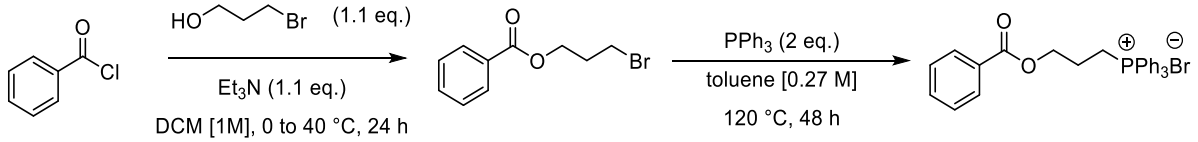

To a solution of 1-bromo-propan-3-ol (3 mL, 33 mmol) and triethylamine (4.6 mL, 33 mmol) in DCM (30 mL) was added benzoyl chloride (3.5 mL, 30 mmol) dropwise at 0 °C. The reaction was heated to 40 °C and stirred for 24 h. After it was cooled to RT, the mixture was poured into water (50ml) and extracted with DCM (3x30 mL). The combined organic was washed with water (3x30 mL) and brine (30 mL), dried over $MgSO_4$, filtered and evaporated. Purification over silica gel (eluting with a gradient of 0% to 2% EtOAc in cyclohexane) afforded 3-bromopropyl benzoate (3.88 g, 53% mass recovered) that was used directly in the next step without further purification.

A solution of 3-bromopropyl benzoate (3.88 g, 16 mmol) and triphenylphoshine (8.39 g, 32 mmol) in toluene (60 mL) was stirred at 120 °C for 48 hours. The resulting suspension was cooled to 0 °C, filtered and triturated with diethyl ether (200 mL). The combined precipitate was dried under vacuum to afford phosphonium bromide (4.36 g, 54%) as an off-white solid.

^{1}H NMR (400 MHz, $CDCl_3$) δ 7.96 (d, J = 7.8 Hz, 2H), 7.89 – 7.80 (m, 6H), 7.80 – 7.74 (m, 3H), 7.65 (m, 6H), 7.54 (d, J = 7.5 Hz, 1H), 7.42 (t, J = 7.7 Hz, 2H), 4.67 (t, J = 6.2 Hz, 2H), 4.18 – 4.06 (m, 2H), 2.23 – 2.09 (m, 2H).

^{13}C NMR (101 MHz, $CDCl_3$) δ 166.3, 135.2 (d, J = 3.1 Hz), 133.8 (d, J = 10.1 Hz), 133.3, 130.6 (d, J = 12.6 Hz), 129.9, 129.7, 128.55, 118.1 (d, J = 86.3 Hz), 63.9 (d, J = 17.8 Hz), 22.6 (d, J = 3.6 Hz), 19.9 (d, J = 52.7 Hz).

^{31}P NMR (162 MHz, $CDCl_3$) δ 24.8.

255 is a known compound and its NMR spectra are in accord with published data.[381]

NMR spectra for Chapter 4

2,4,5,6-Tetra(9H-carbazol-9-yl)isophthalonitrile (4CzIPN)

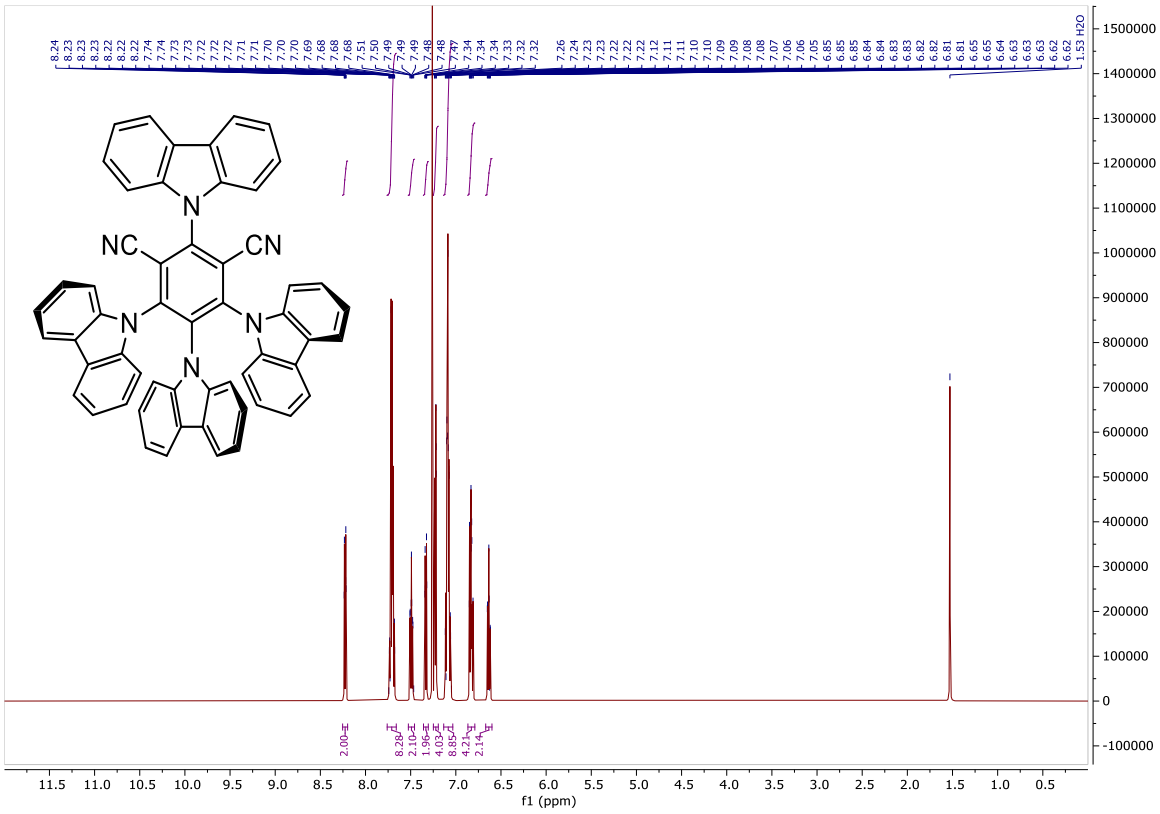

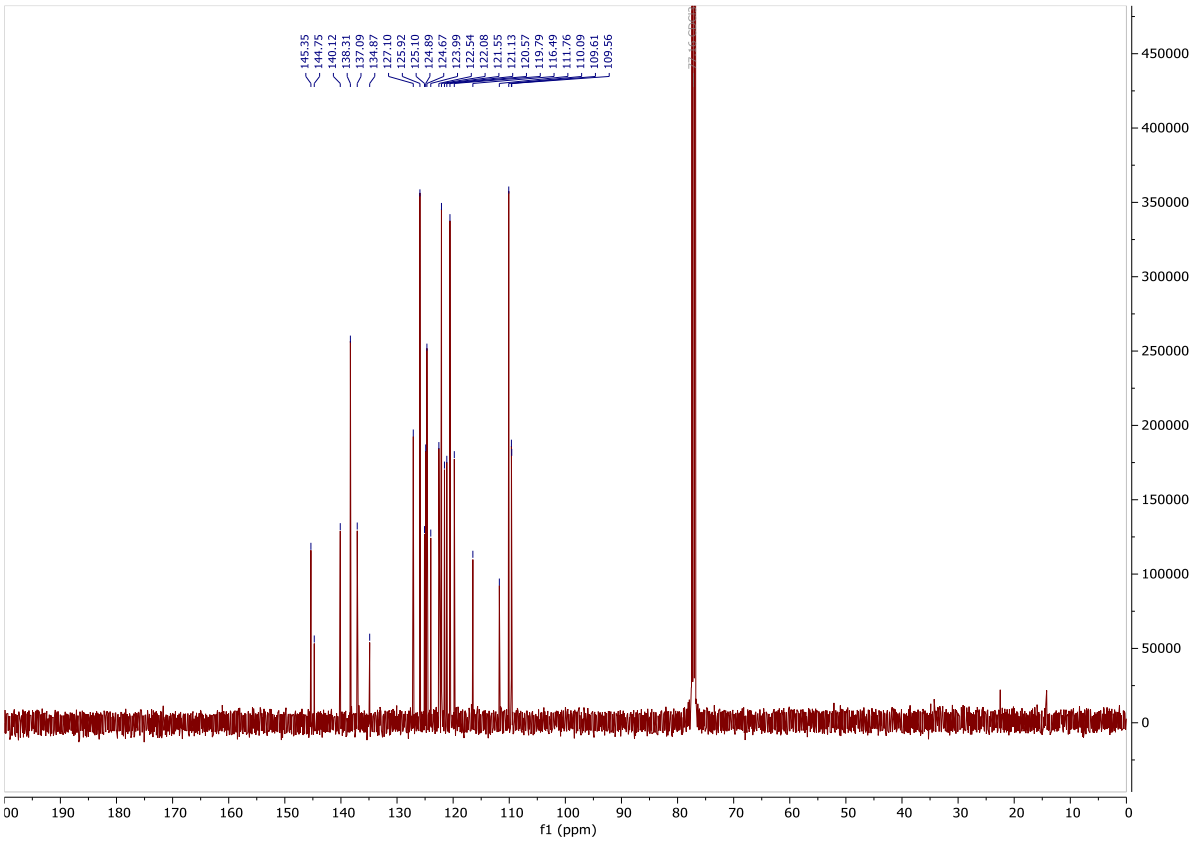

2,4-Dimethylquinoline (164)

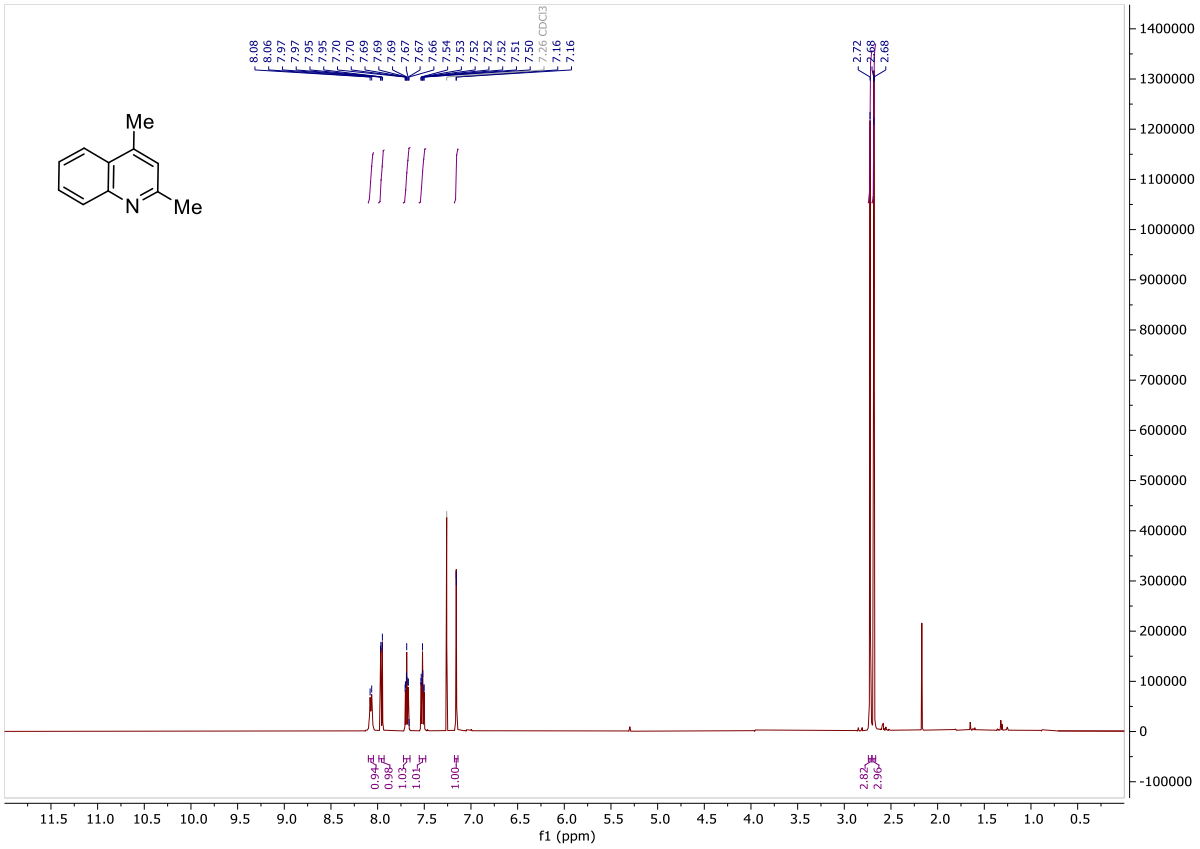

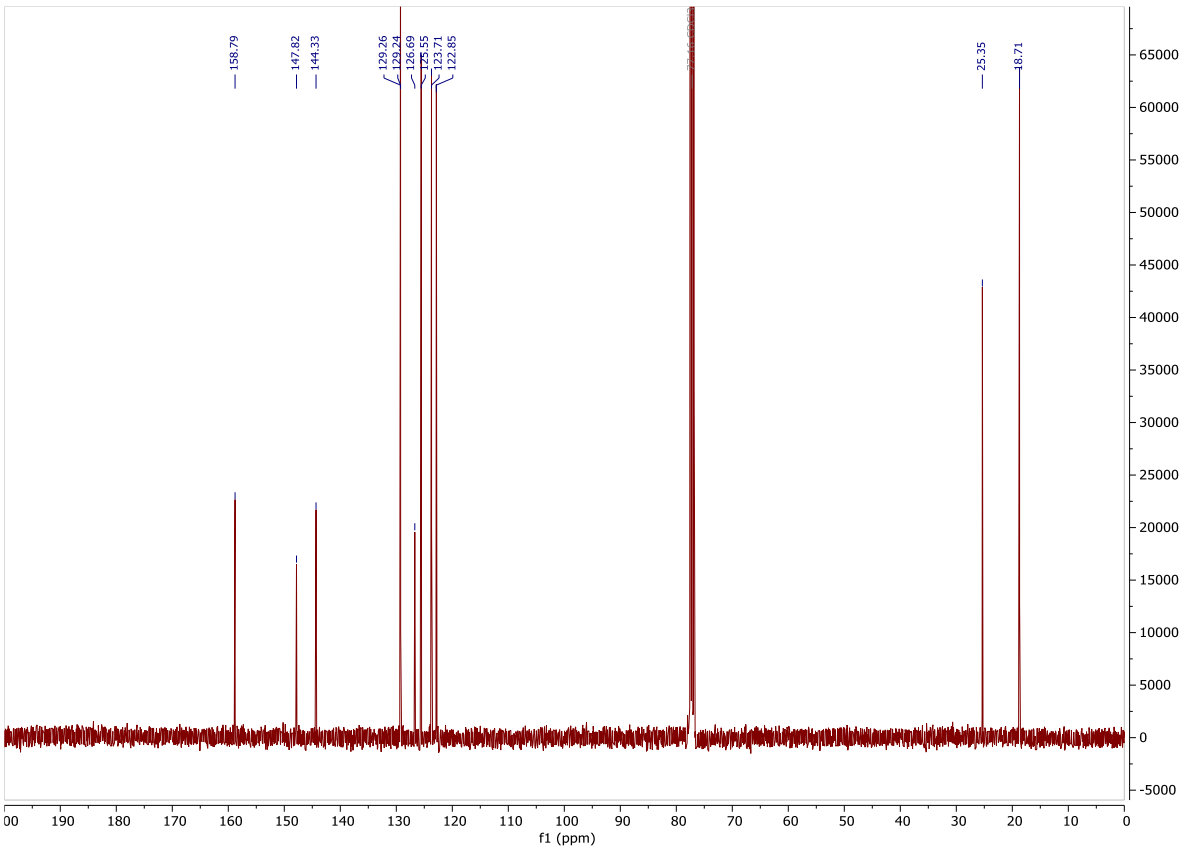

3,3'-Oxybis(tert-butylbenzene) (165)

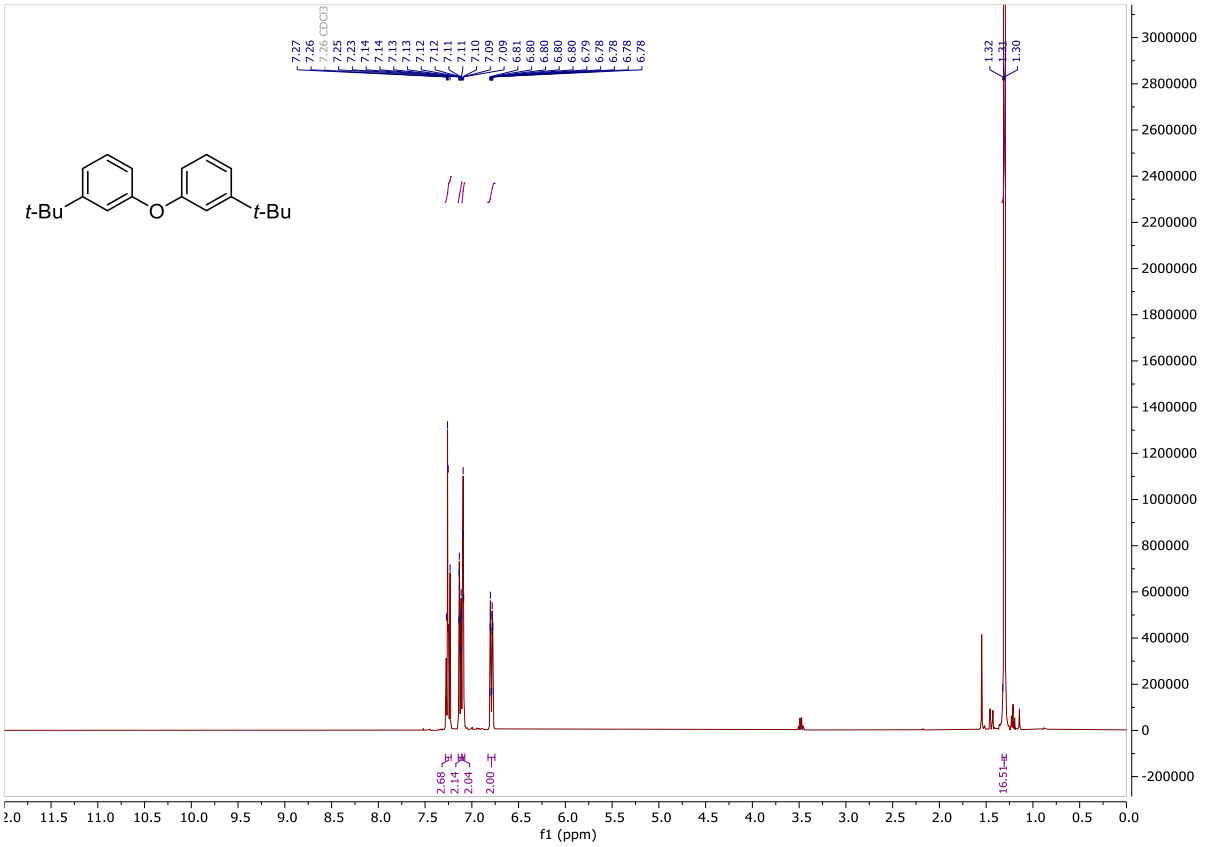

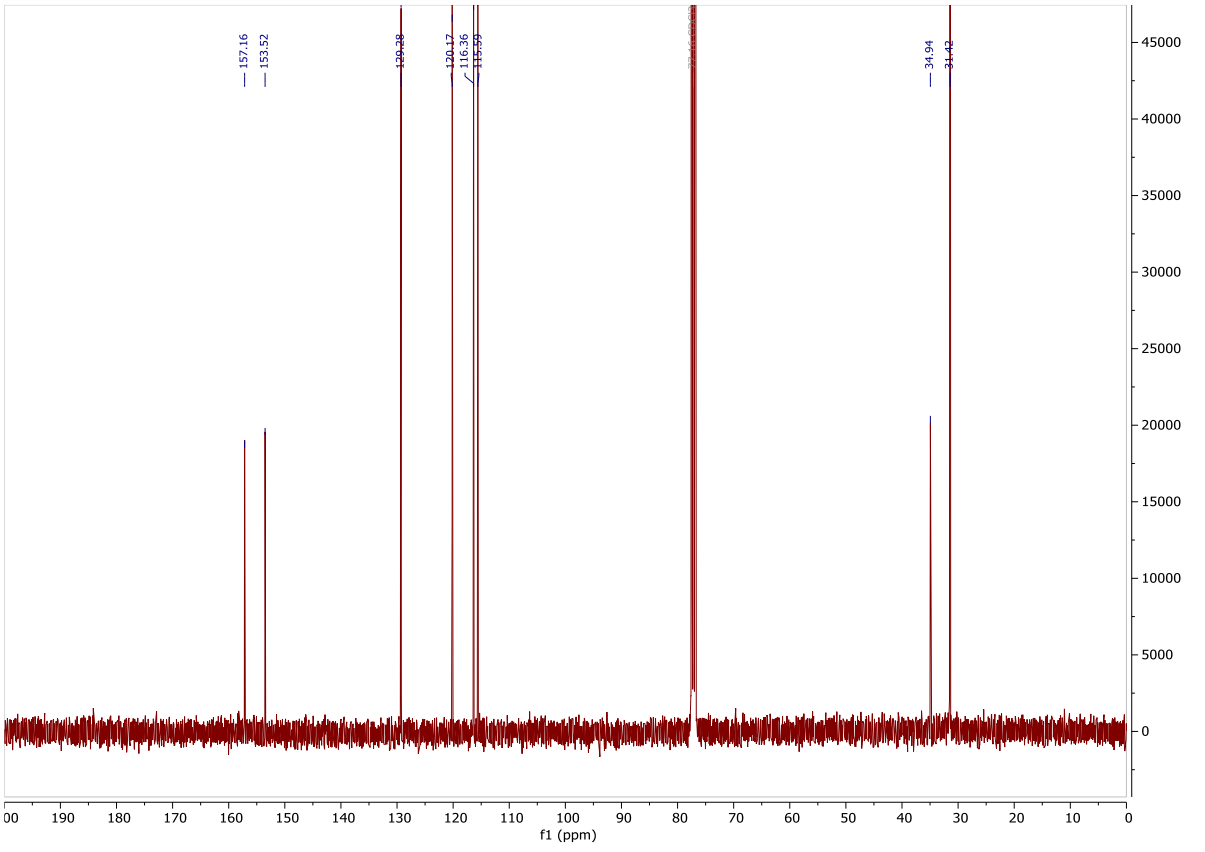

3,6-Di-tert-butyl-9-mesitylxanthylium tetrafluoroborate (166)

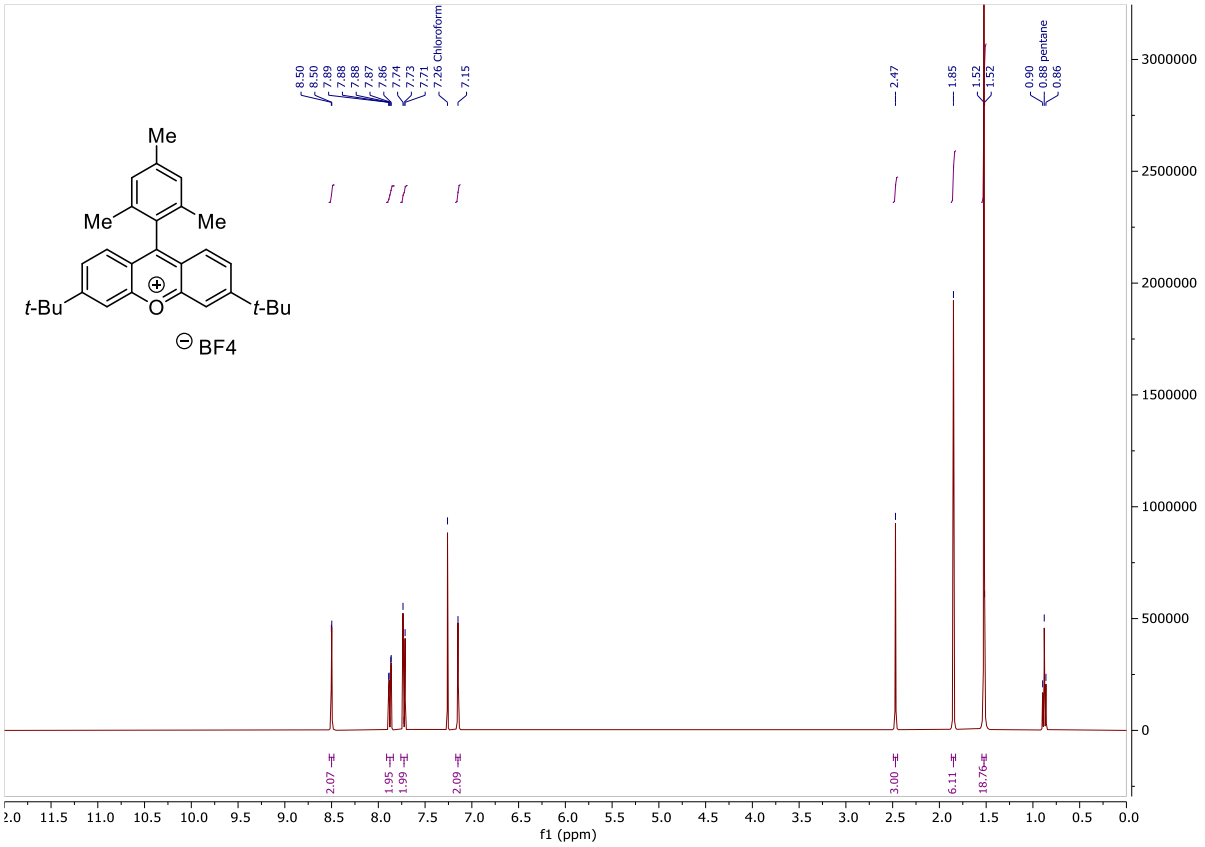

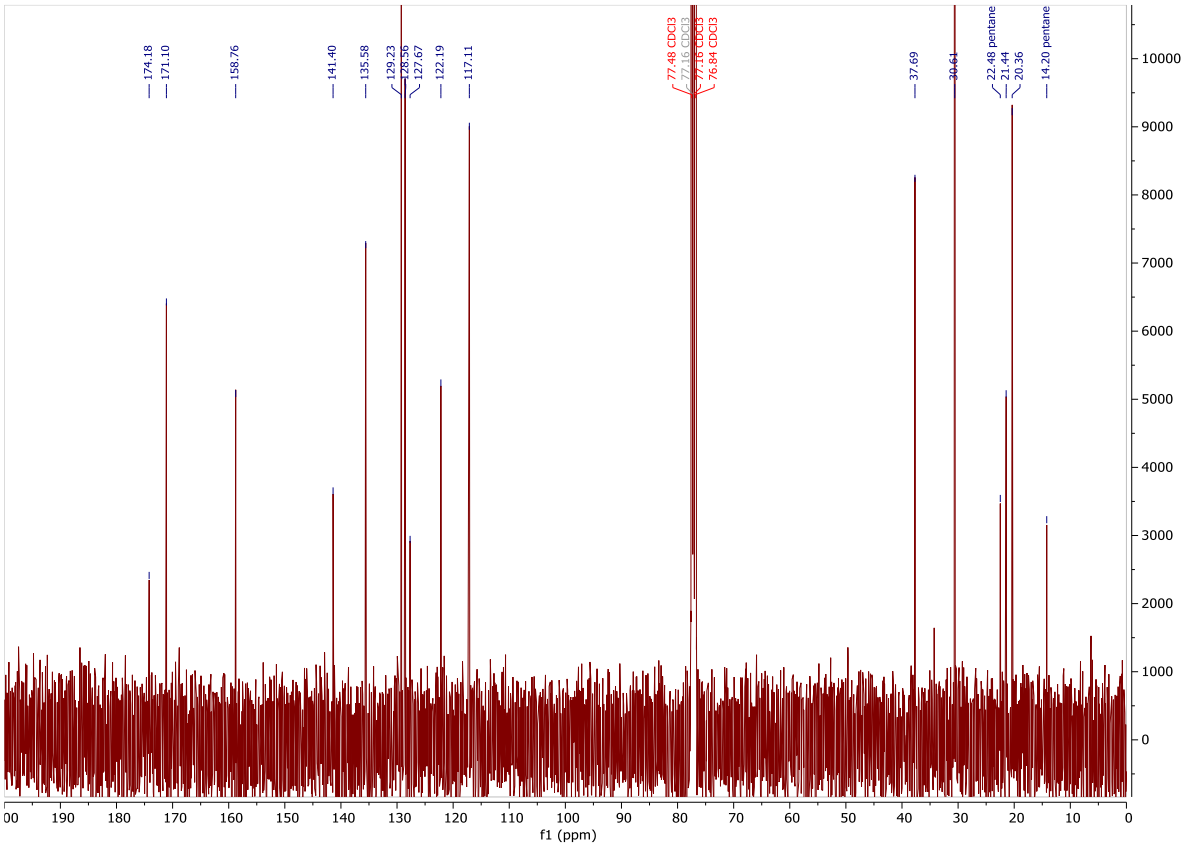

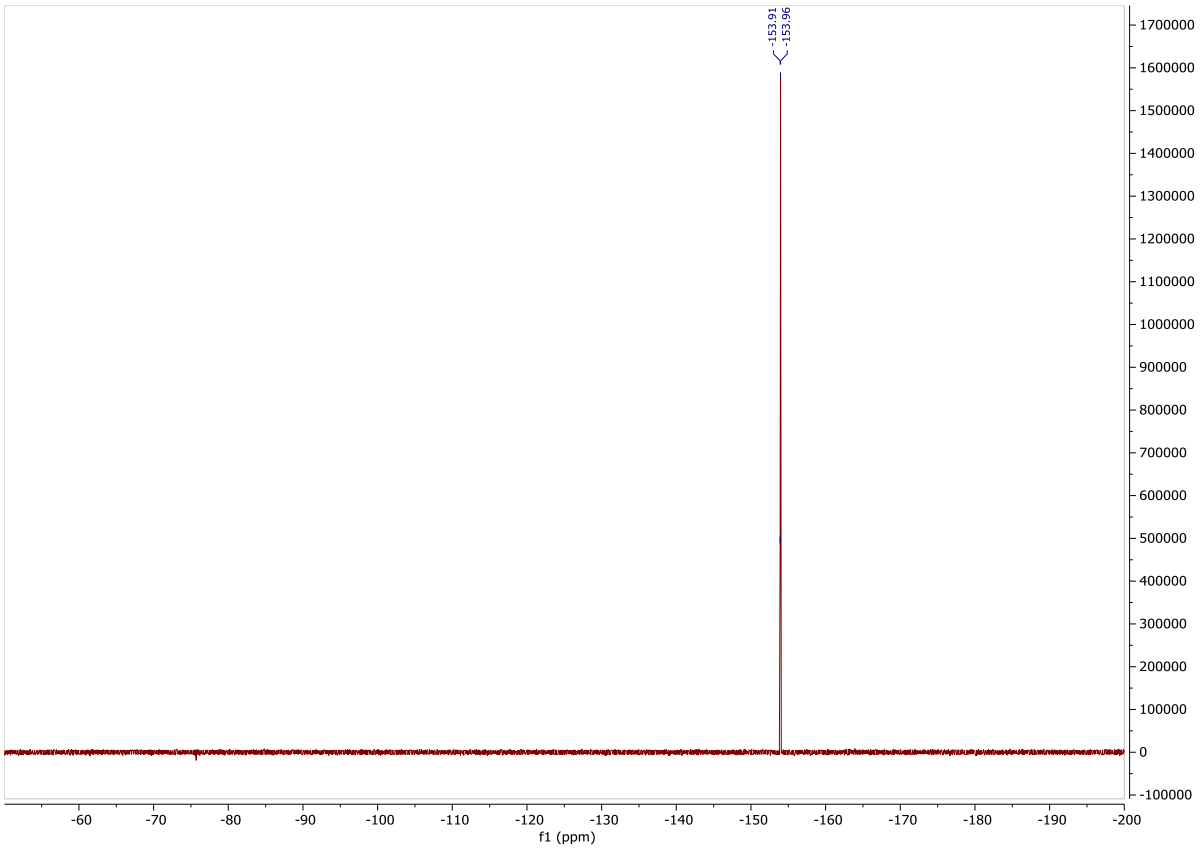
-153.91
-153.96
1700000
1600000
1500000
1400000
1300000
1200000
1100000
1000000
900000
800000
700000
600000
500000
400000
300000
200000
100000
0
-100000
-60
-70
-80
-90
-100
-110
-120
-130
-140
-150
-160
-170
-180
-190
-200
f1 (ppm)

3,6-Di-tert-butyl-9-mesityl-10-phenylacridin-10-ium tetrafluoroborate (PC1)

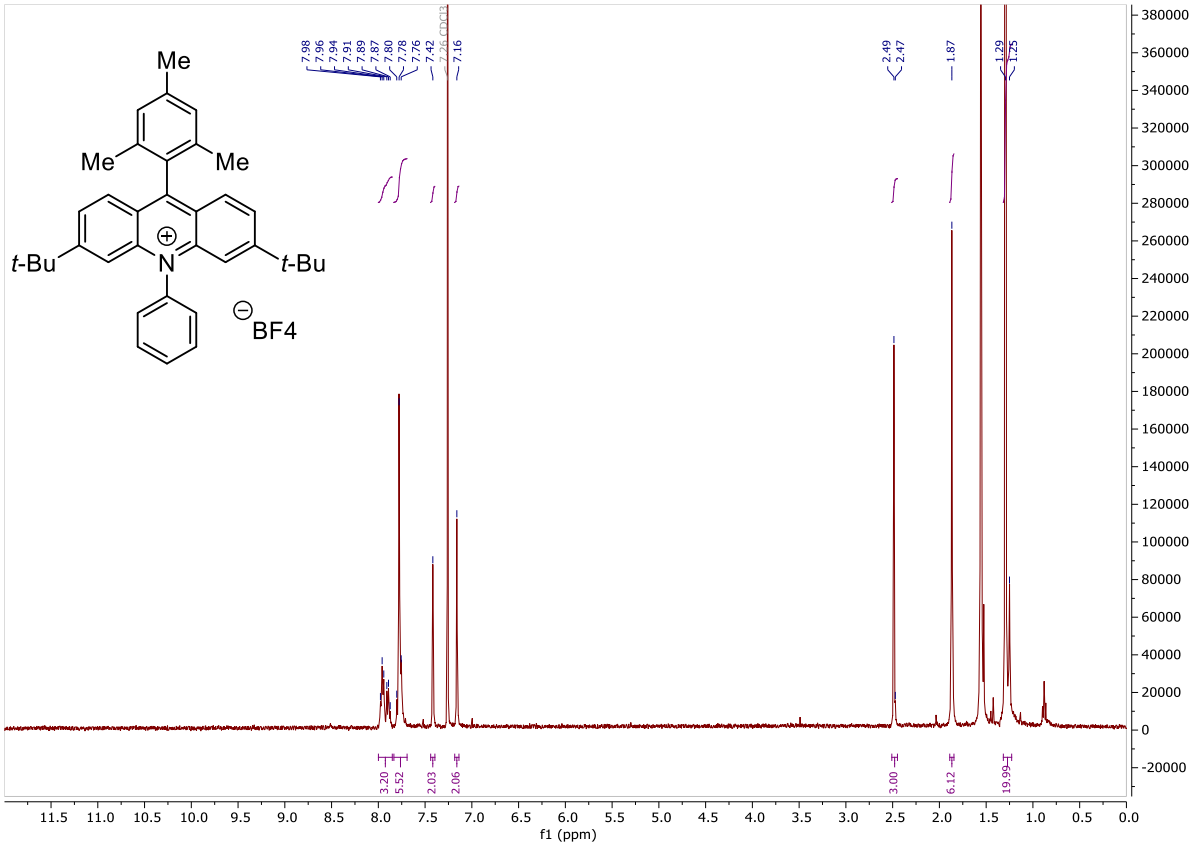

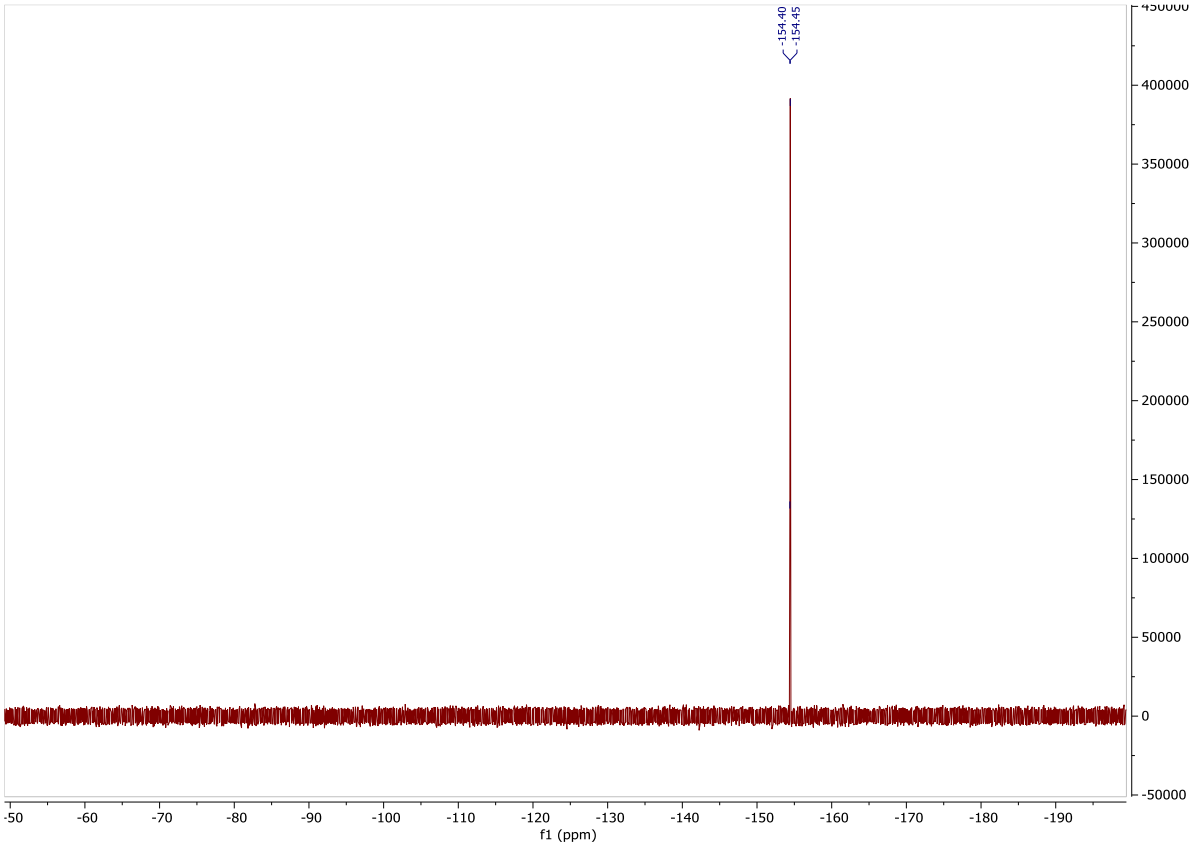

1,2,4,6-Tetraphenylpyridin-1-ium tetrafluoroborate (PC2)

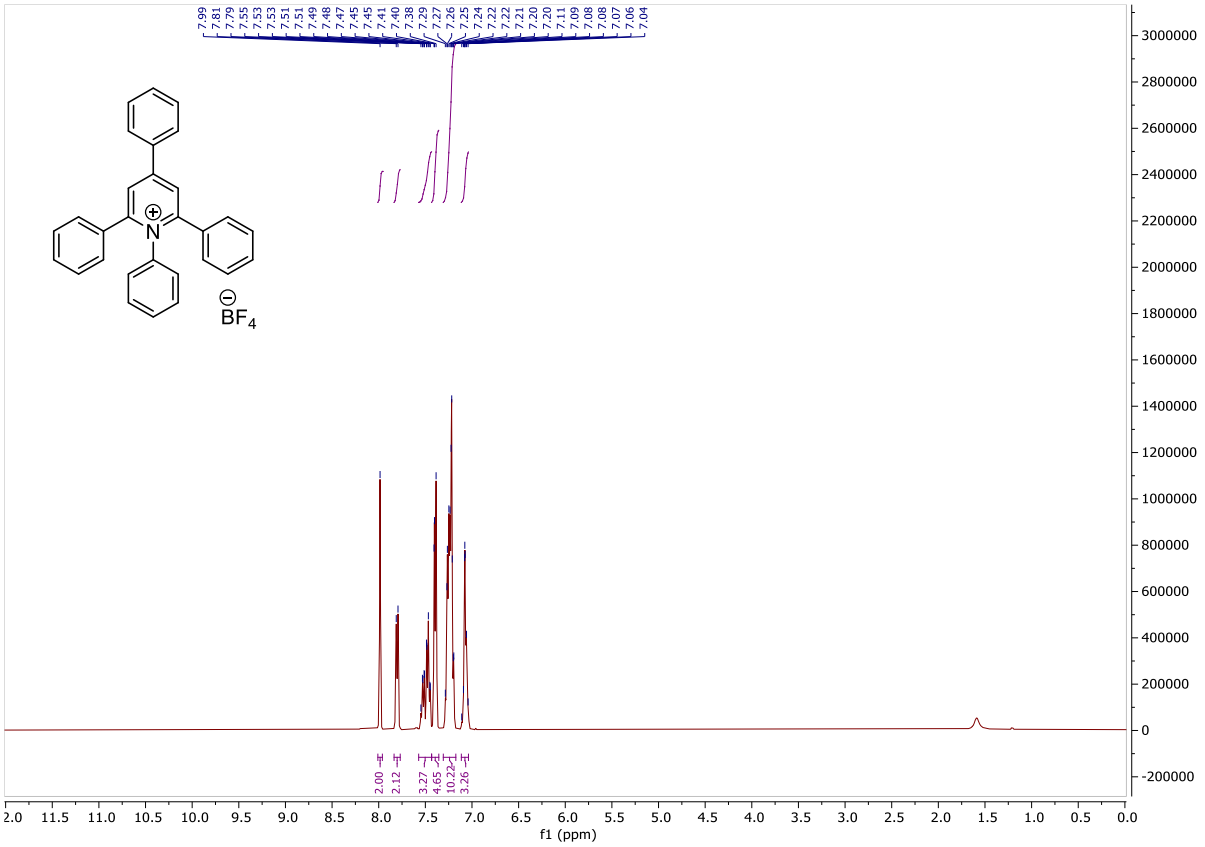

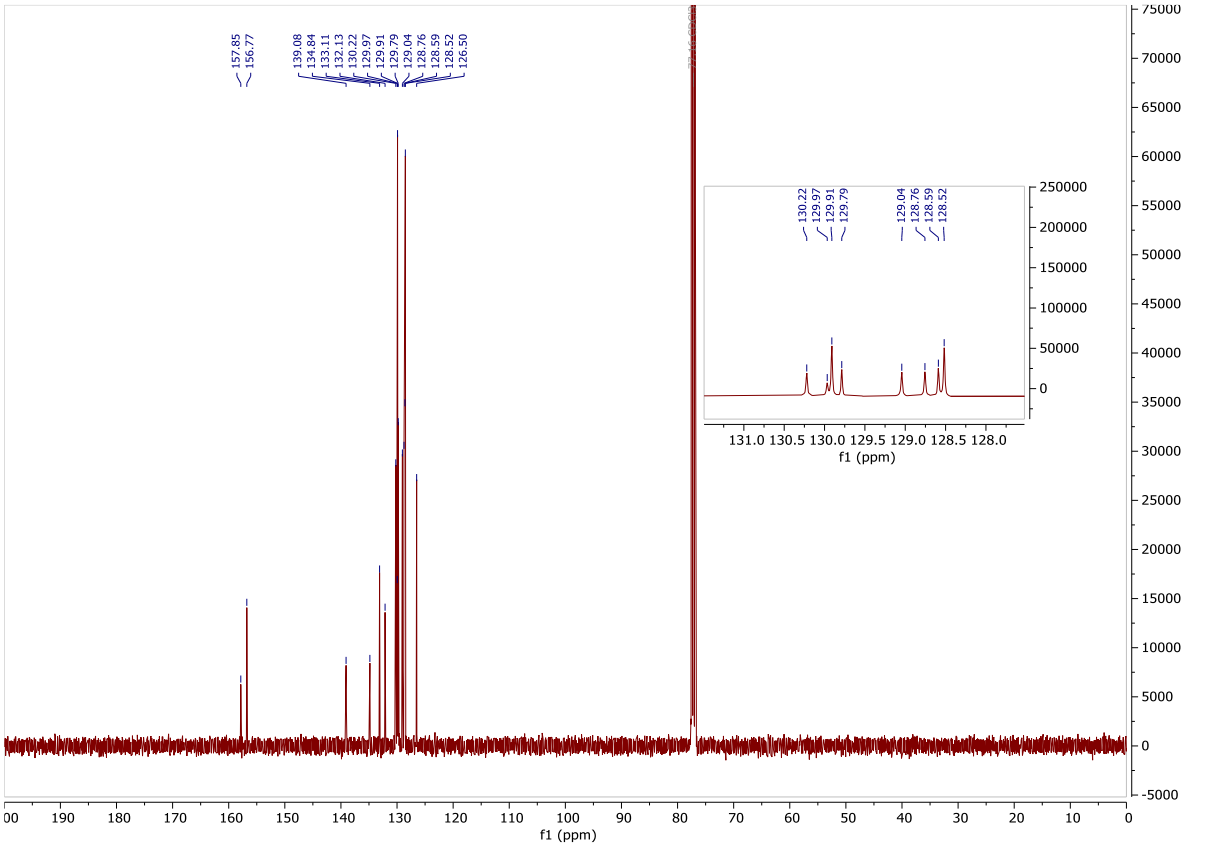

9-(4-(Tert-butyl)phenyl)acridine (202)

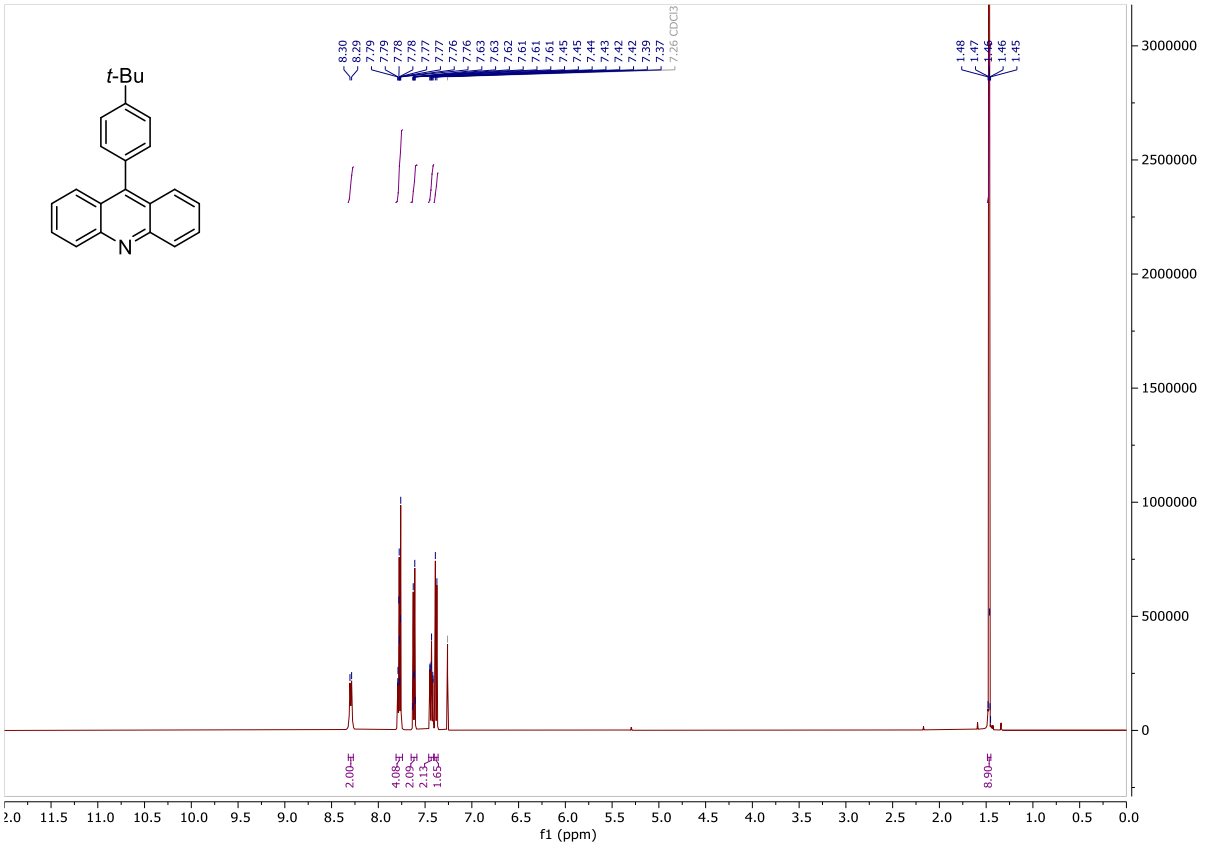

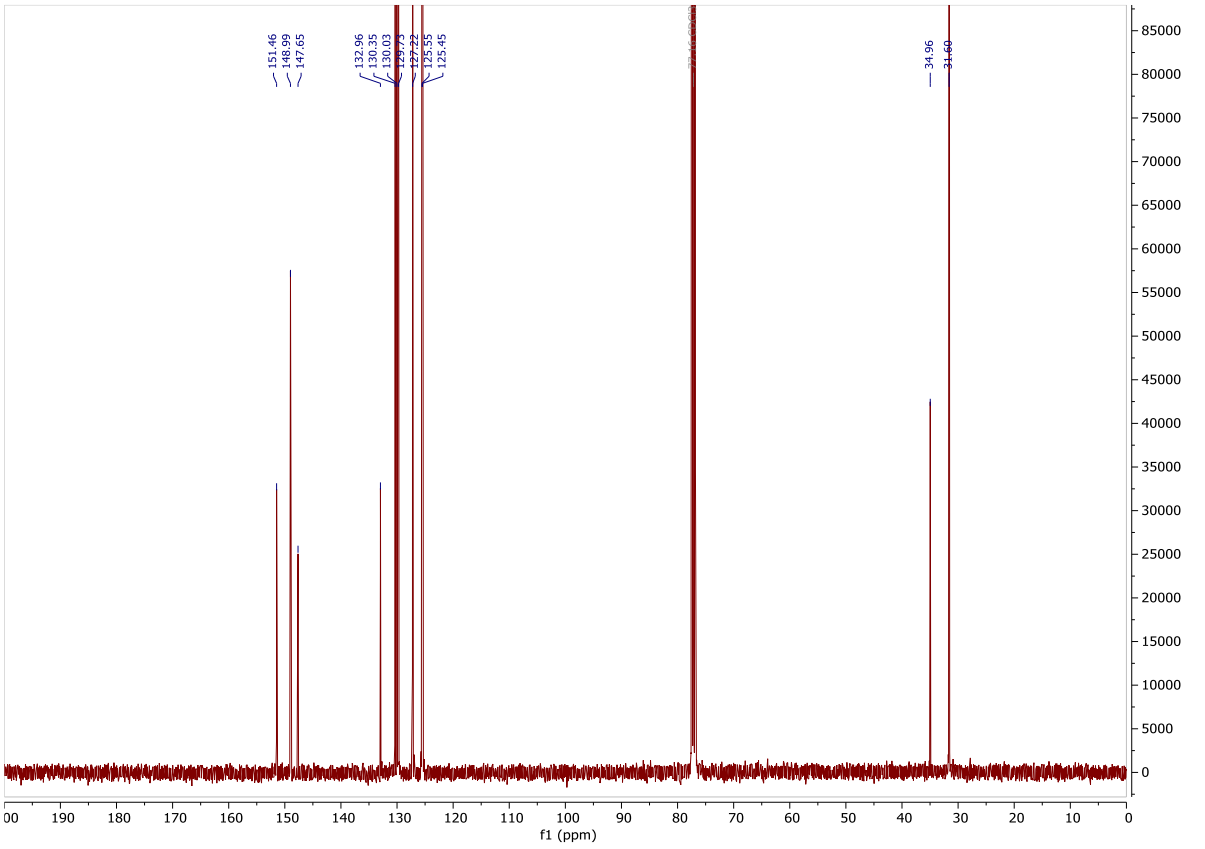

9-Mesitylacridine (203)

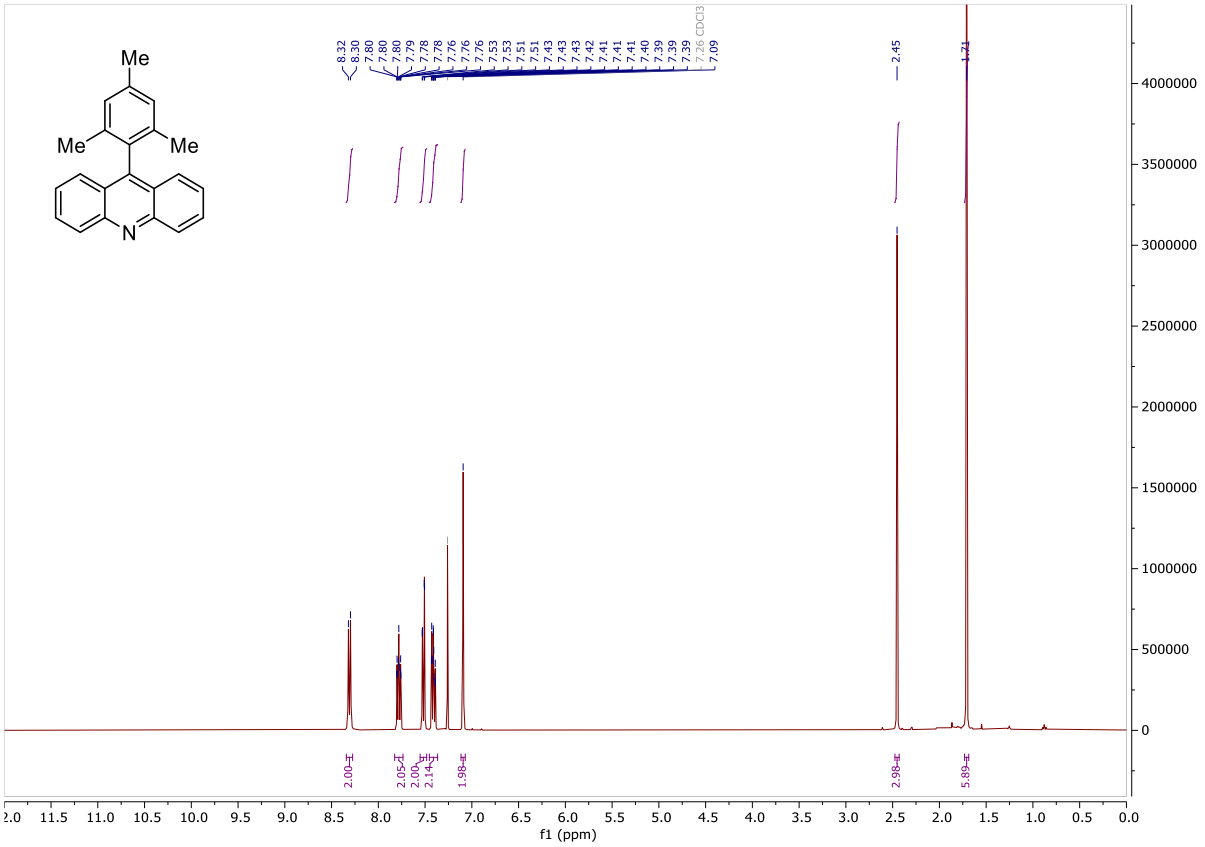

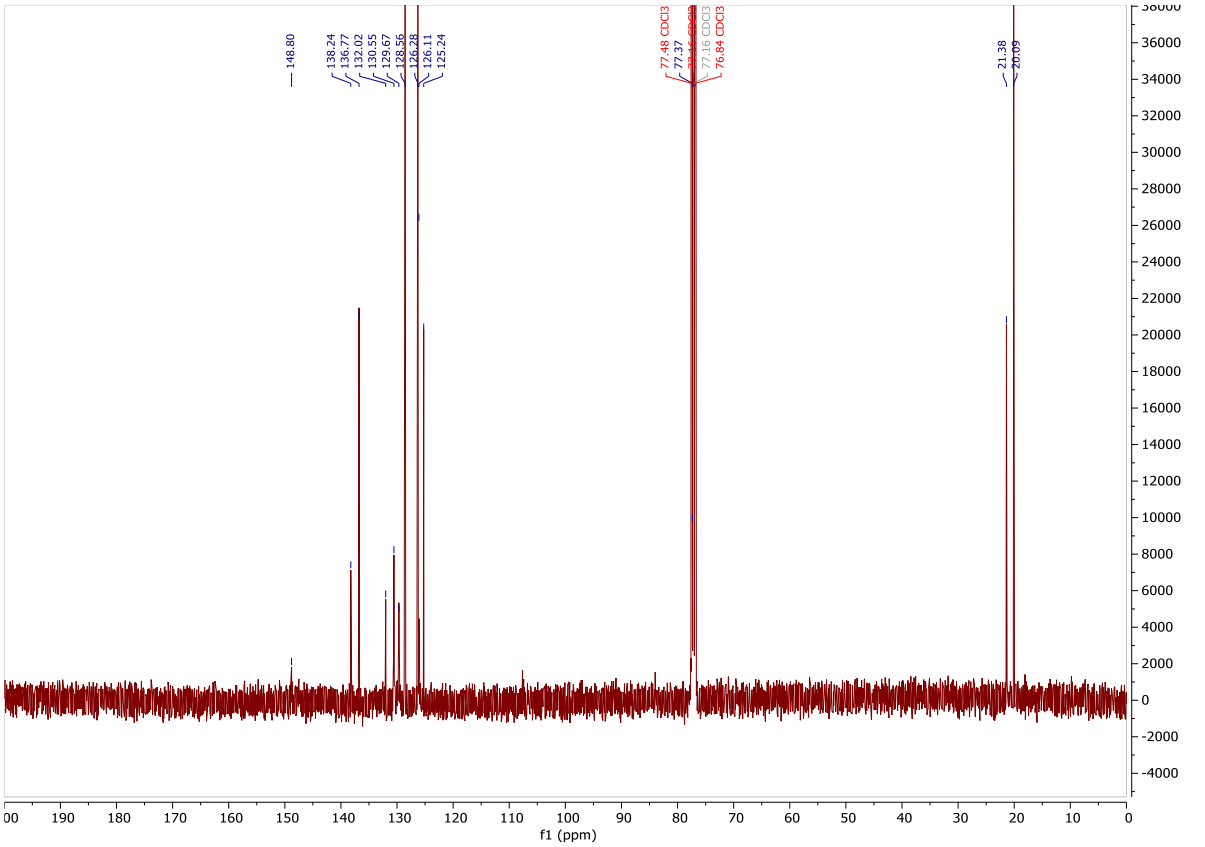

3,6-Di-tert-butyl-9-phenylacridine (204)

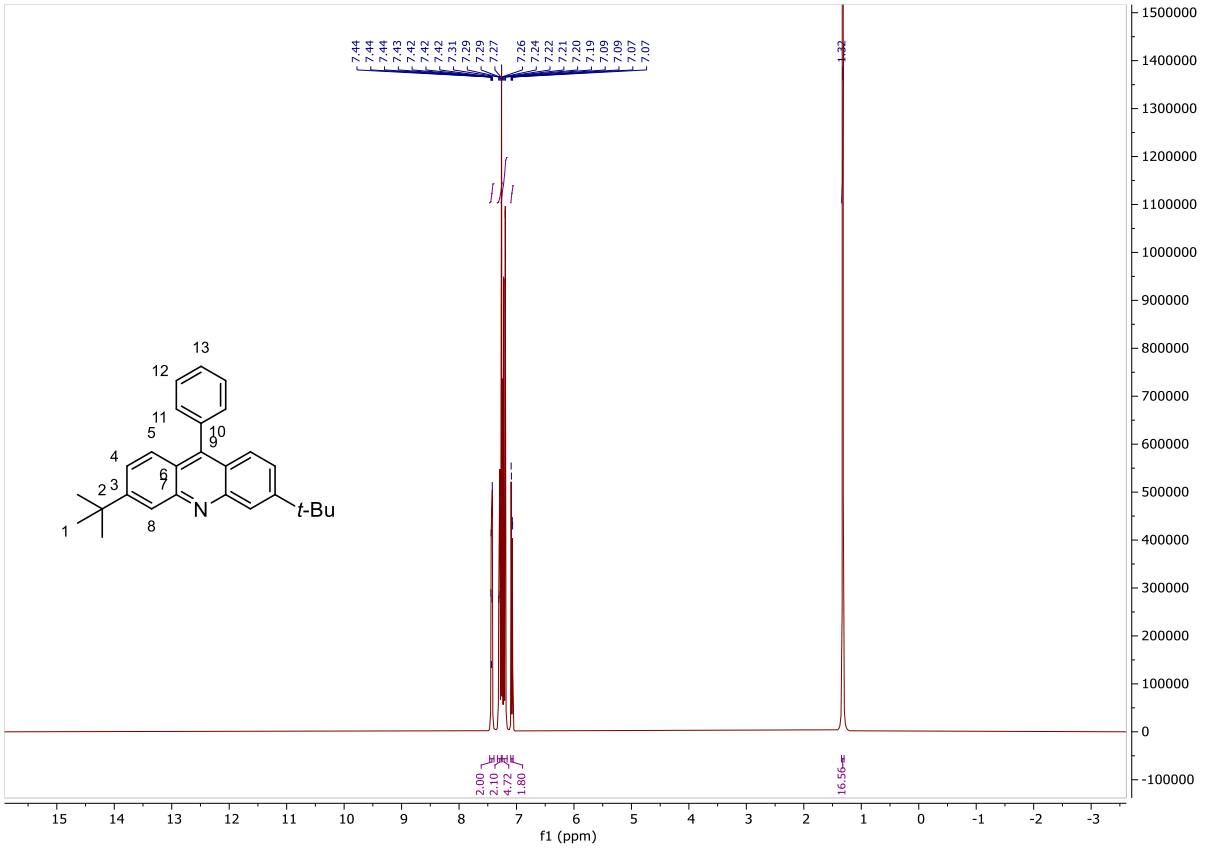

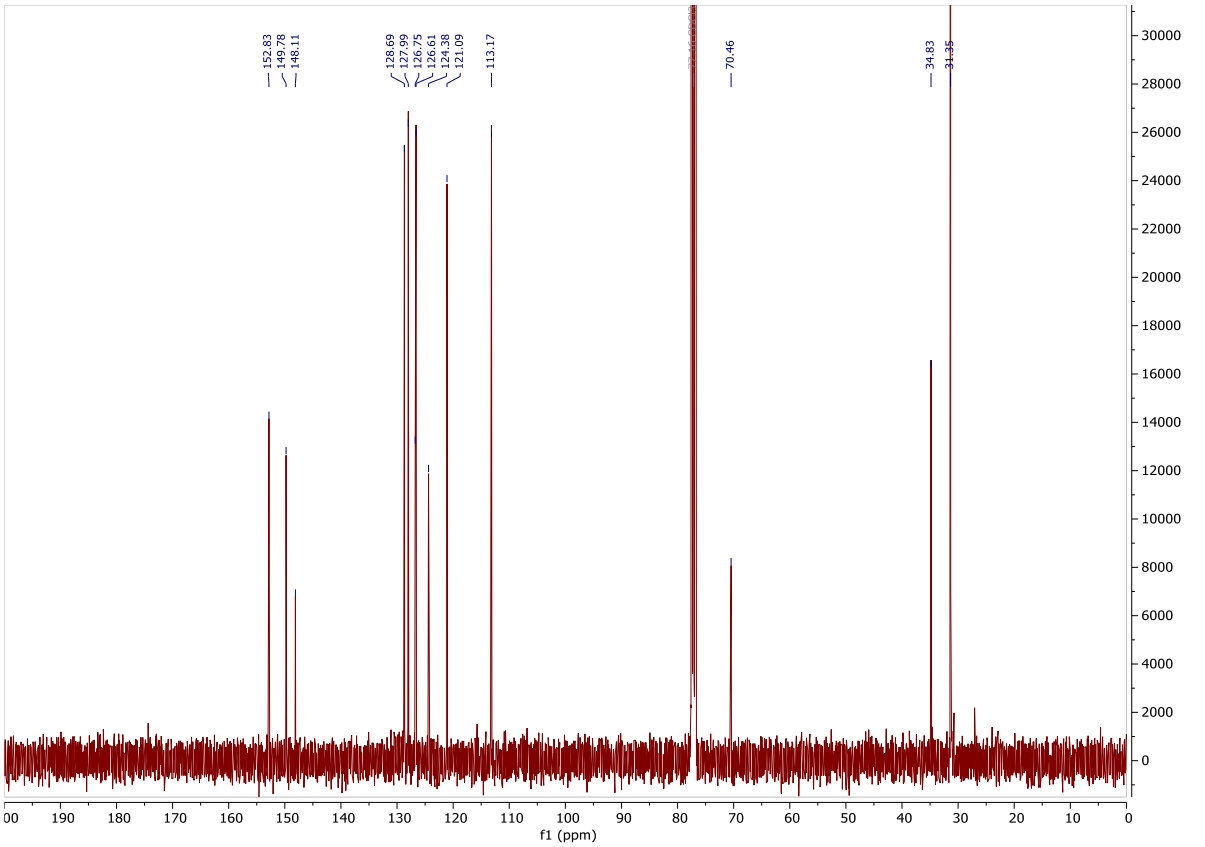

3,6-Di-tert-butyl-9-mesitylacridine (205)

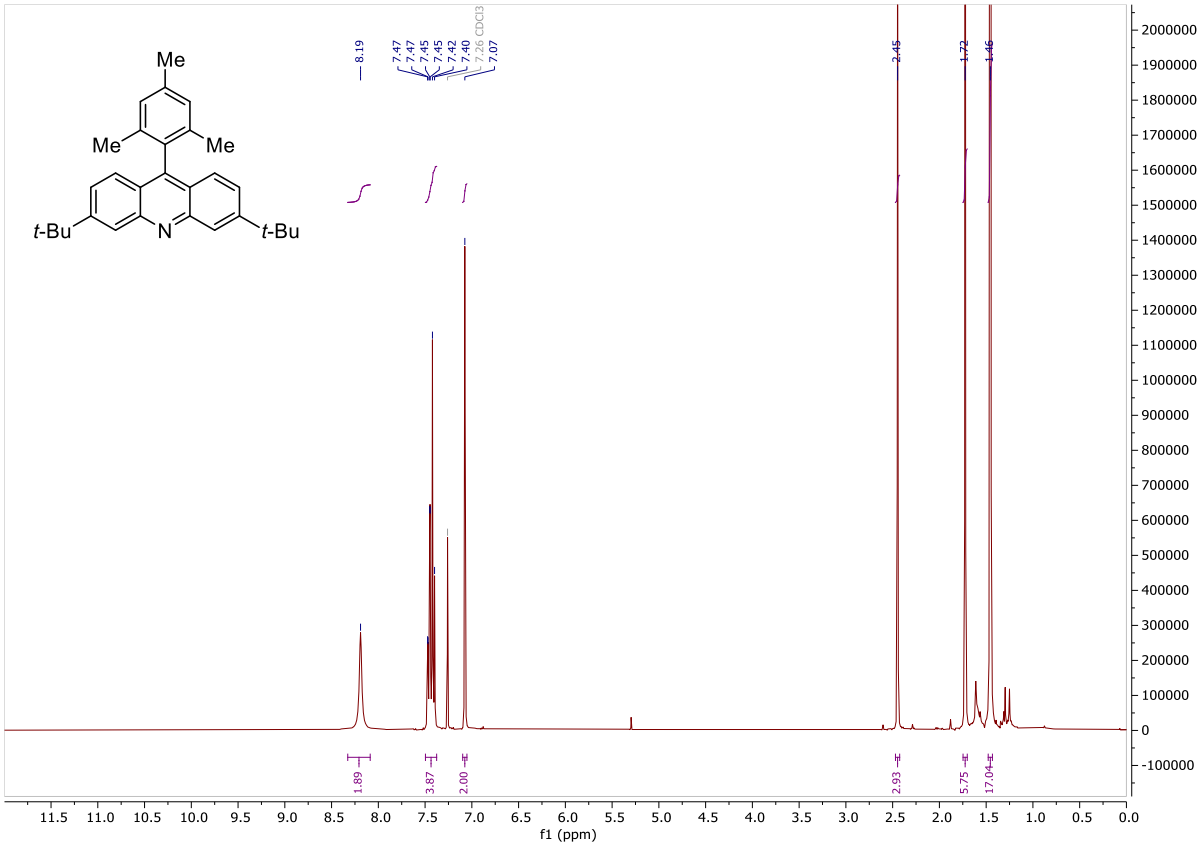

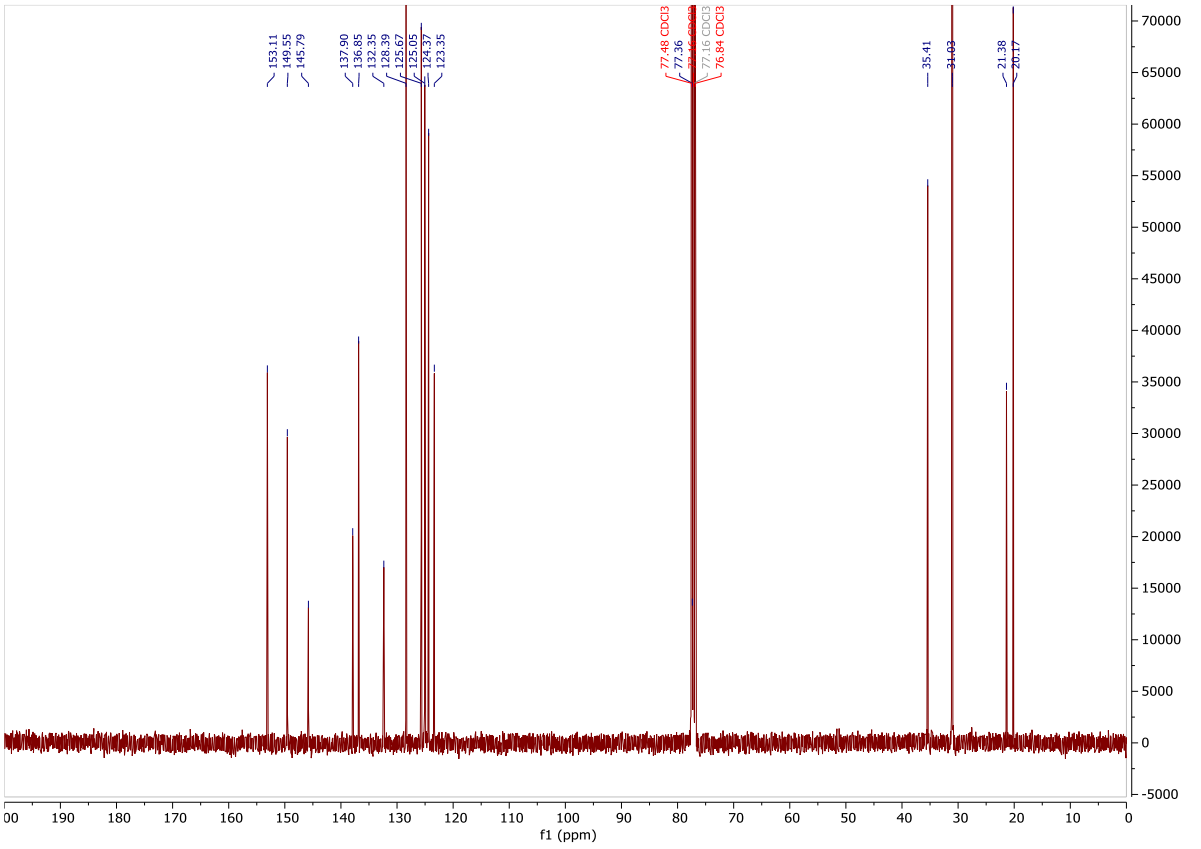

9-(2-Chlorophenyl)acridine (208)

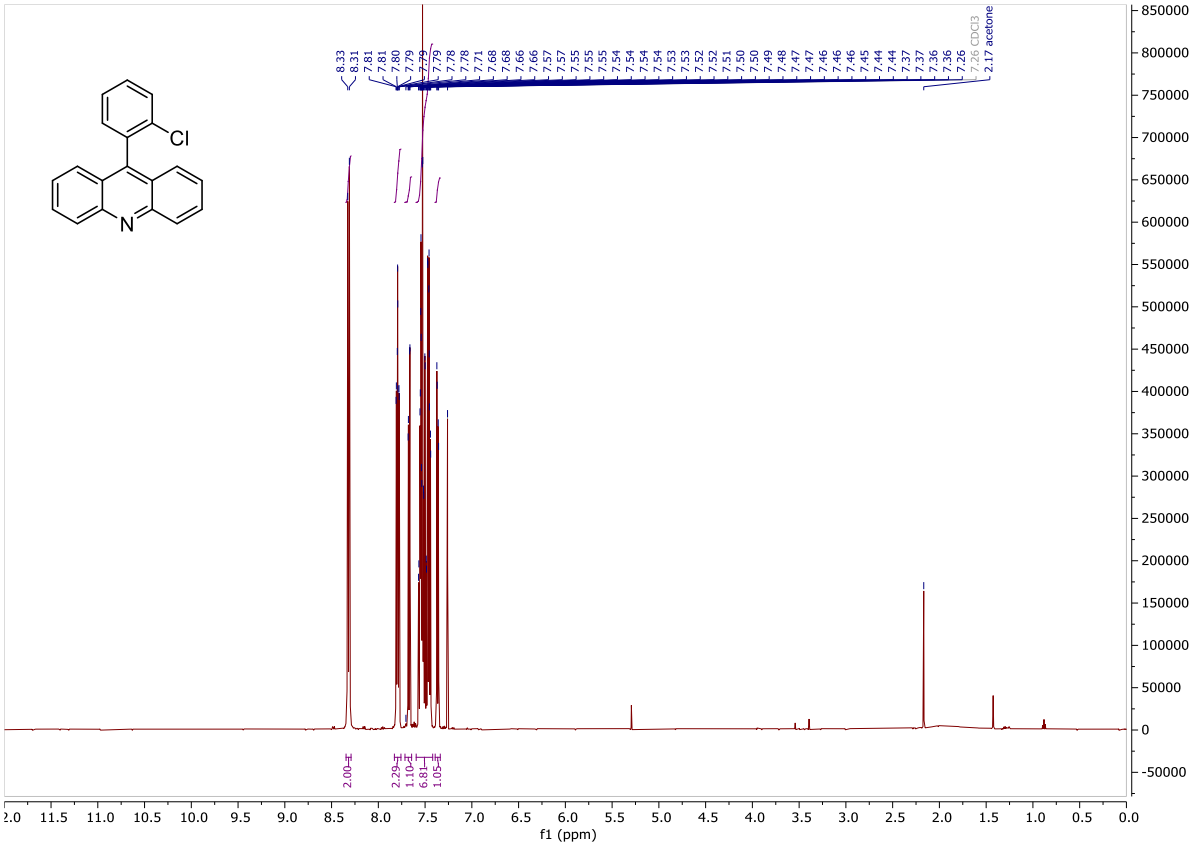

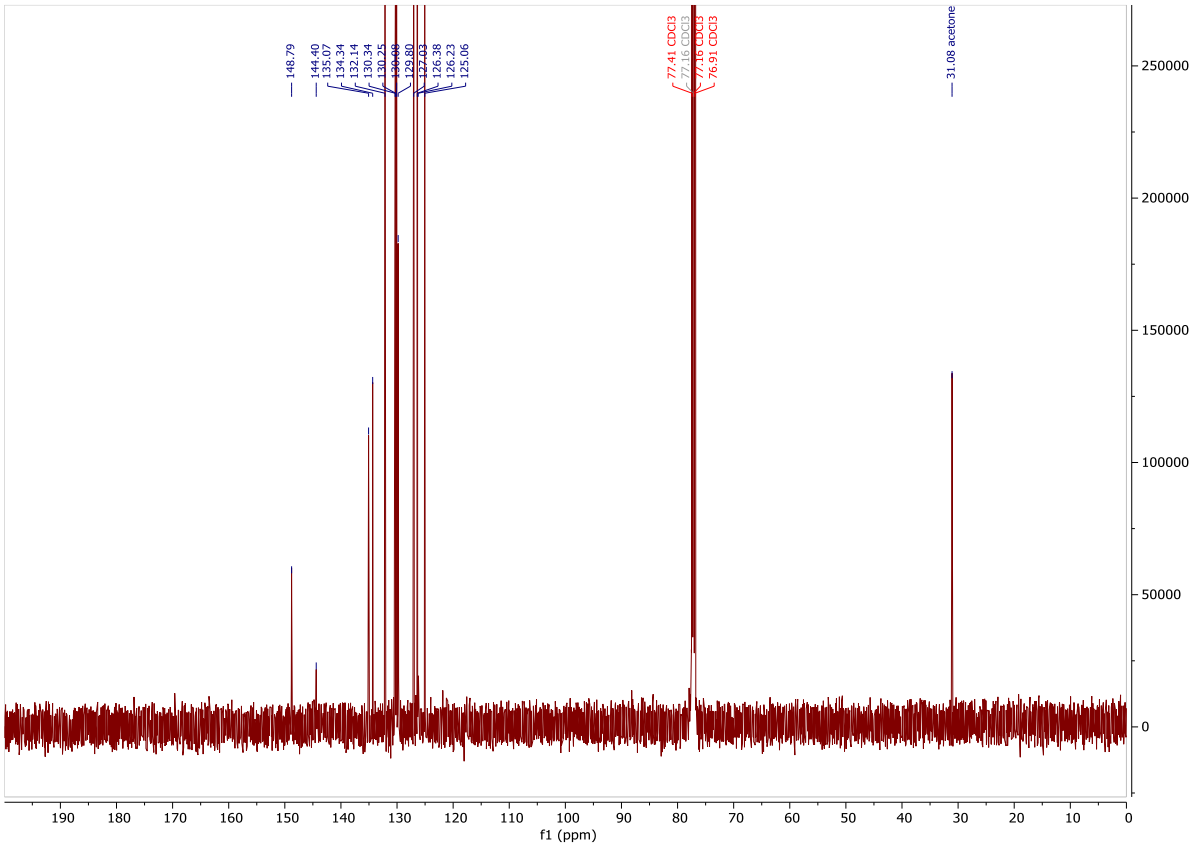

9-Phenyl-9,10-dihydroacridine (244)

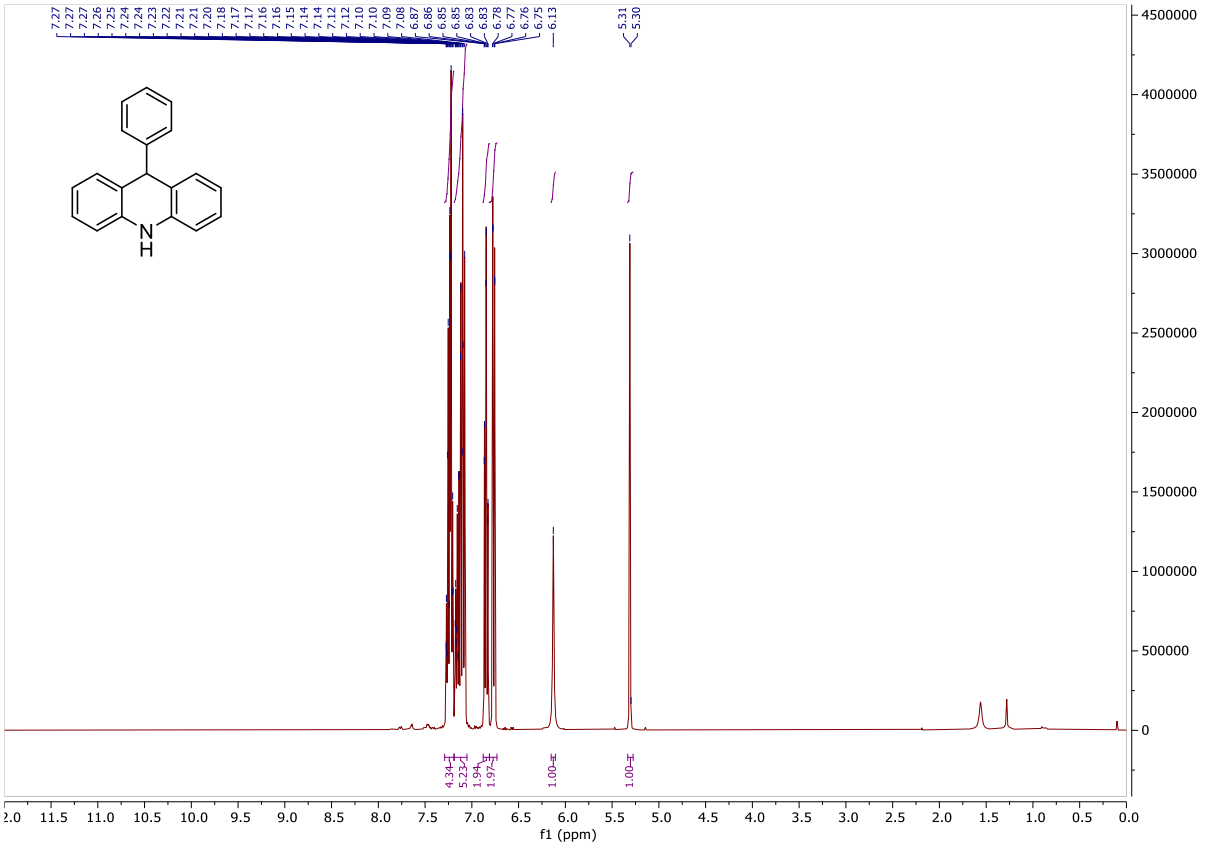

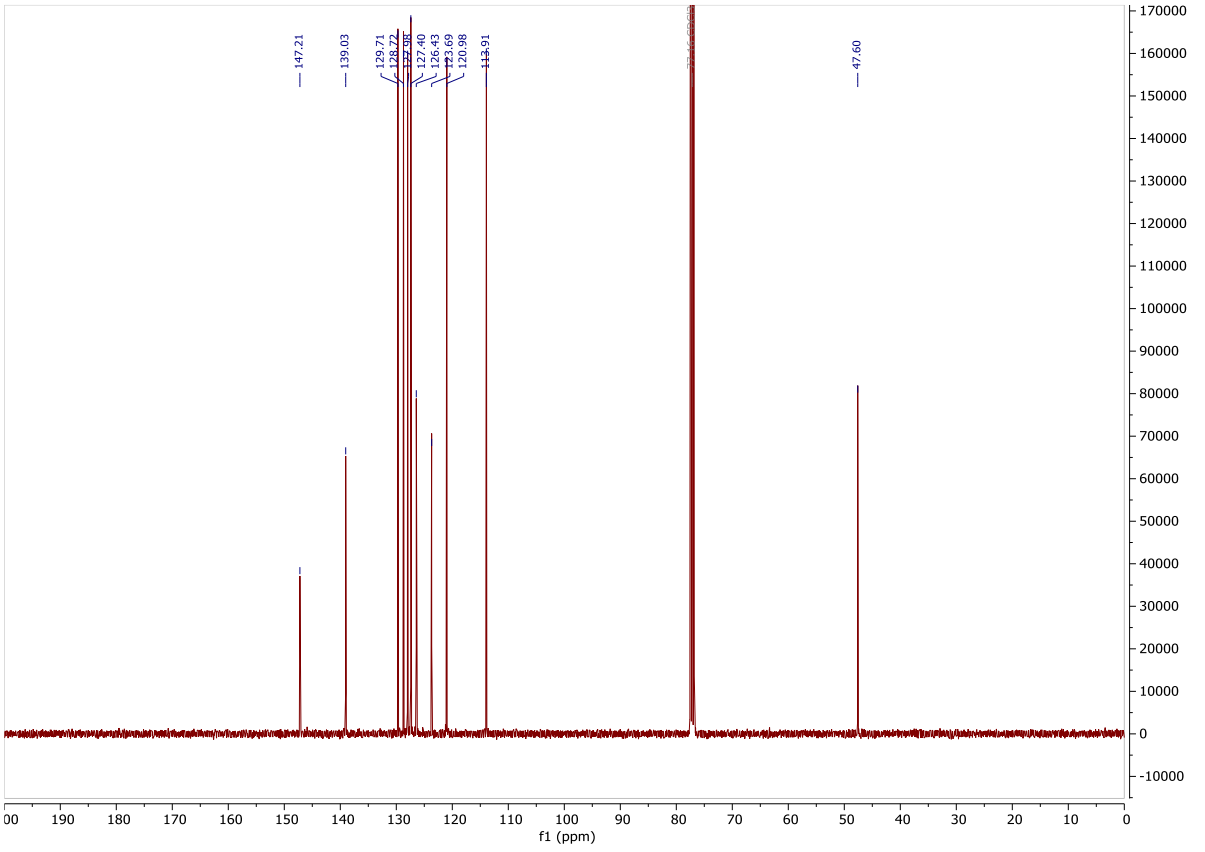

9-(2-Fluorophenyl)acridine (F-PC)

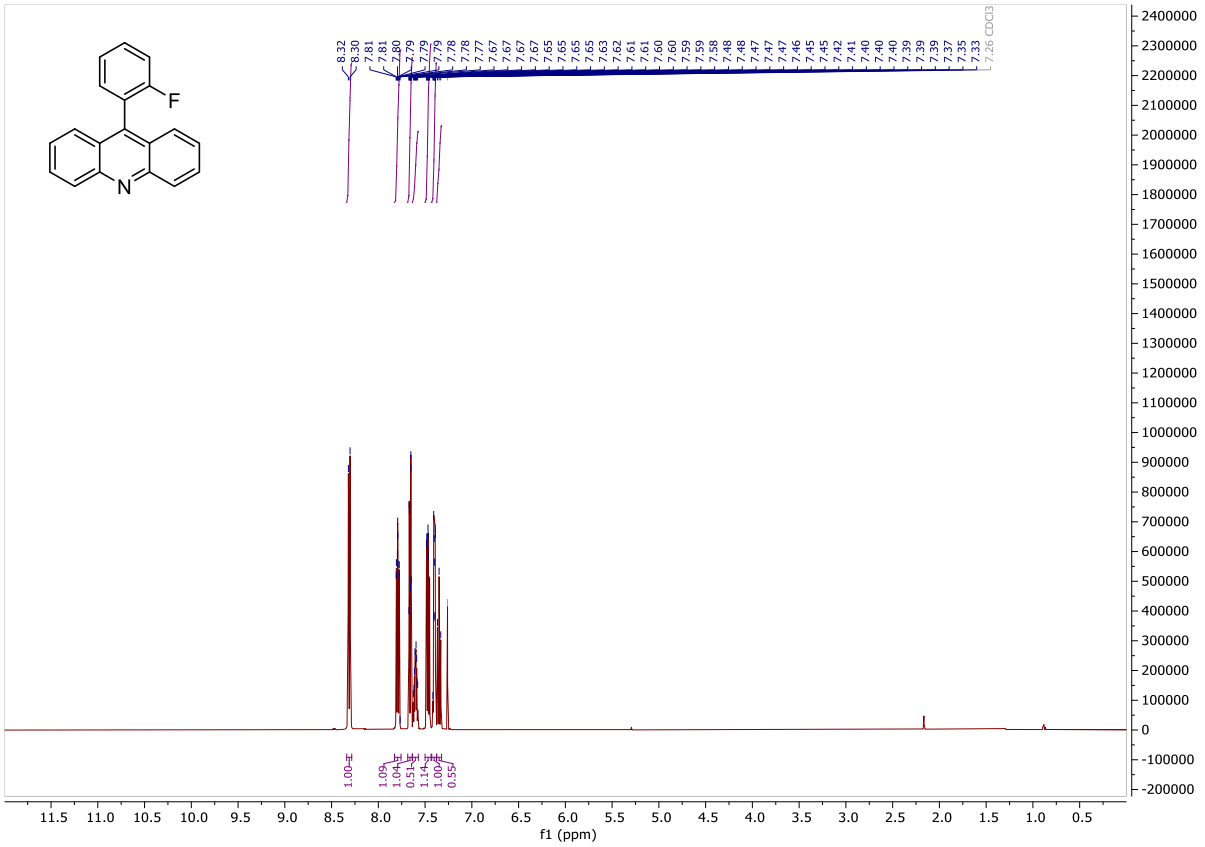

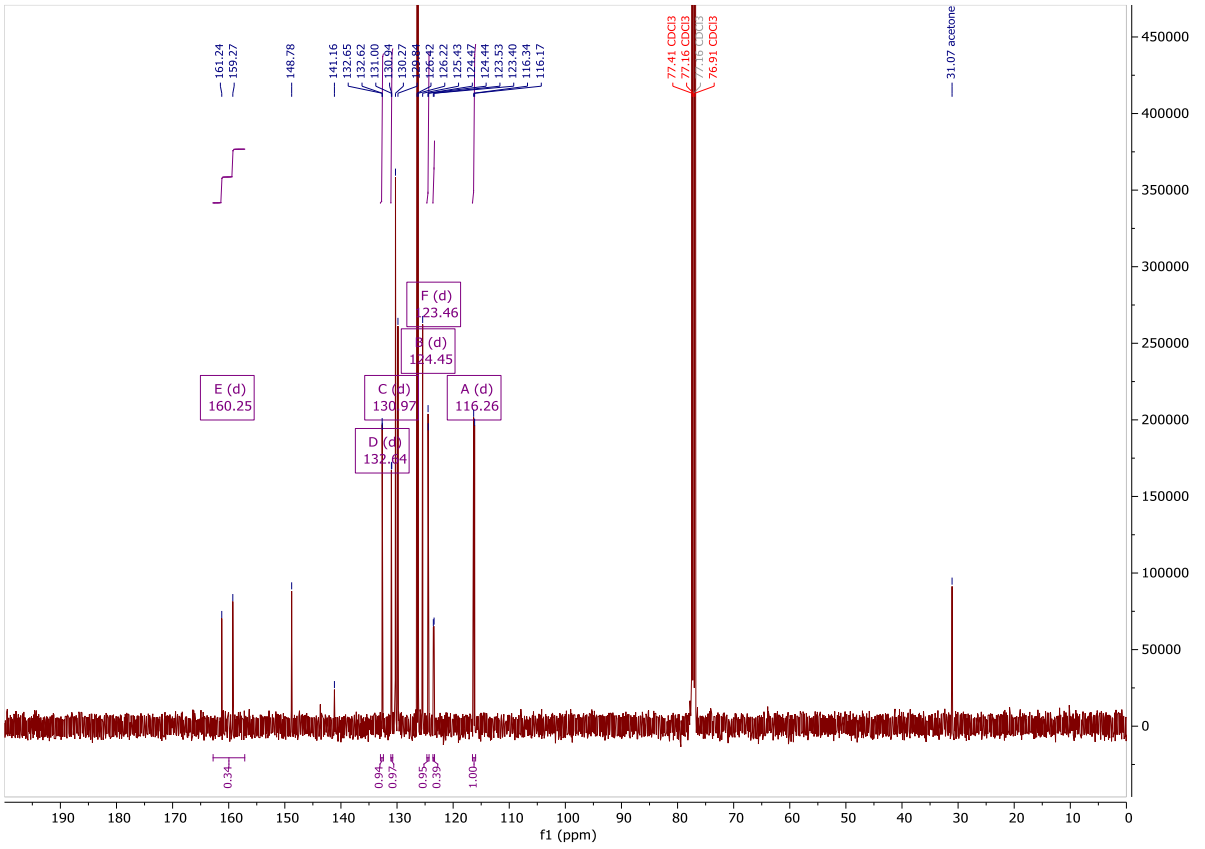

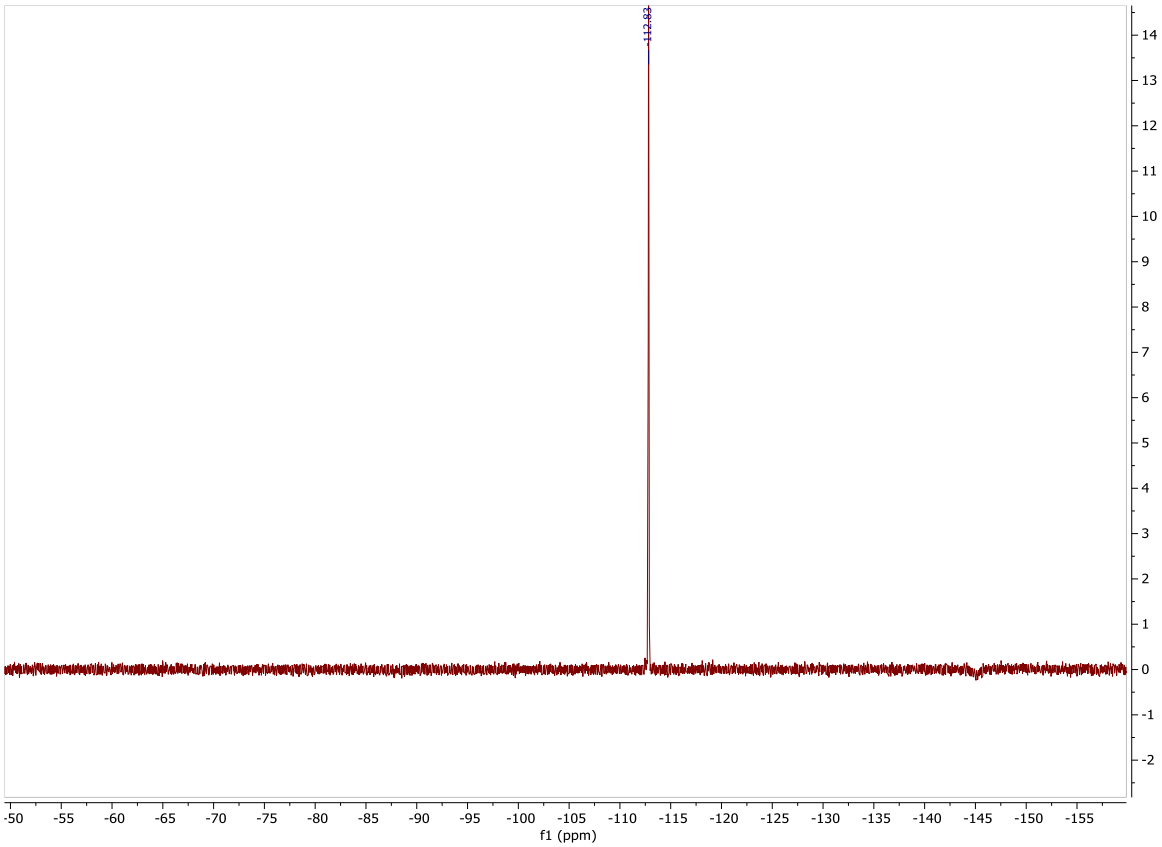
-112.83
14
13
12
11
10
9
8
7
6
5
4
3
2
1
0
-1
-2
-50 -55 -60 -65 -70 -75 -80 -85 -90 -95 -100 -105 -110 -115 -120 -125 -130 -135 -140 -145 -150 -155
f1 (ppm)

9-(2-Fluorophenyl)-9,10-dihydroacridine (245)

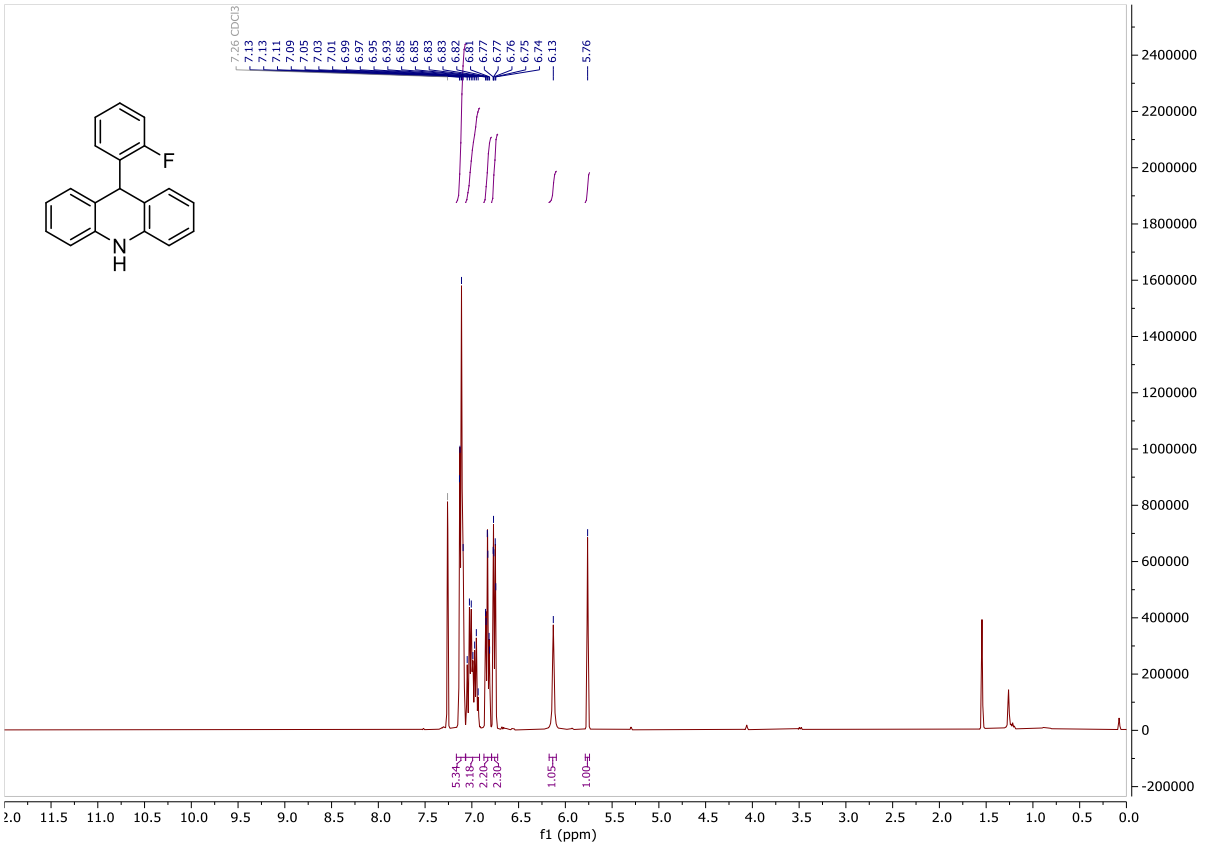

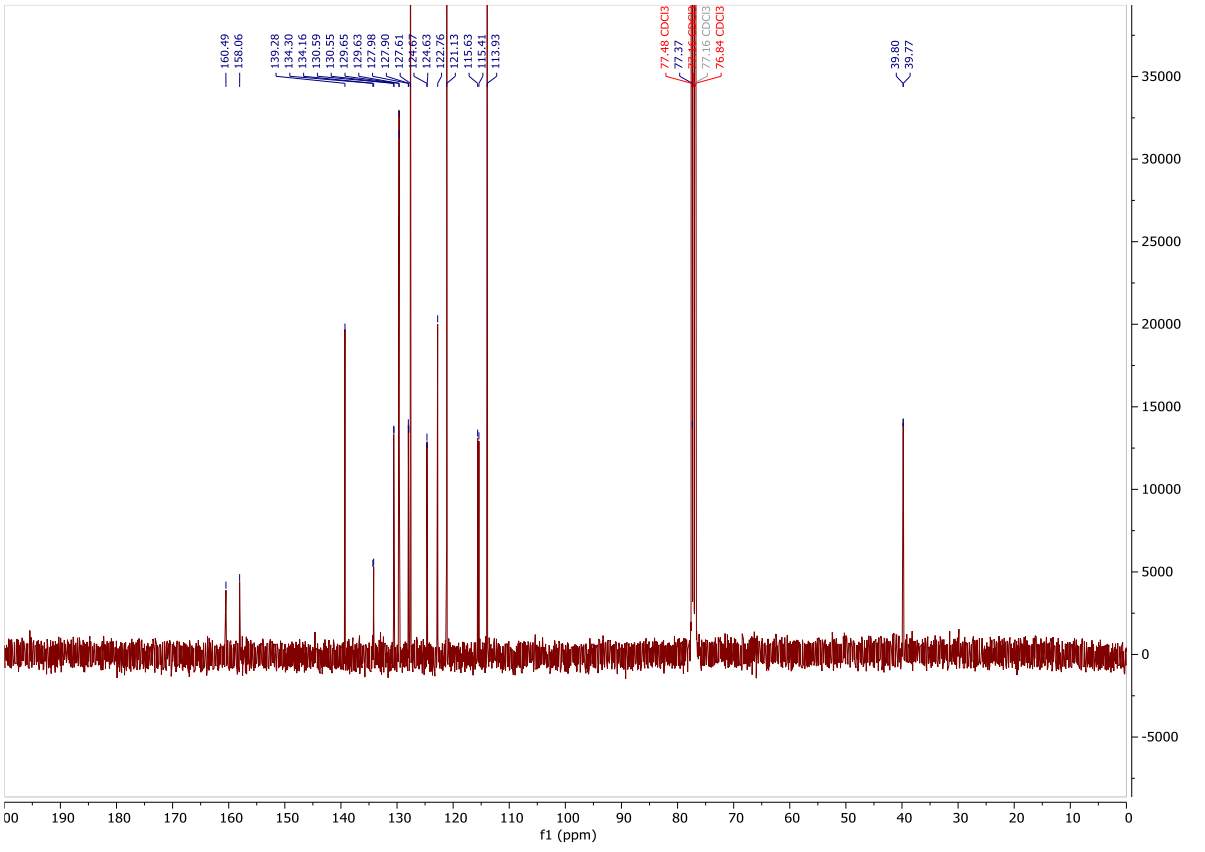

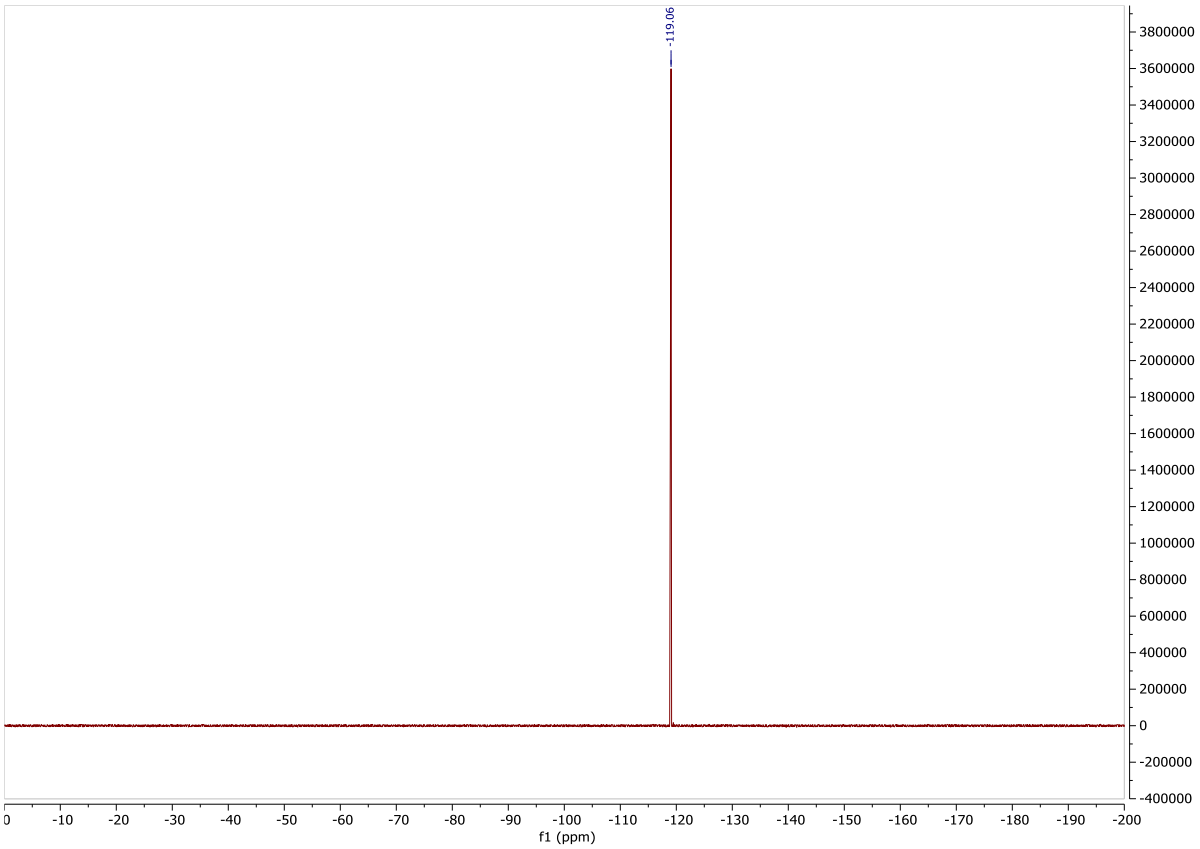
-119.06
3800000
3600000
3400000
3200000
3000000
2800000
2600000
2400000
2200000
2000000
1800000
1600000
1400000
1200000
1000000
800000
600000
400000
200000
0
-200000
-400000
0
-10
-20
-30
-40
-50
-60
-70
-80
-90
-100
-110
-120
-130
-140
-150
-160
-170
-180
-190
-200
f1 (ppm)

9-Cyclobutyl-9-(2-fluorophenyl)-9,10-dihydroacridine (247)

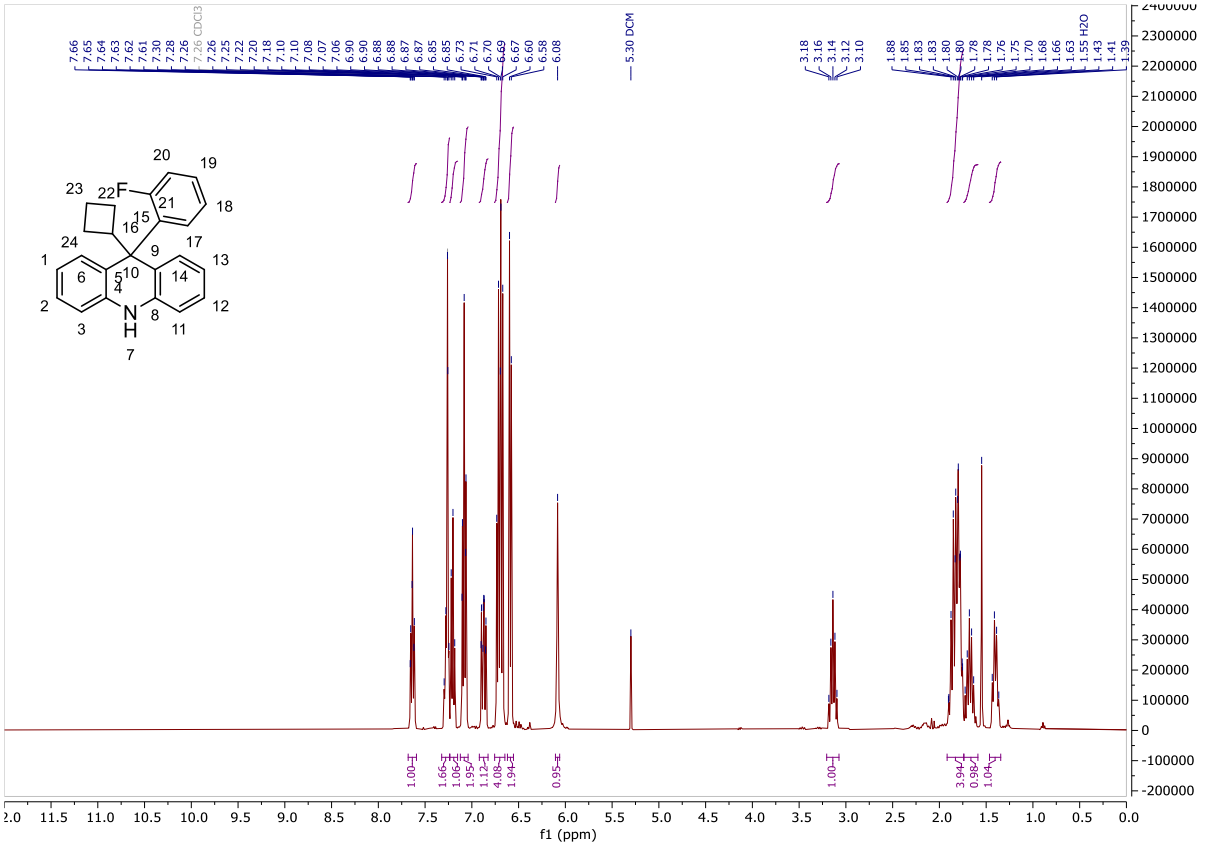

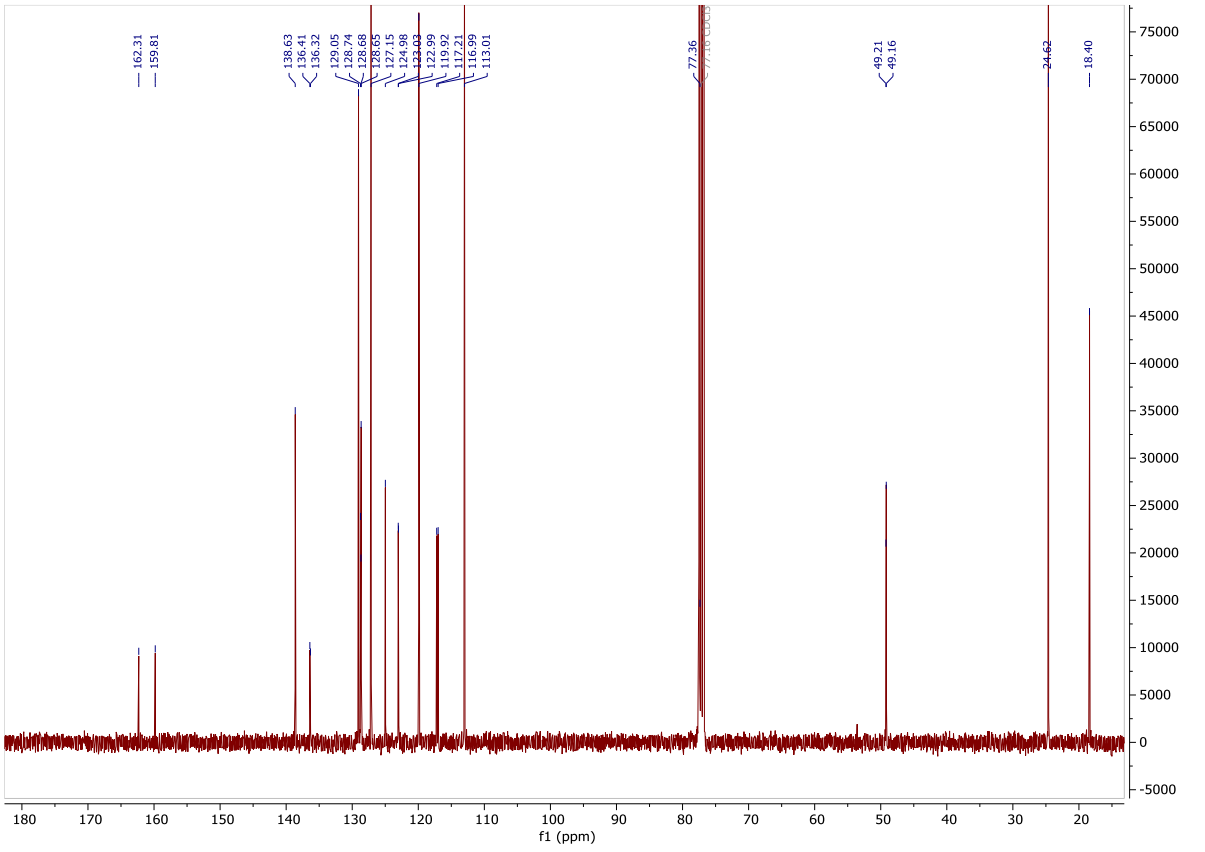

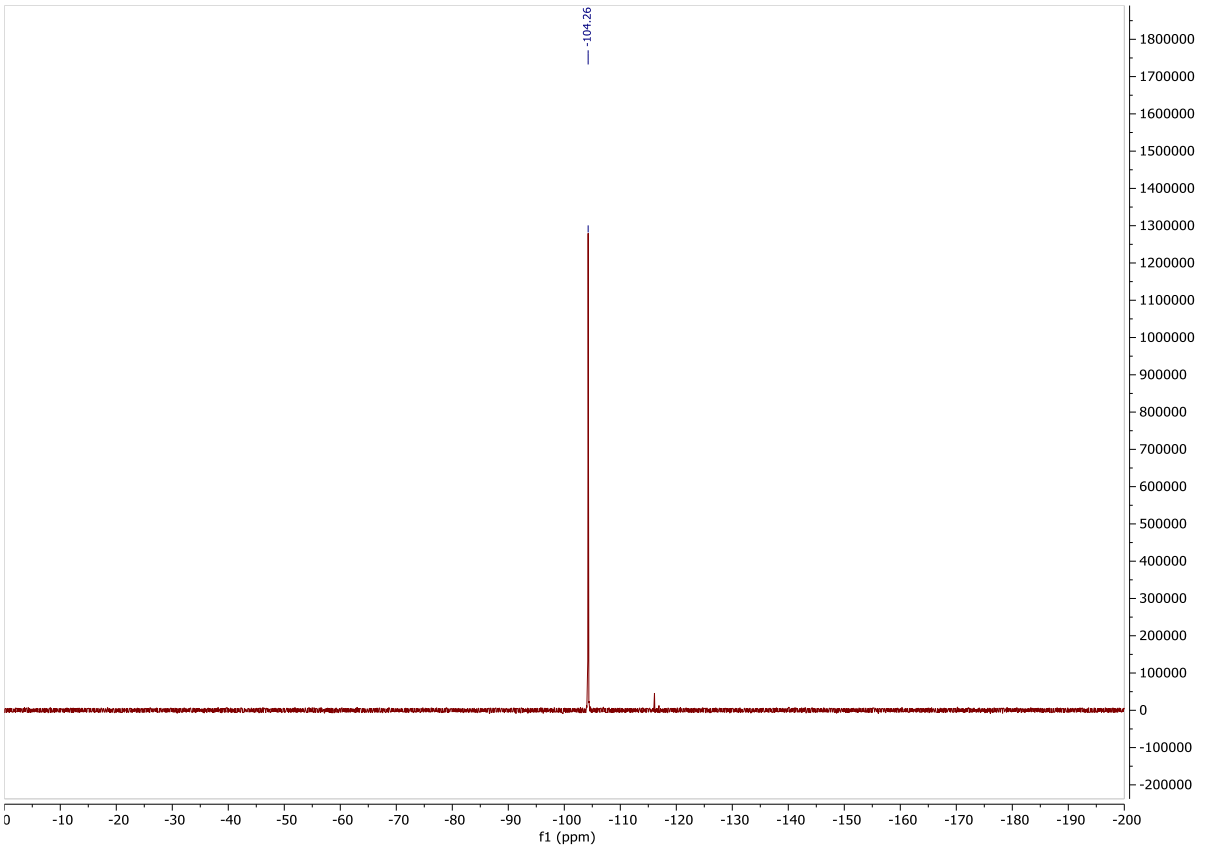
-104.26
1800000
1700000
1600000
1500000
1400000
1300000
1200000
1100000
1000000
900000
800000
700000
600000
500000
400000
300000
200000
100000
0
-100000
-200000
0
-10
-20
-30
-40
-50
-60
-70
-80
-90
-100
-110
-120
-130
-140
-150
-160
-170
-180
-190
-200
f1 (ppm)

HAT catalysts

1,2-Bis(2-chlorophenyl)disulfide (173)

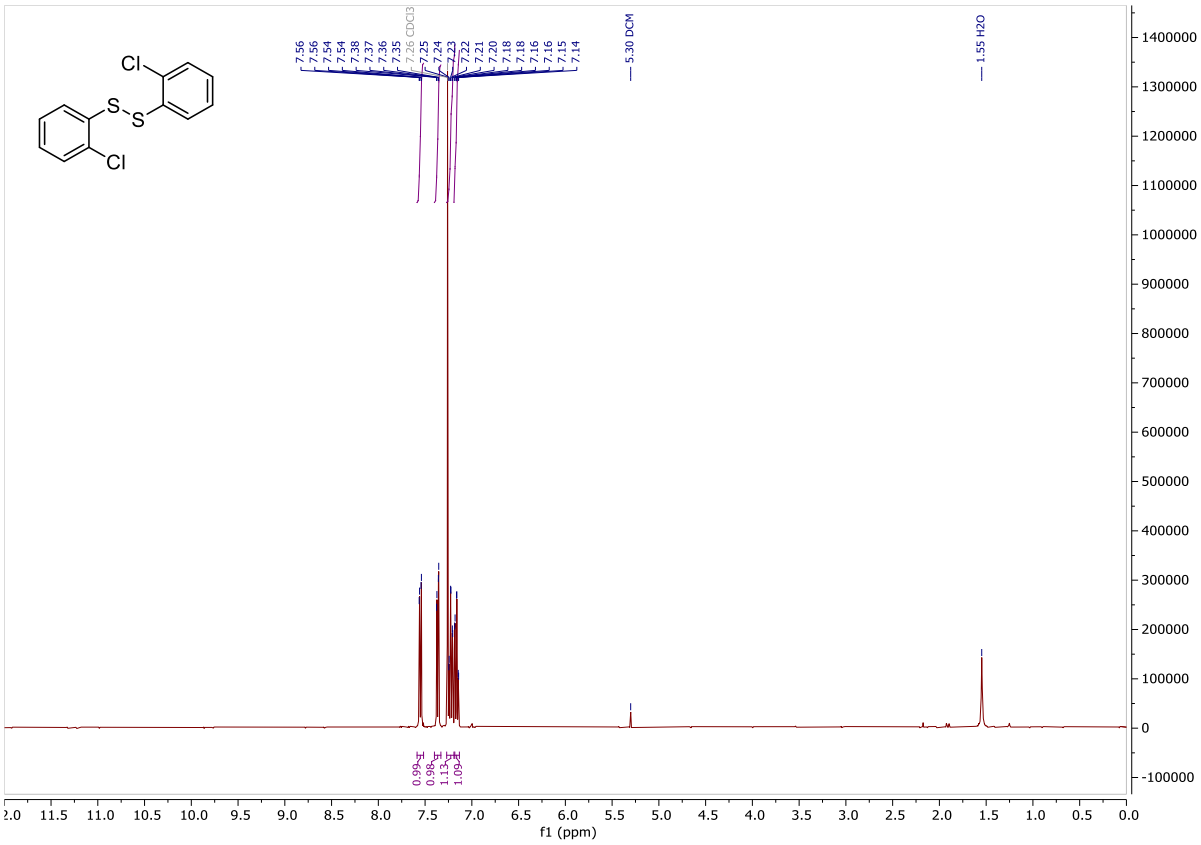

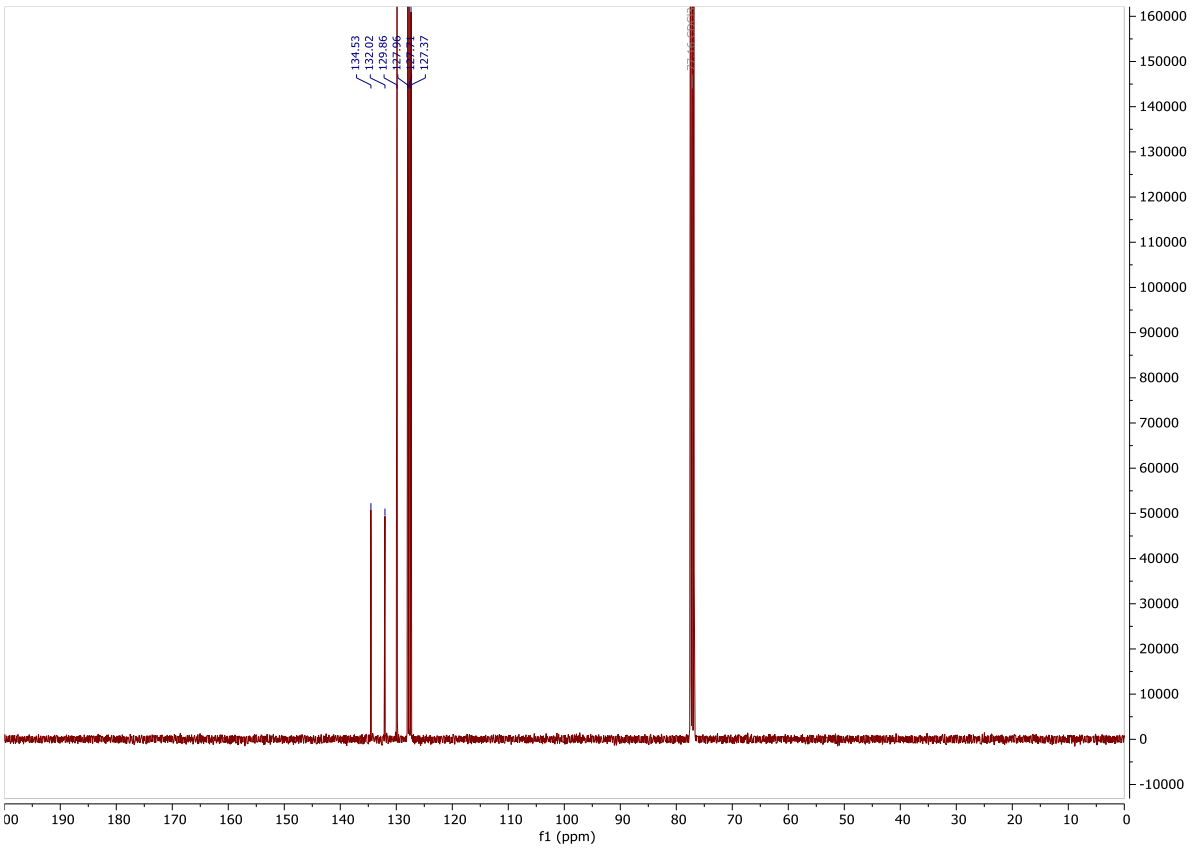

2,2'-Disulfanediyldiphenol (180)

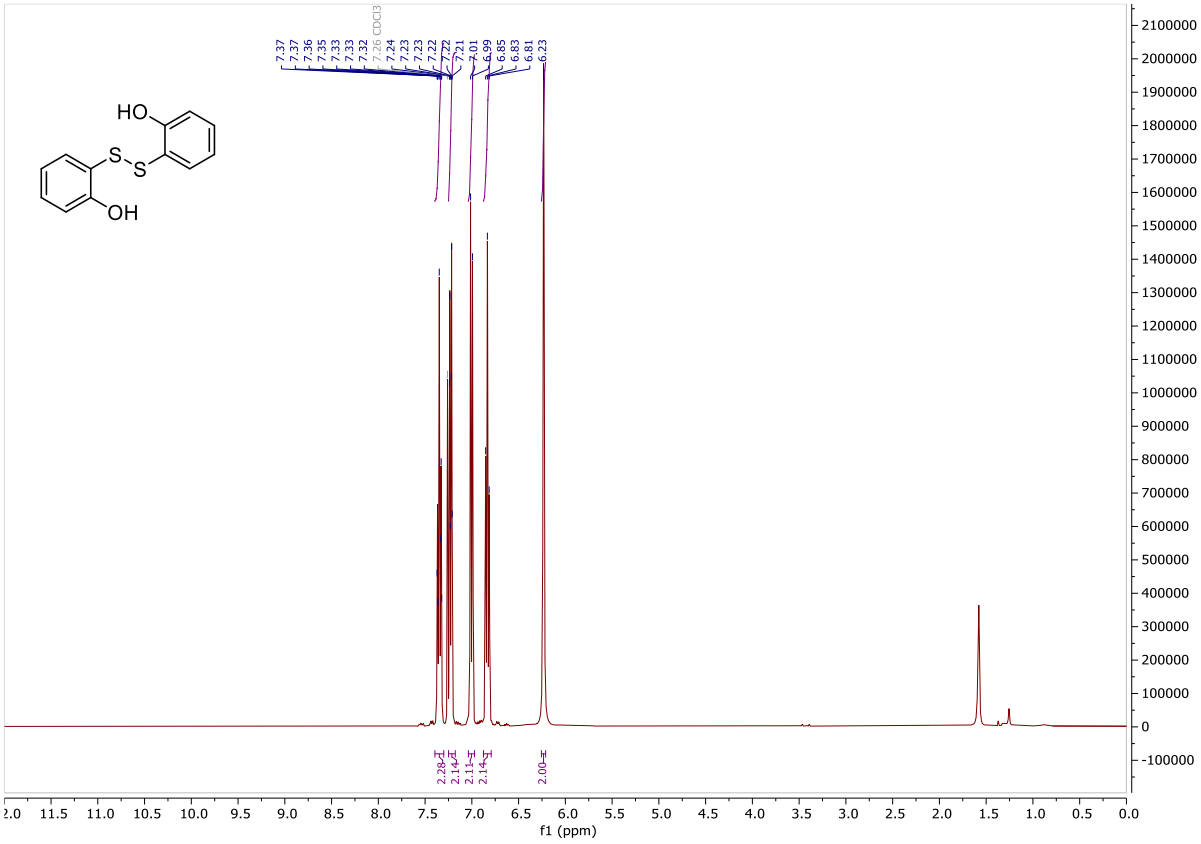

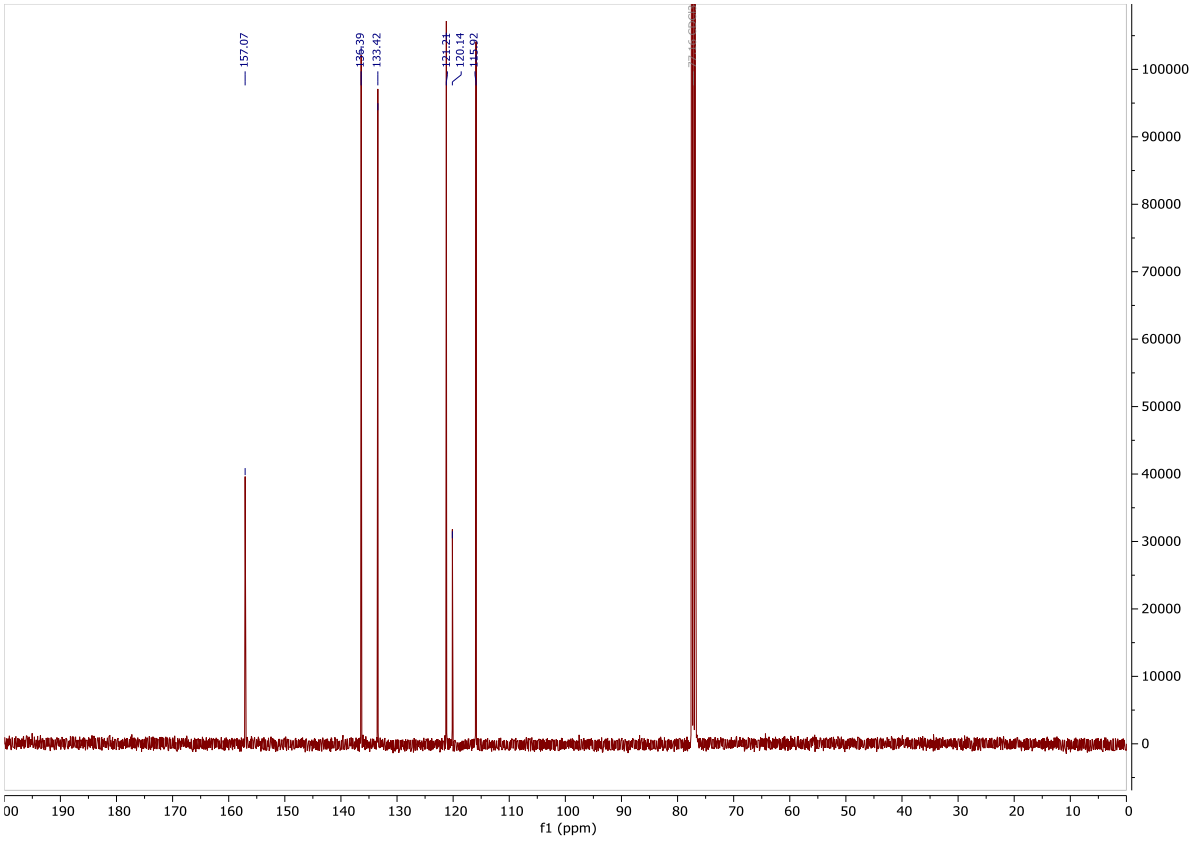

1,2-Di(naphthalen-2-yl)disulfide (181)

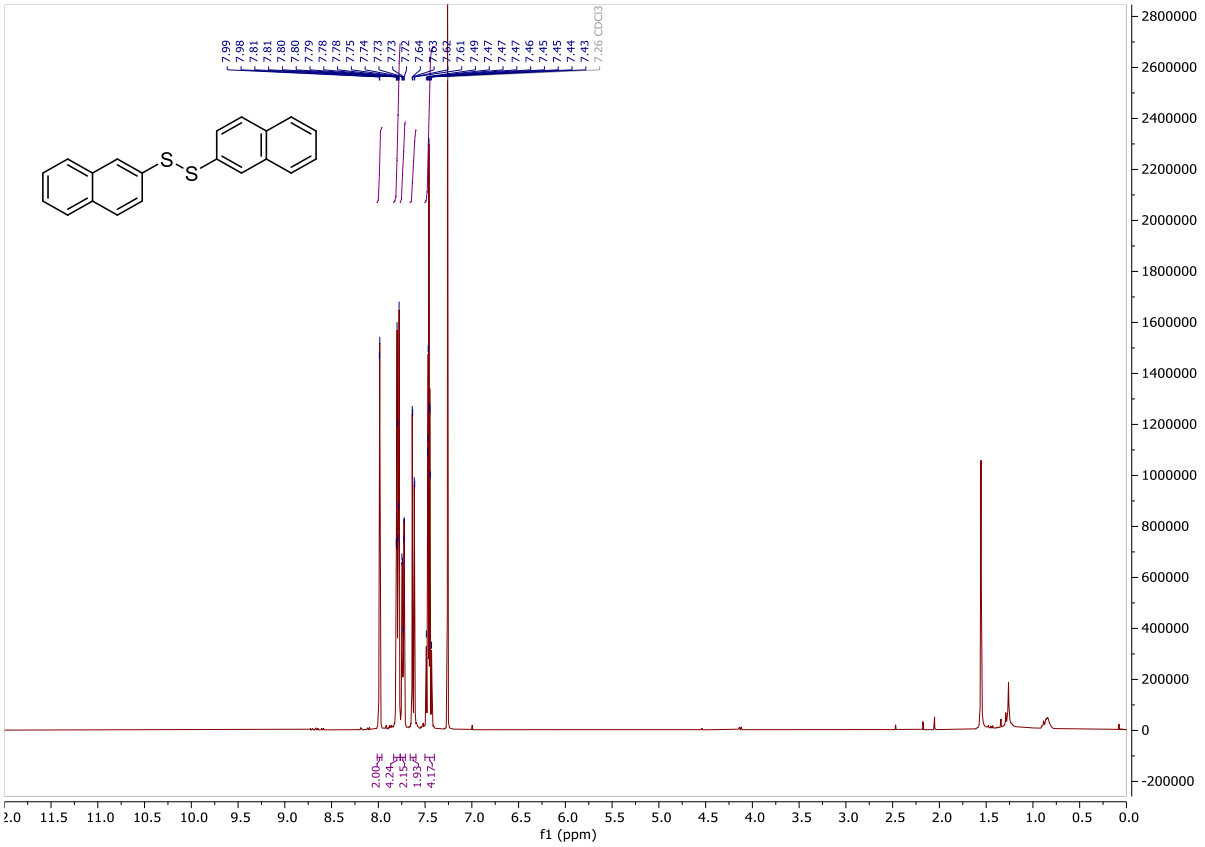

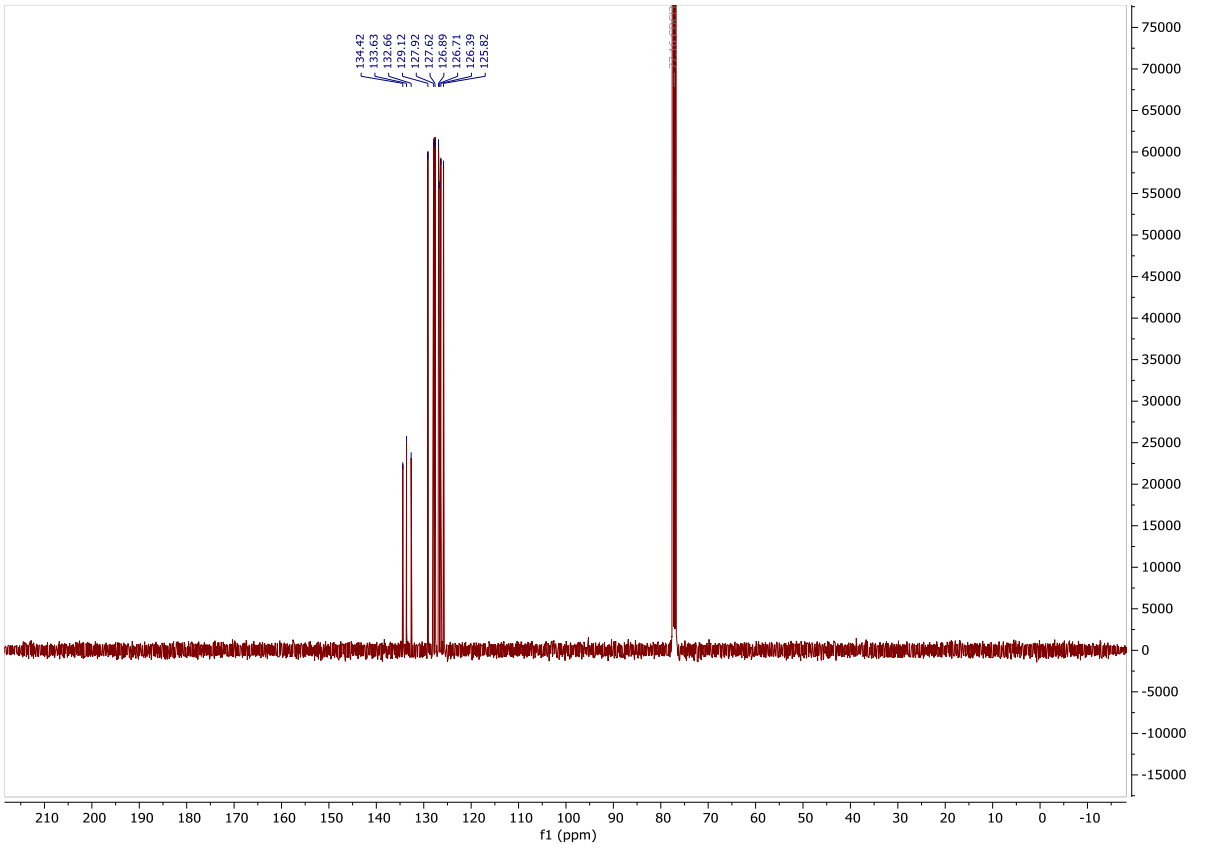

Dinaphtho[2,1-c:1',2'-e][1,2]dithiine (182)

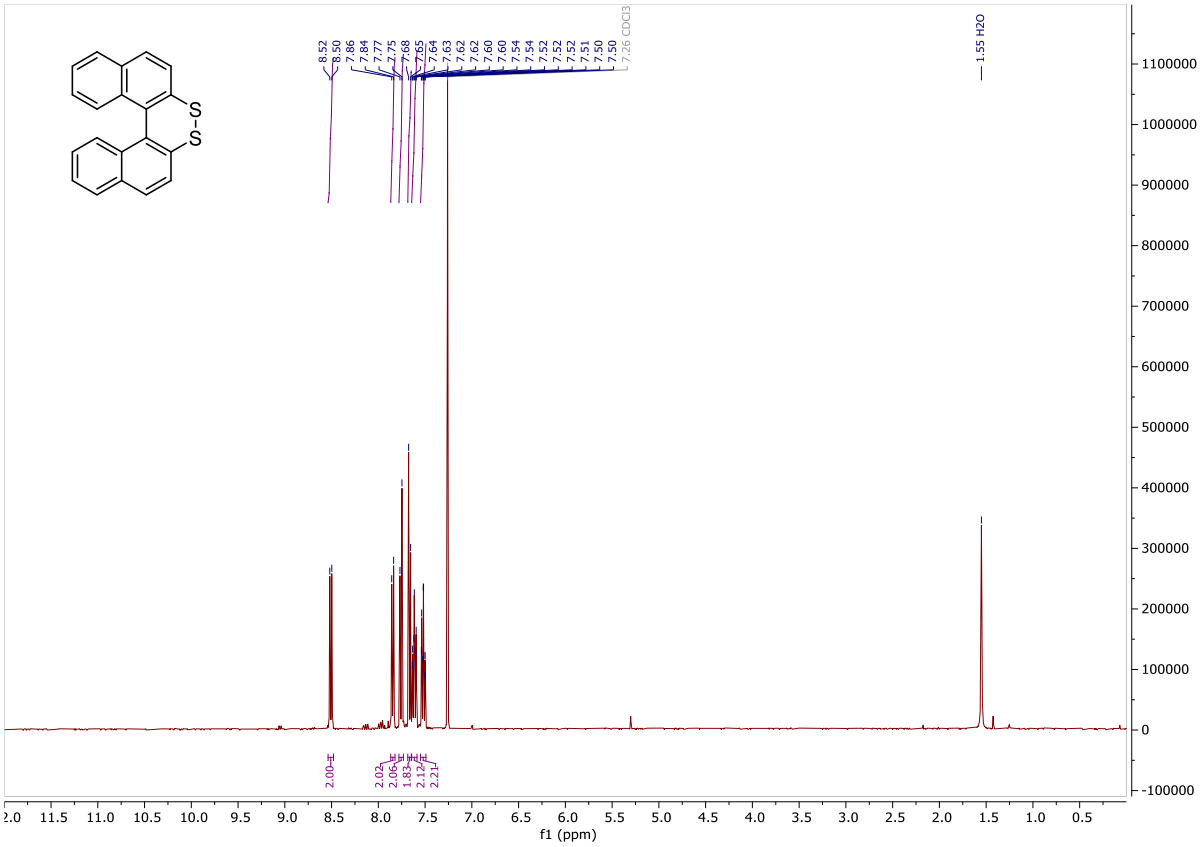

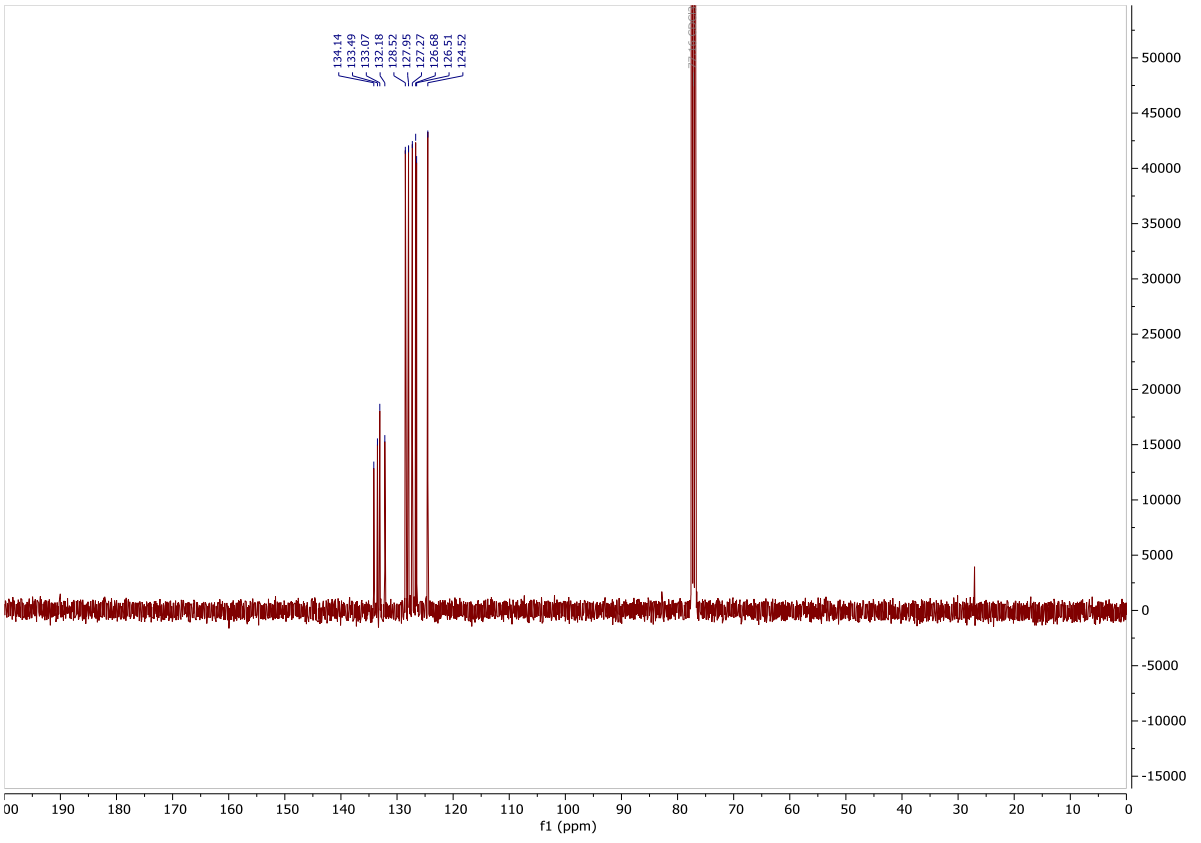

1,2-Bis(2,6-dimethylphenyl)disulfide (188)

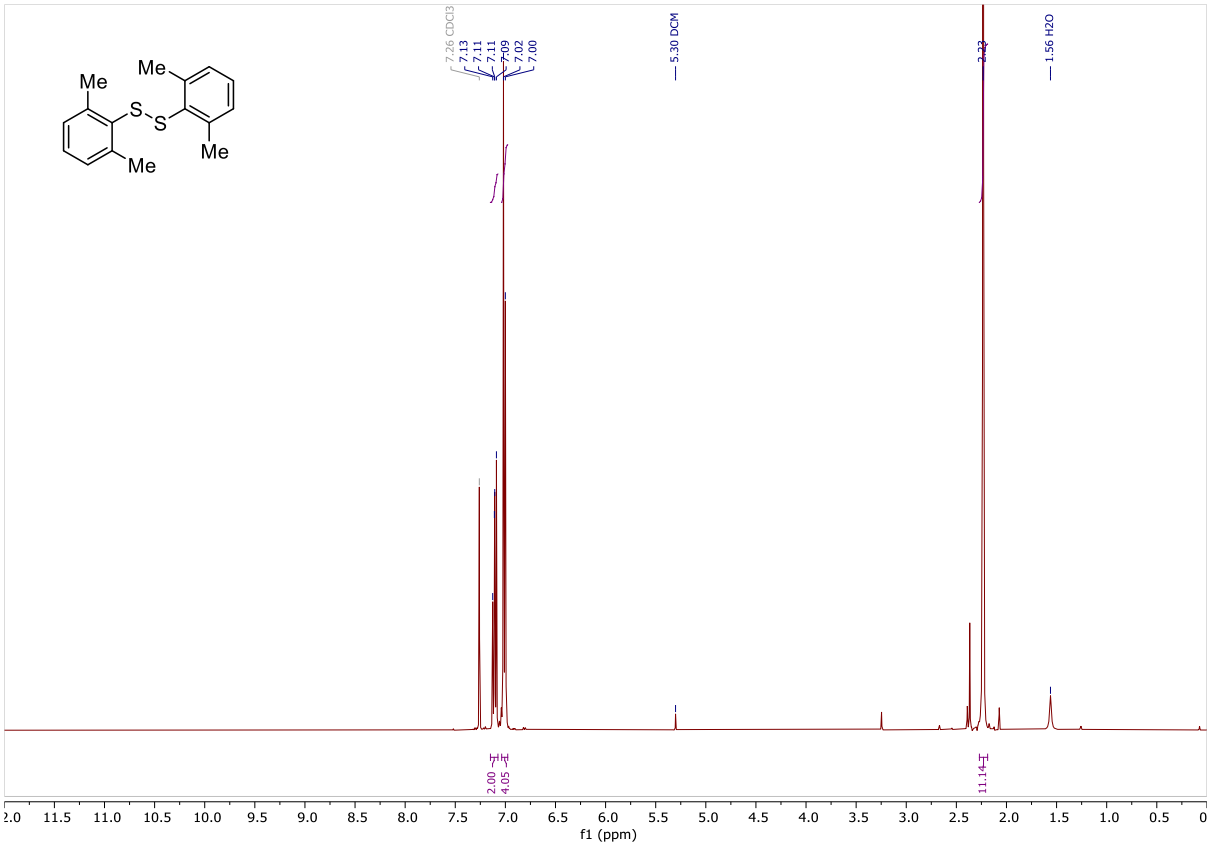

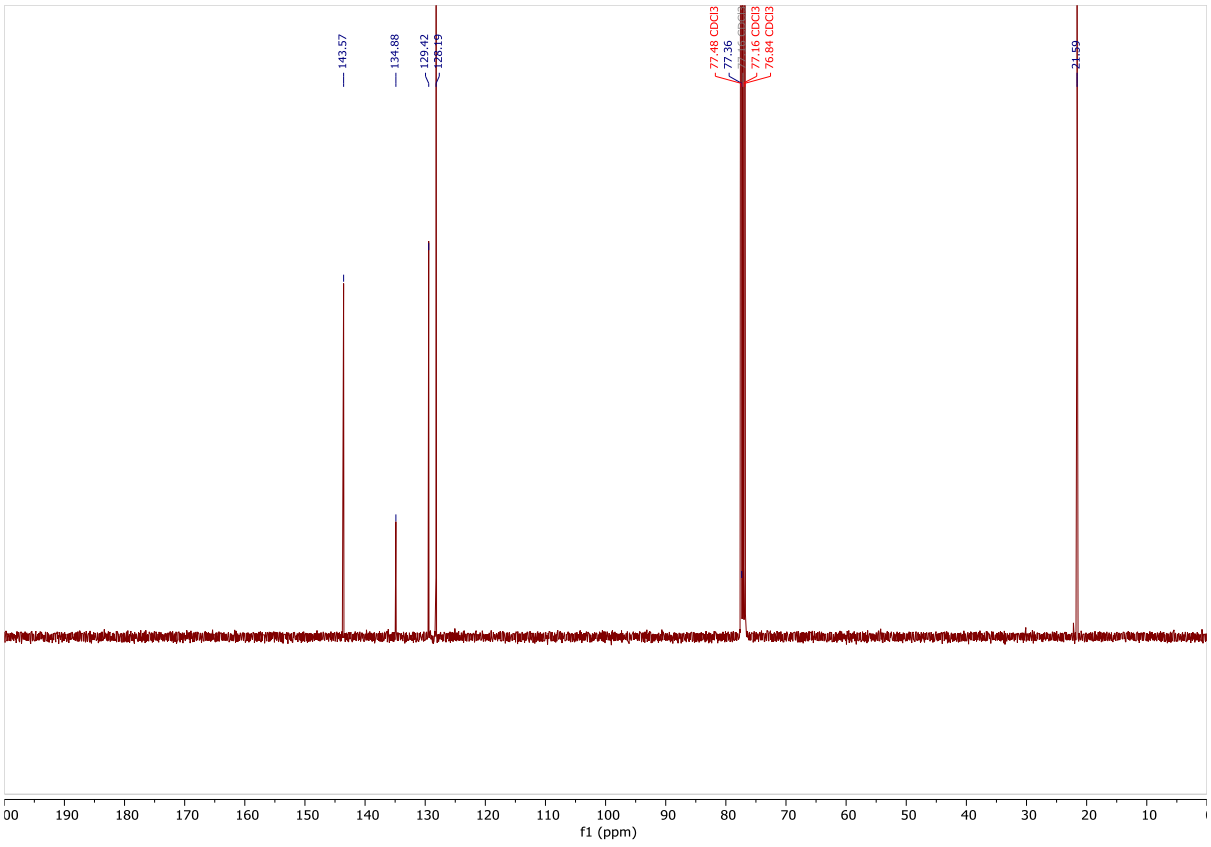

2,2'-Disulfanediylbis(N-methylaniline) (191)

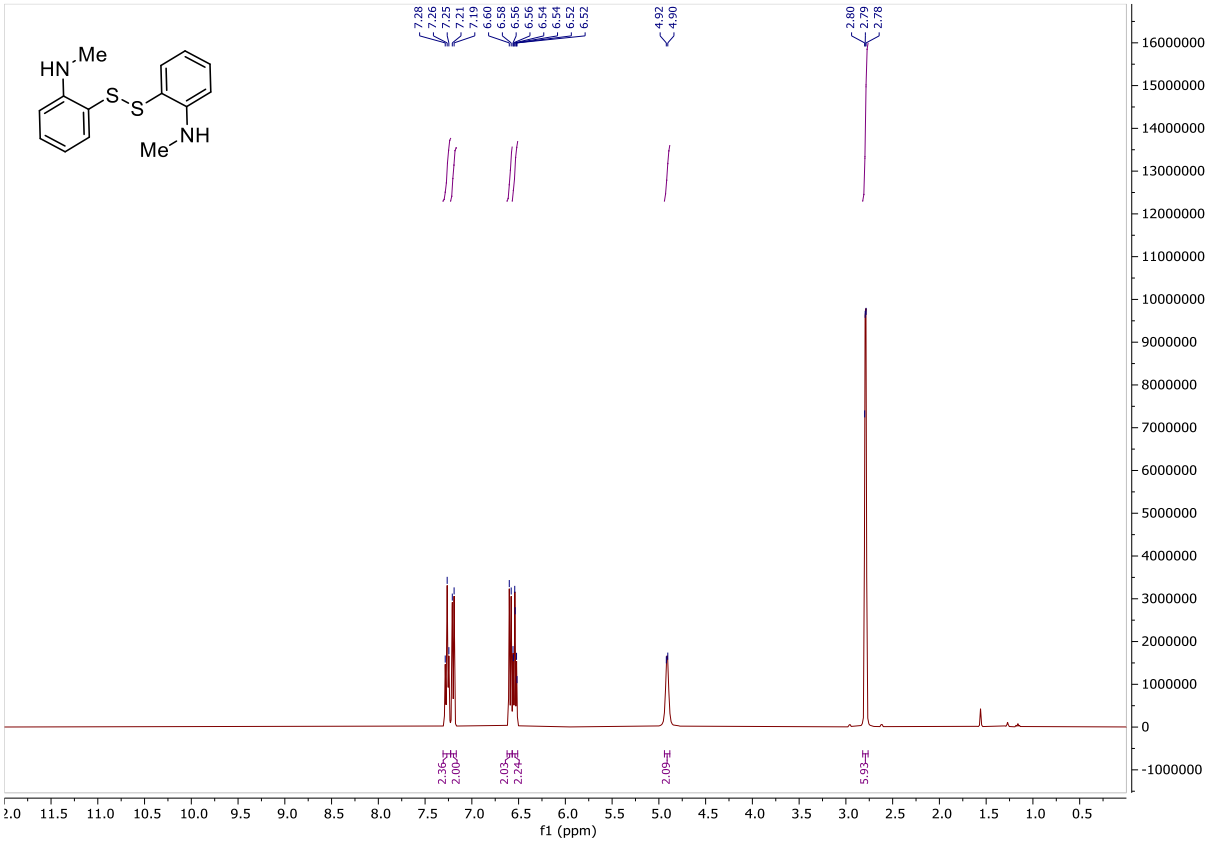

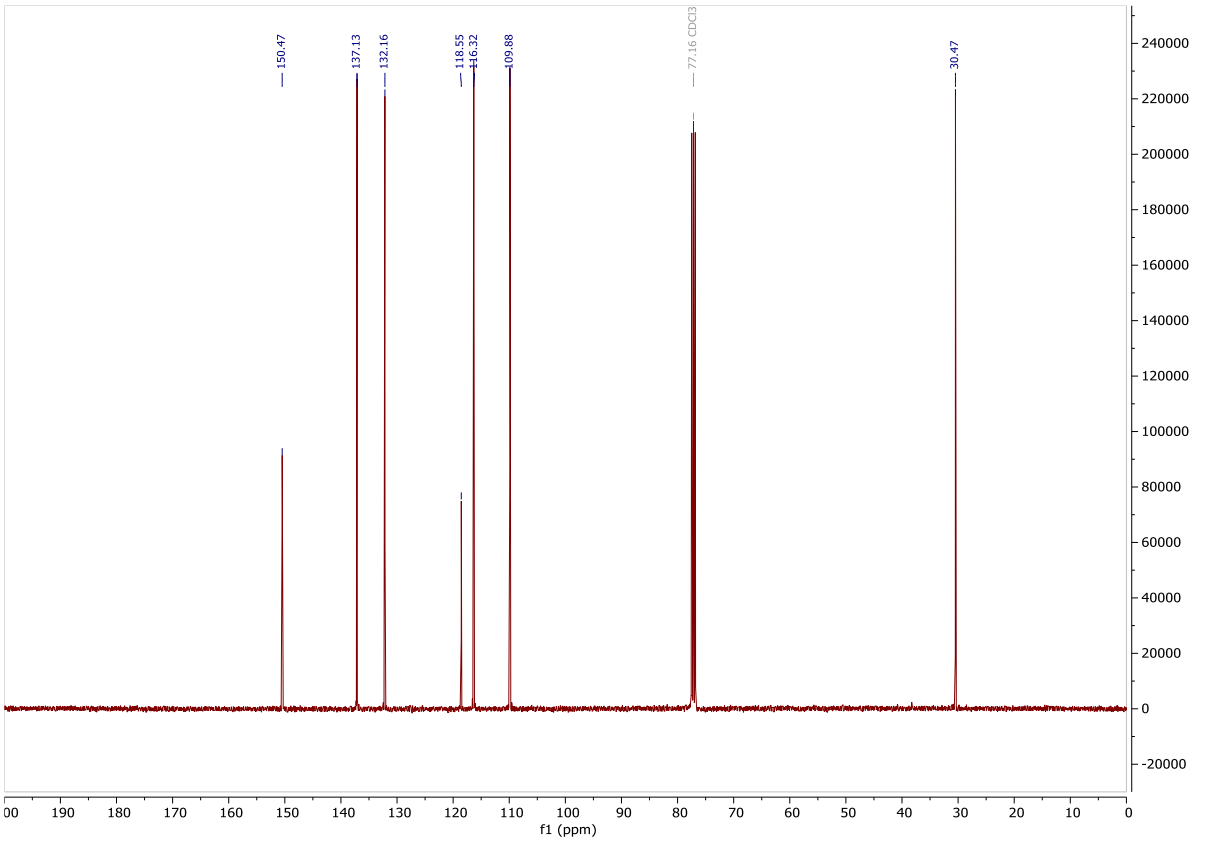

6,6'-Disulfanediylbis(3-methylaniline) (192)

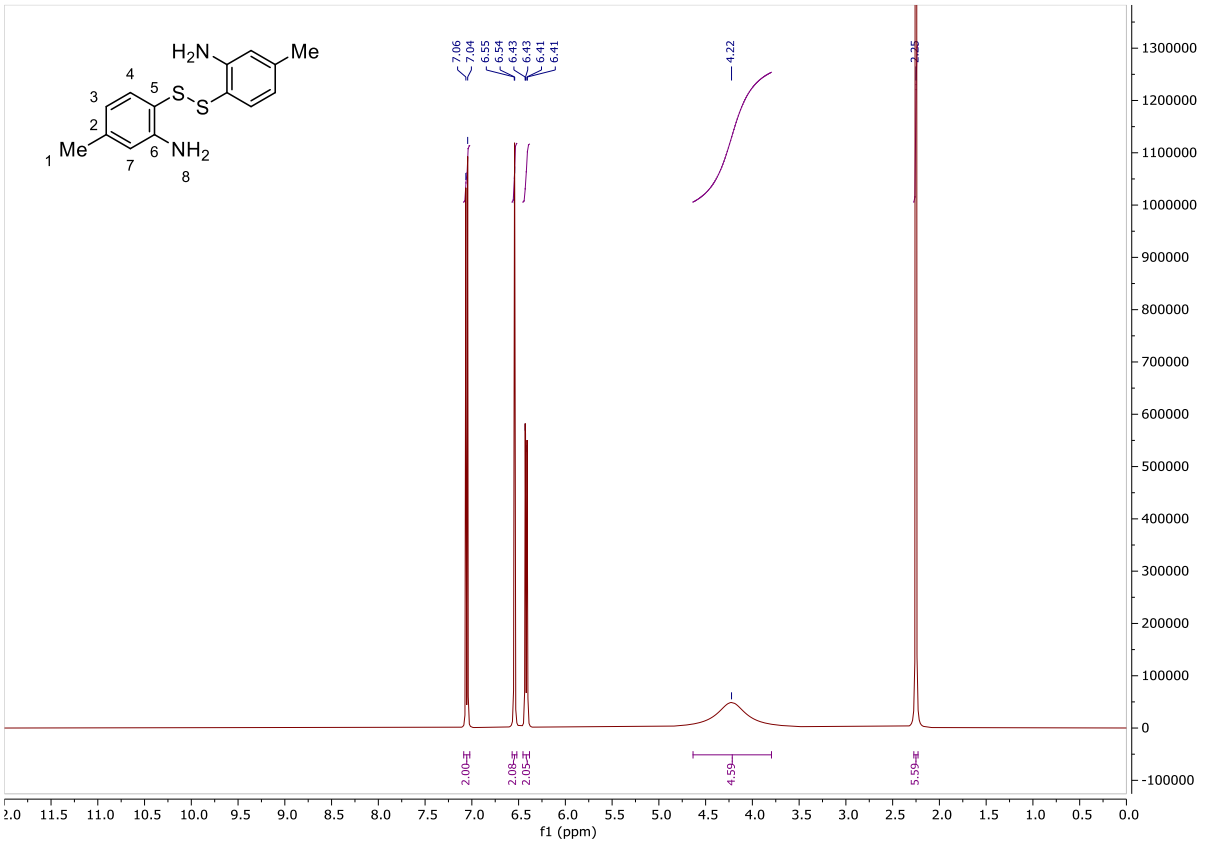

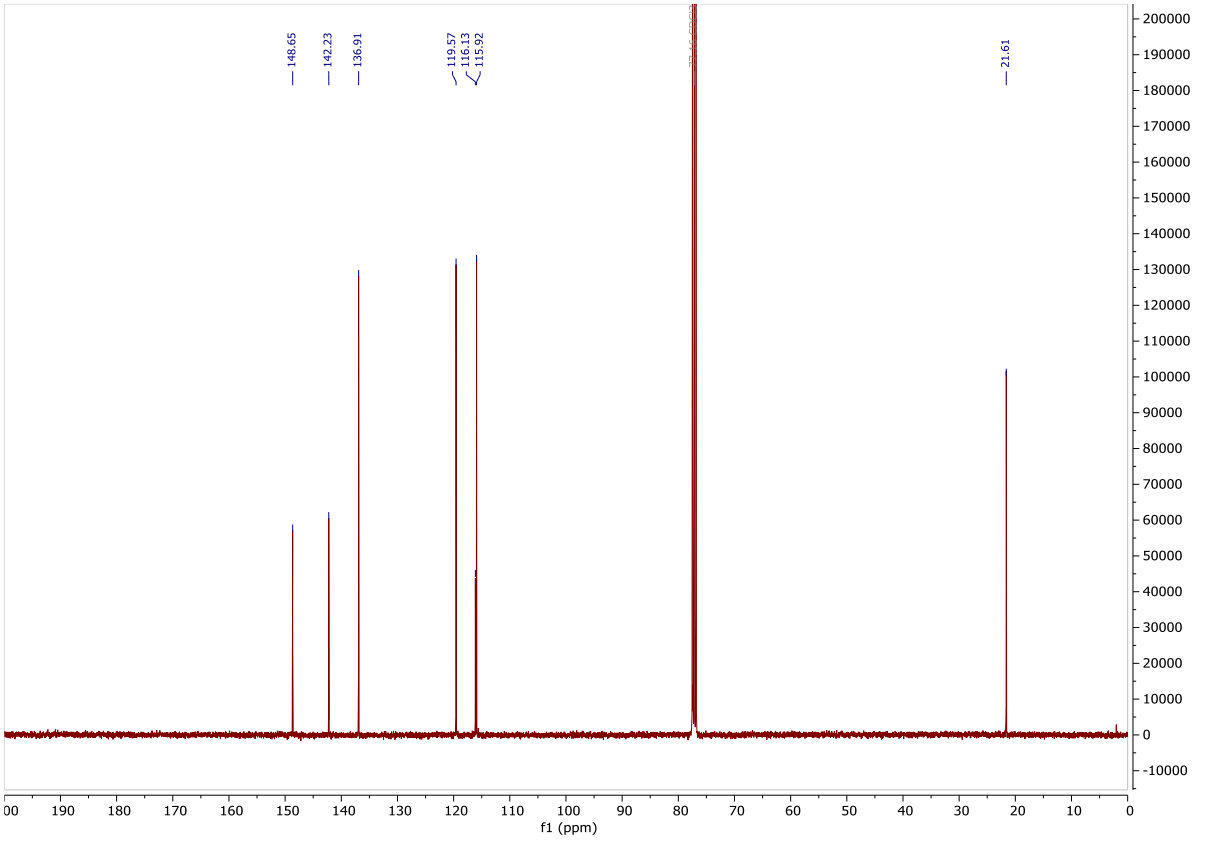

4-(Tert-butyl)-2-nitrophenol (193)

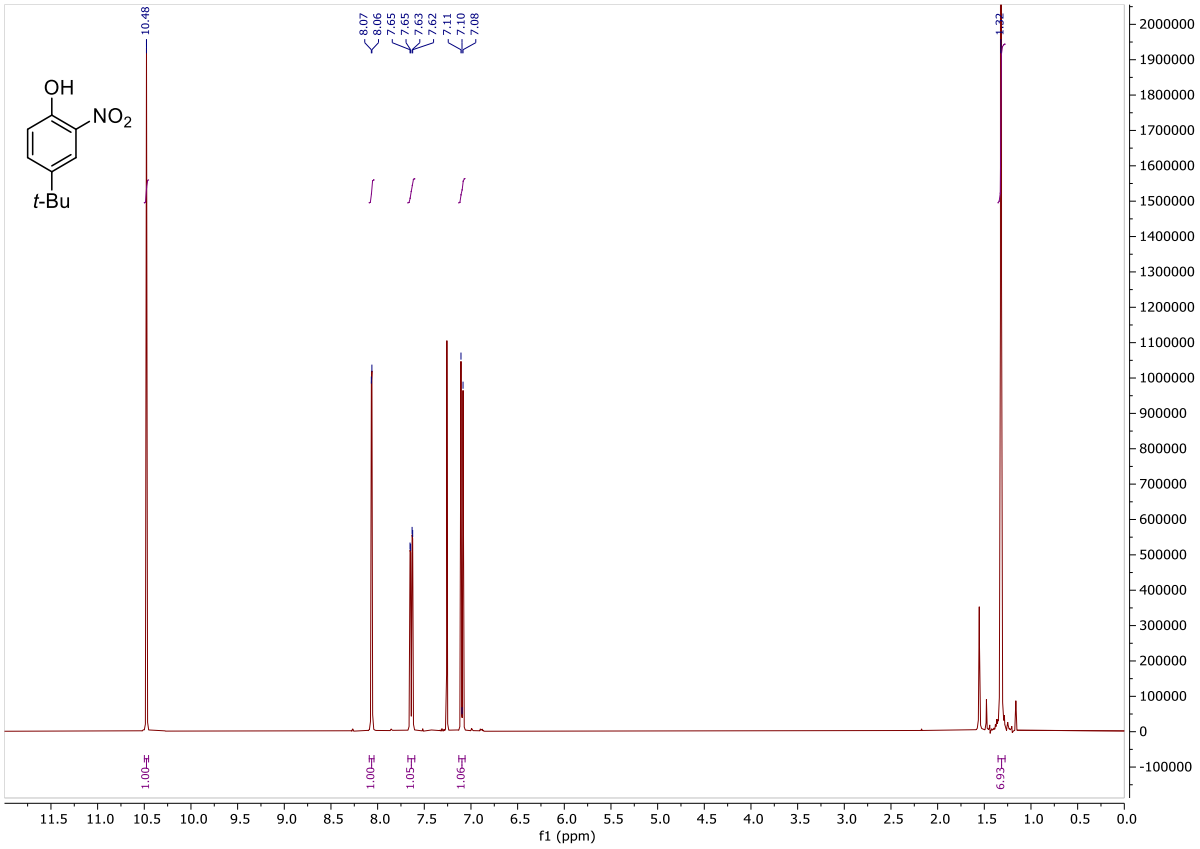

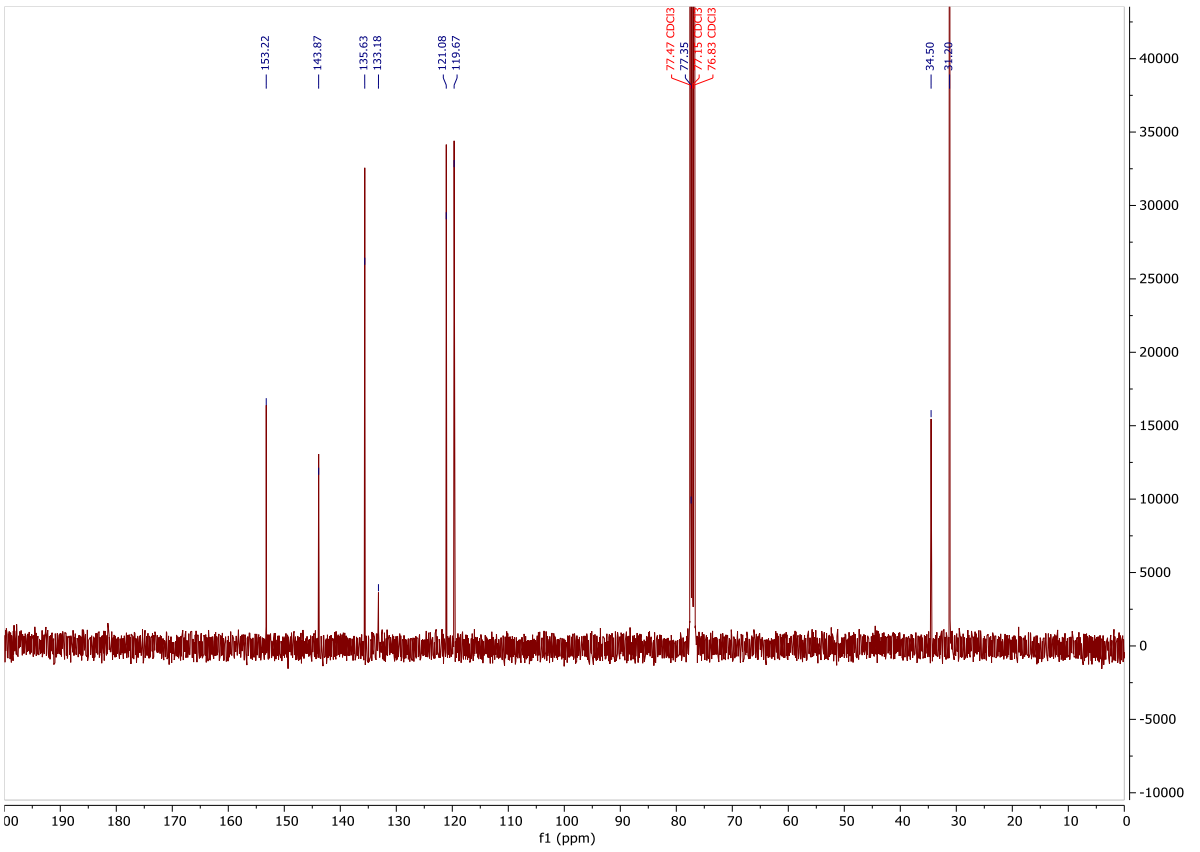

O-(4-(tert-butyl)-2-nitrophenyl) dimethylcarbamothioate (194)

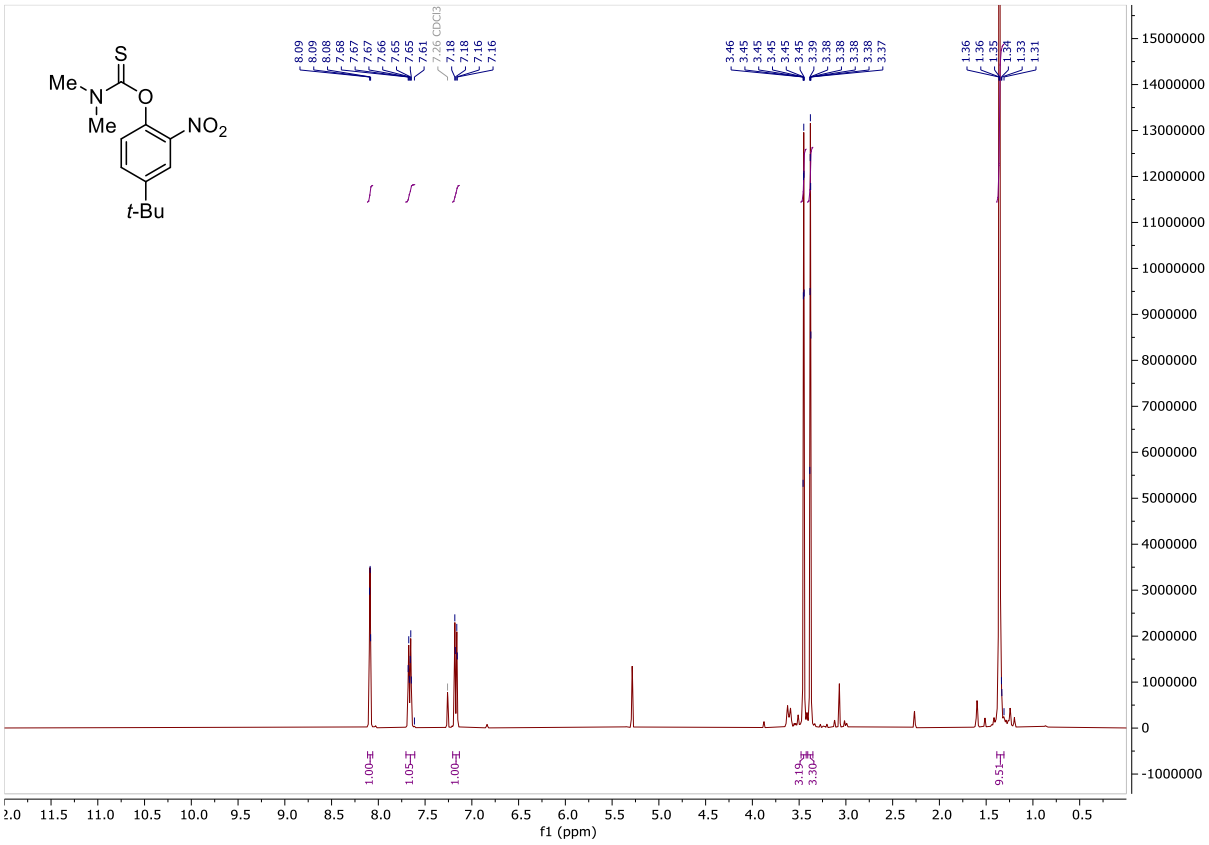

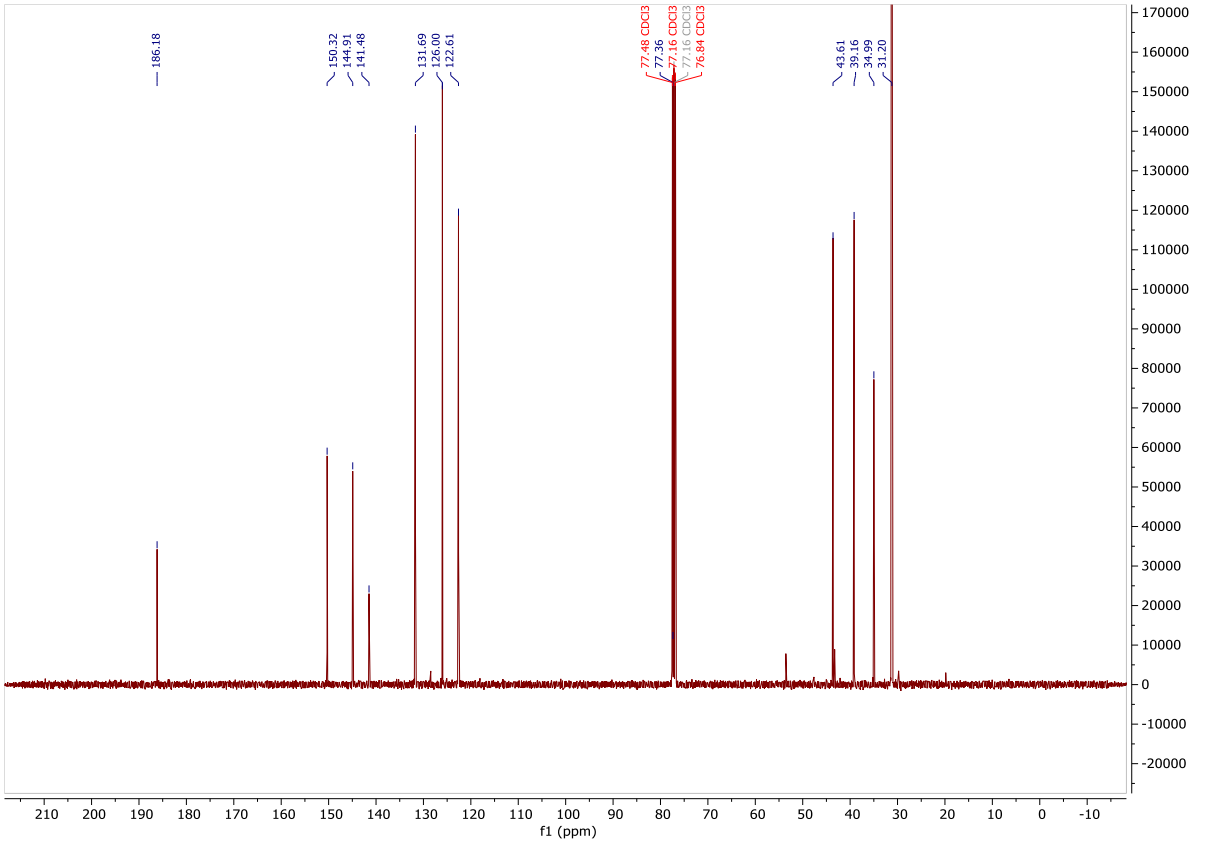

S-(4-(tert-butyl)-2-nitrophenyl) dimethylcarbamothioate (195)

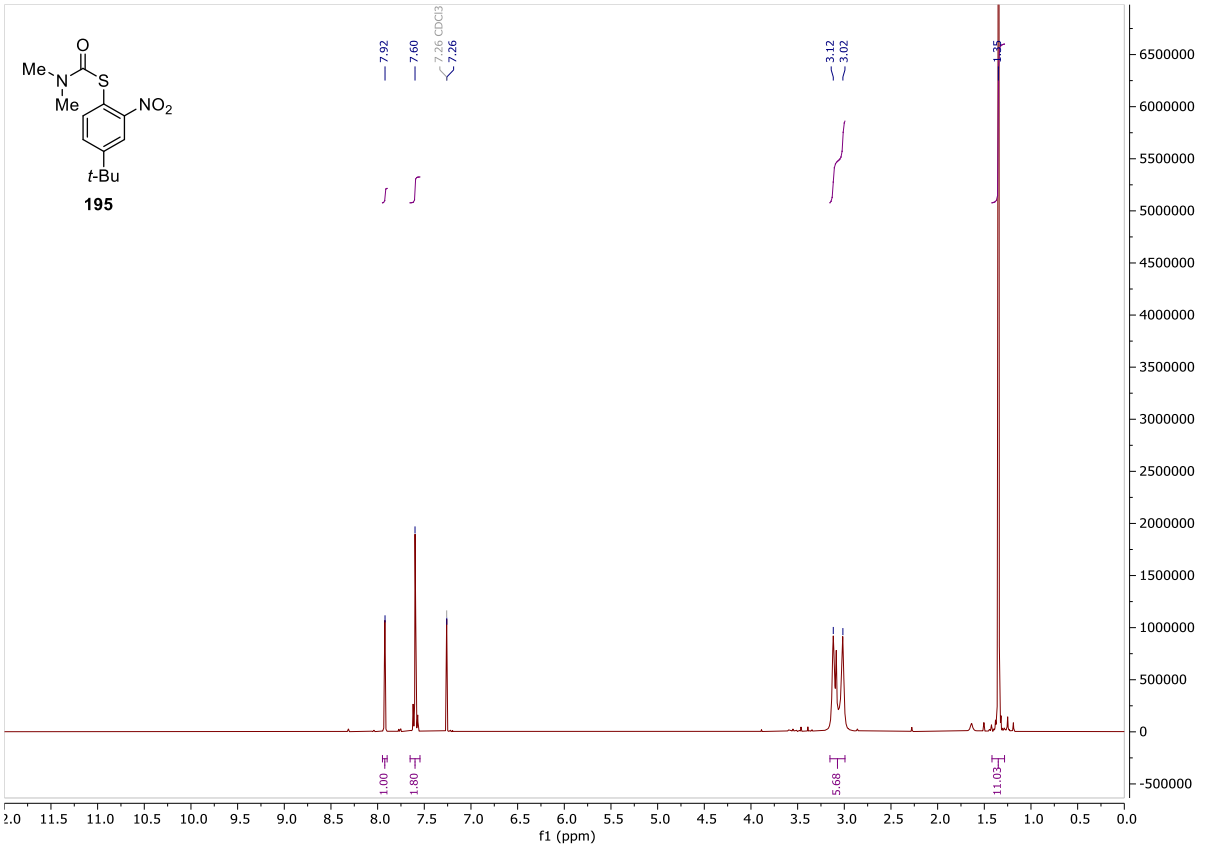

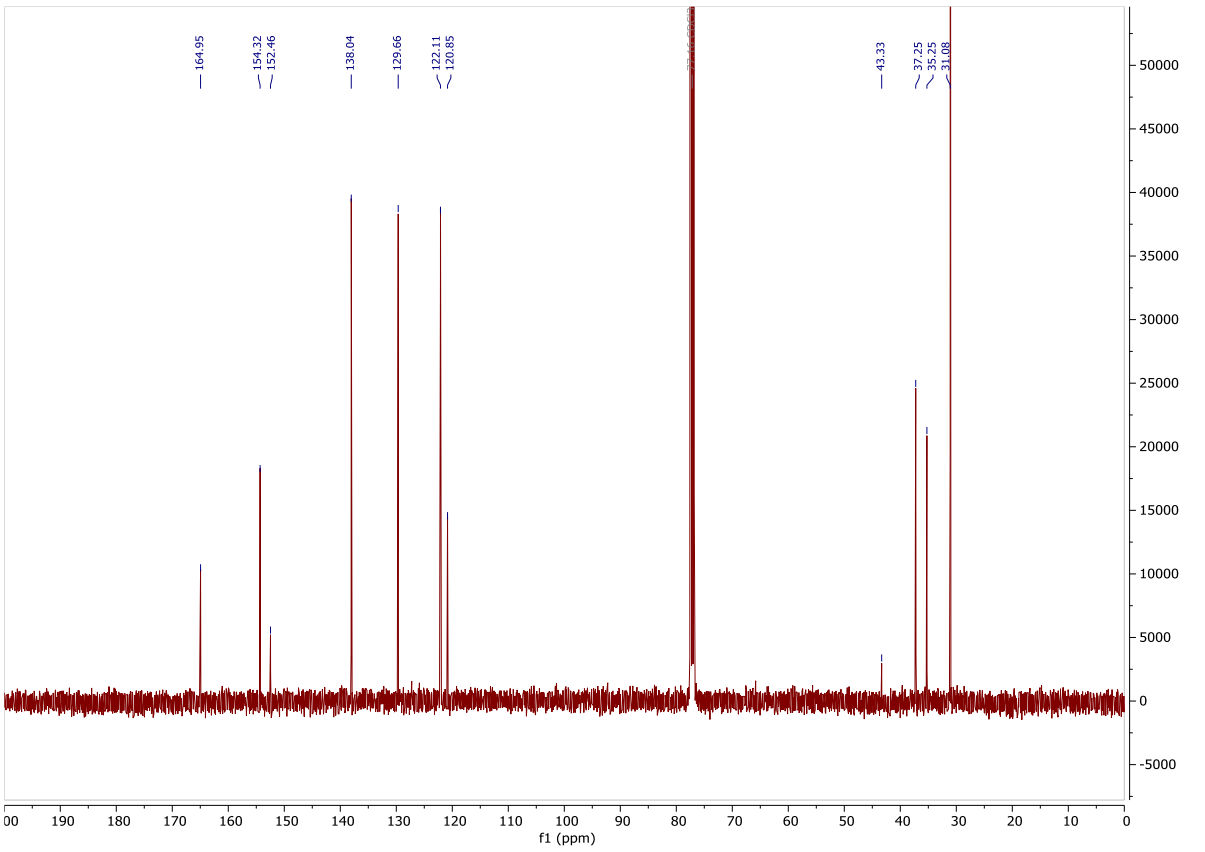

6,6'-Disulfanediylbis(3-(tert-butyl)aniline) (198)

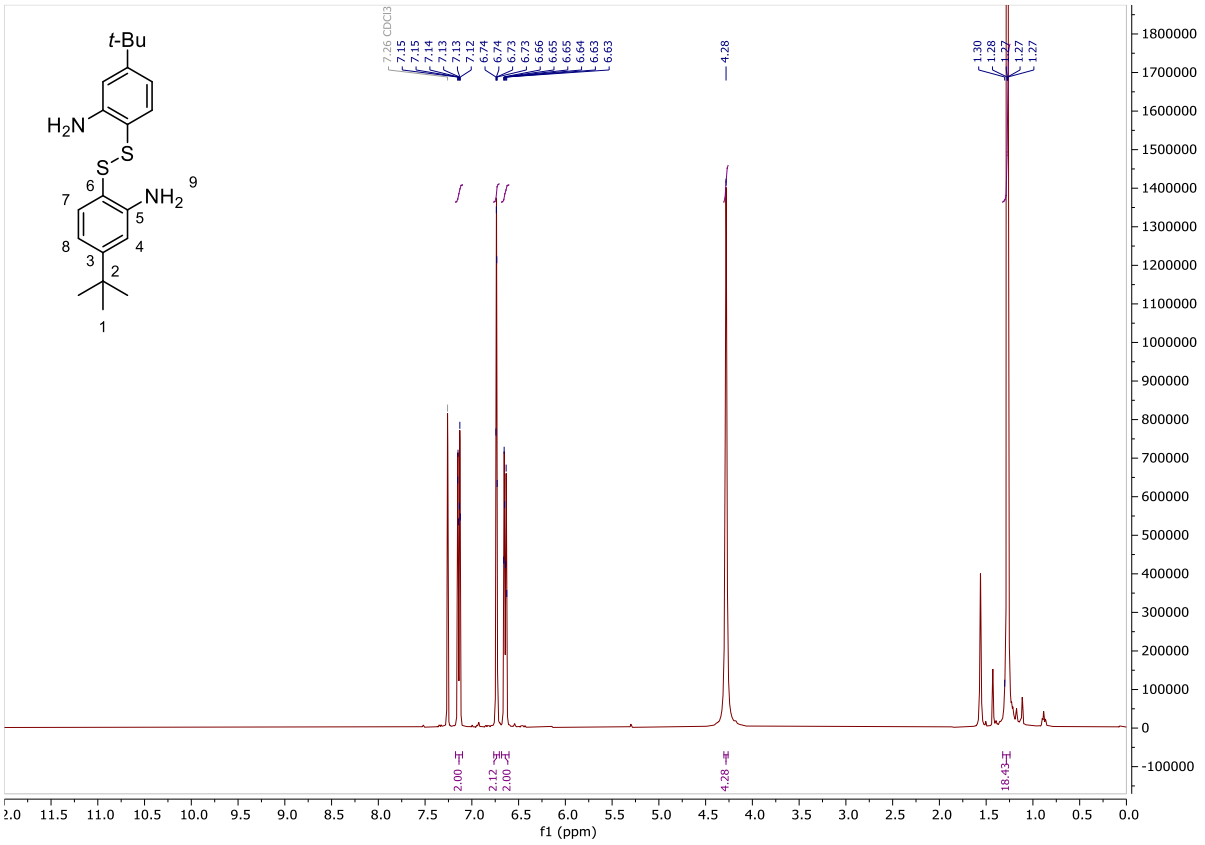

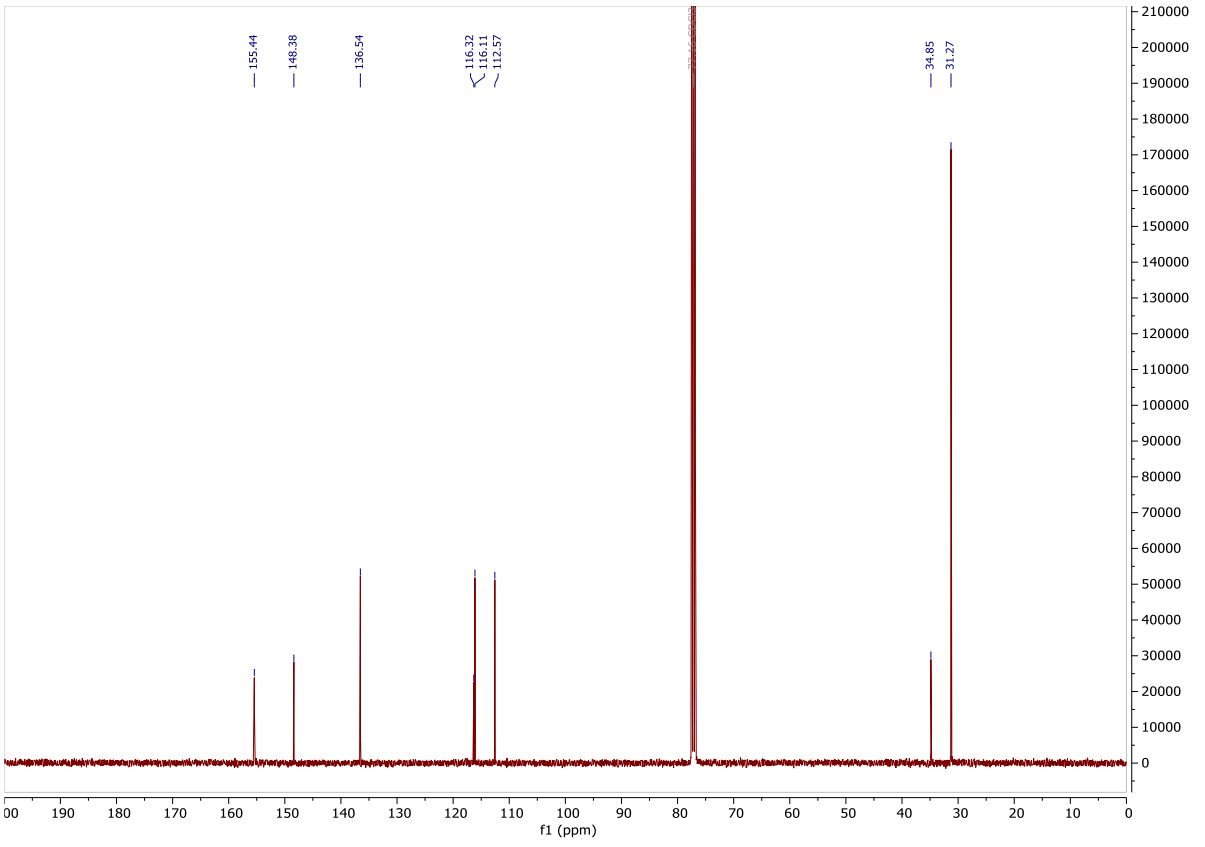

4-Methoxy-2-nitrobenzenethiol (199)

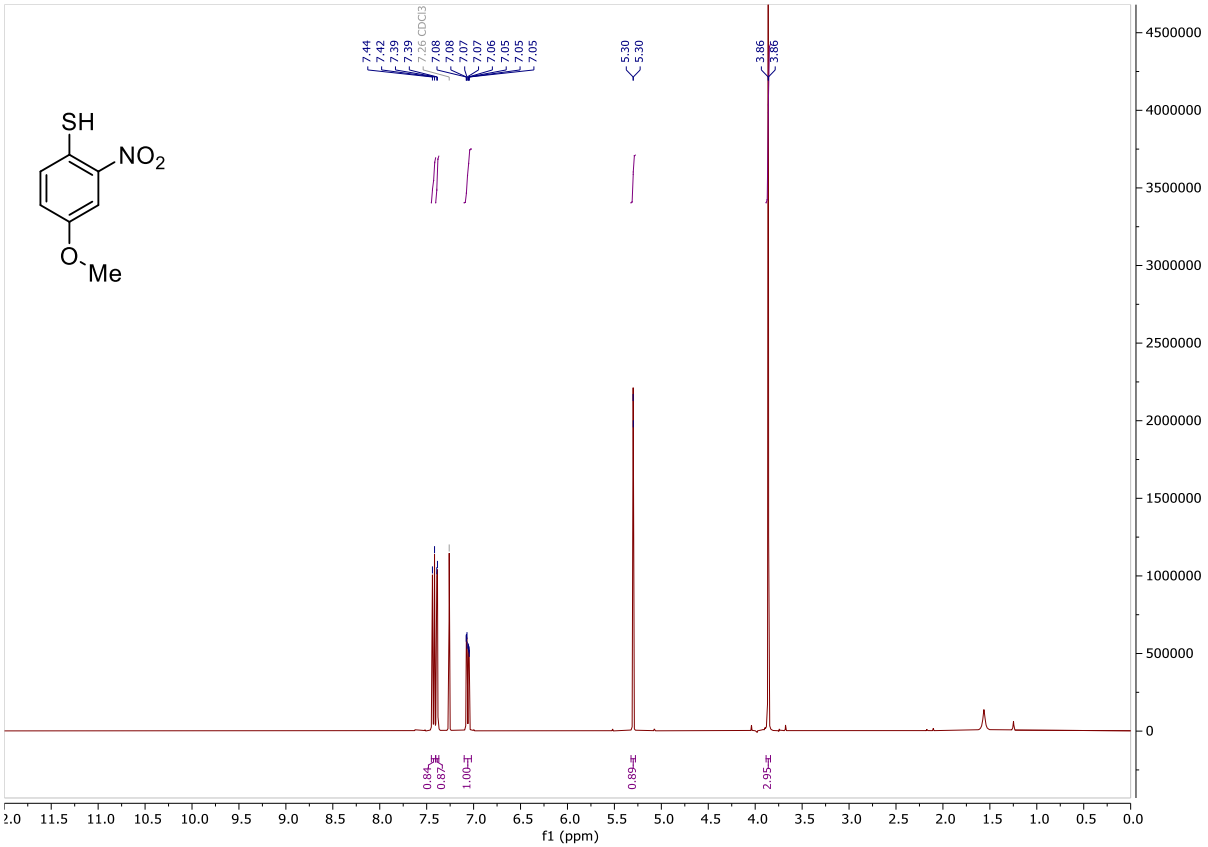

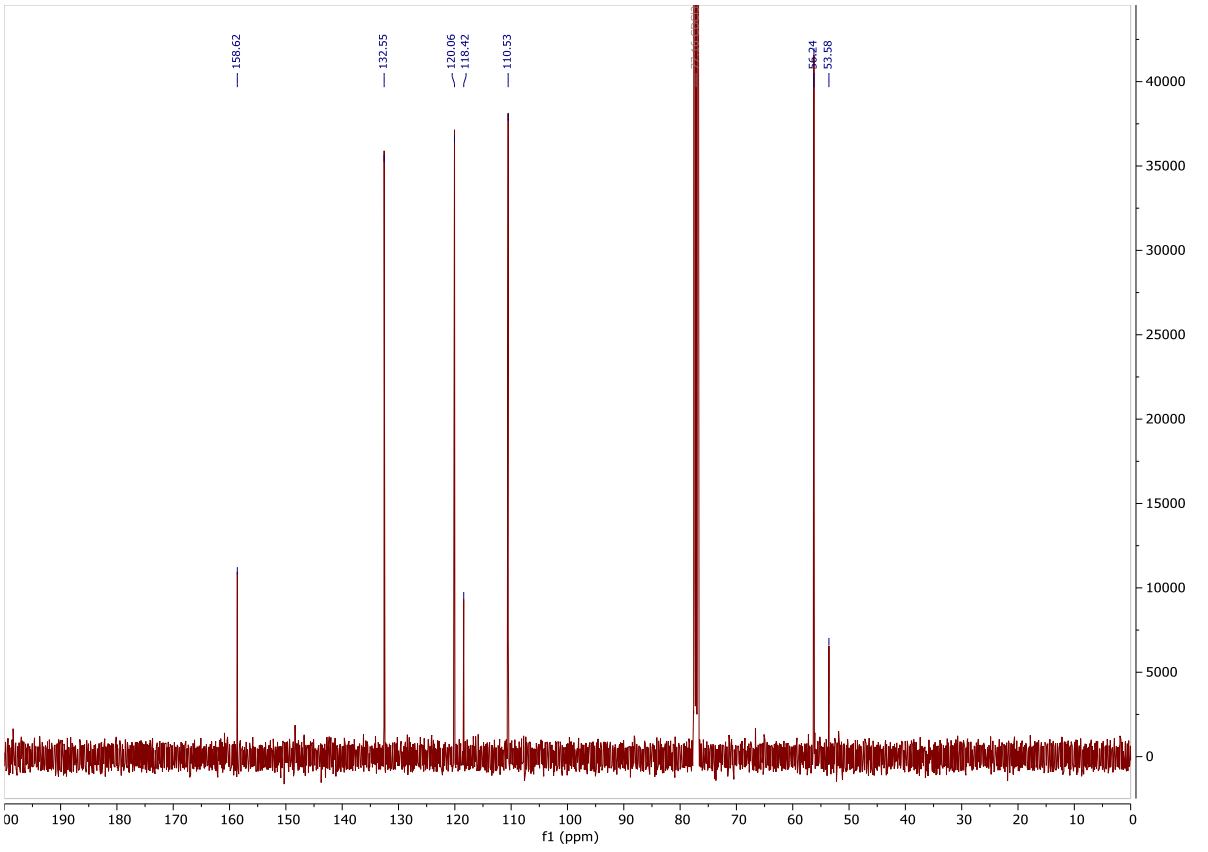

6,6'-Disulfanediylbis(3-methoxyaniline) (201)

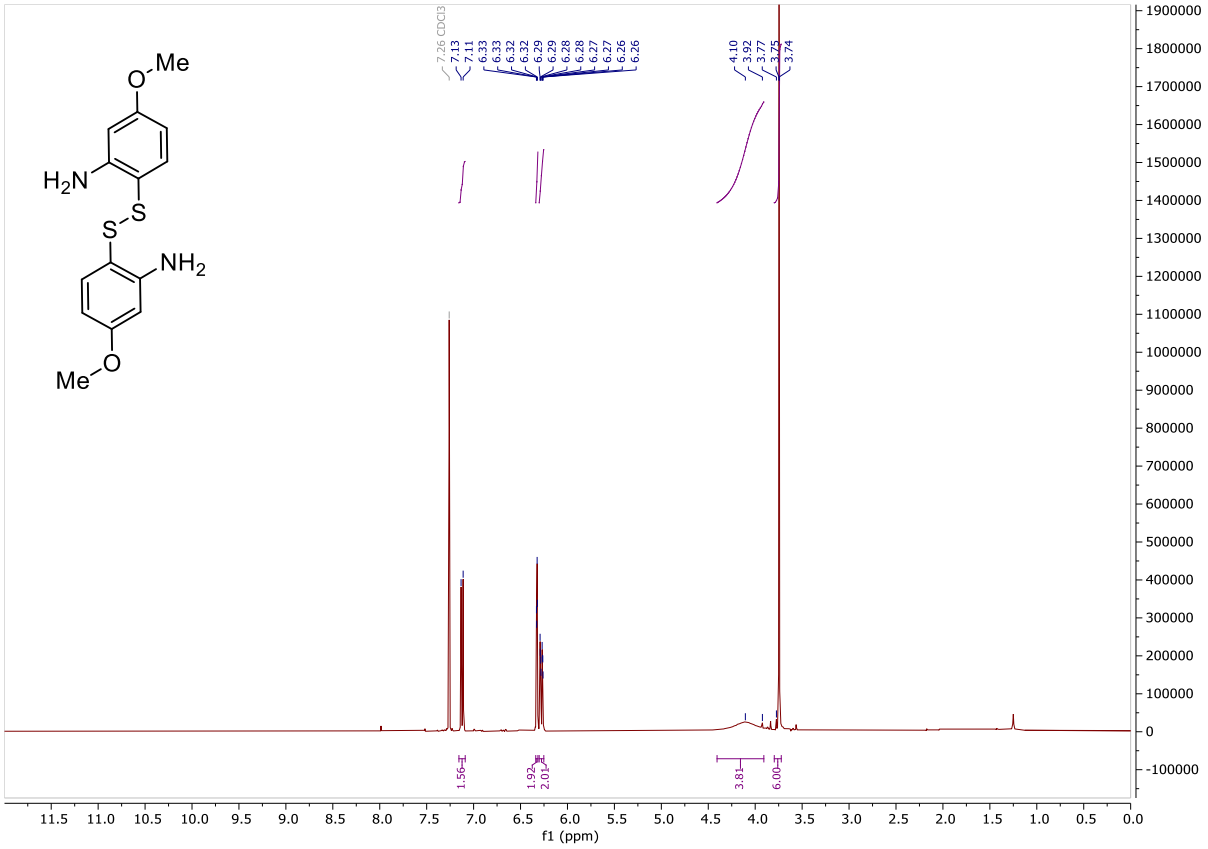

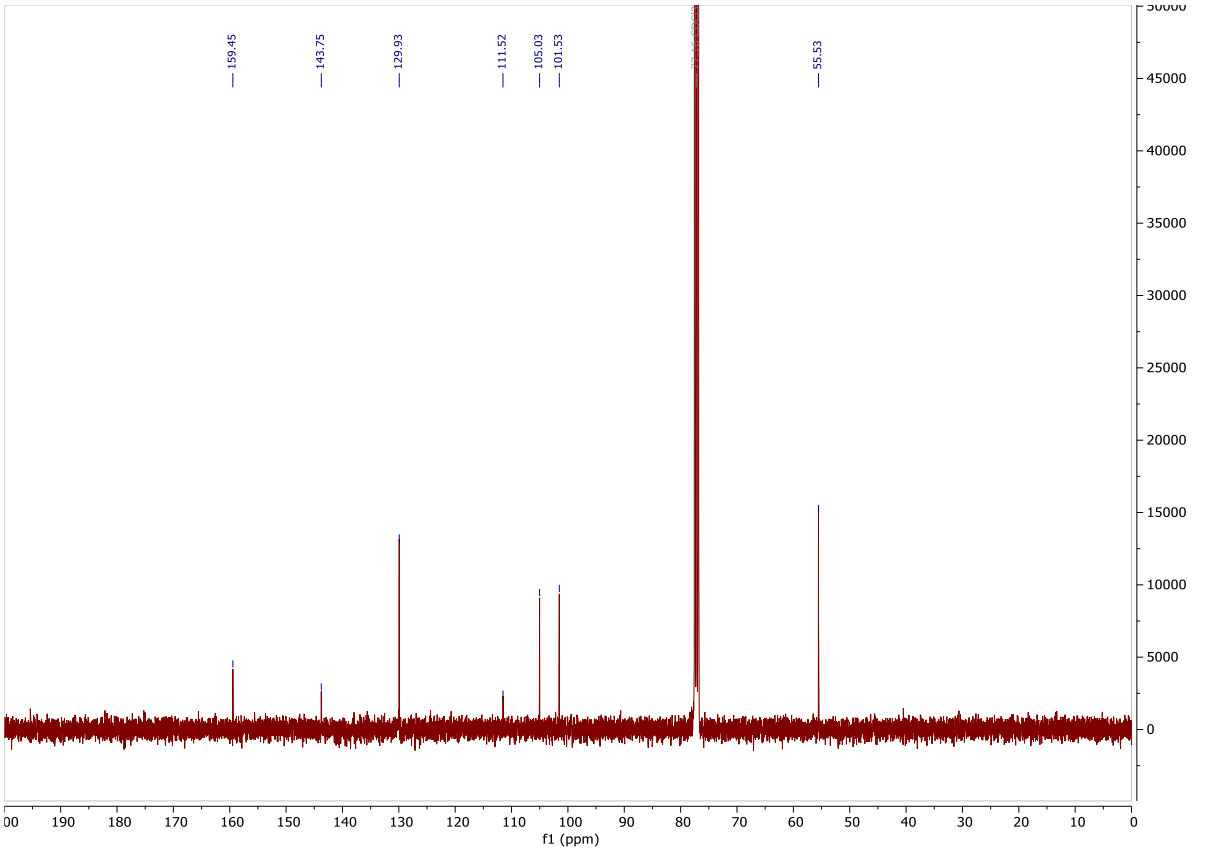

Alkenes

But-3-en-1-ylbenzene (162)

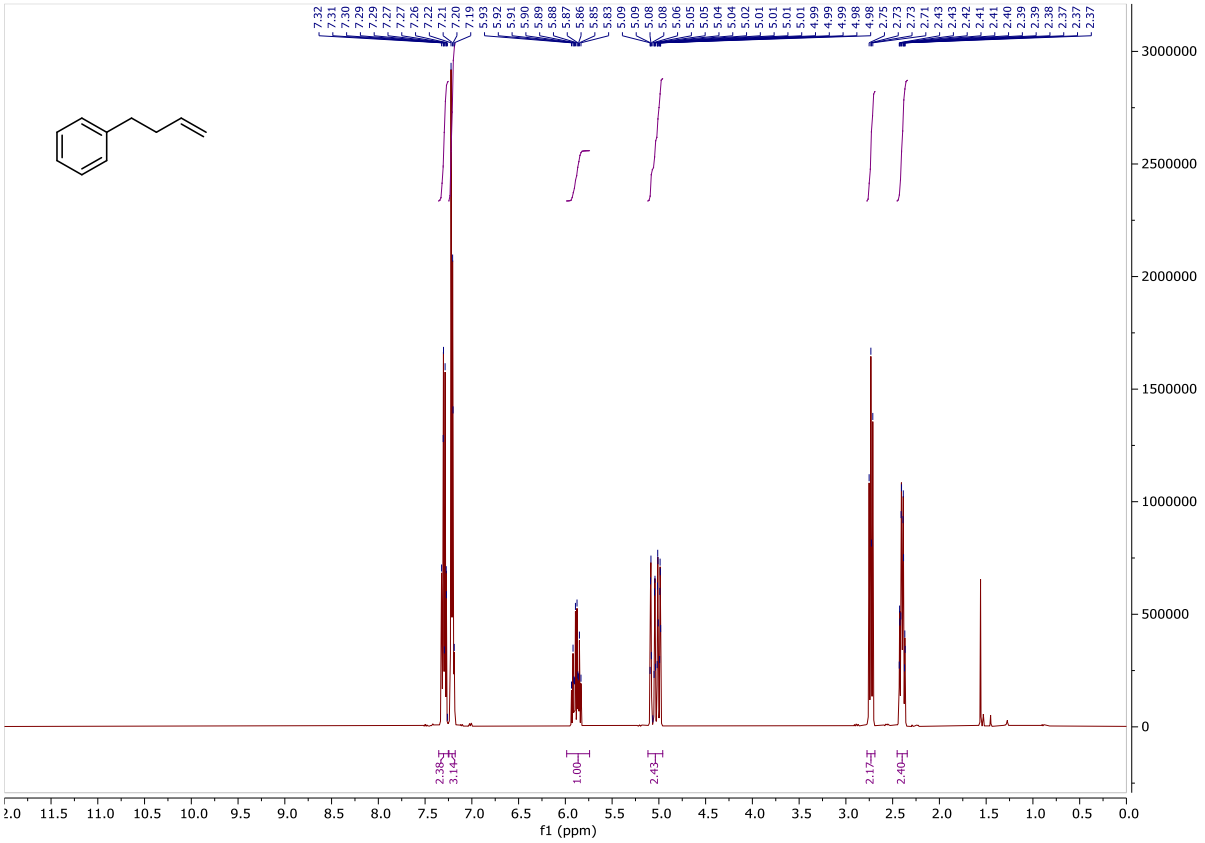

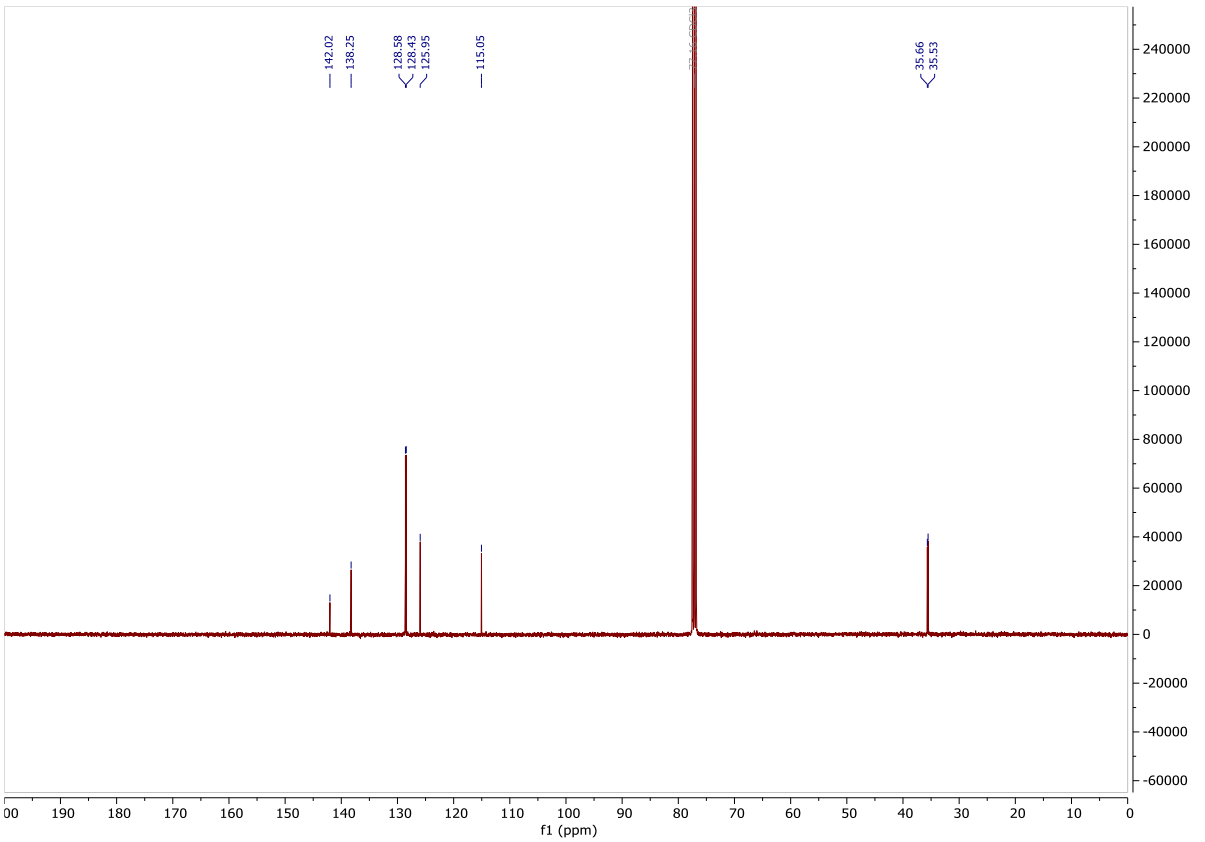

But-3-en-1-yl benzoate (175)

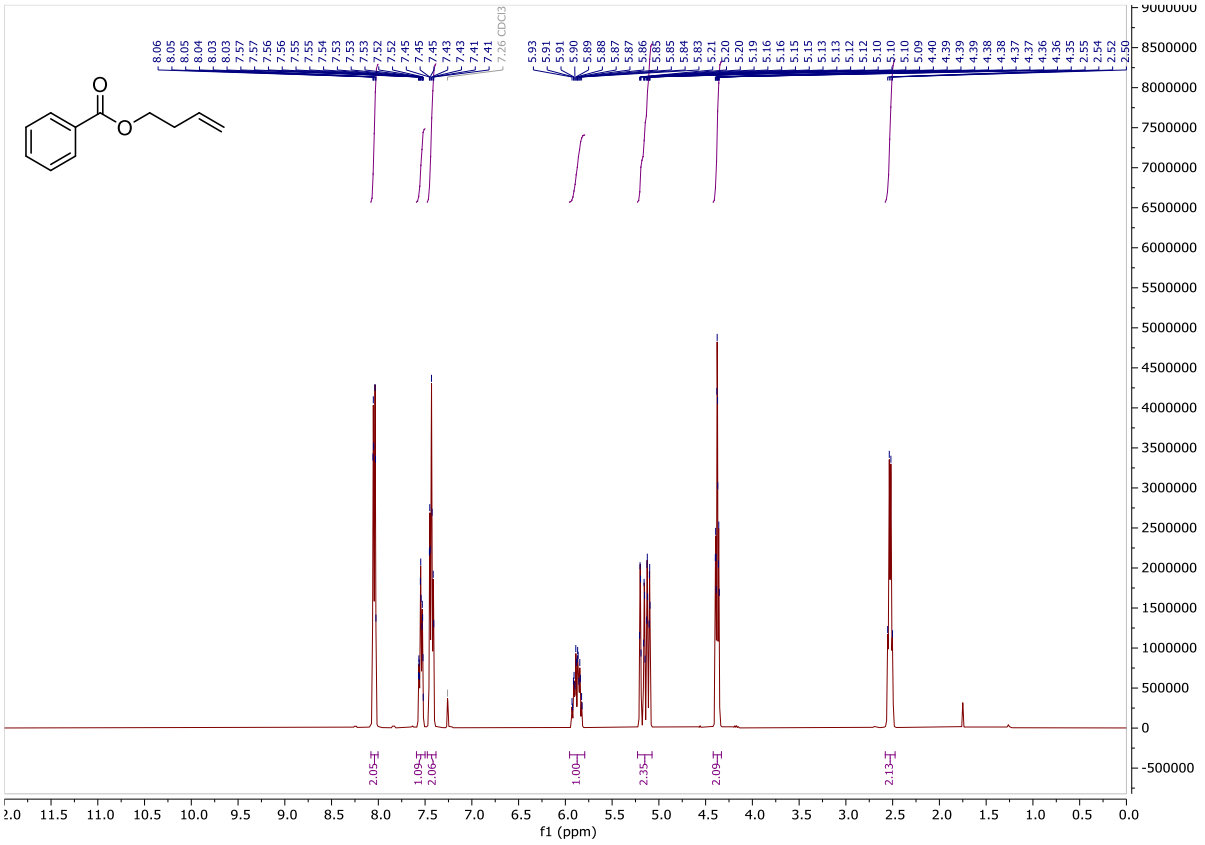

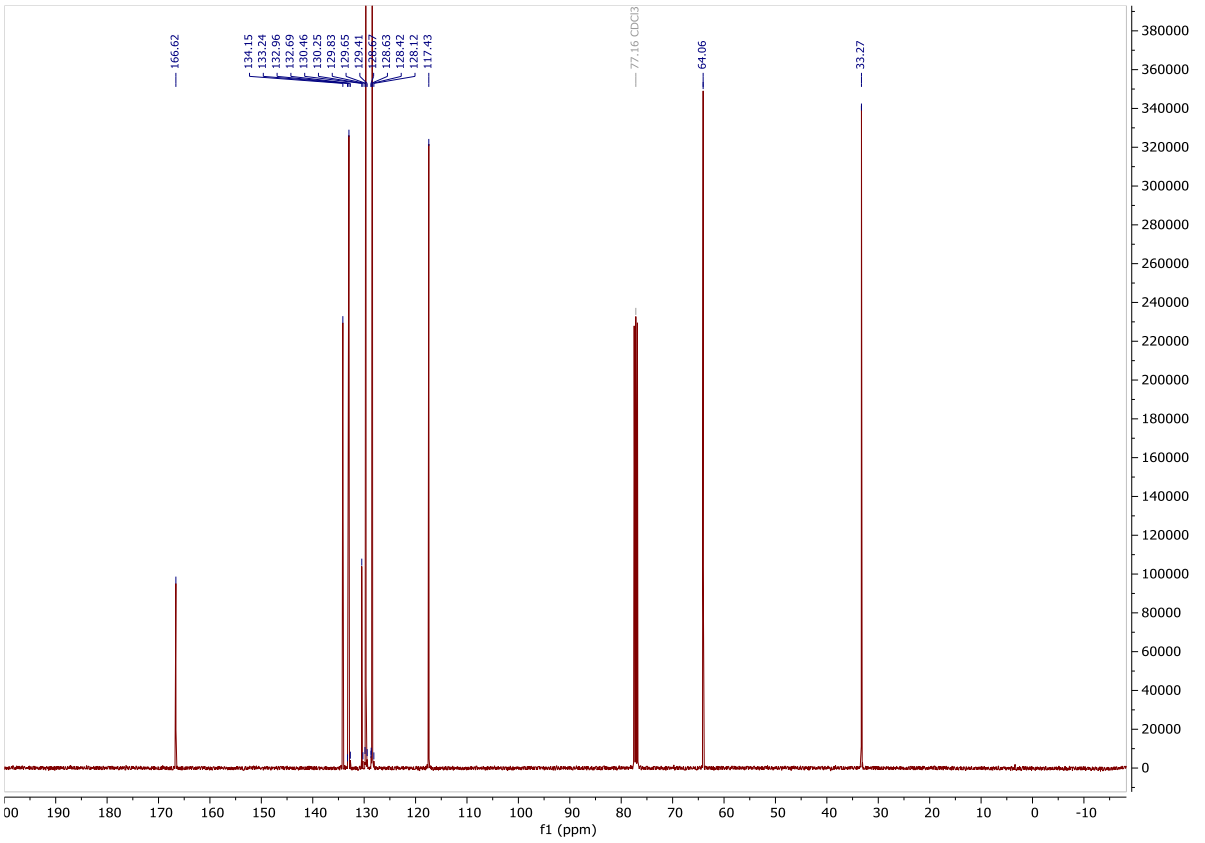

(4-(Pent-4-en-1-yloxy)butyl)benzene (176)

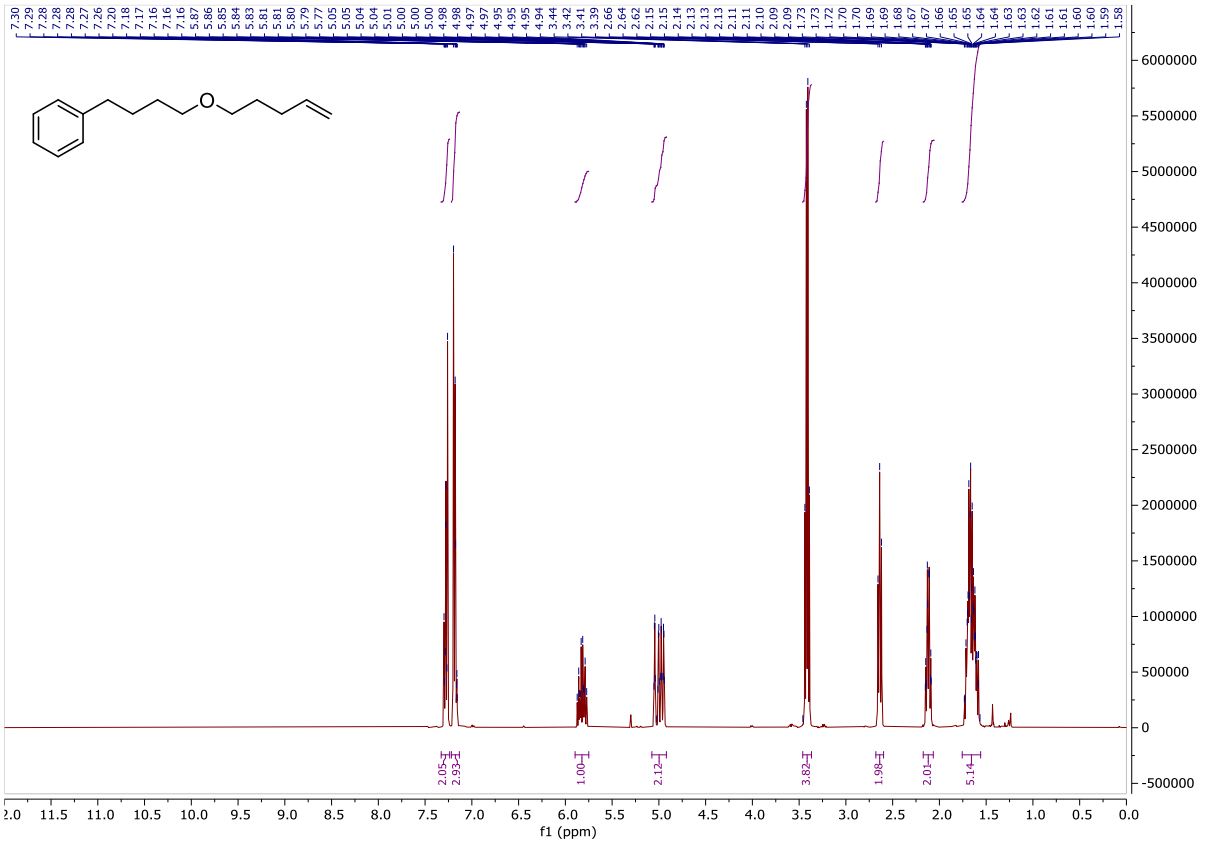

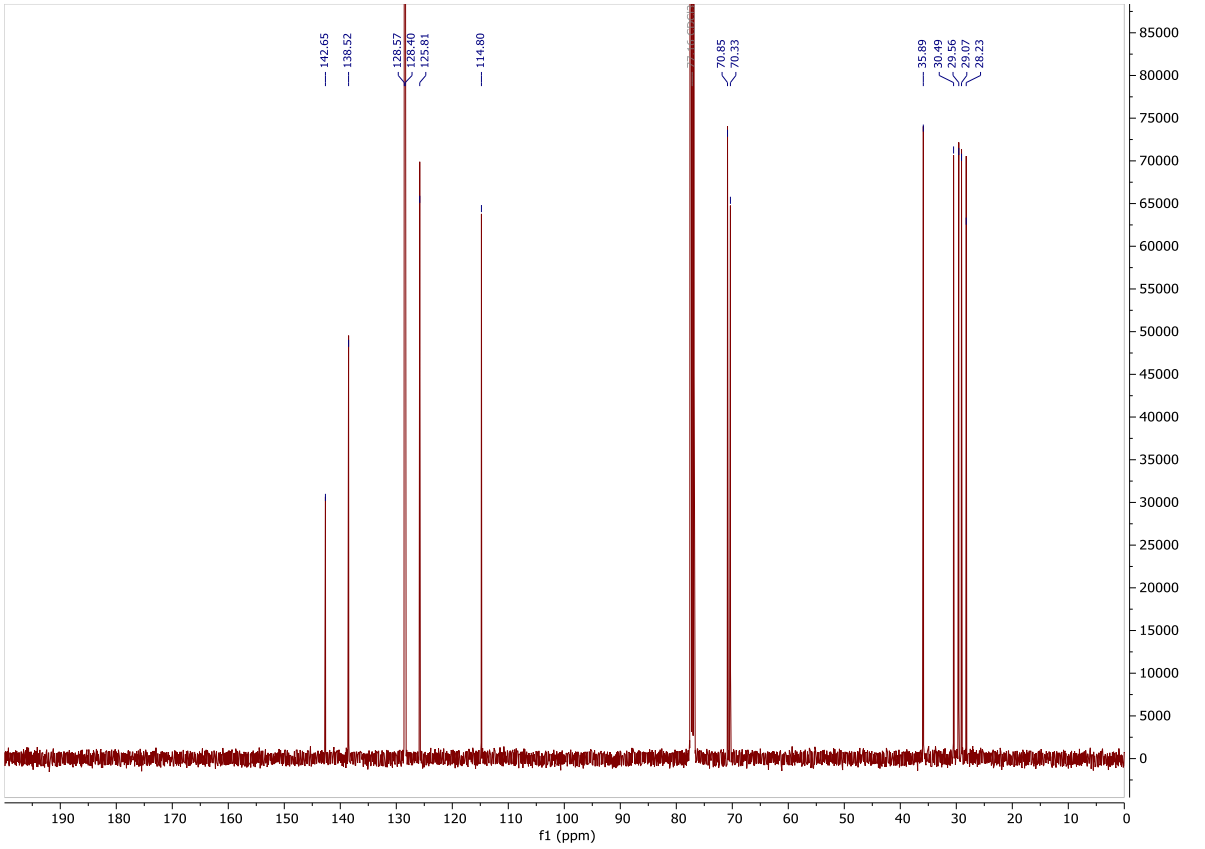

((But-3-en-1-yloxy)methylene)dibenzene (234)

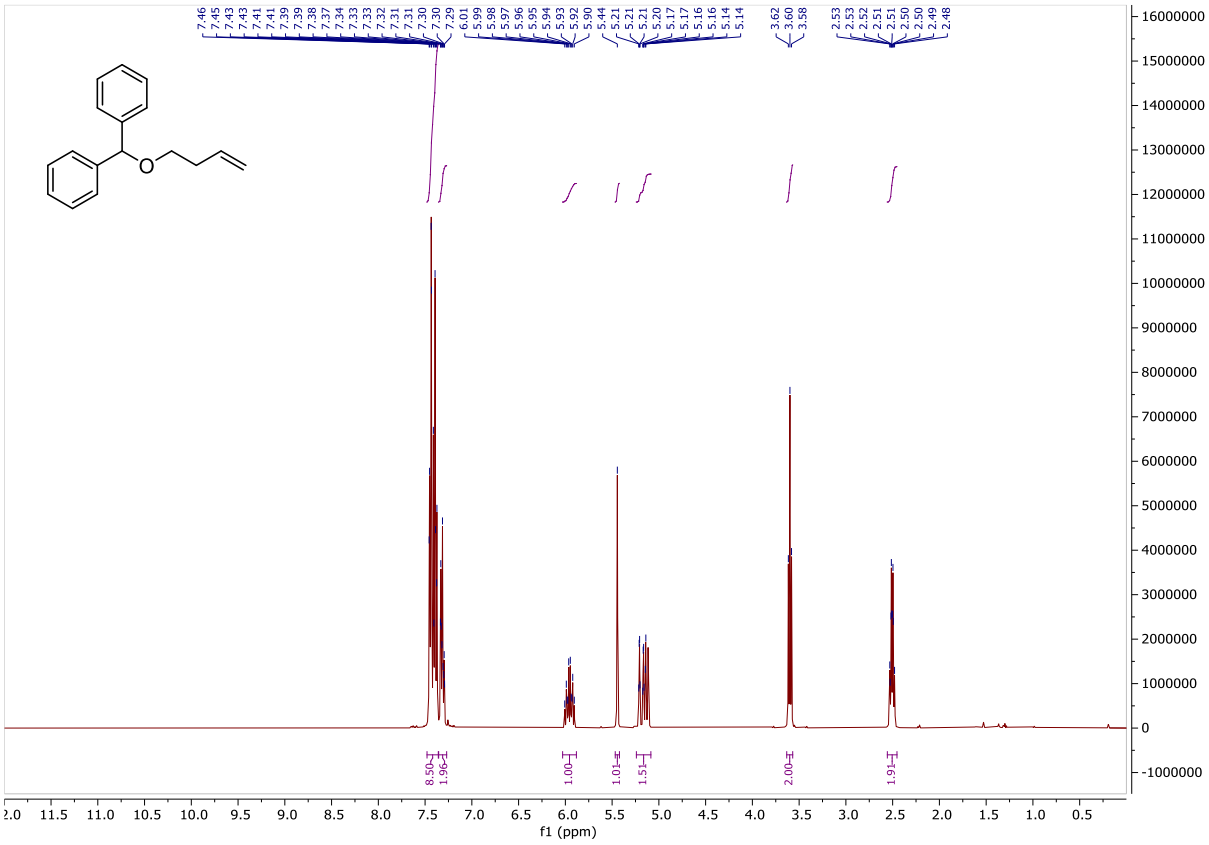

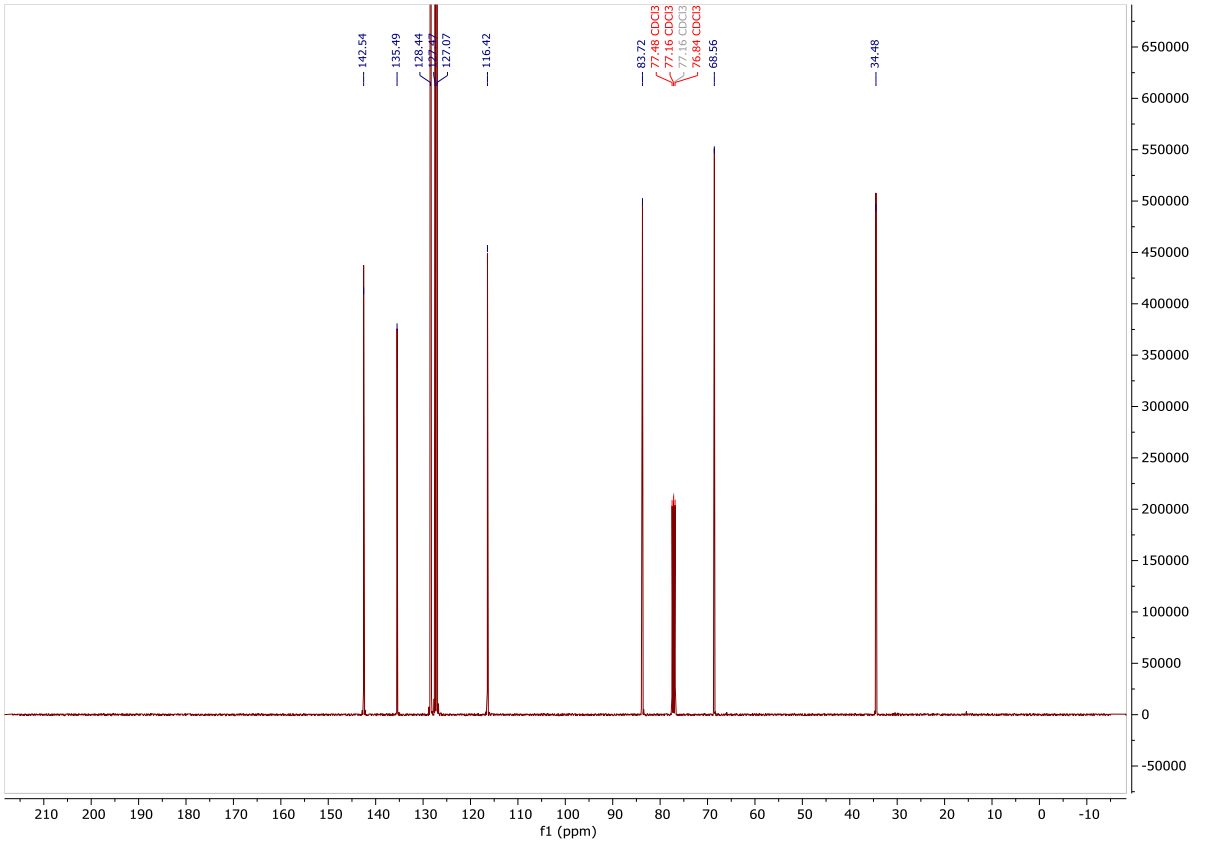

N-(2-bromophenyl)acetamide (240)

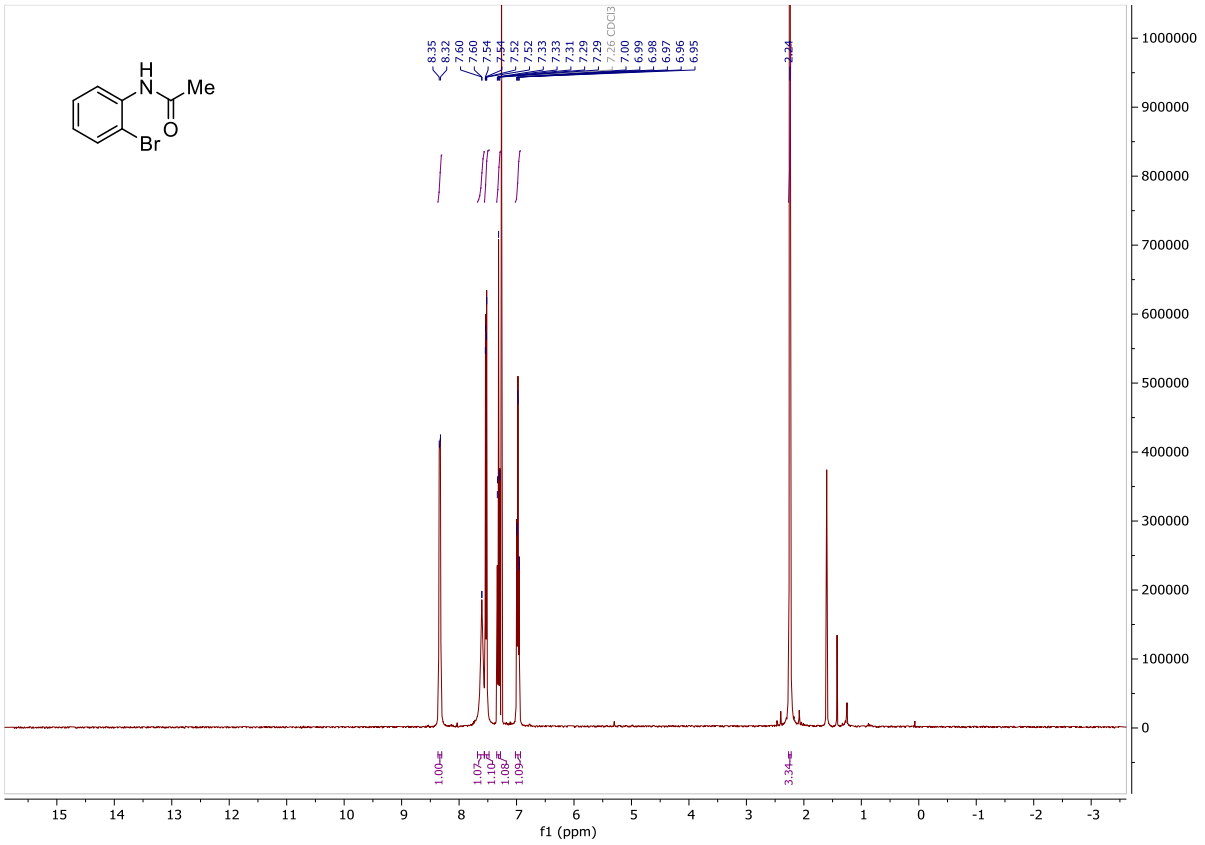

tert-Butyl 3-(3-phenylpropylidene)azetidine-1-carboxylate (233)

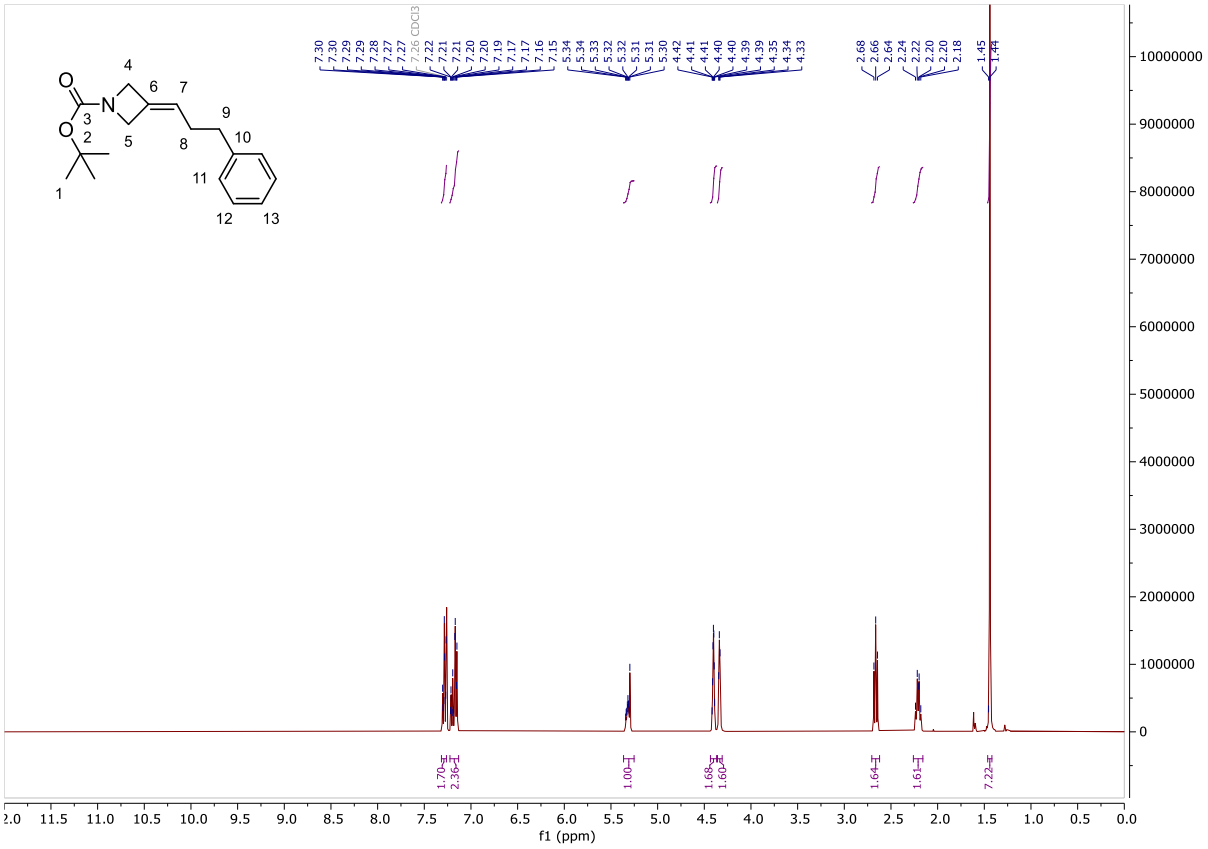

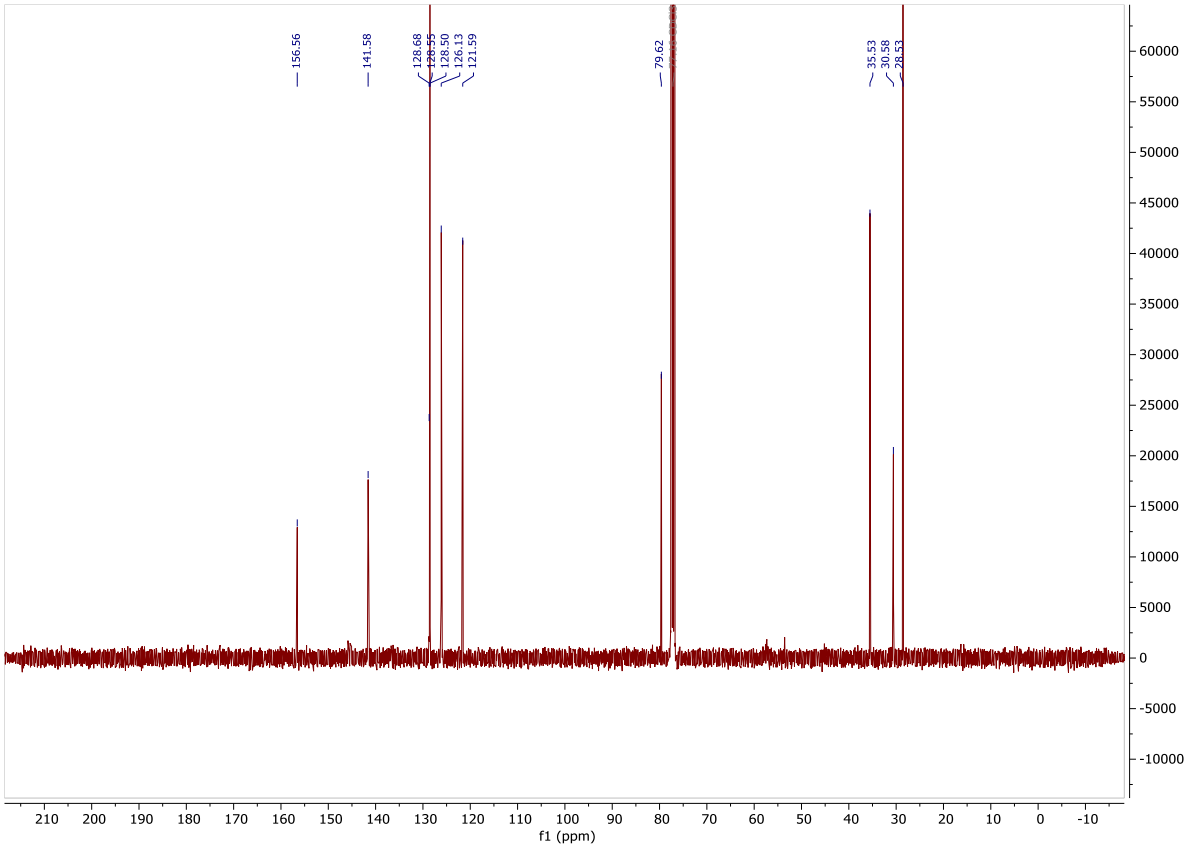

N-allyl-N-(2-bromophenyl)acetamide (235)

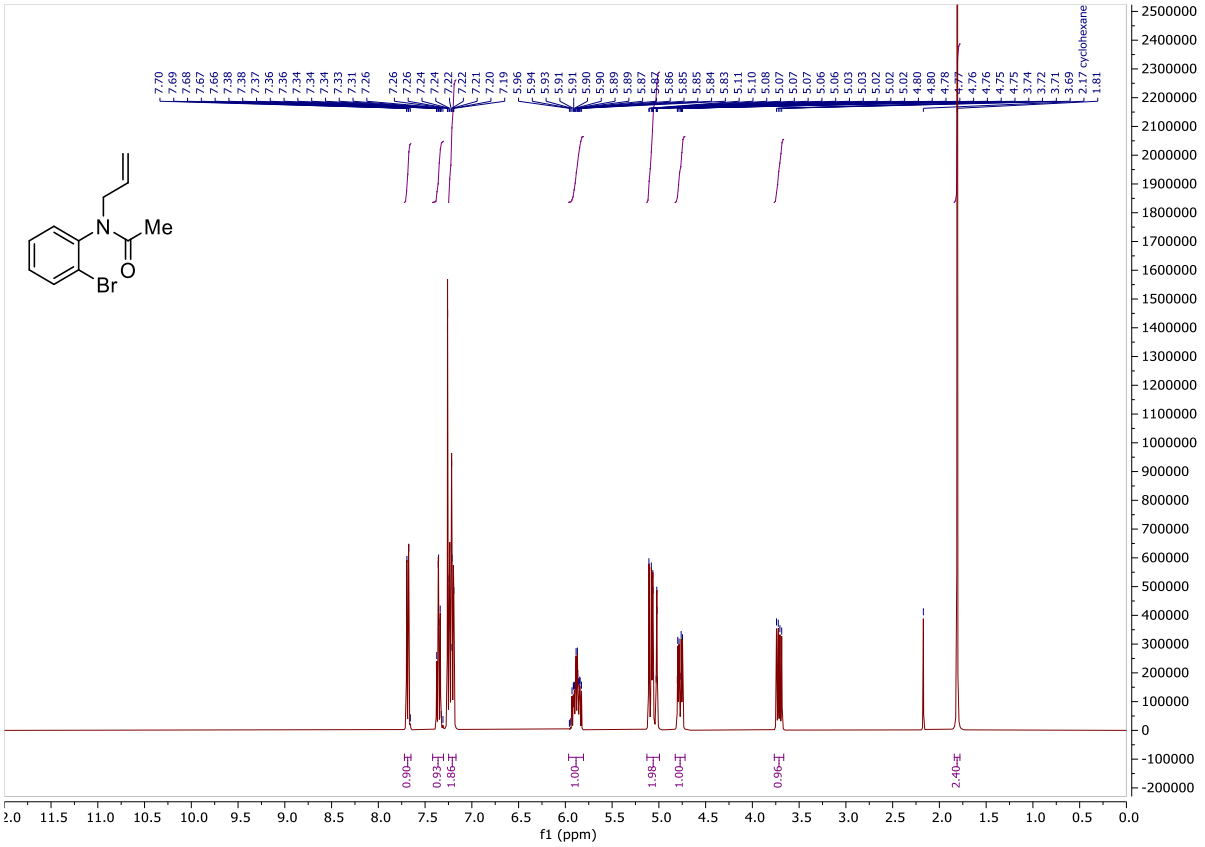

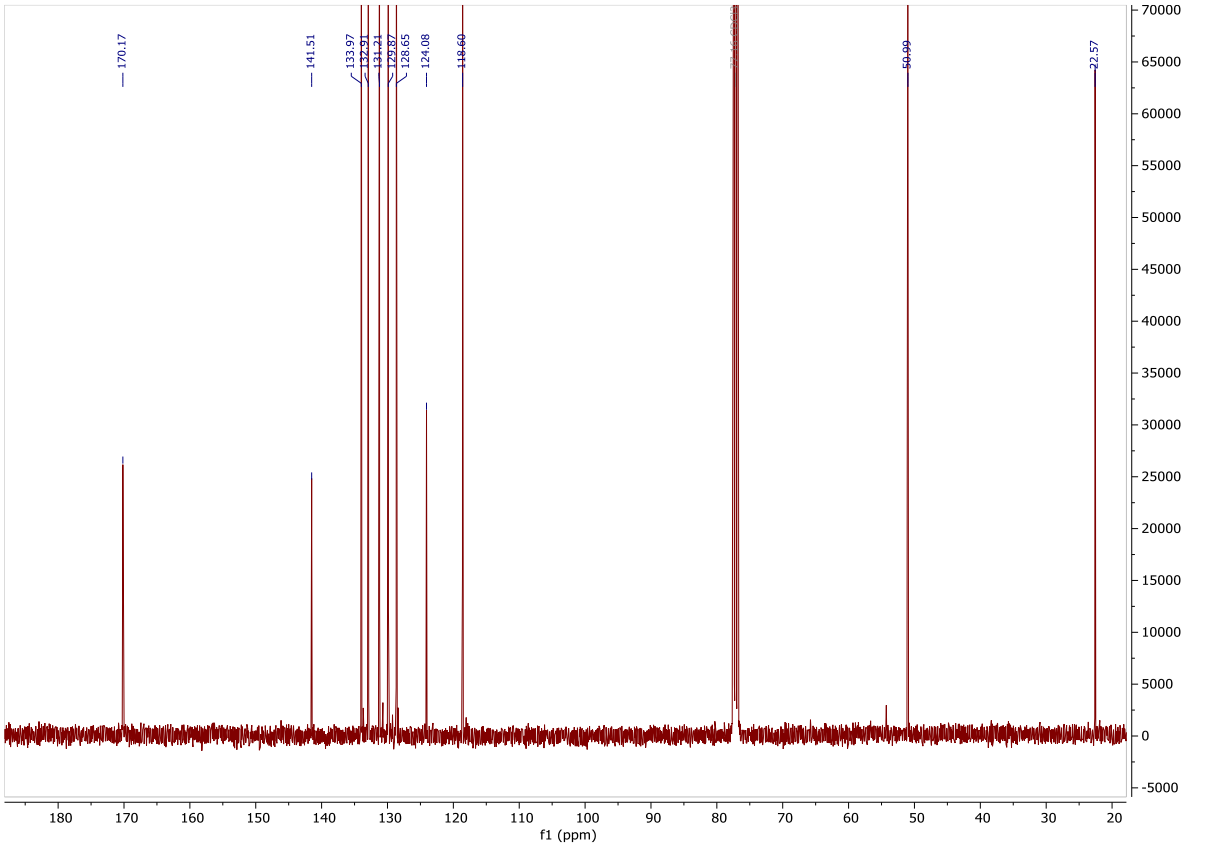

4-Methylpent-3-en-1-yl benzoate (236)

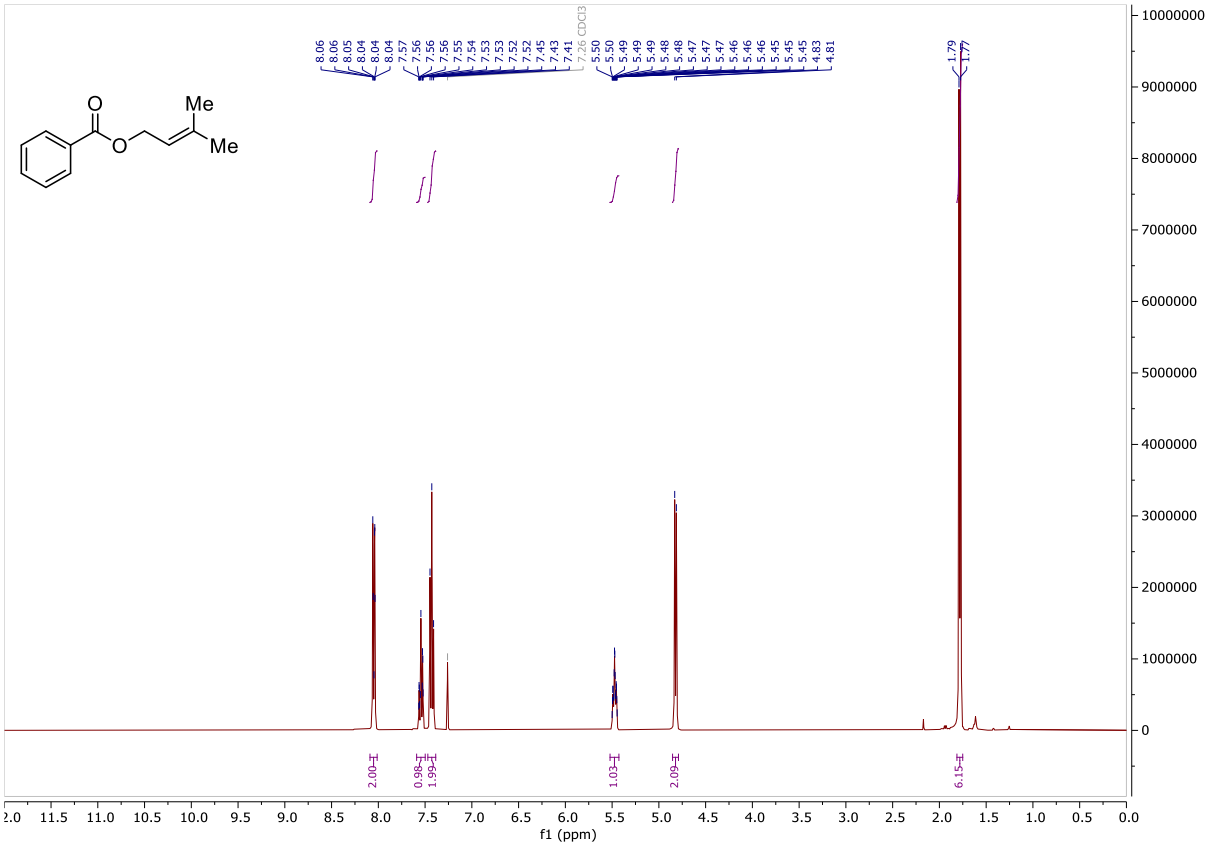

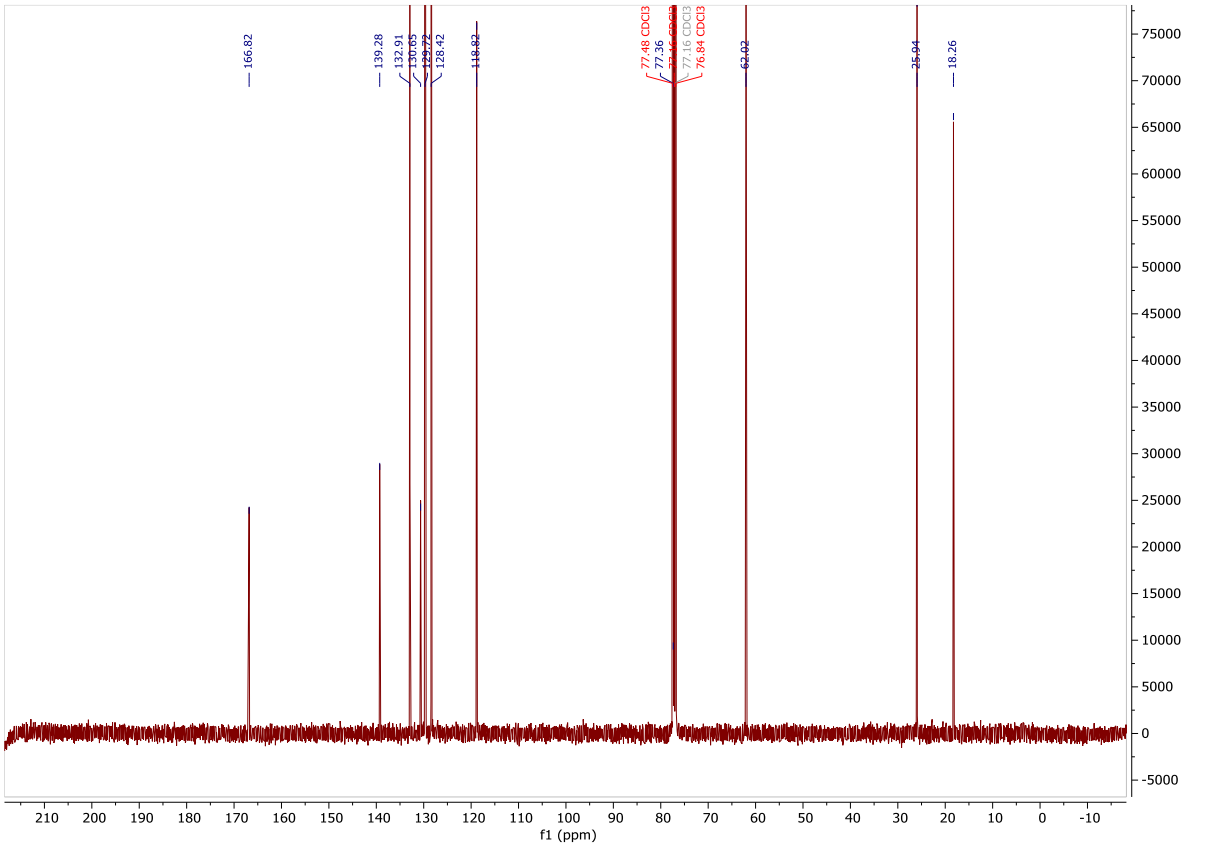

4-Phenylbutyl acrylate (223)

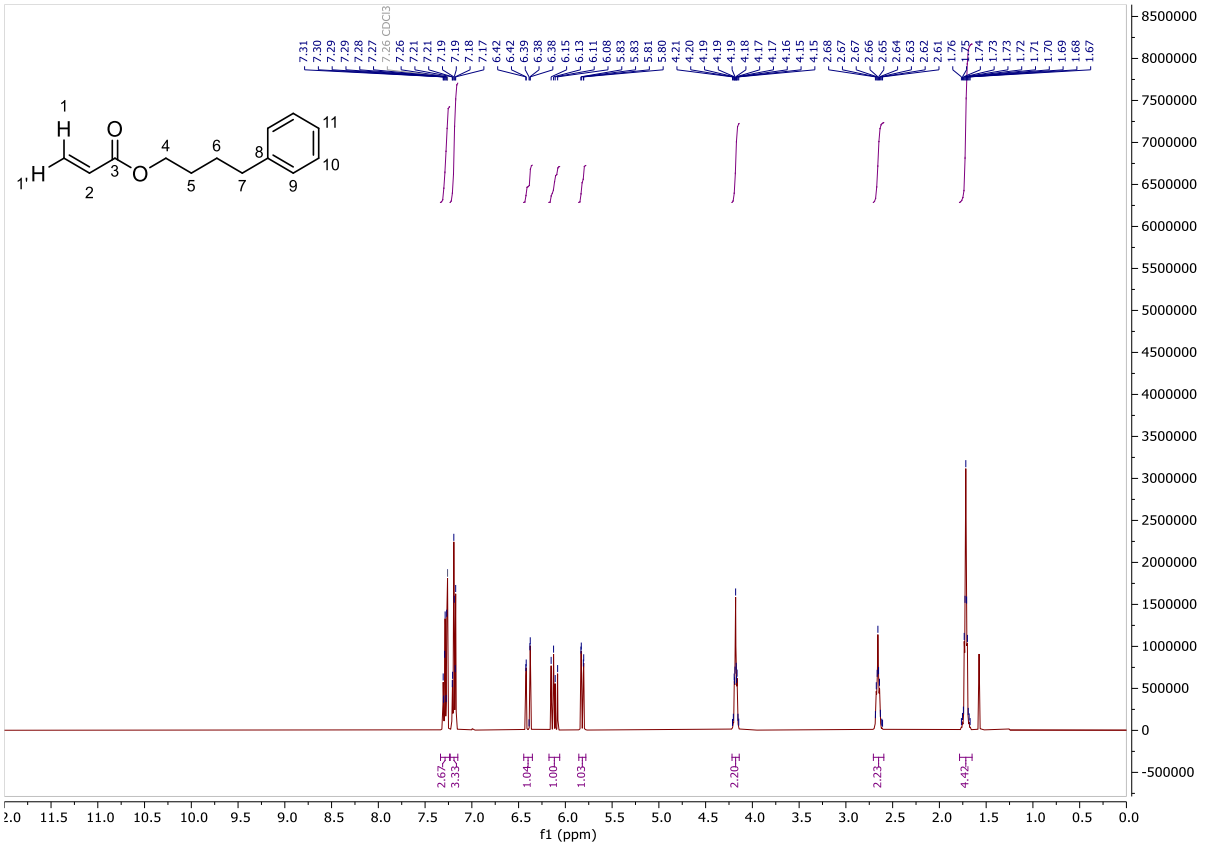

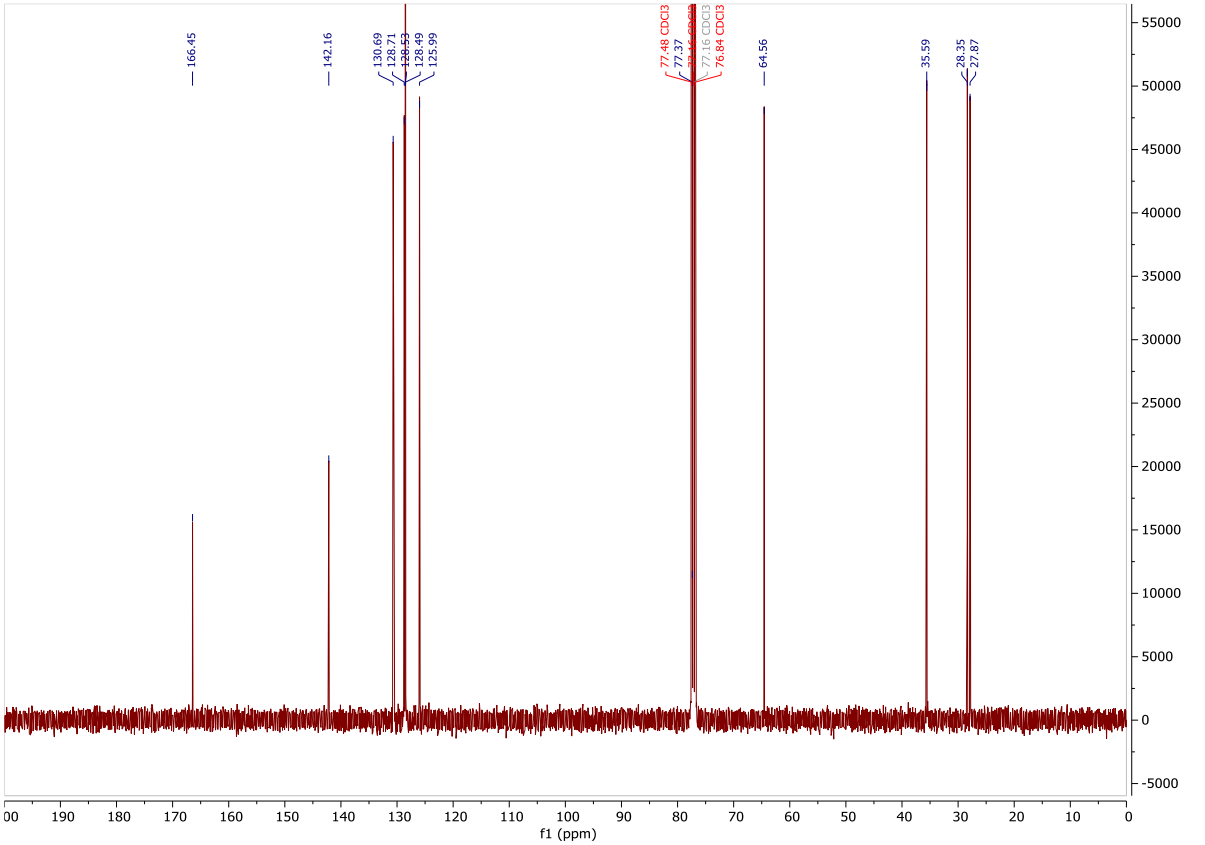

(1R,2S,5R)-2-isopropyl-5-methylcyclohexyl acrylate (225)

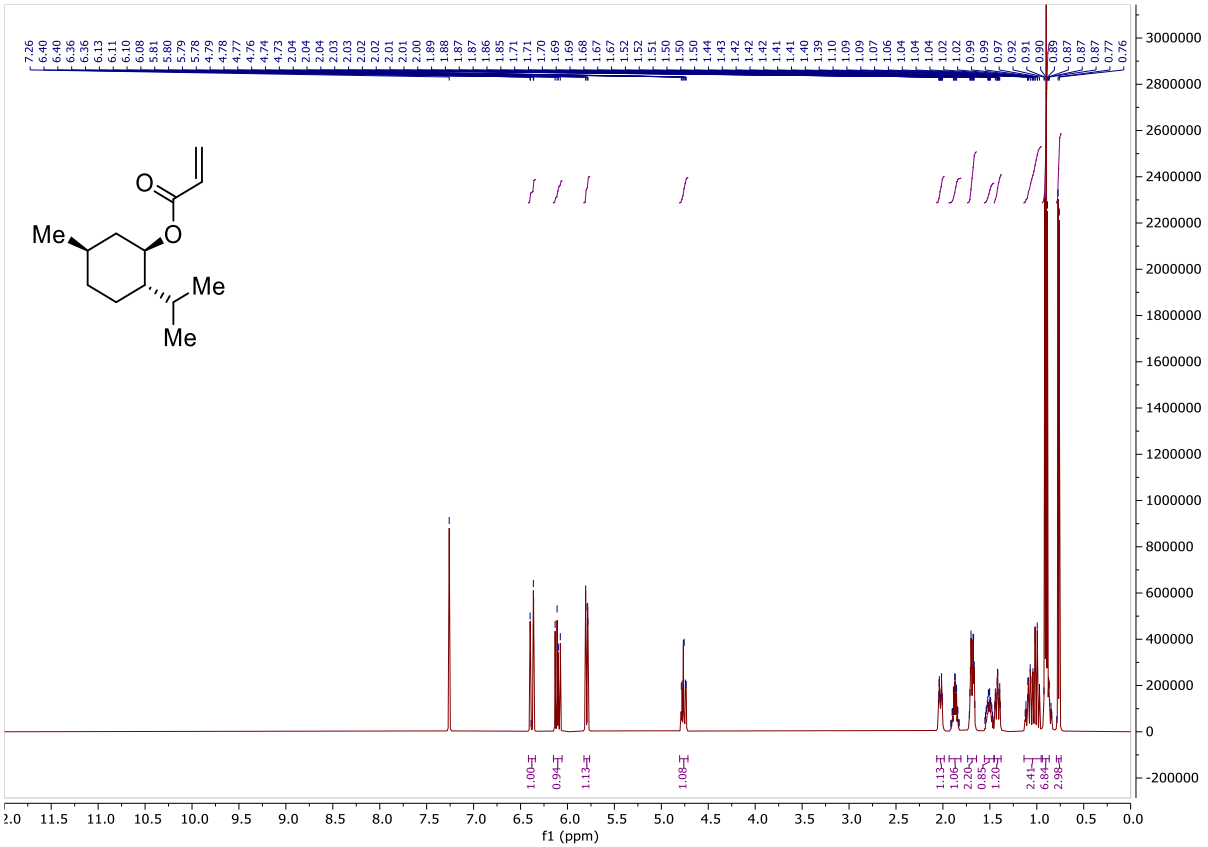

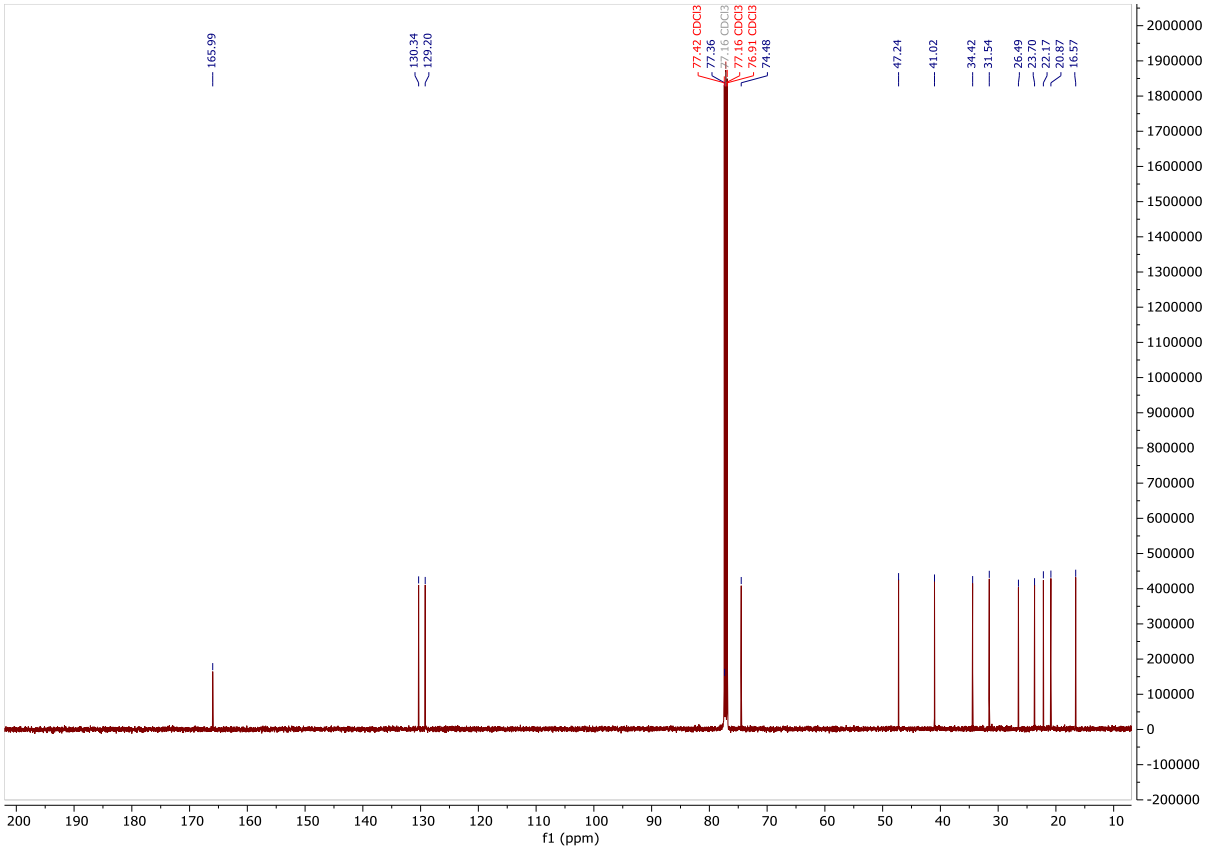

(1S,2R)-1,7,7-trimethylbicyclo[2.2.1]heptan-2-yl acrylate (227)

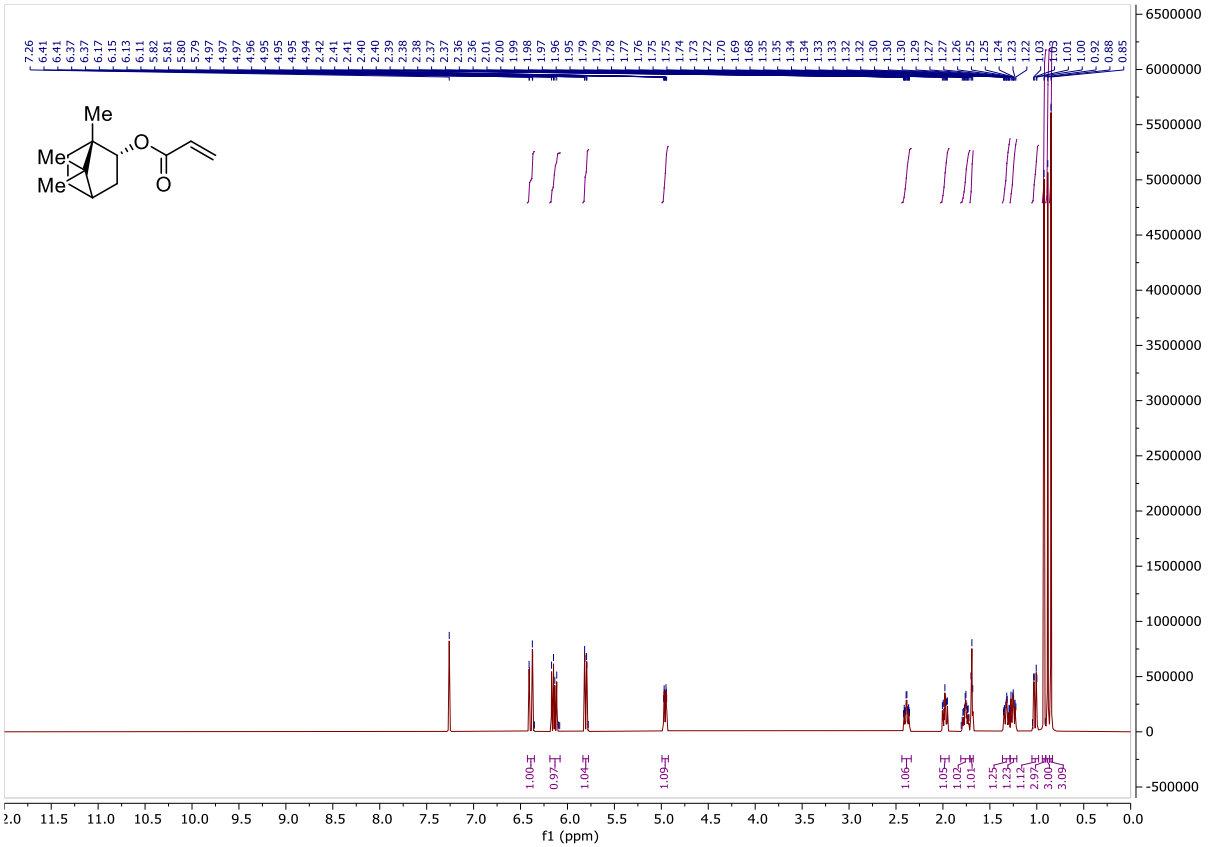

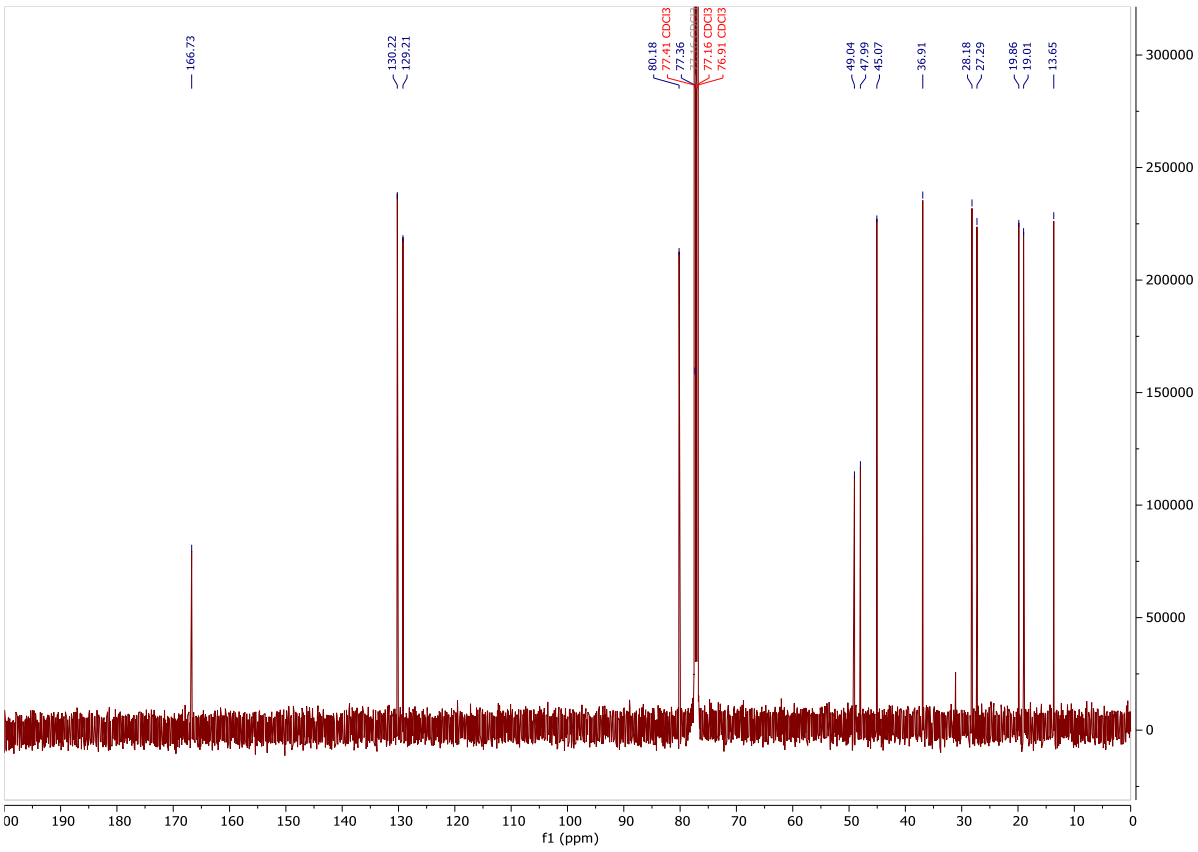

4-(tert-Butyl)phenyl acrylate (237)

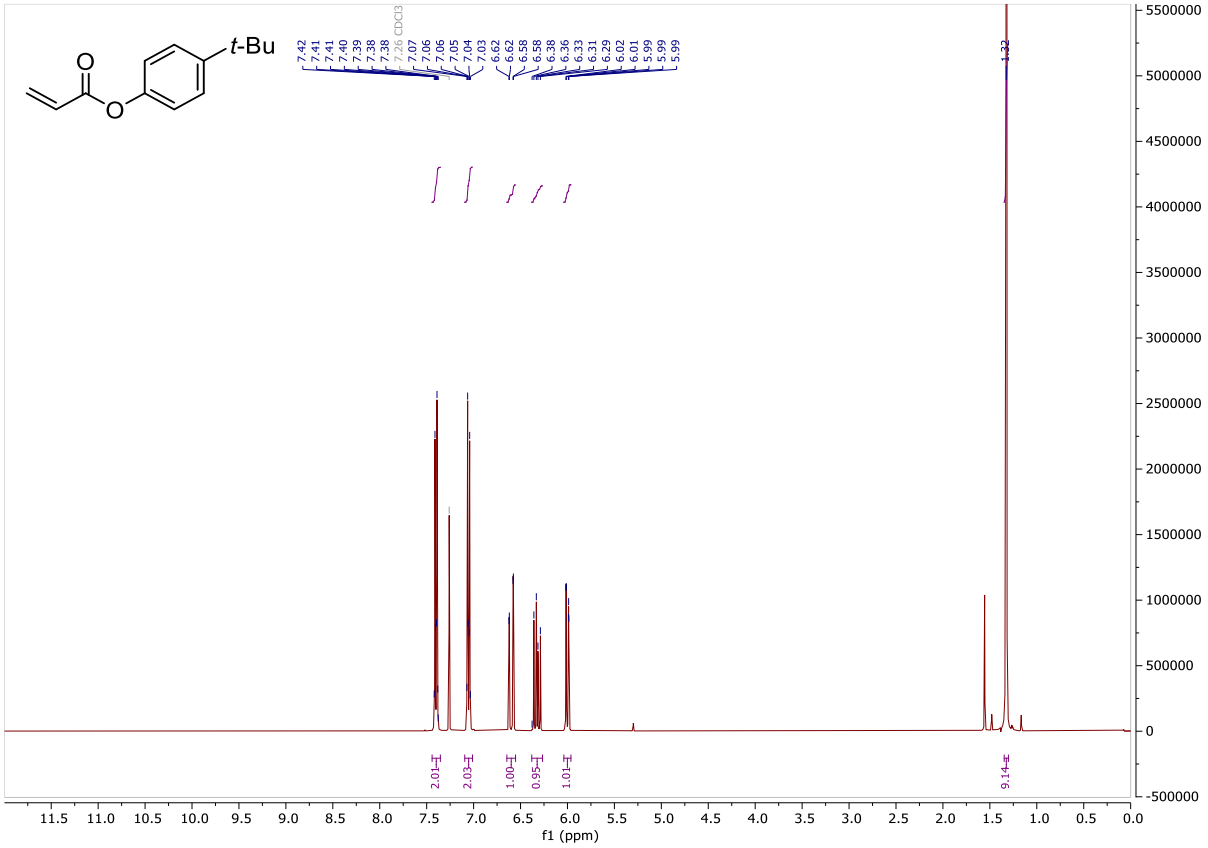

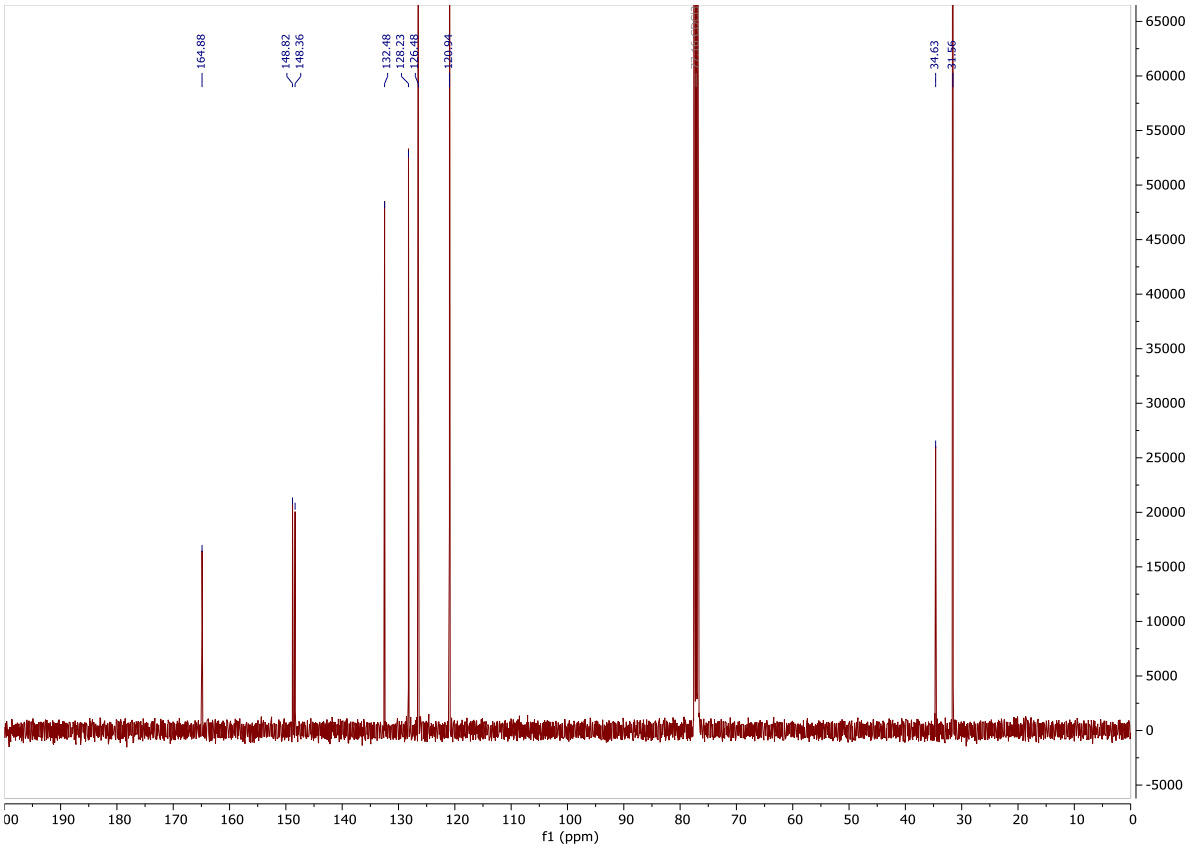

4-Bromophenyl acrylate (238)

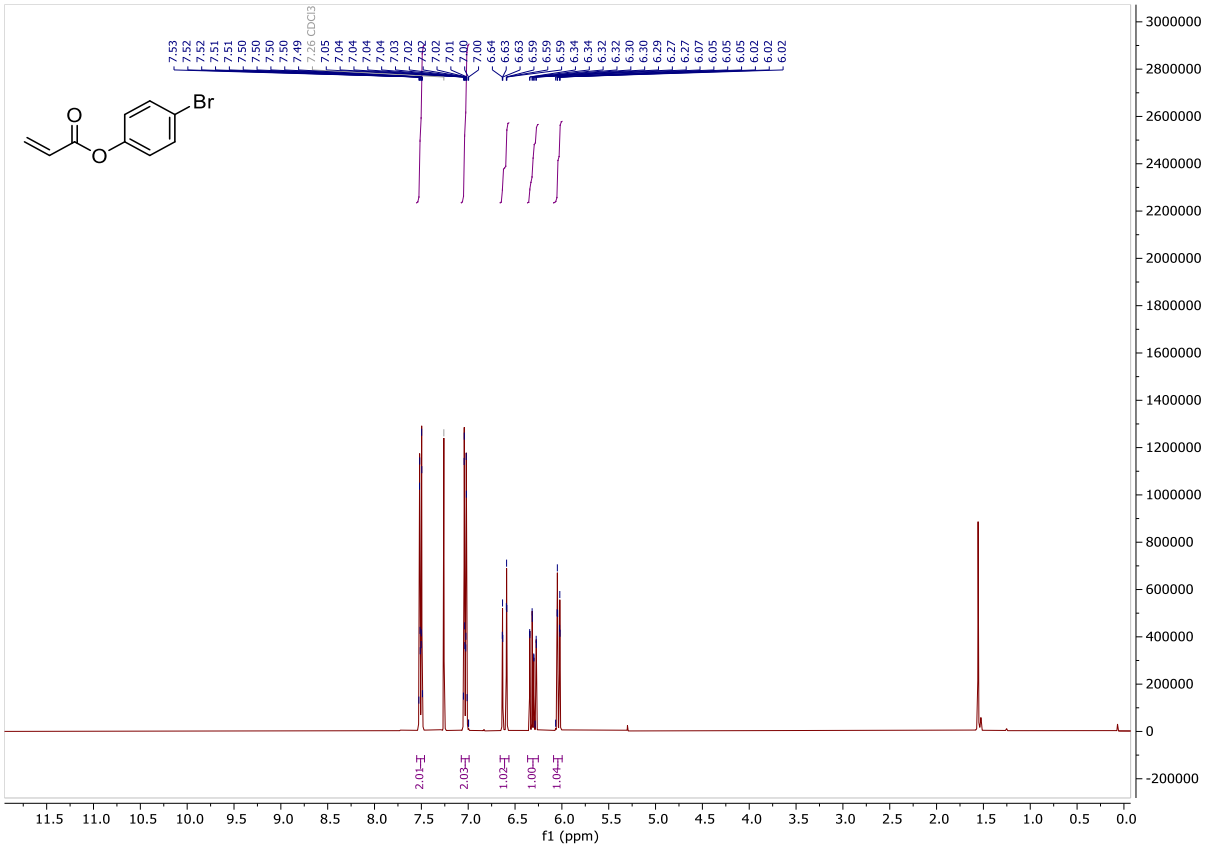

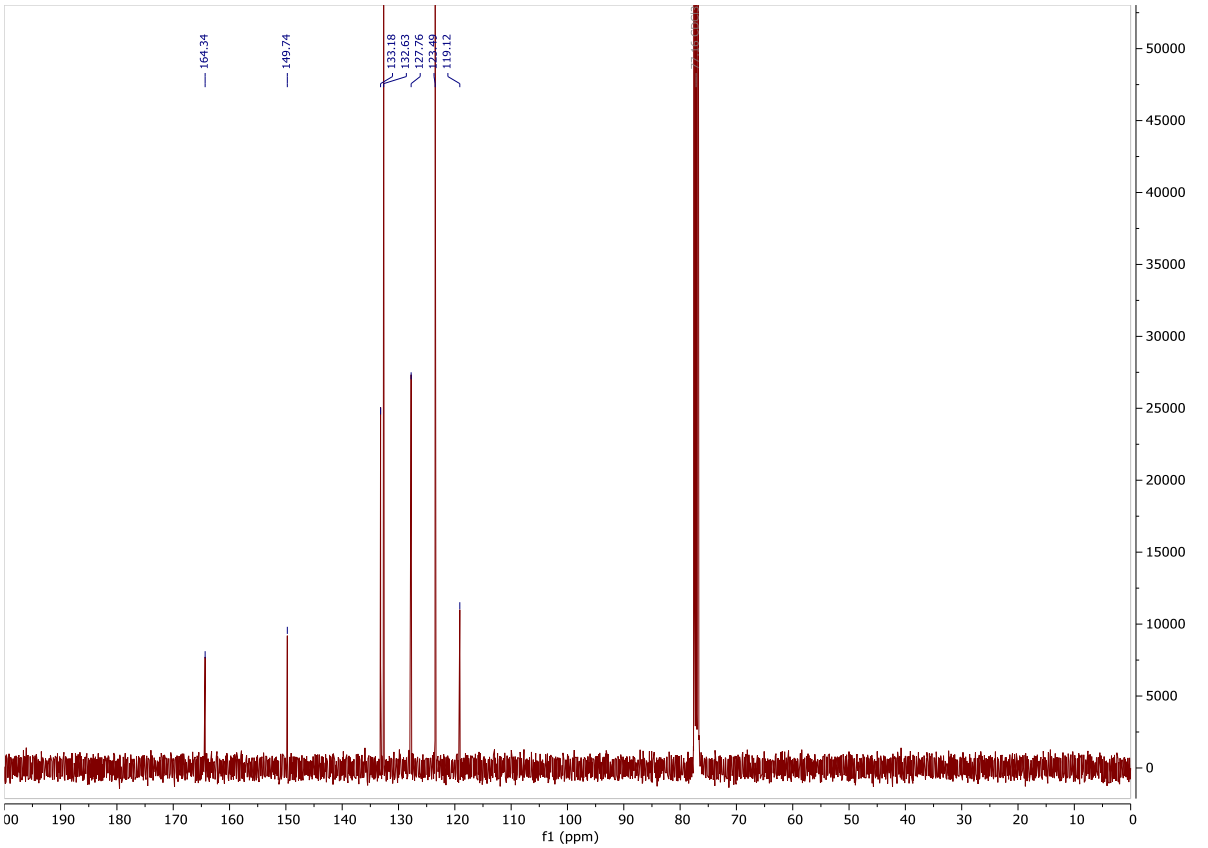

2-Chorophenyl acrylate (239)

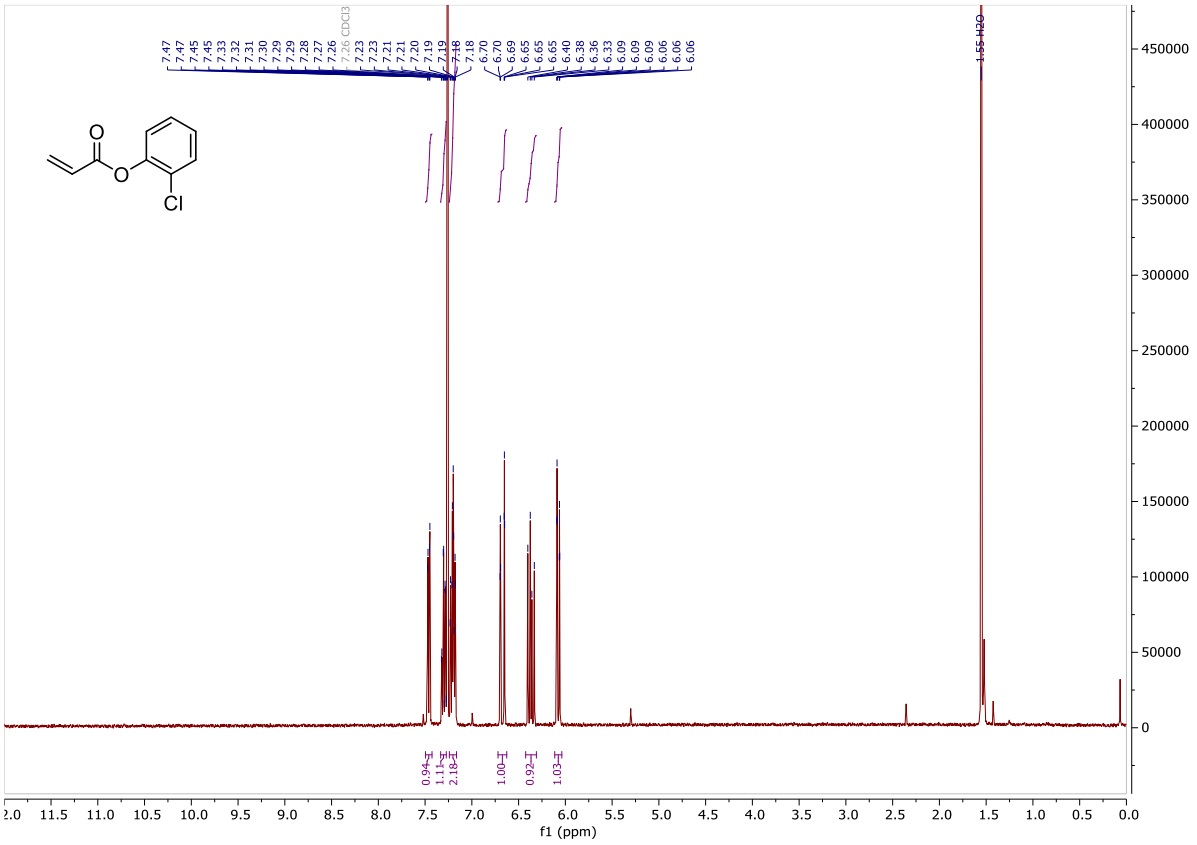

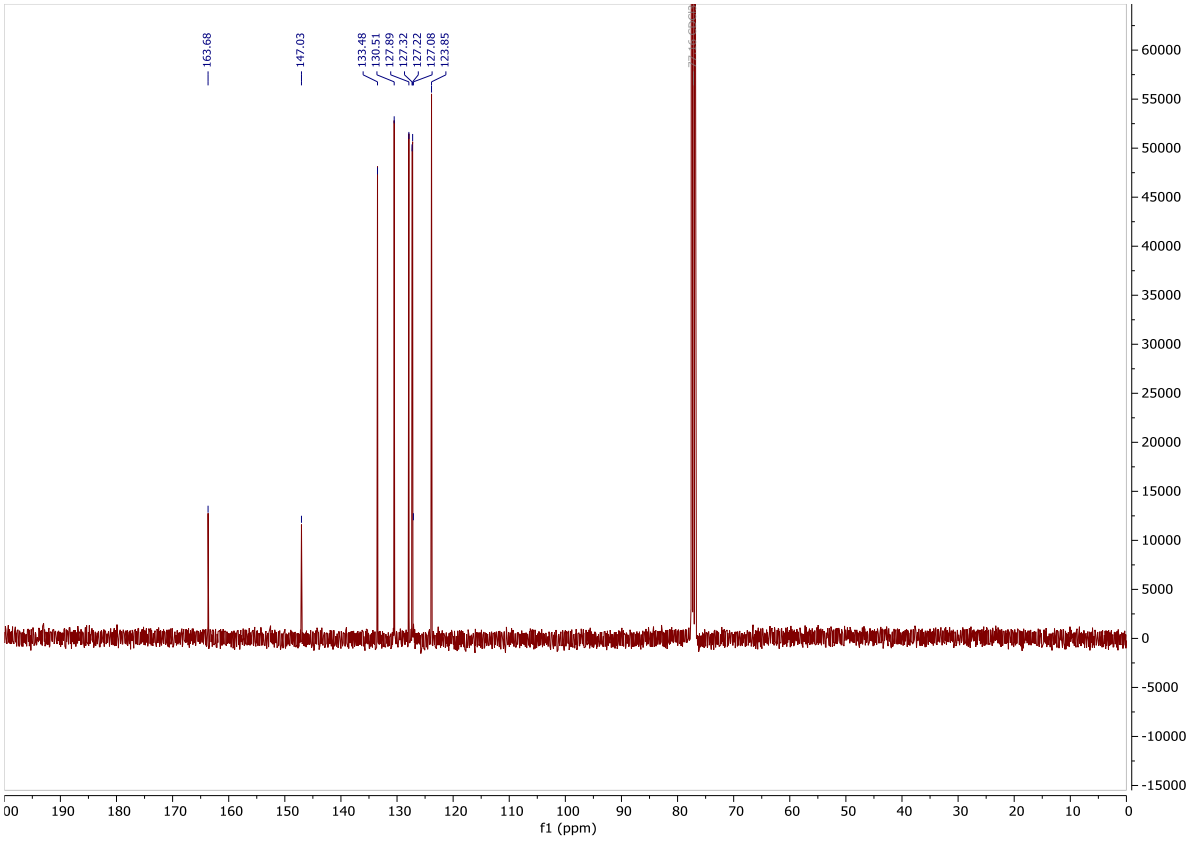

Alkanes

Methyl undecanoate (179)

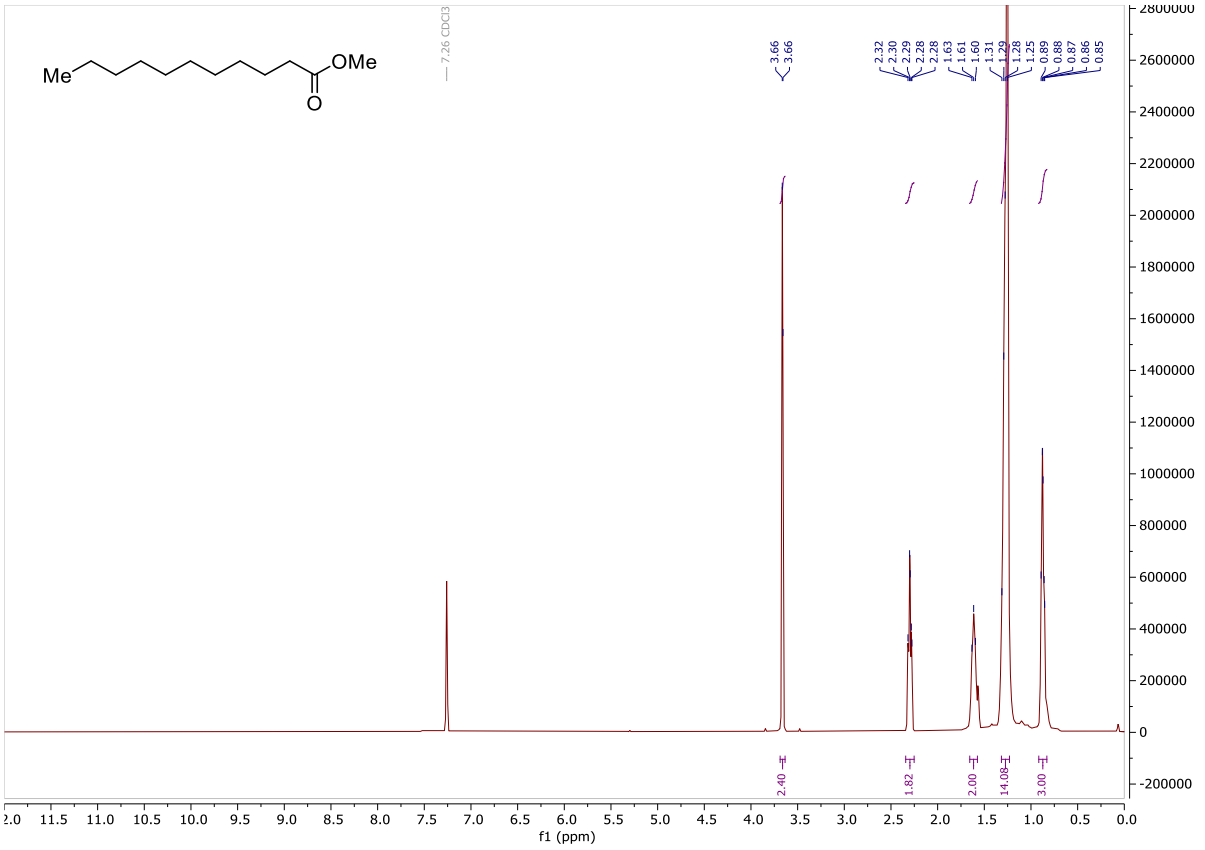

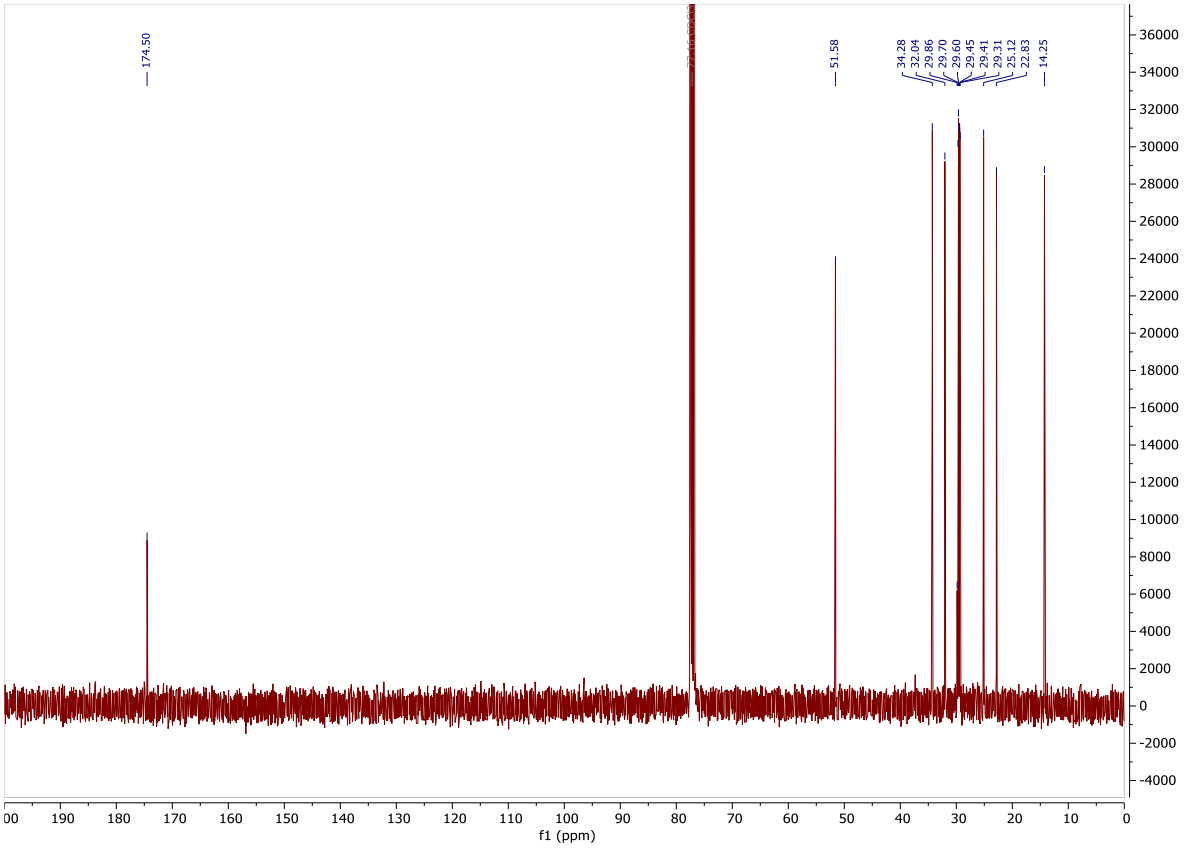

Butyl benzoate (211)

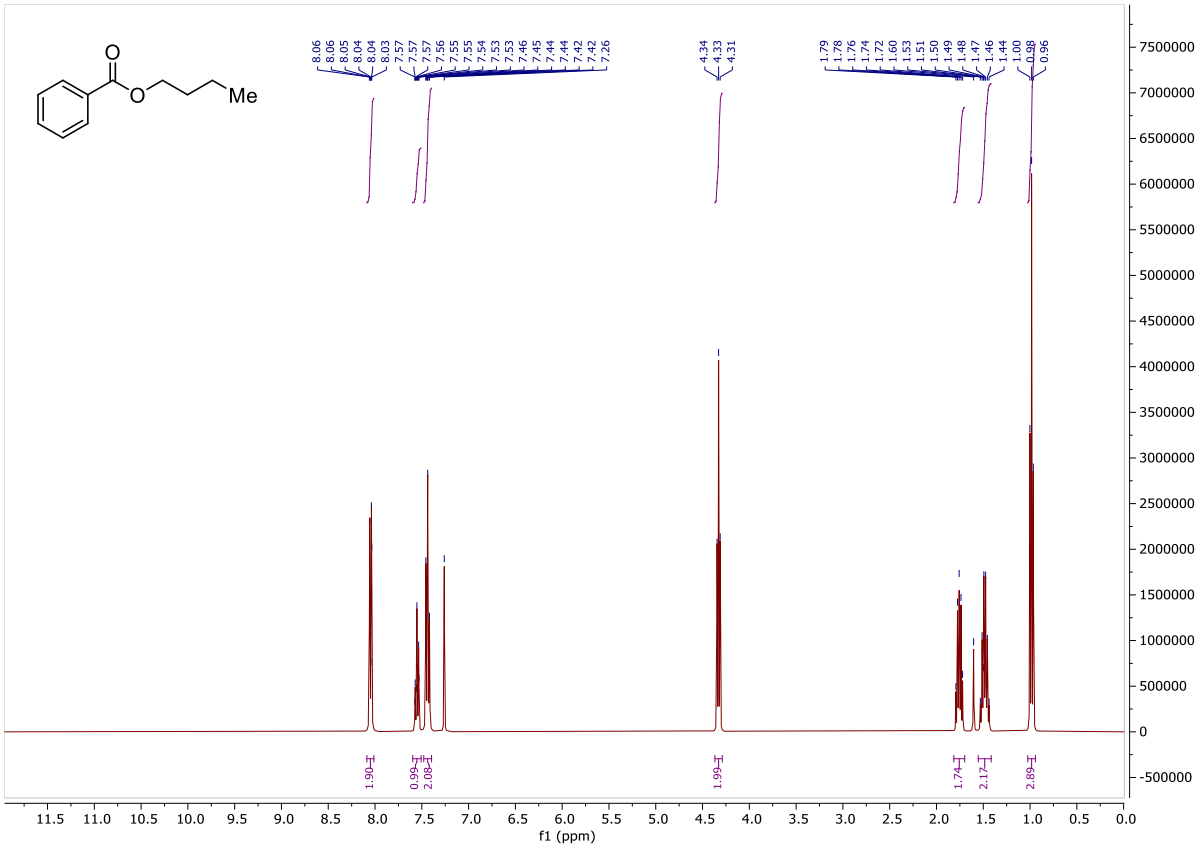

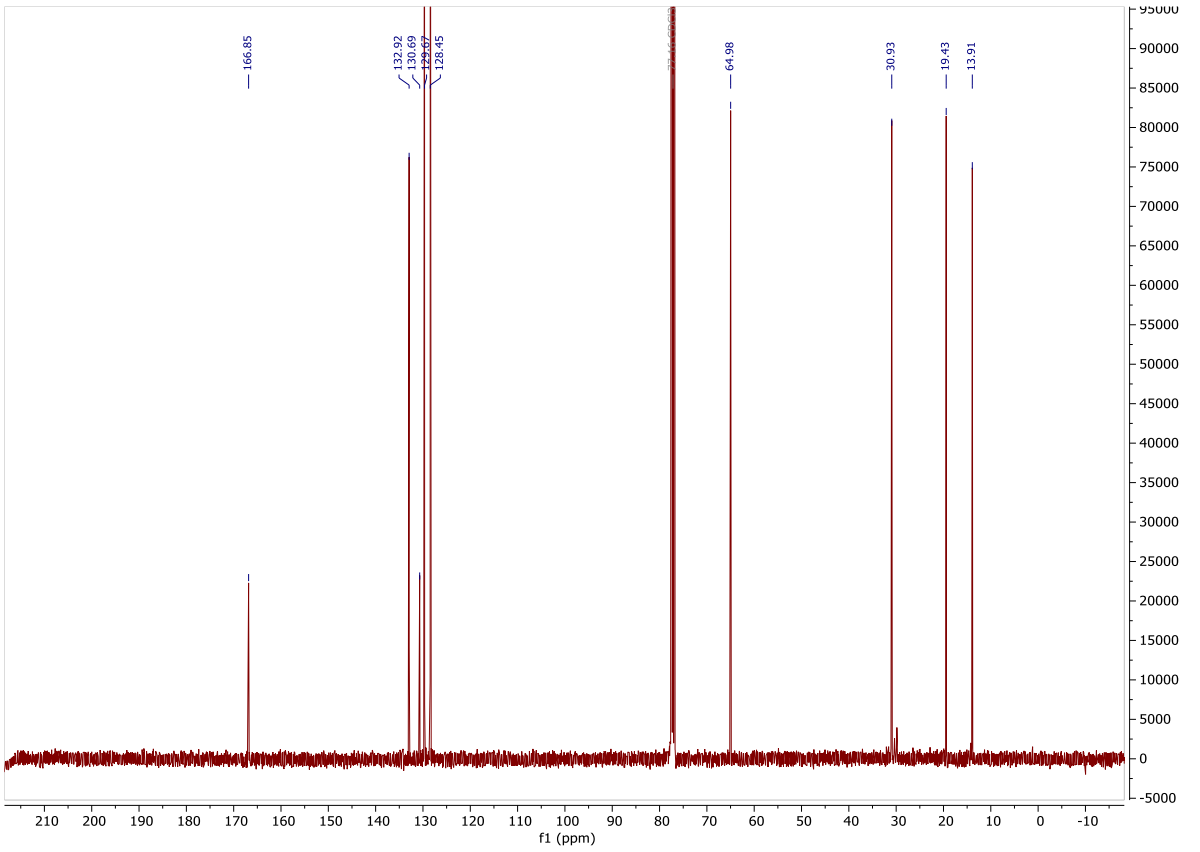

(4-(Pentyloxy)butyl)benzene (212)

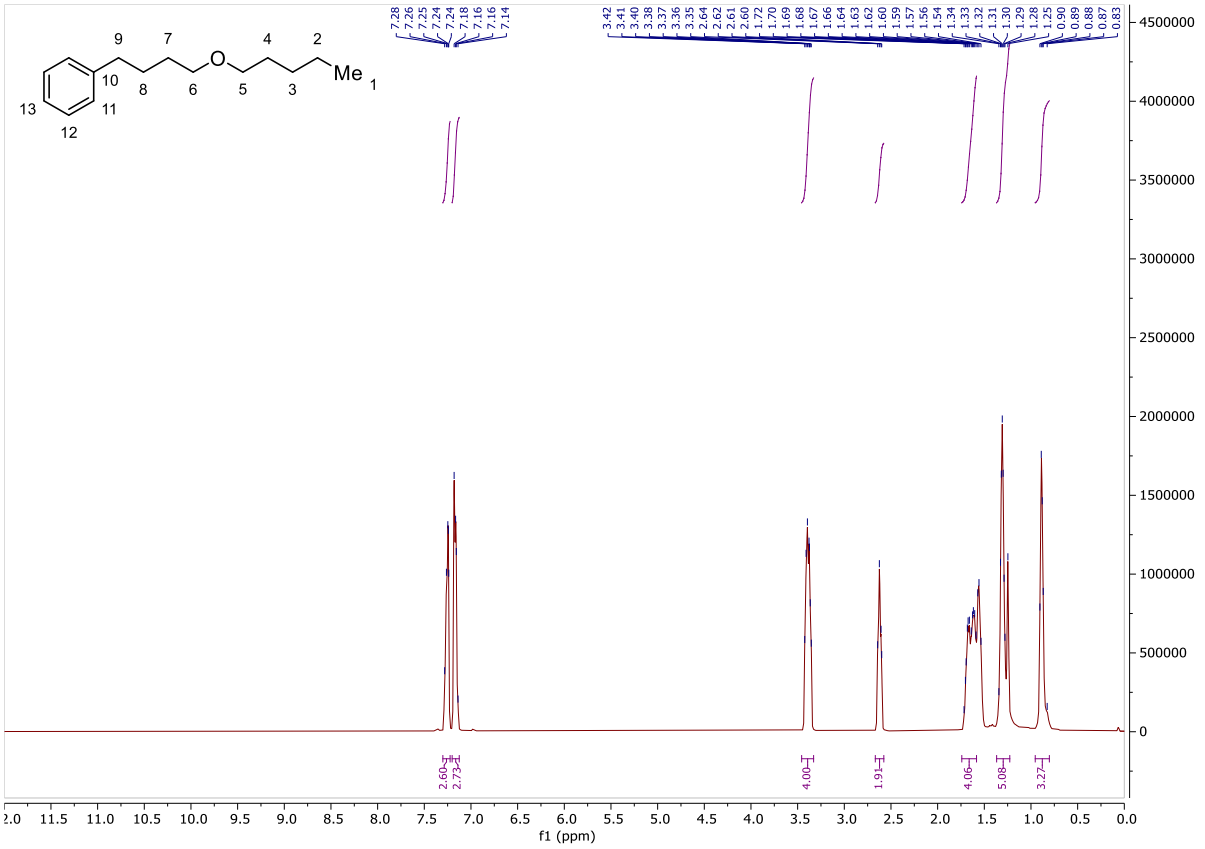

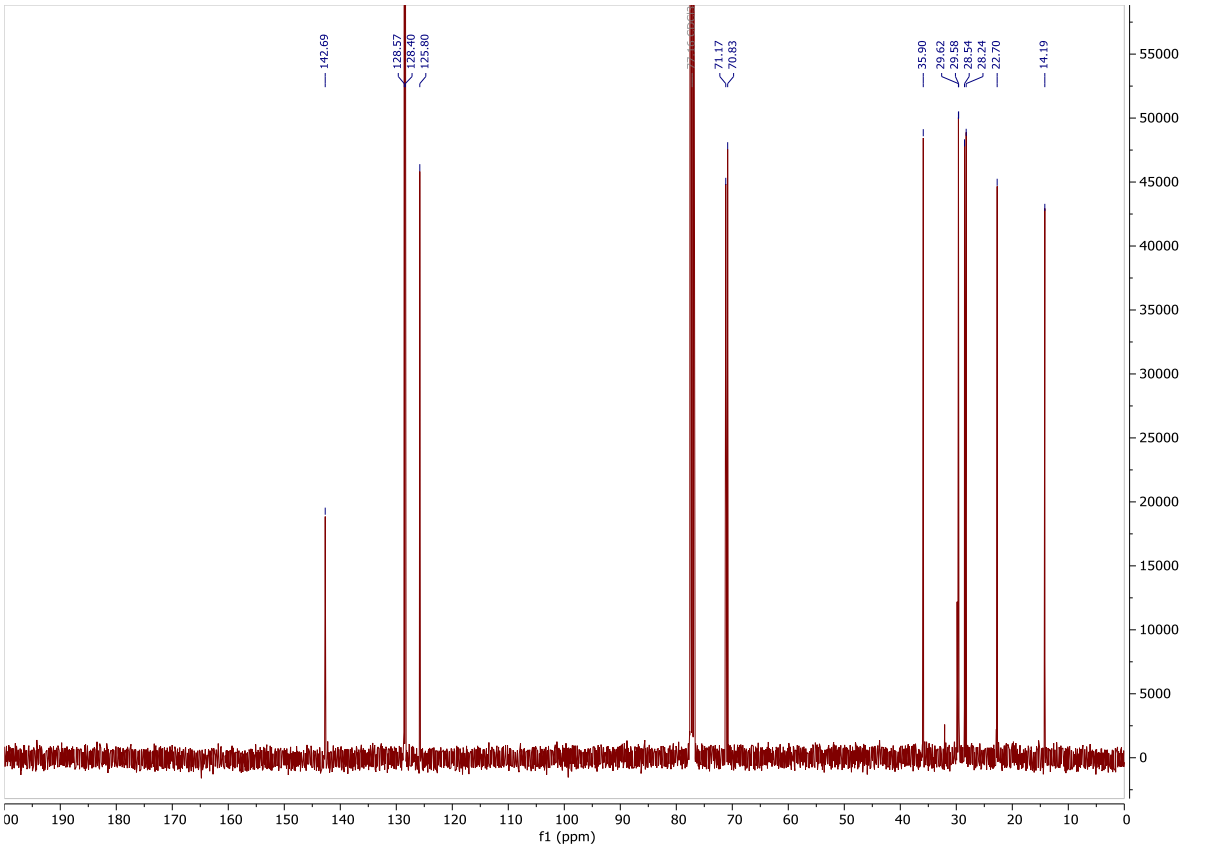

1-Bromo undecane (214)

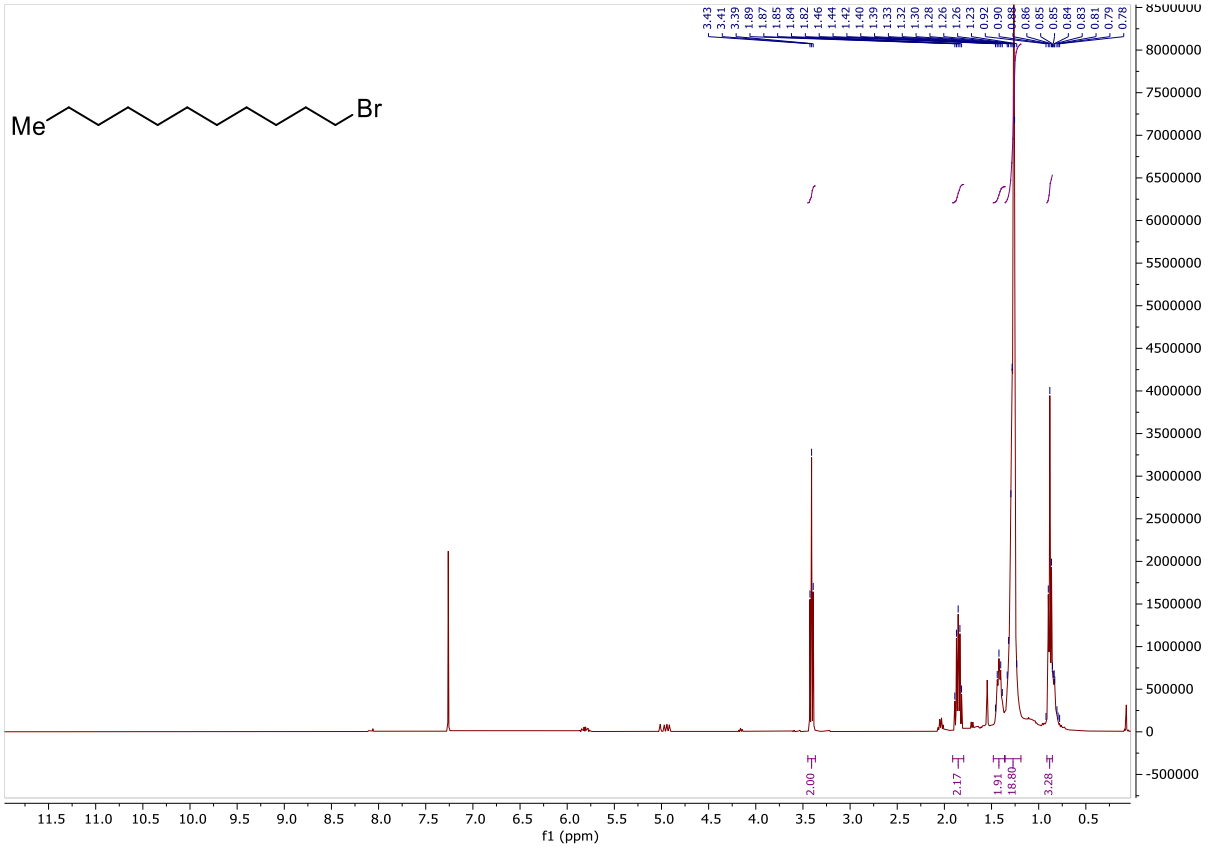

Undecan-1-ol (216)

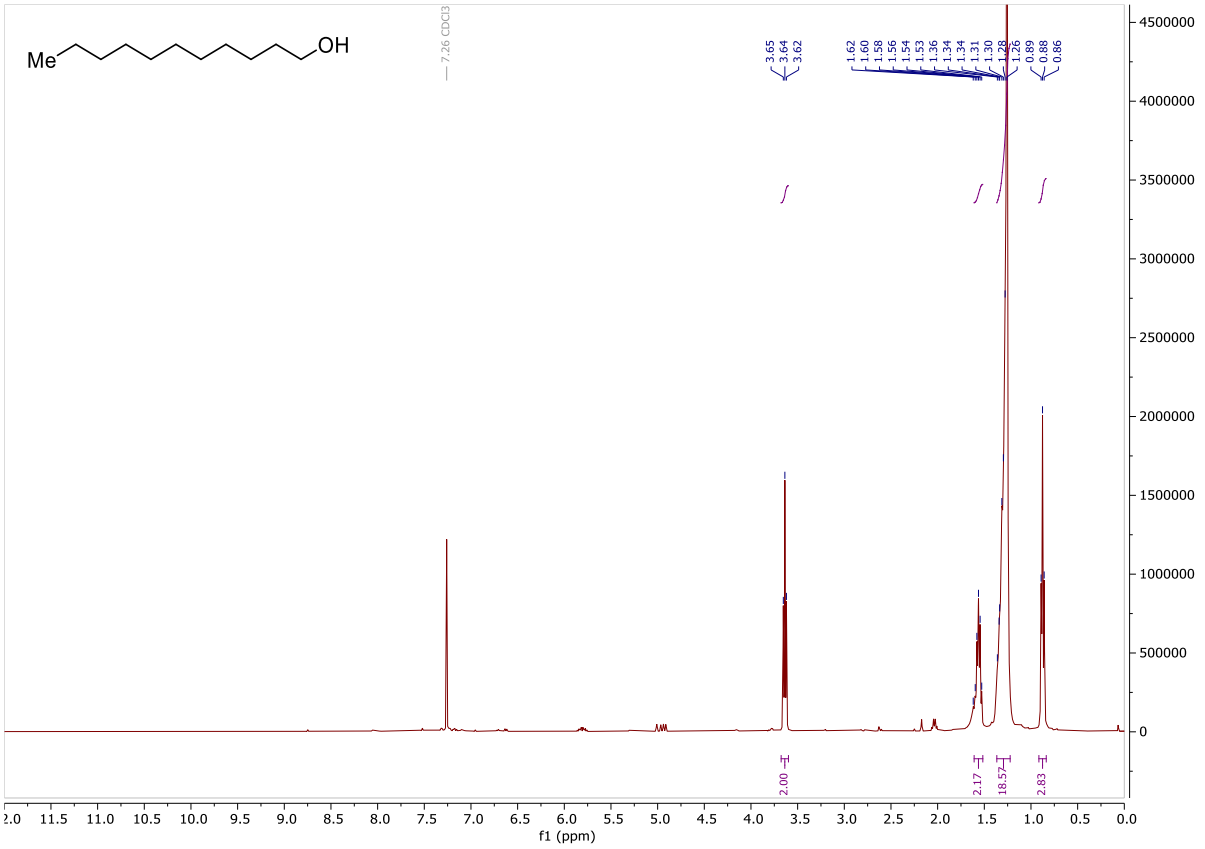

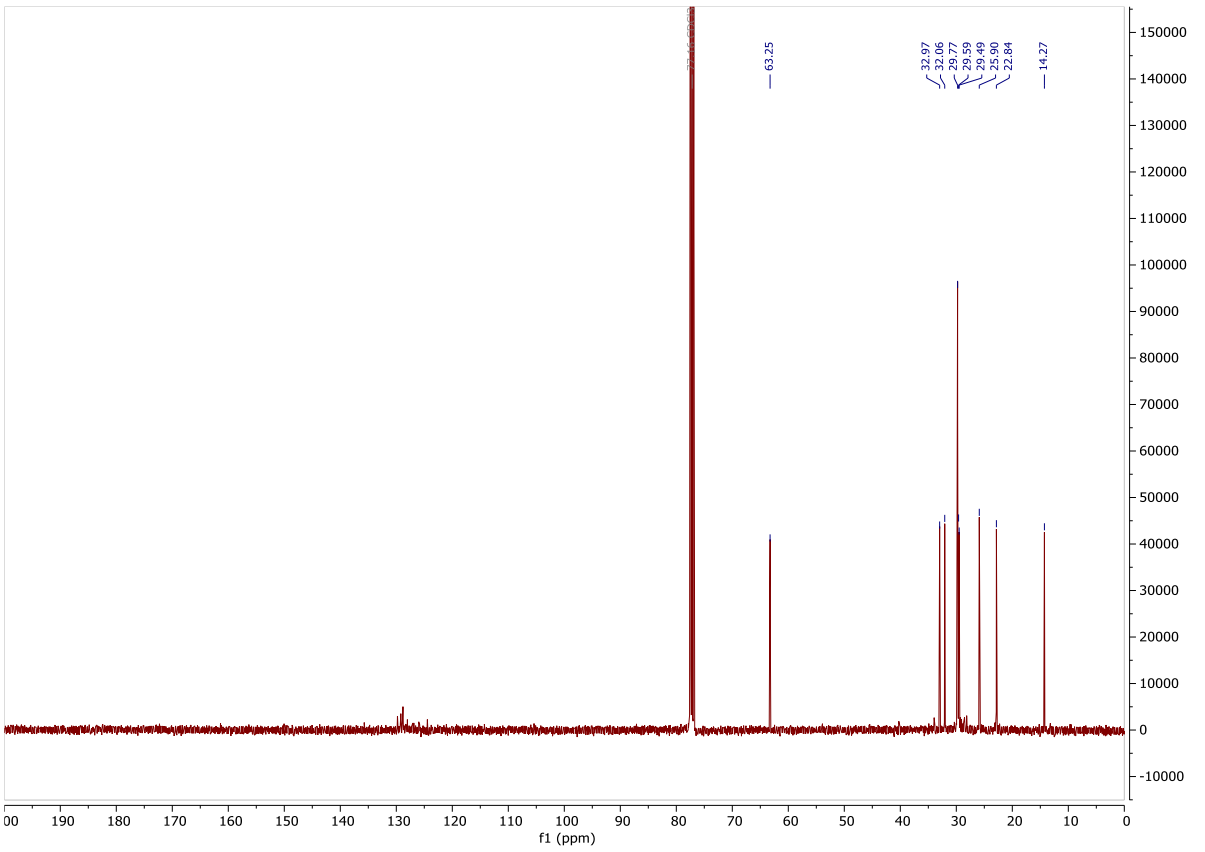

Tert-butyl 4-pentanoylpiperazine-1-carboxylate (218)

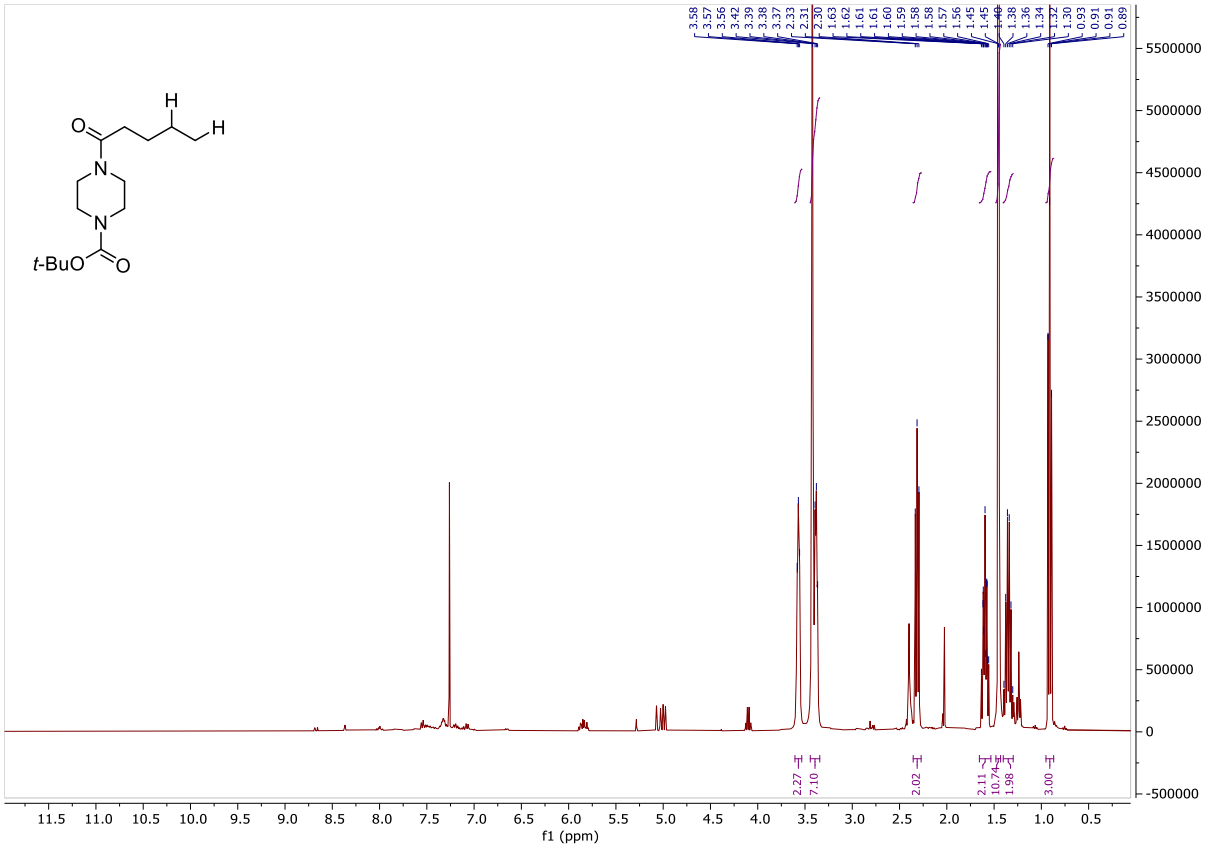

Pentyl nicotinate (220)

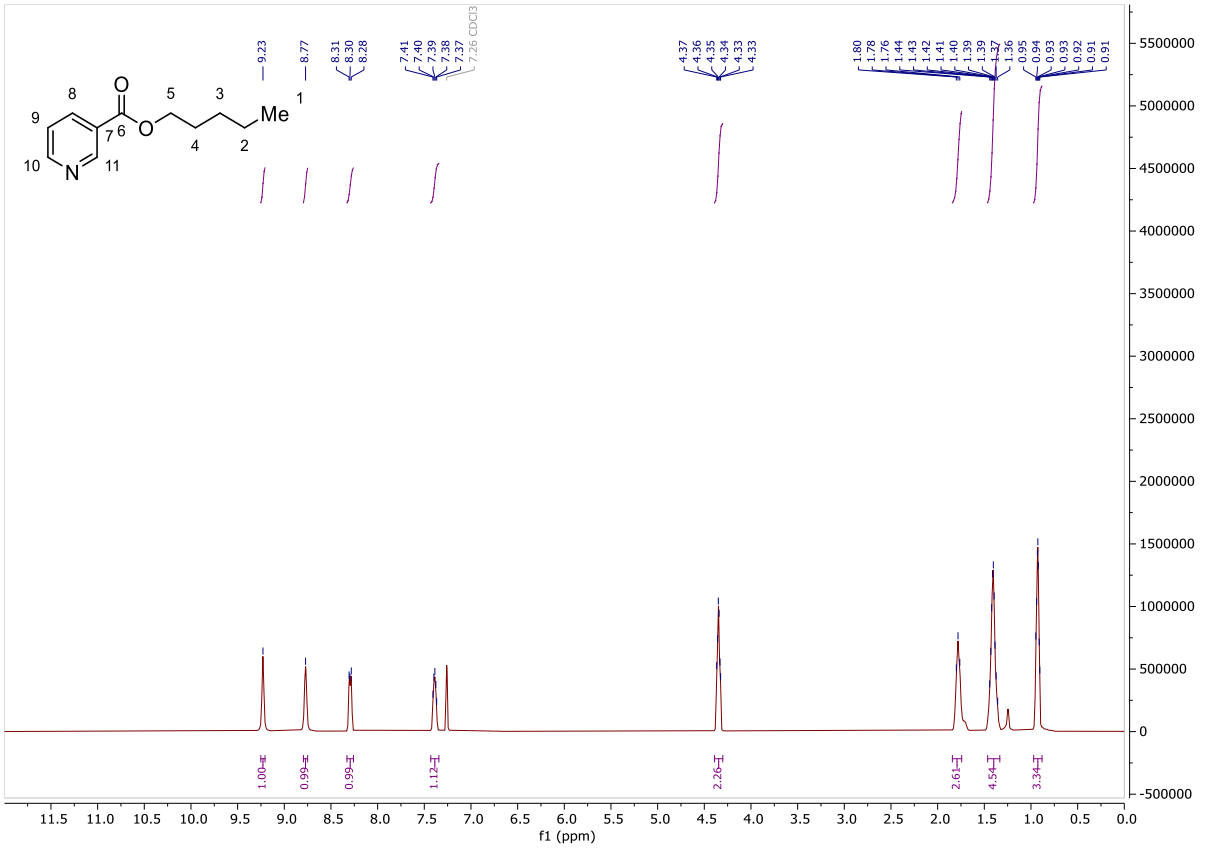

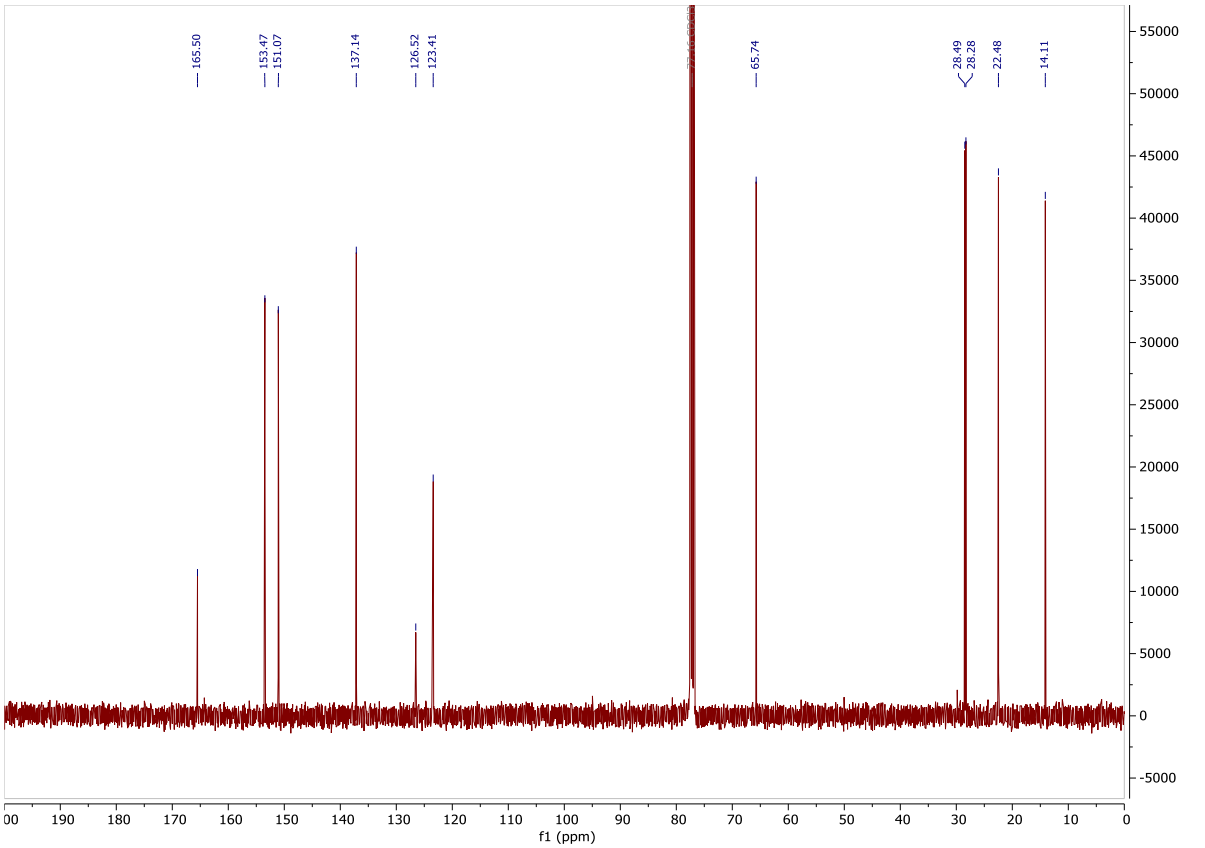

Benzyl piperidine-1-carboxylate (222)

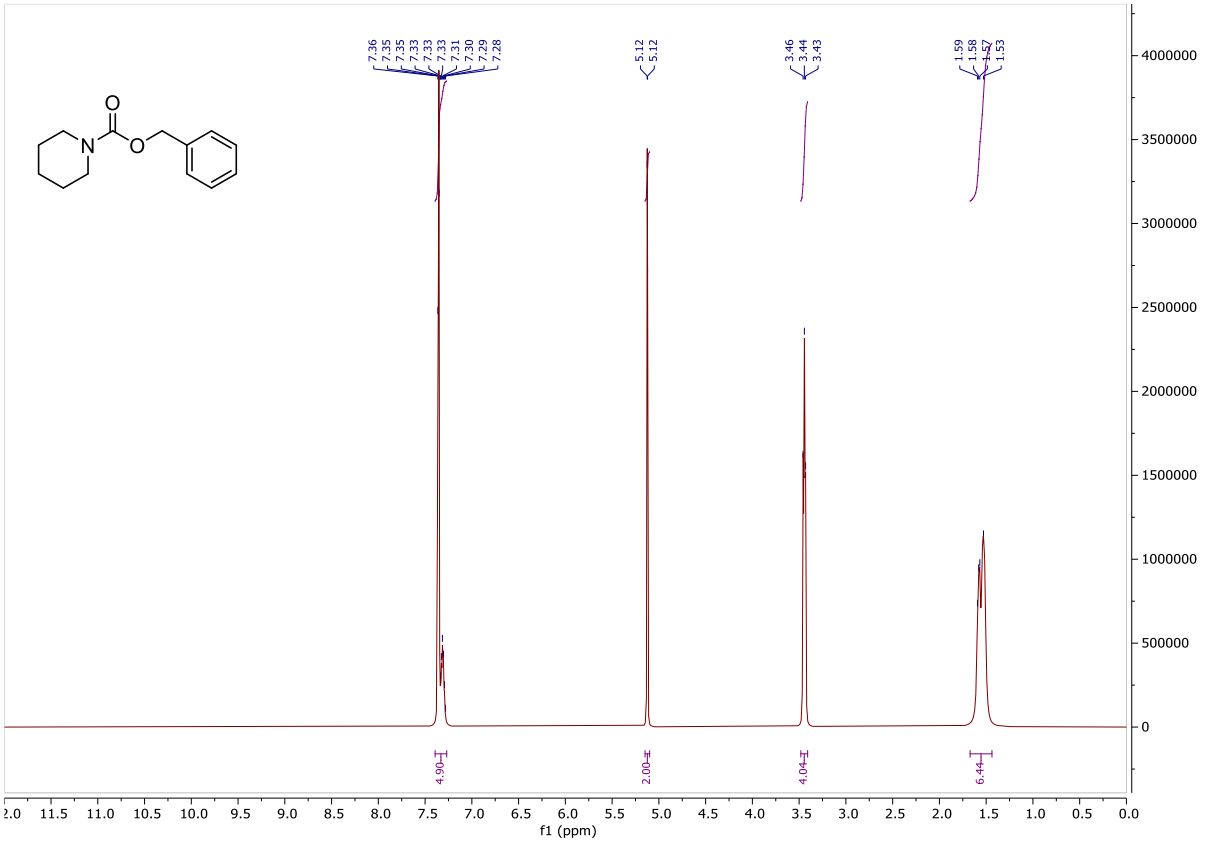

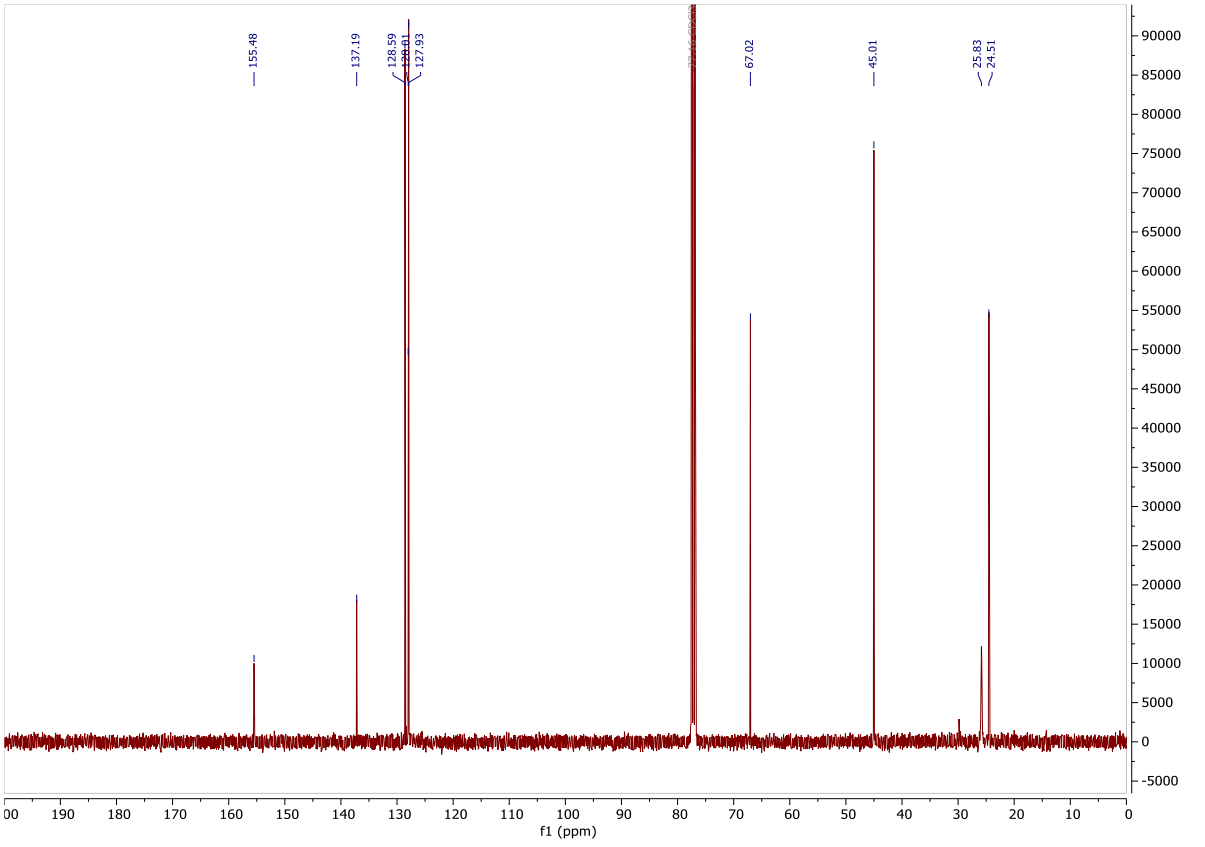

4-Phenylbutyl propionate (224)

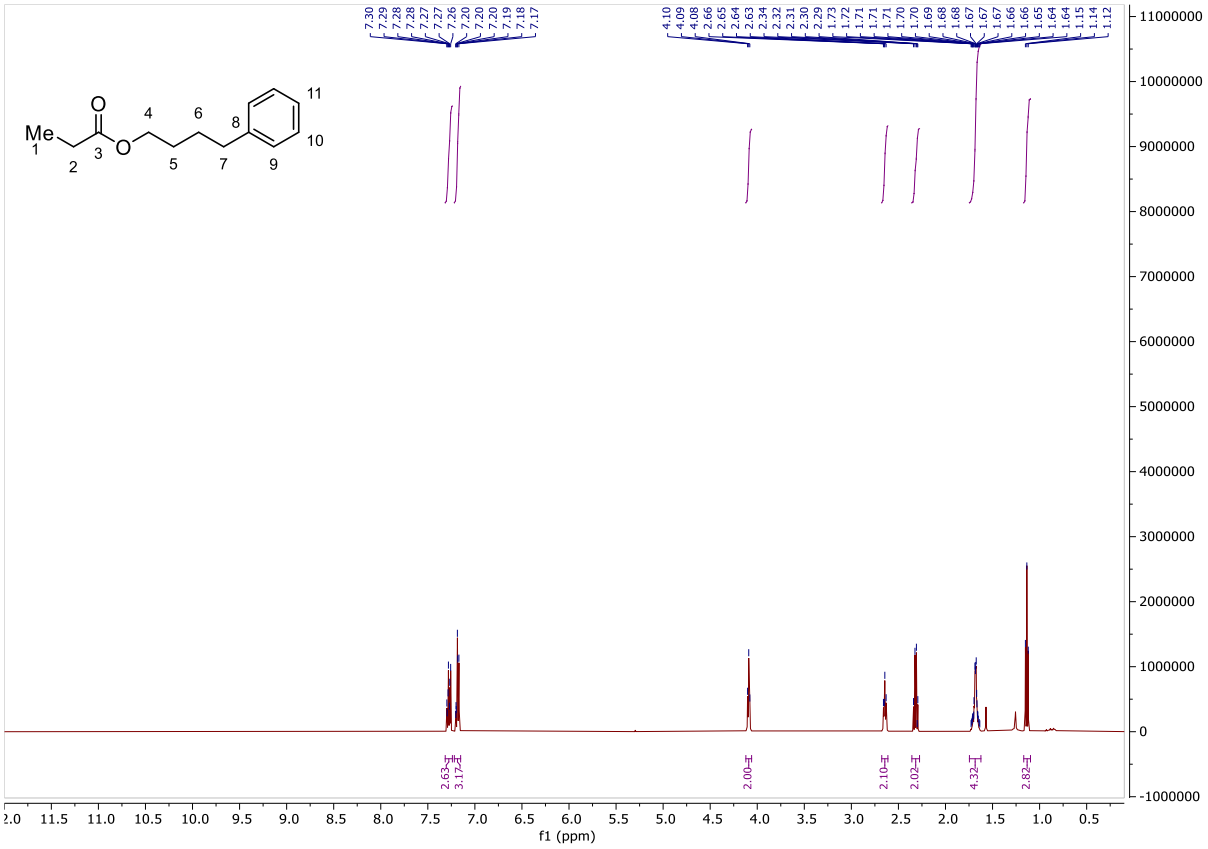

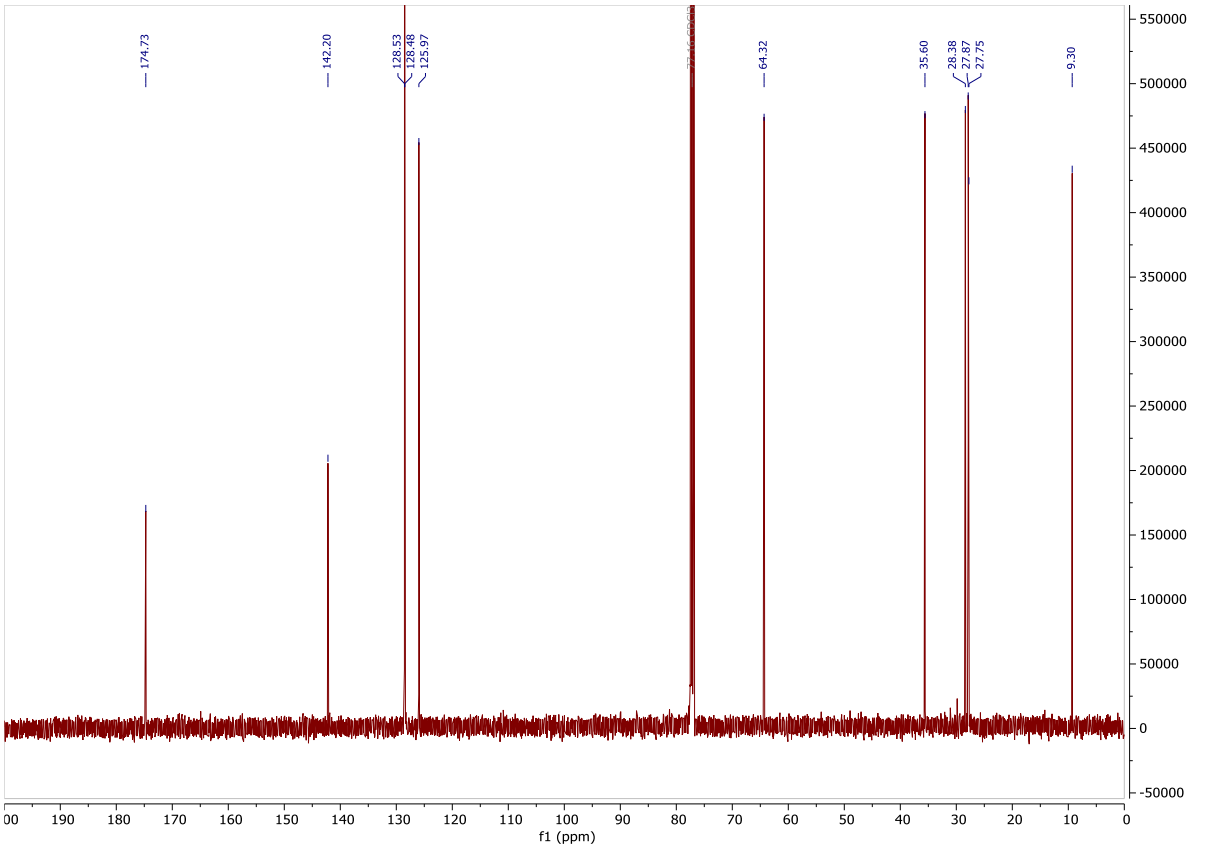

(1R,2S,5R)-2-isopropyl-5-methylcyclohexyl propionate (226)

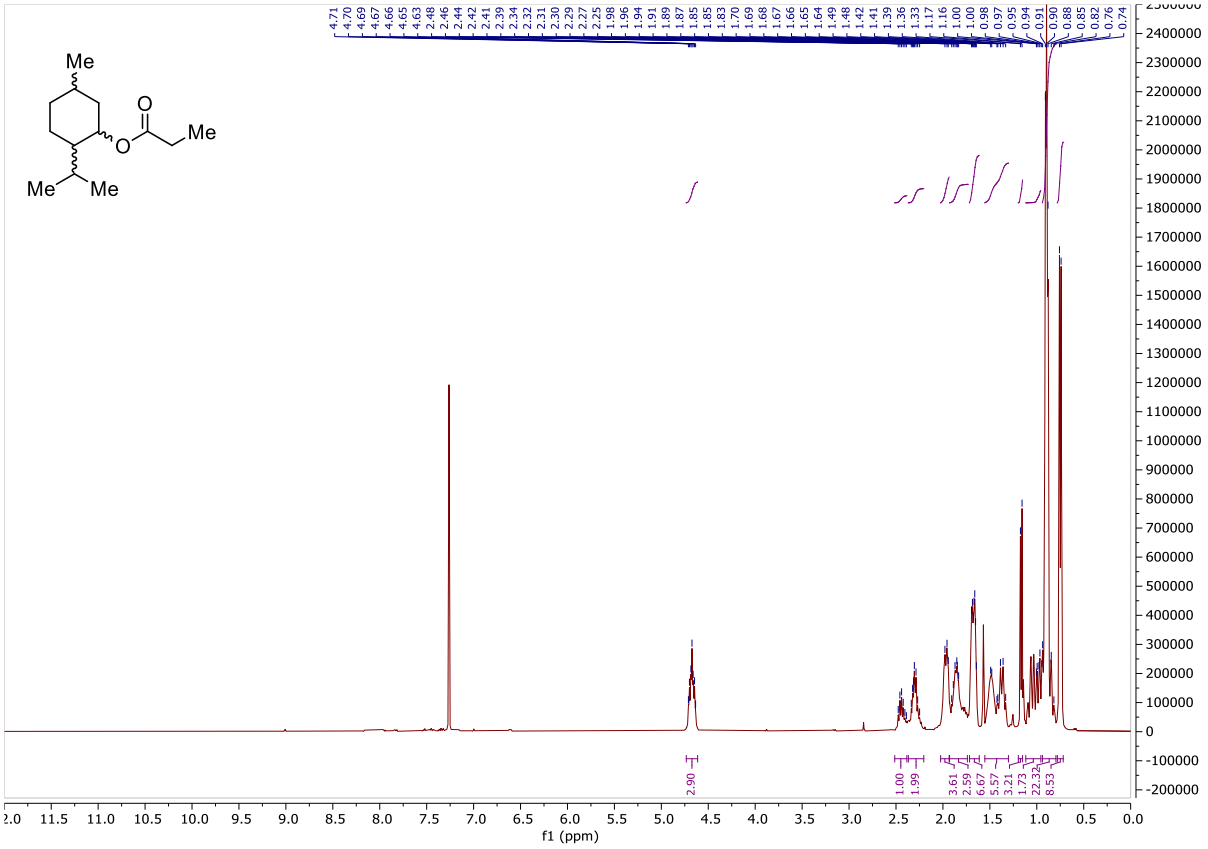

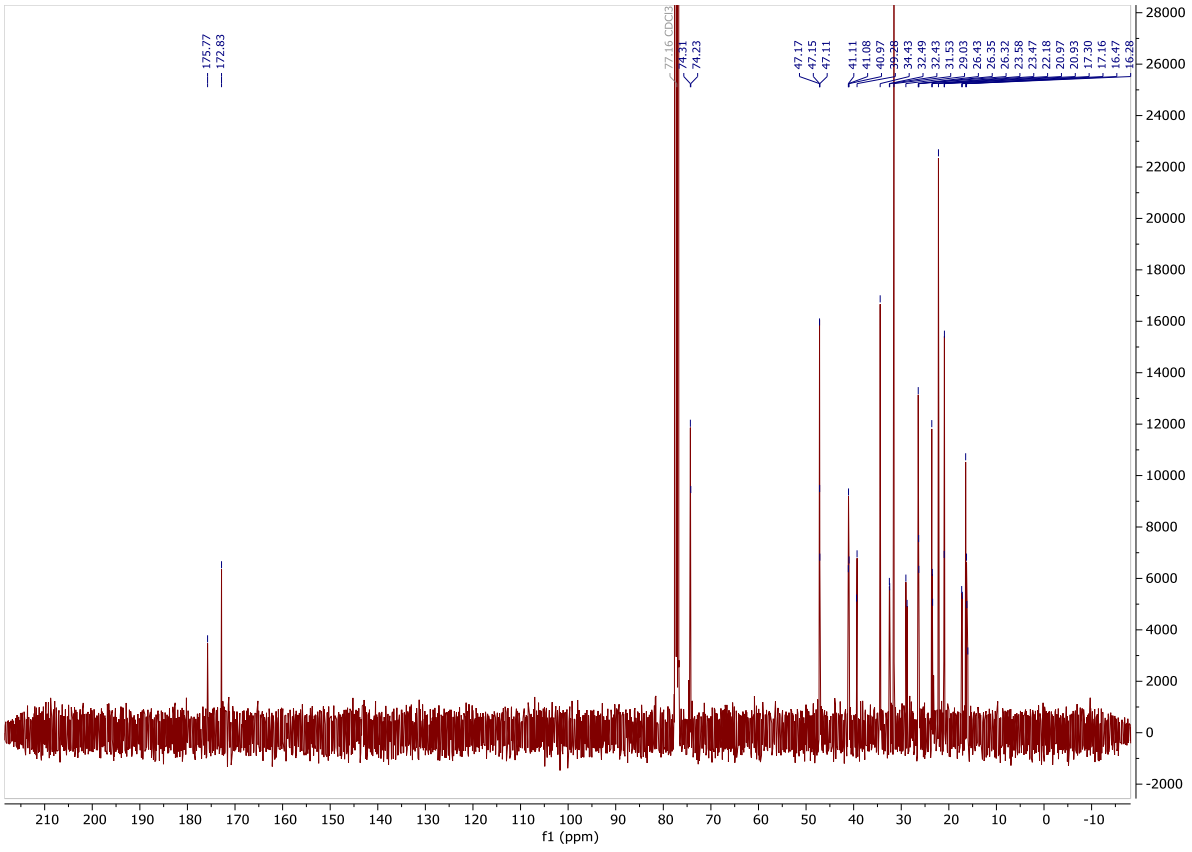

(1S,2R)-1,7,7-trimethylbicyclo[2.2.1]heptan-2-yl propionate (228)

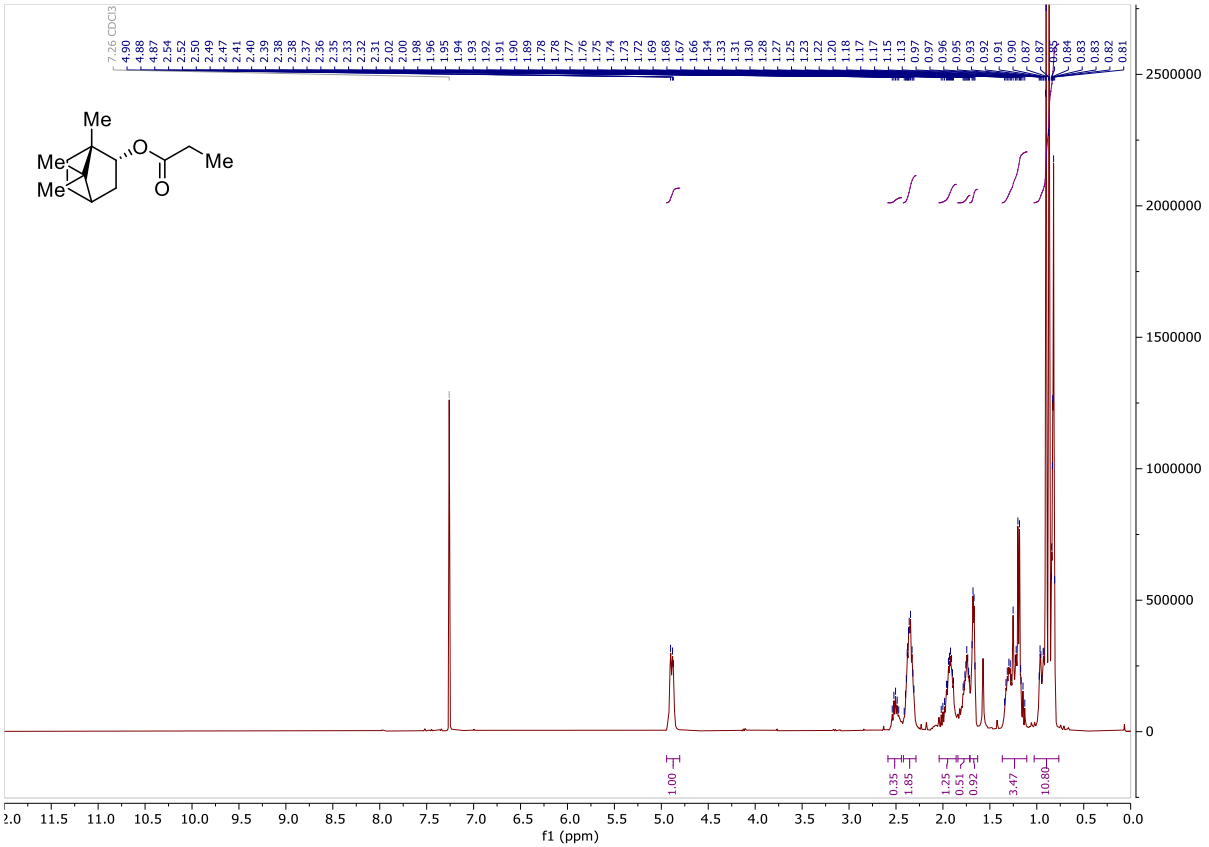

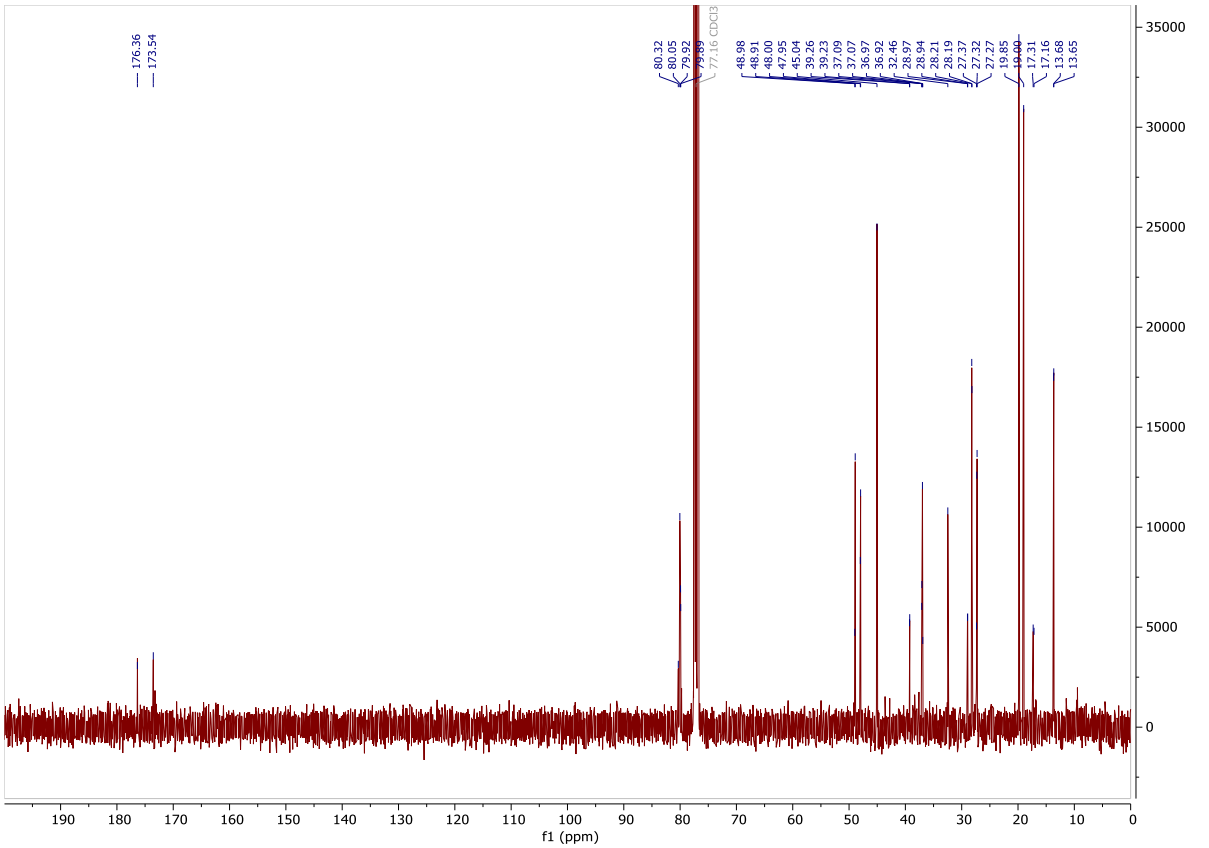

Diethyl (3R,4S)-3,4-dimethylcyclopentane-1,1-dicarboxylate (242)

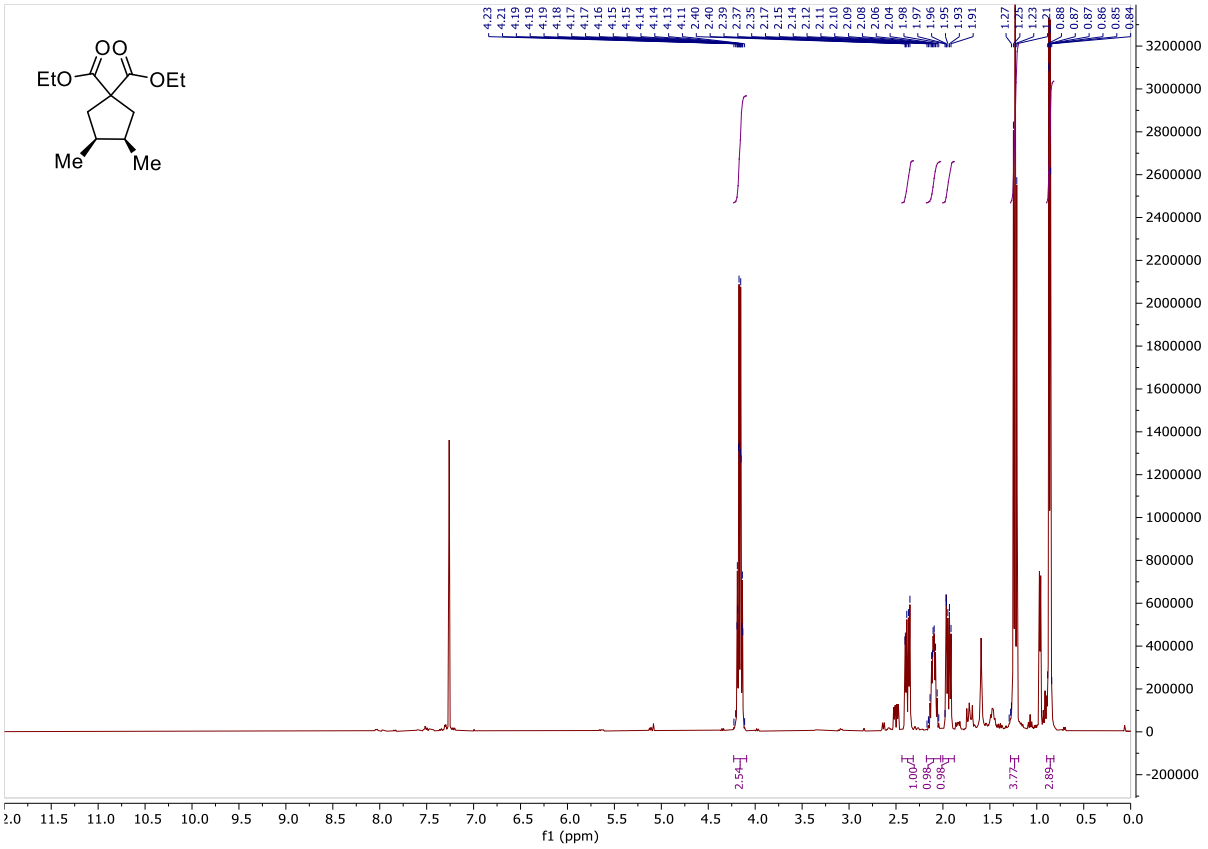

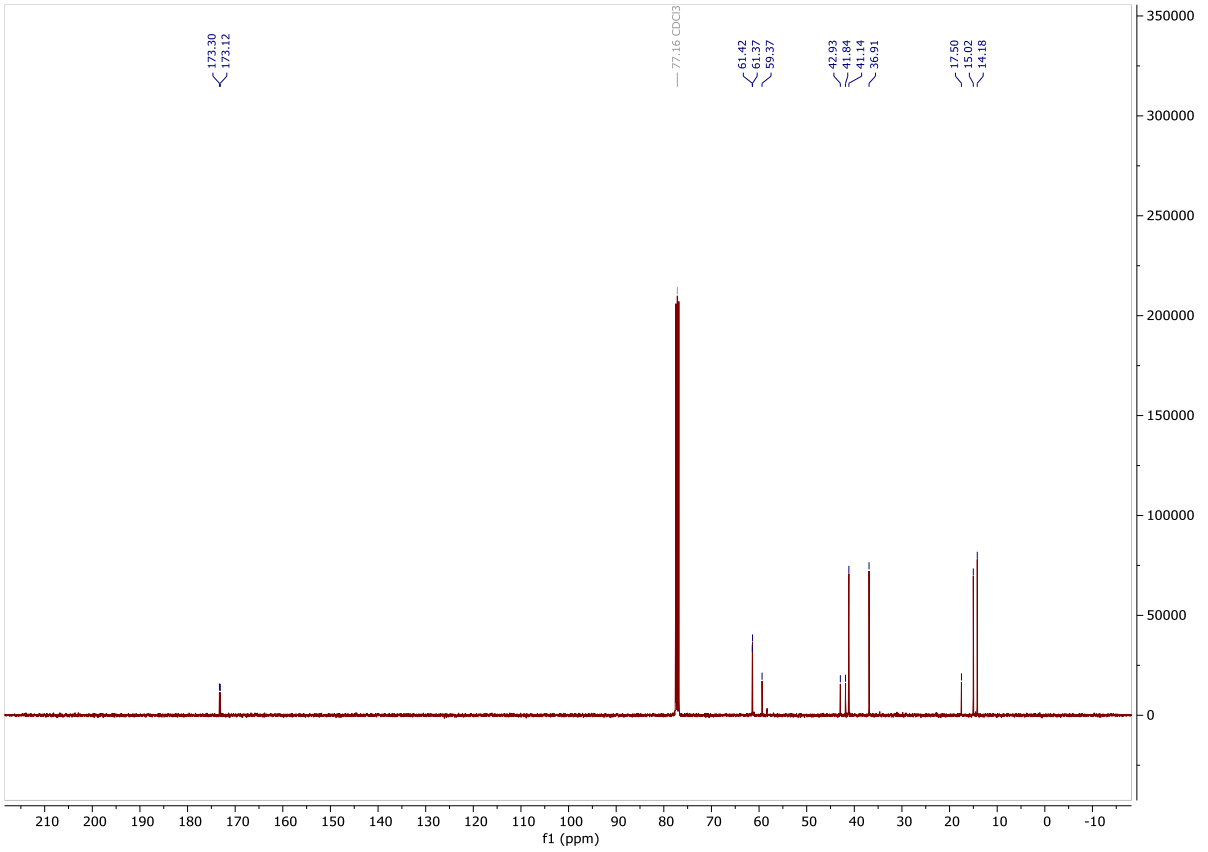

Miscellaneous

Methyl 2,4,6-trimethylbenzoate (250)

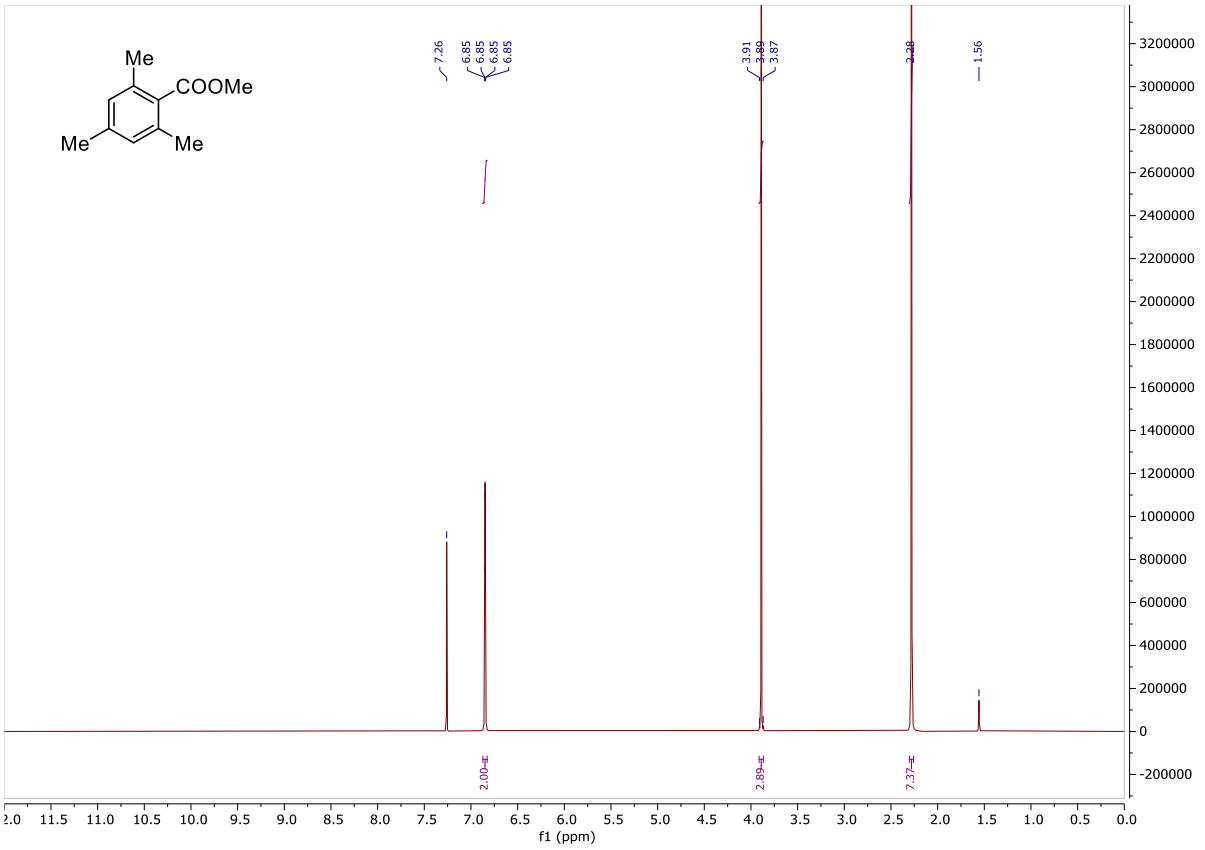

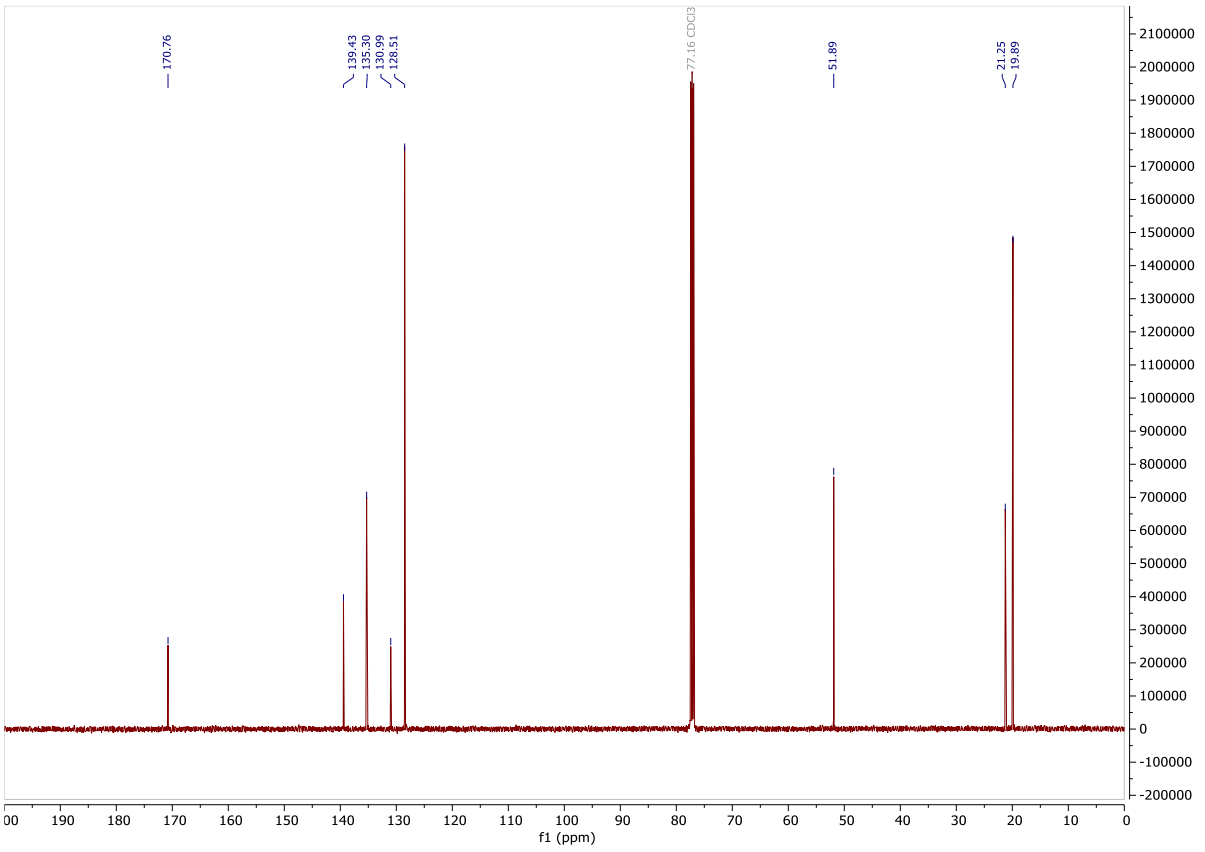

Methyl 2-fluorobenzoate (251)

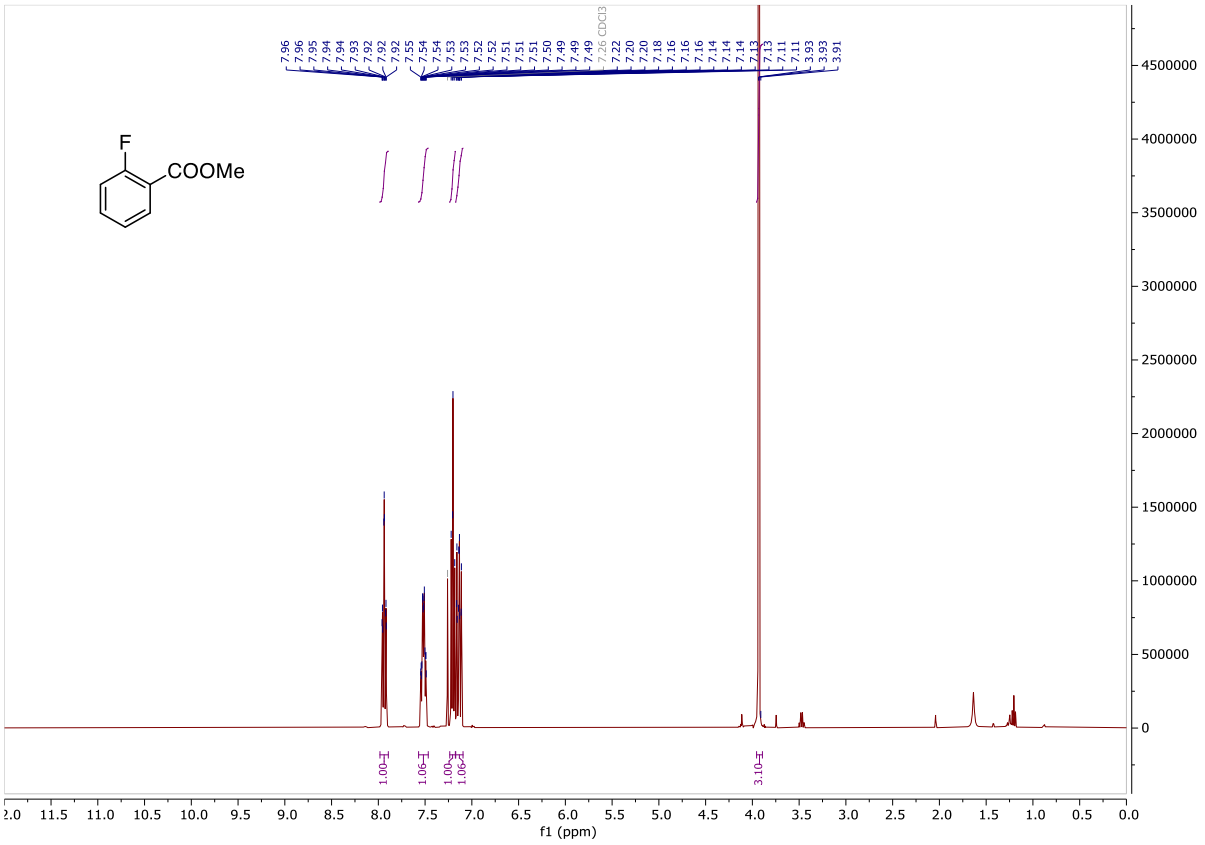

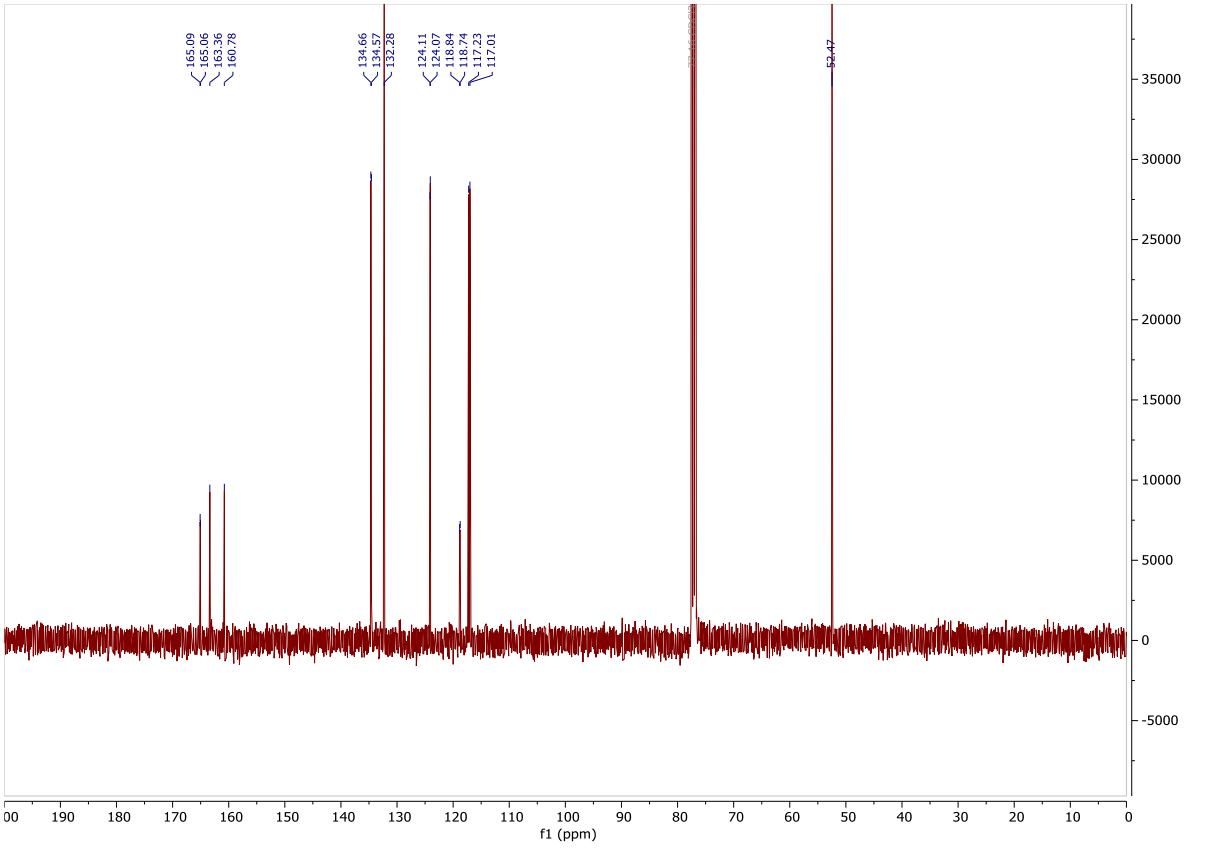

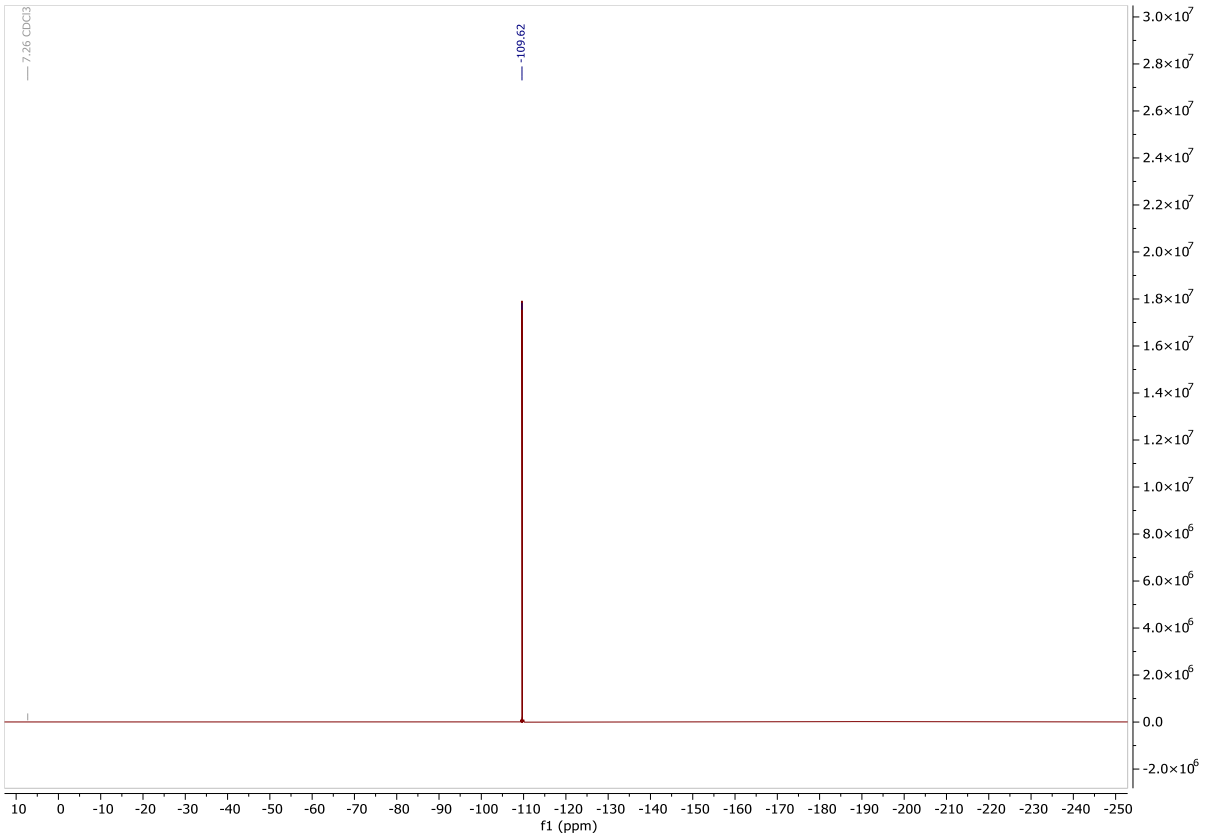
7.26 CDCl3
-109.62
3.0×10^7
2.8×10^7
2.6×10^7
2.4×10^7
2.2×10^7
2.0×10^7
1.8×10^7
1.6×10^7
1.4×10^7
1.2×10^7
1.0×10^7
8.0×10^6
6.0×10^6
4.0×10^6
2.0×10^6
0.0
-2.0×10^6
10 0 -10 -20 -30 -40 -50 -60 -70 -80 -90 -100 -110 -120 -130 -140 -150 -160 -170 -180 -190 -200 -210 -220 -230 -240 -250
f1 (ppm)

Methyl 2,3,4,5,6-pentafluorobenzoate (252)

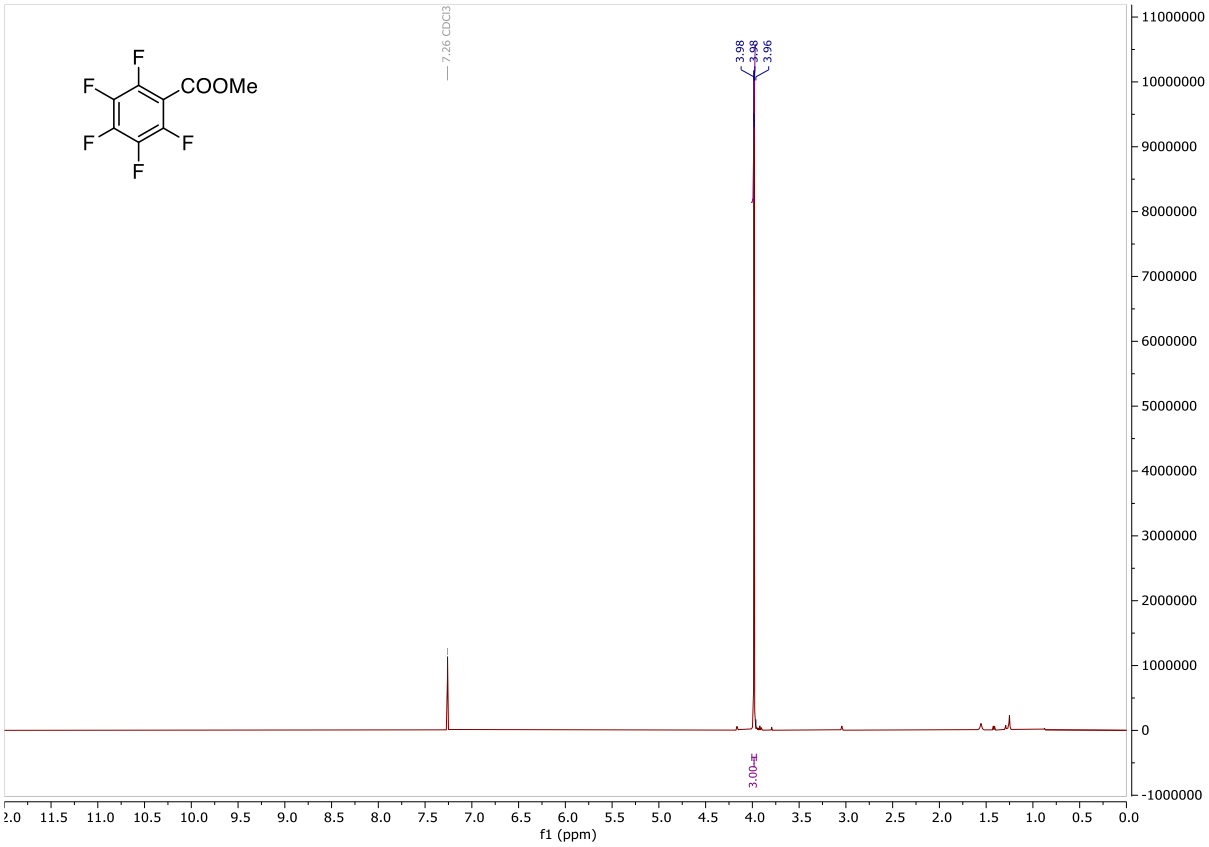

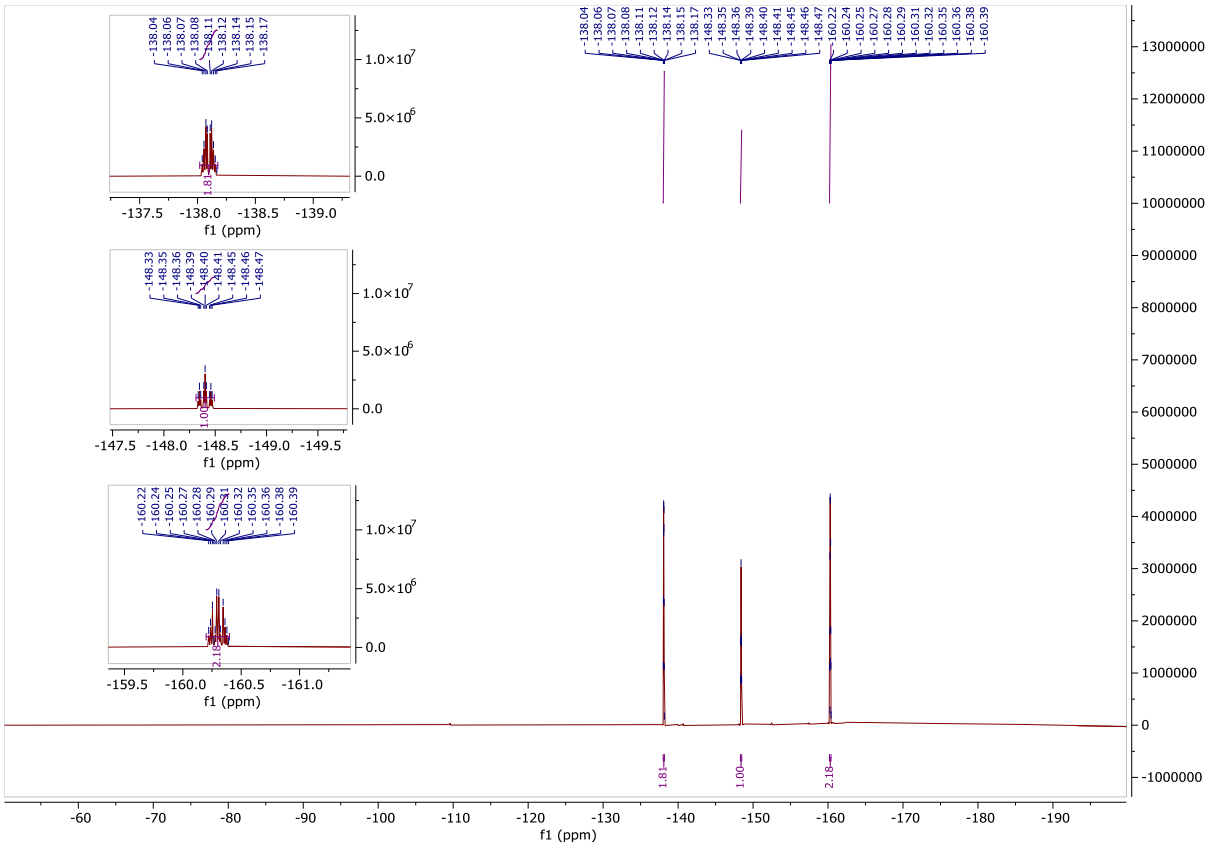

4-Phenylbutyl 4-methylbenzenesulfonate (253)

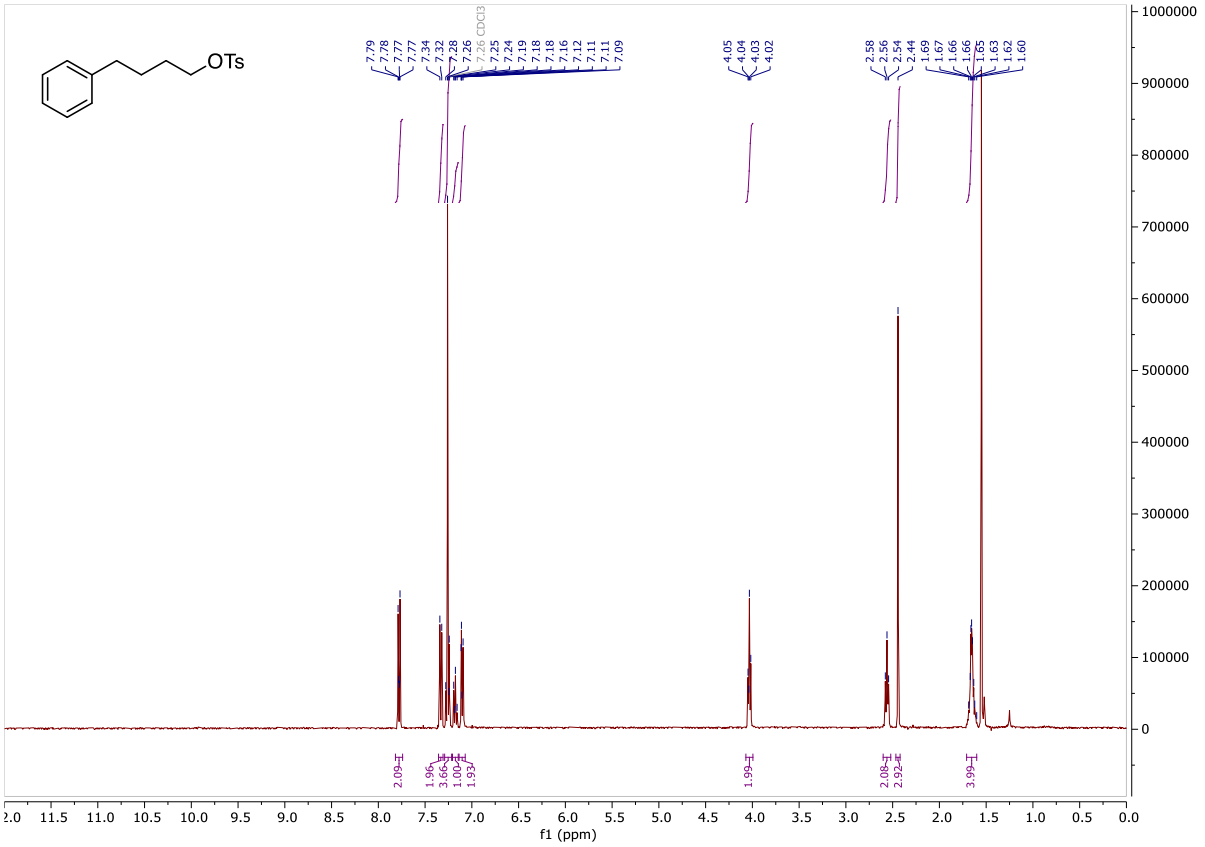

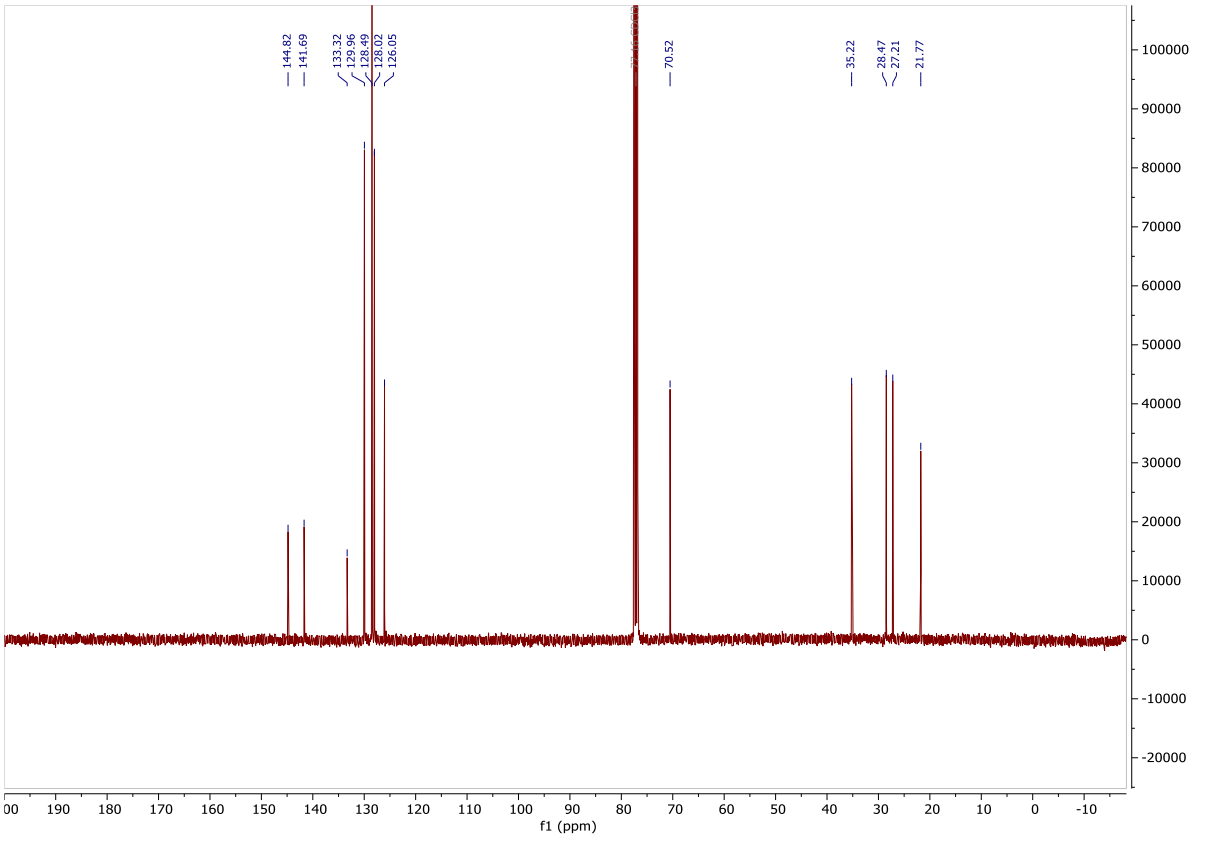

Triphenyl(3-phenylpropyl)phosphonium bromide (254)

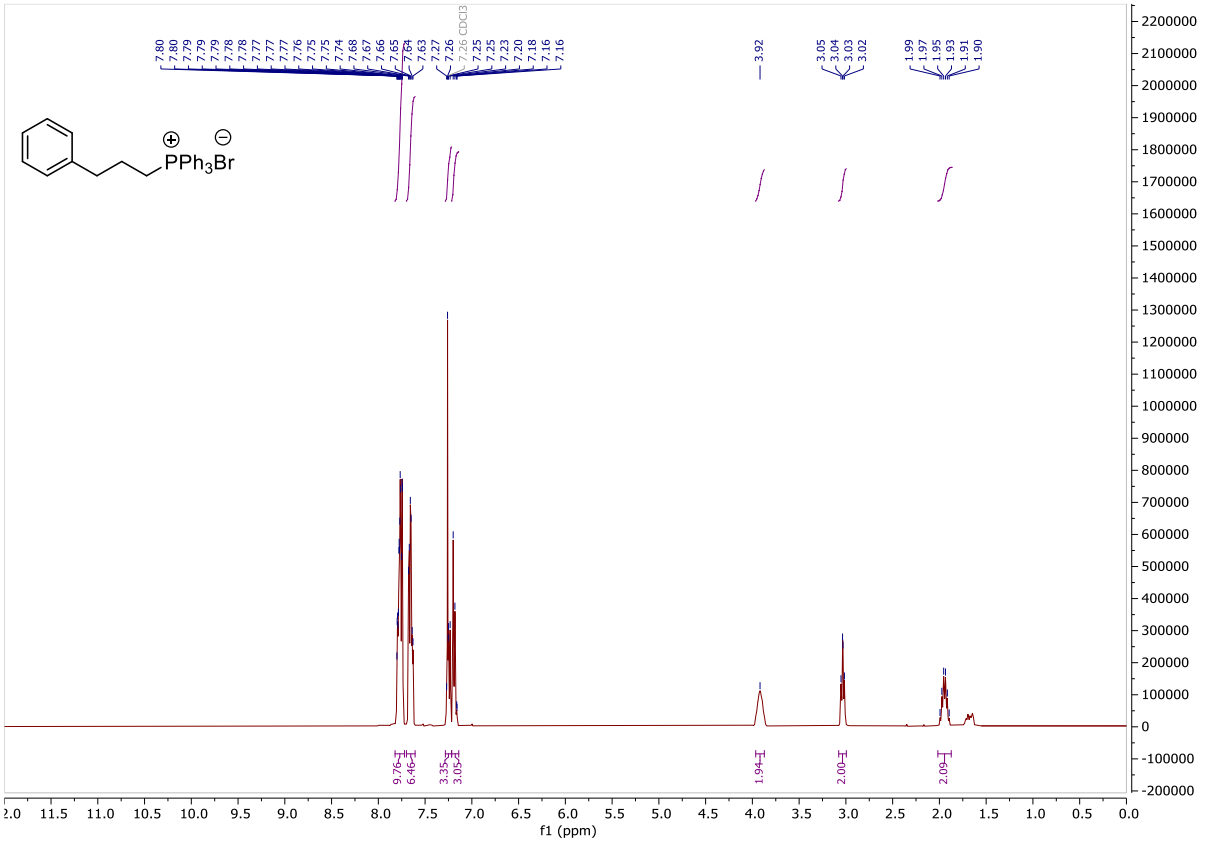

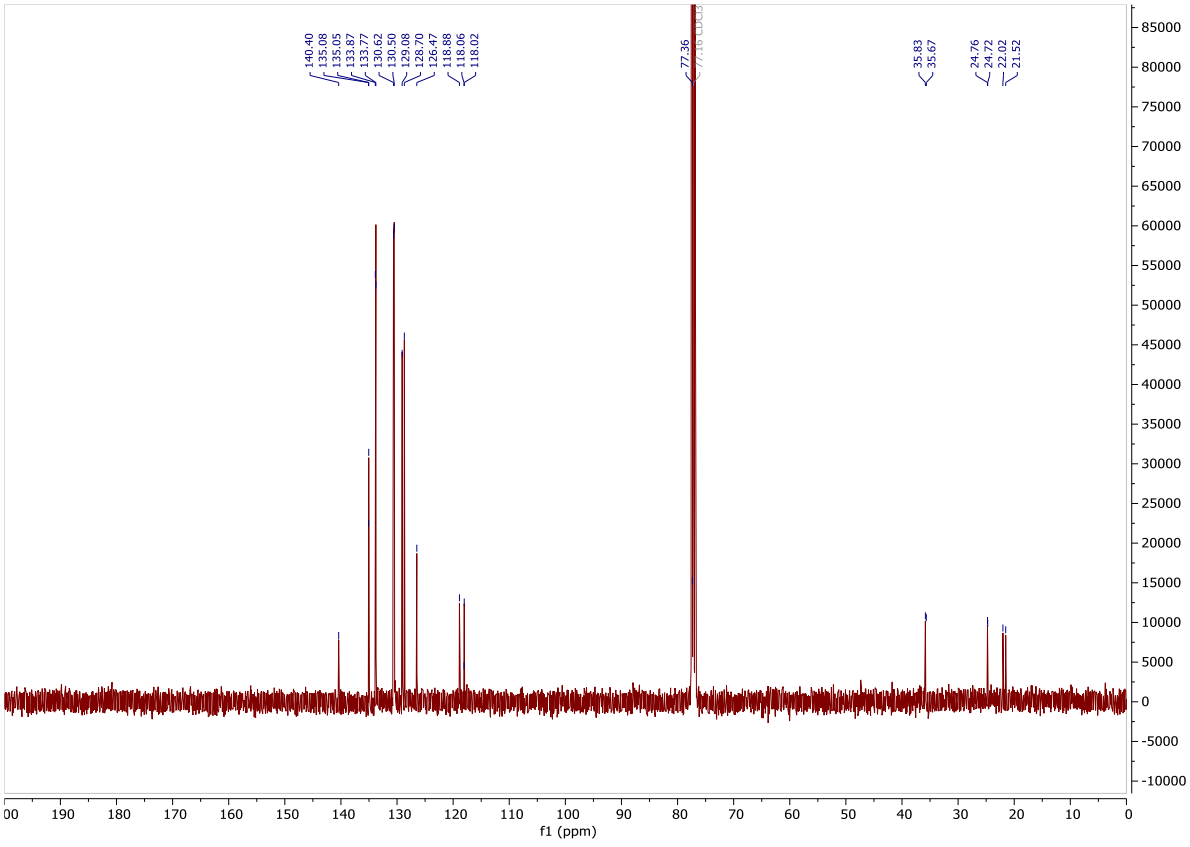

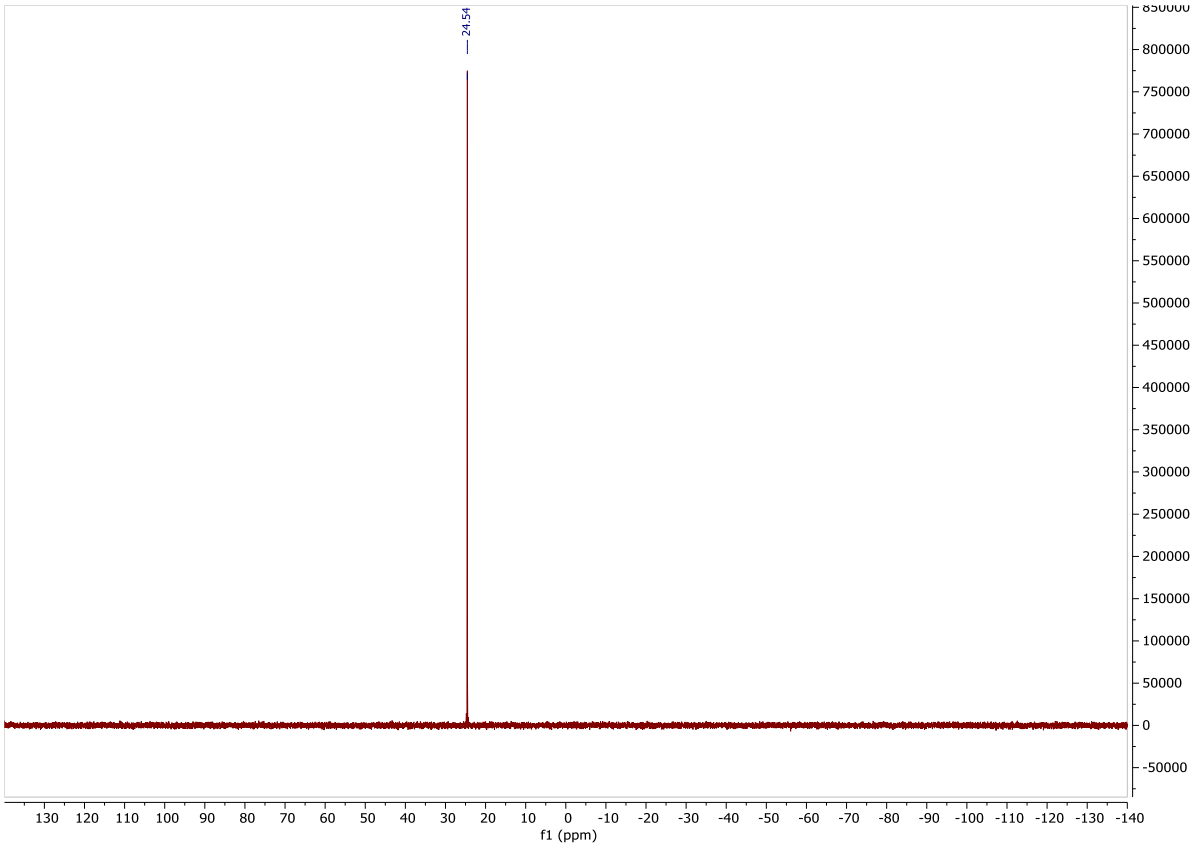
24.54
850000
800000
750000
700000
650000
600000
550000
500000
450000
400000
350000
300000
250000
200000
150000
100000
50000
0
-50000
130 120 110 100 90 80 70 60 50 40 30 20 10 0 -10 -20 -30 -40 -50 -60 -70 -80 -90 -100 -110 -120 -130 -140
f1 (ppm)

(3-(Benzoyloxy)propyl)triphenylphosphonium bromide (255)

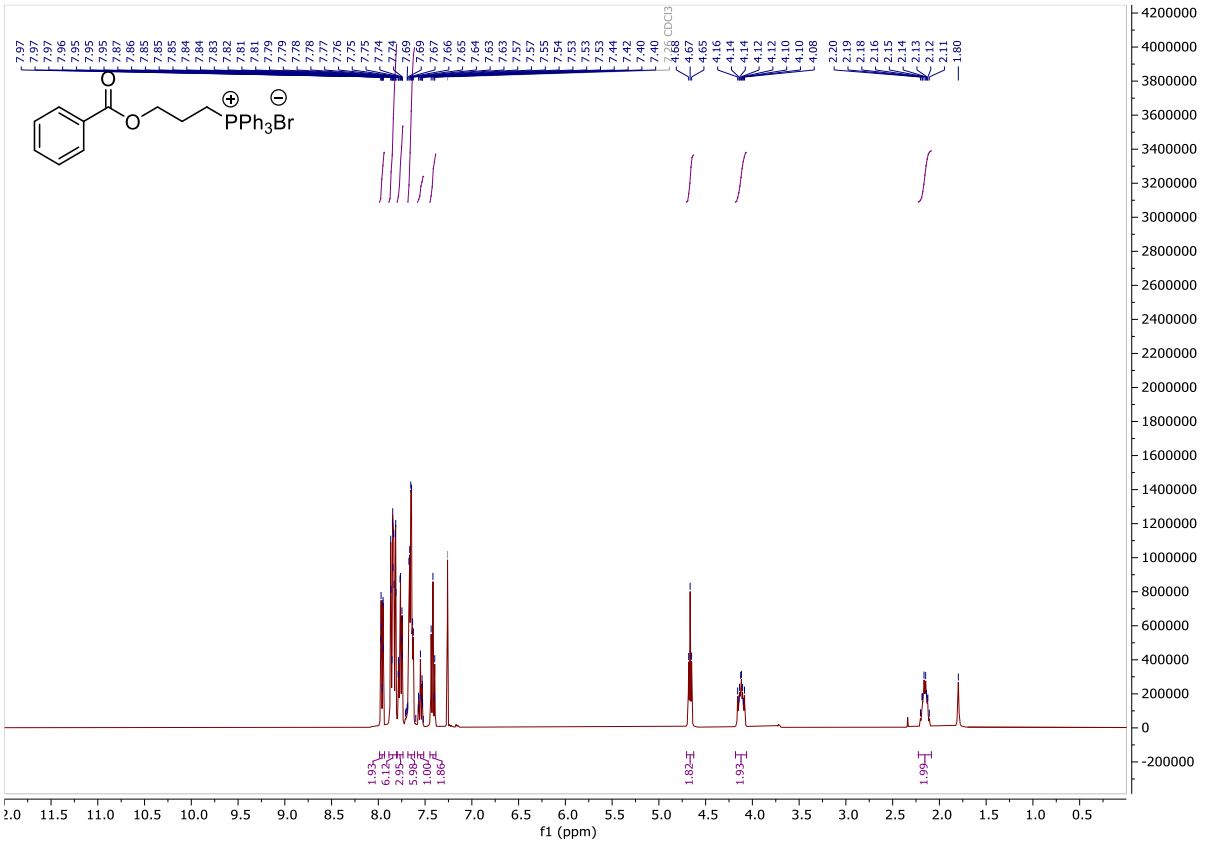

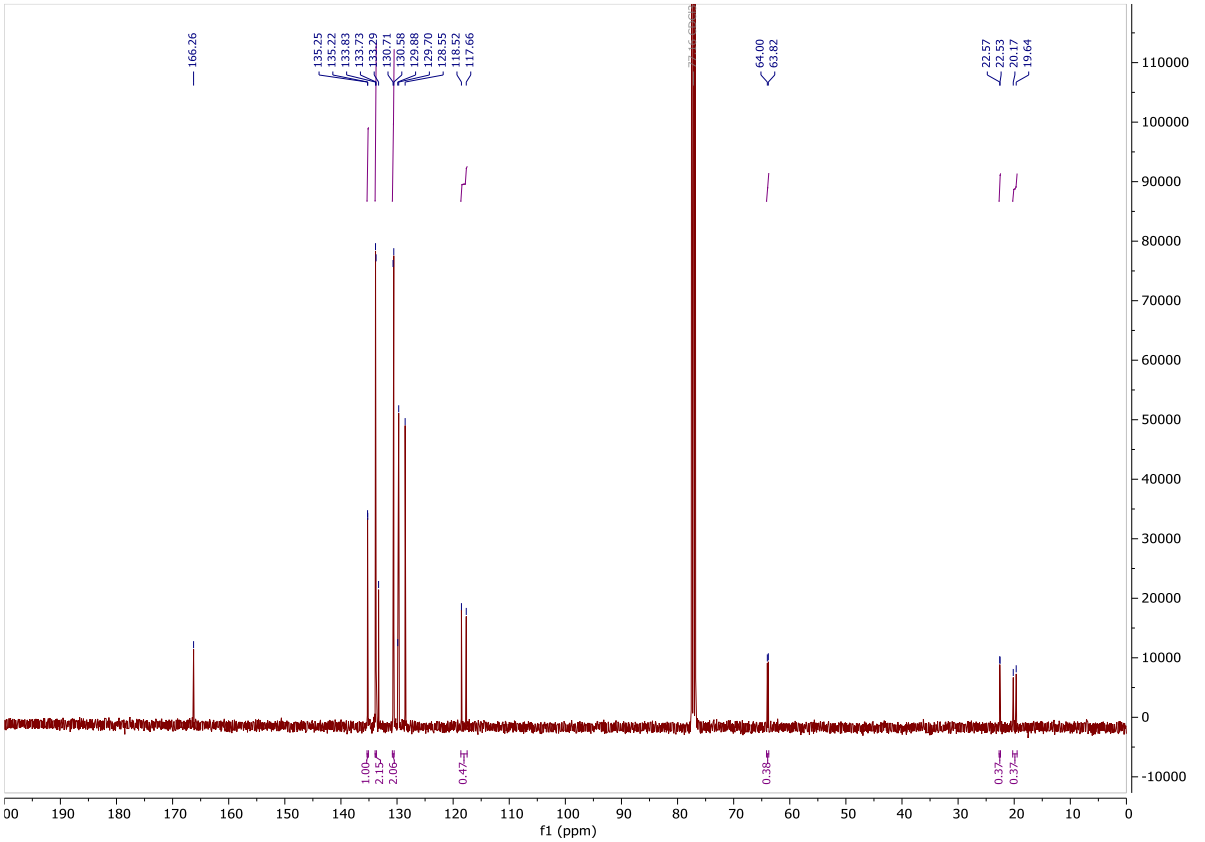

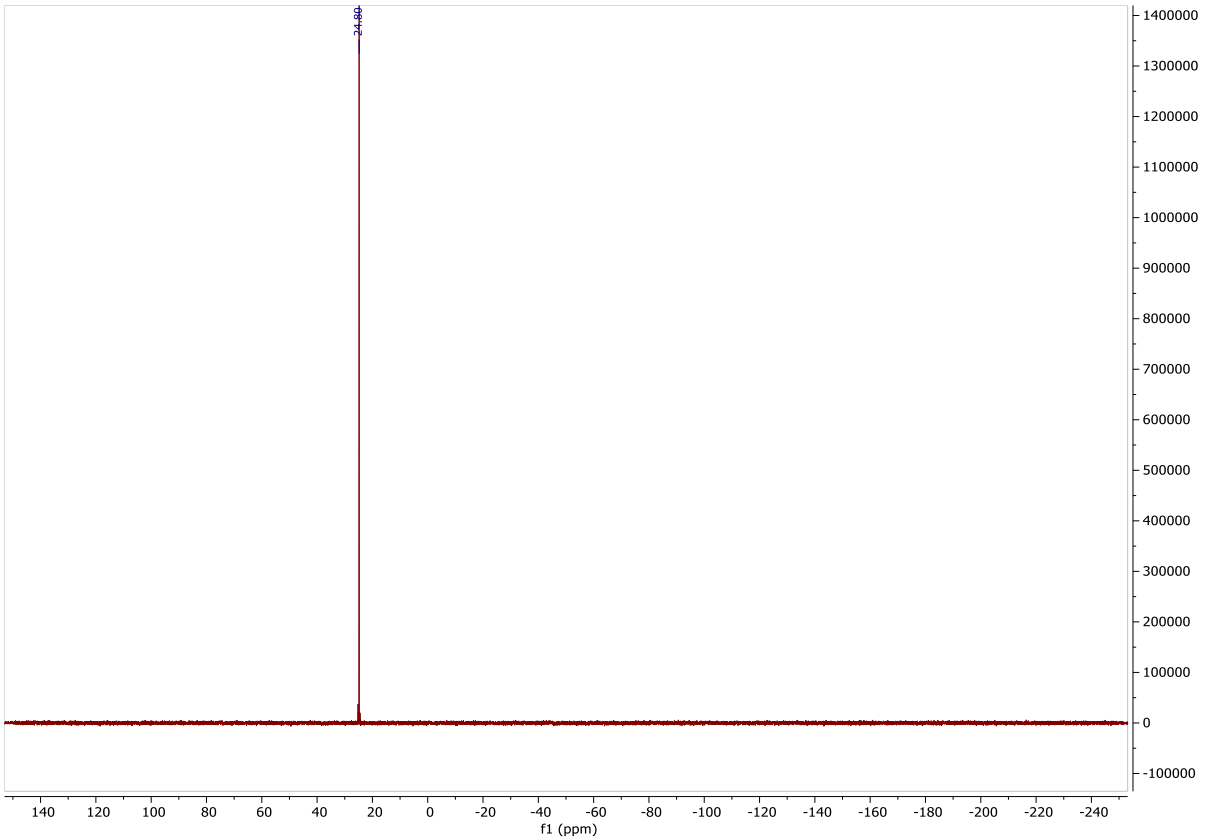
24.80
1400000
1300000
1200000
1100000
1000000
900000
800000
700000
600000
500000
400000
300000
200000
100000
0
-100000
140
120
100
80
60
40
20
0
-20
-40
-60
-80
-100
-120
-140
-160
-180
-200
-220
-240
f1 (ppm)

References

1. H. Kolbe, *Justus Liebigs Ann. Chem.*, 1849, **69**, 257–294.
2. A. Wurtz, *Justus Liebigs Ann. Chem.*, 1855, **96**, 364–375.
3. A. Wurtz, *Ann. Chim. Phys.*, 1855, **44**, 275–312.
4. T. Sandmeyer, *Ber. Dtsch. Chem. Ges.*, 1884, **17**, 2650–2653.
5. T. Sandmeyer, *Ber. Dtsch. Chem. Ges.*, 1884, **17**, 1633–1635.
6. M. Gomberg, *J. Am. Chem. Soc.*, 1900, **22**, 757–771.
7. M. S. Kharasch and F. R. Mayo, *J. Am. Chem. Soc.*, 1933, **55**, 2468–2496.
8. B. Giese and W. Zwick, *Angew. Chem. Int. Ed.*, 1978, **17**, 66–67.
9. D. H. Hey and W. A. Waters, *Chem. Rev.*, 1937, **21**, 169–208.
10. F. Minisci, R. Bernardi, F. Bertini, R. Galli and M. Perchinummo, *Tetrahedron*, 1971, **27**, 3575–3579.
11. W. Bachmann and F. Wiselogle, *J. Org. Chem.*, 1936, **1**, 354–382.
12. D. Griller and K. U. Ingold, *Acc. Chem. Res.*, 1976, **9**, 13–19.
13. C. Walling, *Free radicals in solution*, Wiley, New York, 1957.
14. C. Walling, *Pure Appl. Chem.*, 1967, **15**, 69–80.
15. A. Beckwith and K. Ingold, in *Free Radicals*, ed. J. K. Kochi, Academic Press, New York, 1980, vol. 1, pp. 161–310.
16. M. Yan, J. C. Lo, J. T. Edwards and P. S. Baran, *J. Am. Chem. Soc.*, 2016, **138**, 12692–12714.
17. S. Z. Zard, *Radical reactions in organic synthesis*, Oxford Chemistry Masters, Oxford, 2003.
18. Z. Huang, N. Luo, C. Zhang and F. Wang, *Nat. Rev. Chem.*, 2022, **6**, 197–214.
19. J. K. Matsui, S. B. Lang, D. R. Heitz and G. A. Molander, *ACS Catal.*, 2017, **7**, 2563–2575.
20. Á. Péter, S. Agasti, O. Knowles, E. Pye and D. J. Procter, *Chem. Soc. Rev.*, 2021, **50**, 5349–5365.
21. *Reaxys*, Elsevier, Amsterdam, 2025.
22. L. Capaldo and D. Ravelli, *Eur. J. Org. Chem.*, 2017, 2056–2071.
23. S. Crespi and M. Fagnoni, *Chem. Rev.*, 2020, **120**, 9790–9833.
24. F. Juliá, T. Constantin and D. Leonori, *Chem. Rev.*, 2022, **122**, 2292–2352.
25. J. Koo, W. Kim, B. H. Jhun, S. Park, D. Song, Y. You and H. G. Lee, *J. Am. Chem. Soc.*, 2024, **146**, 22874–22880.
26. Y.-R. Luo, *Comprehensive Handbook of Chemical Bond Energies*, CRC Press, 2007.
27. Z. Zhang, G. Lonardi, T. Sephton, Y. C. Guersoy, C. Stavagna, G. V. A. Lenardon, M. Bietti and D. Leonori, *Nature*, 2025, DOI: 10.1038/s41586-025-09725-1.
28. S. Z. Zard, *Chem. Soc. Rev.*, 2008, **37**, 1603–1618.
29. A. W. Hofmann, *Ber. Dtsch. Chem. Ges.*, 1879, **12**, 984–990.
30. A. W. Hofmann, *Ber. Dtsch. Chem. Ges.*, 1885, **18**, 109–131.
31. E. A. Wappes, S. C. Fosu, T. C. Chopko and D. A. Nagib, *Angew. Chem.*, 2016, **128**, 10128–10132.
32. D. C. Miller, G. J. Choi, H. S. Orbe and R. R. Knowles, *J. Am. Chem. Soc.*, 2015, **137**, 13492–13495.
33. E. Tsui, H. Wang and R. R. Knowles, *Chem. Sci.*, 2020, **11**, 11124–11141.
34. K. Zhang, L. Chang, Q. An, X. Wang and Z. Zuo, *J. Am. Chem. Soc.*, 2019, **141**, 10556–10564.
35. H. Guan, S. Sun, Y. Mao, L. Chen, R. Lu, J. Huang and L. Liu, *Angew. Chem. Int. Ed.*, 2018, **130**, 11583–11587.
36. A. Tursi, *Biofuel Res. J.*, 2019, **6**, 962–979.
37. S. Bera, L. M. Kabadwal and D. Banerjee, *Chem. Soc. Rev.*, 2024, **53**, 4607–4647.
38. A. Williamson, *Justus Liebigs Ann. Chem.*, 1851, **77**, 37–49.
39. A. Cook and S. G. Newman, *Chem. Rev.*, 2024, **124**, 6078–6144.
40. J. Bronsted, *Chem. Rev.*, 1928, **5**, 231–338.
41. Y. Yoshida, K. Shimonishi, Y. Sakakura, S. Okada, N. Aso and Y. Tanabe, *Synthesis*, 1999, 1633–1636.
42. R. Appel, *Angew. Chem. Int. Ed.*, 1975, **14**, 801–811.

43. O. Mitsunobu and M. Yamada, *Bull. Chem. Soc. Jpn.*, 1967, **40**, 2380–2382.
44. P. G. Cozzi, A. Gualandi, L. Mengozzi, E. Manoni and C. M. Wilson, in *Green Chemistry in Drug Discovery: From Academia to Industry*, ed. P. F. Richardson, Springer New York, New York, NY, 2022, DOI: 10.1007/978-1-0716-1579-9_4, pp. 123–154.
45. M. Dryzhakov, E. Richmond and J. Moran, *Synthesis*, 2016, **48**, 935–959.
46. D. H. Barton and S. W. McCombie, *J. Chem. Soc., Perkin Trans. 1*, 1975, 1574–1585.
47. G. L. Lackner, K. W. Quasdorf and L. E. Overman, *J. Am. Chem. Soc.*, 2013, **135**, 15342–15345.
48. C. C. Nawrat, C. R. Jamison, Y. Slutskyy, D. W. C. MacMillan and L. E. Overman, *J. Am. Chem. Soc.*, 2015, **137**, 11270–11273.
49. O. P. Williams, A. F. Chmiel, M. Mikhael, D. M. Bates, C. S. Yeung and Z. K. Wickens, *Angew. Chem. Int. Ed.*, 2023, **62**, e202300178.
50. Y.-X. Wu, M.-R. Chang, Z.-P. Guan, R. Chi, J.-X. Yu, X. Wu and Z.-B. Dong, *Sci. China Chem.*, 2025, DOI: 10.1007/s11426-025-2651-2.
51. H.-M. Guo and X. Wu, *Nat. Commun.*, 2021, **12**, 5365.
52. E. E. Stache, A. B. Ertel, T. Rovis and A. G. Doyle, *ACS Catal.*, 2018, **8**, 11134–11139.
53. Z. Dong and D. W. MacMillan, *Nature*, 2021, **598**, 451–456.
54. H. A. Sakai and D. W. C. MacMillan, *J. Am. Chem. Soc.*, 2022, **144**, 6185–6192.
55. Q. Cai, I. M. McWhinnie, N. W. Dow, A. Y. Chan and D. W. C. MacMillan, *J. Am. Chem. Soc.*, 2024, **146**, 12300–12309.
56. J. J. Großkopf, D. C. Morgan, A. K. Clarke and D. W. C. MacMillan, *J. Am. Chem. Soc.*, 2025, **147**, 35995–36006.
57. X. Pang and X.-Z. Shu, *Chin. J. Chem.*, 2023, **41**, 1637–1652.
58. T. McCallum, X. Wu and S. Lin, *J. Org. Chem.*, 2019, **84**, 14369–14380.
59. E. E. van Tamelen and M. A. Schwartz, *J. Am. Chem. Soc.*, 1965, **87**, 3277–3278.
60. J. E. McMurry and M. P. Fleming, *J. Am. Chem. Soc.*, 1974, **96**, 4708–4709.
61. A. Baumstark, C. McCloskey, T. Tolson and G. Syriopoulos, *Tetrahedron Lett.*, 1977, **18**, 3003–3006.
62. H. Walborsky and H. Wuest, *J. Am. Chem. Soc.*, 1982, **104**, 5807–5808.
63. J. Huang, V. Goedken and H. Walborsky, *J. Org. Chem.*, 1988, **53**, 4128–4131.
64. K. Sharpless, R. Hanzlik and E. E. Van Tamelen, *J. Am. Chem. Soc.*, 1968, **90**, 209–210.
65. E. E. Van Tamelen, B. Akermark and K. B. Sharpless, *J. Am. Chem. Soc.*, 1969, **91**, 1552–1554.
66. H. M. Walborsky and M. P. Murari, *J. Am. Chem. Soc.*, 1980, **102**, 426–428.
67. T. Mukaiyama, T. Sato and J. Hanna, *Chem. Lett.*, 1973, **2**, 1041–1044.
68. S. Tyrlik and I. Wolochowicz, *Bull. Soc. Chim. Fr.*, 1973, **6**, 2147–2148.
69. J. E. McMurry and J. G. Rico, *Tetrahedron Lett.*, 1989, **30**, 1169–1172.
70. J. E. McMurry, T. Lectka and J. G. Rico, *J. Org. Chem.*, 1989, **54**, 3748–3749.
71. J. E. McMurry, *Chem. Rev.*, 1989, **89**, 1513–1524.
72. J. E. McMurry, M. G. Silvestri, M. P. Fleming, T. Hoz and M. W. Grayston, *J. Org. Chem.*, 1978, **43**, 3249–3255.
73. J. E. McMurry, M. P. Fleming, K. L. Kees and L. R. Krepski, *J. Org. Chem.*, 1978, **43**, 3255–3266.
74. J. E. McMurry and L. R. Krepski, *J. Org. Chem.*, 1976, **41**, 3929–3930.
75. J. E. McMurry and M. P. Fleming, *J. Org. Chem.*, 1976, **41**, 896–897.
76. J. E. McMurry and M. Silvestri, *J. Org. Chem.*, 1975, **40**, 2687–2688.
77. J. E. McMurry and M. P. Fleming, *J. Org. Chem.*, 1975, **40**, 2555–2556.
78. J. E. McMurry and M. P. Fleming, *J. Am. Chem. Soc.*, 1974, **96**, 4708–4709.
79. S. Asako and L. Ilies, *Chem. Lett.*, 2020, **49**, 1386–1393.
80. A. Bongso, R. Roswanda and Y. M. Syah, *RSC Adv.*, 2022, **12**, 15885–15909.
81. J. E. McMurry, *Acc. Chem. Res.*, 1983, **16**, 405–411.
82. M. Ephritikhine, *Chem. Commun.*, 1998, 2549–2554.
83. C. Villiers and M. Ephritikhine, *Angew. Chem. Int. Ed.*, 1997, **36**, 2380–2382.
84. E. Block, in *Organic Reactions*, 2005, DOI: 10.1002/0471264180.or030.02, pp. 457–566.
85. T. Suga, S. Shimazu and Y. Ukaji, *Org. Lett.*, 2018, **20**, 5389–5392.

86. T. Suga and Y. Ukaji, *Org. Lett.*, 2018, **20**, 7846–7850.
87. T. Suga, R. Takada, S. Shimazu, M. Sakata and Y. Ukaji, *J. Org. Chem.*, 2022, **87**, 7487–7493.
88. H. Tian, R. Zhang, L. Shi, C. Zhao and X. Wang, *Chin. J. Chem.*, 2023, **41**, 1783–1790.
89. H. R. Dieguez, A. Lopez, V. Domingo, J. F. Arteaga, J. A. Dobado, M. M. Herrador, J. F. Quilez del Moral and A. F. Barrero, *J. Am. Chem. Soc.*, 2010, **132**, 254–259.
90. F. Sato, Y. Tomuro, H. Ishikawa, T. Oikawa and M. Sato, *Chem. Lett.*, 1980, **9**, 103–106.
91. C. Prieto, J. A. G. Delgado, J. F. Arteaga, M. Jaraíz, J. L. López-Pérez and A. F. Barrero, *Org. Biomol. Chem.*, 2015, **13**, 3462–3469.
92. X. Zheng, X.-J. Dai, H.-Q. Yuan, C.-X. Ye, J. Ma and P.-Q. Huang, *Angew. Chem. Int. Ed.*, 2013, **125**, 3578–3582.
93. H. Xie, J. Guo, Y.-Q. Wang, K. Wang, P. Guo, P.-F. Su, X. Wang and X.-Z. Shu, *J. Am. Chem. Soc.*, 2020, **142**, 16787–16794.
94. W. Hao, X. Wu, J. Z. Sun, J. C. Siu, S. N. MacMillan and S. Lin, *J. Am. Chem. Soc.*, 2017, **139**, 12141–12144.
95. H. Xie, S. Wang, Y. Wang, P. Guo and X.-Z. Shu, *ACS Catal.*, 2022, **12**, 1018–1023.
96. Q. Lin, W. Tong, X.-Z. Shu and Y. Chen, *Org. Lett.*, 2022, **24**, 8459–8464.
97. J. M. Cuerva, A. G. Campaña, J. Justicia, A. Rosales, J. L. Oller-López, R. Robles, D. J. Cárdenas, E. Buñuel and J. E. Oltra, *Angew. Chem. Int. Ed.*, 2006, **45**, 5522–5526.
98. B. Giese and J. Dupuis, *Tetrahedron Lett.*, 1984, **25**, 1349–1352.
99. T. Suga, Y. Takahashi, C. Miki and Y. Ukaji, *Angew. Chem. Int. Ed.*, 2022, **61**, e202112533.
100. T. Suga, M. Nakamura, R. Takada and Y. Ukaji, *Bull. Chem. Soc. Jpn.*, 2021, **94**, 1258–1260.
101. K. Daasbjerg, H. Svith, S. Grimme, M. Gerenkamp, C. Mück-Lichtenfeld, A. Gansäuer, A. Barchuk and F. Keller, *Angew. Chem. Int. Ed.*, 2006, **45**, 2041–2044.
102. T. Suga, C. Miki and Y. Ukaji, *ChemistryEurope*, 2023, **1**, e202300033.
103. L. Canali and D. C. Sherrington, *Chem. Soc. Rev.*, 1999, **28**, 85–93.
104. M. N. Hopkinson, C. Richter, M. Schedler and F. Glorius, *Nature*, 2014, **510**, 485–496.
105. S. Díez-González and S. P. Nolan, *Coord. Chem. Rev.*, 2007, **251**, 874–883.
106. H. Jacobsen, A. Correa, A. Poater, C. Costabile and L. Cavallo, *Coord. Chem. Rev.*, 2009, **253**, 687–703.
107. J. Hessevik, R. Lalrempuia, H. Nsiri, K. W. Törnroos, V. R. Jensen and E. Le Roux, *Dalton Trans.*, 2016, **45**, 14734–14744.
108. S. J. Blanksby and G. B. Ellison, *Acc. Chem. Res.*, 2003, **36**, 255–263.
109. J. Dean, *Lange's Handbook of Chemistry*, 1999.
110. A. A. Liori, I. K. Stamatopoulos, A. T. Papastavrou, A. Pinaka and G. C. Vougioukalakis, *Eur. J. Org. Chem.*, 2018, DOI: 10.1002/ejoc.201800827, 6134–6139.
111. A. I. Vogel, *Longman Group Ltd, London*, 1974.
112. J. E. Niklas, K. M. Hunter and A. E. V. Gorden, *Inorg. Chem.*, 2019, **58**, 15088–15100.
113. T. Ohshima, H. Morimoto and Y. Shimizu, US Pat., 9 278 905 B2, 2016.
114. C. Romain, L. Brelot, S. Bellemin-Laponnaz and S. Dagorne, *Organometallics*, 2010, **29**, 1191–1198.
115. T. L. Amyes, S. T. Diver, J. P. Richard, F. M. Rivas and K. Toth, *J. Am. Chem. Soc.*, 2004, **126**, 4366–4374.
116. G. K. S. Prakash, J. Hu, Y. Wang and G. A. Olah, *Org. Lett.*, 2004, **6**, 4315–4317.
117. J. Haggin, *Chem. Eng. News (US)*, 1993, **71**.
118. K. Weissermel and H.-J. Arpe, *Industrial Organic Chemistry*, John Wiley & Sons, 2008.
119. J. B. Levy, R. W. Taft, Jr. and L. P. Hammett, *J. Am. Chem. Soc.*, 1953, **75**, 1253–1254.
120. P. Wiseman, *An Introduction to Industrial Organic Chemistry*, Longman, London, 1972.
121. N. Katada, Y. Iseki, A. Shichi, N. Fujita, I. Ishino, K. Osaki, T. Torikai and M. Niwa, *Appl. Catal., A*, 2008, **349**, 55–61.
122. M. H. W. Sonnemans, *Appl. Catal., A*, 1993, **94**, 215–229.
123. J. M. Adams, D. E. Clement and S. H. Graham, *Clays Clay Miner.*, 1983, **31**, 129–136.

124. G. Zweifel and H. C. Brown, in *Organic Reactions*, 2011, DOI: 10.1002/0471264180.or013.01, pp. 1–54.
125. H. C. Brown and B. S. Rao, *J. Am. Chem. Soc.*, 1956, **78**, 5694–5695.
126. H. C. Brown, E. F. Knights and C. G. Scouten, *J. Am. Chem. Soc.*, 1974, **96**, 7765–7770.
127. K. Takahashi, M. Yamashita, T. Ichihara, K. Nakano and K. Nozaki, *Angew. Chem.*, 2010, **122**, 4590–4592.
128. Y. Yuki, K. Takahashi, Y. Tanaka and K. Nozaki, *J. Am. Chem. Soc.*, 2013, **135**, 17393–17400.
129. G. Dong, P. Teo, Z. K. Wickens and R. H. Grubbs, *Science*, 2011, **333**, 1609–1612.
130. E. M. McGarrigle and D. G. Gilheany, *Chem. Rev.*, 2005, **105**, 1563–1602.
131. T. Katsuki and V. Martin, *Organic Reactions*, 2004, **48**, 1–299.
132. J. D. Cox, *Tetrahedron*, 1963, **19**, 1175–1184.
133. H. C. Chitwood and B. T. Freure, *J. Am. Chem. Soc.*, 1946, **68**, 680–683.
134. T. Hansen, P. Vermeeren, A. Haim, M. J. H. van Dorp, J. D. C. Codée, F. M. Bickelhaupt and T. A. Hamlin, *Eur. J. Org. Chem.*, 2020, **2020**, 3822–3828.
135. D. K. Murphy, R. L. Alumbaugh and B. Rickborn, *J. Am. Chem. Soc.*, 1969, **91**, 2649–2653.
136. H. Sajiki, K. Hattori and K. Hirota, *Chem. Commun.*, 1999, 1041–1042.
137. M. S. Newman, G. Underwood and M. Renoll, *J. Am. Chem. Soc.*, 1949, **71**, 3362–3363.
138. J. Meinwald, S. S. Labana and M. S. Chadha, *J. Am. Chem. Soc.*, 1963, **85**, 582–585.
139. W. Liu, W. Li, A. Spannenberg, K. Junge and M. Beller, *Nat. Catal.*, 2019, **2**, 523–528.
140. W. Liu, T. Leischner, W. Li, K. Junge and M. Beller, *Angew. Chem. Int. Ed.*, 2020, **59**, 11321–11324.
141. X. Liu, L. Longwitz, B. Spiegelberg, J. Tönjes, T. Beweries and T. Werner, *ACS Catal.*, 2020, **10**, 13659–13667.
142. M. Vayer, S. Zhang, J. Moran and D. Lebœuf, *ACS Catal.*, 2022, **12**, 3309–3316.
143. Y.-X. Yao, H.-W. Zhang, C.-B. Lu, H.-Y. Shang and Y.-Y. Tian, *Eur. J. Org. Chem.*, 2023, **26**, e202300111.
144. R. A. Benkeser, A. Rappa and L. A. Wolsieffer, *J. Org. Chem.*, 1986, **51**, 3391–3393.
145. H. C. Brown, S. Ikegami and J. H. Kawakami, *J. Org. Chem.*, 1970, **35**, 3243–3245.
146. E. M. Kaiser, C. G. Edmonds, S. D. Grubb, J. W. Smith and D. Tramp, *J. Org. Chem.*, 1971, **36**, 330–335.
147. T. V. RajanBabu and W. A. Nugent, *J. Am. Chem. Soc.*, 1994, **116**, 986–997.
148. P. Girard, J. Namy and H. Kagan, *J. Am. Chem. Soc.*, 1980, **102**, 2693–2698.
149. A. Gansäuer, H. Bluhm and M. Pierobon, *J. Am. Chem. Soc.*, 1998, **120**, 12849–12859.
150. W. A. Nugent and T. RajanBabu, *J. Am. Chem. Soc.*, 1988, **110**, 8561–8562.
151. M. Paradas, A. G. Campaña, T. Jiménez, R. Robles, J. E. Oltra, E. Buñuel, J. Justicia, D. J. Cárdenas and J. M. Cuerva, *J. Am. Chem. Soc.*, 2010, **132**, 12748–12756.
152. A. Gansäuer, C.-A. Fan and F. Piestert, *J. Am. Chem. Soc.*, 2008, **130**, 6916–6917.
153. C. Yao, T. Dahmen, A. Gansäuer and J. Norton, *Science*, 2019, **364**, 764–767.
154. J. Choi, M. E. Pulling, D. M. Smith and J. R. Norton, *J. Am. Chem. Soc.*, 2008, **130**, 4250–4252.
155. M. Heinz, G. Weiss, G. Shizgal, A. Panfilova and A. Gansäuer, *Angew. Chem. Int. Ed.*, 2023, **62**, e202308680.
156. G. Li and J. R. Norton, *Org. Lett.*, 2024, **26**, 1382–1386.
157. D. S. Hamilton and D. A. Nicewicz, *J. Am. Chem. Soc.*, 2012, **134**, 18577–18580.
158. T. M. Nguyen and D. A. Nicewicz, *J. Am. Chem. Soc.*, 2013, **135**, 9588–9591.
159. A. J. Perkowski and D. A. Nicewicz, *J. Am. Chem. Soc.*, 2013, **135**, 10334–10337.
160. K. A. Margrey and D. A. Nicewicz, *Acc. Chem. Res.*, 2016, **49**, 1997–2006.
161. X. Hu, G. Zhang, F. Bu and A. Lei, *ACS Catal.*, 2017, **7**, 1432–1437.
162. B. A. van der Worp and T. Ritter, *J. Am. Chem. Soc.*, 2025, **147**, 4736–4742.
163. K. Behm and R. D. McIntosh, *ChemPlusChem*, 2020, **85**, 2611–2618.
164. C. Wegeberg and O. S. Wenger, *JACS Au*, 2021, **1**, 1860–1876.
165. T. Huang, P. Du and Y.-M. Lin, *Chin. J. Chem.*, 2025, **43**, 2566–2587.
166. A. M. May and J. L. Dempsey, *Chem. Sci.*, 2024, **15**, 6661–6678.

167. F. Juliá, *ChemCatChem*, 2022, **14**, e202200916.
168. M. R. Hoffmann, S. T. Martin, W. Choi and D. W. Bahnemann, *Chem. Rev.*, 1995, **95**, 69–96.
169. D. Dvoranová, Z. Barbieriková and V. Brezová, *Molecules*, 2014, **19**, 17279–17304.
170. J. Zhang and Y. Nosaka, *J. Phys. Chem. C*, 2014, **118**, 10824–10832.
171. K. Vazdar, D. Margetić, B. Kovačević, J. Sundermeyer, I. Leito and U. Jahn, *Acc. Chem. Res.*, 2021, **54**, 3108–3123.
172. C.-C. Liou and J. S. Brodbelt, *J. Am. Soc. Mass. Spectrom.*, 1992, **3**, 543–548.
173. H. Huang, Z. M. Strater, M. Rauch, J. Shee, T. J. Sisto, C. Nuckolls and T. H. Lambert, *Angew. Chem. Int. Ed.*, 2019, **58**, 13318–13322.
174. R. M. Wilson and T. H. Lambert, *Acc. Chem. Res.*, 2022, **55**, 3057–3069.
175. M. R. Lasky, E.-C. Liu, M. S. Remy and M. S. Sanford, *J. Am. Chem. Soc.*, 2024, **146**, 14799–14806.
176. S.-Q. Lai, B.-Y. Wei, J.-W. Wang, W. Yu and B. Han, *Angew. Chem. Int. Ed.*, 2021, **60**, 21997–22003.
177. L. Leng and J. M. Ready, *ACS Catal.*, 2021, **11**, 13714–13720.
178. L. Quach, S. Dutta, P. M. Pflüger, F. Sandfort, P. Bellotti and F. Glorius, *ACS Catal.*, 2022, **12**, 2499–2504.
179. G. Tan, F. Paulus, Á. Rentería-Gómez, R. F. Lalisse, C. G. Daniliuc, O. Gutierrez and F. Glorius, *J. Am. Chem. Soc.*, 2022, **144**, 21664–21673.
180. C. Ascenzi Pettenuzzo, D. R. Pradhan, J. Singh, L. Liu, G. Cuffel, M. J. Vetticatt and Y. Deng, *J. Am. Chem. Soc.*, 2025, **147**, 10382–10390.
181. I. A. MacKenzie, L. Wang, N. P. R. Onuska, O. F. Williams, K. Begam, A. M. Moran, B. D. Dunietz and D. A. Nicewicz, *Nature*, 2020, **580**, 76–80.
182. M. Schlegel, S. Qian and D. A. Nicewicz, *ACS Catal.*, 2022, **12**, 10499–10505.
183. A. G. Larsen, A. H. Holm, M. Roberson and K. Daasbjerg, *J. Am. Chem. Soc.*, 2001, **123**, 1723–1729.
184. J. Kim, X. Sun, B. A. van der Worp and T. Ritter, *Nat. Catal.*, 2023, **6**, 196–203.
185. M.-F. Nieva and N. Przybilla, *Astron. Astrophys.*, 2012, **539**, A143.
186. W. H. Schlesinger and E. S. Bernhardt, in *Biogeochemistry (Fourth Edition)*, eds. W. H. Schlesinger and E. S. Bernhardt, Academic Press, 2020, DOI: 10.1016/B978-0-12-814608-8.00003-7, pp. 51–97.
187. H. Cavendish, *Philos. Trans. R. Soc. London, Ser. A*, 1766, **56**, 141–184.
188. J. S. Rigden, *Hydrogen: the Essential Element*, Harvard University Press, 2003.
189. W. Ramsay, *The Gases of the Atmosphere, the History of their Discovery*, Macmillan and Company, limited, 1915.
190. S. Mauskop, *Ambix*, 2002, **49**, 185–205.
191. N. Bohr, *Philos. Mag.*, 1913, **26**, 1–25.
192. E. Rutherford, *Philos. Mag.*, 1911, **21**, 669–688.
193. M. Planck, *Ann. Phys.*, 1901, **4**, 1.
194. E. Schrödinger, *Ann. Phys.*, 1926, **386**, 109–139.
195. W. Heisenberg, *Z. Phys.*, 1925, **33**, 879–893.
196. J. N. Brönsted, *Rec. Trav. Chim. Pays-Bas*, 1923, **42**, 718–728.
197. T. Lowry, *J. Soc. Chem. Ind.*, 1923, **42**, 43–47.
198. W. M. Mueller, J. P. Blackledge and G. G. Libowitz, *Metal Hydrides*, Elsevier, 2013.
199. M. Hayward, E. Cussen, J. Claridge, M. Bieringer, M. Rosseinsky, C. Kiely, S. Blundell, I. Marshall and F. Pratt, *Science*, 2002, **295**, 1882–1884.
200. J. S. Vogel, *AIP Conf. Proc.*, 2015, **1655**, 020015.
201. G. Herzberg, *Molecular Spectra and Molecular Structure, Vol. I.*, Read Books Ltd, 2013.
202. M. Weller, M. T. Weller, T. Overton, J. Rourke and F. Armstrong, *Inorganic Chemistry*, Oxford University Press, USA, 2014.

203. C. Mansilla, C. Bourasseau, C. Cany, B. Guinot, A. Le Duigou and P. Lucchese, in *Hydrogen Supply Chains*, ed. C. Azzaro-Pantel, Academic Press, 2018, DOI: 10.1016/B978-0-12-811197-0.00007-5, pp. 271–292.
204. C. G. Santana and M. J. Krische, *ACS Catal.*, 2021, **11**, 5572–5585.
205. P. Sabatier and J. Senderens, *C. R. Acad. Sci., Paris*, 1897, **124**, 1358–1360.
206. F. Haber and G. Van Oordt, *Z. Anorg. Allg. Chem.*, 1905, **44**, 341–378.
207. W. Xu, Y. Zhang, J. Wang, Y. Xu, L. Bian, Q. Ju, Y. Wang and Z. Fang, *Nat. Commun.*, 2022, **13**, 2068.
208. F. Fischer and H. Tropsch, *Brennstoff-Chem.*, 1923, **4**, 276–285.
209. G. P. Van Der Laan and A. A. C. M. Beenackers, *Catal. Rev.*, 1999, **41**, 255–318.
210. J. Halpern, J. Harrod and B. James, *J. Am. Chem. Soc.*, 1961, **83**, 753–754.
211. L. Vaska and J. W. DiLuzio, *J. Am. Chem. Soc.*, 1962, **84**, 679–680.
212. J. Young, J. Osborn, F. Jardine and G. Wilkinson, *Chem. Commun.*, 1965, 131–132.
213. W. S. Knowles and M. J. Sabacky, *Chem. Commun.*, 1968, 1445–1446.
214. R. Crabtree, *Acc. Chem. Res.*, 1979, **12**, 331–337.
215. R. Noyori, T. Ohkuma, M. Kitamura, H. Takaya, N. Sayo, H. Kumobayashi and S. Akutagawa, *J. Am. Chem. Soc.*, 1987, **109**, 5856–5858.
216. P. J. Chirik, *Acc. Chem. Res.*, 2015, **48**, 1687–1695.
217. G. Totarella, R. Beerthuis, N. Masoud, C. Louis, L. Delannoy and P. E. de Jongh, *J. Phys. Chem. C*, 2021, **125**, 366–375.
218. H. Lindlar, *Helv. Chim. Acta*, 1952, **35**, 446–450.
219. C. J. Love and F. J. McQuillin, *J. Chem. Soc., Perkin Trans. 1*, 1973, DOI: 10.1039/P19730002509, 2509–2512.
220. T. Irrgang and R. Kempe, *Chem. Rev.*, 2020, **120**, 9583–9674.
221. I. Langmuir, *J. Am. Chem. Soc.*, 1912, **34**, 860–877.
222. W. Gardiner and G. Kistiakowsky, *J. Chem. Phys.*, 1961, **35**, 1765–1770.
223. R. W. Wood, *Proc. R. Soc. Lond. A*, 1920, **97**, 455–470.
224. H. Smyth, *Phys. Rev.*, 1925, **25**, 452.
225. W. Bleakney, *Phys. Rev.*, 1930, **35**, 1180–1186.
226. T. R. Hogness and E. G. Lunn, *Phys. Rev.*, 1925, **26**, 44–55.
227. A. C. Allisonand and A. Dalgarno, *At. Data Nucl. Data Tables*, 1969, **1**, 91–102.
228. C. Gay, N. Abel, R. Porter, P. Stancil, G. J. Ferland, G. Shaw, P. Van Hoof and R. Williams, *Astrophys. J.*, 2012, **746**, 78.
229. A. Glassgold and W. D. Langer, *Astrophys. J.*, 1973, **186**, 859–888.
230. K. R. Jennings and J. W. Linnett, *Nature*, 1958, **182**, 597–598.
231. D. E. Nagle, R. S. Julian and J. R. Zacharias, *Phys. Rev.*, 1947, **72**, 971.
232. H. P. Broida and J. W. Moyer, *J. Opt. Soc. Am.*, 1952, **42**, 37–41.
233. A. Ding, J. Karlau and J. Weise, *Rev. Sci. Instrum.*, 1977, **48**, 1002–1004.
234. G. Cario and J. Franck, *Z. Phys.*, 1922, **11**, 161–166.
235. C. A. Muedas, R. R. Ferguson, S. H. Brown and R. H. Crabtree, *J. Am. Chem. Soc.*, 1991, **113**, 2233–2242.
236. G. Stein and J. Weiss, *Nature*, 1948, **161**, 650–650.
237. G. Scholes and M. Simic, *J. Phys. Chem.*, 1964, **68**, 1738–1743.
238. G. Nong, Y. Chen, M. Li and Z. Zhou, *Energy Convers. Manage.*, 2015, **105**, 545–551.
239. K. Makino, M. M. Mossoba and P. Riesz, *J. Phys. Chem.*, 1983, **87**, 1369–1377.
240. J. Barrett and J. Baxendale, *Trans. Faraday Soc.*, 1960, **56**, 37–43.
241. A. K. Spiliotis, M. Xygkis, M. E. Koutrakis, D. Sofikitis and T. P. Rakitzis, *Chem. Phys. Impact*, 2021, **2**, 100022.
242. R. M. Martin and J. E. Willard, *J. Chem. Phys.*, 1964, **40**, 3007–3014.
243. R. Penzhorn and B. d. B. Darwent, *J. Chem. Phys.*, 1971, **55**, 1508–1511.
244. B. d. Darwent, R. L. Wadlinger and M. J. Allard, *J. Phys. Chem.*, 1967, **71**, 2346–2347.
245. T. J. Hardwick, *J. Phys. Chem.*, 1961, **65**, 101–108.

246. T. Hardwick, *J. Phys. Chem.*, 1962, **66**, 117–125.
247. R. J. Cvetanović, in *Advances in Photochemistry*, 1963, DOI: 10.1002/9780470133316.ch5, pp. 115–182.
248. P. M. Scott and K. R. Jennings, *J. Phys. Chem.*, 1969, **73**, 1513–1521.
249. P. M. Scott and K. R. Jennings, *J. Phys. Chem.*, 1969, **73**, 1521–1525.
250. O. Strausz and H. Gunning, *Trans. Faraday Soc.*, 1964, **60**, 347–358.
251. M. Meissner and H. Thompson, *Trans. Faraday Soc.*, 1938, **34**, 1238–1239.
252. W. W. Lam, T. Yokota, I. Safarik and O. P. Strausz, *J. Photochem. Photobiol. A: Chem.*, 1989, **47**, 47–63.
253. W. A. Pryor and R. W. Henderson, *J. Am. Chem. Soc.*, 1970, **92**, 7234–7236.
254. Q. Miao, M. Liu, Y.-y. Mou, Y.-f. Zhang, Q. Li, Z.-j. Cao and W. Jiang, *ACS Sustain. Chem. Eng.*, 2024, **12**, 5596–5607.
255. G. Yi, B. Wang, S. Lu, L. Zhang, W. Liu, Z. Chen, L. Yang, X. Luo and A.-J. Wang, *Chem. Eng. J.*, 2024, **483**, 149226.
256. H. A. Schwarz, *J. Chem. Educ.*, 1981, **58**, 101–105.
257. D. A. Armstrong, R. E. Huie, W. H. Koppenol, S. V. Lymar, G. Merényi, P. Neta, B. Ruscic, D. M. Stanbury, S. Steenken and P. Wardman, *Pure Appl. Chem.*, 2015, **87**, 1139–1150.
258. M. Anbar and A. Ross, *Selected specific rates of reactions of transients from water in aqueous solution. II. Hydrogen atom*, Report NSRDS-NBS 51, U.S. Department of Commerce, Washington, DC, 1975.
259. G. V. Buxton, C. L. Greenstock, W. P. Helman and A. B. Ross, *J. Phys. Chem. Ref. Data*, 1988, **17**, 513–886.
260. J. Sweet and J. Thomas, *J. Phys. Chem.*, 1964, **68**, 1363–1368.
261. K. R. Jennings and R. J. Cvetanović, *J. Chem. Phys.*, 1961, **35**, 1233–1240.
262. W. Jones, S. Macknight and L. Teng, *Chem. Rev.*, 1973, **73**, 407–440.
263. T. Hardwick, *J. Phys. Chem.*, 1962, **66**, 2246–2249.
264. T. Hardwick, *J. Phys. Chem.*, 1962, **66**, 291–295.
265. R. J. Cvetanović and L. C. Doyle, *J. Chem. Phys.*, 1969, **50**, 4705–4713.
266. M. Anbar and P. Neta, *Int. J. Appl. Radiat. Isot.*, 1967, **18**, 493–523.
267. F. Parsaee, M. C. Senarathna, P. B. Kannangara, S. N. Alexander, P. D. E. Arche and E. R. Welin, *Nat. Rev. Chem.*, 2021, **5**, 486–499.
268. J. J. A. Garwood, A. D. Chen and D. A. Nagib, *J. Am. Chem. Soc.*, 2024, **146**, 28034–28059.
269. D. S. Urch and R. L. Wolfgang, *J. Am. Chem. Soc.*, 1959, **81**, 2025–2026.
270. A. Beeri, E. Berman, R. Vishkautsan and Y. Mazur, *J. Am. Chem. Soc.*, 1986, **108**, 6413–6414.
271. D. D. Tanner and L. Zhang, *J. Am. Chem. Soc.*, 1994, **116**, 6683–6689.
272. H. W. Melville and J. Robb, *Proc. R. Soc. Lond. A*, 1950, **202**, 181–202.
273. C. A. Muedas, R. R. Ferguson and R. H. Crabtree, *Tetrahedron Lett.*, 1989, **30**, 3389–3392.
274. J. E. Bennett and B. Mile, *J. Chem. Soc., Faraday Trans. 1*, 1973, **69**, 1398–1414.
275. J. Peng, K. Du, J. Sun, X. Yang, X. Wang, X. Zhang, G. Song and F. Feng, *Angew. Chem. Int. Ed.*, 2023, **62**, e202214991.
276. W. A. Pryor, T. Lin, J. Stanley and R. Henderson, *J. Am. Chem. Soc.*, 1973, **95**, 6993–6998.
277. R. Henderson and W. A. Pryor, *J. Am. Chem. Soc.*, 1975, **97**, 7437–7441.
278. T. Autrey, E. A. Alborn, J. A. Franz and D. M. Camaioni, *Energy Fuels*, 1995, **9**, 420–428.
279. D. F. McMillen, R. Malhotra, S.-J. Chang, W. C. Ogier, S. E. Nigenda and R. H. Fleming, *Fuel*, 1987, **66**, 1611–1620.
280. D. F. McMillen, R. Malhotra, G. P. Hum and S. J. Chang, *Energy Fuels*, 1987, **1**, 193–198.
281. D. D. Tanner, L. Zhang, M. Vigneswaran and P. Kandanarachchi, *J. Org. Chem.*, 1995, **60**, 4481–4487.
282. W. A. Pryor, J. P. Stanley and M. G. Griffith, *Science*, 1970, **169**, 181–183.
283. W. Snipes and J. Schmidt, *Radiat. Res.*, 1966, **29**, 194–202.
284. E. W. R. Steacie and N. A. D. Parlee, *Can. J. Res., Ser. B*, 1939, **17b**, 371–384.

285. C. G. Boojamra, R. H. Crabtree, R. R. Ferguson and C. A. Muedas, *Tetrahedron Lett.*, 1989, **30**, 5583–5586.
286. T. Constantin, B. Górski, M. J. Tilby, S. Chelli, F. Juliá, J. Llaveria, K. J. Gillen, H. Zipse, S. Lakhdar and D. Leonori, *Science*, 2022, **377**, 1323–1328.
287. J. Burdeniuc, B. Jedicka and R. H. Crabtree, *Chem. Ber.*, 1997, **130**, 145–154.
288. G. G. Jayson, J. P. Keene, D. A. Stirling and A. J. Swallow, *Trans. Faraday Soc.*, 1969, **65**, 2453–2464.
289. M. Anbar and E. J. Hart, *J. Phys. Chem.*, 1967, **71**, 4163–4165.
290. J. O. Metzger, *Angew. Chem. Int. Ed.*, 1986, **25**, 80–81.
291. R. Jackson and W. A. Waters, *J. Chem. Soc.*, 1958, 4632–4635.
292. J. Zhang, C. Mück-Lichtenfeld and A. Studer, *Nature*, 2023, **619**, 506–513.
293. M. Coellen and C. Rüchardt, *Chem. Eur. J.*, 1995, **1**, 564–567.
294. C.-J. Tso, T. Kasai and K.-C. Lin, *Sci. Rep.*, 2020, **10**, 4769.
295. D. C. Cabanero and T. Rovis, *Nat. Rev. Chem.*, 2025, **9**, 28–45.
296. N. A. Romero and D. A. Nicewicz, *Chem. Rev.*, 2016, **116**, 10075–10166.
297. Z. Zuo and D. W. C. MacMillan, *J. Am. Chem. Soc.*, 2014, **136**, 5257–5260.
298. D. Yin, D. Su and J. Jin, *Cell Rep. Phys. Sci.*, 2020, **1**, 100141.
299. K.-J. Bian, Y.-C. Lu, D. Nemoto, S.-C. Kao, X. Chen and J. G. West, *Nat. Chem.*, 2023, **15**, 1683–1692.
300. S. Tamaki, T. Kusamoto and H. Tsurugi, *ChemCatChem*, 2025, **17**, e202402106.
301. R. Noyori, M. Katô, M. Kawanisi and H. Nozaki, *Tetrahedron*, 1969, **25**, 1125–1136.
302. K. Okada, K. Okubo and M. Oda, *J. Photochem. Photobiol. A: Chem.*, 1991, **57**, 265–277.
303. V. T. Nguyen, V. D. Nguyen, G. C. Haug, H. T. Dang, S. Jin, Z. Li, C. Flores-Hansen, B. S. Benavides, H. D. Arman and O. V. Larionov, *ACS Catal.*, 2019, **9**, 9485–9498.
304. M. O. Zubkov, M. D. Kosobokov, V. V. Levin and A. D. Dilman, *Org. Lett.*, 2022, **24**, 2354–2358.
305. H. T. Dang, G. C. Haug, V. T. Nguyen, N. T. Vuong, V. D. Nguyen, H. D. Arman and O. V. Larionov, *ACS Catal.*, 2020, **10**, 11448–11457.
306. N. A. Romero and D. A. Nicewicz, *J. Am. Chem. Soc.*, 2014, **136**, 17024–17035.
307. S. N. Alektiar and Z. K. Wickens, *J. Am. Chem. Soc.*, 2021, **143**, 13022–13028.
308. J.-M. M. Grandjean and D. A. Nicewicz, *Angew. Chem. Int. Ed.*, 2013, **52**, 3967–3971.
309. H. G. Roth, N. A. Romero and D. A. Nicewicz, *Synlett*, 2016, **27**, 714–723.
310. F. P. Sargent and E. M. Gardy, *Can. J. Chem.*, 1976, **54**, 275–279.
311. R. Marek, A. Lycka, E. Kolehmainen, E. Sievanen and J. Tousek, *Curr. Org. Chem.*, 2007, **11**, 1154–1205.
312. M. Lõkov, S. Tshepelevitsh, A. Heering, P. G. Plieger, R. Vianello and I. Leito, *Eur. J. Org. Chem.*, 2017, **2017**, 4475–4489.
313. B. Yuan, P. Veres, C. Warneke, J. Roberts, J. Gilman, A. Koss, P. Edwards, M. Graus, W. Kuster and S.-M. Li, *Atmos. Chem. Phys.*, 2015, **15**, 1975–1993.
314. M. J. Stirling, G. Sweeney, K. MacRory, A. J. Blacker and M. I. Page, *Org. Biomol. Chem.*, 2016, **14**, 3614–3622.
315. A. J. Bard and L. R. Faulkner, *Electrochemical Methods: Fundamentals and Applications*, 2nd ed., Wiley, New York, 2001.
316. M. Gay, C. Evrard, F. Descamps, P. Carato, N. Renault, M. Coevoet, S. Eddarkaoui, C. Baud, P.-E. Larchanché and L. Buée, *Eur. J. Med. Chem.*, 2018, **159**, 104–125.
317. R. Ding, Q. Liu and L. Zheng, *Chem. Eur. J.*, 2023, **29**, e202203792.
318. C. Pérez-Bolívar, S. y. Takizawa, G. Nishimura, V. A. Montes and P. Anzenbacher Jr, *Chem. Eur. J.*, 2011, **17**, 9076–9082.
319. K.-Y. Jung, K. Vanommeslaeghe, M. E. Lanning, J. L. Yap, C. Gordon, P. T. Wilder, A. D. MacKerell Jr and S. Fletcher, *Org. Lett.*, 2013, **15**, 3234–3237.
320. F. J. Martínez-Martínez, I. I. Padilla-Martínez, M. A. Brito, E. D. Geniz, R. C. Rojas, J. B. R. Saavedra, H. Höpfl, M. Tlahuextl and R. Contreras, *J. Chem. Soc., Perkin Trans. 2*, 1998, DOI: 10.1039/A704640E, 401–406.

321. D. R. Weinberg, N. Hazari, J. A. Labinger and J. E. Bercaw, *Organometallics*, 2010, **29**, 89–100.
322. J. S. Bandar, A. Tanaset and T. H. Lambert, *Chem. Eur. J.*, 2015, **21**, 7365–7368.
323. G. W. Kabalka, T. M. Shoup and N. M. Goudgaon, *J. Org. Chem.*, 1989, **54**, 5930–5933.
324. K. Miyamoto, Y. Sei, K. Yamaguchi and M. Ochiai, *J. Am. Chem. Soc.*, 2009, **131**, 1382–1383.
325. L. Hu and V. H. Rawal, *J. Am. Chem. Soc.*, 2021, **143**, 10872–10875.
326. P. Frei, D. H. Jones, S. T. Kay, J. A. McLellan, B. F. Johnston, A. R. Kennedy and N. C. O. Tomkinson, *J. Org. Chem.*, 2018, **83**, 1510–1517.
327. Y. Hirao, H. Eto, M. Teraoka and T. Kubo, *Org. Biomol. Chem.*, 2022, **20**, 1671–1679.
328. A. E. Cruz-Jiménez, P. A. Argumedo-Castrejón, J. B. Mateus-Ruiz, V. A. Lucas-Rosales, O. A. Valle-González, J. O. C. Jiménez-Halla and J. A. Luján-Montelongo, *New J. Chem.*, 2024, **48**, 9424–9428.
329. Z. R. Bell, G. R. Motson, J. C. Jeffery, J. A. McCleverty and M. D. Ward, *Polyhedron*, 2001, **20**, 2045–2053.
330. S. Pal, S. Das, S. Chakraborty, S. Khanra and N. D. Paul, *J. Org. Chem.*, 2023, **88**, 3650–3665.
331. C. Uncuta, M. T. Căproiu, V. Câmpeanu, A. Petride, M. G. Dănilă, M. Plăveti and A. T. Balaban, *Tetrahedron*, 1998, **54**, 9747–9764.
332. N. Müller, J. Stahl, J. Stoiber and B. König, *Eur. J. Org. Chem.*, 2025, **28**, e202500373.
333. M. H. Çelikoğlu, S. Uçar and B. Nişancı, *J. Heterocycl. Chem.*, 2024, **61**, 1029–1034.
334. W. Verbeet, Y. Husiev and S. Bonnet, *Eur. J. Org. Chem.*, 2024, **27**, e202400054.
335. P. J. Kohlpaintner, N. Schupp, N. Ehlenz, L. Marquart, L. J. Gooßen and S. R. Waldvogel, *Org. Lett.*, 2024, **26**, 1607–1611.
336. P. Mampuys, Y. Zhu, S. Sergeyev, E. Ruijter, R. V. A. Orru, S. Van Doorslaer and B. U. W. Maes, *Org. Lett.*, 2016, **18**, 2808–2811.
337. W.-X. Hu, K.-H. Yu, F.-C. Jia and S.-X. Gu, *J. Org. Chem.*, 2024, **89**, 16531–16541.
338. J. Weweler, S. L. Younas and J. Streuff, *Angew. Chem. Int. Ed.*, 2019, **58**, 17700–17703.
339. T. J. Zähringer, M.-S. Bertrams and C. Kerzig, *J. Mater. Chem. C*, 2022, **10**, 4568–4573.
340. A. S. H. Ryder, W. B. Cunningham, G. Ballantyne, T. Mules, A. G. Kinsella, J. Turner-Dore, C. M. Alder, L. J. Edwards, B. S. J. McKay, M. N. Grayson and A. J. Cresswell, *Angew. Chem. Int. Ed.*, 2020, **59**, 14986–14991.
341. A. Louka, C. Gryparis and M. Stratakis, *Arkivoc*, 2015, **2015**, 38–51.
342. A. R. White, L. Wang and D. A. Nicewicz, *Synlett*, 2019, **30**, 827–832.
343. D. Wu, W. Pisula, V. Enkelmann, X. Feng and K. Müllen, *J. Am. Chem. Soc.*, 2009, **131**, 9620–9621.
344. X. Chen, Y. Xie, C. Li, F. Xiao and G.-J. Deng, *Eur. J. Org. Chem.*, 2017, **2017**, 577–581.
345. J. A. Andrews, J. Kalepu, C. F. Palmer, D. L. Poole, K. E. Christensen and M. C. Willis, *J. Am. Chem. Soc.*, 2023, **145**, 21623–21629.
346. L.-M. Entgelmeier, S. Mori, S. Sendo, R. Yamaguchi, R. Suzuki, T. Yanai, O. García Mancheño, K. Ohmatsu and T. Ooi, *Angew. Chem. Int. Ed.*, 2024, **63**, e202404890.
347. H. Huang, Y. Jiang, W. Yuan and Y.-M. Lin, *Angew. Chem. Int. Ed.*, 2024, **63**, e202409653.
348. A. Srikrishna, T. Jagadeeswar Reddy and R. Viswajanani, *Tetrahedron*, 1996, **52**, 1631–1636.
349. C. Liu, Y. Zhang and R. Shang, *Chem*, 2025, **11**, 102359.
350. J. B. Azeredo, M. E. C. Thedy, M. Godoi, M. H. Keller, B. S. de Souza and J. A. Roehrs, *Tetrahedron Lett.*, 2022, **100**, 153883.
351. S. M. Weierbach, R. P. Reynolds, S. M. Stephens, K. V. Vlasakakis, R. T. Ritter, O. M. White, N. H. Patel, E. C. Hayes, S. Dunmire and K. M. Lambert, *J. Org. Chem.*, 2023, **88**, 11392–11410.
352. Z. Zhang, Y. Wang, X. Pan, M. Zhang, W. Zhao, M. Li and H. Zhang, *Beilstein J. Org. Chem.*, 2025, **21**, 253–261.
353. K. Wang, Y. Hu, Z. Li, M. Wu, Z. Liu, B. Su, A. Yu, Y. Liu and Q. Wang, *Synthesis*, 2010, **2010**, 1083–1090.
354. X. Sun, Y. Zhang, T. Li, K. Li, Q. Sun and Z. Wang, *Org. Lett.*, 2024, **26**, 1566–1572.
355. G. Feng, X. Luo, X. Lu, S. Xie, L. Deng, W. Kang, F. He, J. Zhang, C. Lei, B. Lin, Y. Huang, Z. Nie and S. Yao, *Angew. Chem. Int. Ed.*, 2019, **58**, 6590–6594.

356. Y. Sun, H. Shi, J. He, K. Yang, D. Yin, D. Xiao and Y. Du, *J. Org. Chem.*, 2025, **90**, 2328–2340.
357. J. Cuomo, J. H. Merrifield and J. F. W. Keana, *J. Org. Chem.*, 1980, **45**, 4216–4219.
358. M. S. Newman and H. A. Karnes, *J. Org. Chem.*, 1966, **31**, 3980–3984.
359. B. J. Rodgers, N. A. Elsharif, N. Vashisht, M. M. Mingus, M. A. Mulvahill, G. Stengel, R. D. Kuchta and B. W. Purse, *Chem. Eur. J.*, 2014, **20**, 2010–2015.
360. X. Li, M. Yang, S. Wang, X. Yuan, J. Yin, D. Shi, S. Ma, Q. Zhang and T. Xiong, *Org. Lett.*, 2025, **27**, 4986–4991.
361. T. Tokuyasu, S. Kunikawa, K. J. McCullough, A. Masuyama and M. Nojima, *J. Org. Chem.*, 2005, **70**, 251–260.
362. P. Xu, F. Wang, G. Fan, X. Xu and P. Tang, *Angew. Chem. Int. Ed.*, 2017, **56**, 1101–1104.
363. U. P. Saikia, F. L. Hussain, M. Suri and P. Pahari, *Tetrahedron Lett.*, 2016, **57**, 1158–1160.
364. G. Kundu, T. Sperger, K. Rissanen and F. Schoenebeck, *Angew. Chem. Int. Ed.*, 2020, **59**, 21930–21934.
365. Z. Lu, X. Zeng, G. B. Hammond and B. Xu, *J. Am. Chem. Soc.*, 2017, **139**, 18202–18205.
366. M. Regnier, C. Vega, D. I. Ioannou, Z. Zhang and T. Noël, *Angew. Chem. Int. Ed.*, 2025, **64**, e202500203.
367. A. S. Sokolova, O. I. Yarovaya, A. A. Shtro, M. S. Borisova, E. A. Morozova, T. G. Tolstikova, V. V. Zarubaev and N. F. Salakhutdinov, *Chem. Heterocycl. Compd.*, 2017, **53**, 371–377.
368. J. Song, T. Torigoe and Y. Kuninobu, *Eur. J. Org. Chem.*, 2023, **26**, e202301015.
369. M. Amézquita-Valencia, G. Achonduh and H. Alper, *J. Org. Chem.*, 2015, **80**, 6419–6424.
370. P. Dawar, M. B. Raju and R. A. Ramakrishna, *Synth. Commun.*, 2014, **44**, 836–846.
371. M. Hruzd, S. L. Kleynemeyer, C. Michon, S. Bastin, E. Pollet, V. Ritleng and J.-B. Sortais, *Chem. Commun.*, 2025, **61**, 2969–2972.
372. N. F. Both, A. Spannenberg, H. Jiao, K. Junge and M. Beller, *Angew. Chem. Int. Ed.*, 2023, **62**, e202307987.
373. J. D. Griffin, M. A. Zeller and D. A. Nicewicz, *J. Am. Chem. Soc.*, 2015, **137**, 11340–11348.
374. C.-S. Kuai, L.-C. Wang, J.-X. Xu and X.-F. Wu, *Org. Lett.*, 2022, **24**, 451–456.
375. E. K. Leggans, T. J. Barker, K. K. Duncan and D. L. Boger, *Org. Lett.*, 2012, **14**, 1428–1431.
376. I. Robb and J. A. Murphy, *Org. Lett.*, 2024, **26**, 2218–2222.
377. J. Li, Z. Yu, J. Zhao, C. Ma, L. Duan, Z. Liu, H. Sun, G. Zhao, Q. Liu and Q. Meng, *J. Org. Chem.*, 2025, **90**, 1245–1255.
378. A. C. Albe´niz, P. Espinet and Y.-S. Lin, *Tetrahedron*, 1998, **54**, 13851–13866.
379. D. O'Hanlon, S. Davin, B. Glennon and M. Baumann, *Chem. Commun.*, 2025, **61**, 1403–1406.
380. S. Roediger, A. N. Vieira, C. L. Brudy, M. Trabesinger, J. Hübscher and B. Morandi, *Synthesis*, 2024, **56**, 3923–3928.
381. M. Brovetto and G. Seoane, *J. Org. Chem.*, 2008, **73**, 5776–5785.